Technical Report

TR-98-04

Volume I

MAQARIN natural analogue stydy: Phase III

Edited by J A T Smellie

December 1998

Svensk Kärnbränslehantering AB
Swedish Nuclear Fuel
and Waste Management Co
Box 5864
SE-102 40 Stockholm Sweden
Tel 08-459 84 00
+46 8 459 84 00
Fax 08-661 57 19
+46 8 661 57 19

MAQARIN natural analogue study: Phase III

Edited by J.A.T. Smellie

December 1998

VOLUME I: Chapters 1–13

VOLUME II: Appendices A–R

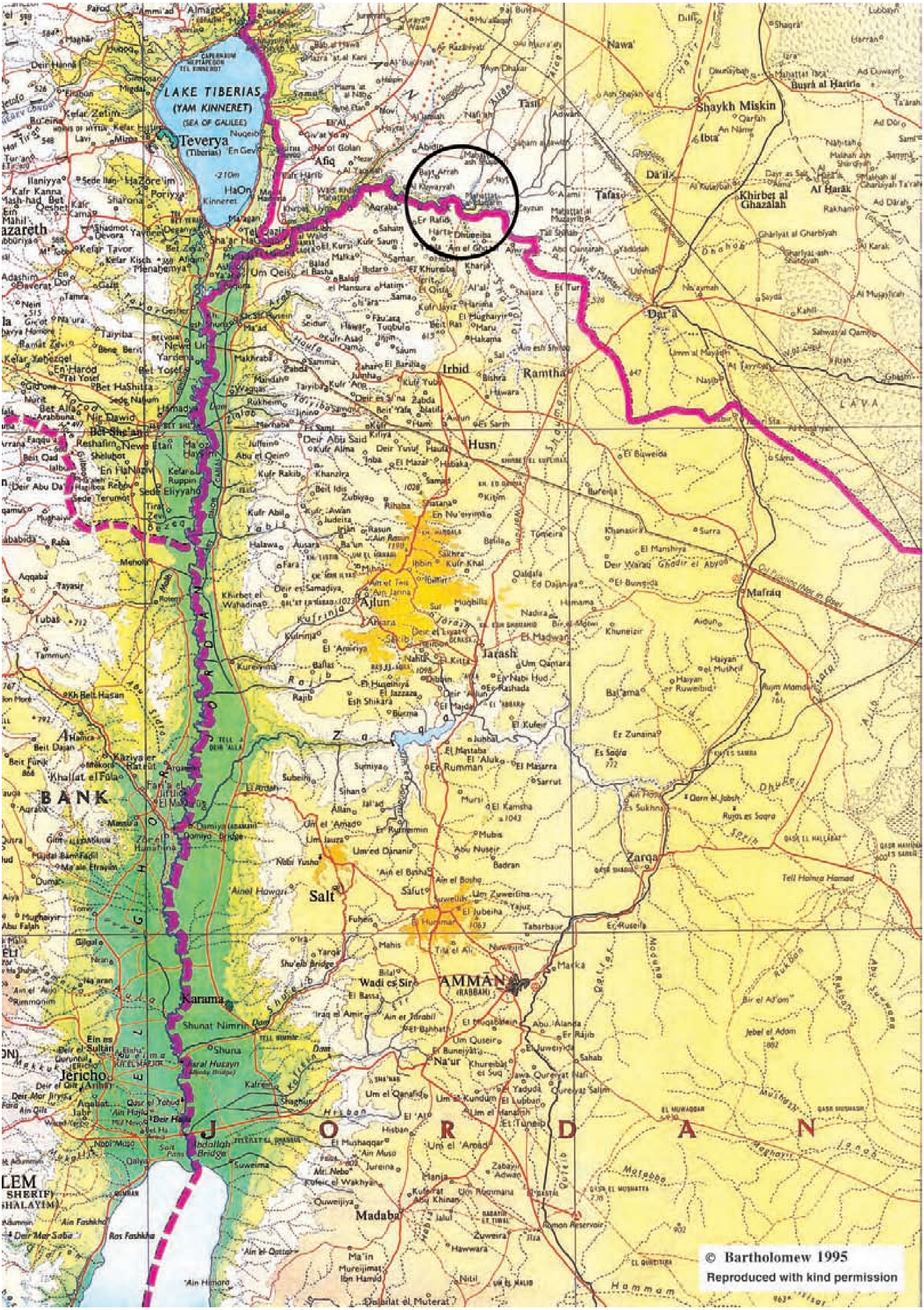

ACKNOWLEDGEMENTS

This study has been funded by Nagra (Switzerland), Nirex (U.K.), SKB (Sweden) and the Environment Agency (U.K.); their active support is gratefully acknowledged.

Special thanks go to Elias Salameh and Hani Khoury (University of Jordan, Amman) for organising the field visits (in particular the excellent excursion to the Jordan sites in conjunction with the Phase III Wrap-up Workshop in Cyprus in November, 1996), for their patience, humour, friendliness and hospitality and, not least, for their considerable scientific contribution to the project.

All the investigators are thanked for their dedicated efforts to make the study a success and, for their valuable technical discussions. The responsible authors are acknowledged for graciously and rapidly responding to the reviewer's comments and queries from the editor. Many thanks also to the reviewers who not only improved the report considerably, but also succeeded in leafing through all the pages without contracting 'tennis elbow'.

Maj-Britt Danielsson (Correcta) is thanked for the laborious task of typing, document formatting, organisation of figures and appendices, and being forever optimistic.

Finally, to Rita at the Amra Hotel, without whom the project would have been impossible.

ABSTRACT

This report represents the conclusion to Phase III of the Maqarin (Jordan) Natural Analogue Study. The main thrust was to establish the origin and chemistry of the Western Springs hyperalkaline groundwaters (Na/K enriched $Ca(OH)_2$ type) and to study their interaction with rocks of different compositions, as natural analogues to key processes that might occur at an early stage within the 'alkali disturbed zone' of cementitious repositories in different host rocks.

Whilst earlier studies at Maqarin were very much site-specific and process-oriented, Phase III provided a regional perspective to the geological evolution of the Maqarin region. This was made possible by greater field access which allowed a more systematic structural and geomorphological study of the area. This has resulted in a greater understanding of the age and spatial relationships concerning formation of the cement zones through spontaneous combustion of the Bituminous Marls, and the subsequent formation of high pH groundwaters at the Eastern and Western Springs locations.

At the Western Springs locality, hydrochemical and hydrogeological evaluation of new and published data (plus access to unpublished data), together with detailed mineralogical and geochemical studies, helped to clarify the very earliest stage of cement leachate/host rock interaction. The data were used also to test coupled flow/transport codes developed to assess the long-term evolution of a cementitious repository.

Additional objectives addressed include: a) rock matrix diffusion, b) the occurrence and chemical controls on zeolite composition, c) the occurrence and chemical controls on clay stability, and d) the role of microbes, organics and colloids in trace element transport.

The Maqarin site now provides a consistent picture explaining the origin of the hyperalkaline groundwaters, and is therefore a unique location for the examination of the mechanisms and processes associated with cementitious repositories. Application of these mechanisms and processes to repository performance assessment are listed and described.

LIST OF CONTRIBUTORS

W.R. Alexander	GGWW, University of Berne, Berne, Switzerland
J. Arlinger	Department of General and Marine Microbiology, Göteborg University, Göteborg, Sweden
W. Boehlmann	Umweltforschungszentrum Leipzig-Halle, Leipzig, Germany
A.V. Chambers	AEA Technology plc, Harwell, U.K.
S.R.N. Chenery	Analytical Geochemistry Group, British Geological Survey, Keyworth, U.K.
I.D. Clark	Department of Geology, University of Ottawa, Ottawa, Canada
A-C. Erlandson	Department of General and Marine Microbiology, Göteborg University, Göteborg, Sweden
P. Fritz	Umweltforschungszentrum Leipzig-Halle, Leipzig, Germany
S. Geyer	Umweltforschungszentrum Leipzig-Halle, Leipzig, Germany
W. Geyer	Umweltforschungszentrum Leipzig-Halle, Leipzig, Germany
L. Hallbeck	Department of General and Marine Microbiology, Göteborg University, Göteborg, Sweden
G. Hanschman	Umweltforschungszentrum Leipzig-Halle, Leipzig, Germany
A. Haworth	AEA Technology plc., Harwell, U.K.
E. Hodginson	Department of Earth Sciences, University of Manchester, Manchester, U.K.
C.R. Hughes	Department of Earth Sciences, University of Manchester, Manchester, U.K.
E.K. Hyslop	British Geological Survey, Murchison House, West Mains Road, Edinburgh, U.K.
D. Ilett	AEA Technology plc., Harwell, U.K.
F. Karlsson	SKB, Stockholm, Sweden

S.J. Kemp	Mineralogy and Petrology Group, British Geological Survey, Keyworth, U.K.
H.N. Khoury	University of Jordan, Amman, Jordan
F-D. Kopinke	Umweltforschungszentrum Leipzig-Halle, Leipzig, Germany
B. Lagerblad	Cement Institute, Stockholm, Sweden
C.M. Linklater	AEA Technology plc., Harwell, U.K.
G. Longworth	Department of Geology, University of Manchester, Manchester, U.K.
M. Mazurek	GGWW, University of Berne, Berne, Switzerland
A.E. Milodowski	Mineralogy and Petrology Group, British Geological Survey, Keyworth, U.K.
J.M. Pearce	Mineralogy and Petrology Group, British Geological Survey, Keyworth, U.K.
K. Pedersen	Department of General and Marine Microbiology, Göteborg University, Göteborg, Sweden
A.F. Pitty	Private consultant, 17, Black Horse Opening, Norwich, U.K.
J. Pörschmann	Umweltforschungszentrum Leipzig-Halle, Leipzig, Germany
S. Reeder	Analytical Geochemistry Group, British Geological Survey, Keyworth, U.K.
C.A. Rochelle	Fluid Processes Group, British Geological Survey, Keyworth, U.K.
E. Salameh	University of Jordan, Amman, Jordan
D. Savage	QuantiSci, Melton Mowbray, Leicestershire, U.K.
J.A.T. Smellie	Conterra AB, Uppsala, Sweden
B. Smith	Analytical Geochemistry Group, British Geological Survey, Keyworth, U.K.
C.J. Tweed	AEA Technology plc, Harwell, U.K.
H.N. Waber	GGWW, University of Berne, Berne, Switzerland
P.D. Wetton	Mineralogy and Petrology Group, British Geological Survey, Keyworth, U.K.
J. Wragg	Fluid Processes Group, British Geological Survey, Keyworth, U.K.

CONTENTS

VOLUME I: Chapters 1–13 (this volume)

CONTENTS

VOLUME II: Appendices A–R

EXECUTIVE SUMMARY

Phase III of the Maqarin natural analogue project was initiated in December 1993 to establish the origin and chemistry of the Western Springs hyperalkaline groundwaters (of type Ca-K-(Na)-OH-SO_4) and study their interaction with host rocks of different compositions. It was hoped that this information, together with existing data from the Eastern Springs groundwaters (of type Ca-(Na, K)-OH), would help to clarify the very earliest stage of the cement leachate/host rock interaction and test current understanding of the long-term evolution of an alkaline disturbed zone around a cementitious repository. With respect to the hyperakaline groundwater environment, additional objectives included: a) the occurrence and chemical controls on zeolite composition at both the Eastern and Western Springs localities, b) the occurrence and chemical controls on clay stability at Maqarin and in Central Jordan, c) the role of colloids, organics and microbes in trace element transport, and d) geomorphological evolution of the Yarmouk River Valley as a control on the hyperalkaline groundwater evolution.

Whilst earlier studies at Maqarin were very much site-specific and process oriented, Phase III was planned to provide a more regional perspective to the geological and hydrogeochemical evolution of the entire cementitious system. Greater field access allowed a systematic structural and geomorphological study of the Maqarin area. This involved the integration of new information from several field visits, from the drilling of strategically placed boreholes, and gaining access to existing data in unpublished reports.

RECENT GEOLOGICAL EVOLUTION OF THE MAQARIN SITE

The Maqarin area (Fig. 1) comprises Cretaceous-Tertiary carbonate rocks overlain by Quaternary basalts, soils and alluvium. The E-W trending Yarmouk River Valley is a relatively recent geomorphological feature, having eroded through some 400 m of the Irbid Plateau exposing the Bituminous Marl Formation which is overlain by the Chalky Limestone Formation, in turn capped by basaltic lava flows. There is no evidence that the Yarmouk Valley is structurally controlled by tectonic events associated with the Jordan Rift Valley system. In general, it seems that the Yarmouk Valley has influenced the evolution of the Maqarin area by serving essentially as a conduit for the transportation of sediment and lava, rather than being the product of dramatically rapid erosion.

Regionally, the exposed strata show very little deformation and are almost horizontal to gently dipping; flexures with very small curvatures are also evident. Locally, at the Eastern Springs locality, the Bituminous Marl Formation has been slightly uplifted by a N-S trending anticline which plunges to the NE. Minor anticlinal bending/

deflection in the marls occurs some 500 m east of the anticline. Detailed structural mapping on a local scale underlines the heterogeneity of the system, in part explained by gravity tectonics (i.e. slumping) facilitated by the steep hillslope angles (~45°). This is supported by widespread evidence of reactivation along the dominant N-S trending joint system by subhorizontal shear movements (seen as slickensides) and an increase in faulting towards the mouth of Adit A-6, the Adit being parallel to the joint system and located at the southern flank of the Yarmouk Valley. Slump features bordering the Yarmouk River Valley are widely observed at the Eastern Springs locality and further upstream.

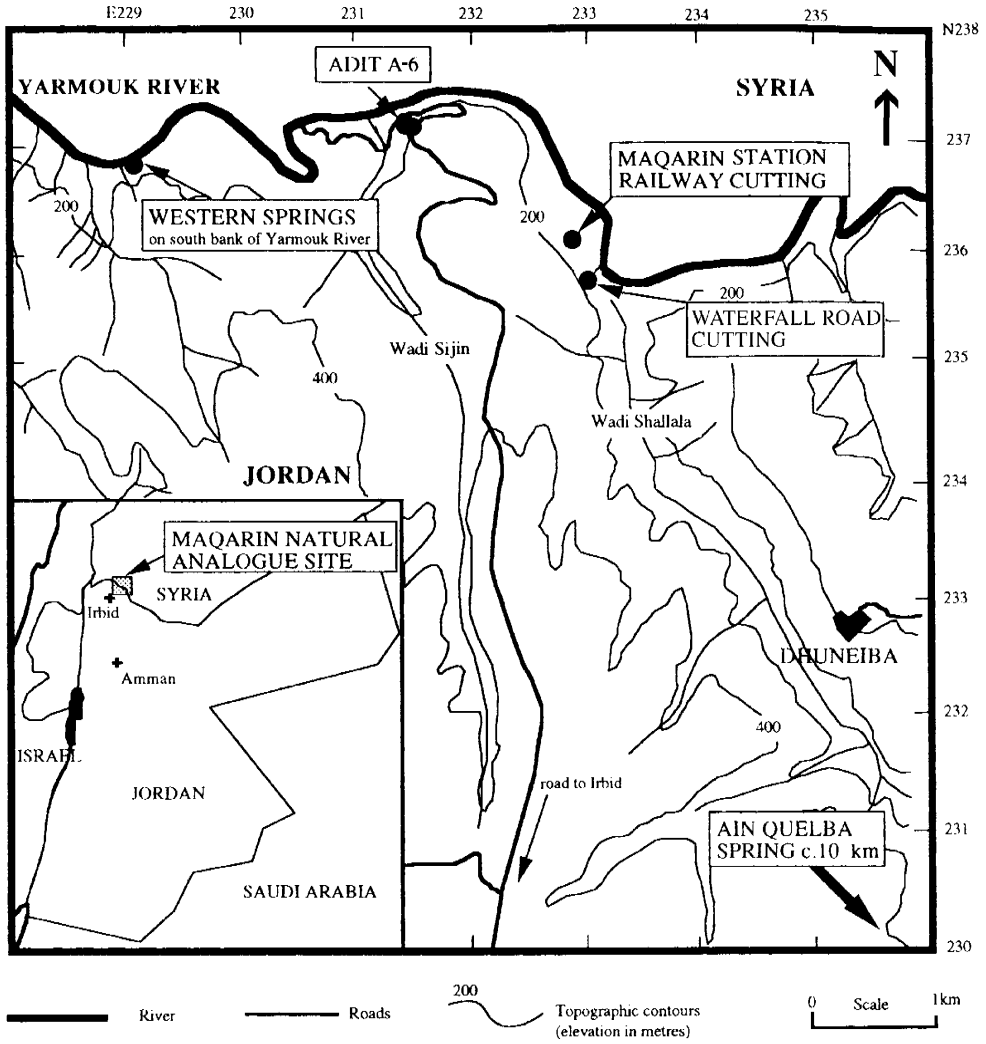

Figure 1. *Location of the Maqarin area in relation to the major wadis and the sampling sites.*

Less is known about the Western Springs locality where talus and colluvium cover most of the hillslopes. There is, however, some indication of a N-S trending fault system and the possibility of localised shear and rotation between such faults. Gravity slumping features on the scale observed at the Eastern Springs locality are not readily observed, but evidence exists of valley bulging on the floor of Wadi Sijin and the presence of a landslide on the western side of the wadi.

Whilst earthquake shock is not seen as a likely mechanism for creating fissures and joints directly in the rock, it may be a significant factor in triggering landslides and causing abrupt rupturing of superficial strata followed by erosional downloading. It is hypothesised that such mechanisms have long typified the Eastern Springs area, and also activated spontaneous combustion in the Bituminous Marl Formation to produce the "cement zones", and subsequently the formation of the hyperalkaline groundwaters in the area. From geomorphological considerations, a probable date of ignition has been set to around 600 ka, and certainly not later than 150 ka. More hypothetically, a second, later phase of triggered landslides, might also be considered to explain the geomorphological features observed at the Western Springs area. Speculatively, such an event might have occurred in the last 100 ka (Late Quaternary), or even as recently as the last 10 ka (Holocene). These two phases of landslip activity indicate that the Eastern Springs system is geologically older than the Western Springs system.

In addition to these two major landslip events, reactivation on a smaller scale may be expected to be recurrent, triggered rapidly by heavy rainfall and more gradually over longer timescales by continued lateral erosion of the Yarmouk River. This may account for the periodic sealing and reactivation of hyperalkaline groundwater conducting fracture pathways indicated from mineralogical studies and field observations.

GROUNDWATER FLOW AND HYDROGEOCHEMICAL EVOLUTION OF THE MAQARIN SITE

The origin and flow features of the groundwaters in the Maqarin area were first studied in the context of the regional flow systems in northern Jordan, and then by constructing a local scale, three-dimensional model for the Maqarin area illustrating the interrelationships between the major stratigraphical units, the important structures, and the general hydrogeological character of the area.

In northern Jordan, regional hydrostratigraphic units dominate with flow generally from the central plateau eastwards to the Jordan River Valley and northwest to the Yarmouk River Valley, with a component from southern Syria flowing southwest towards the Yarmouk Valley (Fig. 2). On the local scale, three main groundwater bodies can be recognised in the Eastern Springs area flowing northwards to the Yarmouk River Valley:

1) Deep confined aquifer water from the Amman Formation (B_2 Unit).

2) Infiltration of meteoric water through the Chalky Limestone Formation in the plateau lying east of Maqarin, penetrating the Bituminous Marl Formation (B_4/B_5

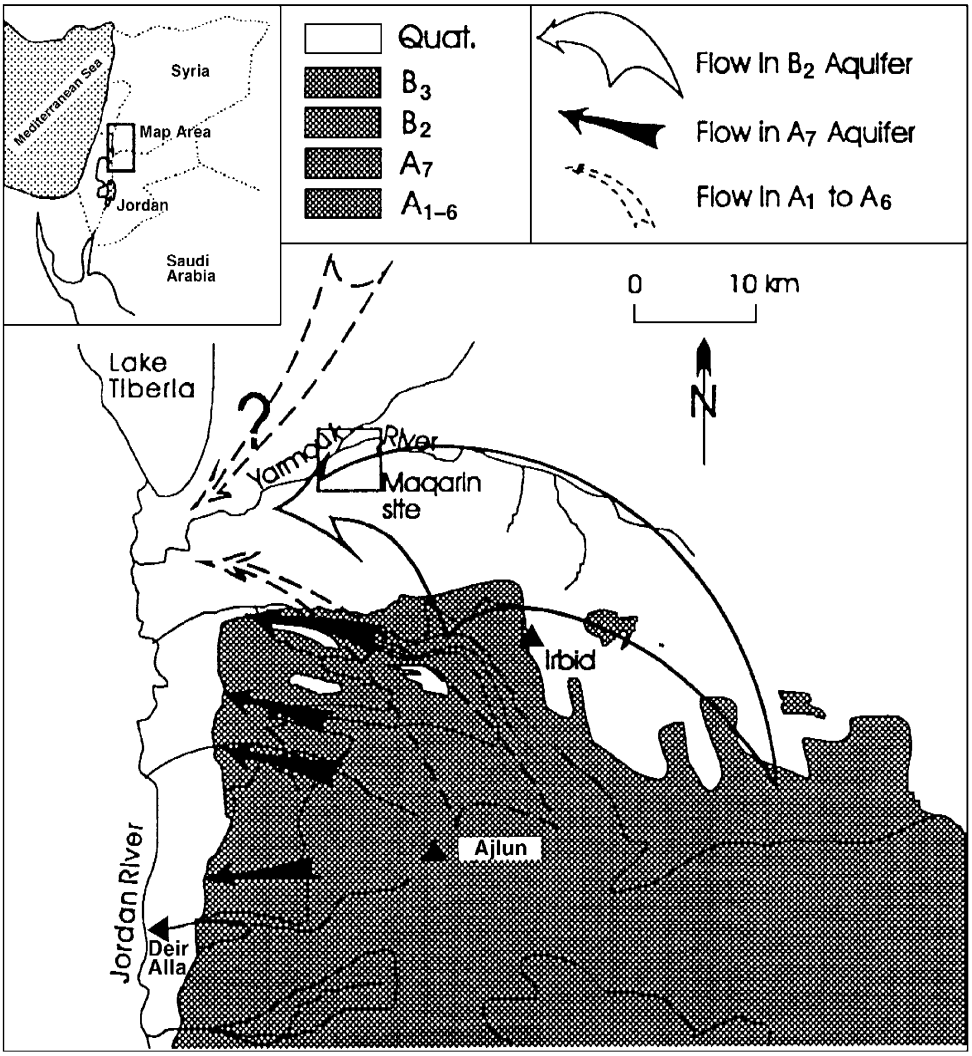

Figure 2. *Regional geology and major groundwater flowpaths in northern Jordan.*

units) down to the contact (B_3) between the cement zones and unmetamorphosed marls. The groundwaters follow this interface eventually discharging as seeps and springs along the Yarmouk Valley sides. In places, groundwater penetrates the cement zone via fractures and joints and passage through this cement zone gives rise to the hyperalkaline groundwaters.

3) Recharge water infiltrates directly into the Chalky Limestone Formation above Adit A-6, down into the cement zone, possibly mixing with type (2), or locally discharging along the roof and walls of the Adit. The maximum extent of the hyperalkaline plume downflow from Adit A-6 to the Yarmouk River is 400–500 m.

In the Western Springs area, the groundwater flow is also northwards towards the Yarmouk River Valley. The waters originate from rapid vertical recharge into the

Chalky Limestone Formation at the plateau south of the Western Springs location facilitated by widespread open karst features. These groundwaters are eventually channelled along the upper part of the underlying Bituminous Marl Formation at the cement/unaltered marl interface, to eventually discharge through a thick colluvium sequence along the Yarmouk Valley at an elevation of 1–4 m above the river bed. A smaller groundwater flow component may penetrate deeper into the unaltered marls controlled by discrete fractures and fissures before discharging. Reaction with the cement zone has also produced the hyperalkaline groundwaters at this locality, although the extent of the hyperalkaline plume downflow to the river is somewhat less than at the Eastern Springs.

Hydrogeochemical and isotope studies largely support the hydrogeological conceptualisation of the major groundwater flow pathways. The recharge groundwaters are meteoric and local in origin, of normal pH and dilute bicarbonate in type, contain measureable tritium, and are the probable precursors to the high pH groundwaters. No significant mixing of groundwaters from the underlying confined Amman Formation aquifer is indicated. Interaction of the normal pH groundwaters with the cement zones in the Bituminous Marl Formation has produced two chemically distinct high pH groundwaters; Eastern Springs Ca-(Na, K)-OH type and the Western Springs Ca-K-(Na)-OH-SO_4 type. Both types are believed to be older than at least 40 years (tritium-free), although minor amounts of tritium (~4 TU) in some samples may indicate mixing with recent recharge waters. The absence of thermonuclear ^{36}Cl is also consistent with an age of >40 years.

Hydrogeochemical modelling suggests that the observed differences in groundwater composition between the Eastern and Western Springs localities can be attributed to different stages of water/rock interaction and evolution (Fig. 3). There is no convincing evidence that the high Na, K and SO_4 concentrations at the Western Springs locality are due to initial differences in the composition of the cement zone, variable infiltration conditions, or anthropogenic contamination. A possible scenario is that the Eastern Springs area groundwater circulation has occurred over a much longer timespan and readily soluble K/Na rich mineral phases (e.g. oldhamite) are already completely dissolved. This compares with the Western Springs area where the groundwater flow system is younger and therefore the system is less involved geochemically. This is consistent with field observations which suggest that the Eastern Springs system is geologically older than the Western Springs system.

It is therefore attractive to consider the Western Springs groundwaters as being analogous to the K/NaOH pore waters (of pH 13 and more) expected to leach from a cementitious repository following the first stages of groundwater/cement interaction (i.e. Region 1). The Eastern Springs, accordingly, may be considered analogous to a more evolved $Ca(OH)_2$ cement pore water (of pH about 12.5) which is produced following complete leaching of the soluble K/NaOH phases (i.e. Region 2). The Maqarin analogy must, however, be treated with some caution. It should be remembered that in a repository situation, the source of Na and Ca in the porewater is highly soluble Na/K hydroxide in the cement. Early repository waters are correspondingly rich in Na and K, but relatively poor in Ca (because the solubility of Ca hydroxide is reduced in the presence of high-hydroxide solutions). At Maqarin, Ca(Na,K) sulphide phases (e.g. oldhamite), present as inclusions in calcite, provide the source of Na and K. In fact laboratory support studies show that high

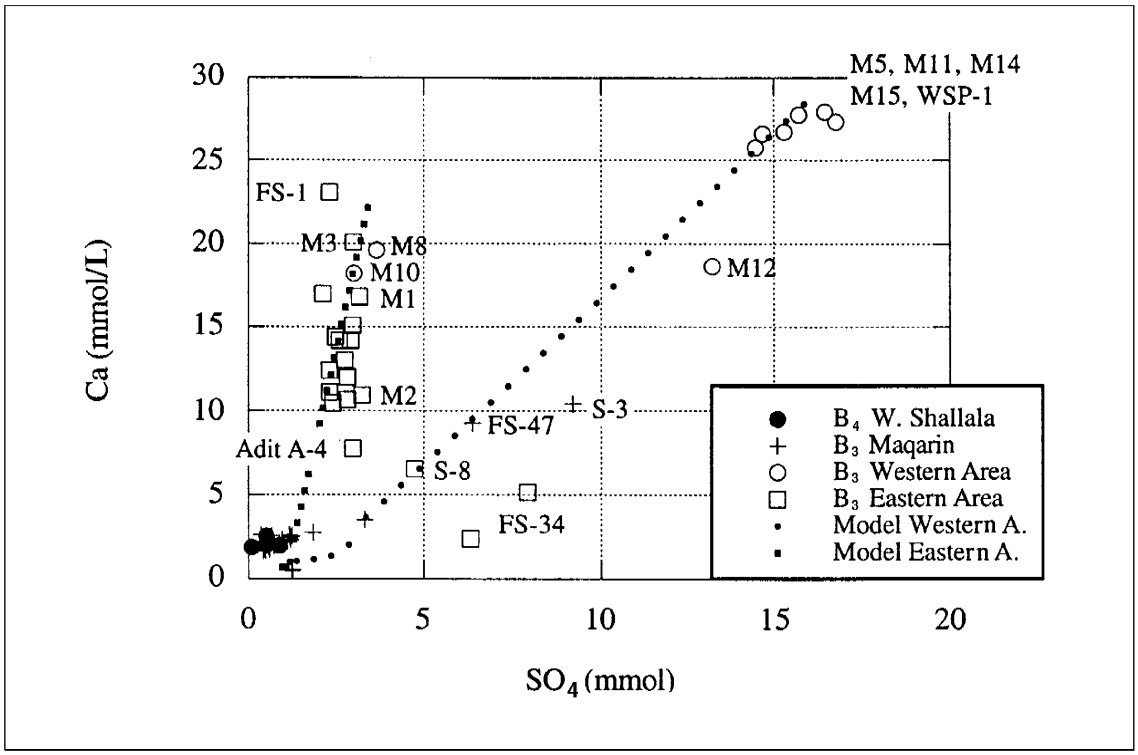

Figure 3. *Modelled evolution of Ca^{2+} and SO_4^{2-} concentrations compared with measured data of high-pH groundwaters from the Eastern and Western Springs areas.*

concentrations of K and Na can be easily leached from samples of calcined marl producing a composition similar to the Western Springs groundwaters. Early Maqarin waters (i.e. Western Springs) are therefore rich in Na, K and Ca.

MINERALOGY AND GEOCHEMISTRY

The main thrust of the mineralogical studies was to study the interaction of discharging high pH groundwaters from the Western Springs locality with unmetamorphosed country rocks (basalt; chert; marl, more accurately described as a limestone/clay biomicrite) contained as fragments, clasts and blocks within the Quaternary colluvium deposits which characterise the Yarmouk River Valley sides above the river bed. Studies included the detailed sedimentology of the colluvium system, provision of major and trace element analyses of whole-rock samples and of individual primary and secondary minerals, modal mineralogy of the colluvium deposits, and porosity characterisation.

The colluvium deposits comprise a lower fluvial boulder/gravel unit, an overlying upper colluvium unit, and a thin soil cover with a poorly defined, thinly weathered transitional zone of weakly cemented colluvium. Since the high pH groundwaters mostly discharge through the lower fluvial unit, the samples for study were selected from this horizon.

In addition, supplementary studies were made on high pH alteration reactions on material from the Eastern Springs locality, in particular Adit A-6. These were carried

out to confirm Phase II observations and conclusions, to elucidate the lateral extent and influence on the country rock during migration of the hyperakaline plume, to investigate the hyperalkaline interaction effect on the host biomicrite porosity, and to determine the trace element mobilisation and distribution adjacent to conducting fractures in the biomicrite (including rock-matrix diffusion).

Hyperalkaline Groundwater Reactions

Basalt, of local derivation, is mostly alkali olivine in type and primary alteration (due probably to weathering) is seen as alteration rims of secondary Fe oxides/ oxyhydroxides around the clasts, as Fe-oxides distributed along the cleavage planes of, for example, augite, as a weak pervasive alteration of feldspar to a white mica, and alteration of interstitial glass to clay minerals and haematite. Of the investigated rock types, the basalt clasts show most reaction with the hyperalkaline waters, being characterised by significant reaction rims comprising major secondary CSH and CASH alteration products. The most reactive phase is the matrix glass, followed by plagioclase and K-feldspar. In contrast, augite, hypersthene and olivine are comparatively unaltered.

The chert clasts are composed of fine-grained or cryptocrystalline quartz, although this may include poorly crystalline or amorphous silica. These show variable reaction with the hyperalkaline groundwaters seen as: a) replacement by fine-grained calcite or aragonite around clast margins, and b) total dissolution and replacement by amorphous (isotropic) gel-like CSH minerals. Most chert reaction products appear to be Al-substituted CSH gels, although some Mg-rich CSH gels were also observed.

The clay biomicrite clasts studied at the Western Springs locality are identical to the Eastern Springs marls investigated during Phases I and II of the Maqarin project. They are composed mostly of fine-grained micrite, chalk and recrystallised microsparrite consisting largely of calcite. Dolomicritic clasts are also present as a minor component probably accounting for the presence of ankerite. The biomicrite clasts show only minor leaching in contact with the hyperalkaline groundwaters. However, those dolomicritic clasts (with an estimated enhanced porosity of ~20%) are associated with the dissolution of the matrix dolomite which is typically infilled by a structureless, microporous Ca-Si-S-Al-rich material, unfortunately too fine-grained for positive identification. By comparison with the Eastern Springs material, these alteration phases may be largely ettringite-thaumasite dominated.

Similar reactivity is observed in the sand-silt matrix which characterises the colluvium. Plagioclase is highly corroded, being present only as trace relicts within a groundmass of fine CASH gel. Detrital quartz and chert grains may also be highly corroded and replaced by CASH minerals.

As a general conclusion, quartz, chert, K-feldspar, glass and plagioclase are the most reactive phases with the hyperalkaline groundwaters, dolomite is moderately reactive, augite, hypersthene (orthopyroxene) and olivine are weakly reactive, and apatite and Ti-Fe oxides appear to be largely unreactive (Table 1).

Table 1. Summary scale of reactivity of different mineralogical components with hyperalkaline groundwater in the Western Springs Quaternary deposits.

BASALT CLASTS
Glass + K-feldspar > Plagioclase >> Augite + Orthopyroxene > Olivine + Fe-Ti oxides
LIMESTONE / CLAY BIOMICRITE CLASTS
Dolomite >> Calcite
MATRIX
Quartz + Chert + K-feldspar-plagioclase > Augite > Olivine + Calcite + Apatite + Ti-Fe oxides
OVERALL SCALE OF REACTIVITY
Quartz Apatite
Chert ≥ Plagioclase > Dolomite >>Augite + Orthopyroxene > Olivine > Calcite
Glass Ti-Fe Oxide
K-feldspar

Mineral paragenesis of the secondary alteration phases indicates the following sequence: a) a very hydrous Ca-K-Na-Al "zeolite-type" phase, b) a CSH gel with a variable Ca:Si ratio covering the range CSH(I) to CSH(II) (i.e. suolinite-afwillite), c) a more Si-rich CSH gel (i.e. okenite-type), and d) a low Ca-Si ratio CSH phase (i.e. truscottite-type). The latest stage of alteration is the replacement of the CSH and CASH phases by calcite or aragonite.

The extent of clast reaction rims seems to be in the order of biomicrite > chert > basalt. However, this does not preclude that clast-specific mineral phases in the chert and basalt may be more altered than in the biomicrite.

Matrix Diffusion Studies

A detailed study of the extent of rock matrix diffusion (in unaltered clay biomicrite) was carried out on four profiles taken perpendicular to water-conducting fractures from Adit A-6; one profile was located close to the cement zone. Each profile was analysed for a suite of major and trace elements and natural decay series radionuclides along with porosity variations; the results are ambiguous.

The elements analysed comprised Al, Ca, Cr, Ni, Co, Se, S, Sr, Zr, Mo, Cs, Ba, Pb, Th and U. Studies showed that geochemical evidence for rock matrix diffusion adjacent to water-conducting fracture zones is influenced by the presence of microfracture networks close to the major fractures, typically extending for several tens of millimetres into the host rock. Accordingly, levels of Cr, Ni, Se, S, Mo, Cs and Ba are commonly enhanced or disturbed for up to 30–40 mm distance from the fracture surfaces, and particularly enriched at the fracture face. These same elements are concentrated in the dominant fracture infill mineralisation (mainly ettringite, thaumasite, jennite and barite). Geochemical enhancement is most likely explained by the presence of the microfracture infill minerals and by the dissolution and replacement of matrix calcite in the host rock, particularly at the fracture face. At

greater distances from the major fractures (>40 mm) the geochemical composition of the host rock is indistinguishable from the background lithological variation, indicating no alteration.

Significant variation in the natural decay series radionuclide background signal has made it impossible to detect any potential perturbations due to hyperalkaline water/rock matrix interaction. However, in two of the profiles there is some indication of a clear signal: the $^{226}Ra/^{238}U$ ratios suggest relatively young water/rock interaction up to 4–7 cm depth. Even so, these depths should be treated cautiously considering the above comments on the influence by microfracture networks and pre-existing lithological variations (e.g. bedding etc.) extending several centimetres into the rock.

Porosity characteristics indicated for all four profiles an enhancement of microporosity in very narrow zones immediately adjacent to the fracture surface in the altered clay biomicrite host rock. These observations confirm earlier data from Adit A-6 and are explained by calcite dissolution adjacent to the fracture. This is followed, in some cases, by a decrease in porosity further into the host rock (e.g. 10–17 mm interval) due to calcite cementation; at a still greater distance from the fracture surface either a constant (or gradual increase in) porosity is observed.

Zeolite Occurrence and Stability

Zeolites are characterised by their large molar volumes and high cation-exchange capacity for alkali and alkaline-earth metals, and are noted for strong sorption of mono- and divalent cations. Sorption of trivalent elements and actinides is somewhat weaker. Since zeolites will occur as products of interaction of hyperalkaline groundwater with aluminosilicate rocks, i.e. as products of the migration of a hyperalkaline plume, their potential to sorb and retard certain migrating radionuclides is of importance to the long-term performance of a cementitious repository. To evaluate the general importance of zeolites, a thorough literature review was first carried out as to their occurrence, stability and behaviour, and then specifically these observations were applied to understanding their origin and occurrence at the Western Springs locality at Maqarin.

All zeolites are generally metastable in nature, transforming over time into more ordered varieties, and ultimately, into feldspars. Zeolite formation in preference to feldspars is favoured by their higher growth rates. They are most abundant in tuffaceous rocks of saline, alkaline lakes; the type and amounts of zeolites formed in all geological systems are strongly controlled by growth kinetics. Phillipsite consistently forms early in the evolution of a diagenetic system, to be replaced by more thermodynamically stable zeolites at later stages of evolution.

A literature compilation of thermodynamic data has been carried out, although no data were found for two minerals, dachiardite (high-silica zeolite) and thaumasite, both of which occur at Maqarin. The hyperalkaline groundwaters at Maqarin are not in thermodynamic equilibrium with zeolites; the concentrations of major aqueous species are probably controlled by equilibrium with portlandite and an ettringite-thaumasite solid solution.

The range of minerals lining groundwater flowpaths at Maqarin (aragonite, gypsum, ettringite-thaumasite, calcium silicate hydrates and zeolites) may be interpreted by the

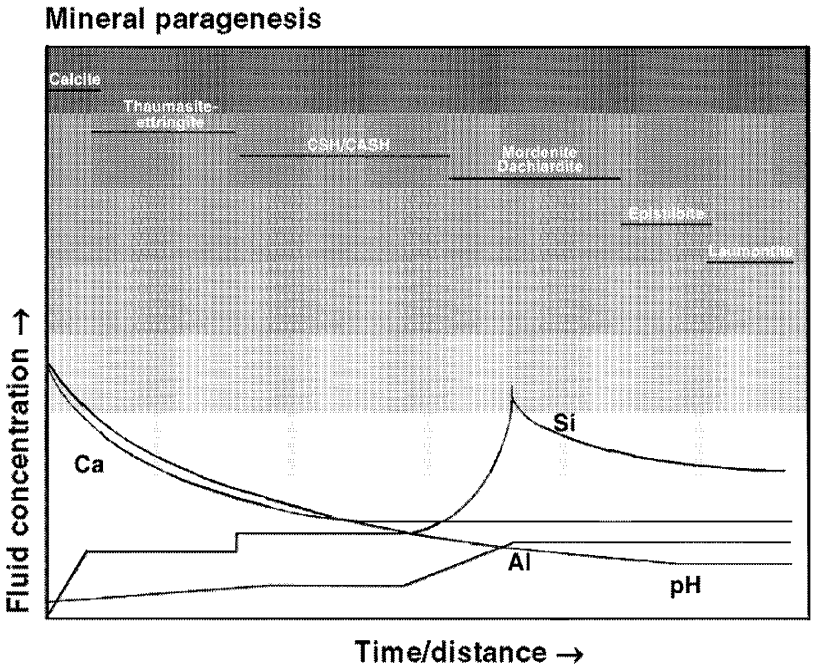

Figure 4. *Schematic diagram of mineral paragenesis and fluid composition evolution within a single fracture in the Maqarin alteration system.*

reaction of a Ca-OH-SO_4 type groundwater with the clay biomicrite, progressively losing Ca, OH and SO_4 ions by the precipitation of CSH, gypsum and ettringite whilst gaining Al and Si by reaction with the biomicrite and ultimately precipitating zeolites (Fig. 4).

The types of zeolites observed at Maqarin are typical of those associated elsewhere with fluids which are either saturated or supersaturated with respect to quartz solubility. Specifically, yugawaralite, mordenite and dachiardite are usually associated with fluids supersaturated with respect to quartz. Laumontite and epistilbite form from solutions saturated with quartz, whereas chabazite is the only zeolite at Maqarin normally associated with fluids undersaturated with respect to quartz. All this evidence suggests that the zeolites found at Maqarin coexisted with pore fluids which were much more siliceous and less alkaline than those currently sampled from groundwater seepages. Such pore fluids may develop only locally, perhaps during the initial and final stages of the sealing of an alteration vein, whilst the bulk of the alteration fluids are of the hyperalkaline type. They may thus represent a small fraction of the pore fluids extant in the Maqarin area.

Conceptual Model of Plume Development

On the basis of geochemical first principles, a conceptual model is presented of the evolution of the host rock as a hypothetical hyperalkaline plume migrates away from a cementitious repository (Fig. 5). The model assumes that the leachates are pushed

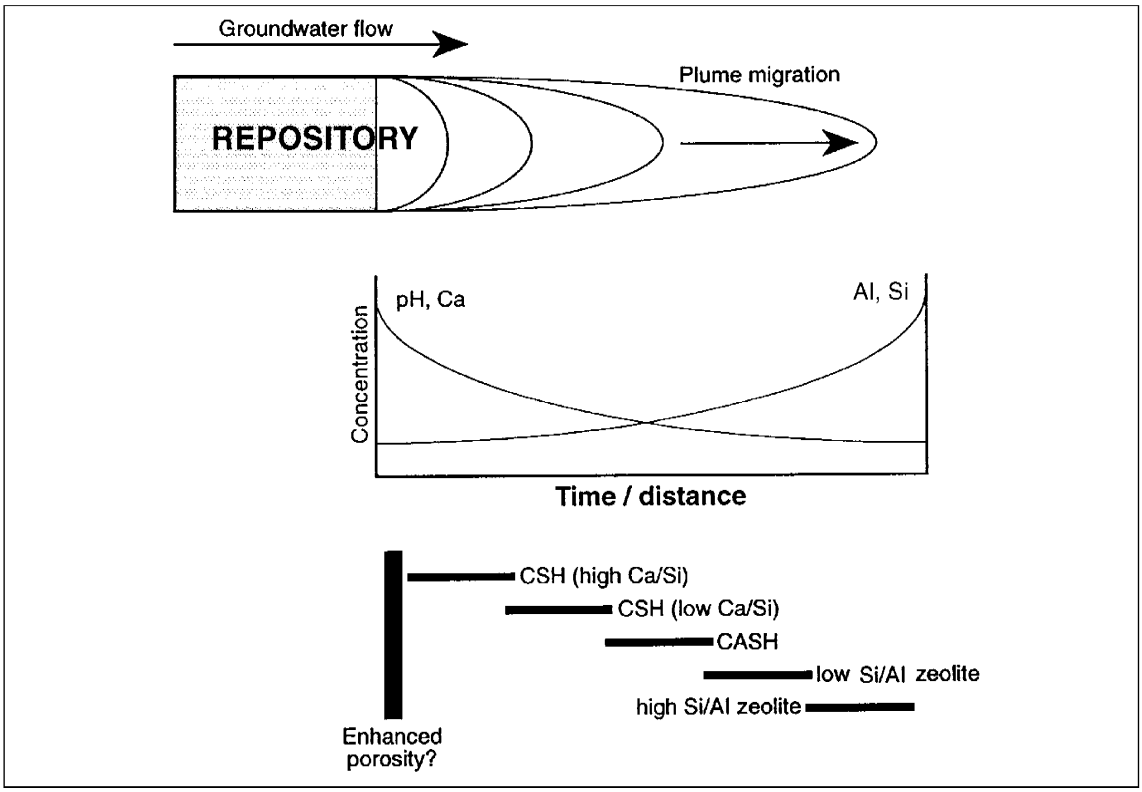

Figure 5. *Schematic diagram of hyperalkaline plume migration from a cementitious repository for radioactive wastes, showing hypothesised variations in fluid composition and alteration mineralogy in space and time.*

from the cement in a piston effect, due to the flow of groundwater into the cement further upstream in the repository. At the cement/host rock interface (the proximal part of the plume), the hyperalkaline leachates have not yet reacted with the host rock and so have a high pH and high concentrations of Na, K and Ca, reflecting the cement porewater chemistry. As the plume reacts with the host (aluminosilicate-bearing) rock, the pH falls, as do the Na, K and Ca concentrations in the groundwater, while the concentrations of Al and Si rise fractionally. Beyond the distal edge of the plume, in the, as yet, undisturbed host rock, the groundwater pH is near neutral, the Na, K and Ca concentrations are low, while the concentrations of both Al and Si are high.

This pattern has consequences for the secondary mineralogy: CSH phases will be found in the fractures (through which the plume has migrated) in the proximal part of the plume, reflecting the fact that the leachate has not yet reacted with the host rock and is equilibrated with the CSH phases which make up the cement. As the leachate moves downstream and interacts with the aluminosilicates in the host rock (and the host rock groundwater and porewater), the Al concentration increases, precipitating CASH phases. At the distal edge of the plume, the leachate has reacted with an even larger volume of host rock (and the host rock groundwater and porewater) and eventually precipitates zeolites as the Al concentration in the groundwater becomes high enough and the pH low enough.

If it is assumed that the plume continues to migrate, then, by analogy with the above argument, the zeolite zone produced by the distal part of the plume will be over-run by the central part of the plume, inducing some re-dissolution of the zeolite phases and replacement by CSH phases. These complex mixtures have been observed in places at Maqarin.

Geochemical Modelling

Based on mineralogical observations and groundwater chemistry, geochemical modelling (involving both equilibrium and kinetic approaches) was carried out to predict the nature of the reaction rims around the different rock fragments/clasts caused by interaction with the hyperalkaline groundwaters, and to compare these predictions with characterisation of the altered clasts. This approach should help build confidence in models of long-term plume evolution (i.e. alkaline disturbed zones; ADZ) around repositories in different geological environments.

Equilibrium (HARPHRQ and CHEQMATE) and kinetic (MARQUISS) modelling approaches were used to model the hyperalkaline water-rock interaction within the colluvium at the Western Springs locality (e.g. Fig. 6). The following conclusions can be made:

- two processes influence the suite of secondary minerals within clast reaction rims: precipitation within the solutions (without any contact with solid phases) and dissolution of primary minerals as a consequence of hyperalkaline water/rock interaction,

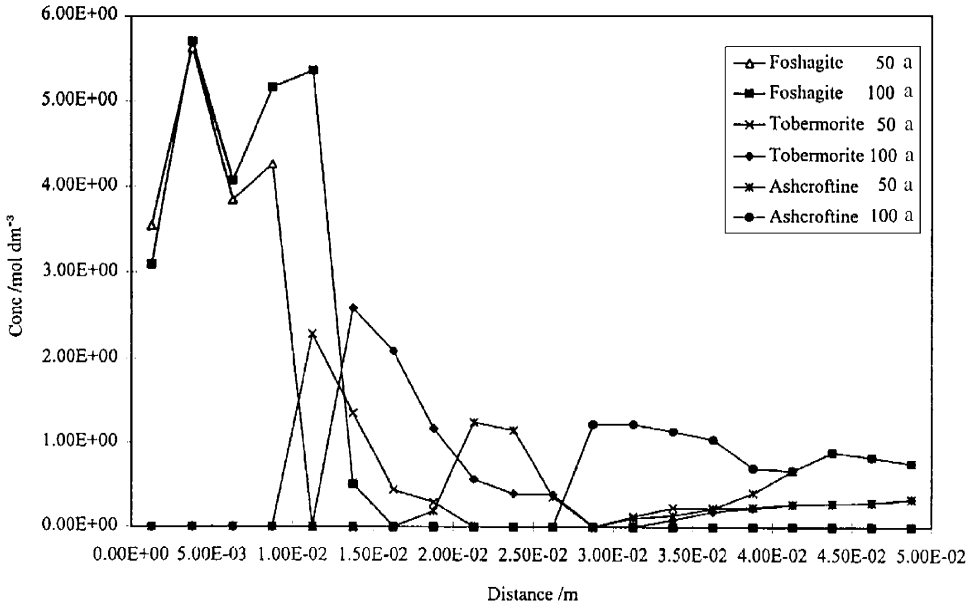

Figure 6. *Predicted evolution in years of the CSH phases and zeolites in Bituminous Marl (CHEQMATE).*

- the secondary minerals predicted to form using an equilibrium model (portlandite, ettringite, calcite, CSH phases and zeolites) were in reasonable agreement with those observed in the field,
- the observed mineral paragenesis could be explained by the outward migration of a high pH plume; initially formed products (coincident with the distal edge of the plume) being replaced by later products as the plume evolves and over-runs itself to greater distances from the source,
- the calculations overpredicted the width of the reaction rims around clasts. Observed rims, although irregular, were typically less than 1 mm. After 100 a of reaction time, calculated rims were already in excess of this (up to several mm's). As well as uncertainty regarding the timescale over which the system has been active, model predictions could be attributed to uncertainty regarding the physical properties of the system, both in terms of: 1) initial diffusion coefficient and porosity of the rock, and 2) changes in porosity occurring as the alkaline water/rock interaction progresses,
- both the mineralogy and the transport properties of the system play an important role in determining the width of reaction rims,
- the transport properties (porosity, diffusivity) of the clasts had the most important influence on the width of the reaction rims.

COLLOIDS

In the case of a cementitious repository, degradation of the cement may provide a significant source of colloids at both the near-field/far-field interface and at the margins of the hyperalkaline plume (which may extend downstream of the repository). Evidence from the Maqarin groundwaters suggests that the numbers of colloids generated in the cement zone will be low. This is supported by the very low amounts of colloids measured from the Adit A-6 (10^7 colloids mL^{-1}). It has been also demonstrated that no uranium (or other trace elements) is associated with the colloidal material characterised. However, as a note of caution, sampling for colloids was conducted under oxidising conditions, and these may not be representative of the reducing conditions expected around a repository

MICROBES

Micro-organisms are present in all the studied hyperalkaline Maqarin groundwaters (~10^5 microbes mL^{-1}), but it could not be demonstrated conclusively that they were *in situ* viable and growing at high pH, rather than just transported to the sampling sites by neutral groundwater. The diversity of the micro-organisms is similar to that recorded from deep groundwater elsewhere using the 16S rRNA gene sequencing method, but none of the sequences found were typical for known alkaliphilic organisms. A possible hypothesis based on the obtained results is that the investigated Maqarin high pH groundwaters may be somewhat too extreme for active life, even for the most adaptable microbes, but this remains to be demonstrated.

ORGANICS

Studies have shown that the high DOC content in the groundwater from the Western Springs locality cannot be fully explained by dissolution of organic matter from the Bituminous Marls by percolating high pH groundwaters. Solution experiments show that only a minor part of the organics could dissolve in the water; in addition, aromatics are found in the DOC whereas organic material is predominantly aliphatic in the marls, which suggests another source for the material. This may include the partial combustion of bitumen during metamorphism, explaining the high aromatic content, and may be a contributary cause to the fact that no soil organics (i.e. no humic compounds) were found in the groundwaters.

CLAY STABILITY

To date, the lack of sufficient identifiable smectite clays in zones of alkaline alteration has precluded an evaluation of clay stability under hyperalkaline conditions. Other, clay-rich areas, need to be identified and studied.

PERFORMANCE ASSESSMENT CONSIDERATIONS

The Maqarin site now provides a consistent picture explaining the origin of the hyperalkaline waters, the persistence of some of the hyperalkaline springs/seepages, and the sequence of alterations occurring when such waters react with various rock-types. Additionally, the studies have produced good quality measurements of the concentration (and general speciation) of some performance assessment relevant elements in high pH groundwaters, microbial and colloidal populations and concentrations of colloidal material.

The Maqarin natural analogue site is therefore a unique location for the examination of the mechanisms and processes associated with cementitious repositories. Evidence from Maqarin shows that:

- hyperakaline pore fluid conditions generated by minerals similar to those found in cements are long-lived (in excess of tens of thousands of years),
- predictive models of the solubility of several elements of interest to radioactive waste disposal provide conservative estimates of solubility (i.e. solubilities are overestimated),
- the amounts of colloidal material generated at the cement zone/host rock interface will be probably no higher than in neutral groundwaters,
- sequences of minerals predicted by thermodynamic and coupled modelling are similar to those observed in hyperalkaline alteration zones,
- the rock matrix may be accessible to diffusion of aqueous species even during the phase of on-going wallrock alteration,
- narrow aperture fractures will probably be self-healing,

- tectonic effects upon fracture sealing and the site hydrology need to be considered on a repository site-specific basis,
- the conceptual model for the evolution of a hyperalkaline plume in a host rock is largely consistent with observations at the site.

1 INTRODUCTION

The Maqarin site in northern Jordan, considered to be an excellent natural analogue for a cementitious low- and intermediate-level radioactive waste repository (also chemo-toxic wastes), was first examined in 1989 in a collaborative research programme jointly funded by Nagra, Nirex and Ontario Hydro. The Maqarin site is unique, situated in bitumen-rich marls which have been thermally altered by natural *in situ* combustion. The rehydrated and recarbonated reaction products are analogous to the mineralogy of Portland cement. The groundwaters discharging at Maqarin are hyperalkaline, and geochemically show some similarities to cement pore water. Phase I of the programme was undertaken to define the cement source term, test geochemical codes predicting safety-relevant heavy element solubility and mobility under highly alkaline conditions, to examine microbiological activity in this environment, and to establish the overall applicability of the Maqarin site as an analogue to a cementitious environment. These studies showed the Maqarin site to be a most interesting and relevant analogue for early and later stage leachate discharge from the near-field environment of a cementitious repository in marls. The results of Phase I were presented at a Workshop hosted by Nagra in March, 1991, and are compiled in a Nagra Technical Bulletin, NTB 91-10, published in 1994.

In July, 1991, a second phase of the Maqarin natural analogue study was proposed. This involved the collaboration of project members jointly funded by Nagra, SKB and Nirex.

The main thrust of the Phase II programme was to expand the Phase I study by looking at geochemical modifications and transport phenomena in the zone of interaction between the near-field leachates and far-field marls. Consequently, principal aspects included an extended hydrochemical (including trace element speciation) and isotopic characterisation of the groundwaters and detailed mineralogy and geochemistry of the bedrock and fracture zones typical of the near- and far-field environments. These data were then used to test coupled flow-transport models in a hyperalkaline environment. Additional aspects included a preliminary synthesis of available hydrogeological data of the Maqarin region, assessing the stability of clay in the interaction zone, the presence of microbes and their potential influence on the physico-chemical properties of trace elements, an examination of the stability of steel and kerogen-rich material, and small-scale petrographic studies of ancient high pH fossil reaction zones in Central Jordan.

To achieve these objectives, an extended geochemical sampling and analytical programme focussed on aqueous and petrological samples from the Eastern Springs discharge zone (analogue for late stage near-field discharge) and from the Western Spring zone (analogue for early stage near-field discharge). Petrological samples from fossil reaction zones in Central Jordan were also collected to compare with present on-going hyperalkaine reactions at Maqarin.

Whilst Phase I database testing examined essentially pure end-member mineral species, in the Phase II study, more effort was given to provision of relevant field data for testing the model predictions (aqueous speciation data was improved; more details

regarding trace element sources/sinks etc.). Modelling was also extended to test coupled flow-transport codes in the hyperalkaline environment, and to test a microbiological code developed to predict the influence of microbiological activity in a repository near-field.

The results from Phase II were first compiled in 1994 and the final report published in 1998 as a Nirex Science Report, S/98/003.

This present Phase III study was initiated in December 1993. In contrast to the Ca-dominated seepage groundwaters which typify the Maqarin Eastern Springs localities, studied in detail in Phases I and II, the Western Springs locality, which appears to be characterised by Na/K/Ca-dominated seepage waters, was not yet fully understood. Further investigation of such groundwater interactions, which may be somewhat analogous to the earliest hyperalkaline leachates from a repository, was therefore the focus of the Phase III study. Four funding organisations participated: Nagra, SKB, the Environment Agency (formerly UKHMIP) and Nirex.

The major objectives of Phase III were to confirm the presence of Na/K-hydroxide-rich groundwaters at the Western Springs locality, establish their origin and chemistry, and study the water/rock interactions. It was hoped that, by comparing and integrating these data with existing data from the Eastern Spring localities, the work would help to expand existing knowledge on the very earliest stage of the cement leachate/host rock interaction and contribute to the validation of the current conceptual models of the repository/host rock evolution. In addition, the data could be used to test those coupled codes employed in assessing the long-term evolution of the repository as part of a repository safety assessment, indicating both the applicability of the codes in a repository analogous environment and identifying those areas where further code development may be necessary.

Additional objectives included a literature review of zeolite mineral phases, their occurrence and genesis, and their potential relevance to the Maqarin area. Zeolite mineral phases have been identified at the Eastern Springs localities. These occurrences in a hyperalkaline environment are significant in relation to the repository concept because of their (relatively) high molar volumes (and thus may occlude porosity as replacements for clays, micas and feldspars) and high cation exchange capacity (and thus of relevance to retardation of cations in groundwater). Mineralogical studies of the Western Springs localities provided added insight into the stability of these zeolite phases under different hyperalkaline conditions.

Restricted petrographic studies of fossil cement zones and their associated hyperalkaline plumes were carried out in Central Jordan to allow the late-stage evolutionary end-members of the cement leachate series to be studied, thus complementing the Phase II studies at Maqarin of the earlier-stage evolutionary members.

The role of organic material and microbes, for example, in influencing the transport of radionuclides in and around a cementitious repository, was also addressed at the Western Springs localities.

To try and reach a broad understanding of geological occurrences at the Maqarin Site, geomorphological studies were carried out to establish the recent evolution of the Yarmouk River Valley with the aim of identifying different timed events (i.e. number and duration) which may explain the observed water/rock reaction mineral assemblages

within and outside the cement zones, and also to shed some light on the origin of the cement zones.

Finally, an effort was made to integrate groups involved in cement and construction research, as an attempt to further develop the analogy between Maqarin and a cementitious repository. This resulted in a general review of the nature and use of cement in repository construction, and its relevance to the Maqarin analogue study (see Appendix R).

Phase III studies at Maqarin required the drilling of three strategically located boreholes to facilitate groundwater sampling and analysis. One further objective behind the drilling of these new boreholes, besides access to deeper groundwaters, was to derive hydrogeological and hydrochemical data to support the Phase II groundwater flow conceptual model. There is still some uncertainty as to the origin of the Ca/Na/K-hydroxide groundwaters at the Western Springs locality. It is not known whether they simply result from water/cement zone interaction (i.e. early-stage evolution reactions), or whether they are the product of mixing between Eastern Springs high pH water (late-stage evolution reactions) within the cement zones, with deeper, upwelling aquifer groundwater from the Amman Formation. Furthermore, it is not known whether unusual sources of contamination (i.e. from nearby village or agricultural activities) may contribute to the groundwater chemistry. The possibility of a mixing origin was further tested by evaluating existing hydrogeological and chemical data from the Maqarin area (i.e. those data resulting from the Jordanian-Syrian Dam Project on the Yarmouk River) obtained from the Jordan Valley Authorities in Amman.

Specific objectives of the Phase III study included:

1. Establishing the origin and chemistry of the Western Springs groundwaters using hydrogeological, hydrogeochemical and isotopic data.

2. Carrying out petrographical studies of mineral phases resulting from high pH (13.5) water/rock reactions. Rocks included unmetamorphosed marls and various other rock types (e.g. basalt, limestone, chert etc.) incorporated in the consolidated lacustrine and fluviatile gravels and conglomerates (colluvium) at the Western Springs locality.

3. Examination of the effects of the hyperalkaline groundwater/host rock interaction on the accessibility of the host rock matrix to radionuclides. In Phase II the results suggested that, as a consequence of alteration of the original host rock mineralogy, the full matrix may be isolated from the advective flow paths. This could have a significant impact on radionuclide retardation, especially for non- or weakly-sorbing elements, in some repository concepts.

4. The testing of coupled flow/transport codes employed in assessing the long-term evolution of an alkaline disturbed zone.

5. Investigation of the occurrence and geochemical controls on zeolite composition at the Eastern and Western Springs localities, and to compare results with a literature assessment of zeolite formation under hyperalkaline conditions.

6. Investigation of the occurrence and geochemical controls on clay stability at Maqarin (active Eastern and Western Springs reaction series) and in Central Jordan (older fossil end-member reaction series).

7. The study of the role of colloids, organics and microbes in trace element (including radionuclide) transport at the Eastern and Western Springs localities.

8. Geomorphological studies of the Yarmouk River Valley with special reference to the geological events and timescales involved in the origin of the Eastern and Western Springs areas.

2 GEOLOGY AND HYDROGEOLOGY OF THE MAQARIN AREA

(H.N. Khoury, E. Salameh, M. Mazurek and W.R. Alexander)

2.1 GEOLOGY

2.1.1 Introduction

The Maqarin area (E232.250:N237.900) (Fig. 2-1) is located along the Yarmouk River Valley at the Syrian-Jordanian border, 16 km north of Irbid. There is a variation in altitude from 40–400 m and the exposed rocks comprise Cretaceous-Tertiary carbonates overlain by Quaternary basalts, soils and alluvium. The most interesting and characteristic features of the area are the presence of the brecciated, highly altered metamorphic zone (i.e. the cement zone) and the associated hyperalkaline groundwaters (pH >12.5). The cement zone is restricted to the lower part of the Chalky Limestone Formation and the upper part of the Bituminous Marl Formation. Although the general geology of the area has been described in detail elsewhere (e.g. Khoury et al., 1992; Milodowski et al., 1998), this present version incorporates new information obtained during field visits in 1994/95, from newly drilled boreholes, and from unpublished reports obtained from the Harza Engineering Company and the Jordan Valley Authorities.

2.1.2 Physiography

The Maqarin area lies adjacent to the south bank of the Yarmouk River about 25 km east of the Jordan Rift Valley. The gorge of the Yarmouk River is a relatively recent geomorphological feature created by headward erosion initiated in the Jordan Rift Valley (see Chapter 3) and eventually extending eastwards into Jabel El-Arab where thick basalt flows rise to some 1 300 m.a.s.l. Maqarin is bounded on its southern side by an anticline (Fig. 2-2) with a width (i.e. wavelength) of 2 700 m and an amplitude of 100–120 m. On the southern flank of the Yarmouk River Valley the anticlinal axis bears NNE-SSW at the river, becoming oriented NE further to the north on the Syrian side. To the east Maqarin is bounded by Wadi Shallala and to the west by Wadi Sijin (Fig. 2-1).

In general the valley sides are steep; from river level the slopes rise uniformly (25 degrees) to an elevation of 240 m where the topography flattens to form an almost horizontal terrace of some 500 m width. The terrace between elevations 240–400 m consists of a series of hummocks of limestone rubble which are separated by red-brown soils. Further to the south the hummocky terrain is bounded by the level of the Irbid plain.

To the south of the Western Springs area the topography rises very steeply (45–60 degrees) from the wadi bottom (-50 m) to a level of 400 m.a.s.l. At this level a

peneplain (formed prior to the incision of the Yarmouk) extends for a few kilometres eastward and southeastwards. Overlying the peneplain is a soil horizon of a few metres thickness. The slopes forming part of the Western Springs location are covered by an angular rock talus to an elevation of 100–150 m above the wadi.

Along the Yarmouk River Valley, rocks from different formations form the valley bottom. In some places the valley floor is covered by alluvial deposits, recent rock debris and consolidated conglomerates.

Alluvial terraces are well preserved at the mouth of Wadi Sijin (elevation 90 m), extending to the Maqarin railway station (elevation 100 m).

2.1.3 Lithological Features

The geology of the Maqarin area is illustrated in Figures 2-2 and 2-3. This information is based on data from existing maps of the area (e.g. Weiseman and Abul Latif, 1963) modified from recent field visits, and drillcore logs dating from the 1950s to the 1970s (Fig. 2-4; Harza, 1982 and the Jordan Valley Authorities, 1980).

Amman Formation

The oldest unit of interest to the present study is the Amman Formation which consists of thinly-bedded limestones, cherty limestones and cherts with a total thickness of 90 m. The unit does not crop out in the mapped area, but was identified from drillcore logs resulting from the Jordanian-Syrian Dam Project investigations in the 1970s; the projected top of the Amman Formation is shown in Appendix A; Figure A-1. On a regional scale the Amman Formation is a major aquifer; at Maqarin it forms a confined aquifer. Worth mentioning is the presence of broken shells, pisoliths, eoliths and current bedding in the formation.

Bituminous Marl Formation

The Bituminous Marl Formation is exposed only to a distance of 1.5 km to the east of Maqarin along the river bed where it is covered by younger rocks. It also crops out in a narrow and limited area in Wadi Shallala and upper Wadi Sijin (Fig. 2-2) at a distance of a few kilometres from the Maqarin site. Outcrops also occur at the southern side of the Yarmouk River at Maqarin, representing the core of an anticline trending NNE-SSW and plunging in a NNE direction. The projected top of the Bituminous Marl Formation, as deduced from drillcore data, is shown in Appendix A; Figure A-2.

The marls consist of clay biomicrites with a relatively high hydrocarbon content. They conformably overlie the Amman Formation and in the upper horizons large spheroidal limestone concretions (up to 180 cm in diameter) containing thin bands of cherts are found. The thickness of the formation in the study area is 220 m.

The argillaceous nature of the formation results in it forming both an efficient aquiclude and also providing a "lubricating surface" allowing movement of the overlying sediments. In places, the upper part of the formation and the overlying lower Chalky

Limestone Formation are highly metamorphosed and brecciated; these have been mapped as the cement zone.

Chalky Limestone Formation

This is the main lithological unit of the Maqarin study site with a thickness of 300–390 m (Fig. 2-3). It outcrops on both sides of the Yarmouk River and conformably overlies the Bituminous Marl Formation. The Chalky Limestone Formation consists mainly of limestones, chert beds and chalks, and is subdivided into three members:

Lower Chalky Limestone Member: The lower 50 m of this 190 m thick member consists of a massive, homogeneous limestone; locally the lower parts are bituminous. The overlying beds consist of a sequence of white micritic and crystalline limestones.

Chert Chalky Limestone Member: This member conformably overlies the Lower Chalky Limestone Member. It is 30–40 m thick and consists of chalk limestone beds with numerous thin chert beds.

Upper Chalky Limestone Member: It conformably overlies the Chert Chalky Limestone Member and has a total thickness of 170 m. Lithologically it is very similar to the Lower Chalk Limestone Member, but is softer and less resistant to weathering. Fresh outcrops are olive-brown to grey in colour, becoming cream-coloured (i.e. chalk-like) when weathered.

The Chalky Limestone Formation is highly karstified, as observed 1 km to the south of the Western Springs, with sink holes of up to 40 m in diameter and 20 m depth commonly occurring. In addition, in areas affected by metamorphism, the formation is highly fractured, jointed and shows a large reduction in volume, not only vertically but also laterally. This considerably increases the permeability of the limestones at these locations.

Volcanic Rocks

Volcanic rocks are found in the Maqarin area (Fig. 2-2) at two locations:

1) peneplain basalts (referred to as the Syrian or Hauran Basalts dated to 5.0–3.5 Ma; Fig. 2-3) of limited areal extent 500x500 m and a thickness of 150 m, thinning out towards the east and south, and

2) at the west side of the mouth of Wadi Shallala, although it is not certain whether this occurrence is *in situ* or has been transported there. The peneplain basalts directly overlie either the Chalky Limestone Formation or a palaeosoil horizon which may have a thickness of up to 3 m. These soils may comprise a solid red-brownish rock as a result of baking, shrinkage, consolidation and secondary fillings.

The basalt outcrops have a maximum thickness of 100 m and outcrop at elevations ranging from 165–265 m.a.s.l. About 1 km south of Maqarin remnants of a weathered basalt are found at an elevation of 360 m.a.s.l., and, further to the west, basalts cover an old peneplain at 400 m.a.s.l. The basal elevation of the basalt just south of the Maqarin site is shown in Appendix A; Figure A-3.

Another basalt flow (Raqqad Basalt) covers the lower reaches of the Yarmouk River. It is similar in type to the Hauran flows, but is much younger in age (0.48–0.35 Ma). It is not clear whether the Maqarin basalt belongs to the older Hauran flows (5.0–3.5 Ma) or to the more recent Yarmouk flows (0.83–0.79 Ma). Its elevation (flow bottom at 165 m.a.s.l.), when compared with the Hauran or Syrian flows to the north, is at least 60 m lower in elevation, even though it is some 100 m higher than the younger basalts. This cannot be accounted for by slope extensions and extrapolation.

Palaeosoils

A horizon of palaeosoils, red in colour and up to 3 m in thickness, underly the area covered in basalts. The soil is solidified and includes clasts of the surrounding rocks such as chert limestone and chalk. The mineralogical constituents of the palaeosoils are quartz, illite and kaolinite, together with calcite as a secondary filling material. These palaeosoils, and their significance in the geological evolution of the area, are described in more detail in Chapter 3.

Cement Zone (Metamorphic Unit)

Sporadic spontaneous combustion of the Bituminous Marl Formation has resulted in an irregular distribution of metamorphic calcined rocks (i.e. cement zone). The main extent of these altered and brecciated rocks in the Maqarin area has been described and illustrated by Khoury and Nassir (1982) and Harza (1982).

The contact between the cement zone and unaltered marl is well shown in the two Adits (A-6 and A-7; Fig. 2-2). The contact is transitional and the typical rock sequence is from a fresh brown/grey marl through a black marl to a soft light-grey marl and eventually to a fine-grained, cream coloured chalky material. In the adits the transition from unaltered to altered is 1–2.5 m wide. In the cement zone the original sedimentary textures are absent except for some nodular chert bands which have undergone some transformation, including colour changes (Khoury and Salameh, 1986).

Distribution of the unaltered Bituminous Marl Formation

The boundary between the unaltered marl and the overlying cement zone is shown in Figure 2-5. The contact is irregular and lower in elevation than one would expect by projecting the stratigraphy as seen on the Syrian side of the Yarmouk River. The top of the unaltered Bituminous Marl Formation rises towards the south and, at a point 1.8 km south of the river, is higher than 170 m.

Distribution of the cement zone (Metamorphic Unit)

Individual cement zone types are generally discontinuous, being typically lenticular in shape; consequently, correlation between boreholes to construct a three-dimensional picture is difficult. The generalised distribution of the cement zone (Metamorphic Unit) at Maqarin is shown in Appendix A (Figs. A-4 to A-7). Despite the difficulty of

correlation, a general pattern between the top of the unaltered Bituminous Marl Formation and the base of the cement zone can be distinguished (Fig. 2-6):

- ***Zone of weathering***; the upper part of the cement zone (2–6 m) is characterised by a low percentage of soluble compounds. This may reflect leaching by meteoric water, or, perhaps this part of the zone did not achieve the high temperatures which led to calcining elsewhere. Figure A-8 in Appendix A shows the top of the unaltered Bituminous Marl Formation; the marl contact dips about 20 degrees to the west from a 130 m+ elevation high, centred along the direction of Adit A-7.
- ***Zone of brecciation.***
- ***Intact zone***; *in situ* rock with only localised brecciation.

In general, the strength and quality of the cement zone rock components appear to improve to the west (i.e. Zone A to C; Appendix A (Figs. A-9 to A-14); Table 2-1), i.e. downstream, with the weakest metamorphism apparently located towards Adit A-7. A zone of relatively insoluble rock parallels the unaltered marl/cement zone contact throughout the whole area (Harza, 1982).

The elevation of this contact increases to the south (Appendix A; Figs. A-2 to A-8). Towards the Yarmouk River Valley, the top of the contact occurs at a relatively high elevation of 120–133 m. The shape of the top of the contact is interpreted as forming a north- to south-trending ridge which separates the upstream and downstream low-lying areas as observed on the alteration surface. The low-lying area upstream is probably around 100–110 m in elevation, whilst that downstream is less than 100 m elevation and is probably larger in areal extent.

In the area south of the Adit A-7, the contact constitutes a saddle of around 120–125 m elevation (near borehole HQ-18; Appendix A; Fig. A-7) and then rises to 157 m in borehole HQ-10. South of this point the gradient of the contact is thought to level off to form a broad plateau between 152–155 m elevation. This plateau extends south to at least the limit of the cement zone shown in the line of the cross-section, but certainly not as far south as borehole HQ-41 (Appendix A; Fig. A-7). At the cement zone contact with the unaltered marl, a 2–6 m thick unit containing no evidence of mineral dissolution reflects a metamorphic transition.

2.1.4 Structural Features

General

The E-W trending valley of the Yarmouk River cuts through the Irbid Plateau and exposes the Bituminous Marl Formation, overlain by the Chalky Limestone Formation and basaltic lava flows on the top. Although regional tectonic controls have sometimes been postulated, no positive evidence exists that the 400 m deep river incision is related to tectonic features, such as faults (see Chapter 3). Regionally, the strata exposed in the Maqarin area show very little deformation and are almost horizontal to gently dipping. Flexures with very small curvatures are also evident in the area.

Locally, at the Eastern Springs area, the Bituminous Marl Formation has been slightly uplifted by a N-S trending anticline parallel to longitude 232° which plunges to the NE

(Fig. 2-2; Khoury et al., 1985). It shows a deflection to the east in the Yarmouk River area; on the northern side of the river the axial trend becomes NE-SW. The structural contour lines of the top of the Amman Formation (Appendix A; Figure A-1) shows an anticlinal bending at a distance of some 500 m to the east of the anticline in the Bituminous Marl Formation. This deflection is similarly towards the east where the trend becomes NE-SW in the Yarmouk River bed area, i.e. in the area of Adit A-6. On the SE flank of the anticline, the strata dips 18–20° to the SE for a distance of 2 km before becoming horizontal, whereas the NW limb dips gently to the NW. Both anticlinal bendings may be considered to belong to one anticline which is asymmetric with a fold plane inclined to the east by 25°. The fold plane deflects gradually to the east where it trends to the NE-SW instead of N-S.

The hillslopes are covered by talus and colluvium, and so observations of structural features within the Bituminous Marl Formation and the Chalky Limestone Formation are mostly limited to two localities: the Waterfall Road Cutting at the mouth of Wadi Shallala near the Yarmouk River and Adit A-6 (Fig. 2-1).

Eastern Springs Area

Structural Features at the Waterfall Road Cutting

Two very regular, near-vertical systems of joints with E-W and N-S strikes are observed, with joint spacings in the range of decimetres (Fig. 2-7). Both systems cut discordantly through bedding, which is subhorizontal. No indications of faulting, either along steep or bedding-parallel structural elements, were observed. Joint infill is evident in places, but it is not yet known if this represents secondary cement phases produced by interaction with hyperalkaline waters.

Structural Features at Adit A-6

The horizontal, N-S trending Adit A-6 provides a long profile (120 m currently accessible) through the Bituminous Marl Formation in the southern flank of the Yarmouk River Valley. The N-S trending joint system observed at the Waterfall Road Cutting is prominent in the whole section, while the E-W system is largely absent, possibly due to the different positions of the two sites relative to the anticline structure. In addition, faults are prominent structural features in the Adit (see Fig. 2-7):

- The N-S trending joints are reactivated by subhorizontal shear movements, as indicated by slickensides. The spacing of the fractures is in the range of decimetres; fracture length mostly exceeds 5 m. In detail, many fractures consist of sets of parallel planes along which shear movement has occurred, and these planes are interconnected by networks of short cracks of the fault damage zone. This description is representative for the fracture geometry of water sampling site M1.
- The inner part of the Adit (50–110 m) contains N-dipping, listric faults cross-cutting bedding (which generally dips at 35–45° to ENE) and then rotating into a bedding-parallel position. The trace lengths of these structures are limited to only a few metres.

- The M2 site (45 m from the adit entrance) also contains a secondary fault system dipping 15°-40° (with a few much steeper at 80°–90°) towards the NE. This fault system is much more strongly developed in the outer (0–50 m) part of the Adit. The faults contain sets of subparallel shear planes, mostly longer than 10 m, and an accompanying network of small joints along which no shear movement has occurred and most likely represent tensile features (Fig 2-8).

  The joints do not cross cut the shear fractures, but can be observed interconnecting them in many cases at angles of approx. 45°. The observed fault geometries closely conform with the mechanistic principles of brittle fault development described by Martel and Pollard (1989). In their terminology, the shear planes are called master faults, and the accompanying joint network are splay cracks, and the whole structure is a fault zone. On the basis of the geometric arrangement of masters and splays, a sinistral shear-sense can be derived in Figure 2-8, i.e. a movement of the upper block towards the valley bottom (down-slope normal faulting). Water sampling site M2 is situated within a major fault zone of this type.

- The master faults are structurally relatively simple, parallel to sub-parallel features. Most faults do not contain any unconsolidated fault rocks (fault breccia, fault gouge), so the amount of slip along a single shear surface probably is very limited. Secondary mineralisations are very common but heterogeneously distributed in the fractures.

Interpretation of Structures

The differences in structural patterns between the Waterfall Road Cutting and Adit A-6 localities underlines the local heterogeneity of the system. In part, the faulting observed in the Adit is best attributed to gravity tectonics, locally facilitated by 45° hillslopes. The clear increase of faulting towards the Adit mouth indicates that the driving force for faulting could be gravity sliding or spreading, and this is also consistent with the shear-sense (hanging-wall moving towards the valley) determined in some of the faults in the Adit. Such movements may be expected to be recurrent, triggered rapidly by heavy rainfall and more gradually over longer timescales by lateral erosion of the Yarmouk River (see Chapter 3). This may account for the periodic sealing and reactivation of hyperalkaline groundwater conducting fracture pathways (see Milodowski et al., 1998).

Water-conducting Features in Adit A-6 (Sampling Sites M1, M2)

Sealed and open fractures can be observed in the Adit A-6, including both the N-S and N-E dipping fault sets. A detailed fracture map of the Adit wall is shown in Figure 2-9. Some fault planes may contain secondary infills of up to 1 cm thickness, persisting over the entire studied area, while others have no infill at all (Fig. 2-10). The latter fractures often discharge water into the Adit and may represent the youngest phases of tectonic activity. All discharge is concentrated into fractures, and no matrix flow can be observed. In places, the fractures occur as abundant, closely-spaced, fine anastomosing networks of veinlets and, at M1 (140 m from the adit entrance), the precise zone of water discharge is an array of, often connected, microfractures covering an area of 0.1 to 0.2 m^2. The average fracture spacing in the vicinity of sampling site M2 is in the

order of 10–20 cm (somewhat less on the eastern side of the tunnel wall) on the basis of Figure 2-8 and less than 10% are currently water-conducting. The majority of the fractures are sealed with secondary cement phases (Milodowski et al., 1998), and so must have been water-conducting at some point, and those which contain no secondary infill appear tight.

Within a typical 1 m E-W section of the Adit A-6 roof at sampling site M2, numerous water-conducting features can be observed including both the steep N-S fault set and the N-E dipping shear system. The fracture spacing varies from 0.05 to 0.40 m and the aperture ranges from 0.5 to 5 mm. One major fracture conducts a significant portion of the water at this site and it is a very regular, linear feature, 5 to 6 mm wide. It has been largely infilled with white to cream-coloured secondary minerals forming a complex symmetrical banded/crustiform- and locally colloform-textured vein. Several closely spaced parallel hairline fractures within a 10 to 20 mm wide zone on either side of the main fracture also produce minor seepages.

Western Springs Area

Structural observations are very limited because talus and colluvium cover most of the hillslope. Small outcrops observed in a couple of gullies expose a N-S trending fault system and a superficial investigation of bedding in the Chalky Limestone Formation to the south of the springs suggests the possibility of localised shear and rotation between such faults. A more prolonged period of field investigation with associated drilling is necessary before anything more definitive can be stated on the Western Springs site.

2.2 HYDROGEOLOGY

In the Maqarin area (i.e. Eastern Springs) the relationship between the groundwater level and the major stratigraphic units is illustrated in Figure 2-11; in general the groundwater level lies just below the contact between the cement zone (Metamorphic Unit) and the underlying unaltered Bituminous Marl Formation.

2.2.1 Amman Formation (B_2)

Figure 2-12 shows the 1980 groundwater piezometric surface of the Amman Formation measured in the Maqarin study site. Compared with Appendix A; Figure A-1, it can be easily observed that the piezometric head lies at least at an elevation of 100 m greater than the top of the Amman Formation. Generally this produces an upward gradient along the Yarmouk River Valley, producing artesian discharges downstream from the Wadi Shallala confluence. At the Eastern Springs location, evidence of artesian flow occurs from a well opposite to Adit A-6 on the Jordanian side (M-13; Fig. 2-4), which is still producing Amman Formation groundwater since it was drilled in the 1970s. Downstream at the Western Springs location, the artesian head increases relative to the Yarmouk Valley floor and reaches an elevation of 30–50 m above ground-level.

Although the Bituminous Marl Formation forms an aquiclude, secondary porosity along secondary joints and fissures may allow groundwater to rise up from the Amman Formation through the Bituminous Marl Formation to the surface. This has been observed just opposite to Adit A-6 on the Syrian side of the Yarmouk River.

The permeability of the Amman Formation ranges from $10^{-5} - 10^{-7}$ ms^{-1} and the groundwater is generally alkaline with significant amounts of sulphate and chloride. Water discharging through springs and wells has a characteristic smell of H_2S. Groundwater compositions vary from one spring/well to another, but tend to be quite stable at a single source over time. The variation in composition is attributed to mixing of different waters from the overlying groundwater bodies.

2.2.2 Bituminous Marl Formation (B_3)

The Bituminous Marl Formation itself acts as an aquiclude, possessing little appreciable primary permeability. The permeability of the marls, as calculated from pumping tests, ranges from $10^{-7} - 10^{-9}$ ms^{-1}, and is considerably influenced by secondary permeability caused by fracturing and fissuring. These joints and fissures may be caused by tectonic activity (upward movements) or by unloading due to weathering and erosion. As a result of this secondary porosity, groundwater samples collected from wells in the Bituminous Marl Formation may originate from different sources, for example:

- water seeping downwards from overlying units, including the cement zone (Metamorphic Unit);
- water rising up from the Amman Formation; as evidenced by the discharging artesian Amman Formation groundwaters found on the Syrian side of the Yarmouk River Valley and further downstream in the Muhkeiba area.
- mixtures of both water types.

Consequently, groundwaters heterogeneous in composition may be expected. However, hydrochemical studies (see below and Chapter 6) indicate that any groundwater component from the underlying Amman Formation is insignificant, except potentially at the seepage locations close to the edge of the Yarmouk River.

2.2.3 Chalky Limestone Formation (B_{4-5})

As a whole, the Chalky Limestone Formation forms a good aquifer (Fig. 2-13); the lower and central parts represent aquifers of intermediate character, and regionally there is much spring discharge; some shallow wells produce moderate water volumes (up to 20 Ls^{-1}). The permeability of the formation ranges from $10^{-5} - 10^{-8}$ ms^{-1}. As mentioned above, karst features and increased fracturing of those areas affected by metamorphism all contribute to increased rock permeability and groundwater discharge. The groundwaters are generally of alkaline type with significant bicarbonate.

In some of the exploration wells drilled on the plateau overlying Adits A-6 and A-7, basaltic rocks were encountered at greater depths than expected. Sometimes the basalts were recorded below the Chalky Limestone Formation or mixed with boulders from the cement zone. Recent studies have indicated that karst sink holes have probably formed

prior to the basalt flows, thus allowing the basalt to locally penetrate deeper into the Chalky Limestone Formation during eruption. Other processes may have also contributed, for example, large and small basalt boulders on or near the plateau surface are presently segregating through the soil along the large soil cracks to reach the bottom of the karst sink holes. A further mechanism may arise from the collapse of large solution cavities or caverns (possibility existing in the altered cement zone) bringing down the overlying basaltic rocks to greater depths.

The Eastern Springs Groundwaters

The groundwater level in the Chalky Limestone Formation lies at an elevation of 206.2 m.a.s.l. in borehole HQ-41 (2 km south of the Adit A-6 entrance; Fig. 2-4) with a gradient to the N, NW and NE (Fig. 2-14). At the entrance to Adit A-6 the groundwater level is ~40 m.a.s.l. (entrance level is at ~100 m.a.s.l.). At the surface of the plateau overlying Adits A-6 and A-7 (elevation 245 m.a.s.l.) thick, highly permeable desiccated soil covers have developed. Precipitation (450 $mmyr^{-1}$ average) seems to infiltrate totally into these soil layers and find its way to the groundwater aquifers in the Chalky Limestone Formation. At a distance of 100–150 m from the Adit A-6 entrance towards the south, two possible points of recharge have developed; one over the Adit A-6 area, and one in its immediate surroundings (Fig. 2-14). It is considered that the water collected from Adit A-6 at a distance of 50–200 m from the entrance originates from recent recharge (i.e. meteoric water which has reacted with the cement zone). If this is the case, residence times are still about 50 years as indicated by ^{36}Cl and ^{3}H interpretation (see Chapter 6).

This recent recharge groundwater either enters the adit (i.e. flows along the adit) to discharge at the slopes of the Yarmouk River Valley or as seepages near the valley floor back into the aquifer, or percolates deeper to join the groundwater flow from the Chalky Limestone Formation which originates from recharge over the highlands lying a few kilometres south of Maqarin.

The Western Springs Groundwaters

In the Western Springs area recharge into the Chalky Limestone Formation takes place further to the south, along the plateau lying at an elevation of 360–400 m.a.s.l. and extending for a few kilometres to the south. On this plateau surface, fractures may have an average separation of around 15 cm and an observed penetration of around 2 m. A thick, very dessicated soil horizon has developed, typical for highly karstified rocks. In the immediate vicinity, where the rocks are barren, large karst holes (i.e. sink holes) have developed with an average diameter of around 40 m and with a depth of at least 20 m. Infiltration rates are consequently very high and the greatest portion of precipitation either remains in the soil as moisture, or finds its way into the bedrock and the groundwater body, but does not concentrate as surface flow.

The infiltrated water percolates down and flows in a northerly direction where it eventually reacts with the cement zone rocks of the Metamorphic Unit, located at the top of the Bituminous Marl Formation and at the bottom of the Chalky Limestone Formation, eventually finding its way to the Western Springs locality at the contact

between the unaltered Bituminous Marl Formation and the overlying colluvium (Fig. 2-15).

The composition of the Western Springs groundwaters may be influenced by other external sources, for example farmers on the plateau use fertilisers, mainly K, NO_3, Urea and PO_4, in the form of sulphates, nitrates and/or II or III phosphates. There arises the possibility that these can percolate down into the groundwater table and eventually to the Western Springs locality. Furthermore, the groundwater catchment area which lies to the south of the Western Springs locality receives the domestic discharge from Hartha village (3 km to the south), contained in cesspits dug into the Chalky Limestone Formation. Such cesspits may have hydraulic connections via karst features (i.e. fissures and holes) which may lead the waste water into the main groundwater body and then to the Western Springs locality. These different hypotheses have been tested by sampling the various sources of contamination (see Appendix Q). No strong evidence was found that links anthropogenic contamination to the chemistry of the Western Springs groundwaters.

2.2.4 Groundwater Flow

For the purpose of the Maqarin study, the area has been divided into the two sub-areas of groundwater flow; the Eastern and Western Springs. The regional geological setting and the general recharge features of these subareas have been described above.

Eastern Springs

In the Eastern Springs sub-area (Fig. 2-1) the many wells, adits, shafts etc. drilled and excavated in the late 1970s have provided a considerable amount of hydrogeological data described and interpreted by Khoury et al. (1985). In brief, based on hydrogeological criteria, three main groundwater bodies can be recognised:

1. The deep aquifer water from the Amman Formation (B_2) which, at certain locations, may move upwards along discontinuities in the Bituminous Marl Formation where the artesian head is in excess.

2. Infiltration of water along the plateau lying east of Maqarin, penetrating the B_4/B_5 units of the marls (Fig. 2-3) down to the B_3 contact to discharge northwards along this interface to the Eastern Spring localities along the Yarmouk River Valley slopes. These meteoric waters interact with the cement zone giving rise to the hyperalkaline groundwaters.

3. Water infiltrates into the bedrock above Adit A-6, down through the cement zone, and may join groundwater body (2) above, or locally discharge along the roof and walls of the Adit.

The unusual chemistry of the Adit A-6 water is believed to be the result of precipitation infiltrating through the basaltic-rich soils and rocks into the cement zone (see Chapter 6 for discussion). In contrast, the waters seeping from the Maqarin Station Railway Cutting (see Fig. 2-1) may represent a mixture of groundwater bodies (1) and (2) above. This also applies to the high pH water encountered in the colluvium deposit

lying to the west of the Maqarin bridge at the river edge (sample M10; see sub-section 4.4.5). Present studies indicate that at the Maqarin Station Railway Cutting the seepage waters originate mainly from groundwater body (2), with a possible component from (3), whereas the colluvium seepages at the river edge (M10) appear to be a mixture of groundwater bodies (1) and (2).

Western Springs

These springs discharge small amounts of water along a distance of about 100 m on the Jordanian side of the Yarmouk River Valley, at an elevation of 1–4 m above the level of the river bed (Fig. 2-1). The rocks at the discharge sites comprise cemented alluvium (colluvium) covered by rock debris and river sediments. On the valley slopes the colluvium in turn covers the outcropping Bituminous Marl Formation (Fig. 2-15). Since the marls form an aquiclude, the discharged groundwater may have different origins and pathways:

1. The waters may totally originate from recharge into the Chalky Limestone Formation on the plateau south of the Western Springs. These recharge waters may flow vertically downward to the impermeable Bituminous Marl Formation, subsequently discharging along the interface of the cement zone/unaltered marls to the Western Springs location. A smaller groundwater flow component may penetrate deeper into the unaltered marls controlled by discrete fractures and fissures before discharging.

2. The waters may originate in the Amman Formation rising upward via discontinuities in the Bituminous Marl Formation (B_3) to the colluvium, eventually discharging along the riverbank.

3. The derivation of the groundwaters may be a combination of origins (1) and (2). The chemistry of the groundwaters strongly supports the importance of origin (1) (see Chapter 6 for discussion).

2.3 SYNTHESIS OF DATA

Using available information on well and borehole logs from the Maqarin area (archives of the Water Authority and the Jordan Valley Authorities; Appendices B and C), and data collected in the course of remapping, a three-dimensional model was constructed manually to illustrate the interrelationships between the major stratigraphical units, the important structures, and the general hydrologeological character of the area (Fig. 2-16). The area chosen to be modelled was bordered to the east by Wadi Shallala, to the west by Wadi Sijin, to the north by the Yarmouk River, and to the south by an extension of the highlands of Jordan.

The model shows the extension of the cement zone (Metamorphic Unit) which underlies the area from Wadi Shallala in the east to Wadi Sijin and beyond to the west, and from the Yarmouk River in the north to a line coinciding with Latitude 236.200, about 2 km

to the south. Here the cement zone wedges out suddenly along a E-W line where it is sharply separated from the Chalky Limestone Formation.

The topography indicates three distinguishable levels:

A. The original level plain of the Chalky Limestone Formation 380–400 m.a.s.l.; erosional surface.

B. A level plain (1x1 km) 300 m.a.s.l. with karst topography and collapse structures; these overly the Metamorphic Unit/cement zone.

C. A level plain (0.5x1 km) 250 m.a.s.l. covered by basalts partly overlain by recent soils and underlain by palaeosoils up to 3 m in thickness. The Metamorphic Unit/ cement zone underlying the palaeosoils has a thickness of 150–170 m.

Integrating the hydrological information shows a fresh, normal pH groundwater (pH 7) flowing due north in the most southern area of the model, eventually entering the cement zone where reaction results in a high pH groundwater. The high pH water continues flowing in a northerly direction with a small component branching off to Wadi Shallala in the east and Wadi Sijin to the west. During this passage mixing with some infiltrating meteoric water occurs in area (B) referred to above.

At level C referred to above, infiltrated meteoric water mixes with the same groundwater flow from the south at a table elevation of 60–80 m.a.s.l. However, there is evidence of two local recharge areas of meteoric water above the level of Adit A-6 which formerly used to completely infiltrate to the original groundwater level. This infiltration is now interrupted by Adit A-6 such that; a) part of the meteoric waters first reach Adit A-6 and then infiltrate deeper from the adit floor, or b) the meteoric water flows as surface water along the axis of the adit to the entrance where it evaporates along the slopes of the Yarmouk River Valley.

2.4 REFERENCES

Alexander, W.R. and Mazurek, M., 1996. The Maqarin natural analogue: Possible implications for the performance of a cementitious repository at Wellenberg. Nagra Unpubl. Int. Rep. (NIB 95-59), Nagra, Wettingen, Switzerland.

Harza, 1982. Harza Overseas Engineering Co.: Jordan Valley Irrigation Project, Stage II. Final Report.

Jordan Valley Authorities, 1980. Jordan Valley Authority and Water Authority, Internal Reports (JVA) and (WA).

Khoury, H.N. and Nassir, S., 1982. High temperature mineralisation in the bituminous limestone in the Maqarin area – northern Jordan. N. Jb. Miner. Abh., 144:2, 197–213.

Khoury, H.N., Salameh, E. and Abdul-Jaber, O., 1985. Characteristics of an unusual highly alkaline water from the Maqarin Area, north Jordan. J. Hydrol., 81, 79–81.

Khoury, H.N. and Salameh, E., 1986. The origin of high temperature minerals from the Sweileh area, Jordan. Dirasat, 13, 261–269.

Khoury, H.N., Salameh, E., Clark, I.D., Fritz, P., Bajjali, W., Milodowski, A.E., Cave, M.R. and Alexander, W.R., 1992. A natural analogue of high pH waters from the Maqarin area of northern Jordan. I: Introduction to the site. J. Geochem. Explor., 46, 117–132.

Martel, S.J. and Pollard, D.D., 1989. Mechanics of slip and fracture along small faults and simple strike-slip fault zones in granitic rock. J. Geoph. Res., 94, B7, 9417–9428.

Milodowski, A.E., Hyslop, E.K., Khoury, H.N. and Salameh, E., 1998. Site description and field sampling programme. In: C.M. Linklater (Ed.), A natural analogue study of cement-buffered, hyperalkaline groundwaters and their interaction with a repository host rock: Phase II. Nirex Science Report, S/98/003, Nirex, Harwell, U.K., p. 10–47.

Wieseman, G. and Abdul Latif, A., 1963. Geology of the Yarmouk area, northern Jordan. Unpubl. Int. Rep., BGR, Hannover, Germany.

Table 2-1. Engineering and geochemical properties of the cement zone (Metamorphic Unit). After Harza (1982) and Jordan Valley Authorities (1980).

Geotechnical Division	Rock Classification	Unconfined Compressive Strength, (kg/cm^2)	E Modulus (kg/cm^2)	Dry Unit Weight (gm/cc)	Porosity (%)	Permeability (cm/sec)	Solubility (%)
A Weak Rock	Highly altered marble into soft material	2.6–19.0	330–15 000	094–1.75	84–68	$5x10^{-3}$–$5x10^{-4}$	<10
	Commonly veined	Av. 21.0	Av. 4 500	Av. 1.37	Av. 53		
B Moderately Weak Rock	Marble altered to a soft material	62.0–103.1 Av. 79.0	15 900–23 000 Av. 20 000	1.39–2.19 Av. 1.80	–	10^{-4}–10^{-5}	<10 10-20 >20
C Moderately Strong to Strong Rock	Crystalline marble with veins filled by secondary mineralisation	131.0–653.0 Av. 283.8	27 800–105 000 Av. 62 000	Av. 1.94	–	$<10^{-5}$	<10 10-20 >20

FIGURES

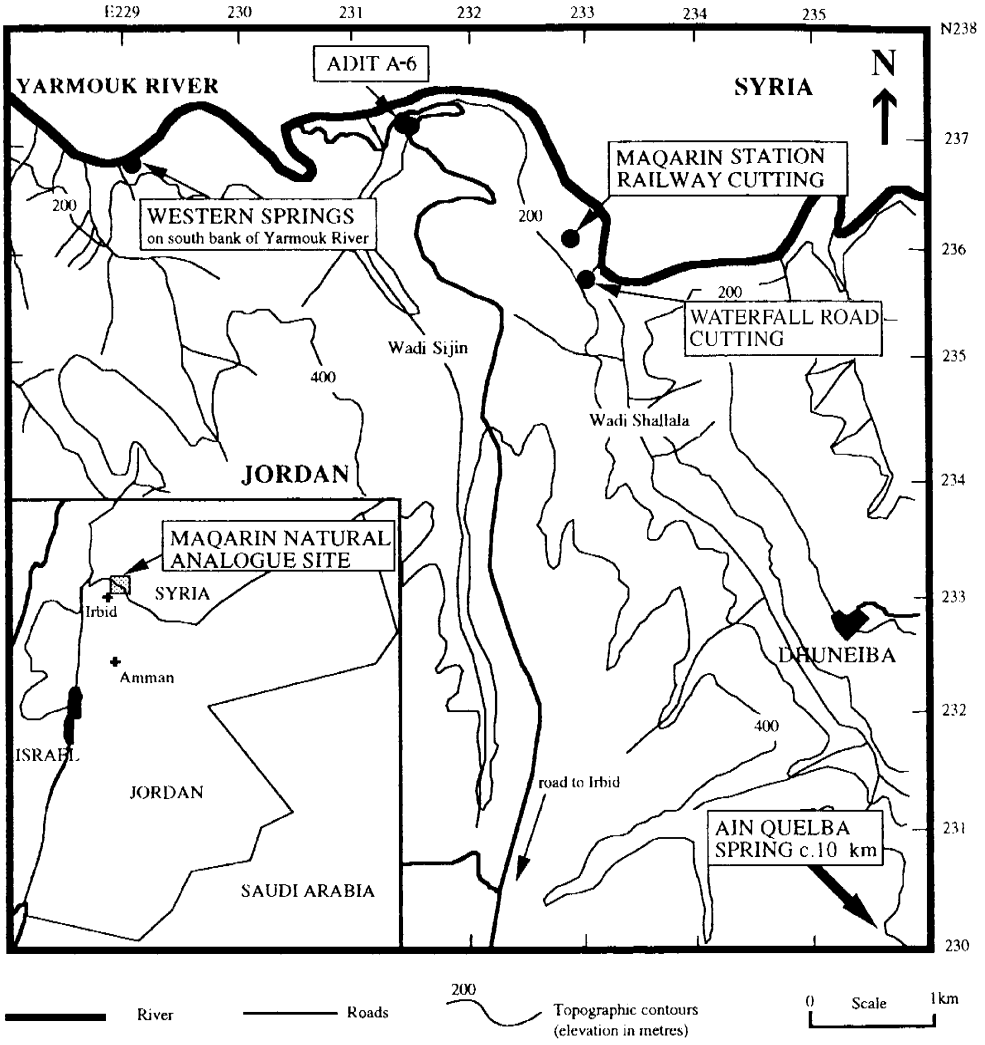

Figure 2-1. *Location of the Maqarin area in relation to the major wadis and the sampling sites.*

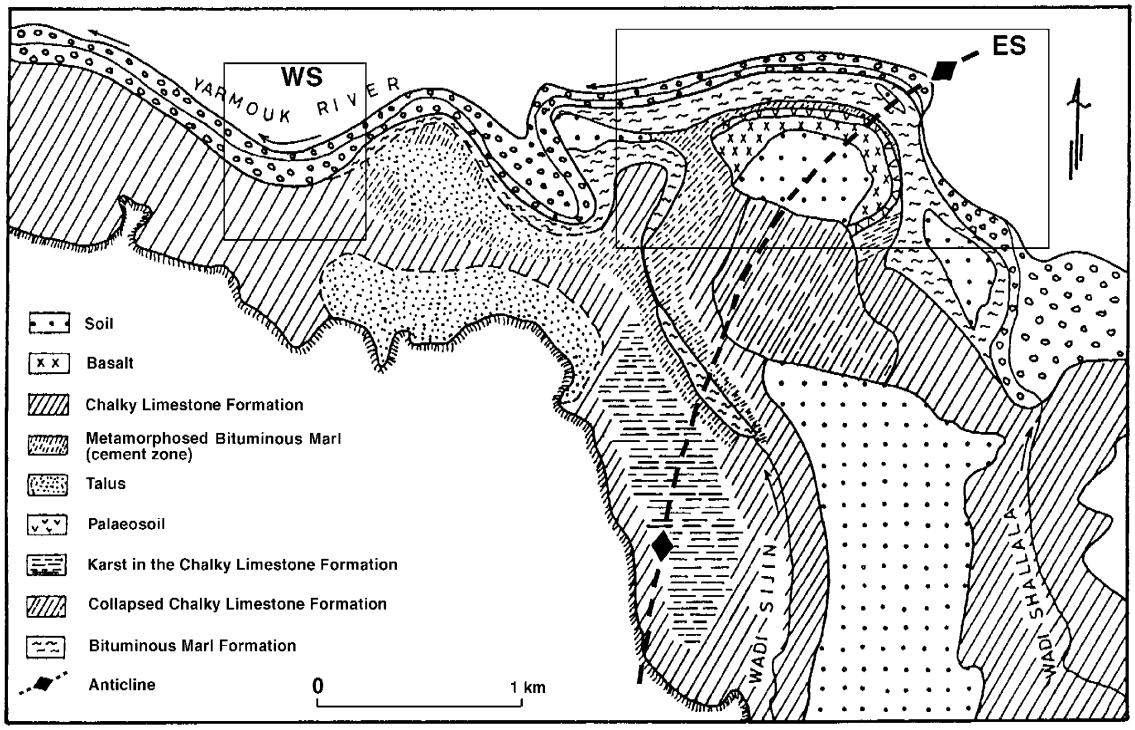

Figure 2-2. *The general geology of the Maqarin area. (ES = Eastern Springs locality; WS = Western Springs locality)*

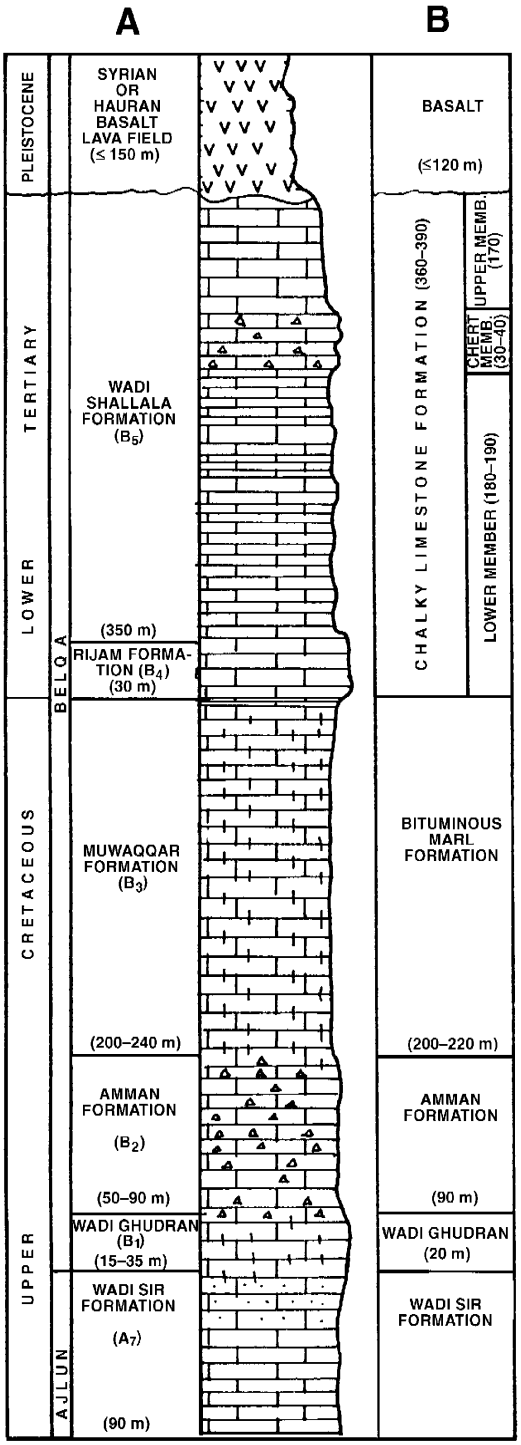

Figure 2-3. *Generalised stratigraphical column showing the major geological units. Nomenclature used regionally (together with the hydraulic units: B_1, B_2 etc.), and locally at Maqarin, is given in columns A and B respectively.*

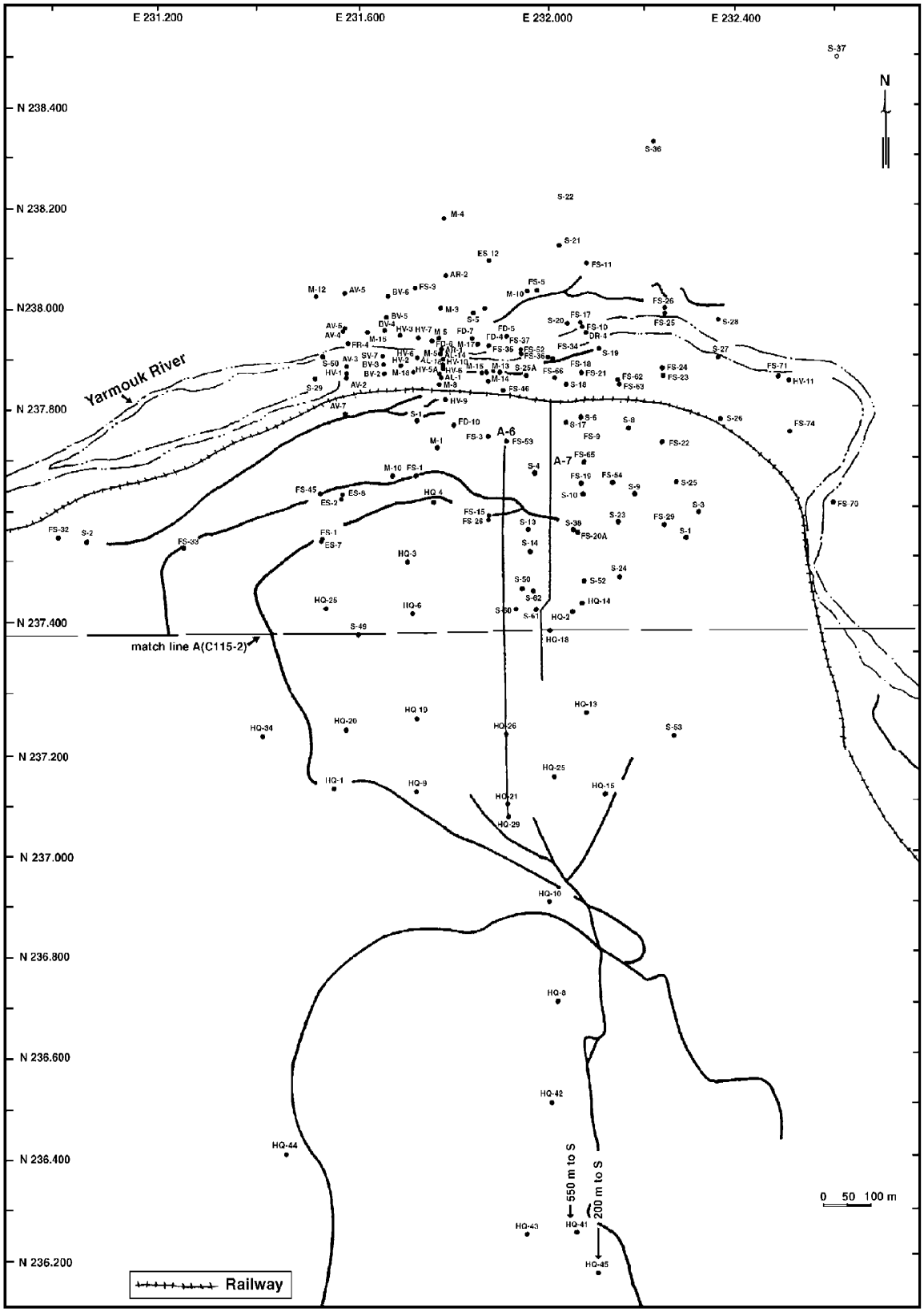

Figure 2-4. *Locations and identification labels of existing boreholes used to construct lithological profiles referred to in the text and shown in Appendices A and B. Also shown are the positions of Adits A-6 and A-7. After Harza (1982) and Jordan Valley Authorities (1980).*

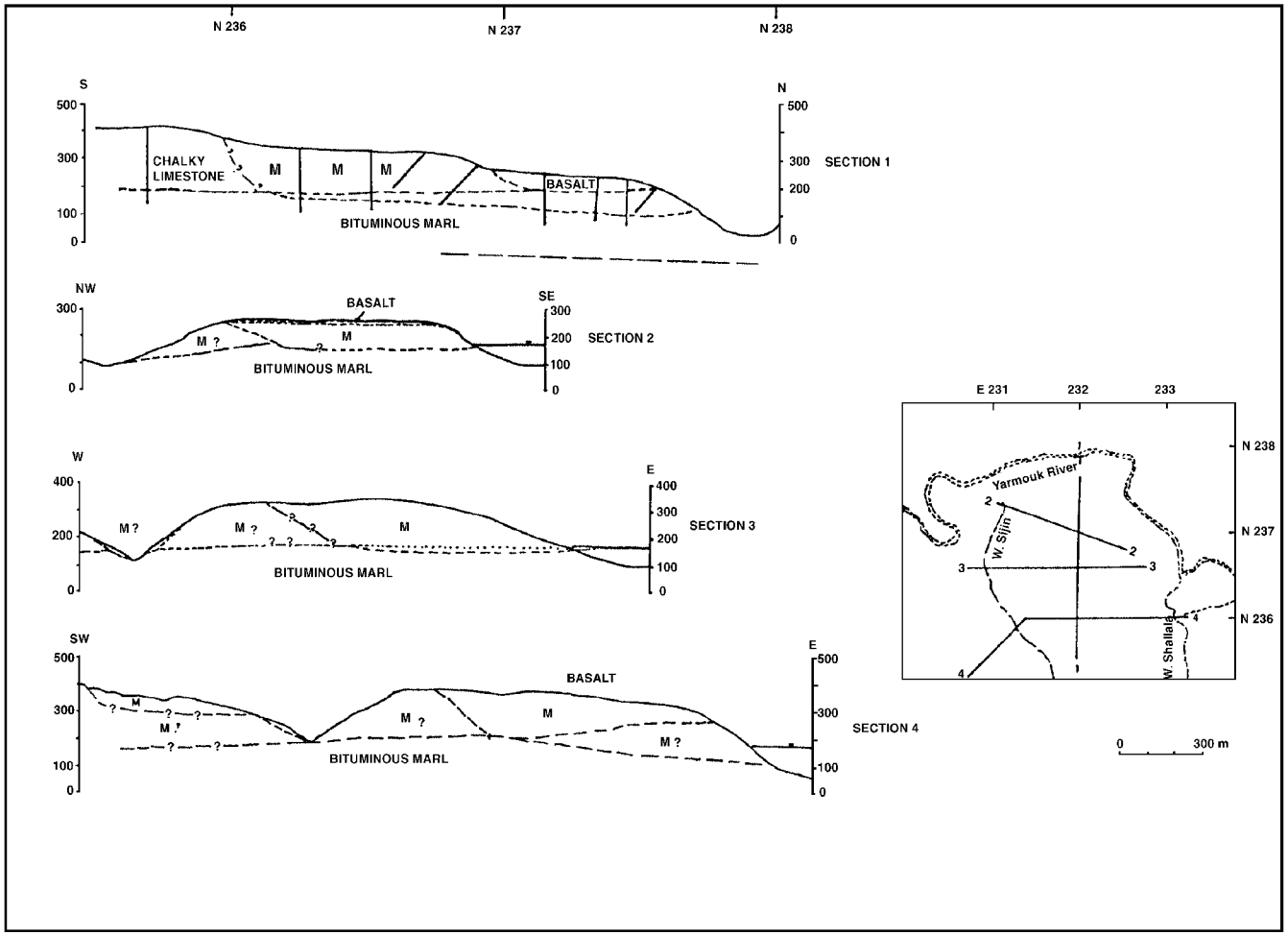

Figure 2-5. *Locations of cross-sectional profiles (1-4) from the Maqarin area showing the contact between the unaltered Bituminous Marl Formation and the overlying cement zone (Metamorphic Unit) ("M"). After Harza (1982) and Jordan Valley Authorities (1980).*

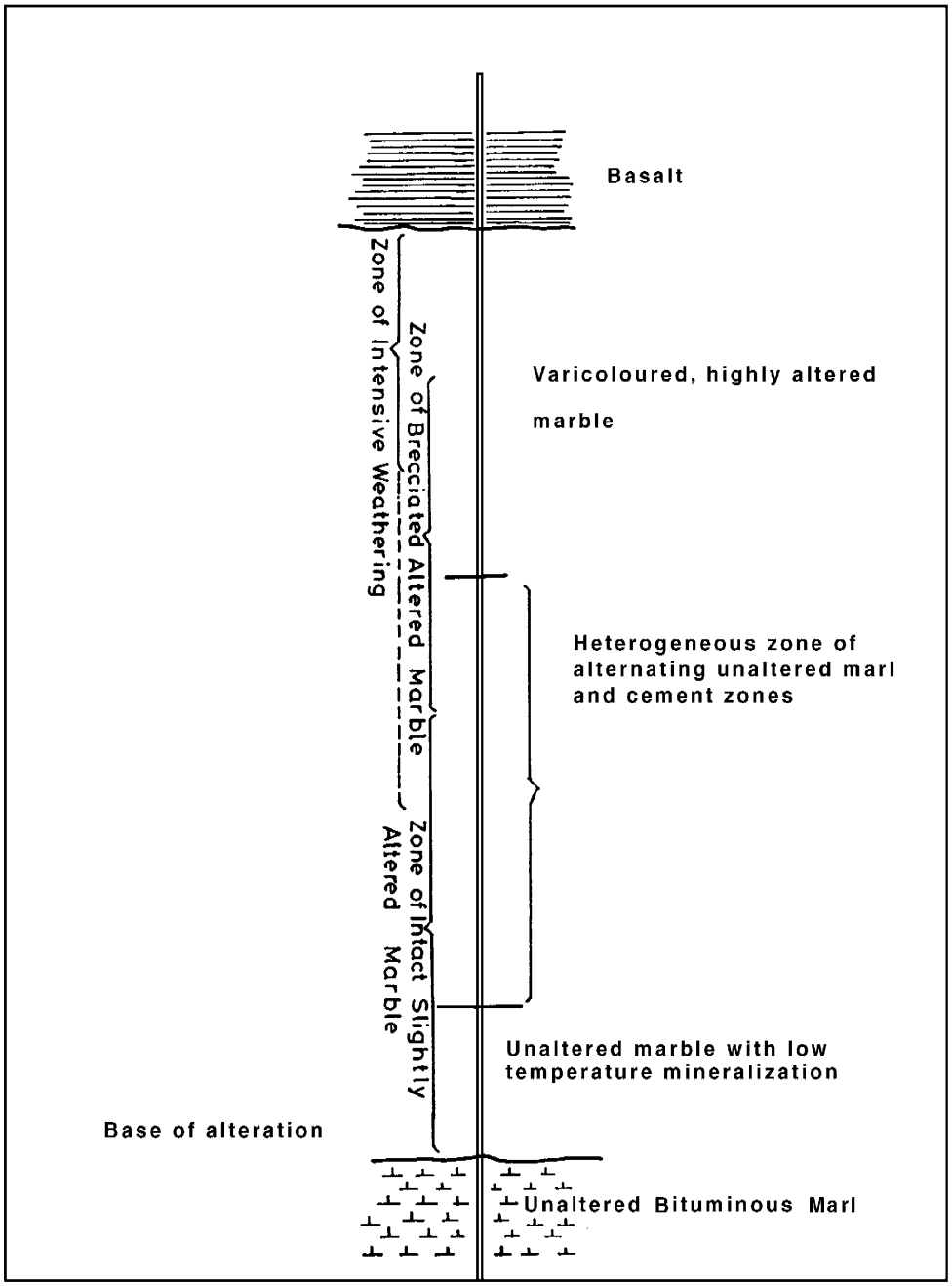

Figure 2-6. *General features of the cement zone (Metamorphic Unit) overlying the unaltered part of the Bituminous Marl Formation. After Harza (1982) and Jordan Valley Authorities (1980).*

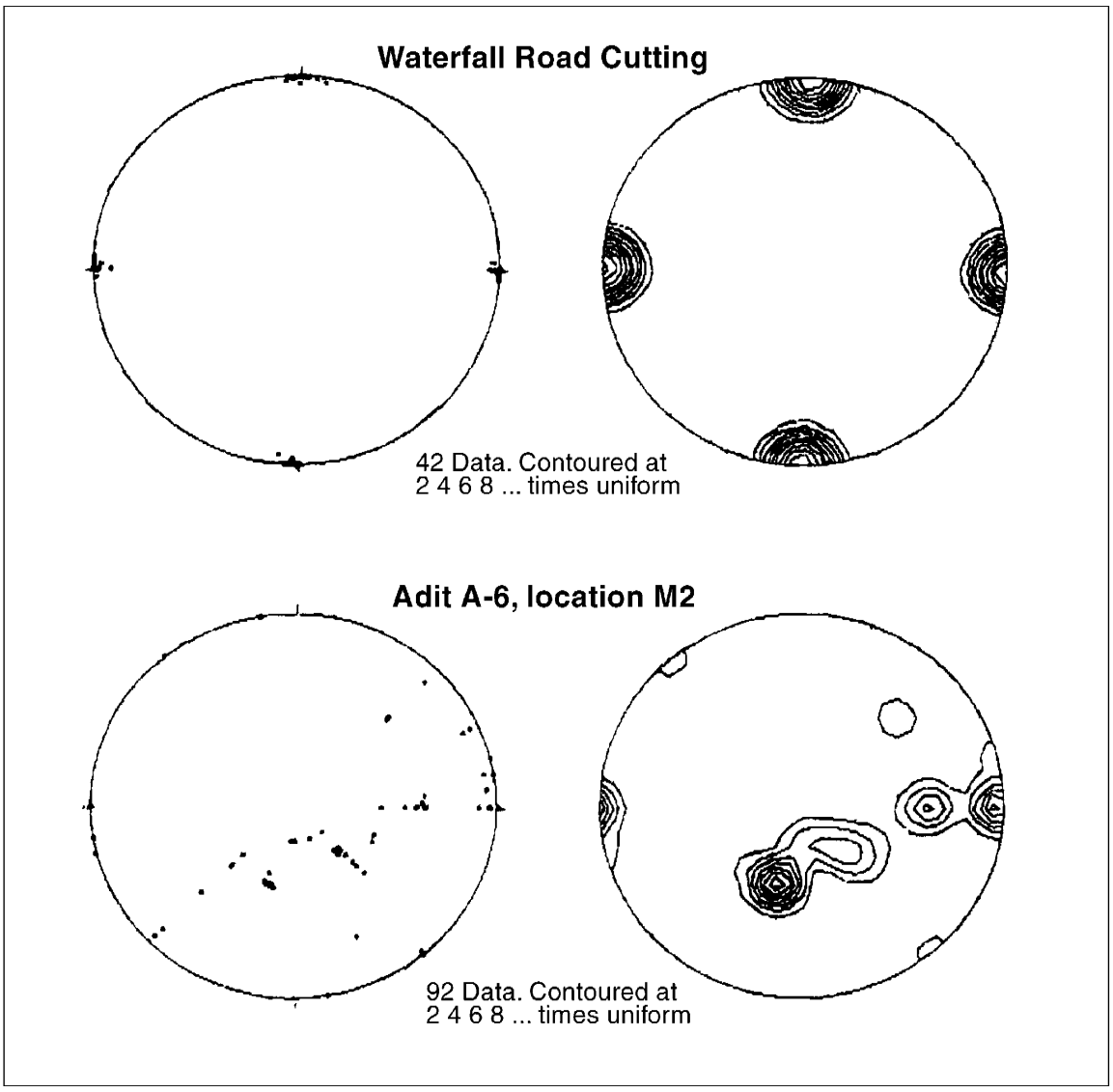

Figure 2-7. *Orientations of structural elements in the Waterfall Road Cutting and in Adit A-6 (see Fig. 2-1 for locations).*

(Equal area projections of the lower hemisphere).

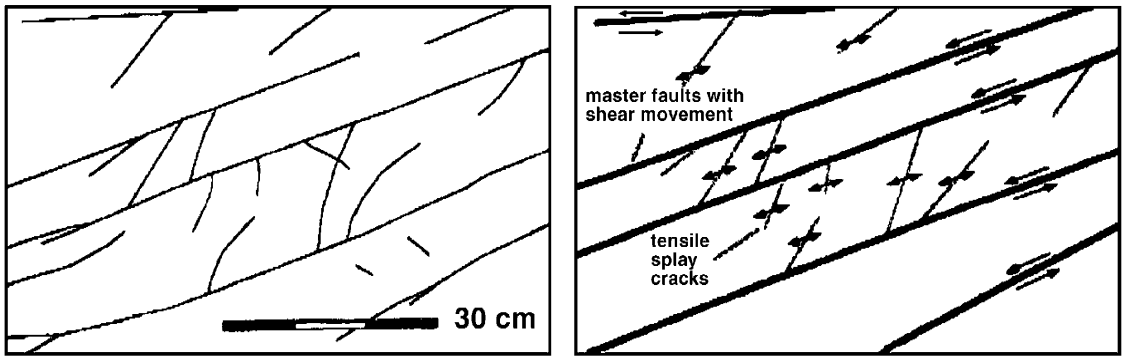

Figure 2-8. *Geometry and mechanistic interpretation of NE-dipping faults in Adit A-6.*

(View of the NE Adit wall).

Figure 2-9a. *Typical infilled fractures at sampling site M2, Adit A-6. Several main fractures, 2–10 cm apart, with fine anastomosing network of veinlets between them (from Alexander and Mazurek, 1996).*

Figure 2-9b. *Bedding plane parallel shear zone in a N-E dipping bedding plane at sampling site M2, Adit A-6. Note otherwise massive nature of the Bituminous Marl Formation (from Alexander and Mazurek, 1996).*

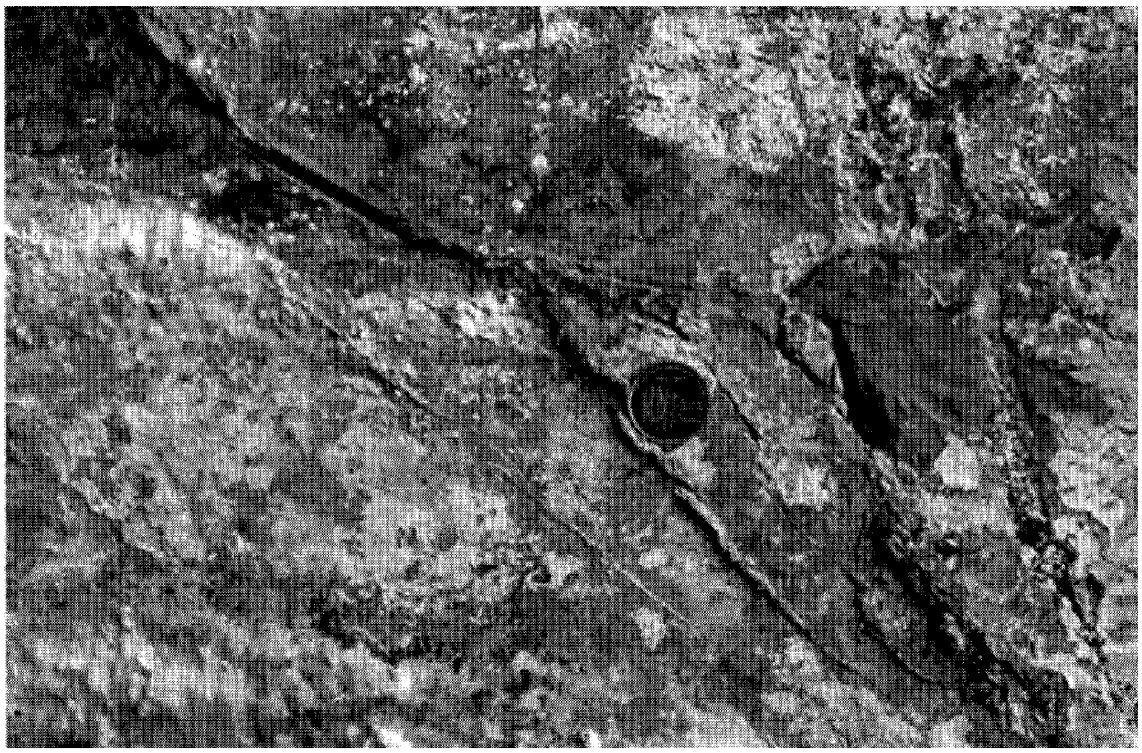

Figure 2-10. *Partially mineralised fracture set at the Maqarin Station Railway Cutting (steep master fault with a set of diverging splay cracks). Openings with apertures of several millimetres remain open. Coin size approx. 2 cm.*

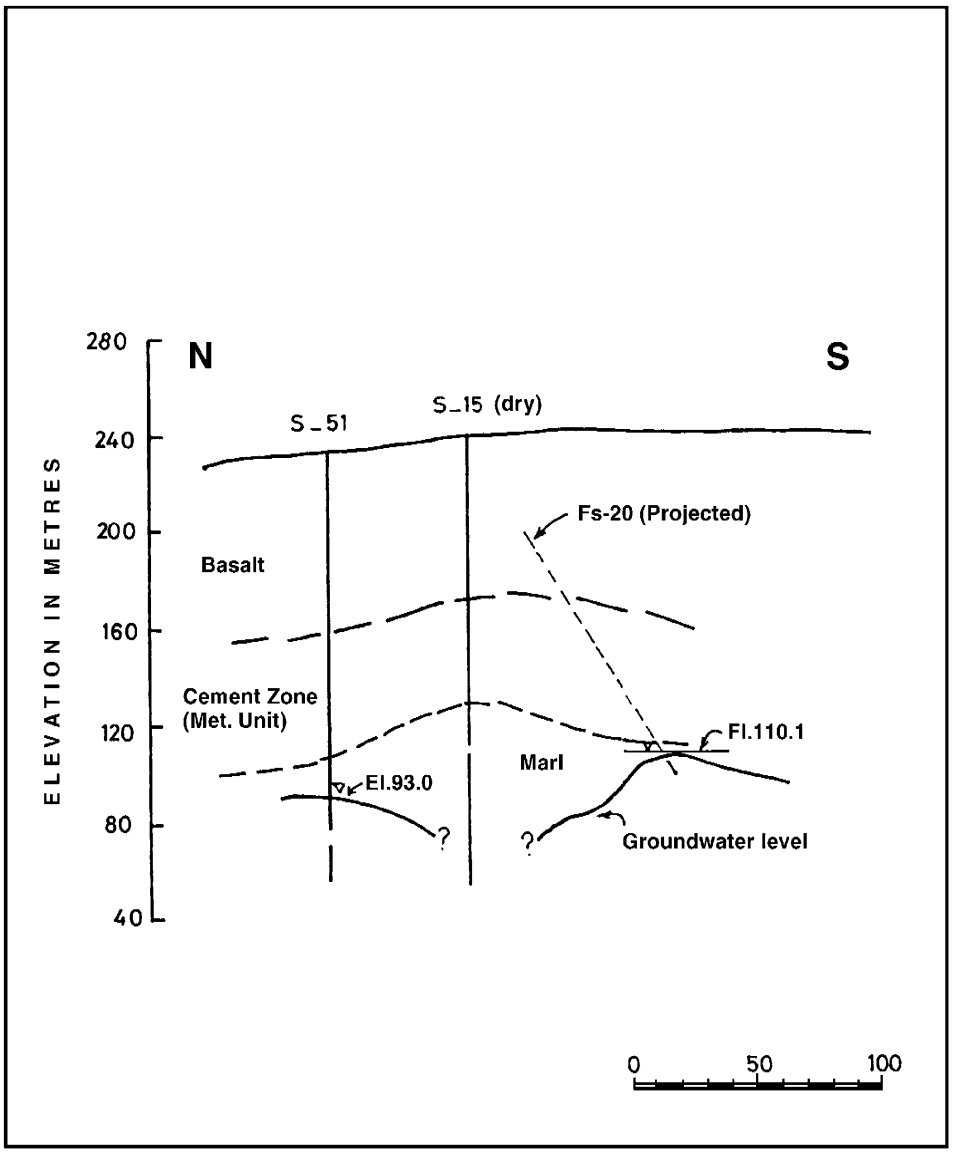

Figure 2-11. *Relationship between groundwater levels and the Maqarin stratigraphy along a N-S profile at the Eastern Springs location close to the Yarmouk River. After Harza (1982) and Jordan Valley Authorities (1980).*

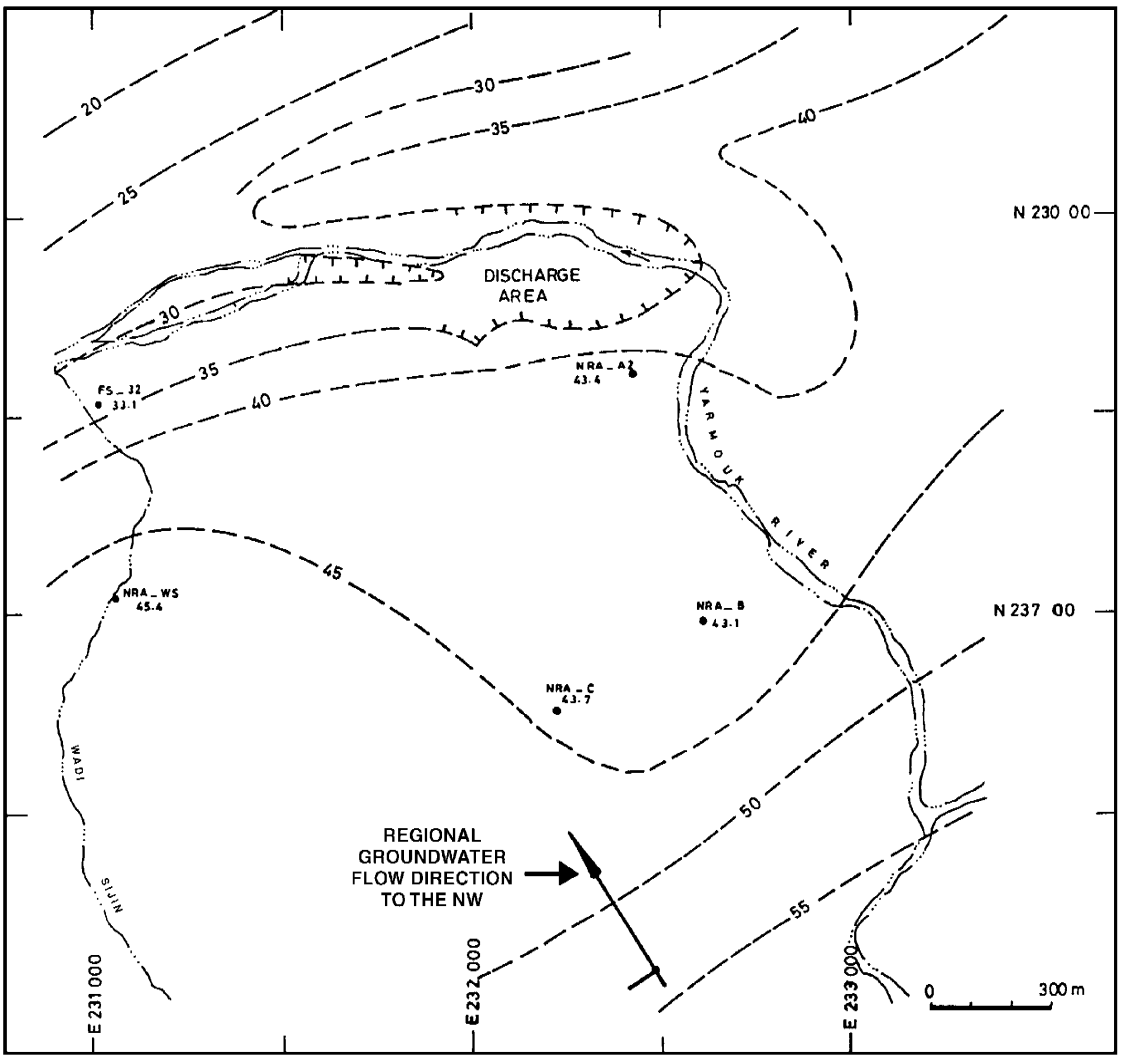

Figure 2-12. *Groundwater piezometer contours of the Amman Formation measured from the Maqarin area. Modified after Harza (1982).*

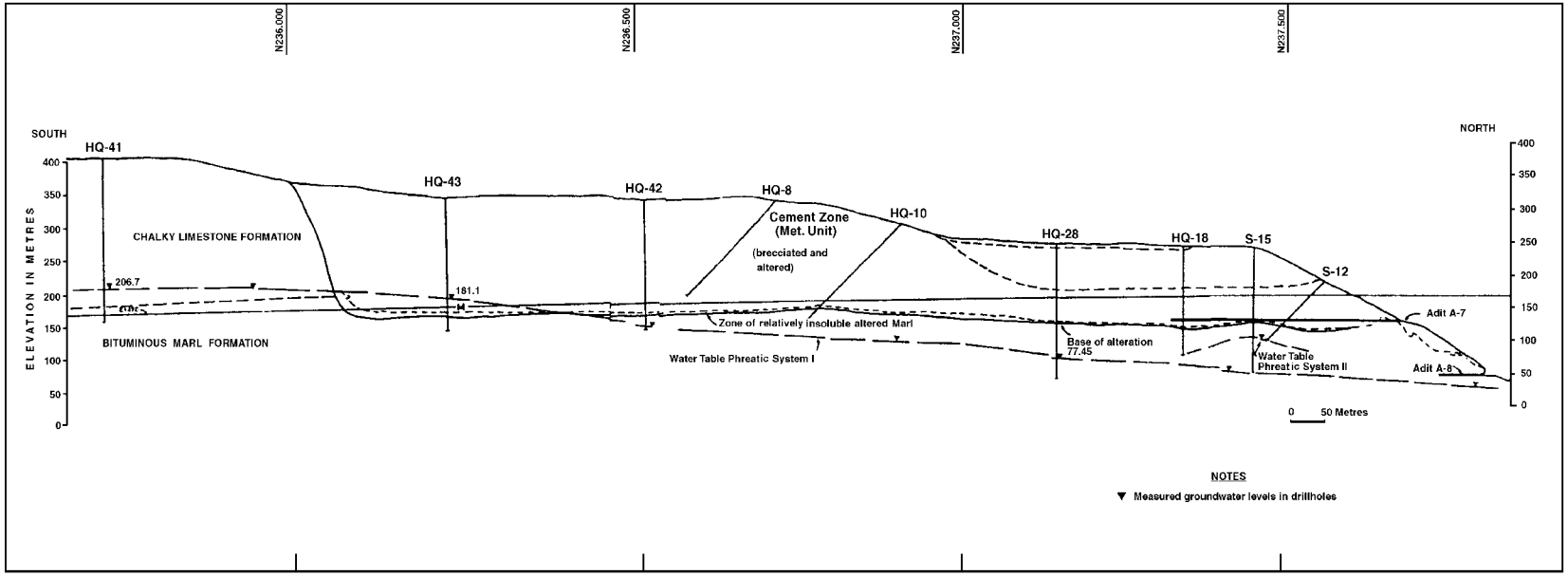

Figure 2-13. *Groundwater levels measured in the Chalky Limestone Formation along a S-N cross-sectional profile parallel to Adit A-7. Modified after Harza (1982).*

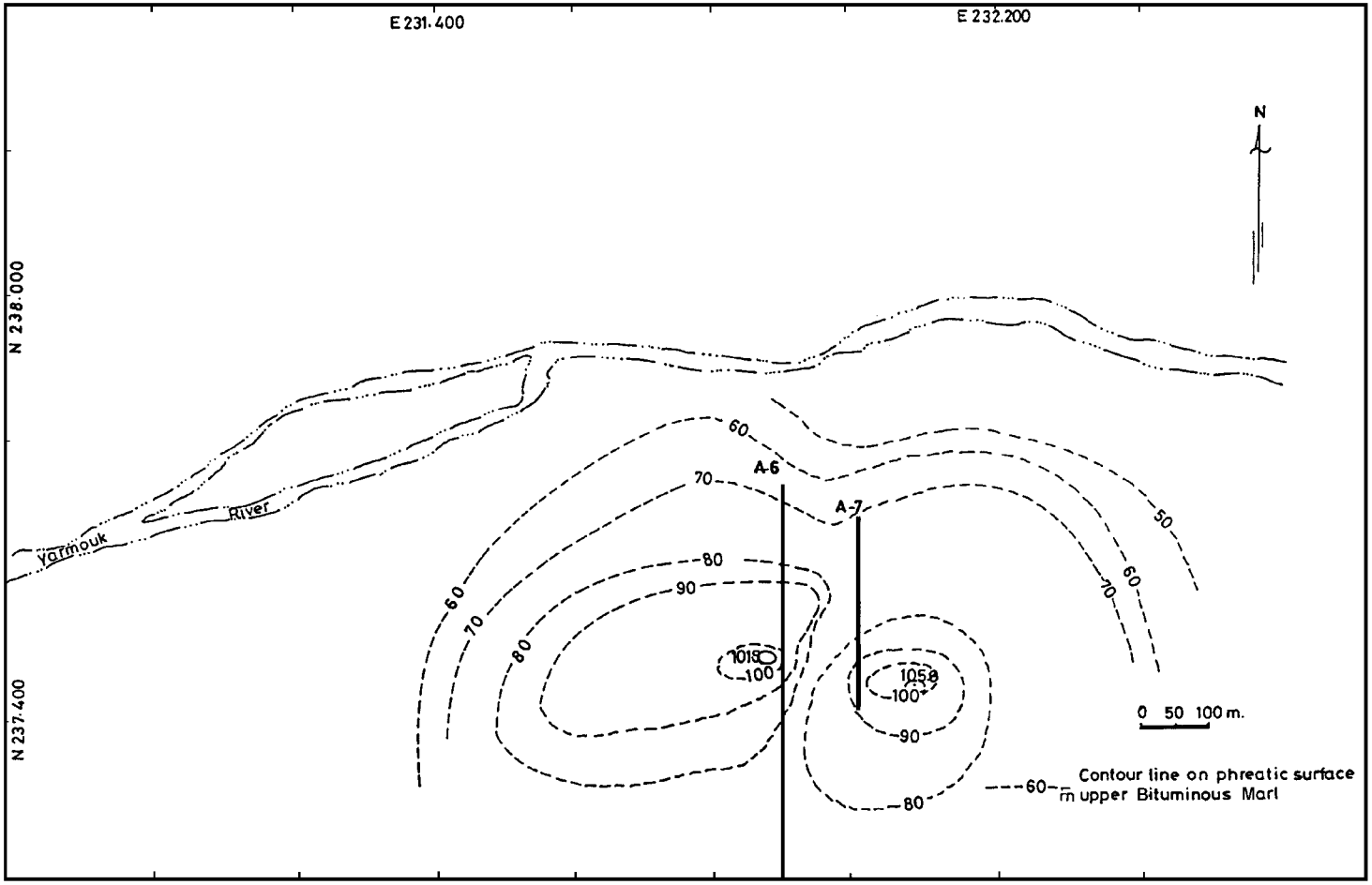

Figure 2-14. *Location of two possible recharge points in the vicinity of Adits A-6 and A-7. After Harza (1982).*

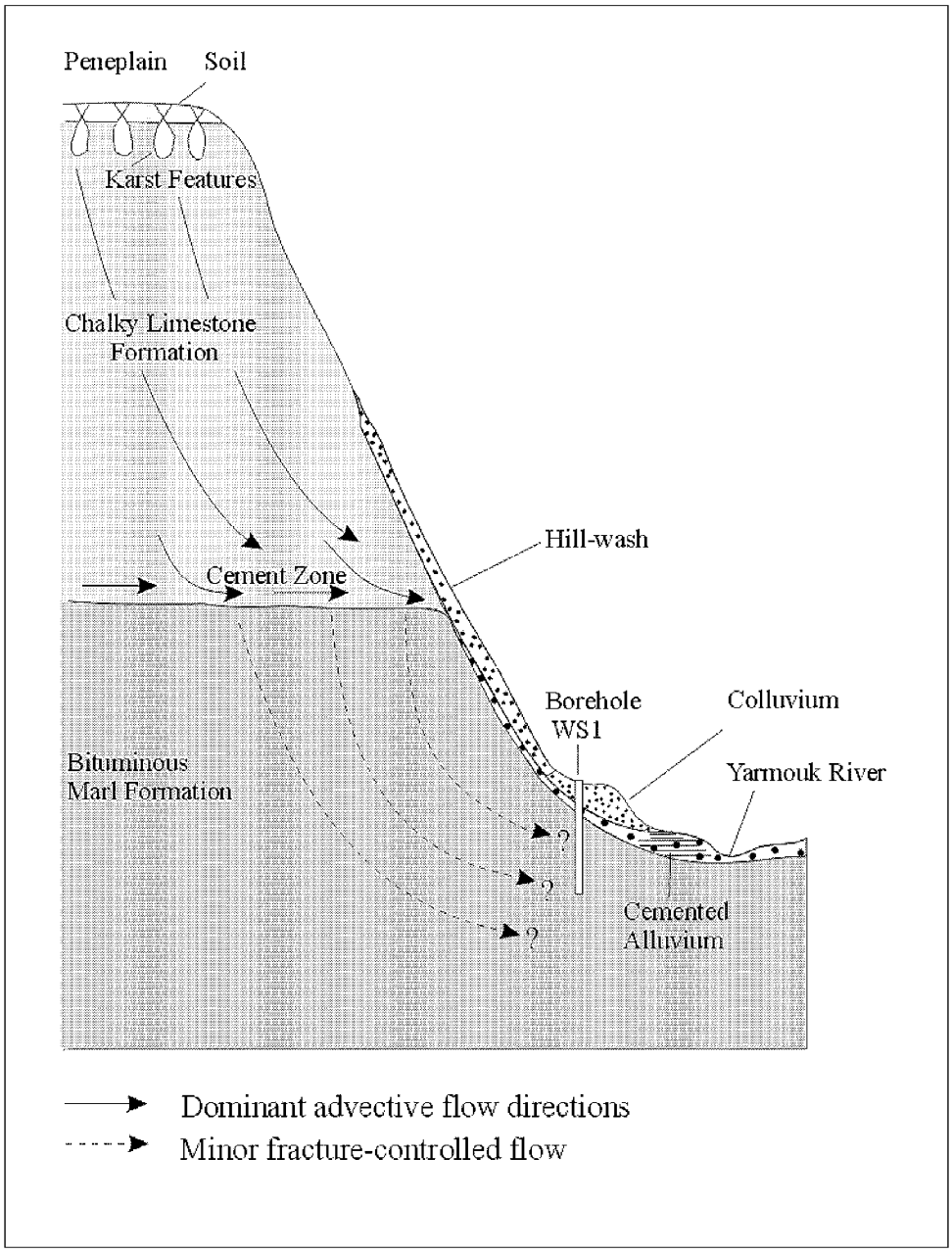

Figure 2-15. *Schematic diagram of the hydrogeologic situation in the Western Springs area. Discharge seepages at the bottom of the Yarmouk River Valley occur mostly at the Colluvium – Cemented Alluvium interface.*

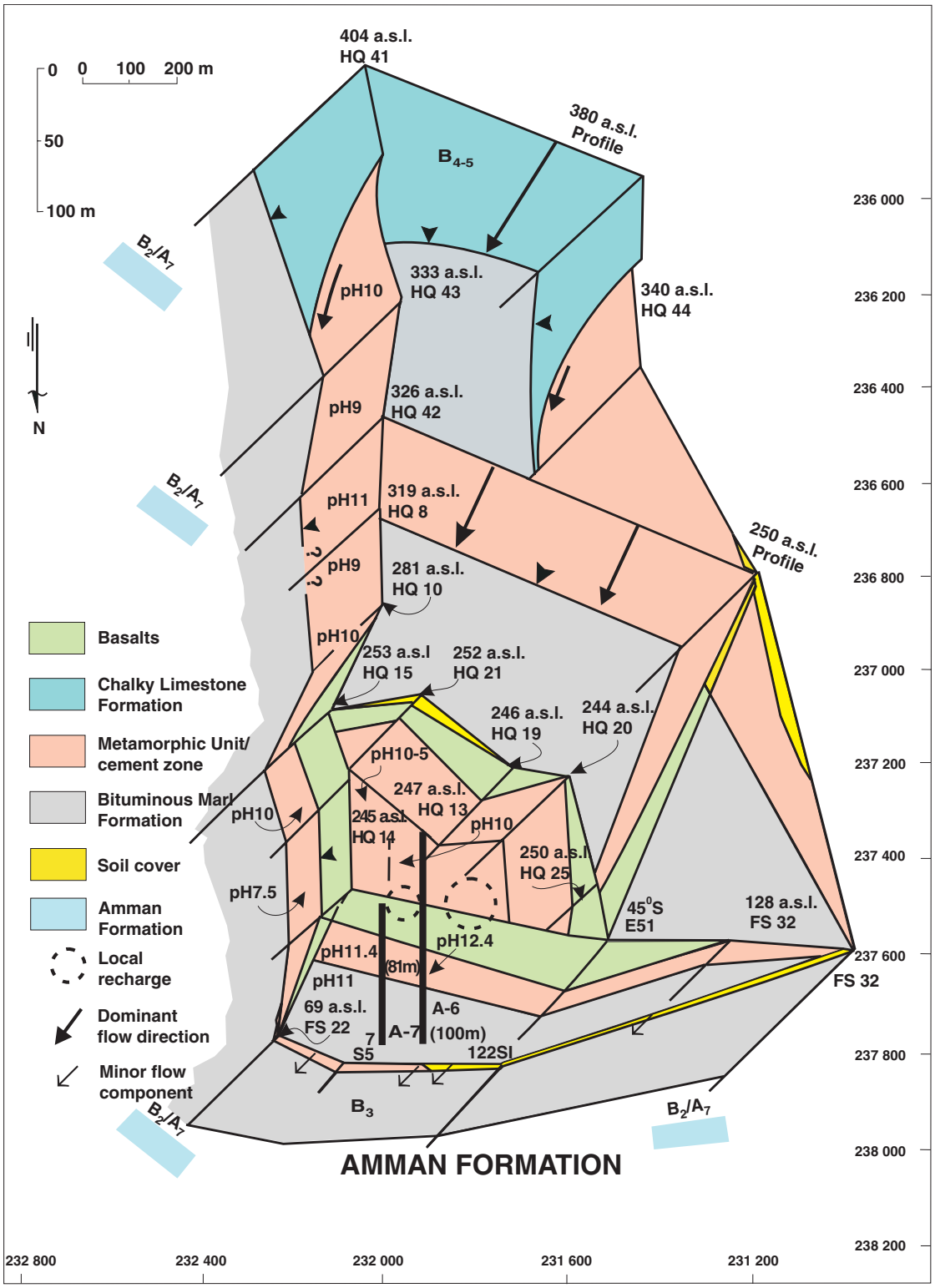

Figure 2-16. *Three-dimensional illustration of the Maqarin area, integrating major stratigraphical units, important structures and the general hydrogeological character of the area. The illustrated area is bounded by the Yarmouk River to the north, Wadi Shallala to the east and Wadi Sijin to the west, and by latitude 236.200 to the south. (Note: e.g. 250 a.s.l. = 250 metres above sea level).*

3 GEOMORPHOLOGY OF THE MAQARIN AREA

(A.F. Pitty)

3.1 INTRODUCTION

The Yarmouk River, the main tributary of the River Jordan, drains an area of approx. 6 800 km^2, of which 1 800 km^2 is in Jordan and 5 000 km^2 is in Syria (Fig. 3-1; Appendix D; Plates D-1 and D-2). Its tributaries, in turn, are extensive; for example, one major tributary, the river Midaneh, rises south of Damascus. The Maqarin section of the Yarmouk River lies at the northern end of an extensive tract of Cretaceous/Tertiary limestones, covered with 'terra rossa' soils. As such, it is typical of many parts of Mediterranean lands.

Otherwise, the area is geologically outstanding, for two reasons. First, it is bounded to the north and east by part of the world's most extensive flood-basalt field. Within the Jebel Druze-Wadi Hauran volcanic province of southern Syria and northern Jordan, continental flood basalts cover some 48 000 km^2. The full extent, from Yemen to Turkey, covers some 80 000 km^2. Second, the study area is bounded, to the west, by a sector of the 6 000 km long African-Syrian rift, the Jordan Rift System (Fig. 3-2). The Maqarin study area is only 20–25 km east of an eastern branch of this rift, a newly formed plate boundary which separates the Sinai microplate from the Arabian plate.

The focus of interest in the Maqarin study is the Bituminous Marl Formation, and the high-temperature, low-pressure metamorphic rocks (i.e. the cement zone) created by ignition of these organic-rich rocks (Khoury et al., 1985; Clark et al., 1993). The probability of a bituminous rock combusting increases the closer it is to the surface, where the bedrock is unsaturated and an oxygen supply is therefore available via cracks and joints in the bedrock.

Clearly, erosional unroofing of the overlying strata is critical in exposing the bituminous rocks to atmospheric oxygen. Therefore, the purposes of the present geomorphological study are to:

- review the structural and denudational geohistory of the Maqarin area,
- estimate erosion rates,
- examine the connection between erosion, oxygen supply, and the likelihood of combustion of the bituminous rock,
- relate this information to explain the occurrence and distribution of hyperalkaline groundwaters at Maqarin.

3.2 STRUCTURE

3.2.1 Plate Tectonics

In post-Cretaceous time, the Arabo-Nubian shield rifted and, about 24–22 Ma ago, parted along the Red Sea and Gulf of Aden, forming a divergent plate margin. This cratonic break-up, drift, and spreading of the Red Sea floor impelled the Arabian sub-plate northwards and also induced its largely NNE counterclockwise rotational movement. The Dead Sea – Jordan rift system originated from these plate motions (Kashi and Croker, 1987).

In plan view, the rift system changes direction, so that blocks along its two sides cannot fit together after strike-slip motion has occurred (Kovach et al., 1990). As a result, gaps are opened up along some sections, producing the structurally controlled 'rift valleys'. In other sections, local compression occurs and ridges may be produced. This contrast between these features explains why 'baselevel' varies both in time and space along the Dead Sea – Jordan rift system

3.2.2 Regional Dip

In its lower reaches, the Yarmouk River appears to lie close to a large-scale structural low between the anticline of the Ajlun Dome, some 40 km to the south, and the Mt. Hermon anticline, approx. 70 km to the north (Fig. 3-1). It is, therefore, possible that the Yarmouk has followed its present alignment for much of its geohistory. In the Maqarin area, the dip of the strata is generally low (Appendix D; Plate D-3).

Subhorizontal Neogene and Quaternary strata overlie the NW-dipping flank of the broad anticlinal structure of the Ajlun dome. They are separated from the underlying Cretaceous and Early Tertiary rocks by several angular and erosional unconformities (Mor and Steinitz, 1985).

3.2.3 Faulting

The Dead Sea-Jordan rift system is characterised throughout its length by master strike-slip faults, arranged in an en echelon pattern (Fig. 3-2). Shear for the initial 60 km of left-lateral offset averaged 0.4 cm/a between 20 and 5 Ma, accelerating to 0.9 cm/a over the past 5 Ma. Rates during the past 1.5 ka range between 0.15 and 0.35 mm/a. (Garfunkel et al., 1981).

In the Pliocene, and particularly during the Pleistocene, vertical displacement was very large, attaining 2 000 and 4 000 m, respectively. However, despite its proximity to one of the world's great rift systems, faulting is not common in the Maqarin area. Evidence of tensional stress occurs only within a zone about 4 km wide on either side of the rift (Arkin, 1989).

3.2.4 Uplift

Uplift to produce the Afro-Asian dome did not occur until ca. 10 Ma ago (Almond, 1986), possibly reflecting a response to the ascent and accumulation of magma at the

crust-mantle boundary. It is also possible that the earliest drainage lines were established at this time.

3.3 INITIAL DRAINAGE AND BASE LEVELS

An ancestral Yarmouk River, as postulated for several river valleys to the south (Freund et al., 1968), may have extended westwards to the Mediterranean coast before the Jordan Rift system was initiated. If so, the fact that the Mediterranean was approx. 1 000 m below present sea-level during the Messinian salinity crisis, ca. 6 Ma ago, may have initiated some incision at that stage.

The alignment along which such an extension may have occurred – the Bet Shean-Yizre'el Valley-Qishon graben – is offset to the south of the present Yarmouk River outlet by some 40 km, similar to the amount of offsetting by strike-slip faulting.

In the Dead Sea area, the Jordan Rift Valley formed as a morphotectonic depression ca. 6 Ma ago (Steinitz and Bartov, 1991). When the rift was activated, only some areas within the rift acted as baselevels, as a result of extension, whilst other zones developed much later (Kafri and Heimann, 1994). Eastward reversal of westward palaeodrainage in east Galilee, established 5–3 Ma ago, took place not earlier than 2 Ma ago. This means that this part of the Jordan Rift system in the Sea of Galilee area did not form a baselevel prior to 2 Ma ago (Kafri and Heimann, 1994).

Further south, the extension which formed the Rift Valley was probably initiated 4 Ma ago (Heimann, 1990). The lower valley of the Zarqa river, some 60 km south of Maqarin, was already incised at this time (Baubron et al., 1985). Further south, the Wadi Zerqa Ma'in, the major drainage to the Dead Sea, started to incise ca. 6 Ma ago, reaching sea-level at 4.0–3.4 Ma ago (Steinitz and Bartov, 1991).

Near the Jordan Rift Valley, there is no apparent evidence of a pre-Cover basalt stage in the geohistory of the Yarmouk Valley (Mor and Steinitz, 1985). However, in the Maqarin area, two clear examples of palaeowadis of pre-Cover basalt age are evident. The first is the sediment-filled Dhuneiba (Fig. 3-3) palaeochannel (Appendix D; Plate D-4). The second is a clearly defined valley palaeomeander, high on the southern shoulder of the present Yarmouk gorge (3.7 km ESE of Maqarin Station). The altitude of the palaeochannel floor is approx. 370 m.a.s.l.

3.4 IGNEOUS INTRUSIONS

3.4.1 Plateau Basalts

Several extensive lava flows within the Jebel Druze volcanic province (Fig. 3-1), the type area for 'plateau basalts', are dated at 12.3 Ma. Subsequently, in north-west Arabia, there was a lull in volcanic activity between 12 and 7 Ma, with renewed activity peaking 5–4 Ma ago (Barberi et al., 1980). After 3 Ma, the ESE alignment of fissure

eruptions may correspond with displacements within the Arabian plate, related to the alignment of spreading of the Red Sea rift.

To the north of Maqarin, the lava flows again developed at about 400 m across south-west Syria. The so-called 'Cover Basalt' (also referred to as the Syrian or Hauran Basalts), originally dated at 1.8 Ma, are now dated at 5.3–3.5 Ma (Mor, 1993). Made up of several flows, the Cover Basalts are 100–150 m thick in the Sea of Galilee area. These flood basalts extended to, or just across, the line of the Maqarin Valley (Fig. 3-4). Possibly, lava crossed a gravel fill in the ancestral valley, probably already developed prior to the eruption of the Cover Basalt.

3.4.2 Yarmouk Basalt

The Yarmouk Basalt is dated at 0.83–0.79 Ma (Mor, 1993). It spilled into the ancestral valley floor (Fig. 3-4), re-excavated or created below the level of the plateau, when it was about 200 m higher than its present-day level in the Maqarin area. A basalt terrace, where the Yarmouk-Raqqad valley section of the Yarmouk drainage enters the Jordan Rift Valley, is some 100 m above the present-day river level.

3.4.3 Raqqad Basalt

The key fact about the Yarmouk River valley is the age of the Raqqad basalt, now revised (Mor, 1993) to ca. 0.48–0.35 Ma ago (about five times older than previously thought). This means that the lower reaches of the Yarmouk River Valley were already incised to within 30 m of their present level nearly 0.5 Ma ago.

It seems that the Raqqad basalt, flowing down the Wadi Raqqad (Figs. 3-3, 3-4), ponded back drainage within the Maqarin Valley, upstream from the confluence of these two valleys. A long, narrow lake was formed which was gradually filled by sediment, with increasingly coarse material dumped near the head of the former lake. These deposits may include the cemented boulders, banked against the base of the valley side and appearing, in turn, to pond back groundwater outflow at the Western Springs area. Locally, groundwater levels were probably raised after ca. 0.5 Ma.

3.5 AGE OF THE MAQARIN VALLEY

3.5.1 Erosion Rate

Considering the erodibility of the chalk bedrock in the Maqarin area, the minimum age for the valley may seem remarkably old. The comparative slowness of "incision" is probably due to:

1. The repeated infilling of the valley floor by debris from upstream areas during climatic episodes favouring greater sediment yield, with much stream power, during subsequent episodes of downcutting, merely reworking and re-excavating this material.

2. The flooding of the valley with lava, perhaps on several occasions, prior to the Raqqad basalt phase. The lava is comparatively resistant to erosion, as evident by the bar across the Jordan Valley, created by the outflow of the Yarmouk Basalt. This is still undergoing downcutting, 0.8 Ma after its deposition.

Since the Cover Basalt was deposited, incision at the outlet of the Yarmouk Valley has been <13 cm/ka, almost balanced by the rate of sedimentary infill of the rift floor in this region of 11 cm/ka (Mor, 1993). Concurrently, the mean rate of tectonic lowering of the Dead Sea – Jordan rift, south of the Sea of Galilee, was 24 cm/ka. At the Maqarin study site, the age and altitude of the Yarmouk Basalt suggest a mean rate of incision of 25 cm/ka over the past ca. 0.8 Ma. However, since the lower Yarmouk Valley, below the Wadi Raqqad confluence, was cut down to within 30 m of its present level before the deposition of the Raqqad basalt, an erosion rate of approx, 57 cm/ka may have prevailed between 0.8 and 0.5 Ma.

At the point where the Yarmouk gorge enters the Jordan Rift Valley, the difference in altitude from the top of the Cover basalt on the Um Qeis and Mevo-Hama plateaux (Fig. 3-3) to the present-day river bed is 545 m (Mor and Steinitz, 1985). Averaged over a timespan of the 3.5 Ma, this gives a mean erosion rate of 15.6 cm/ka. This figure is unexceptional, since "...several examples suggest that an average rate of bedrock channel lowering in middle latitudes might be roughly of the order of 15 cm/1 000 years" (Pitty, 1971).

Although the former ponding back of the Yarmouk River by the Raqqad basalt seems inevitable, it is worth noting that, similarly, the Hula lake basin (approx. 60 km NNW of Maqarin Station) was dammed by the Yarda basalt. Deposited about 0.9 Ma ago, the Yarda basalt is chronologically equivalent to the Yarmouk Basalt (Heimann and Ron, 1993). The volcanic events causing the damming were complicated, with an intercalation of basalt and gravel layers. After some alternation of peat and open-water and marly sediments, a deep lake formed which filled up with calcareous mud (Cowgill, 1969). In addition, a littoral facies of coarse clastic sediment, the Benot Ya'akov formation, was introduced by tributary wadis. Boulders up to 0.5 m in diameter are dominant in highly cemented, resistant layers, which form bar-like structures across the Jordan River. Archaeological materials in the "bar" are assigned to the Acheulian Industrial Complex, thus constraining the age of the Benot Ya'akov formation between 0.73 and 0.24 Ma (Goren-Inbar et al., 1992a, b). Some comparable features are probably recognisable in the Yarmouk Valley after ponding by the Raqqad basalt.

3.5.2 Longitudinal Profiles

The "Cycle of Erosion"

Longitudinal profiles (Figs. 3-5, 3-6 and 3-7) trace the changing gradient of stream channels from source to mouth. Traditionally, abrupt points of increased gradient ('knickpoints'), together with smoothly declining ('graded') segments of a profile between knickpoints, were seen as diagnostic features of the geohistory of a stream valley and the upland surfaces of its interfluves.

The classic study on the geomorphic evolution of the Jordan Rift system by Quennell (1958) was one of the last examples of this approach. Meanwhile, it became

increasingly admitted that erosional lowering of structural relief occurs only to a very approximate degree. Reduction to a specific and widely recognisable flat surface at a specific altitude – a 'peneplain' in 19th century terminology – is now believed to be unrealistic.

Examples in North Jordan

The longitudinal profiles of the Yarmouk, and its main neighbour to the south, the Zarqa (Figs. 3-3, 3-5), can be examined with reference to specific geological structures and lithologies. In the Yarmouk, the uppermost 'knickpoint', at approx. 420 m.a.s.l., illustrates the degree to which incision into the Cover basalt plateau has proceeded. In the Maqarin area, this is clearly seen in detail, up-valley from the sheer-cliff gorge at Amrawa, 6.5 km SE of Maqarin Station (Figs. 3-3, 3-7).

In the Maqarin area, the knickpoint on the Wadi Shallala profile (Figs. 3-3, 3-7) is the clearest illustration of how this locally steepened gradient ('knickpoint'), created by a renewed phase of river downcutting, advances upvalley. This profile, at the knickpoint, also suggests that a thickness of approx. 30 m of strata would be exposed by downcutting.

In the more general longitudinal profile (Fig. 3-5), both the Cover Basalt and the Raqqad Basalt knickpoints are clearly evident, at 420 and -90 m.a.s.l., respectively. In the more detailed profile (Fig. 3-6), the knickpoint at 270 m.a.s.l. may be linked to the former Yarmouk Basalt valley fill. From these data, estimates of horizontal distances from topographic maps, and the revised radiometric ages of the basalts (Mor, 1993), rates of headward retreat of the knickpoints can be suggested (Table 3-1).

The calculated rates appear proportional to the thickness of the basalts. Extrapolation of the Yarmouk Basalt retreat rate suggests that its knickpoint could have reached the Maqarin anticline, approx. 39–41 km up-valley from the Rift Valley, about 600 ka ago. One plausible date for initiation of combustion metamorphism at both the Eastern and Western Springs would, therefore, be soon after 600 ka ago.

3.6 MASS MOVEMENTS

The jointed rocks of the Smoking Hills formation in northern Canada burn in locations where they are exposed to air, mainly on hillslopes and where landslides occur (Mathews and Bustin, 1984). Mass movements in the Maqarin area, therefore, are a particular focus of interest. Three main factors – earthquakes, joints, and erosional rebound – will be considered in the following sections.

3.6.1 Lower Valley

Landslides are a significant feature in the Maqarin area, and are developed on a spectacular scale downvalley, particularly in the Raqqad-Yarmouk section, to the north

of Um Qeis (Fig. 3-3). Oversteepening by lateral erosion may be a critical erosional factor, rather than the rate of vertical incision.

3.6.2 Maqarin Interfluve

An ancient rockslide is a dominant feature of the upper valley side, due south from the adit site. The displaced, crushed, and re-cemented strata descend from just below the 400 m contour to approx. 220 m. It terminates on the southern margin of the laterite-covered Adh Dhlla bench, with a remnant of the Yarmouk Basalt on its northern margin.

3.6.3 Wadi Sijin

Much of the west side of the lower part of the Wadi Sijin has collapsed, involving an area of approx. 1.5 km^2, now composed of irregular, low hills.

3.7 EARTHQUAKES

3.7.1 General

Much of the history of earth-surface processes is usually seen as the result of gradual change by slow but persistent processes. However, when the "Holy Land" region is the epicentre of interest, catastrophes have to be anticipated.

3.7.2 Localisation of Seismic Events

Figure 3-2 shows that seismic activity is clearly concentrated along the Jordan Rift system, with epicentre alignments appearing to correlate well with the fault pattern, including faults branching off the transform. About 76% of the total energy from the earthquakes over the last 4 000 years seems to have been released from the transform proper (Bayer et al., 1989).

Within the rift, the last major earthquake, with a 'local magnitude' (ML) of 6.2, caused much damage to Jericho and other nearby towns in 1927 (Marco and Agnon, 1995). Structural damage affects old and/or poorly constructed buildings, set on relatively loose ground, whilst those built on solid bedrock remain intact. For example, beyond 70 km from the epicentre, the Sept. 2, 1973 earthquake was generally not felt (seismic intensity I on the Modified Mercalli Scale (MMS)) in structures built on rocky exposures, even within the Jordan Rift Valley. In contrast, seismic intensities of III-IV (MMS) were experienced all along the soil-covered Shefala, up to 180 km from the epicentre (Arieh et al., 1977). Generally, landslides in solid bedrock are not reported until an MMS intensity of VII is attained (Brazee, 1979). The strongest earthquake in the Jordan Rift Valley since 1834, which occurred on July 11, 1927, yielded a maximum intensity of MM = IX close to Damia Bridge on the Jordan River (Shapira et al., 1993). Of some 40 reported earthquakes over the past 2 ka, 10–15 were comparable to the 1927 event (Ben-Menahem et al., 1976).

3.7.3 Seismic Risk in the Maqarin Area

The risk of seismic activity in the Levant is clearly related to the main geological faults in the region, and associated fault movements (Shapira et al., 1986). As it is only at such loci that earthquakes might actually initiate ground rupture, this is not a mechanism which could create primary rock dislocation in the fault-free Maqarin area. Also, earthquakes in the Levant are mostly of comparatively small magnitudes (Ben-Menahem et al., 1976). Further, the number of earthquakes associated with faults outside the Jordan Rift system is small (Shapira et al., 1986).

It must be stressed that earthquake 'damage' in the Holy Land usually refers to fragile buildings rather than to bedrock structure, and that Maqarin is too remote from epicentres (Fig. 3-2) to invite speculation about catastrophic' changes in groundwater systems due to seismic shock.

3.7.4 Earthquake-triggered Landslides

In aseismic areas, occasional extremes of heavy rainfall are usually and demonstrably the trigger for landslipping. However, landslipping, of critically unstable valley sides could be triggered by earthquakes in seismic areas. This is a particular feature of the lowest reaches of the Yarmouk Valley, and is suggested in an engineering study of landslips nearby, in the Jordan River gorge, north of Lake Tiberias (Harash and Bar, 1988).

The Sept. 2. 1973 earthquake, although only 4.5 Richter magnitude, is particularly noteworthy. The hypocentre was on the southern shore of Lake Tiberias. Three landslides were apparently triggered at this time, in marly slopes or cliffs of the Lisan formation, incohesive materials "...most vulnerable to landslides, which could be triggered by even relatively minor earthquakes" (Arieh et al., 1977). In contrast, the Yarmouk Valley rock avalanche comprised hard Eocene limestone exposures on the northern slope of the Raqqad-Yarmouk Valley near El Hamma (Fig. 3-3). During such an event, hillsides would indeed appear to 'skip like lambs'. The occurrence of such an event, at the present-day, confirms both the importance of mass movements on valleysides of the Yarmouk and the role of earthquakes in triggering mass-movement mechanisms.

The topography of the Wadi Sijin landslide probably remains too irregular to be older than Holocene. Conversely, the degree to which soil has accumulated in the depressions within the slipped mass suggest that it is older than a few centuries. One possibility is that it was triggered at the time when the Roman towns, Gadara (Um Qeis) and Abilda (near Ain Quelbe) were destroyed. Ain Quelbe is probably the only spring 3–5 km south of the Wadi Sijin landslide. These events may have been due to an earthquake (Wieseman and Abdul Latif, 1963). More probably, like the Mount of Olives during the Uzziah event (Wachs and Levitte, 1984), such damage could be attributed essentially to landsliding associated with the seismic event.

Some similarities between the Mount of Olives during the Uzziah earthquake and the Wadi Sijin landslip may be worth noting, as that part of Jerusalem also consists of soft chalk, and is a similar distance away from the major fault zones in the Jordan Rift Valley. The "splitting" of the Mount of Olives, as described in Zachariah 14, also involved the formation of a large valley, the filling up of an existing valley nearby, and

the appearance of new springs (Wachs and Levitte, 1984). Possibly, a large landslide, like that on the western flank of Wadi Sijin, could have been triggered by this earthquake, one of the strongest recorded in Jerusalem's long history. The Uzziah event probably happened between 2740 and 2695 B.P. (Wachs and Levitte, 1984).

In the absence of pollen analysis or the discovery of datable material, there is no factual evidence to support a specific date for the Wadi Sijin landslide. However, its appearance, as a slightly regularised but basically chaotic topography, is consistent to an event which occurred 3–2 ka ago.

3.8 JOINTS

According to Price (1966), "...despite the fact that joints are so common and have been studied widely, they are perhaps the most difficult of all structures to analyse". However, joints (Fig. 3-8A) are clearly an influence on, and are modified by, mass movement. Both primary and modified joint characteristics are probably a fundamental consideration in combustion metamorphic processes. Therefore, certain facts about joints are worth listing.

1. At Maqarin, the main joint trends of 10° and 130° are clearly unrelated to the SW-NE trend of the Maqarin fold. Similarly, in the northern Negev, the "...pattern of the joints seem to bear no simple relationship to ...monoclines" (Reches, 1976).

2. It seems that a basic joint pattern is acquired at a comparatively early stage after lithification. Thus, in Eocene chalks, widespread joints which cut successive beds possibly developed after induration had been well advanced (Bahat, 1987).

3. By definition, there is no displacement laterally or vertically along joints. However, they may become more prominently expressed near the ground surface, due to extension induced by denudational unloading. Thus, some larger-scale joint structures may become sub-divided into smaller rhomboids by interactions on smaller scales (Bahat, 1987).

   An instructive regional analogy to the Maqarin area may be the water-yielding open spaces in Carboniferous Limestone of southern Kentucky (Fig. 3-8B). Here, 25% of wells reach water-bearing crevices within 15 m, and crevices become progressively smaller and fewer below 25 m depth (Walker, 1956).

4. Extension of pre-existing joints is facilitated by erosional processes, with the vertical motion of rebound due to erosional unloading of superincumbent strata (Fig. 3-8C), and laterally, due to valley incision or cliff retreat (Fig. 3-8D). For example, joint sets increase in abundance with proximity to the Niagara escarpment (Gross and Engelder, 1991).

In the case of the Kentucky wells (Fig. 3-8B), the zone of most active solution ends below depths of 25–30 m (Walker, 1956). This is the same order of magnitude as the estimated 30–50 m of sedimentary sequence that underwent combustion metamorphism in the "Mottled Zone" in the Hatrurim basin (Burg et al., 1991).

3.9 REBOUND AND 'VALLEY BULGING'

Superficial, non-tectonic 'anticlines' have been reported where stream incision begins to cut down into a less competent strata, termed 'valley bulges' (Hollingworth et al., 1944). Significantly, such superficial anticlines can develop so abruptly, that witnesses have reported an accompanying explosive sound. One eye-witness near Stanford, Kentucky, "...saw that the disturbance advanced upstream...at the rate of a slow walk...During the rest of the day there were frequent sounds as of further rending of the rocks at depths beneath the upheaved surface; but by nightfall the sounds had all ceased..." (Shaler, 1877, quoted by Simmons, 1966). This graphic account suggests a very plausible mechanism for igniting bituminous strata. Notably, a valley-bulge structure is apparently developed along the narrow line of sharply anticlinal strata, in the channel floor of the Wadi Sijin (Wieseman and Abdul Latif, 1963; Fig. 3-7).

3.10 QUATERNARY PALAEOENVIRONMENTS

3.10.1 General

The three basalt flows – Cover, Yarmouk, and Raqqad – are three decisive, dated, and irreversible changes in the geohistory of the Maqarin locality. Superimposed on these local changes are the global palaeoenvironmental changes that accompanied the glacial-interglacial cycles during the Quaternary. These are discernible in a wide variety of indicators, each of which requires careful evaluation before drawing even tentative conclusions, particularly when the former conditions at a specific locality are being envisaged.

For present purposes, the scattered data and conflicting interpretations on the palaeoenvironments of the Levant have been reviewed exhaustively and evaluated systematically. However, comparatively little has been identified which could have some bearing on the processes of combustion metamorphism. The following notes illustrate some themes which might be noted or developed further.

3.10.2 Present-day Environment

In several ways, the character of the present-day environment emphasises why palaeoclimatic reconstructions in the Levant must be, at best, uncertain. As Figure 3-9 illustrates, there are precipitation gradients as steep as 100 mm/a within a 10 km E-W traverse around the Maqarin area. Clearly, even quite minor shifts in precipitation belts could have a dramatic effect.

The palaeoenvironments on the valley sides and uplands in the Maqarin area, influenced by local conditions, should be distinguished from changes in the hydrological regime of the Yarmouk River itself. As evident from the generalised relief in Figure 3-1, headwater tributaries of the Yarmouk rise in uplands and mountains with significant altitude. Notably, the Jebel Druze in Syria rise to over 1 500 m.a.s.l., and the summit of Mt. Hermon exceeds 2 100 m.a.s.l. Even at the present-day, snow melt is a significant component of spring discharge on the western flank of Mt. Hermon.

3.10.3 Fossil Pollen

Palynological evidence gathered in the Near East over the past 35 years indicates that the vegetation of the region was subject to many fluctuations during Late Quaternary times. The main indicator taxa are sagebrush *(Artemisia)*, of steppe and semi-desert conditions, and oak (*Quercus*) park forest, corresponding to an increase in annual precipitation. At the present-day, the *Artemisia herba-alba*, a species totally resistant to summer drought, is characteristic of the semi-desert which occupies large tracts of the Syro-Jordanian plateau, where an annual precipitation of 150–300 mm prevails. The evergreen trees *Olea* and *Pistacia* are more sensitive to frost than *Quercus*. The olive does not flower when winter temperatures are <3°C. From the continental pollen record, it seems that the Last Glacial Maximum (LGM), despite being cooler, "...was generally dry in all regions of the Near East" (Baruch, 1994).

Detailed studies of the palynological record in the Hula and Dead Sea basins, mainly by Horowitz (1979; 1989) and co-workers, shows that these basins acted as isolated niches, periodically favourable for tree growth. Perhaps not surprisingly for such a distinctive location, the Dead Sea fossil pollen record is difficult to synchronize with more generalised conclusions on palaeoenvironments in the eastern borderlands of the Mediterranean. Some workers appear to circumvent this difficulty by not referring to Horowitz's work.

3.10.4 Global Climate Change

There are many steep environmental gradients in both the present and the past in the Levant. For present purposes, the generalised findings of Global Climatic Models (GCMs) are probably the most instructive guide to the major changes which might have occurred in the Levant. GCMs simulate the influence of continental ice sheets on the global climate. They offer some generalised scales for change which are useful yardsticks, even when considering local conditions. For example, the model of Manabe and Broccoli (1985) shows an air temperature in the central Mediterranean lower by 4°C in winter and by 4–0°C in summer. The CLIMAP (1976) simulation for the Last Glacial Maximum (LGM), July-August temperatures at 18 ka BP shows air-surface temperatures in the Mediterranean down by 4–8°C, and the precipitation rate down by 1 mm/day. These figures are compatible with the fossil pollen record.

3.10.5 Some Features of the Yarmouk Palaeoenvironment

Duricrust

A hard biogenic calcrete, locally termed 'nari', veneers much of the outcrops of chalky formations within the semi-arid fringe of Mediterranean climates in the Near East. Most radiocarbon datings fall in the 20–13 ka range (Kaufman et al., 1973). It seems that the Last Glacial Maximum (LGM) favoured episodic veneering of the surface with the relatively impermeable crust. In fact, 'nari' might be one of the most significant palaeoenvironmental changes for consideration in geochemical studies of natural waters.

The crust itself, although only 0.2–3 cm thick, has considerable compressive strength (500–800 kg/cm^2). It is not breakable by hammer blow and does not soften when wet

(Yaalon and Singer, 1974). A critical feature of the 'nari' crust is its relative impermeability. A significant percentage of this material is silt-sized quartz, now attributed to an aeolian source. Biogenic processes appear to be critical in lithification.

The laminar 'nari' crust is erosion-resistant and preserves the rolling relief of a chalky limestone landscape. Many hillslopes with 'nari' crust are very stable and quite old (Dan et al., 1972). On many lower parts of hillslopes, however, the indurated 'nari' may disintegrate, exposing underlying, soft chalk (Yaalon and Singer, 1974).

In the Maqarin area (Appendix D; Plate D-1), the location and persistence of 'nari' may be an important difference between present-day and past infiltration rates. It is prominent on much of the upper slopes of the Maqarin anticlinal spur and especially in smoothing the surface of the ancient rockslide.

The impermeability of 'nari' not only reduced infiltration of rainwater, but also may confine shallow-depth groundwater below the surface of a hillside. The outflow at the Western Springs may include a component of sub-nari seepage.

Alluvial deposits

Two contrasted alluvial deposits are identifiable in the Maqarin area, and probably reflect contrasted environmental conditions and/or geomorphological processes:

(i) The fluvial gravel and boulder fill of the present Yarmouk channel is approx. 15 m thick below the confluence with the Wadi Raqqad (Michelson, 1973). Similar depths have been reported through the Maqarin anticline, but with maximum depths at certain points of 53 m (Wieseman and Abdul Latif, 1963). Some of the valley floor and river bank gravels are cemented. This is a regionally recognised phenomenon, particularly in the Hula basin (Picard, 1965). Also, in the lower Yarmouk, below the confluence with the Wadi Raqqad, cemented gravels underlie the Raqqad Basalt (Michelson, 1973); the formation is, therefore, older than 0.48 Ma. Cementation suggests greater importance of calcareous groundwaters to river flow, perhaps reflecting a drier period in the regional climate about 0.5 Ma ago. Notably, a drier climate about the beginning of the Upper Quaternary has been inferred from extensive calcrete development in the neighbouring Zarqa Valley (Baubron et al., 1985).

(ii) Loose, coarse gravels, up to 40 m above the present valley floor, are noted both upstream, near Maqarin Station, and downstream (Al Arqub terrace: Appendix D; Plate D-5) from the Maqarin anticline. The upper surface of such remnants might be the remains of a formerly continuous valley fill of boulders (Fig. 3-6). Alternatively, both occurrences could simply be localised deposits, remnants of former alluvial fans, dumps of coarse clastics on the main valley floor deposited from tributary wadis. These materials may be equivalent to the 2–10 m thick Khirba Samra formation in the neighbouring Zarqa Valley, which is attributed to a former episode of greater humidity (Baubron et al., 1985). Artefacts in the Zarqa Valley suggest that this phase could have begun sometime after 75 ka ago (Besancon and Hours, 1985).

As in the Zarqa Valley, the altitude of the sediments does not necessarily reflect chronological sequence. The lower, cemented gravels on the valley floor are probably

significantly older than the coarse gravels, up to 40 m higher up the valley side. This non-tiered arrangement reflects the repeated filling and re-excavation, a typical feature of the wadi environments.

Structure and Sediments at the Yarmouk-Jordan Confluence

This area is critical to an understanding of the role and evolution of the Yarmouk River Valley; the altitude of this confluence sets a hypothetical 'baselevel' – a lower limit for erosion – in the Yarmouk River upstream. Notably, at this point in the Jordan River Valley, there is a remarkable structural 'hole', the Kinnerot Basin, (i.e. Lake Tiberias). It is only 4–6 km wide, and over 4.5 km deep (Marcus and Slager, 1985).

This area is the site of the Naharayim Formation, 30–40 m thickness of fluvial sediments, mainly coarse conglomerates (Fig. 3-10). It represents a huge fan-delta, deposited in times of much greater sediment transport. Possibly, the depth of the Kinnerot Basin, nearly as great as its width at this point, may be due to sediment loading by the continued and large-scale deposition from the Yarmouk River. If so, the Yarmouk may control, rather than be controlled by, this 'baselevel'.

The Naharayim Formation overlies the Yarmouk Basalt and is, in turn, overlain by the Raqqad Basalt. Therefore, it reflects fluvial activity in the 0.8–0.5 Ma time period, the episode when erosion rates were 2–3 times higher than the longer-term average.

3.11 SELF-COMBUSTION OF THE BITUMINOUS MARLS

The north-central part of Jordan is characterised by heterogeneous occurrences of metamorphosed Bituminous Marl Formation rocks, formed by high temperature (>1 000°C) alteration caused by spontaneous combustion. As stated in the introduction, the probability of the marls self-combusting increases the closer the rock is to the surface; here the bedrock is unsaturated and an oxygen supply is available via cracks and joints. A balance between rock exposure and the level of the local groundwater table is therefore a necessary prerequisite for combustion.

Figure 3-11 (modified after E. Salameh; written comm., 1997) attempts to explain the relationship between self-combustion of the marls and the recent geological development of the Yarmouk River bottom elevation under relatively "equilibrium conditions". The present Yarmouk River Valley at Maqarin lies at an elevation of +50 m.a.s.l. whereas 10 km to the west in the Yarmouk Basalt the valley bottom lies at -100 m.a.s.l. If this same gradient is extrapolated to locate the river valley bottom elevation at the time of the Yarmouk Basalt flows (~0.8 Ma) which lie at ~100 m.a.s.l. in the area 10 km west of Maqarin, then the valley bottom must have been 200 m.a.s.l. at that time (i.e. point X in Fig. 3-11). Furthermore, at this same time the Bituminous Marl Formation at Maqarin was still covered by at least 70 m of Chalky Limestone Formation rocks, which means that the marls were below the regional groundwater level. Combustion was thus very unlikely to occur.

If it is assumed that the self-combustion processes could only have occurred subsequent to draining the groundwater overlying the Bituminous Marl Formation, and assuming

that the erosion rate since deposition of the Yarmouk Basalt was constant, then self-combustion of the marls could only have occurred after erosion of the Yarmouk Basalt and an additional 150 m of the older Cretaceous, Chalky Limestone Formation. However, in all probability, even when the marls in the river bed were exposed, combustion would have been prohibited due to frequent floodings and bank storage of water (see section 3.4.3). Therefore, it is estimated that the free exposed marls would have required an exposed thickness of at least 10–20 m to initiate and maintain combustion. This means that the elevation of the river bed at the time of combustion must have been initiated when the marls were 80–90 m.a.s.l.

What kind of timescale can be deduced from this hypothesis? Based on the observation that the marls have been eroded a further 30–40 m since the assumed time of combustion to the present day, and assuming that a total of 200 m of rock have been eroded by the Yarmouk River during the past 0.8 Ma, then a period of 120–160 ka would be required to erode this 30–40 m of marl. Accordingly, combustion could not have started earlier than, say, about 150 ka ago.

Present studies at Maqarin, however, show two important observations that require a modification of the above hypothesis. The first is the deposition of the Bituminous Marl Formation on the nose of the anticline, which has two significant implications, and the second is the reassessment of erosion rates of the overlying strata by the Yarmouk River during recent geological time. With respect to the former, the marl outcrop is at its highest valleyside altitude along the axis of the anticline. This point appears to coincide with the knickpoint in the longitudinal profile, just downvalley from the Maqarin Station locality (Fig. 3-6). Secondly, the pitch of the anticlinal nose means that the altitude of the top of the Bituminous Marl Formation rises towards the south. In consequence, the uppermost strata of the Bituminous Marl Formation on the southern flank of the Yarmouk Valley were higher than the zone where the marls were first exposed by incision along the valley floor. Being above groundwater levels, therefore, oxygen could have been admitted to such valleyside strata soon after the earliest exposure of the Bituminous Marl Formation in the valley floor, i.e. significantly earlier than 150 ka ago. Finally, considering more realistic erosion rates, for example the calculated rates of headward retreat of knickpoints along the Yarmouk River profile (see sub-section 3.5.2), a date of combustion soon after 600 ka ago is suggested.

Gradually revealing the marls during erosion is, however, unlikely to result in combustion. An abrupt exposure to oxygen seems essential to achieve spontaneous combustion, and a steady oxygen supply is probably required to reach and maintain the high temperatures known to have been generated during combustion metamorphism. The potential impact of sudden geological events is supported by the widely recognised association of combustion metamorphism with landslides and related mass movements (e.g. Appendix D; Plates D-6 and D-7). As discussed in Section 3.7, earthquakes are not a prerequisite to trigger such mass movements, as illustrated by the Smoking Hills of northern Canada (Mathews and Bustin, 1984). Also, some instances of combustion metamorphism are in areas of generally subdued relief, notably the Daba-Siwaqa area, 50 km south of Amman (Nassir and Khoury, 1982). Abrupt rupturing of superficial strata by valley bulging on channel floors, following erosional unloading, may be an equally probable mechanism for igniting organic-rich rocks. It seems that both mechanisms could have admitted oxygen abruptly to the Bituminous Marl Formation in

the Maqarin anticline area. The date of ignition soon after 600 ka at both the Eastern and Western springs localities seems possible, if not probable.

An additional hypothesis relates to the existence of karst-type sink holes (up to 20–30 m deep) in the Chalky Limestone Formation overlying the Bituminous Marl Formation, which may have facilitated ingress of oxygen and subsequent combustion. These features probably formed prior to the deposition of the overlying basalt flows (see sub-section 2.2.3). This supported by the occurrence of basalt at the bottom of some of the sink holes (E. Salameh, per. comm., 1996), although this does not preclude the possibility of the downward collapse of the overlying basalt into the sink holes at a later stage. However, the main point is that the formation of the sink holes themselves is the result of very long geomorphological processes, certainly over spans of tens to hundreds of thousands of years. It is unlikely therefore that erosion of such features has initiated combustion by accessing oxygen to the underlying Bituminous Marl Formation, since combustion is more likely to be linked to a sudden exposure of the marls to oxygen and water, as discussed above. On the other hand, combustion could conceivably have been triggered by the flow of basalt into the sink holes, which would tie the combustion coevally with the deposition of the Yarmouk Basalt flows some 0.8 Ma ago.

A further and important final comment on the age of combustion and the formation of the metamorphic cement zones is referred to in sub-section 4.3.3. Observations of the fluvial boulder gravel deposits (i.e. the earliest Quaternary deposits) at the Western Springs locality show the presence of reworked cement zone clasts. This clearly indicates that the Metamorphic Unit (cement zone) was already exposed and undergoing erosion prior to deposition of these Quaternary sediments (A.E. Milodowski, written comm., 1997). Since these sediments predate the extrusion of the Raqqad Basalt flows (see sub-section 3.4.3), the Quaternary sediments (and therefore age of combustion) must be therefore older than ca. 500 ka.

3.12 CONCLUSIONS

In general, it seems that the Yarmouk River Valley at Maqarin has served essentially as a conduit for the transportation of sediment and basalt lava, rather than being the product of dramatically rapid erosion. Further, the sediment loading of the Jordan Rift Valley floor by the Yarmouk River might be a contributary cause to its progressive sinking, as much as a control on that river's erosional history.

There seems good evidence that combustion has been initiated sometime between 0.5–0.8 Ma, and around 0.6 Ma would appear to be a reasonable compromise. Furthermore, lateral erosion undercutting by the Yarmouk River, resulting in landslides and/or slumping, either triggered by seismic activity or simply gravitational mechanisms associated with heavy periods of rainfall, would provide the necessary conditions for sudden oxygen (and water) ingress and subsequent spontaneous combustion of the Bituminous Marl Formation. In all probability, land movements have occurred at various times during the last 0.6 Ma. Present studies suggest the possibility that land movements and combustion in the area which includes the Eastern Springs occurred

soon after 0.6 Ma. More hypothetically, a second, later phase of triggered landslides at the Western Springs area might also be considered. This could be attributed to slab failure of an undercut meander scar in the Yarmouk Valley, to valley bulging on the floor of Sijin, or to landslips on the western valley side of Wadi Sijin. Speculatively, such an event might have occurred in the last 100 ka of Late Quaternary time (?slab failure), or even as recently as the last 10 ka, i.e. within the Holocene (?landsliding).

These two phases of landslides, representing, respectively the Eastern and Western Springs localities, may lend support to other indications (e.g. hydrochemistry) that the Eastern Springs system is older and more evolved than the Western Springs system.

3.13 REFERENCES

Almond, D.C., 1986. The relation of Mesozoic-Cenozoic volcanism to tectonics in the Afro-Arabian dome. J.Volcanol. Geothermal Res., 28, 225–246.

Arieh, E., Peled, U., Kafri, U. and Shaal, B., 1977. The Jordan Valley earthquake of September 2, 1973: Isr. J. Earth Sci., 26, 112–118.

Arkin, Y., 1989. Large-scale tensional features along the Dead Sea-Jordan Rift Valley. Tectonophysics, 165, 143–154.

Bahat, D., 1987. Jointing and fracture interactions in Middle Eocene chalks near Beer Sheva, Israel. Tectonophysics, 136, 299–321.

Barberi, F. et al., 1980. Recent basaltic volcanism of Jordan and its implications on the geodynamic history of the Dead Sea shear zone. In: B. Zanettin (Ed.), Geodynamic evolution of the Afro-Arabian rift system. Accad. Nazionale dei Lincei, Rome, 667–683.

Baruch, U., 1994. The Late Quaternary pollen record of the Near East. In O. Bar-Yosef and R.S.Kra (Eds.), Late Quaternary chronology and paleoclimates of the Eastern Mediterranean. Radiocarbon, 14, 103–119.

Baubron, J-C., Besancon, J., Copeland, L., Hours, F., Macaire, J-J. and Sanlaville, P., 1985. Evolution de la moyenne vallee du Zarqa (Jordanie) au Neogene et au Quaternaire. Rev. Geol. Dyn. Geog. Phys., 26, 273–283.

Bayer, H-J., El-Isa, Z., Hotzl, H., Mechie, J., Prodehl, C. and Saffarini, G., 1989. Large tectonic and lithospheric structures of the Red Sea region. J. Afr. Earth Sci., 8, 565–587.

Ben-Menahem, A., Nur, A. and Vered, M., 1976. Tectonics, seismicity and structure of the Afro-Eurasian junction – the breaking of an incoherent plate. Phys. Earth Planet. Inter., 12, 1–50.

Besancon, J. and Hours, F., 1985. Prehistory and geomorphology in northern Jordan: a preliminary outline. Studies in the history and archaeology of Jordan, ii, 59–66.

Brazee, R.J., 1979. Reevaluation of Modified Mercalli Intensity Scale for earthquakes using distance as determinant. Bull. Seismol. Soc. Am., 69, 911–924.

Brink, T., Schoenberg, U.S., Kovach, R.L. and Ben-Avraham, Z., 1990. Uplift and a possible Moho offset across the Dead Sea transform. Tectonophysics, 180, 71–85.

Burg, A., Starinsky, A., Bartov, Y. and Kolodny, Y., 1991. Geology of the Hatrurim Formation ("Mottled Zone") in the Hatrurim basin. Isr. J. Earth Sci., 40, 107–124.

Clark, I.D., Fritz, P., Seidlitz, H.K., Trimborn, P., Milodowski, T.E., Pearce, J.M. and Khoury, H.N., 1993. Recarbonation of metamorphosed marls, Jordan. Appl. Geochem., 8, 473–481.

Clark, I.D. and Fritz, P., 1998. Isotope hydrogeology of the Maqarin hyperalkaline groundwaters. In: C.M. Linklater (Ed.), 1998. A natural analogue study of cement-buffered, hyperalkaline groundwaters and their interaction with a repository host rock: Phase II. Nirex Science Report, S/98/003, Nirex, Harwell. U.K., p. 200–212.

CLIMAP, 1976. The surface of the ice-age earth. Science, 191, 1131–1137.

Cowgill, V.M., 1969. The waters of Merom: A study of Lake Huleh. I. Introduction and stratigraphy of a 54 m core. Arch. Hydrobiol., 66, 249–272.

Dan, J., Yaalon, D.H. and Koyumdjisky, H., 1972. Catenary soil relationships in Israel, 2. The Bet Guvrin catena on chalk and nari limestone crust in the Shefela. Isr. J. Earth-Sci., 21, 99–118.

Freund, R., Zak, I. and Garfunkel, Z., 1968. Age and rate of the sinistral movement along the Dead Sea Rift. Nature, 220, 253–255.

Garfunkel, Z., Zak, I. and Freund, R., 1981. Active faulting in the Dead Sea rift. Tectonophysics, 80, 1–26.

Goren-Inbar, N., Belitzky, S., Goren, Y., Rabinovich, R. and Saragusti, I., 1992a. Gesher Benot Ya'aqov – the "bar": an Acheulian assemblage. Geoarchaeology, 7, 27–40.

Goren-Inbar, N., Belitzky, S., Verosub, K., Werker, E., Kislev, M., Heimann, A., Carmi, I. and Rosenfeld, A., 1992b. New discoveries at the Middle Pleistocene Acheuilan site of Gesher Benot Ya'aqov, Israel. Quat. Sci., 38, 117–128.

Grass, M.R. and Engelder, T., 1991. A case for neotectonic joints along the Niagara Escarpment. Tectonics, 10, 631–641.

Harash, A. and Bar, Y., 1988. Faults, landslides and seismic hazards along the Jordan River gorge, northern Israel. Eng. Geol., 25, 1–15.

Heimann, A., 1990. The development of the Dead Sea Rift and its margins in northern Israel during the Pliocene and the Pleistocene. GSI/28/90.

Heimann, A. and Ron, H., 1993. Geometric changes of plate boundaries along part of the northern Dead Sea Transform: geochronologic and paleomagnetic evidence. Tectonics, 12, 477–491.

Hollingworth, S.E., Taylor, J.H. and Kellaway, G.A., 1944. Large-scale superficial structures in the Northampton Ironstone Field. Quart. J. Geol. Soc., 100, 1–44.

Horowitz, A., 1979. The Quaternary of Israel, Academic Press, New York, 394 pp.

Horowitz, A., 1989. Palynological evidence for the Quaternary rates of accumulation along the Dead Sea Rift and structural implications. Tectonophysics, 164, 63–71.

Kafri, U. and Heimann, A., 1994. Reversal of the palaeodrainage system in the Sea of Galilee area as an indicator of the formation timing of the Dead Sea Rift valley base level in northern Israel. Palaeogeog., Palaeoclim., Palaeoecol., 109, 101–109.

Kashai, E.L. and Croker, P.F., 1987. Structural geometry and evolution of the Dead Sea – Jordan rift system as deduced from new subsurface data. Tectonophysics, 141, 33–60.

Kaufman, A., Carmi, I. and Schlesinger, R., 1973. Rehovot radiocarbon measurements II. Radiocarbon, 15, 179–184.

Khoury, H.N., Salameh, E. and Abdul-Jaber, Q., 1985. Characteristics of an unusually highly alkaline water from the Maqarin area, northern Jordan. J. Hydrol., 81, 79–91.

Kovach, R.L., Andreasen, G.E., Gettings, M.E. and El-Kaysi, K., 1990. Geophysical investigations in Jordan. Tectonophysics, 180, 61–69.

Manabe, S. and Broccoli, A.J.J., 1985. The influence of continental ice sheets on the climate of an ice age. J. Geophys. Res., 90, 2167–2190.

Marco, S. and Agnon, A., 1995. Prehistoric earthquake deformations near Masada, Dead Sea graben. Geology, 23, 695–698.

Marcus, E. and Slager, J., 1985. The sedimentary-magmatic sequence of the Zemah-1 well (Jordan-Dead Sea rift, Israel) and its emplacement in time and space. Isr. J. Earth-Sci., 34, 1–10.

Mathews, W.H. and Bustin, R.M., 1984. Why do the Smoking Hills smoke? Can. J. Earth Sci., 21, 445–462.

Michelson, H., 1973. "Yarmouk Basalt" and "Raqqad Basalt" – two volcanic phases which flowed through pre-exiting gorges. Isr. J. Earth-Sci., 22, 51–58.

Mor, D., 1993. A time-table for the Levant Volcanic Province, according to K-Ar dating in the Golan Heights, Israel. J. Afr. Earth Sci., 16, 223–234.

Mor, D. and Steinitz, G., 1985. The history of the Yarmouk River based on K-Ar dating and its implications on the development of the Jordan Rift. Geol. Surv. Isr. Rep., GSI/40/85. 18 pp.

Nassir, S. and Khoury, H., 1982. Geology, mineralogy and petrology of Daba marble, Jordan. Dirasat (Nat. Sci.), 9, 107–130.

Picard, L., 1965. The geological evolution of the Quaternary in the Central-Northern Jordan graben, Israel. Geol. Soc. Am. Spec. Pap., 84, 337–366.

Pitty, A.F., 1971. Introduction to geomorphology. Methuen, London, 526 pp.

Price, N.J., 1966. Fault and joint propagation in brittle and semibrittle rocks. Pergamon, Oxford, 176 pp.

Quennell, A.M., 1958. The structural and geomorphic evolution of the Dead Sea rift. Quart. J. Geol. Soc. Lond., 114, 1–24.

Reches, Z., 1976. Analysis of joints in two monoclines in Israel. Bull. Geol. Soc. Am., 87, 1654–1662.

Shapira, A., Manor, O., Oman, D. and Sheshinsky, R., 1986. The empirical relation of earthquake epicenters to mapped faults in Israel. Isr. J. Earth Sci., 35, 149–157.

Shapira, A., Avni, R. and Nur, A., 1993. A new estimate for the epicenter of the Jericho earthquake of 11 July 1927. Isr. J. Earth Sci., 42, 93–96.

Simmons, G.C., 1966. Seam anticlines in central Kentucky. U.S. Geol. Surv. Prof. Pap., 550-D, 9–11.

Steinitz, G. and Bartov, Y., 1991. The Miocene-Pliocene history of the Dead Sea segment of the Rift in light of K-Ar ages of basalts. Isr. J. Earth-Sci., 40, 199–208.

Wachs, D. and Levitte, D., 1984. Earthquake risk and slope stability in Jerusalem. Environ. Geol.Water Sci., 6, 183–186.

Walker, E.H., 1956. Reservoir capacity of Mississippian limestones in the Hopkinsville quadrangle, Kentucky. Bull. Geol. Soc. Am., 67, 1431–1440.

Wieseman, G. and Abdul Latif, A.A., 1963. Geology of the Yarmuk area, North-Jordan. Unveroff. Ber. Dtsch. Geol. Mission Jordanien, Arch. Bundesanst. Bodenforsch., Hanover, 120 pp., mimeo.

Yaalon, D.H. and Singer, S., 1974. Vertical variation in strength and porosity of calcrete (nari) on chalk, Shefela, Israel and interpretation of its origin. J. Sed. Petrol., 44, 1016–1023.

TABLE

Table 3-1. Estimates of retreat rates of basalt knickpoints in the longitudinal profile of the Yarmouk Valley.

Basalt Unit	Upper Age *(Ma)*	Thickness *(m)*	Knickpoint Distance Upvalley *(km)*	Retreat Rate *(m/ka)*
Raqqad	0.35	40	15	43
Yarmouk	0.79	30	53	67
Cover	3.5	approx. 100	62	18

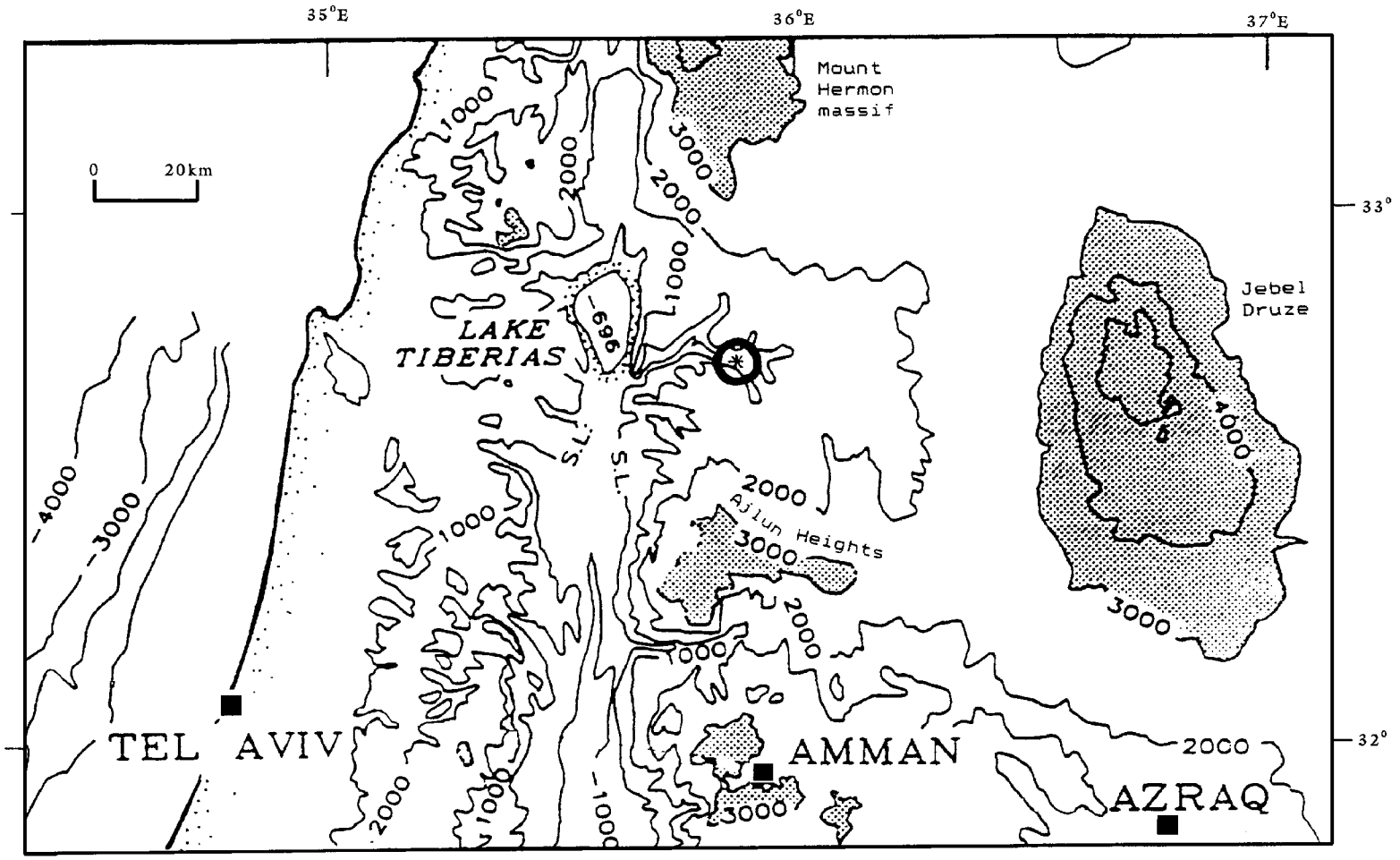

Figure 3-1. *Generalised relief of the Yarmouk River catchment and surrounding area (after Brink et al., 1990) . Circled asterix indicates location of the Maqarin site. Note: Contour values are in feet.*

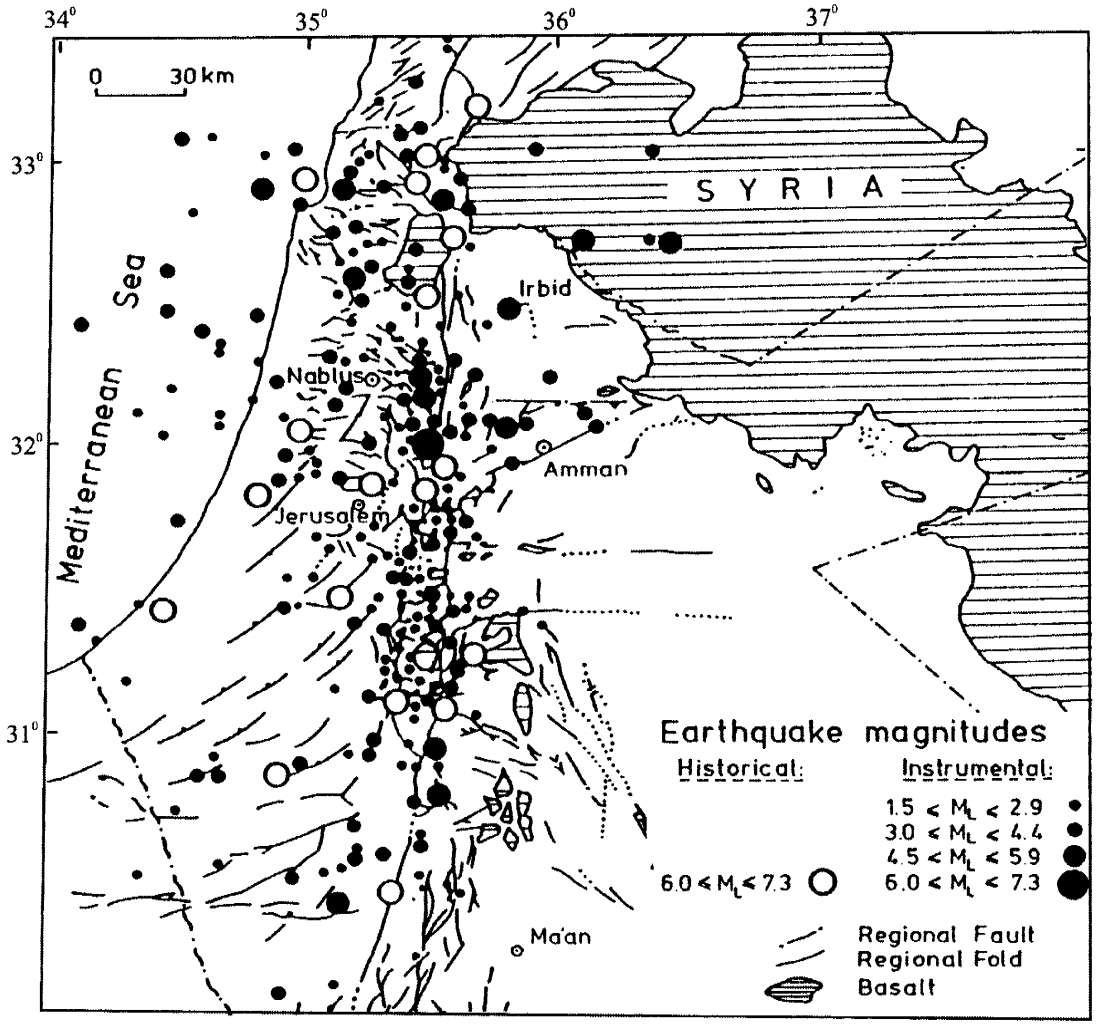

Figure 3-2. *A seismicity map showing how the trends of the Jordan Rift system and flood-basalt province converge just north of the Maqarin study area (from Bayer et al., 1989). Maqarin is approx. 30 km north of Irbid, where neither major faults nor epicentres are recorded.*

The map features seismicity for the period 2150 B.C. to 1984.

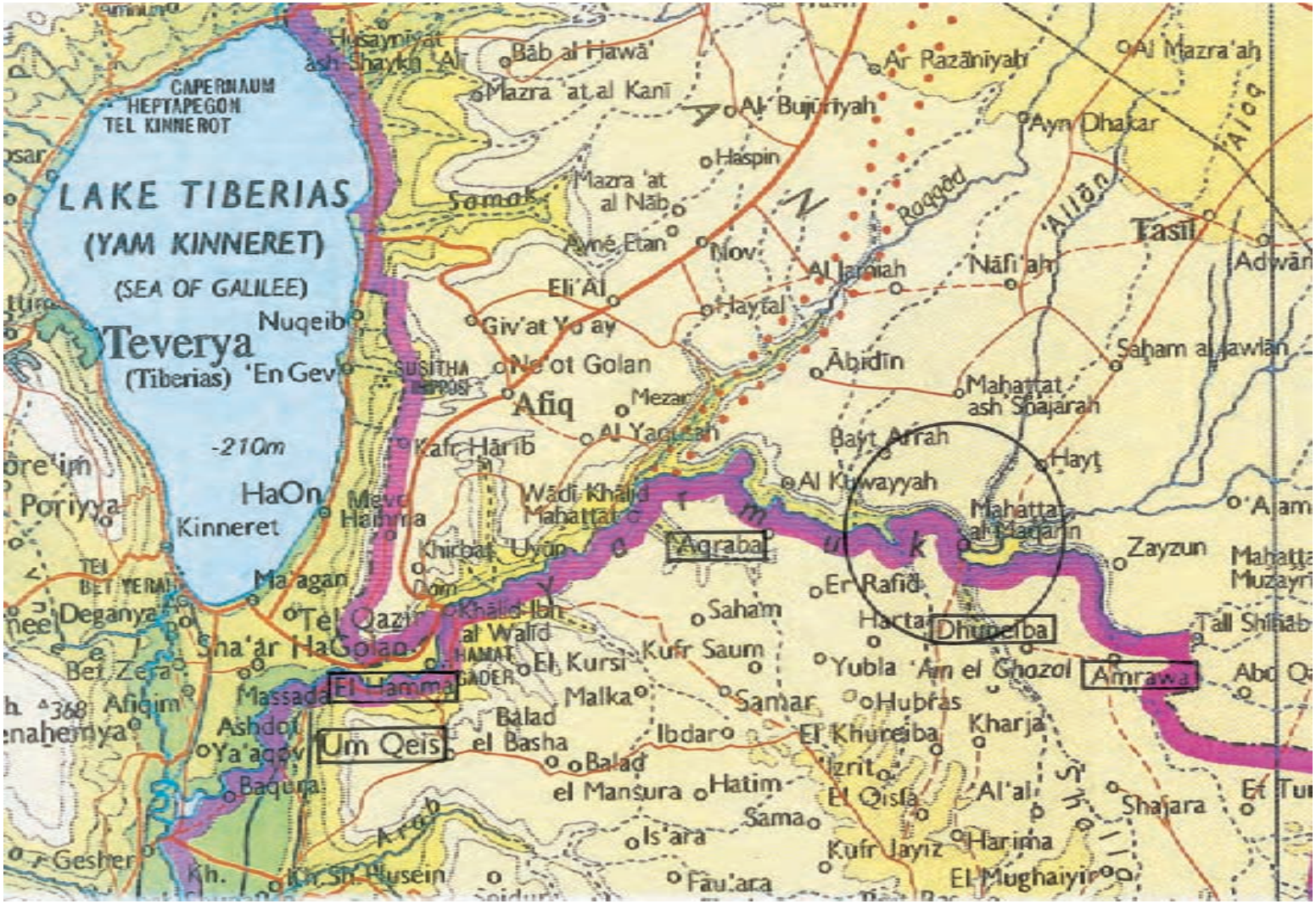

Figure 3-3. *Enlarged map of the Maqarin / Yarmouk River Valley region showing locations of some of the place names (boxed) mentioned in the text.*

(© *Bartholomew 1995. Reproduced with kind permission*).

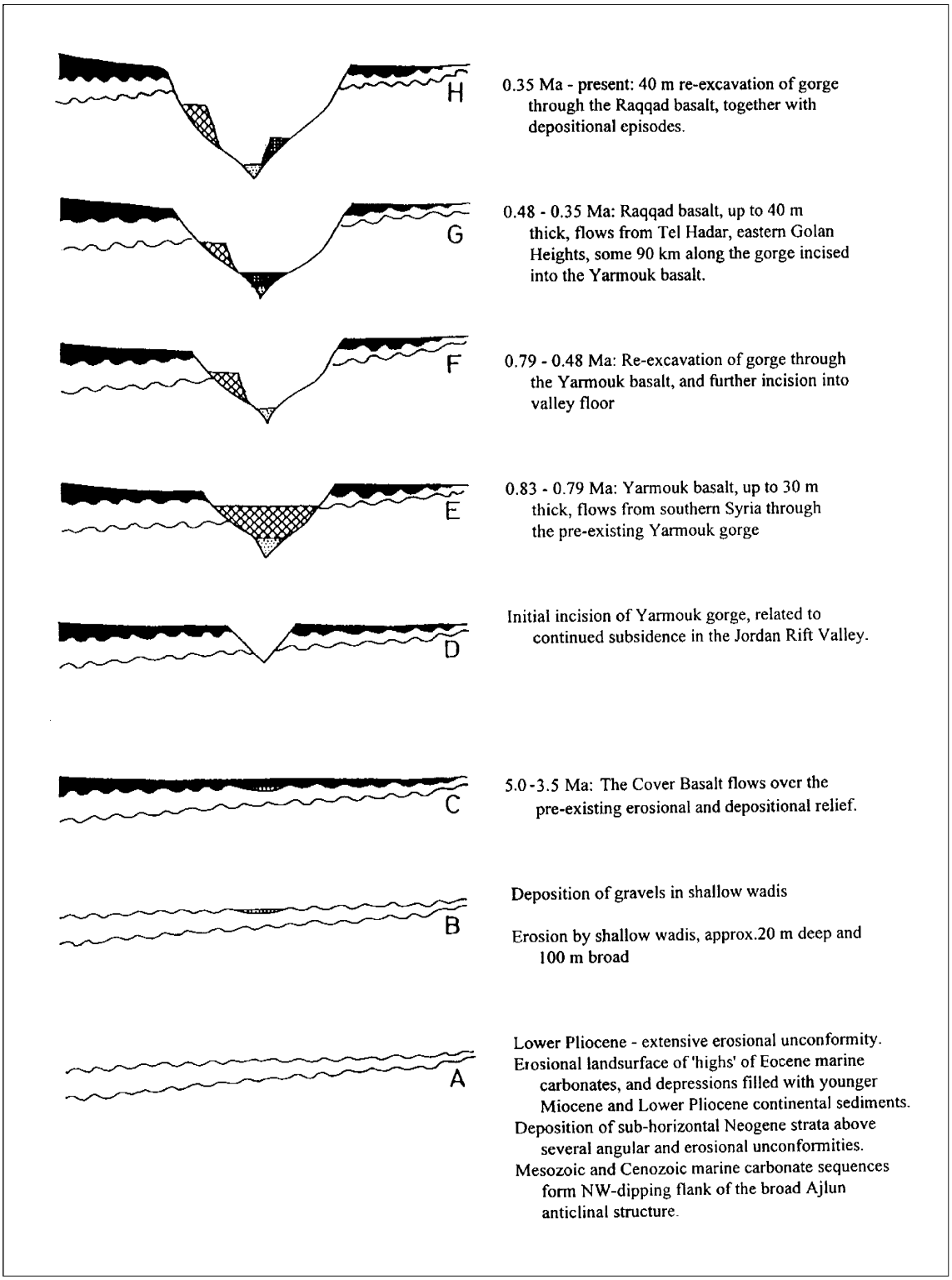

Figure 3-4. *Geohistory of the lower Yarmouk River Valley (modified from Mor and Steinitz, 1985).*

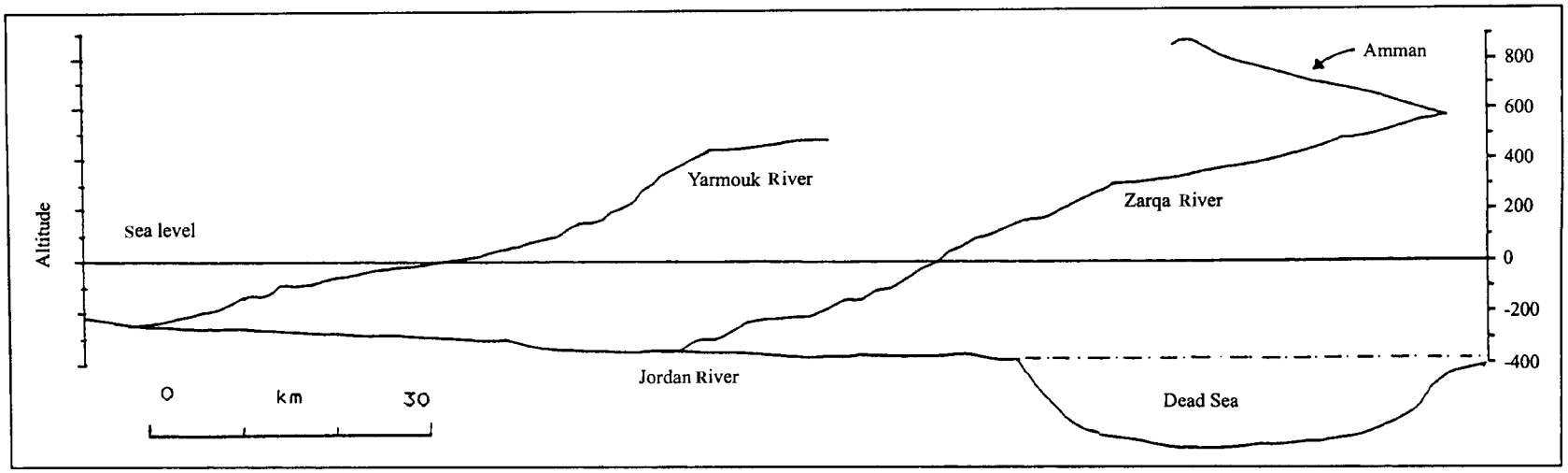

Figure 3-5. *Longitudinal profiles of the Yarmouk and Zarga Rivers (modified after Quennel, 1958).*

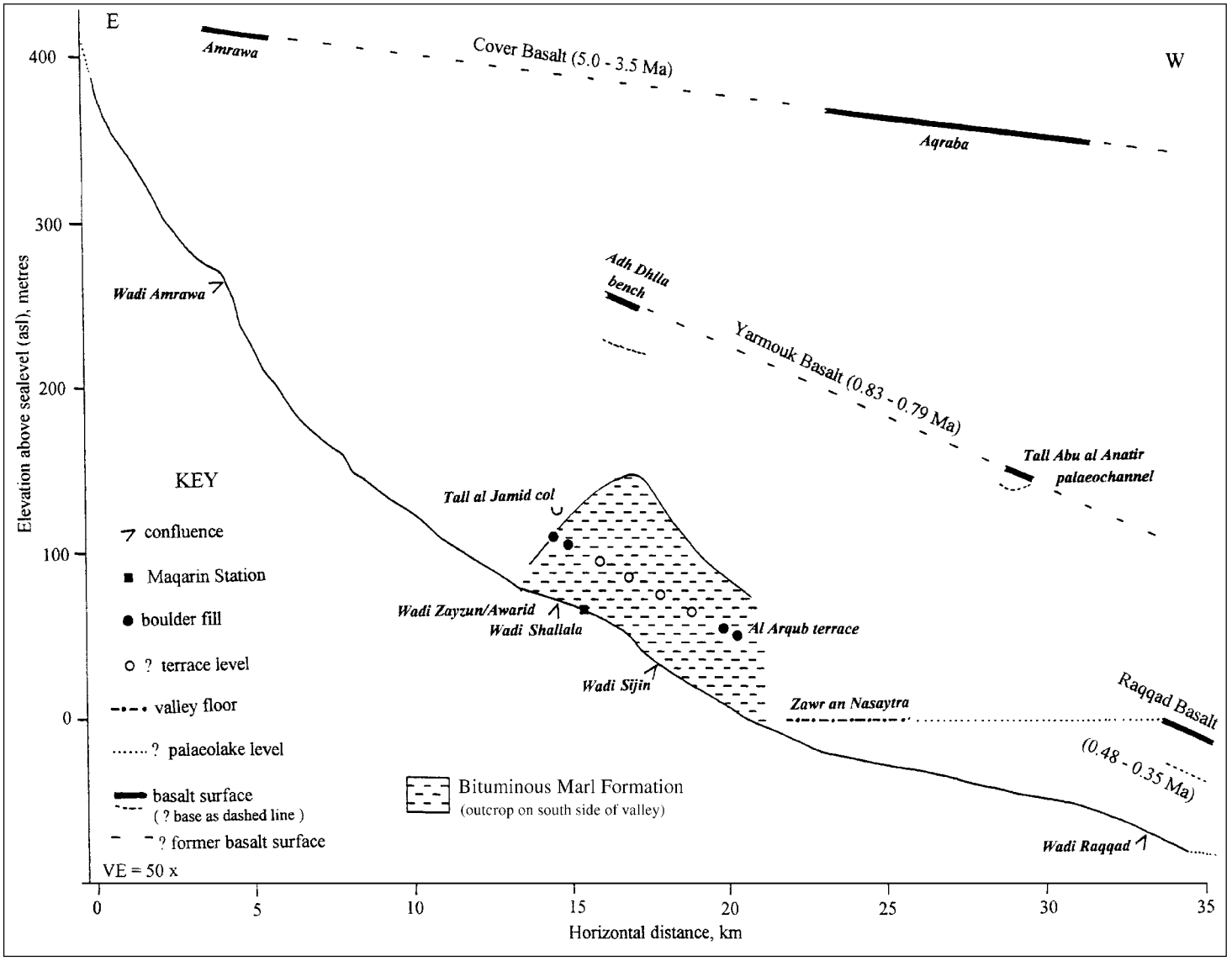

Figure 3-6. *Longitudinal profile of the Yarmouk River and of the Zarqa River (modified after Quennell, 1958).*

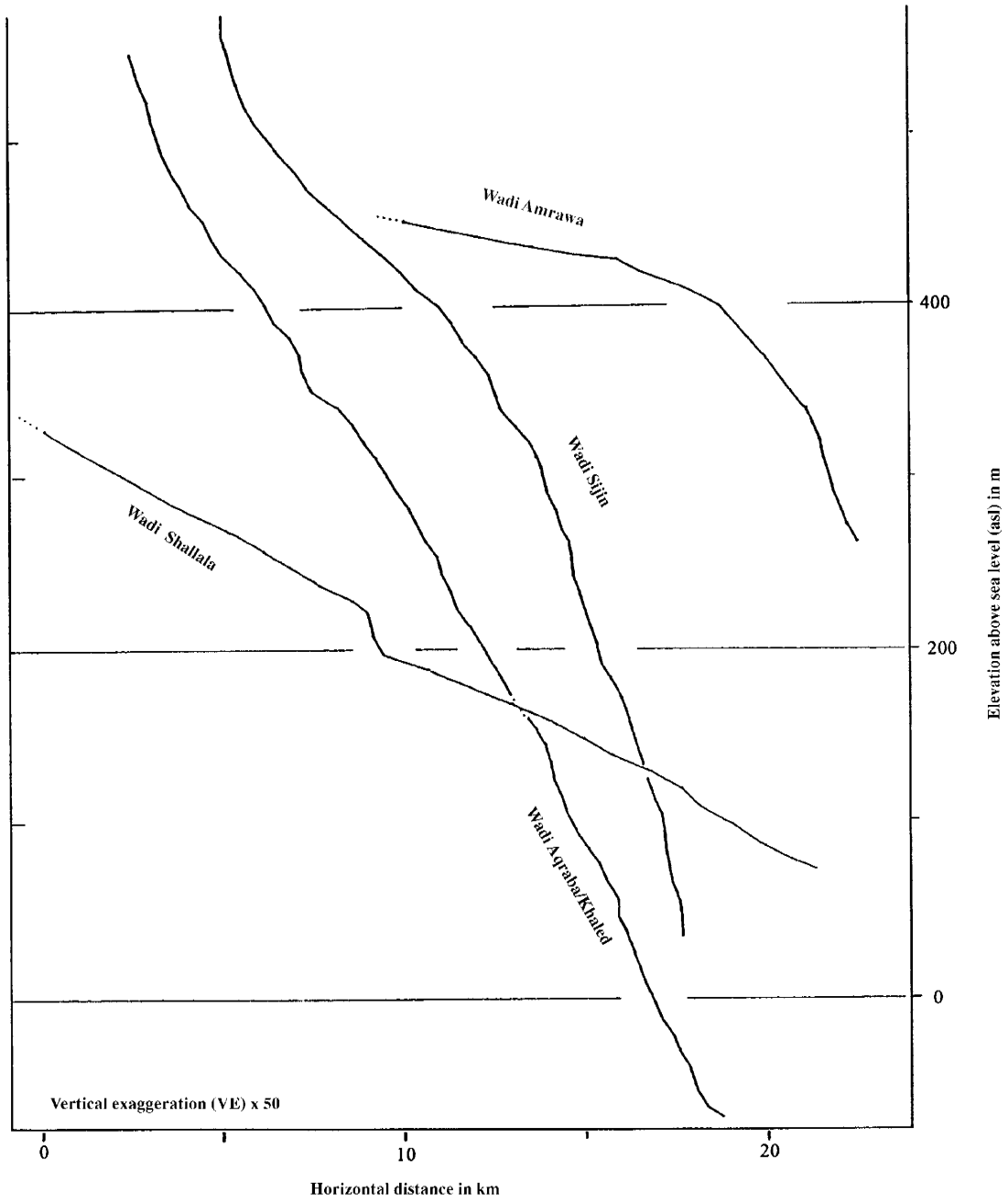

Figure 3-7. *Longitudinal profiles of the left-bank tributary valleys of the Yarmouk River in the Maqarin area.*

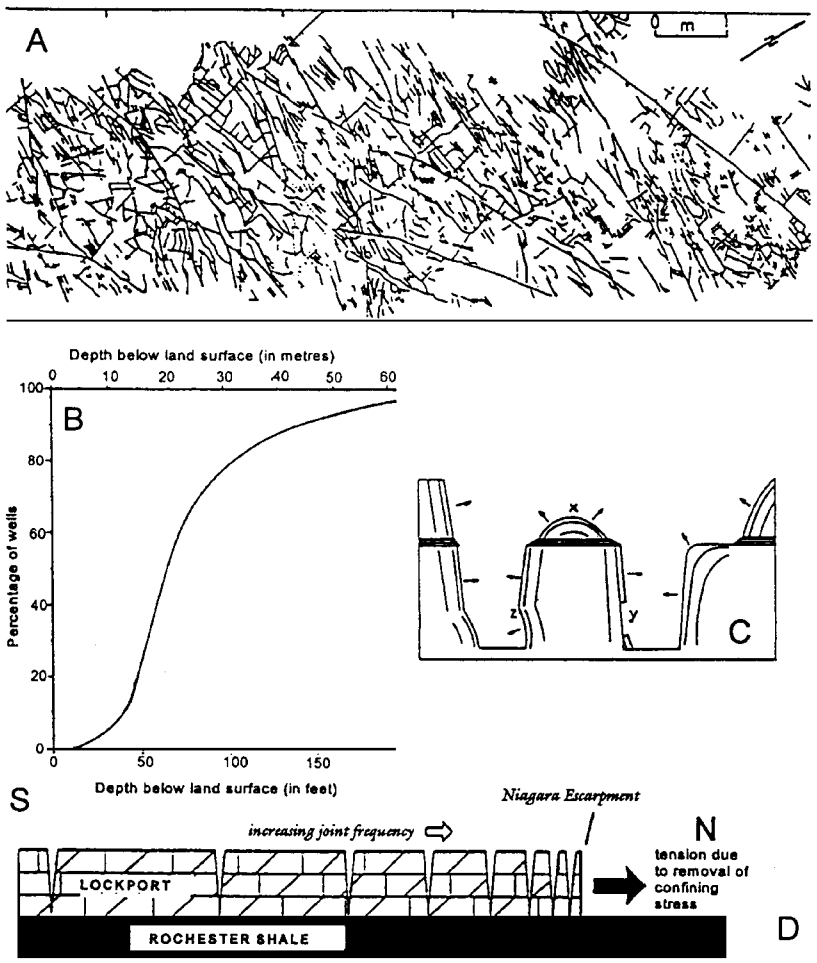

A. Map of joints on an exposed surface of dolomitic limestone in the Hazeva monocline (*from* Reches, I976. Fig.10).

B. Cumulative curve of depth to water-bearing crevices in limestone in Kentucky wells, showing that some 70 percent of the wells meet water-bearing crevices before penetrating more than 25 m (*from* Pitty, 1971, p.96). There are very few crevices below 50 m (*after* Walker, 1956).

C . Large-scale sheet structures and joints, produced by expansion of massive sandstones in the Colorado Plateau (*after* Bradley, 1963). Arrows indicate inferred direction of expansion:

x is an exfoliation dome

y is an exfoliation cave

z is an overhanging exfoliation plate in a meander scar (*from* Pitty, 1971, p.97). . Z-type expansion may be particularly significant in the widening of the Yarmouk Valley e.g. in the vicinity of the Western Springs.

D. Schematic cross-section through the limestones of the Niagara Escarpment, showing an increase in fracture frequency with proximity to the escarpment face (*from* Grass and Engelder. 1991) . A similar tendency may be present on the oversteepened valleyside in the proximity of the Maqarin adit. (A-6)

Figure 3-8. *Illustrations of joints (A) and their association with shallow-depth groundwaters (B) and with the effects of erosion on rock mechanics (C and D).*

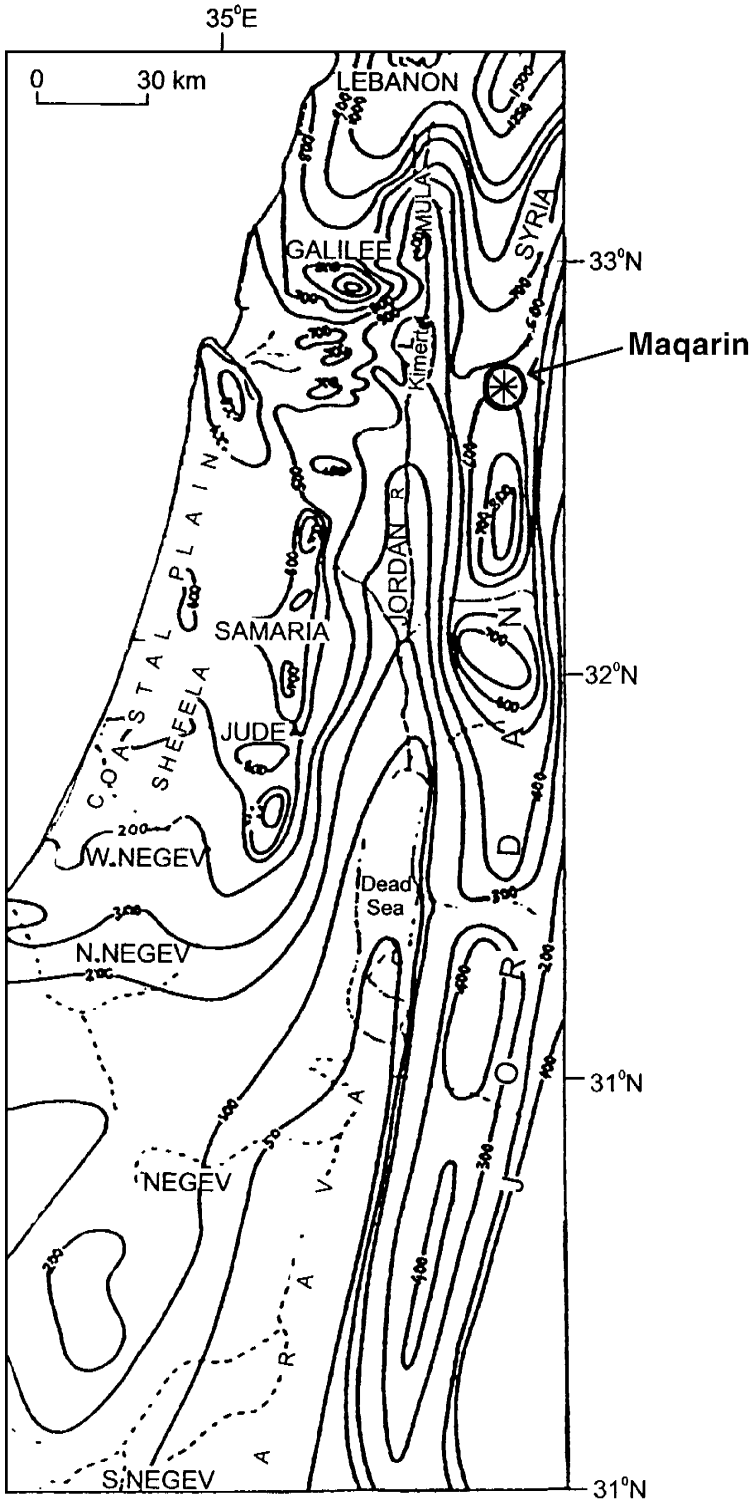

Figure 3-9. *Map of present-day precipitation isohyets, showing steep gradients around the Maqarin area [circled asterisk].*
(From Horowitz, 1979).

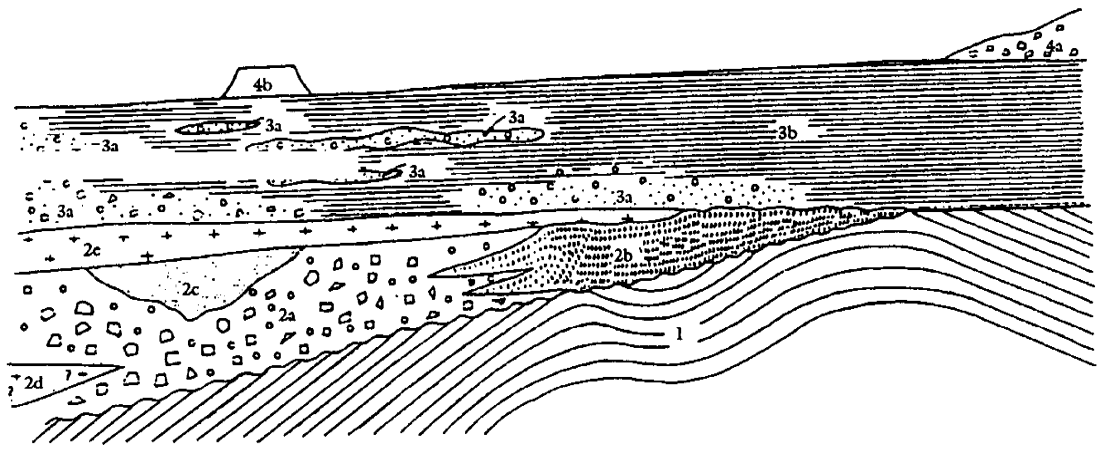

	LITHOLOGY	FORMATION	AGE	CULTURE
4b 4a	"Tell" culture Scree	4 Recent	Holocene	Natufian to Recent
3b 3a	limnic-brackish fluvial	3 Lisan	Late Quaternary	Levalloiso-Mousterian to Aurignacian
2e 2d 2c 2b 2a	basalt (Raqqad)* basalt (Yarmouk)* loessial soil red-brown loam Naharayim gravel and boulders	2 Naharayim	Mid- Quaternary	Acheulian s.s.
1	limnic/fluvial	1 Ubeidiya	Early Quarternary	" Pebble Culture" (inc.Abbevillian)

* The names of the basalts replace those used by Picard (1965), prior to the aid of radiometric dating. His 2e " Yarmouk basalt " is almost certainly, the Raqqad basalt.

Figure 3-10. *Generalised section (west-east) through Quaternary deposits, evacuated from the Yarmouk River Valley, in the Jordan-Yarmouk confluence area of the Jordan Rift Valley (from Picard, 1965).*

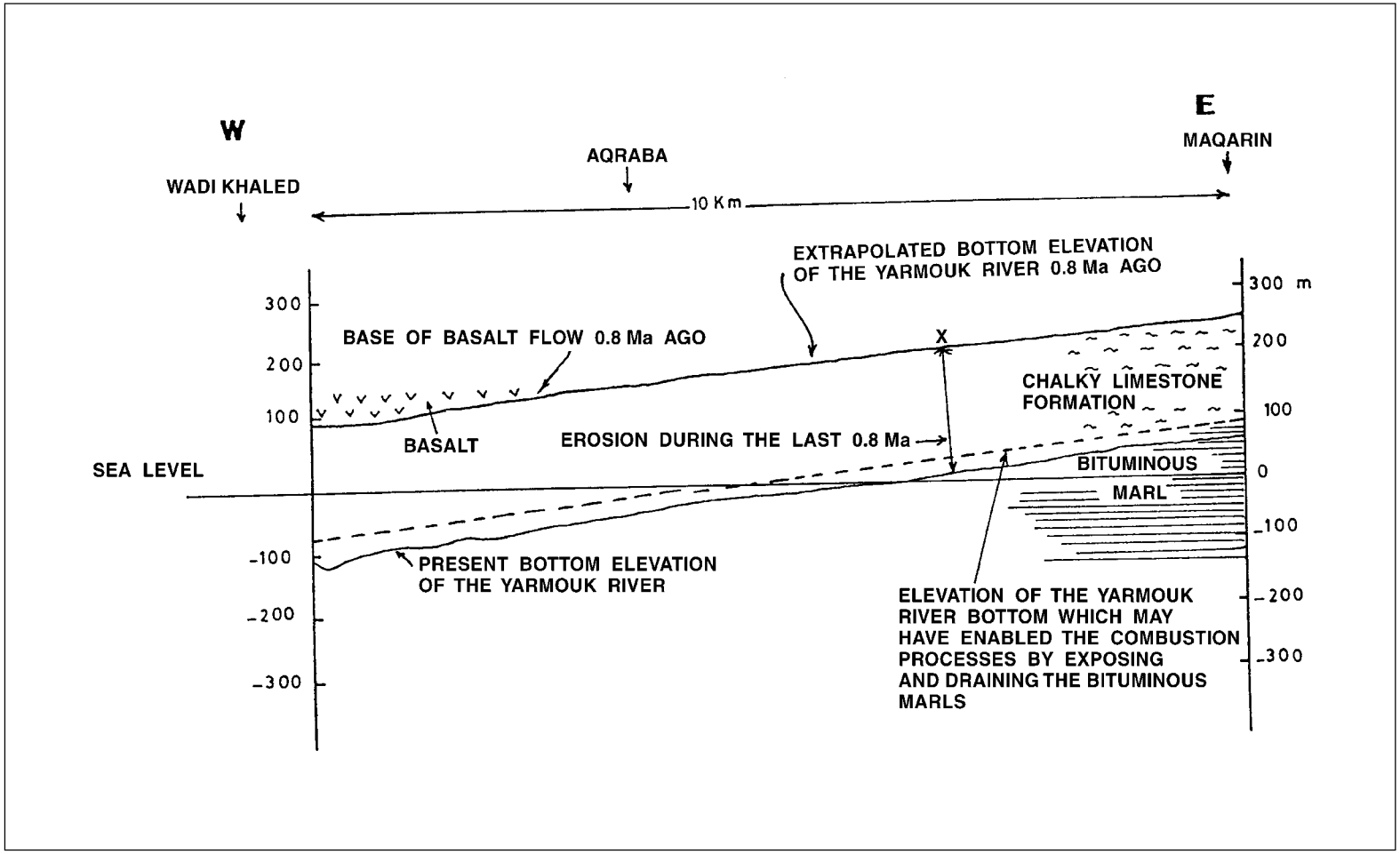

Figure 3-11. *Schematic illustration of the possible relationship between the Yarmouk River bottom elevation, and the earliest initiation of combustion of the Bituminous Marl Formation (E. Salameh, written comm., 1997).*

4 SITE DESCRIPTION SAMPLING PROGRAMME AND GROUNDWATER ANALYSIS

(A.E. Milodowski, E.K. Hyslop, J.A.T. Smellie, E. Salameh and H.N. Khoury)

4.1 INTRODUCTION

This chapter describes the sampling programme, locations and local geology of the sites for groundwater and rock/ mineral samples, and presents a summary of the Phase III groundwater analyses obtained from the Maqarin site. This enables the data obtained from the groundwater and solid samples to be correlated, and provides the geographical and geometrical context for the subsequent mineralogical and geochemical interpretations. The geology and hydrogeology of the Maqarin and central Jordan areas has been described already in detail in previous reports for Phase I and Phase II (Alexander, 1992; Linklater, 1998) and in Chapter 2 and Chapter 3 of this present report.

Three areas (Fig. 4-1) were studied:

(a) the Maqarin area in northern Jordan where hyperalkaline springs associated with retrograde hydration of thermally metamorphosed Bituminous Marl Formation rocks, i.e. bituminous limestone and clay biomicrite (argillaceous limestone formerly referred to as "marl");

(b) the Daba-Siwaqa area of central Jordan where metamorphosed bituminous limestone (and their retrograde hydrated and altered equivalents) similar to those found at Maqarin also occur, but on a much larger scale and which are no longer associated with hyperalkaline groundwater;

(c) the Sweileh area near Amman in central Jordan where metamorphosed clay biomicrites similar to those at Maqarin, but also including significant metamorphosed kerogenous phosphorite, have recently been sampled.

The field work for the Phase III study was undertaken in several stages. Three short, cored boreholes were drilled in December 1993 at Maqarin consisting of: a) borehole RW1 in the Eastern Springs area, at the Maqarin Station Railway Cutting site, b) borehole WS1 at the Western Springs site immediately above the M5 spring site, and c) borehole BH3 near the Western Springs area at Wadi Sijin (Fig. 4-1). The cores were initially assessed macroscopically for evidence of hyperalkaline rock-water interaction before selecting samples for further analysis. Unfortunately, apart from one small sample, most of the drillcore recovered lacked any hyperalkaline water-rock interaction, and consequently these cores were not examined further. Borehole BH3 was dry and groundwater sampling was confined therefore to boreholes WS1 and RW1.

The main field sampling was undertaken in November 1994. The programme concentrated on sampling and field data acquisition at Maqarin in northern Jordan, but two short visits were also made to examine and sample fossil rock-water interaction sites in the Daba-Siwaqa and Sweileh areas in central Jordan. Further colloid sampling was undertaken at Maqarin during May 1995 (see Chapter 10) and supplementary sampling of representative background lithologies for geochemical analysis was carried out during September and October 1995. Sampling for microbes was conducted in November 1996 (see Chapter 11).

4.2 MAQARIN AREA

4.2.1 Background to the Sampling

A few days prior to the main sampling visit in November 1994, extremely heavy rainfall produced a major flash-flood along the Yarmouk River Valley. As a result, vegetation and small trees along the river bank and the narrow flood plain of the Yarmouk had been destroyed. In addition, large areas of the bedrock along the valley floor had been exposed by stripping off of the soil and colluvium. At the Eastern Springs locality, the flooding had exposed limestone bedrock overlain by well-cemented wadi colluvium and fluvial gravels through which hyperalkaline spring seepages were actively discharging along the river bank terrace, approximately 400 m north of Adit A-6. Within this area, a number of old water resource exploration boreholes (drilled during the 1950s) had also been exposed. At the Western Springs locality, the flooding had exposed wadi colluvium and alluvial deposits affected by hyperalkaline groundwater discharge for a distance of over 250 m along the river terrace.

It had not been possible to observe these areas during Phase I or Phase II due to military restrictions and because of the former soil cover and dense vegetation. Consequently, a number of new sites of hyperalkaline groundwater-rock interaction were sampled. The same sampling site code system used in Phase II (Milodowski et al., 1998a) was used for the Phase III programme. The numbering of the new groundwater sites examined in Phase III simply follow on from the site numbers used in Phase II. It should be noted however, that this numbering system differs from that followed in Phase I.

Details of the rock and mineral samples collected are presented in Appendix E and the groundwater sampling and analytical protocols are described in Appendix F.

4.3 WESTERN SPRINGS AREA

4.3.1 General

The Western Springs area was the main focus of the Phase III programme. This site (characterised by groundwaters with higher pH, and higher Ca, Na, K, NH_3, Sr, SO_4 and NO_3 concentrations than the Eastern Springs area) is of particular interest as an analogue for the early stages of the repository alkaline plume evolution when Na and K

hydroxide concentrations are relatively high. In addition, the site presents an opportunity to study the reaction of hyperalkaline groundwaters with silicate-rich lithologies (i.e. interaction with basalt-rich colluvium, as opposed to interaction with limestone and the clay biomicrites in the Eastern Springs area).

4.3.2 Site Location

The Western Springs area, located about 2.5 km west of Adit A-6, represents the westernmost extent of hyperalkaline groundwater activity at Maqarin (Fig. 4-1). Natural hyperalkaline springs discharge as a series of seepages through colluvial (slope-wash debris flow) deposits and fluvial gravels and boulders (Plate 4-1). The present discharge occurs at about 1 m above river level, along a 200–250 m section of river bank on the southern (Jordanian) side of the Yarmouk (Fig. 4-2). There is no recorded evidence of hyperalkaline groundwater on the northern (Syrian) side of the Yarmouk River. Prior to the recent flood-scouring of the valley-floor, hyperalkaline groundwater activity and associated rock-water interaction was only evident at the westernmost end of the section (area between M5 and M16; Fig. 4-2). The M5 spring site was sampled previously during Phase I and Phase II (Clark et al., 1992a; Milodowski et al., 1998a). However, the flooding had removed a considerable area of vegetation and soil cover from over 200 m of river bank on the Jordanian side of the Yarmouk. This revealed an additional area of hyperalkaline spring seepage, extending from M16 to approximately 150 m upstream of M16 (Fig. 4-2), through alluvial boulder gravels and colluvium forming a low river-cut platform at about the same level as the M5-M16 site (i.e. approx. 0.5–1 m above present river level). The hyperalkaline seepages in this freshly-exposed area are very diffuse, and it was impractical to sample the very weak flows from these springs under the heavy rainfall conditions which prevailed during the field visit. However, the marked greenish-yellow colouration of the spring waters in this area indicates that the springs are probably very similar in chemistry to (i.e. high chromate), and continuous with, the main active spring area between M5 and M16, in contrast to the colourless (lower chromate) waters of the Eastern Springs area.

4.3.3 Sedimentological Model

The Quaternary sediments in the Western Springs area are highly heterogeneous, particularly along the banks of the Yarmouk River where they comprise intercalated colluvial deposits (slope-wash debris flow material) and fluvial boulder gravels. Further away from the river the deposits are largely colluvium with a thin, organic-poor, chalky ("marly") soil veneer. Within the area, the colluvium and soil are also influenced by landslip activity.

A schematic summary of the Quaternary sediment sequence at the M5-M16 site is shown in Figure 4-3. Here three discrete sedimentological units can be distinguished:

(i) thin soil cover, with a poorly-defined transitional zone of thin weathered, weakly cemented colluvium ("nari") grading into the underlying colluvium;

(ii) colluvium unit;

(iii) basal fluvial boulder-gravel unit.

Previously (Milodowski et al., 1992; 1998a) all of this sequence had been referred to as "colluvium". However, more detailed examination during Phase III revealed this to be an over-simplification. These three units are quite clearly geologically distinct and have significantly different mineralogical and sedimentological characteristics. The sedimentological characteristics of the Western Springs are illustrated schematically in Figure 4-4, and are described in detail below:

Fluvial Boulder-Gravel Unit

This is the lowermost Quaternary unit seen in the Western Springs area. It comprises very coarse, clast-supported alluvial boulder gravel (clast size varying from <1 cm to >1 m), with well-rounded water-worn clasts (indicative of a significant distance of water transport) of basalt, clay biomicrite/limestone and chert (Plate 4-2). Some clasts are imbricate, with orientation consistent with the present river drainage direction.

The composition of the boulder gravel was estimated by counting clasts along a 20 m stretch of representative gravel between sites M11 and M12. A measuring tape was laid along the ground in traverses parallel to the river, and the intersection of every "component" >0.5 cm (whether clast, or matrix or void space, and component type) along the traverses was recorded. The clast count data are given in Table 4-1.

The boulder-gravel is dominated by basalt clasts, with a subordinate amount of micritic limestone and chert. It has a sandy matrix, or locally it may lack matrix altogether, and is well-cemented by calcite, aragonite and other fine-grained hyperalkaline groundwater mineralisation products, to form a hard, tough, very coarse conglomerate. The high content of basalt clasts clearly distinguishes it from the overlying poorly-sorted colluvium.

At least 1 m of boulder gravel is present at outcrop along the bank of the Yarmouk River, but its maximum thickness is not known since its base was not seen in the immediate area. However, it was encountered in the nearby borehole WS1 (see Fig. 4-2 for location), which proved that the basalt-rich gravels, beneath the colluvium, rest directly on bedrock (Bituminous Marl Formation) between 9.50–11.20 m depth below ground level. This indicates that the boulder gravels are of the order of at least 1.7 m thick about 10–20 m south of their outcrop. The boulder gravel unit probably represents a gravel side-bar deposited along the outside edge of the river bend at the Western Springs, and probably rests directly on bedrock. Similar gravels can be seen to crop out on the Syrian side of the river where they form a generally flat lying alluvial terrace which has been developed for agriculture. The schematic relationship of the fluvial boulder-gravel to the other Quaternary sediments at the Western Springs is illustrated in Figure 4-4.

Basalt-rich fluvial boulder-gravels, recently exposed, also occur approximately 150 m upstream of M16 (Fig. 4-2). These form part of a longitudinal gravel bar, which may in part be overlain and obscured by colluvium. In contrast to the boulder gravels between M5 and M16, these gravels lack any evidence of hyperalkaline spring-related alteration and cementation. In this respect, they are similar to the gravels encountered in borehole WS1, which also lack evidence for significant hyperalkaline groundwater interaction. These gravels appear to have similar composition and stratigraphic relationship (with respect to the colluvium), as the gravels occurring between M5 and M16, and it seems

likely that the two areas are correlated. However, evaluation of the precise relationship of the two areas of fluvial boulder gravel (Fig. 4-2) requires more detailed sedimentological mapping.

The main hyperalkaline spring discharge occurs along the interface between the basal fluvial boulder gravels and the overlying colluvium (Figs. 4-2 and 4-4; Plate 4-1). It is also obvious that hyperalkaline groundwater has permeated through the fluvial gravels, resulting in extensive cementation of the intergranular porosity and matrix. Flow of hyperalkaline groundwater from the springs over the surface of the boulder gravel has resulted in the deposition of extensive laminated calcareous tufa (travertine) which coats and encrusts the exposed surfaces of the river-cut gravel platform.

Occasionally, water-worn fragments of reddened and altered micritic limestone were also seen within the boulder gravels (grouped with micritic limestone in the clasts counts). These relatively uncommon clasts appear to be broadly similar to the reddened and baked rocks of the cement zone exposed locally 1–2 km upstream in Wadi Sijin and Adit A-6. These clasts are clearly only locally-derived, since they are unstable and are therefore unlikely to have survived long-distance fluvial transport. Their presence in the fluvial boulder gravels is very significant for constraining the age relationships of the Metamorphic Unit (i.e. cement zone) at Maqarin. The inclusion of cement clasts in the fluvial gravels clearly demonstrates that the cement zone pre-dates the earliest of the Quaternary sediments at the Western Springs site. Furthermore, they demonstrate that the cement zone was exposed and was being eroded actively in the Yarmouk Valley at the time that this basal fluvial boulder gravel unit was being deposited. In contrast, the hyperalkaline springs, which have produced the alteration and cementation of the fluvial gravel unit (and overlying colluvium) must have developed since the deposition of the gravels.

These observations are in accordance with the geomorphological development of the Yarmouk River Valley and have been referred to in Section 3.11.

Colluvium Unit

This unit largely comprises poorly-sorted, angular fragments of weathered grey-white and creamy-coloured chalky limestone and clay biomicrite, in a fine chalky matrix. It represents debris-flow or slope-wash material derived from the adjacent hillside. The deposit is for the most part matrix supported and lacks the basalt-derived detritus that typifies the underlying fluvial gravels. Clasts of mottled, orange, purple and reddish-brown, altered metamorphosed micrite are common in the colluvial deposits. In borehole WS1 varicoloured clasts of altered marble are particularly abundant between 5.50 and 6.20 m depth below surface. The presence of such clasts in the colluvium is indicative of the close proximity of the site to the cement zone.

Borehole WS1 indicated a 9.50 m thickness of colluvium resting on basalt-rich fluvial gravels. Between M5 and M16 (Fig. 4-2), the colluvium forms a very steep undercut at the river bank leading down to the narrow platform of fluvial boulder gravels, from which the colluvium has been eroded. However, upstream of M16, the colluvium spreads out as a sheet over the low fluvial gravel platform (Fig. 4-2), and part of this may represent debris-flow material fanning out and moving downstream of the Wadi Sijin area. For the most part, the colluvium is poorly consolidated and uncemented.

Hyperalkaline springs discharge at the base of the unit, at the interface with the underlying gravels between site M5 and M16 (Figs. 4-2 – 4-4). The colluvium above this level is typically unconsolidated and dry. However, the colluvium displays some evidence of minor mineralisation and cementation by hyperalkaline groundwater for up to 1 m above the present-day spring line (Fig. 4-4). Here, hyperalkaline alteration is evident as alteration rims around clasts, and as precipitates of white, powdery secondary calcite and ettringite-thaumasite mineralisation along fissures and coating clast fragments. No active groundwater seepage has been observed at this level in the colluvium, but the presence of hyperalkine groundwater alteration effects suggests that the hyperalkaline groundwater flow has occurred at a higher level in the past.

Between 80 m to approximately 150 m upstream of M16, hyperalkaline discharge occurs through the matrix of the colluvium. Here the colluvium is strongly cemented by secondary calcareous mineralisation. Whilst it is evident that major hyperalkaline discharge has occurred in the past, in this area of the Western Springs, the activity has waned and is now restricted to very small and diffuse flows. The distribution of present and past hyperalkaline spring activity suggests that as alteration products have sealed up fluid pathways through the Quaternary deposits, the groundwater flow may have been diverted further downstream to the present main area of discharge.

Regolith and Soil

An irregular, diffuse, weathered and weakly calcareous cemented horizon 0–0.2 m thick marks the transition between the present-day, thin, friable chalky ("marly") soil cover (variable thickness). It contains plant root channels with diffuse concretionary haloes of calcareous cementation, and is cut by irregular, hairline fissures lined by fine micritic calcite. Much of cementation seems locally expansive and locally disrupts the soil structures. In part, some of these cements may be related to past hyperalkaline groundwater activity, but most probably represents evaporitic carbonate precipitation from capillary water. In this respect, the cementation is probably akin to calcrete formation (or "nari" as described in Chapter 3) typical of many arid and semi-arid climates (e.g. Arakel and McConchie, 1982). However, a stable isotope study of these cements would be required to be certain in distinguishing cements formed by capillary-evaporative calcrete formation (Salomons et al., 1978) and calcite precipitated from capillary hyperalkaline porewater reacting with soil or atmospheric CO_2 (Clark and Fontes, 1990; Clark et al., 1992b).

4.3.4 Sampling Sites

Samples were taken from all the main lithotypes along a profile bordering the Yarmouk River (E228.600:N237.250 to E228.800:N237.250) and subsequently subjected to mineralogical and geochemical analysis; sample details are summarised in Appendix E. Groundwater sampling sites are shown on Figure 4-2. Groundwater samples for geochemical analysis were collected from borehole WS1 (M17) and the following five spring discharges:

M5: Spring discharge occurring at the interface between the colluvium unit and the basal fluvial boulder gravels. Seep sampled by inserting plastic tubing up to 30 cm into a fissure at the interface between the two lithologies.

M11: Small, low-flow seep approx. 10 m east of M5, at the interface between the colluvium unit and the basal fluvial boulder gravels. Seep sampled directly at outflow point.

M12: Standing pool of hyperalkaline water, fed by numerous small spring flows, 15 m east of M11. Sample taken directly from pool.

M14: Spring discharge occurring at the interface between the colluvium unit and the basal fluvial boulder gravels. Seep sampled by inserting plastic tubing up to 10 cm into a fissure at the interface between the two lithologies.

M15: Spring discharge occurring at the interface between the colluvium unit and the basal fluvial boulder gravels. Seep sampled by inserting plastic tubing up to 10 cm into a fissure at the interface between the two lithologies.

Samples for microbiological analyses (DNA and epifluorescence analysis) were collected from M1, M17 and M18 on the same day, and stored in a cool-box in the field. On return to Amman in the evening, these were then re-packed into a cold-box, together with dry ice, and air-freighted to Sweden within 48 hours, for analysis (see Chapter 11).

Full details of the groundwater sampling protocols and field analyses undertaken are described in Section 4.5 and Section 4.6.

4.3.5 Comments on Sample Quality

It should be noted that adverse weather conditions prevailed throughout the sampling of the Western Springs area. Very heavy rainfall limited the practicality of sampling and field analysis. Although attempts were made to sample seepage sites M13 and M16 (Fig. 4-2), representative sampling proved impossible due to a combination of contamination by rainfall and the very slow flows from the springs at these two sites. However, measured pH was very similar to adjacent sampling sites. The adverse weather also affected the field operation of the pH, Eh and conductivity meters. Consequently, some field measurements (marked with an asterix in Table 4-1) failed and calibration proved difficult. In this respect it is notable (Table 4-1) that "Field pH" is consistently lower by 0.5–0.7 pH units, than the corresponding "Laboratory pH" determination. In contrast, pH measurements for the other sites at Maqarin, which were sampled under dry conditions, show good agreement between "Field pH" and "Laboratory pH" (Table 4-1). Comparison of data from Phase II for site M5 (Milodowski et al., 1998b) with Phase III data for the same site shows that the Phase III data exhibit slightly lower values for pH and other ionic components, suggesting that the Phase III sampling might be diluted by the heavy rainfall. In respect of these problems, the field measurements for sites M5 and M11-M15 should perhaps be regarded with caution.

It had been intended to measure pH and Eh using a Perspex flow-through cell, when sampling from the spring sites, in order to minimise effects of sorption of atmospheric CO_2 and O_2 (Ball and Milodowski, 1989). However, except for site M5, the flows were

too slow to enable this to be used effectively and consequently pH and Eh had to be measured by placing the specific ion electrodes directly into the springs.

Borehole WS1 was completed with a slimline inflatable packer system, which had been installed to isolate flow from the Bituminous Marl Formation from flow from the overlying unconsolidated Quaternary sediments. The original intention had been to isolate the contact zone between the underlying Bituminous Marl Formation and the colluvium sequence, i.e. to sample the high pH groundwaters. This proved impossible because the high permeability of the colluvium short-circuited the upper packer seal leading to dilution of the groundwater in the packed-off section. The packed-off interval was subsequently adjusted to sample water specifically from the Bituminous Marl Formation. Prior to sampling, the borehole was pumped dry three times, and then allowed to recover for two days before sampling. The borehole was then pumped, and the pH and Eh of the groundwater monitored with specific ion electrodes via a purpose-built Perspex flow-through cell (referred to above). Eighteen litres of groundwater were pumped out before the pH reading stabilised, followed by sampling (sample M17).

4.4 EASTERN SPRINGS AND ADIT A-6

4.4.1 General

The Eastern Springs area (Fig. 4-1) has been studied in detail during Phases I and II, where work focussed on the cement zone alteration and on the marl-hyperalkaline groundwater interaction in Adit A-6 and the Maqarin Station Railway Cutting sites respectively (Alexander, 1992; Linklater, 1998). Initially, there were three main reasons for re-examining the Eastern Springs sites during Phase III:

(i) to sample colloids produced at the cement/host rock interface (M1) and to validate the findings of the Phase I colloid study (M2).

(ii) to sample groundwater from the new borehole (RW1 – sample M18; Fig. 4-1) drilled to intersect the hyperalkaline groundwater flow in the Maqarin Station Railway Cutting.

(iii) to collect further samples of fracture alteration in the clay biomicrite ("marl") host-rock in Adit A-6, in order to further evaluate trace element mobility, rock-matrix diffusion and porosity changes in response to reaction with hyperalkaline groundwater along fracture flow-paths.

However, during Phase III, a number of new hyperalkaline spring sites in the Eastern Springs area were discovered which warranted additional close examination during the main field visit programme. These included:

(i) a new road cutting exposing hyperalkaline seepages 100 m west of the original Maqarin Station Railway Cutting;

(ii) an extensive area of hyperalkaline groundwater seepage through alluvial boulder gravels approx. 400 m north of the entrance to Adit A-6;

(iii) several new road cuttings between Adit A-6 and the Maqarin Station where exposed colluvium and fluvial gravels have been cemented by palaeo-travertine deposits.

4.4.2 Adit A-6

Adit A-6 was only sampled for colloids and for microbiology during Phase III. The site is described in detail by Alexander (1992) and Linklater (1998), and the reader is referred to these earlier reports for further details of the sampling locations.

To ensure that the waters were sampled without air contact, a specially-constructed teflon sample collection cup was emplaced over a major seep at each of the two sites in the adit wall, after cutting a mounting platform into the tufa coating (Plate 4-3). The teflon cup / tufa contact was sealed with a teflon O-ring. To ensure an airtight seal, the cup and surrounding tufa was coated with a flexible silicone sealant. To further reduce the risk of carbon dioxide contamination, the seal and cup were coated and packed with a paste of tufa saturated with hyperalkaline water which was allowed to set. It was hoped that any carbon dioxide would first react with the calcium hydroxide (portlandite) in the tufa and thereby be prevented from infiltrating into the collecting system. The sampling cup was connected to a collecting vessel with teflon tubing. To prevent back-diffusion of carbon dioxide into the sampling system, a bubble-trap filled with hyperalkaline groundwater was connected at the outlet of the sampling vessel. The system was then left to flush through with hyperalkaline groundwater for 48 hours before sampling. All sampling was carried out under a nitrogen atmosphere (Plate 4-4). Although colloids were collected successfully from the M1 site during the November 1994 field visit, and then subsequently during a later visit in 1995, insufficient flow was obtained from the M2 site, and collection here had to be abandoned. Further details of the colloid sampling programme are given in Chapter 10.

Samples of clay biomicrite host rock were collected from the M2 site and from other fractures between M1 and M2. Sampling involved collecting a series of rocks taken progressively away from the main conducting fracture. Samples were taken to enable rock matrix diffusion effects and the disturbance of the U-decay series system to be evaluated in wallrock up to 10 cm away from the fracture wall. Obtaining diffusion profiles over longer distances was limited by the close-spacing of fracture sets in Adit A-6. Additional fracture mineralisation samples associated with hyperalkaline groundwater seeps in Adit A-6 were also collected.

4.4.3 Maqarin Road Cutting Site

A new exposure of hyperalkaline seepages (M8 site) is located in organic-rich clay biomicritic limestone, about 100 m west of the Maqarin Station Railway Cutting (M3 site sampled in Phase II). The exposure has been produced as a result of widening the former railway line cutting to construct a new metalled road through the area. The road construction has exposed a number of large bedrock and colluvial deposits in cuttings between Adit A-6 and the Maqarin Station Railway Cutting Site (M3).

The M8 site road cutting has excavated 3–4 m into the side of the wadi, creating a face 5–6 m high which intersects fractures carrying hyperalkaline groundwater. This has

resulted in new hyperalkaline groundwater seeps. The clay biomicrites at this site are organic rich and black in colour. Heavy staining of the tufa precipitates by dark-brown to black organic matter is apparent at all seepages (Plate 4-5), indicating the possibility that organics have been mobilised in the hyperalkaline groundwater. Seeps occur through low-angle bedding-plane fractures spaced 60–100 cm apart. The main seeps are from a zone of fractures 0.5–1 m beneath the soil-bedrock interface at the top of the cutting. Groundwater discharges occur along 12 m of the cutting face but the seeps rapidly decrease in flow eastwards over a distance of 6 m. In contrast, the development of tufa associated with the seeps is most extensive at the eastern end of the cutting. Observations suggest that flow was originally much greater at the eastern end of the cutting, but with time the flows have become reduced as a result of progressive sealing of fractures by secondary precipitates, and the seepages have subsequently migrated westwards along the cutting. It is clearly evident that the tufa development on the cutting face (Plate 4-5), and the sealing up of fractures in the eastern end of the exposure and the westward migration of seeps, has occurred over a very short timescale (<2 years) since development of the cutting. At the western end of the exposure, the bedrock is obscured by colluvial breccias and there is no evidence of past or present hyperalkaline groundwater flow.

The horizontal fractures in the upper 0.5 m of the cutting face are very heavily mineralised by carbonates and possible ettringite. Some fractures have developed vein fills up to 1 cm thick. This mineralisation is probably much older than that seen associated with the active seeps lower down the face. A steep grassed slope developed on colluvium overlies the cutting. The slope leads to an unstable cliff or crag of variably-cemented colluvium situated 6–8 m further up the wadi wall. The colluvium is cemented with carbonate and ettringite associated with local seeps of hyperalkaline groundwater. Most of the seepages in this overlying colluvium are now inactive, but alkaline groundwater (pH ~12.5) still drips from a few small stalactites at the base of the crag. It would appear that alkaline groundwaters have been flowing along the bedrock-colluvium interface. At the M8 cutting face, these groundwaters penetrate through the fractured bedrock just beneath the colluvium-bedrock interface. Further observations made during the Phase III field visit also suggest that the same situation exists at the Maqarin Station Railway Cutting locality (Site M3) 100 m to the east. At this location, hyperalkaline groundwaters were seen seeping also along the bedrock-soil (or colluvium) interface overlying the railway cutting. Recent observations suggest that the cement zone which feeds seepages M8 and N3 may be located some 500 m due south of the sampling sites (W.R. Alexander, per. comm., 1997). The hyperalkaline groundwater appears to flow from the cement zone into the unaltered Bituminous Marl Formation where flow is then re-directed along the colluvium bedrock interface.

Samples of groundwater for major minor and trace element analyses were collected from M8. The results of chemical analyses of groundwater from this site are presented in Tables 4-2 and 4-3.

4.4.4 Borehole RW1

Borehole RW1 (M18 site) represents the borehole drilled in December 1993 at the Maqarin Station Railway Cutting (E233.060:N236.625). Unfortunately, since completion, the packer system became dislodged such that only the open hole could be

sampled. Prior to sampling, the borehole was pumped out completely and allowed to recover over a period of 3 days. Samples were then collected for analysis after 25 litres of water had been removed. Samples were taken for microbiology analysis (DNA and epifluorescence) and for major, minor and trace element analysis. The results of the geochemical analyses are presented in Tables 4-2 and 4-3.

Because of the open-hole conditions, observations indicate significant mixing with rainwater or water from the upper aquifer or colluvium, i.e. a mixture of hyperalkaline groundwater with background bicarbonate groundwater. (Laboratory pH 8.18; Field pH 8.97–9.63). The water level in the borehole was unusually close to the surface due to very heavy rainfall recharge at the time of sampling.

4.4.5 New Seepage Sites Along the Yarmouk River Valley

Adjacent to the Yarmouk River directly beneath (and north of) Adit A-6, large areas of the bedrock and well-cemented Quaternary fluvial boulder gravels had been exposed as a result of the recent flooding

Several old (1940s to 1950s) hydrogeological borehole sites were also re-located in this area. One open borehole in particular was exposed in the bedrock on the Jordanian bank about 25 m downstream from the old road bridge. This borehole appears to be uncased, with significant artesian flow and corresponds to the Maqarin Unity Dam-Site Investigation Borehole M-13 which samples water from the deep artesian Amman Formation (B_2) aquifer. It had not been possible to sample groundwaters from this aquifer during previous (Phase I and Phase II) investigations. The well was sampled (sample M9) via tubing placed to a depth of 5m from the surface, to minimise contamination from surface water.

The groundwater chemical analyses (sample M9) are given in Tables 4-2 and 4-3. It represents a bicarbonate-type groundwater significantly more saline than the water from the upper B_4/B_5 aquifer sampled (during Phase II) at the Ain Quelba Spring (compare M9 data with data for Ain Quelba Spring in Milodowski et al., 1998b).

Well-cemented colluvial deposits are exposed around the M9 borehole site and extend for approx. 100 m downstream from the old bridge across the Yarmouk River (E231.500:N237.750). These deposits are cemented by travertine deposits; a small area of small actively-flowing hyperalkaline seeps were found about 75 m downstream from the old bridge, and about 400 m north of Adit A-6. The seeps emanate through small fissures within the colluvial deposits and underlying fluvial boulder gravels. The sedimentological setting of this site appears to be similar to that of the Western Springs area. Samples of the hyperalkaline groundwater seepages were collected for chemical analysis (M10) as described for the Western Springs localities (see Section 4.3).

The groundwaters discharging at M10 are still highly alkaline (pH 12.44; see Tables 4-2 and 4-3). The pH is only slightly lower than groundwaters discharging from the cement zone and biomicrite rocks in Adit A-6 (Phase II). Compared to Adit A-6, M10 is slightly enriched in K and Cl compared to Adit A-6 samples, although Na and SO_4 are broadly similar. There is no obvious evidence of a cement zone located between Adit A-6 and the M10 site. This suggests that the alkaline plume may extend for at least 400 m from the cement-zone in the Eastern Springs area. However, it should be noted

that the hydrogeology is complex, with flow occurring through the matrix of the colluvium (which contains some clasts of cement zone rocks) as well as through fracture conduits in the clay biomicrite host rocks within this area.

4.5 CENTRAL JORDAN

4.5.1 General

Of the other cement zone rocks (i.e. combustion-related thermally-metamorphosed "marls" and limestones) similar to those at Maqarin but which cover central Jordan, the occupied West Bank and Israel, two areas have been sampled: (i) Daba-Siwaqa area, and (ii) Sweileh area (Fig. 4-1).

Neither area is now associated with present-day hyperalkaline activity. The marbles of the Daba-Siwaqa area are worked commercially, and the area has been examined by several studies, including the Phase II programme (Milodowski et al., 1998a). In contrast, the Sweileh metamorphic area (Khoury and Salameh, 1986) has received little attention.

The objective of the Phase III programme was to try to find evidence of hyperalkaline rock/water interaction with clay-rich (unmetamorphosed) host rocks to test the stability of clay as an analogy to the performance of bentonite seals in a cementitious repository.

4.5.2 Daba-Siwaqa Area

The Daba-Siwaqa area is located 30-50 km south of Amman, lying east of the Desert Highway which runs from Amman to Aqaba (E36°.15′:N31°.30′). The region is at an altitude of 680–918 m.a.s.l. and is characterised by a semi-arid to desert climate, with very low winter rainfall (annual rainfall <100 mm). Streams are ephemeral and the area supports minimal vegetation.

A cement zone (i.e. high-temperature combustion-metamorphosed marbles; Daba Marble Zone), similar to that at Maqarin, underlie some 375 km^2 of the Daba-Siwaqa area. The development of the metamorphic Daba Marble Zone is structurally-controlled and is strongly associated with areas of gentle folding linked to the development of three major fault zones:

(i) Zarqa-Ma'in-Daba-Dhiban Fault Zone;
(ii) Wadi El Hammam Fault Zone;
(iii) Siwaqa Fault Zone.

Large areas of travertine were developed at hyperalkaline spring sites associated with extensive silicification and replacement of tufa by opaline silica (Milodowski et al., 1998a). The travertines are much more resistant to erosion and ablation than the surrounding rocks and now exist as relict caps on many of the hills in the area (e.g. Khan-ez-Zabib Hills). The geology of the area is described in detail by Milodowski et al. (1998a).

Several sites were visited in the area during Phase III sampling. This included the working Daba Marble quarries at El Hammam, several road cuttings along the Desert Highway 3 km either side of Daba village, and several of the railway cuttings along the old mineral railway between Siwaqa in the south and Khan-ez-Zabib in the north.

Most of the sites (except the railway cuttings) had been examined and sampled during Phase II. In common with Phase II, no evidence could be found in this area for the interaction of hyperalkaline groundwaters with clay-rich lithologies. Smectite alteration products – volkonskoite (chrome smectite) – have been recorded from many localities in this area (Khoury et al., 1982; Milodowski et al., 1998c). However, the smectite appears to be an exogenic precipitate (Milodowski et al., 1998c) within hyperalkaline-altered chalks and hydrated marbles, rather than an in situ reaction product of primary clay-rich lithologies. The only host lithologies that are present within the hyperalkaline alteration halo around with the Daba Marble Zone, are essentially very low-clay content chalks and fine biomicrites. There is little or no evidence for any clay-rich lithologies in this area.

The samples collected from the Daba-Siwaqa area are described in Appendix E.

4.5.3 Sweileh Area

An area of palaeohyperalkaline groundwater interaction was examined in a new cutting for the Abu-Tara to Sweileh road, 2 km west of Sweileh, near Amman (E35°.10′:N32°.01′). Early reconnaissance of the area during the December 1993 visit had suggested that the site might furnish samples in which the interaction of hyperalkaline groundwater with clay-rich lithologies could be examined. The area was revisited briefly during November 1994, but unfortunately sampling and observations were limited by weather conditions.

The site presents a sequence of interbedded bituminous (kerogenous) phosphorites, fissile chalk and micritic limestone and massive chert, overlying interbedded micritic limestones and chalks with discontinuous nodular cherty horizons. The main metamorphic zone appears to be related to the combustion of the bituminous phosphorite horizon, and was not exposed in the road cutting. Samples collected previously from the area demonstrate that the metamorphic assemblage is dominated by apatite-rich rocks (in contrast to the Maqarin area). Within the road cutting, some of the chalky micrites appear to be slightly baked and reddened, suggesting that the study area is at the limits of the Metamorphic Unit/cement zone. However, the precise position of the Metamorphic Unit/cement zone in relation to the study site is poorly understood, and a detailed mapping study of the area is required before this relationship can be resolved.

The sequence is summarised below:

Thickness	Brief Description
>1.5 m	Bituminous phosphorite (top not seen).
0.55 m	Shaley chalk or friable laminated micritic limestone.
0.3 m	Blocky to massive phosphorite.

Thickness	Brief Description (contd.)
0.22 m	Fine massive micritic limestone, replaced by, or grading from massive chert in the basal 0–10 cm.
0.22 m	Fine massive micritic limestone, replaced by, or grading from massive chert in the basal 0–5 cm.
0.35 m	Apparently marly or shaley micrite or chalk, displaying greenish staining or alteration for up to 6 m along bedding planes away from steep vertical fissures containing travertine-like calcareous mineralisation products.
0.1–0.2 m	Silicified micrite with traces of bedding.
0.35 m	Massive micritic limestone with scattered chert nodules, grades up from a phosphoritic base.
0.18 m	Massive chert.
0.02 m	Thin phosphoritic micrite grading upwards into the overlying chert.
0.27 m	Limestone with scattered cherts.
0.22 m	Shaley or fissile chalk displaying greenish staining or alteration along bedding planes, away from steep fissures mineralised by calcite and ?silicate phases.

A series of steeply inclined fractures, spaced at intervals of 0.5–3 m apart, appear to have been conduits for hyperalkaline groundwaters. A highly disturbed and faulted area at the southwestern end of the section is associated with the development of a soft, mamillated and laminated calcite travertine deposit. Here, extensive calcite flowstone coats the surfaces of wide, steep fissures. Elsewhere, pale greenish staining or alteration is evident in some shaley micritic limestone horizons. The alteration is developed away along bedding planes fractures, adjacent to steep, thin (1–2 cm) fractures mineralised by secondary calcareous phases. The green alteration resembles the volkonskoite mineralisation seen in the Daba-Siwaqa area.

No truly "clay-rich" lithologies are present at this site. However, samples of the green matrix alteration associated with the palaeohyperalkaline fracture mineralisation were collected for analysis. The samples collected from the Daba-Siwaqa area are described in Appendix E.

4.6 SUMMARY AND CONCLUSIONS

In Phase I the "colluvium" grouped together all recent sedimentary units. Phase III studies showed the colluvium to comprise two units: a lower unit of fluvial gravels and an upper unit of colluvium *senso stricto*. The main Western Spring discharges occur at the interface between these two lithologies.

Phase III groundwater sampling was successfully accomplished with one major reservation; the objective of drilling three boreholes to establish the extent and composition of the Western Springs hydrochemistry was not totally successful. The high pH cement source zone has still not been located, and the hope of sampling deeper hyperalkaline groundwaters from packed-off borehole sections at the colluvium/marl contact was not realised because of the high friability and porosity of the colluvium. The drilling, however, emphasised the impermeability of the underlying marls, and that advective flow through the marls was fracture controlled.

On the other hand, the flooding along the Yarmouk Valley exposed additional hyperalkaline seepages, especially at the Eastern Springs locality, which helped considerably in establishing the extent of the hyperalkaline plume from the vicinity of Adit A-6 to be at least 400 m.

As the rainy season coincided with the major sampling mission, and some contamination may have occurred, care is required in interpreting the groundwater data, especially the near-surface samples.

The sampling of rock specimens for hyperalkaline water/rock interaction studies was successful. However, problems were still encountered in finding clay-rich marl samples for clay/high pH groundwater stability studies. More detailed, regional-scale geological surveys are necessary, but this fell outside the scope of Phase III.

Colloid and microbial sampling was successfully carried out using more sophisticated methods than in previous studies. In common with the hydrochemical sampling, there is still a need to sample from more anoxic groundwater conditions. This requires a more systematic drilling campaign than hitherto possible.

4.7 REFERENCES

Alexander, W.R. (Ed.), 1992. A natural analogue study of the Maqarin, hyperalkaline groundwaters. I: Source term description and thermodynamic database testing. Nagra Tech. Rep. (NTB 91-10), Nagra, Wettingen, Switzerland.

Arakel, A.V. and McConchie, D., 1982. Classification and genesis of calcrete and gypsite lithofacies in palaeodrainage systems of inland Australia and their relationship to carnotite mineralization. J. Sed. Petrol., 52, 1149–1170.

Ball, T.K. and Milodowski, A.E., 1989. The geological, geochemical, topographical and hydrogeological characteristics of the Broubster natural analogue site, Caithness. Brit. Geol. Surv.Tech. Rep., Fluid Proc. Res. Gr., (WE/89/37), Keyworth, UK.

Clark, I.D. and Fontes, J-Ch., 1990. Paleoclimatic reconstruction in northern Oman based on carbonates from hyperalkaline groundwaters. Quat. Res., 33, 320–336.

Clark, I.D., Fritz, P., Milodowski, A.E. and Khoury, H.N., 1992a. Sampling and analytical methods. In: W.R. Alexander (Ed.), A natural analogue of the Maqarin hyperalkaline groundwaters. I: Source term description and thermodynamic database testing. Nagra Tech. Rep. (NTB 91-10), Nagra, Wettingen, Switzerland, p. 19–40.

Clark, I.D., Khoury, H.N., Salameh, E., Fritz, P., Göksu, Y., Wieser, A., Causse, C. and Fontes, J-Ch., 1992b. Travertines in central Jordan: implications for palaeohydrology and dating. Proc. IAEA/ UNESCO Symp. Isotope Tech. in Water Res. Devel., Vienna, 11–15 March 1991. IAEA, Vienna, Austria.

Linklater. C.M. (Ed.)., 1998. A natural analogue study of cement-buffered, hyperalkaline groundwaters and their interaction with a repository host rock: Phase II. Nirex Science Report, S/98/003, Nirex, Harwell, U.K.

Milodowski, A.E., Pearce, J.M., Hughes, C.R. and Khoury, H.N., 1992. A preliminary mineralogical investigation of a natural analogue of a cement-buffered hyperalkaline groundwater interaction with marl, Maqarin, northern Jordan. Nagra Int. Rep. (NIB 92-50), Nagra, Wettingen, Switzerland.

Milodowski, A.E., Hyslop, E.K., Khoury, H.N. and Salameh, E., 1998a. Site description and field sampling programme. In: C.M. Linklater (Ed.), A natural analogue study of cement-buffered, hyperalkaline groundwaters and their interaction with a repository host rock: Phase II. Nirex Science Report, S/98/003, Nirex, Harwell, U.K., p. 10–47.

Milodowski, A.E., Cave, M.R., Reeder, S., Smith, B., Chenery, S.R.N. and Cook, J.M., 1998b. Aqueous geochemistry at Maqarin. In: C.M. Linklater (Ed.), A natural analogue study of cement-buffered, hyperalkaline groundwaters and their interaction with a repository host rock: Phase II. Nirex Science Report, S/98/003, Nirex, Harwell, U.K., p. 48–63.

Milodowski, A.E., Pearce, J.M., Hyslop, E.K., Hughes, C.R., Inglethorpe, S.D.J., Strong, G.E., Wheal, N., MacKenzie, A.B., Karnland, O. and Khoury, H.N., 1998c. Mineralogy and Petrology. In: C.M. Linklater (Ed.), A natural analogue study of cement-buffered, hyperalkaline groundwaters and their interaction with a repository hot rock: Phase II. Nirex Science Report, S/98/003, Nirex, Harwell, U.K., p. 70–145.

Khoury, H.N. and Salameh, E., 1986. The origin of high temperature minerals from the Sweileh area, Jordan. Dirasat, 13, 261–269.

Salomons, W., Goodie, A. and Mook, W.G., 1978. Isotopic composition of calcrete deposits from Europe, Africa and India. Earth Surface Processes, 3, 43–57.

TABLES

Table 4-1. Clast-count analysis: Alluvial boulder gravel (M5–M16 sies).

Clast type	Proportion %
Basalt	47
Biomicrite/Limestone	8
Chert	11
Matrix (< 0.5 cm material)	34
Voids	0

Table 4-2. Major Element Chemistry of the Maqarin Groundwaters.

Sample	Blank	M5	M8	M9	M10	M11	M12	M14	M15	M17	M18
Field Temperature (°C)$^{+}$	n.d.	22.0	25.0	25.0	25.0	22.0	22.0	22.0	22.0	26.5	18.5
Field Eh (mV)$^{+}$	n.d.	202	262	409	250	n.d.*	n.d.*	n.d.*	n.d.*	-55	390
Field pH^{+}	n.d.	12.2	12.44	7.40	12.3	12.0	11.86	12.06	12.09	7.67	8.97
Laboratory pH^{+}	4.86	12.70	12.50	7.61	12.40	12.70	12.50	12.70	12.70	7.24	8.81
Conductivity (µS/cm)$^{+}$	n.d.	n.d.*	6010	947	580	n.d.*	n.d.*	n.d.*	n.d.*	n.d.*	n.d.*
Diss. Oxygen (mg/L)	n.d.	n.d.*	6	4.5	6	n.d.*	n.d.*	n.d.*	n.d.*	0.9	4
Ca (mg/L)	<0.05	1067	786	93.0	729	1033	747	1072	1113	87	113
Mg (mg/L)	<0.10	<0.10	<0.10	28.7	<0.10	<0.10	<0.10	<0.10	<0.10	38.2	2.26
Na (mg/L)	0.04	129	25.3	64.1	53.6	124	118	130	135	56.5	38.1
K (mg/L)	<0.50	491	3.10	4.52	20.8	502	452	531	528	57.0	13.6
NH_4 (mg/L)	<0.05	2.81	0.16	<0.05	0.23	2.68	1.89	3.20	3.14	5.84	0.81
Sr (mg/L)	0.001	15.500	3.810	0.870	11.900	14.320	12.020	14.900	15.300	3.470	3.390
CO_3 (mg/L)^{z}	n.d.	16	8	n.d.	11	19	30	47	23	n.d.	n.d.
HCO_3 (mg/L)	<20	n.d.	n.d.	319	n.d.	n.d.	n.d.	n.d.	n.d.	79	27
Field HCO_3 (mg/L)	n.d.	n.d.	n.d.	89	n.d.	n.d.	n.d.	n.d.	n.d.	94	n.d.*
OH (mg/L)	n.d.	637	449	n.d.	474	625	394	600	657	n.d.	n.d.
Cl (mg/L)	0.42	34.9	40.3	108	83.2	39.9	39.7	39.3	50.2	46	47.3
SO_4 (mg/L)	0.27	1410	352	68.8	290	1390	1270	1470	1510	449	280
NO_3 (mg/L)	0.33	34.8	7.13	11.6	3.09	29.1	18.0	30.2	32.6	<0.20	0.8
Major cation total (meq/L)	0.00	71.99	40.50	9.93	39.53	70.32	54.40	73.32	75.51	11.81	7.97
Major anion total (meq/L)	0.02	68.98	35.29	9.93	36.67	68.01	52.27	69.19	72.90	12.07	7.66
Balance (%)	-86.18	2.14	6.87	0.00	3.75	1.67	2.01	2.89	1.76	-1.10	1.96
TOC (mg/L)	<1.00	6.08	7.64	<1.00	1.83	5.43	2.87	5.11	5.91	1.65	7.38
TIC (mg/L)	0.41	2.95	1.38	60.2	1.29	2.87	1.37	1.85	1.32	15.5	4.28

Note: (i) n.d. = not determined;
(ii) n.d.* = not determined in field due to adverse weather conditions preventing any practical measurement;
+ = refer to Section 4.3.5 for discussion;
z = titrated values, which are higher than obtained by acid extraction for ^{13}C analysis (see Table 6-4); TIC values also differ.

Table 4-3. Trace Element Chemistry of the Maqarin Groundwaters.

Sample	Blank	M5	M8	M9	M10	M11	M12	M14	M15	M17	M18
Br (mg/L)	<0.04	<0.04	<0.04	0.34	<0.04	<0.04	<0.04	<0.04	<0.04	0.19	0.21
NO_2 (mg/L)	0.03	1.47	<0.04	0.07	0.51	2.88	9.89	2.94	3.19	<0.04	0.16
HPO_4 (mg/L)	<0.05	0.55	0.10	<0.05	<0.05	0.54	0.44	0.57	0.60	<0.05	<0.05
F (mg/L)	0.02	0.92	0.43	0.62	0.26	0.95	0.74	0.96	0.97	2.44	0.63
Reduced S (mg/L)	<0.005	0.030	<0.005	<0.005	<0.005	0.023	<0.005	0.017	0.028	0.894	0.072
B (mg/L)	<0.02	0.14	0.03	0.11	<0.02	0.12	0.07	0.12	0.12	0.09	0.02
Li (mg/L)	<0.01	0.46	<0.01	<0.01	0.05	0.43	0.38	0.47	0.50	0.04	0.01
Ba (mg/L)	<0.001	0.024	0.036	0.197	0.051	0.024	0.032	0.026	0.025	0.040	0.031
Si (mg/L)	<0.02	0.07	0.04	10.71	0.26	0.18	0.37	0.14	0.13	15.00	3.06
Al (mg/L)	<0.02	<0.02	<0.02	0.03	<0.02	<0.02	<0.02	<0.02	<0.02	<0.02	0.09
V (mg/L)	<0.02	<0.02	<0.02	<0.02	<0.02	<0.02	<0.02	<0.02	<0.02	<0.02	<0.02
Mn (mg/L)	0.001	<0.001	<0.001	0.004	<0.001	<0.001	<0.001	0.001	0.001	0.010	0.001
Total Fe (mg/L)	<0.01	<0.01	<0.01	<0.01	<0.01	<0.01	<0.01	<0.01	<0.01	<0.01	0.02
Reduced Fe (mg/L)	<0.02	<0.02	<0.02	<0.02	<0.02	<0.02	<0.02	<0.02	<0.02	<0.02	<0.02
Co (mg/L)	<0.02	<0.02	<0.02	<0.02	<0.02	<0.02	<0.02	<0.02	<0.02	<0.02	<0.02
Ni (mg/L)	<0.02	<0.02	<0.02	<0.02	<0.02	<0.02	<0.02	<0.02	<0.02	<0.02	<0.02
Cu (mg/L)	<0.005	<0.005	<0.005	<0.005	<0.005	<0.005	<0.005	<0.005	<0.005	<0.005	<0.005
Zn (mg/L)	<0.005	0.028	0.015	0.034	0.012	0.018	<0.005	0.005	0.022	<0.005	<0.005
Cr (mg/L)	<0.01	5.24	0.95	<0.01	0.36	5.14	4.38	5.36	5.46	<0.01	<0.01
Mo (mg/L)	<0.02	0.21	0.09	<0.02	0.05	0.18	0.16	0.18	0.20	<0.02	0.06
Cd (mg/L)	<0.005	<0.005	<0.005	<0.005	<0.005	<0.005	<0.005	<0.005	<0.005	<0.005	<0.005
Pb (mg/L)	<0.10	<0.10	<0.10	<0.10	<0.10	<0.10	<0.10	<0.10	<0.10	<0.10	<0.10
As (µg/L)	<0.4	<0.4	<0.4	1.3	<0.4	<0.4	<0.4	<0.4	<0.4	0.5	0.5
Sc (µg/L)	<0.5	1070	55.5	4.5	52.0	1070	1030	1140	1310	<0.5	0.6
Th (µg/L)	n.d.	<0.018	<0.018	<0.007	<0.018	<0.018	<0.018	<0.018	<0.018	<0.007	0.010
U (µg/L)	n.d.	0.082	0.041	2.52	<0.022	0.023	<0.022	<0.022	<0.022	0.079	0.834

FIGURES

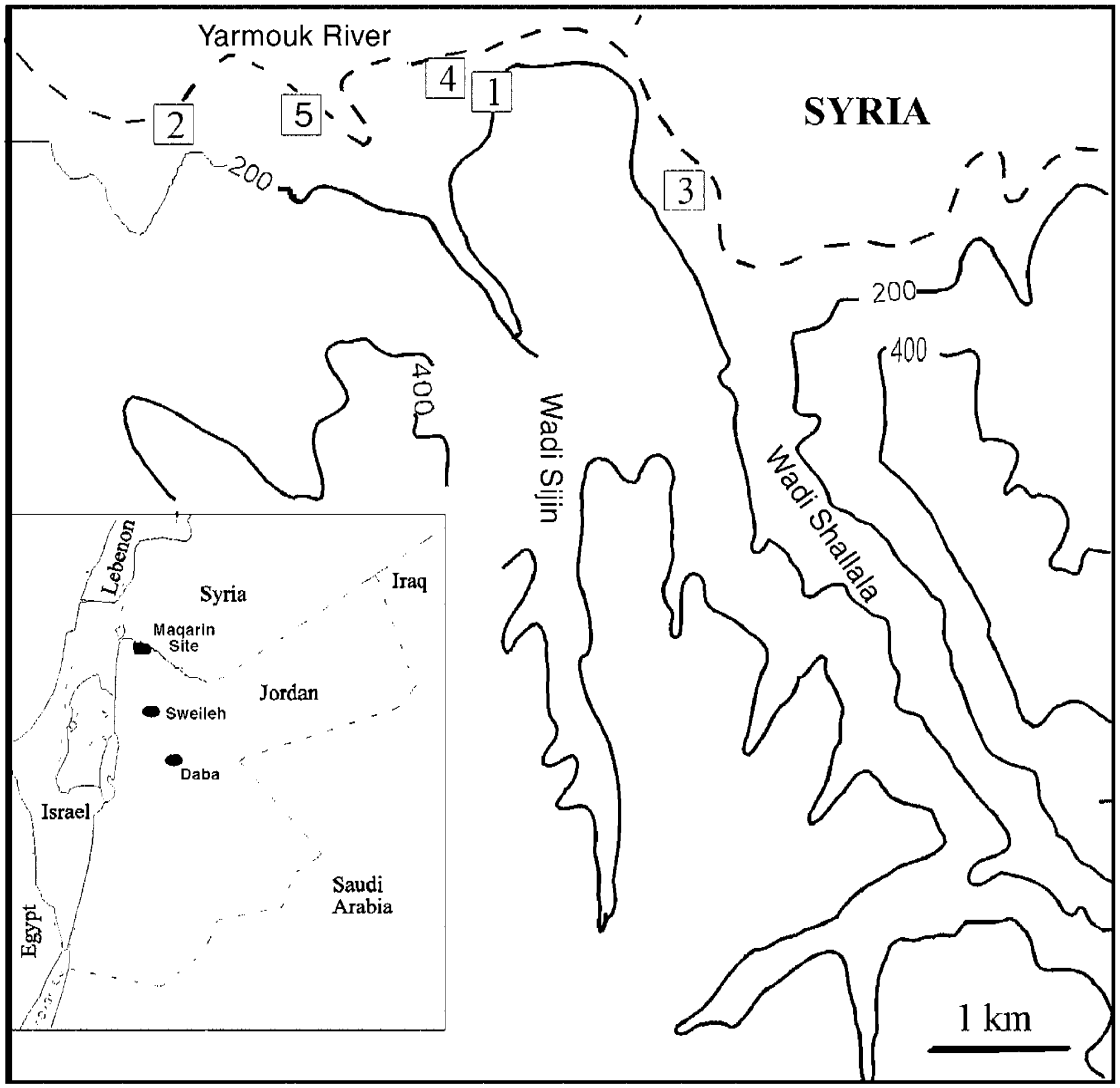

Figure 4-1. *Location of the Maqarin Natural Analogue Site, northern Jordan, and the main sites sampled (1 = Adit A-6; 2 = Western Spring seepages and Borehole WS1; 3 = Maqarin Station Railway Cutting and Borehole RW1; 4 = Eastern Spring seepages and Borehole M13; 5 = Borehole BH3). Inset shows the Sweileh site (near Amman) and the Daba site in central Jordan.*

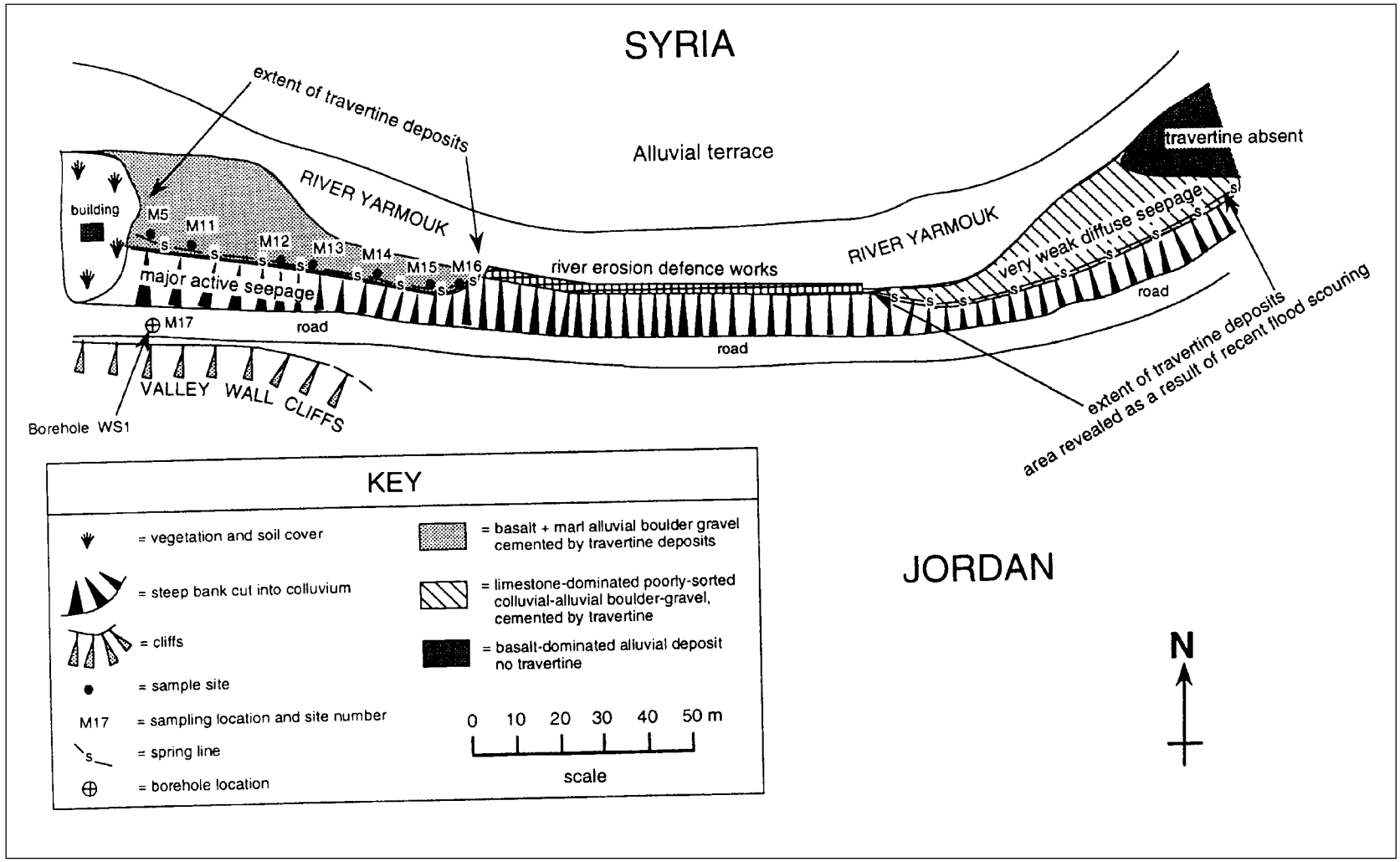

Figure 4-2. *Sketch-map of the Western Springs area showing the location of sampling points and the position of the hyperalkaline spring discharges, and the distribution of principal sediment types.*

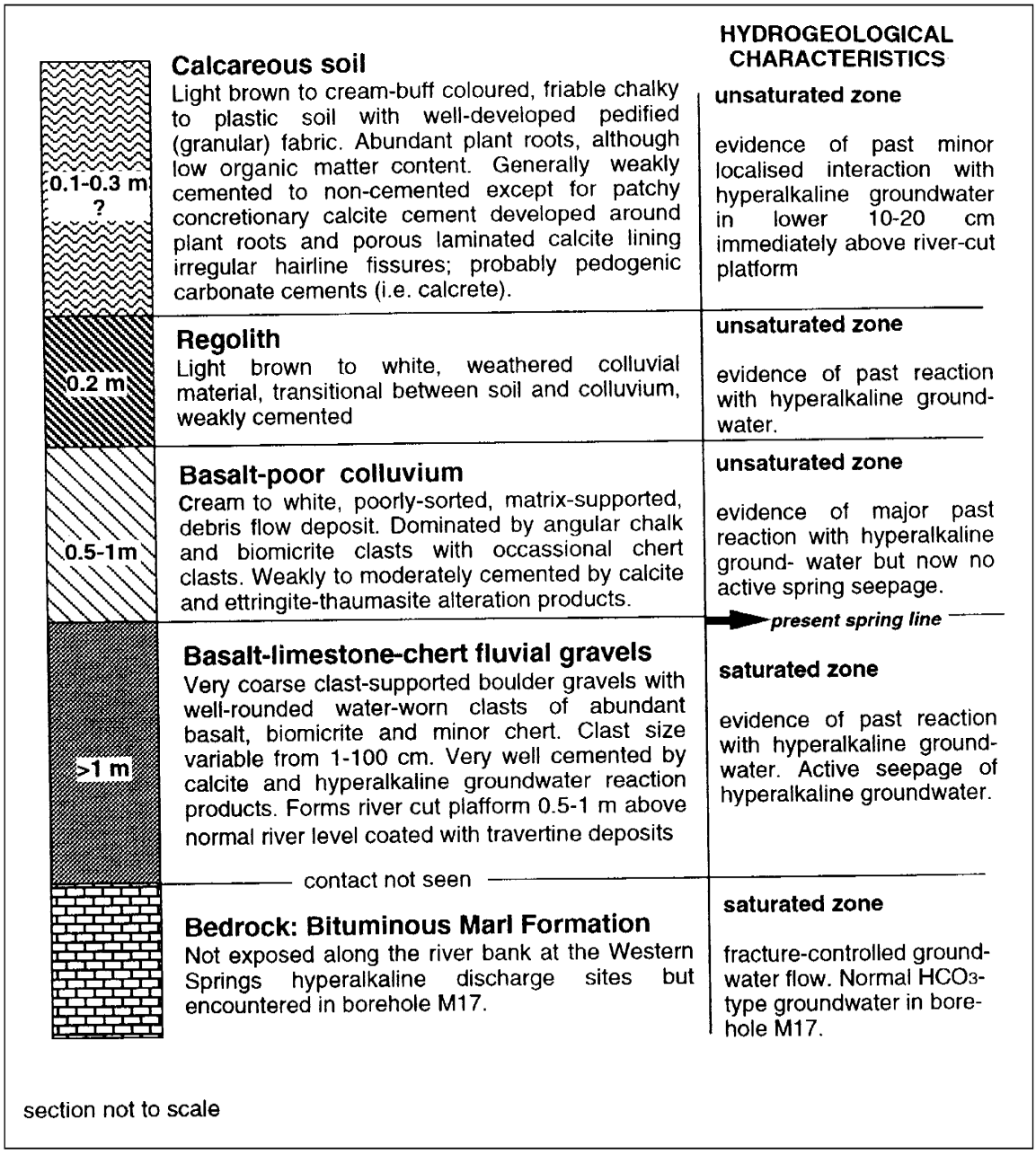

Figure 4-3. *Summary geological section of the Quaternary deposits at the M5 and M11-M16 sites, Western Springs area, Maqarin.*

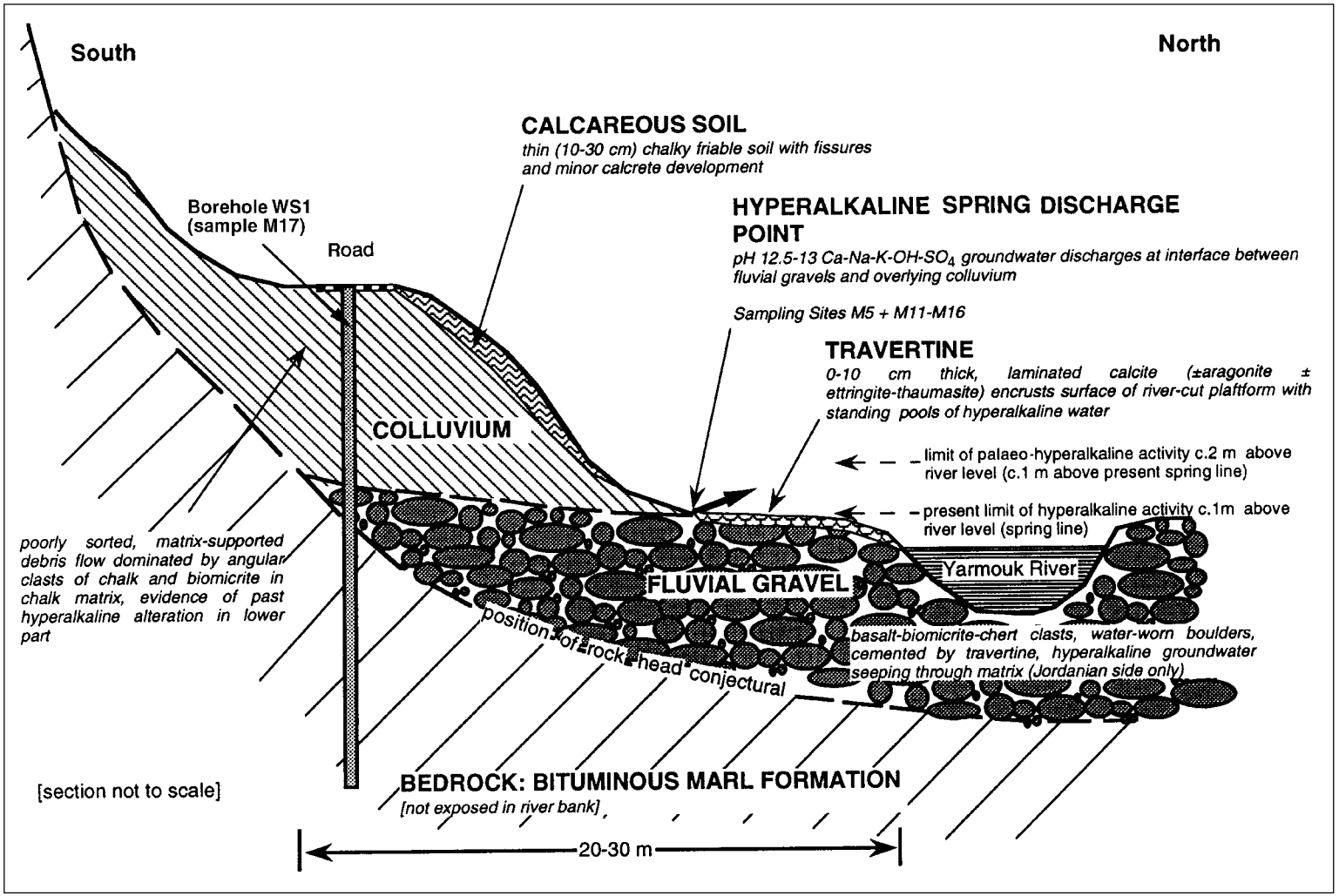

Figure 4-4. *Conceptual model of the Quaternary deposits at the Western Springs area, Maqarin.*

PLATES

Plate 4-1. *Hyperalkaline groundwater discharge from intergranular porosity and fractures in Quaternary colluvium and fluvial deposits on the bank of the Yarmouk River (Maqarin "Western Springs" – Sampling Site M5), and associated travertine deposits. The high pH water accumulates in pools in the surface of the zeolite-carbonate cemented colluvium and has a yellow-green coloration due to high chromate ion concentration.*

Plate 4-2. *Alluvial gravels containing large water-worn boulders of basalt (dark coloured), clay biomicrite limestone (cream coloured) and cherts (white) tightly cemented by zeolites and travertine (calcite, aragonite + ettringite-thaumasite). Maqarin Western Springs (Sampling Site M5 – camera lens cap shown for scale).*

Plate 4-3. *Teflon colloid sampling funnel installation, inserted into an alcove specifically cut into the tufa coating on the wall to intersect a major hyperalkaline flow at site M1 in Adit A-6. The teflon funnel is sealed into place with silicon sealant and coated with crushed and moulded tufa to prevent atmospheric contamination of the groundwater.*

Plate 4-4. *Sampling colloids under nitrogen overpressure at site M1, in Adit A-6.*

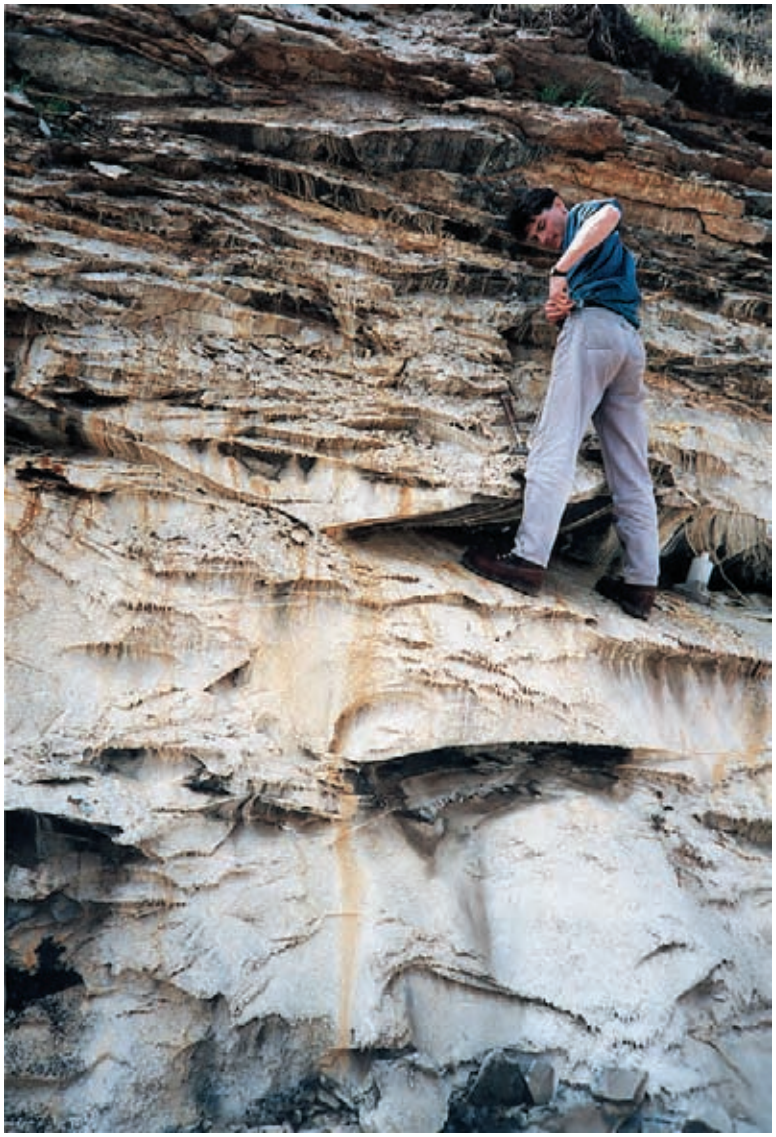

Plate 4-5. *Recent exposure of Bituminous Marl Formation clay biomicrite at site M8; a new road cutting about 100 m west of the Maqarin Station Railway Cutting. The rock face displays extensive seepage of hyperalkaline groundwater from numerous bedding-parallel fractures. The white tufa precipitates have developed in less than two years, and are stained brown by organic matter transported in the hyperalkaline water.*

5 MINERALOGY, PETROLOGY AND GEOCHEMISTRY

(A.E. Milodowski, E.K. Hyslop, J.M. Pearce, P.D. Wetton, S.J. Kemp, G. Longworth, E. Hodginson and C.R. Hughes)

5.1 INTRODUCTION

This chapter describes the detailed mineralogical, petrological and geochemical observations on the rockwater interaction associated with the active high-pH (pH up to 12.9) groundwater sites at Maqarin, and also of the now fossilised (palaeo) high-pH groundwater interaction sites from Daba, central Jordan. The study focusses primarily on the alteration of the silicate-rich lithologies represented within the Quaternary colluvium and fluvial deposits of the Maqarin Western Springs area, in contrast to the earlier Phase II investigations which largely examined the alteration of silicate-poor clay biomicrites from the Eastern Springs site. The principal objective of the study was to provide a detailed mineralogical and petrographic description of the effects of the system of rock-water interaction with the high pH Ca-K-Na-OH-SO_4 type hyperalkaline springs discharging through conglomerates and gravels containing silicate-rich rocks (basalt, chert), clay biomicrite ("marl") and limestone clasts. Specific objectives included:

(i) description of the alteration mineralogy and mineral paragenetic sequence;

(ii) provision of major and trace element mineral chemistry data for primary and secondary minerals;

(iii) provision of data on modal mineralogy of the colluvium and its components;

(iv) provision of data for whole-rock geochemistry;

(v) observations on the porosity characteristics of the system.

In addition, further mineralogical and petrological observations were made of the Eastern Springs area alteration associated with the high pH Ca-OH type groundwaters. In particular, Adit A-6 was studied to provide further information to:

(i) confirm and verify Phase II observations and conclusions;

(ii) attempt to elucidate the lateral extent of the migration and influence of the hyperalkaline plume;

(iii) investigate the effect of hyperalkaline groundwater-rock interaction on porosity in the clay biomicrite wallrock of the Bituminous Marl Formation;

(iv) obtain data on the mobilisation and distribution of uranium and other trace elements adjacent to flowing fractures in the Bituminous Marl Formation and an

assessment of rock-matrix diffusion characteristics in Adit A-6, This included the following observations:

- further information on fracture alteration mineralogy in Adit A-6;
- uranium mineralogy and quantitative distribution in the clay biomicrite and altered fracture wallrock;
- uranium distribution profiles in rock matrix away from fracture walls;
- U-series disequilibrium data for alteration profiles adjacent to fractures in the clay biomicrite.

5.2 MINERALOGY AND PETROLOGY OBSERVATIONS

5.2.1 General

The bulk and clay fraction (<2 μm) mineralogical data (determined by XRD) for the samples from both Maqarin and central Jordan areas are summarised in Tables 5-1 to 5-3. Whole-rock geochemical data for the Quaternary sediments (fluvial gravels and colluvium) at the Western Springs, and limited background data for the Amman Formation, Chalky Limestone Formation and Quaternary plateau basalts in the Maqarin area, are given in Table 5-4. The mineralogical and analytical protocol is detailed in Appendix G. For further information for background whole-rock lithogeochemistry of the Bituminous Marl Formation and the cement zone rocks (Metamorphic Unit) from Maqarin, the reader is referred to the Phase I and Phase II reports edited by Alexander (1992) and Linklater (1998).

5.2.2 Western Springs

General

The hyperalkaline groundwater of the Western Springs area discharges through a highly heterogeneous assemblage of Quaternary sediments. The sedimentology of the system is described in Chapter 4 and broadly comprises three discrete lithological types:

(i) a thin soil cover with a poorly-defined transitional zone of thin weathered, weakly-cemented colluvium ("regolith" or "nari") grading into the underlying colluvium;

(ii) an upper colluvium unit;

(iii) a lower fluvial boulder-gravel unit.

Most of the hyperalkaline groundwater discharge in the Western Springs area occurs through the lower fluvial boulder gravel unit. Consequently, most of the mineralogical investigations have been focussed on this lithology. The mineralogical characteristics of these units are described below.

Primary Mineralogy and Petrology of the Fluvial Boulder Gravels

General

This unit comprises coarse, clast-supported alluvial boulder gravel (clast sizes <1 cm to >1 m) with well-rounded water-worn boulders, cobbles and pebbles with an interstitial sandy matrix. Field clast counts in the M5-M16 area show that basalt is the dominant clast type (47%) with chert (11%) and micrite and microsparrite limestones (8%) as subordinate to minor components. A matrix of granule-grade clasts and sand to silt-grade material forms 34% of the volume of the gravel unit. An overall modal composition for the gravel has been estimated by combining the results of field clast counting (Chapter 4; Table 4-1) with results from point-counting analysis of two thin sections (samples C375 and C362) of the interstitial matrix material (Table 5-5). This indicates that the gravels comprise 58% basalt detritus, 12% micrite/limestone, 12% chert and 16% fine-grained matrix. Thin section point counting suggests that the gravels now possess only about 3% intergranular porosity in the Western Springs area.

Chert clasts are composed of fine-grained or cryptocrystalline quartz, although this may also include poorly crystalline or amorphous silica. No cherts were separated for geochemical analysis because they are considered to be essentially monominerallic silica. The limestone clasts are mostly fine-grained micrite, chalk and recrystallised microsparrite composed largely of calcite. Dolomicritic clasts are also present as a minor component and probably account for the presence of "ankerite" (essentially a ferroan dolomite) during XRD analysis of matrix material (Table 5-3). The limestone clasts are mineralogically and petrographically identical to the local *in situ* micritic limestones and chalks which were examined in detail during earlier Phase I and Phase II studies (Milodowski et al., 1992, 1998).

Varicoloured (reddish, yellow-orange and greenish) clasts of highly altered metamorphic cement zone rocks are also present as a minor component of both the fluvial gravels and the overlying colluvium deposits. These clasts are highly altered rocks which comprise an assemblage of fine-grained calcite, intimately intergrown with cryptocrystalline or amorphous Ca-S-Si-Al-rich material. The Ca-S-Si-Al-rich material could not be identified positively, but it is most probably ettringite or thaumasite. Corroded relicts of very altered fine-grained metamorphic calc silicate minerals (possibly spurrite, larnite or wollastonite) are present in some of these clasts. These metamorphic rock clasts are usually strongly leached and are microporous. It is not clear from the petrographic observation, whether the leaching and alteration of these clasts occurred before, or after, their deposition, in the Quaternary sediments. Clearly, this indicates that the gravels and colluvium contain detrital material that has been derived from the erosion of the cement zone. The inclusion of cement zone rocks within these sediments demonstrates, equivocally, that the combustion metamorphism at Maqarin must pre-date the deposition of these Quaternary deposits. However, the presence of altered metamorphic rock fragments within the Quaternary deposits complicates any interpretation of the water-rock interaction and evolution of the high pH plume in the Western Springs area. If the clasts were already altered (perhaps by hydration and leaching at their source) prior to deposition, then it is unlikely they are contributing to the development high pH groundwater within the Western Springs area. However, if the metamorphic clasts are actively altering and hydrating within the colluvium and gravel, then they represent the presence of a "cement-zone" locally within the Western Springs Quaternary deposits.

BSEM-EDXA and optical petrographic observations reveal that much of the sandy matrix of the gravels consists of sand- and silt-grade calcite, quartz, and chert with subordinate to minor amounts of augite, olivine and plagioclase derived from basaltic detritus. Detrital grains of apatite-rich material (probably derived from local phosphorite horizons interbedded with the sequence of Cretaceous and Tertiary chalks and micritic limestones at Maqarin) are common accessory minerals in the matrix.

Petrology of the Basalt Clasts

Three representative basalt clasts (C362, C368 and C375) were selected from the gravels for detailed modal analysis. The objective was to characterise the mineralogical and geochemical variation in the basalts to provide primary data for interpretation of alkali alteration. The modal analyses of these clasts are given in Table 5-5 and their chemical composition is shown in Table 5-4.

Most of the basalt clasts present in the gravel deposits are alkali olivine basalt but lesser amounts of an olivine-free enstatite variety of basalt (e.g. C375) are also present. The basalt clasts typically have a fine-grained groundmass of randomly-orientated plagioclase laths (typically <0.4 mm long) with interstitial anhedral granular greenish augitic clinopyroxene (<0.3 mm grains), and finely-disseminated Fe-Ti oxides (magnetite, ilmenite). Fine-grained Fe oxides are commonly developed along the cleavage planes of the augite. Olivine (intermediate Mg-Fe variety) is present in most basalt clasts, varying in size from macroscopic single crystal phenocrysts and glomerocrysts up to 1.7 mm across to very fine microscopic groundmass material. In olivine-free basalt, enstatite phenocrysts are present in place of olivine. Apatite is present as a trace primary mineral; trace to minor interstitial K-feldspar was also identified in some cases. Some clasts display weak pervasive alteration of feldspar to white mica, giving the feldspar a dusty appearance. The matrix in some clasts may also contain interstitial glass, which locally is altered to very fine-grained secondary? clay minerals and haematite. Clay minerals are green-brown in colour and are typically concentrated around primary vesicles (cavities formed by gas bubbles in the original lava). Vesicles can comprise 0–15% of the basalt volume; they are irregular in shape and are commonly interconnected, at least on a thin section scale, and are typically about 0.5–1 mm in size. Calcite as well as clay minerals may line vesicular cavities. Many basalt clasts also show a fine alteration rim of secondary Fe oxide or oxyhydroxide. In section, this can be seen to be partly due to the oxidative alteration (with liberation of Fe) of primary Fe-Ti oxides and augite at the margins of the clast. This alteration is evident on clasts within and outside the areas influenced by hyperalkaline groundwater discharge; therefore, the alteration is probably related to weathering phenomena.

Comparison with Background In Situ Quaternary Basalt

Two samples representative of the local *in situ* Quaternary plateau basalt in the Maqarin area were also examined in thin section (C782 – massive basalt, and C783 – vesicular basalt). Both samples are similar in mineralogy and are olivine basalt with olivine as the sole phenocryst phase (3–5% by volume). Olivine phenocrysts are subhedral to euhedral, varying in size from 1.5 mm down to grains which cannot be distinguished

from the fine microcrystalline groundmass. Glomerocrysts, composed of small clusters of olivine microphenocrysts, are present in C782. The olivine is essentially unzoned and Mg-rich, close to Fo_{89} (forsterite-rich) in composition. Most olivines are fresh, although some crystals display some red staining at their margins due to oxidative weathering. Chromite or magnetite inclusions are present in most olivine crystals. The groundmass of the basalts is also fresh and unaltered, and shows an intergranular to intersertal texture. It is composed dominantly of plagioclase, with interstitial augite and minor Ti-Fe oxides (magnetite and ilmenite) and small patches of cryptocrystalline material (?glass). Plagioclase laths vary from randomly orientated to patches showing flow-alignment, and reach up to 0.5 mm in length. Compositionally, they appear to be oligoclase to andesine. Augite is generally anhedral, either rounded or lath-like, and reaches 0.2 mm in length. It is mostly pale brown in colour and may show some zonation, becoming more Fe-rich at the margins. Augite becomes the dominant component in the groundmass around vesicles, suggesting segregation of the residual dregs of melt during the final stages of crystallisation there.

In C782, vesicles comprise <5% of the basalt volume. However, in C783, vesicles are much more abundant, comprising 10–15% of the rock volume. Fine clay-like alteration is evident around the margins of some vesicles and it is tentatively suggested here that this is probably smectite or smectite-chlorite intergrowths. However, more detailed investigation is required to confirm the identity of the clay alteration. A chemical analysis of the massive basalt (C782) is included in Table 5-4.

Chemically and mineralogically, the dominant olivine basalt clasts in the fluvial gravels and the local *in situ* plateau basalts are very similar. Therefore, it is considered that the basalt clasts are most probably only of local derivation.

Primary Mineralogy and Petrology of the Colluvial Deposits

The colluvium is dominated by clasts of micritic limestone and chalks. The deposits are typically poorly-sorted and variable in fabric from matrix- to clast-supported material. The clasts are mineralogically similar to the local micritic host rocks from which they are largely derived (Chalky Limestone Formation). However, basalt fragments are also present in the lower part exposed in the river bank. In part this probably represents admixture with material from the top of the underlying basalt-rich fluvial boulder gravel unit. The colluvium has a sticky (when wet), fine-grained, chalky, silty, micritic, calcite and clay matrix, probably largely derived from weathering of the dominant chalky and micritic carbonate local rocks.

XRD analyses (Tables 5-2 and 5-3) show the matrix material to be composed of calcite with minor quartz, ankerite, fluorapatite and very small amounts of clay minerals. The clay mineralogy includes: kaolinite, mica (including illite) and possibly traces of smectite. This is broadly comparable with the mineralogy reported previously for the local micritic limestones and chalks by Milodowski et al. (1998).

Secondary Alteration Characteristics of the Quaternary Sediments

General

XRD analysis of the untreated matrix material from the fluvial gravel (Table 5.2) indicates that it is predominantly composed of calcite. Minor constituents include quartz, augite, ankerite, hematite and fluorapatite, which are all part of the primary assemblage. Ettringite, thaumasite, bentorite and gypsum represent the dominant (crystalline) secondary alteration minerals (in addition to major calcite). A diffraction peak at approx. 8.8 Å was tentatively attributed to the zeolite epistilbite in one of the samples (C372). Unfortunately, this mineral could not be identified unambiguously. Nevertheless, it is consistent with the previous observations of poorly-crystalline zeolitic material of dachiardite composition – which were also tentatively detected by XRD during a more limited examination of Western Springs alteration assemblages within the Phase II study (Milodowski et al., 1998). In an attempt to try to concentrate and improve XRD detection and identification of the silicate phases, samples of gravel matrix were acid leached to remove calcite. This removed most, but not all, of the calcite present. However, the leaching did enable the positive identification of trace detrital constituents such as albite, K-feldspar, kaolinite and 'mica'.

The acid leached, <2 μm fraction XRD analysis, produced disappointing results. Although kaolinite was identified in most of the samples, with 'mica' and possible smectite in C370 and C372, the XRD patterns generally presented a broad indistinct diffraction band from approx. 17 to 10 Å making identification of clay minerals difficult or impossible. The broad band may reflect the presence of poorly-ordered clay minerals in the gravel matrix samples, or may have been caused by the alteration of CSH/CASH phases (known to be present from the petrographic observations) that may have been de-stabilised under the laboratory acid-leaching protocol.

The gravel matrix is essentially cemented by very fine-grained secondary minerals that are largely the result of precipitation from, and reaction with, the hyperalkaline groundwaters. All the samples of fluvial gravel examined from the Western Springs displayed variable degrees of alteration of basalt, clay biomicrite and chert clasts, and of the matrix. Most of the alteration is too fine-grained to be observed in detail by optical petrographic techniques. However, detailed observations by BSEM-EDXA revealed a complex alteration fabric. Compositional data, obtained by EMPA and ATEM, for the high-pH groundwater alteration products in the fluvial gravels and colluvium, are tabulated in Appendix H. These data have been plotted also as molar proportions $[Ca+Na_2+K_2]$:Si:Al in Appendix H, for comparison with the compositional fields of known minerals. This approach was used effectively in Phase II (Milodowski et al., 1998) to help define and constrain the identities of the poorly crystalline CSH, CASH and zeolitic gels that are typical of the low-temperature alteration products associated with these high-pH groundwater systems at Maqarin.

Reactivity of the Primary Components

The clay biomicrite clasts generally show relatively minor leaching. However, some clasts have apparently significant secondary porosity (visually estimated at approx. 20% in some cases). This secondary porosity is associated with the dissolution of matrix dolomite and is typically infilled by a structureless, microporous, Ca-Si-S-Al-rich

material (Appendix I; Plates I-1 and I-2). Dolomicrite fragments are particularly susceptible to dissolution and secondary porosity formation. Generally, the style of alteration seems to be similar to that described in earlier studies of altered fractured "Bituminous Marl" wallrocks in Adit A-6 and the Maqarin Station Railway Cutting (Milodowski et al., 1998), and is probably largely ettringite-thaumasite dominated. Unfortunately, in the Western Springs samples examined, this alteration is too fine-grained and too intimately admixed with the host rock minerals to enable reliable compositional information to be obtained by EMPA or BSEM-EDXA.

Chert clasts show variable reaction with the high pH fluids. In sample C362, the alteration appears to be largely dissolution of the cryptocrystalline silica and its replacement by fine-grained calcite or aragonite around clast margins (Appendix I; Plate I-3). In other samples (e.g. C365, C374), BSEM observations revealed that some cherts have been completely dissolved and replaced by amorphous (isotropic) gel-like CSH minerals. Most chert reaction products appear to be Al-substituted CSH gels broadly similar to those seen cementing the matrix of the basal colluvium and fluvial gravels. Any Al present in the alteration products must have been derived externally to the chert clasts, since these are essentially pure silica. It is most likely that the Al is locally derived from the porewaters, and was liberated to the porewaters during alteration of adjacent basalt and/or clay biomicrite clasts. However, in the case of C374(2), ATEM data indicate that the alteration product is a Mg-rich CSH gel of variable composition (Appendix H; Table H-11).

Basalt clasts are the most reactive components, both in lower part of the colluvium sequence, where it is affected by hyperalkaline groundwater (e.g. C365), and in the fluvial boulder gravels. The clasts commonly develop significant reaction rims with the formation of major secondary CSH and CASH alteration products. The most reactive phase in the basalt is the interstitial glass. The glass is extensively dissolved and corroded, or replaced by CASH minerals and Fe oxides/oxyhydroxides, around the margins of clasts, and adjacent to vesicles filled by hyperalkaline alteration products (Appendix I; Plates I-4 – I-6). Plagioclase is also very reactive (Appendix I; Plates I-7 – I-9), but less so than glass (Appendix I; Plates I-5 and I-6). Typically it is severely corroded with a gel-like CSH/CASH alteration product replacing it (Appendix I; Plate I-10) for up to 3 mm into some clasts. Dissolution of plagioclase occurs preferentially along cleavage planes. Some basalt clasts also contain minor amounts of K-feldspar. This too, is highly reactive and where exposed at the clast surface is largely replaced by secondary CASH minerals. Possibly, it is more reactive than plagioclase. Augite, hypersthene and olivine are comparatively unaltered (e.g. Appendix I; Plate I-11). These minerals are commonly fresh, although they may exhibit some minor dissolution and corrosion effects where exposed at clast margins (Appendix I; Plate I-12).

Similar reactivity is seen in the sand-silt matrix. Plagioclase is invariably highly corroded, and is often present only as trace relicts within a groundmass of fine CASH gel. Detrital quartz and chert grains may also be highly corroded and replaced by CASH minerals (e.g. Appendix I; Plate I-13). Apatite, augite, olivine and calcite microfossil detritus are comparatively unaltered (Appendix I; Plates I-8 and I-9).

Organic fragments (largely abraded detrital woody plant stems) are common components in the fluvial gravel matrix. These fragments are variably altered; some showing no evidence of alteration, whilst other fragments exhibit calcite infilling of cellular cavities (Appendix I; Plate I-14), and partial replacement of cellulose cell wall

tissure by calcite (Appendix I; Plate I-15) and a Cr-rich ettringite-like mineral (Appendix I; Plate I-16). Calcite, apatite and Ti-Fe oxide material in the matrix and clasts of these sediments are largely unaffected by dissolution. Calcitic microfossil detritus is often fresh and well preserved (Appendix I; Plate I-17), although, microfossil cavities are commonly lined by fibrous CSH minerals (Appendix I; Plate I-18) and/or ettringite-thaumasite-like calcium sulphosilicate.

From a qualitative visual comparison of all the samples studied, an overall scale of reactivity of the different mineralogical components within the colluvium and fluvial gravels has been summarised in Table 5-6. Overall, it appears that quartz, chert, K-feldspar, glass and plagioclase are the most reactive minerals or phases present in the Quaternary sediment; dolomite is moderately reactive; augite, hypersthene (orthopyroxene) and olivine are weakly reactive; and calcite, apatite and Ti-Fe oxides appear to be largely unreactive. The width of the reaction rims on the different clasts, developed by the hyperalkaline interaction, varies considerably from clast to clast, between clasts around a single pore, and even within a single clast. Basalt clasts show the narrowest alteration rims, typically between 100 mm and 1 mm wide. Clay biomicrite (marl) clasts are often altered over a wider interval (up to several millimetres), the alteration affecting the interstitial clay and silica, but leaving the major calcite largely unaltered. The wider alteration rim in the marl appears to be due to its high degree of microporosity (of the order of 30%), which allows greater fluid access to the rock matrix. In contrast, the basalt and chert clasts have little matrix porosity. Consequently the depth of alteration is much more limited, although their individual mineral components may be more reactive than the marl minerals.

Early Colluvium Fabrics

The colluvium has a texturally very complex fabric. Petrographic observations reveal that the matrix has a well-developed close-packed and compacted "granular" fabric. The "granules" themselves comprise a close-packed aggregate of finer silt, sand and clay-grade detritus (Appendix I; Plates I-19 and I-20). The "granules" display irregular "intragranular" shrinkage cracks. Observations also show that the aggregate granules appear to have suffered multiple shrinkage and fracturing, disaggregation and re-agglomeration. Fine (<1 mm), irregular, "extra-granular" fractures cut through the colluvium. These are filled with fine micritic calcite or silica-rich clay-like detritus largely washed-in. In many cases, these show evidence of repeated fracturing and filling. In more porous domains, "bearded" fabrics (i.e. fines deposited on the underside of clasts) may be developed. This suggests physical internal sedimentation of elutriated fines from meniscii films of pore water. These fabrics are interpreted to be related to pedogenic (soil-forming) processes in which the "agglomerated granules" (peds) are probably formed by complex and repeated wetting, drying and shrinkage, accompanied by elutriation and mobilisation of fines under unsaturated conditions.

Some of the colluvium contains fine (<1 mm) irregular fissures lined by micritic, powdery calcite. Calcite cementation also occurs locally in the matrix, in diffuse irregular patches, and more commonly is concentrated around *in situ* plant roots. This type of alteration and mineralisation fabric development is also probably pedogenic in origin, rather than related to interaction with the hyperalkaline groundwater. It is texturally very similar to the soil carbonate cementation (calcrete/nari or caliche

formation), under evaporative conditions in the unsaturated zone or in a zone of fluctuating groundwater level, typical of arid and semi-arid environments described from both fossil and modern systems (e.g. Arakel and McConchie, 1982; Strong and Milodowski, 1987; Chapter 3, this report). However, the fabric is overprinted in the lower part by the high pH groundwater alteration effects.

Phase Chemistry

The secondary alteration products are largely poorly crystalline. With the exception of ettringite and calcite, they give virtually no X-ray diffraction pattern, suggesting that they have limited structural order. Most are generally difficult to distinguish by qualitative BSEM-EDXA and optical techniques. However, they exhibit a range of morphologies including: isotropic low birefringent gels, fine sheet-like morphology, and fibrous morphology. ATEM and EMPA analyses show that the compositions of the hyperalkaline alteration products (Appendix H; Figs. H-1 to H-3) identified in the Western Springs area fall into four quite distinct compositional groups (calcite is not included here):

(i) Gel phases with compositions falling within the range of compositions expected for zeolites (Appendix H; Figs. H-1a, H-1b and H-2a). These range from high-Si phases close to dachiardite (ideally $[Ca,Na,K]_3Al_4Si_{18}O_{45}\cdot 14H_2O]$), to Ca-rich phases close to wairakite (ideally $CaAl_2Si_4O_{12}\cdot 2H_2O$).

(ii) Gel-like Al-poor calcium silicate hydrate (CSH) phases with compositional range from approx. Ca:Si = 0.67 – i.e. close to gyrolite, to approx. Ca:Si =1.63, i.e. close to afwillite or jennite (Appendix H; Figs. H-2c, H-2d and H-3b). Most compositions show a small amount of Al in the structure. Occasionally these compositions exhibit fibrous morphology. Possibly these are analogous to the tobermorite- and jennite-structured gels, CSH(I) and CSH(II) respectively, found in hydrated Portland cements (Lea, 1970).

(iii) Gel-like and fibrous, but Al-substituted CSH phases (CASH) showing ranges in composition broadly parallel to the CSH gels (see (ii), above), but intermediate in composition between: zeolites and CSH gels at the low Ca:Si end of the range; and hydrogarnet and CSH gels at the high Ca:Si end of the range (Appendix H; Figs. H-1d to H-2c).

(iv) Fibrous ettringite with some Si substitution suggesting compositions intermediate between ettringite and thaumasite (Appendix H; Figs. H-2b and H-2c).

Both ATEM and EMPA data for the same samples are in general agreement, and the compositions of these alteration products are broadly similar to those identified during Phase II – from the alteration of clay biomicrite in Adit A-6 and from preliminary analyses of colluvium alteration in the Western Springs (Milodowski et al., 1998). However, the preliminary analyses of the basalt colluvium alteration products, undertaken during Phase II, suggested that the major alteration products were restricted to calcite, ettringite-thaumasite and zeolitic, gel-like to fibrous, CASH phases with a composition restricted to the high-Si dachiardite and calcium mordenite (ideally $[Ca,Na_2,K_2]\ Al_2Si_{10}O_{24}\cdot 7H_2O]$) end of the spectrum. Discrete crystalline CSH and Al-

substituted CSH minerals were not recognised. The new data presented in this report indicate that there is a much wider range of phases and compositions than previously expected, and that, despite the marked difference in primary mineralogical assemblage, the alteration products of the basalt-rich gravels and colluvium are broadly similar to those encountered during the alteration of clay biomicrite in Adit A-6. The alteration products typically exhibit the complete range of compositions within a small area (typically a few tens of microns of the same sample).

The major difference in alteration assemblages is the greater abundance of "zeolitic" material in the Western Springs. This probably reflects the greater availability of Al in the primary source material (major basalt component). In contrast, the Al source in the primary clay biomicrites was very restricted; clay minerals comprising typically <5% of the total rock mass.

Porosity Characteristics

Attempts were made to quantify porosity fabrics by Image Analysis (IA) of optical fluorescence microscopy images. In both the colluvium and fluvial gravel samples from the Western Springs, it was found that the UV-resin pervasively stained large areas (e.g. Appendix I; Plate I-20). In addition it was found that the flourescence from resin, which had penetrated extensively into the sub-micron microporosity within and between fibrous and gel-like, CSH, CASH and ettringite-thaumasite, could not be resolved optically to discrete pores. It produced a background "continuum" of "body" fluorescence from this microporous (?nanoporous) material, obscurring any fine detail. Under UV-fluorescence microscopy, the larger clasts can be clearly identified as non-fluorescent areas. However, large areas of the matrix are extensively stained by the UV-resin This is due to its very fine-grained nature with abundant microporosity. Therefore, discrimination of truly open voids is difficult as many areas have fluorescence intensities very similar to the resin such that the fine-grained zeolitic laths that line many of these pores are typically obscured. Nevertheless, although much of the fine structure of the colluvial matrix cannot be observed by UV-fluorescence microscopy, clearly this must contain significant interconnected microporosity.

Mineral Paragenesis

The earliest alteration seen in both the colluvium and fluvial gravel is the formation of a thin veneer of iron oxide or oxyhydroxide or iron-stained clay which coats clast surfaces. This probably formed, not as a result of alkali groundwater interaction, but as a result of weathering oxidation in the colluvium and infiltration of clay detritus through the sediments.

Within the replacement alteration rims of component clasts it is extremely difficult to determine the mineral paragenesis. Many of the alteration products are too fine to resolve as discrete crystals under BSEM or optical microscopy, and petrographic relationships determined from ATEM observations are limited to very small areas and the observations are somewhat ambiguous. However, the mineral/phase relationships can be seen relatively clearly within the coarser intergranular porosity between clasts, or within vuggy cavities in the basalt. Mineral paragenetic fabrics are particularly well-

developed in sample C365, which contains an irregular mineralised fissure network within the basal part of the colluvium (e.g. Appendix I; Plate I-21).

The earliest secondary phase formed is a very hydrous, Ca-K-Na-Al-silicate ("Phase 1", Appendix I; Fig. I-5) which has a very low backscatter coefficient (i.e. appears dark on BSEM images). It occurs as fibroradiate to acicular to prismatic crystals growing from the surfaces of basalt clasts and other silicate detritus, and rests on the early iron oxide or oxyhydroxide veneer (Appendix I; Plate I-22). Electron microprobe (EMPA) analyses show that compositionally this phase falls within the zeolite compositional field (Appendix H; Figs. H-1, H-2 and H-3). Although the composition ranges from mordenite to laumontite/wairakite, most of the analyses are much more tightly clustered and fall between laumontite/wairakite-type and epistilbite-type compositions.

The "zeolitic" phase is followed by the precipitation of a CSH gel with variable Ca:Si ratio covering the range CSH(I) to CSH(II) (or their crystalline equivalents e.g. suolinite to afwillite), or its Al-substituted equivalent CASH phase ("Phase 2", Appendix H; Fig. H-2a). In some samples this phase is Al-rich, in others it is Al-poor, probably reflecting the local availability of Al. This phase occurs as colloform "gel-like" coatings on clasts, or forming an intergranular pore-filling cement, which also encloses and replaces the earlier-formed zeolitic material (Appendix I; Plates I-21 and I-22). Most compositions fall largely within the Ca:Si range expected for tobermorite-type CSH(I) compounds. However, the more Al-rich variants are significantly more aluminous than the previously described natural aluminous tobermorite-structured mineral – tacharanite (e.g. Appendix H; Fig. H-2a). This in turn is followed by the precipitation of a progressively more Si-rich CSH gel with an okenite-like composition ("Phase 3") and is finally encrusted with a low Ca:Si ratio CSH phase, with well-developed fibrous morphology (Appendix I; Plates I-21 and I-22), similar in composition to truscottite or an Al-substituted equivalent compound ("Phase 4", Appendix H; Fig. H-2a).

The latest stage of alteration observed is the replacement of the CSH and CASH phases by calcite or aragonite. The carbonate forms a skin encrusting the outer surface of the CSH or CASH minerals where they are exposed to the open porosity. Here the calcite (or aragonite) locally fills between, or replaces the fibres of the CSH/CASH mineral. Carbonate replacement possibly results from reaction of the CSH/CASH minerals with atmospheric carbon dioxide, which may diffuse into the surface of the colluvium and gravel as the system seals up and the groundwater flux through the sediments is reduced

The paragenesis is summarised below:

(1) ZEOLITE GEL

Mainly Ca-rich – laumontite/wairakite and epistilbite

(2) CSH(I)-TYPE GEL or Al-SUBSTITUTED CASH EQUIVALENT

Ca:[Si+Al] = 0.67 to 1.63

(3) LOW Ca:Si CSH or CASH GEL

Ca:[Si+Al] = 0.67 to 0.5

(4) VERY LOW Ca:Si CASH GEL

Ca:[Si+Al] $\leq$ 0.5

(5) CALCITE or ARAGONITE + ETTRINGITE-THAUMASITE

The overall paragenesis and alteration process affecting the Western Springs is summarised in Figure 5-1. Although the alteration mineralogies are similar, the paragenetic sequences of minerals observed in the Eastern (see Phase II study) and Western Springs areas of Maqarin are reversed. The paragenesis at the Western Springs can be interpreted as follows:

(i) The "First Impact of Alkaline Plume" (Figure 5-1) resulted in the formation of Ca-rich zeolite or zeolitic gels as early-formed products at the "front-edge" of the alkaline plume.

(ii) As the plume front migrated forward and pH rose at the Western Springs, and the zeolitic alteration products became unstable, they were partially replaced and enclosed beneath a reaction rim of CSH or Al-substituted CSH minerals ("High pH Overprint"; Figure 5-1). The early-formed zeolites were preserved by the formation of the layer of CSH alteration products which armoured them, protecting the zeolite from complete reaction.

(iii) The porosity and permeability of particular horizons of colluvium and gravel decreased through cementation by secondary alteration products. Consequently, with a reduced flow, the groundwater became more rock-buffered, and pH decreased and sulphate increased. This resulted in the formation of ettringite and thaumasite mineralisation (Waning System; Figure 5-1).

(iv) Eventually, further cementation of gravels and colluvium reduced groundwater flow to the point where atmospheric CO_2 could "back-diffuse" into the cemented colluvium and gravel, reacting with the CSH alteration products to form secondary carbonate mineralisation (Waning System; Figure 5-1).

In the Eastern Springs fracture mineralisation (Phase II study; Milodowski et al., 1998), CSH minerals were formed early in the paragenesis, close to the cement zone. The groundwaters discharging from the cement-zone, into fractures in the immediately adjacent marl, would probably have achieved a high pH very rapidly. Consequently, CSH phases formed rather than zeolite, which is stable at lower pH (see also Chapters 7 and 8). Zeolite could only form late in the paragenesis, in a waning fracture flow-system, when the groundwater flow decreased through fracture mineralisation and cementation. During this late stage, the pH would have decreased and the aqueous concentrations of Si and Al would have increased in the slower-flowing fracture

porewaters, through increased residence time (i.e. longer rock-water interaction). Consequently, zeolite precipitation became stabilised.

Sr Isotopes

Strontium isotope data for a limited suite of samples representing some of the rock-types in the area are presented in Table 5-7. Data for Western Springs hyperalkaline groundwater (Site M5), and bicarbonate-type groundwaters from the underlying Amman Formation aquifer (Site M9) and from the background Chalky Limestone Formation aquifer (Site M17), are also shown for comparison. Strontium isotope data were also obtained for the Quaternary basalts, which represent the uppermost aquifer system. It was hoped that the strontium isotopic signatures in groundwaters might be of value in reflecting the isotopic composition of lithologies along the flow-path of the hyperalkaline groundwater, and so help constrain the origin of its geochemical characteristics (in particular, the source of the high K and high Na).

In reality, the data-set is too limited to fully evaluate the range of lithologies in the Maqarin area. Nevertheless, the data do suggest that the different formations are isotopically distinct. The $^{87}Sr/^{86}Sr$ ratio increases (i.e. becomes more radiogenic) from the Amman Formation (represented by the datum for the silicified limestone), through the Chert Chalky Limestone Member to the cement zone (Adit A-6). Comparison between the data clearly indicates that the Western Springs groundwater $^{87}Sr/^{86}Sr$ signature is very similar to that of the cement zone.

Nevertheless, there is nothing to indicate any significant component of any other groundwater, either the Amman Formation, or high-level groundwaters from the Quaternary basalts, reflected in the Sr signature of M5 (Western Springs). This is discussed in more detail in Chapter 6.

5.3 MATRIX DIFFUSION STUDIES IN FRACTURED CLAY BIOMICRITE

5.3.1 Introduction

The objective of this part of the programme was to test whether the matrix of the clay biomicrite host rock in Adit A-6 has been affected by hyperalkaline groundwaters, and in particular whether the host rock around water-conducting fractures has undergone mineralogical and geochemical changes caused by hyperalkaline groundwater interaction. To this end, a series of actively flowing fractures in Adit A-6 were sampled (Fig. 5-2) to obtain profiles perpendicular to the fracture orientation through the host clay biomicrite. It was intended to collect large profiles of up to a metre in length, but it was not possible to obtain fracture-free host rock over distances greater than 10 cm before another fracture, or water-conducting joint, was encountered.

Four individual profiles were selected for study, primarily on the basis of observed macroscale wallrock alteration around the fractures (Figs. 5-3 – 5-5; Appendix J). Two profiles were examined in detail, and the remaining two in less detail. A series of

polished thin sections (PTS) were prepared along each profile for uranium and optical petrological studies. This involved the use of the following techniques: Fission Track Registration (FTR), Electron Microprobe Analysis (EMPA), Laser Ablation Microprobe – Inductively Coupled Plasma – Mass Spectrometry (LAMP-ICP-MS) and Backscattered Scanning Electron Microscopy – Energy Dispersive X-ray Spectra (BSEM-EDXA).

A series of rock slices were cut from the profiles for bulk-rock geochemical analysis for major and selected trace elements by XRF and ICP-MS. Porosity/permeability studies were undertaken on these same materials.

The four samples used in the diffusion profile studies (Fig. 5-2) are C353, from 108 m into Adit A-6 (2 m outside the cement zone), C357 and C358, both from 53 m into the adit, and C359 from the M2 groundwater sampling site at 45 m distance. Locations of the samples analysed and a graphical presentation of the geochemical data are detailed in Appendix J.

Uranium values were determined by track-counting from FTR prints at 1 mm intervals along profiles from the vein or wallrock edge into the enclosing host rock. The results were then plotted up as a U profile for each of the four samples. The PTS were then analysed using LAMP-ICP-MS along the same profiles for the elements Al, Ca, Cr, Co, Se, Sr, Zr, Mo, Cs, Ba, Pb, Th and U. These data were plotted as profiles also. Data from FTR, bulk rock geochemical analysis and EMPA results were compared with the LAMP-ICP-MS data and used for ICP-MS calibration purposes. Bulk geochemical data were also plotted as a series of profiles, so that all the data could be easily compared (Appendix J).

The bulk geochemical data (Table 5-8) shows that the geochemistry of the sample from close to the cement zone (C353) is different from the other samples from nearer the adit entrance. The C353 analyses have higher Si, Ti, Al, Fe, Mn, K, P and lower S and Loss-on-ignition (LOI; representing volatiles). The trace elements are also higher (commonly twice as much) in Cr, Co, Ni and Sr, and very much higher in Zr, Cs, U and Th. Although it is possible that rock this close to the cement zone has been affected by hyperalkaline fluids, which have significantly changed the bulk composition of the clay biomicrite, it seems more likely that many of the differences are primary compositional differences due to changing stratigraphic levels of the clay biomicrite intersected by the adit.

5.3.2 Sample C353

General

Sample C353 consists of a complex banded vein approx. 15 mm thick, with a highly altered wallrock zone (14–20 mm wide) where the grey-coloured clay biomicrite host rock is altered to a mottled brown colour, containing fine banding parallel to the fracture. Small dark spots are present throughout the altered zone. The 0–15 mm geochemistry subsample contains this alteration zone and includes a single ettringite-bearing microvein (<0.2 mm thick) perpendicular to the main vein. The 15–30 mm subsample includes the outer part of the mottled brown zone, and contains two small perpendicular microveins (0.1–0.2 mm thick) also containing ettringite vein infill. The

30–45 mm subsample is grey-coloured, apparently unaltered clay biomicrite containing a single planer ettringite microvein (<0.5 mm wide) parallel to the main vein. The 45–60 mm, 60–75 mm and 75–90 mm geochemistry subsamples are grey-coloured clay biomicrite host rock with no indication of alteration or veining.

The PTS profile is 120 mm in length, beginning with the complex vein approx. 20 mm thick which contains wallrock inclusions. The wallrock itself is banded with an alteration zone (30–40 mm thick) fringing the vein. Bedding in the clay biomicrite is aligned perpendicular to the main vein.

The vein contains major coarse calcite with abundant fibrous ettringite, neither of which contain significant U. Thin bands of dull granular thaumasite contain approx. 20 ppm U. The vein contains significant barite as elongate bands up to 600 microns long but generally <10 microns thick. Barite contains high U ranging from 50–150 ppm. Large areas of the vein consist of included host rock fragments. The clay biomicrite has undergone intense alteration and is partly converted to ettringite and thaumasite. Relict areas of clay biomicrite have a spongy texture and contain abundant small grains of barite and Ti-Fe-V. They are enriched in P, and normally contain 20–30 ppm U, though >100 ppm U is recorded in places. Some large (>1mm) rafts of wallrock are almost completely replaced by fibrous ettringite aligned perpendicular to the vein margins (i.e. parallel to the original bedding). Patches of relict clay biomicrite within the rafts contain relict microfossils replaced by FeS with colloform Fe, Cr and Zn phases.

Along the wallrock edge a zone of ?calcification is present about 1–2.5 mm thick. The actual junction with the vein is irregular, with ettringite penetrating into the clay biomicrite, and incorporation of partially dissolved clay biomicrite material within the vein.

The host clay biomicrite rock is micritic limestone containing abundant foram tests and fossil debris. Tests are replaced by calcite, pyrite, Fe-oxide and rare CSH. The sample is cut by two sets of microfractures. The earliest are mineralised by calcite and rare strontianite, and the second set contain ettringite, with occasional CSH, and many are open. Fracture wallrocks show irregular dissolution of calcite with replacement by ettringite to a depth of typically approx. 10 microns, but up to 400 microns in places.

Wallrock Profiles (not including vein material)

Bulk rock geochemical profiles (Appendix J; Figs. J-4 to J-9) show that of the major elements Si, Fe, Mg, P and S appear to be enhanced close to the vein. Elements apparently depleted in the altered wallrock are Ca and LOI. The trace elements Cr, Ni and Se are enhanced at the wallrock edge. Mo and Ba show high levels in the 15–30 mm zone, suggesting that a "front" may be present at the edge of the visibly altered zone. The main problem in interpreting the geochemical data is assessing the influence of pre-existing "background" variation caused by lithological variation in the sample.

LAMP analysis (Appendix J; Table J-2, Figs. J-10 to J-12) shows that Al levels are enhanced at the altered wallrock edge and in a zone for at least 2 mm depth in to the wallrock. Levels are particularly high at the immediate edge (<0.25 mm) where ettringite mineralisation and replacement has occurred. Enhancement of Al for a 2 mm

wide zone is confirmed by EMPA data. Background variation of Al is relatively high and considerable variation is observed between the three PTS used for the profiles.

Thorium also shows clear enhancement at the wallrock edge. The highly altered wallrock at the immediate edge which is partially replaced by ettringite has very low Th (1 ppm), whilst levels in the wallrock zone for up to 2 mm are up to 4.2 ppm Th compared to background host rock levels of approx. 2 ppm. This shows good agreement with the bulk geochemical data. Uranium shows a very similar distribution with levels of up to 38 ppm U compared to background values of approx. 22 ppm. FTR analysis shows lowering of U levels at the wallrock edge (Appendix J; Fig. J-13), probably due to ettringite replacement. Higher levels of U around 30 ppm are detected by FTR, but are masked within the greater background variation detected by the FTR method.

Chromium shows extreme enrichment along the wallrock edge, and is also significantly enriched in the wallrock to a depth of 4 mm. Nickel is similar with very high levels at the altered edge, but a more complex enrichment in the wallrock, defining a possible enrichment front centred at 3 mm distance. The bulk geochemistry profiles show similar trends for both Ni and Cr.

Cobalt is also very enriched at the altered edge and in the wallrock for 0.5 mm distance. Some unusually high levels in the host rock are not easily explained. The LAMP Co data are different from the geochemical data, in that the latter have higher levels in the host rock, probably influenced by the unusual high levels in the host rock. Selenium also shows extreme enrichment at the altered edge. There is a suggestion of enhancement for several millimetres into the wallrock, but this is masked by the host rock variation. Geochemical data have lower overall levels of Se, but confirm high levels close to the fracture.

Lead levels are dominated by enhanced levels and greater variation in the middle of the profile. The very high variation from 14–41 mm relates entirely to one PTS (C353BP2) which shows unusual levels compared to the other sections. If the other two sections are used to define the background variation then the apparent enhancement at the wallrock edge is genuine. It is possible of course that the very high Pb levels represent alteration fronts, since discoloured alteration zones are observed at distances of up to 24 mm from the fracture. Barium is similar to Pb, with some enhancement at the immediate edge, but masked by very high levels and variation between 13 and 51 mm. Again it is difficult to determine if these are genuine element migration fronts or differences in background host rock levels between different PTS. Zr is similar and whilst not enhanced at the altered edge, it shows relatively high background levels and some high variable levels in a broad band up to 20 mm. This corresponds well with the geochemistry profile which is also dominated by high Zr levels at 0–20 mm.

Strontium and Cs are strongly related. Both are present at low levels at the altered wallrock surface (i.e. ettringite-replaced interface), but have enhanced fringes for several millimetres into the wallrock. They are highly enriched in single analysis points at distances of 40 and 50 mm, probably reflecting analysis of a component other than clay biomicrite groundmass (likely to to be strontianite in microveins). The geochemistry data confirm the LAMP results for Cs and Sr, being dominated by higher levels in the host rock.

Iron levels are highly variable throughout the profile, and it is not possible to relate them to any features related to the fracturing. This is probably due to the abundance of small grains of pyrite throughout the clay biomicrite host rock.

Trace Element Composition of Vein Material in C353

Uranium content of vein components derived by FTR analysis has been described earlier. LAMP analysis of trace elements in the vein is tabulated in Appendix J; Table J-3. Note that these data have not undergone the full calibration procedures and are thus semi-quantitative only (indicates order of magnitude concentrations). Most of the clay biomicrite material in the vein is highly altered and this is reflected in the trace element concentrations which are enriched in Cr and Se. Barite has high Cr, Se, Ni and Pb. Chromium and Se are also enriched in ettringite, though present at higher levels in calcium silicate. Uranium is also present in moderate amounts in the latter phase. Calcite appears to be enriched in Se also.

5.3.3 Sample C357

Sample C357 (Appendix J; Figs. J-16 to J-18) is a large clay biomicrite block containing a single planar fracture with occasional braided offshoots. The fracture is aligned approx. 45° to bedding in the clay biomicrite host rock. The fracture is mineralised by a 2 mm thick vein composed mainly of ettringite. On either side of the vein is a prominent zone 0–15 mm wide of intense braided microveins, commonly <5 mm long. The microveins are intense and typically 1–3 mm apart. The host rock appears uniform outside the zone of microfractures.

The host rock is a biomicrite containing abundant forams, some infilled by CSH. Minor apatite and framboidal pyrite are present throughout the rock and irregular aggregates of sphalerite up to 20 microns across are also occasionally present.

The vein is typically 400 microns to 1 mm wide and is dominated by ettringite which forms well developed radiating crystals some up to 1 mm length. The outer edges of the vein contain later veinlets <50 microns thick of a Ca-Si phase (probably jennite) which cuts across the ettringite. The jennite contains small <5 microns Fe-rich grains. The wallrock edge is gradational in detail with both ettringite and jennite replacing the biomicrite host rock. Ettringite replacement is observed in a zone up to 400 microns wide.

The microfractures are dominated by ettringite, with some later jennite also present. Most veins are typically <50 microns wide. Alteration zones around the microfractures appear to have less calcite, with ettringite and jennite infilling the porosity. The outermost microveins (furthest from the main vein) contain abundant aggregates up to 50 microns across of poorly formed celestite laths.

Two sub-samples were taken for geochemistry from the rock, the immediate wallrock at 0–10 mm, and an apparently unaltered host rock sample at 50–75 mm distance from the vein edge. The results show apparent enhanced Si, Se, Mo, Cs and Ba and lower LOI in the fracture wallrock (Appendix J; Table J-5, Figs. J-20 to J-25).

Uranium FTR analysis (Appendix J; Fig. J-29) shows that no U is present in the vein phases. Levels of U are enhanced in a symmetrical fringe with the highest levels of 30 ppm U at approx. 3 mm on either side of the vein. The average background host rock U content is 20–25 ppm. The LAMP data (Appendix J; Table J-6, Figs. J-26 to J-28) confirm the very low U in the vein phases. Thorium shows a very similar LAMP profile to U, though no patterns are observed in the host rock because of the relatively high background variation.

Aluminium determination by LAMP shows little variation throughout the sample. The highest levels are present in ettringite and jennite. In the latter, EDXA analysis shows that no Al is present in the pure phase, so the LAMP data may be detecting contamination by ettringite with which it is intimately associated.

Selenium levels are extremely high in the vein phases (>100 ppm), and also enhanced in the wallrock for approx. 7 mm distance. The rest of the rock has lower and relatively uniform values. The geochemistry data confirm the enrichment. Note that two datum points at 0.25 mm and 0.5 mm from the immediate wallrock edge do not contain enhanced Se levels, suggesting there may be a more complex detailed enhancement pattern at the wallrock edge.

Caesium is absent from ettringite, but present at enhanced levels in the jennite vein phase (note only 2.7 ppm but still significant compared to the uniform host rock background levels of around 1 ppm). Caesium is also enhanced in the fractured wallrock zone for 10 mm distance, and perhaps greater. The wallrock analyses do not include vein material, although it is possible that jennite replacement around the microveins has caused the high caesium levels. The geochemistry data support the enhanced levels identified by LAMP.

Barium is present at enhanced levels in the wallrock, with levels double that of the background host rock decreasing over about 10 mm distance away from the vein. Negligible Ba is present in the vein ettringite, whilst jennite contains very high levels of 850 ppm Ba. The geochemical data profile match that from LAMP analysis.

LAMP analysis of Pb confirms the low levels obtained by bulk geochemistry, with no variation distinguished between the wallrock and host rock. High Pb is present in the jennite vein phase (12 ppm). Some moderate enhancements occur throughout the host rock (up to 7 ppm) but these do not appear to be related to the veining.

Zirconium shows a relatively high variation along the profile, with no relationship to the altered wallrock and very low in the vein. It has a similar variation to U and Cr. The variation of Co throughout the host rock is larger than any changes in the wallrock. The vein minerals have very low (<5 ppm) to negligible levels of Co.

Molybdenum shows low levels in the immediate wallrock which are similar to the host rock distant from the vein, resulting in a wallrock composition not distinct from the background host rock. Low levels of Mo (15 ppm) are present in the vein.

Chromium is very low <10 ppm in the vein. It shows a high variation throughout the profile, and although low in the wallrock, this is not significant from the "background" variation. The low levels close to the vein are supported by the geochemical data which have low Cr at 0–10 mm and higher levels >50 mm, suggesting that Cr could have been removed from the fracture wallrock.

As with the geochemical data, there is little variation in Sr on the LAMP profile. The vein phases have similar Sr levels to the host rock, suggesting substitution for Ca in ettringite and jennite. Very high levels in a single analysis at the end of the profile may represent a celestite grain.

5.3.4 Sample C358

The sample is a pale brown-grey clay biomicrite with an open uncoated fracture surface showing an alteration zone up to 19 mm wide around the fracture surface (Appendix J; Figs. J-31 and J-32). The alteration zone consists of multiple parallel banding with dark bands alternating with lighter whitish bands. When freshly broken the rock has a bituminous smell. The maximum visual alteration is 19 mm from the main fracture. The clay biomicrite is uniform with very poorly developed bedding.

The broad bands appear to have formed as a result of calcite dissolution (dark bands) and reprecipitation (light bands). Calcified bands are typically 6 mm wide, though many different thicknesses are present. Where removed, calcite has been replaced by ettringite, thaumasite and probable CSH.

Results of the bulk geochemistry suggest that the altered wallrock has higher Si, Al and Ba, and lower LOI, Cr, Co, Ni and possibly U. LAMP data show that the area of the zones has very enhanced Al, Ba and Pb (Appendix J; Table J-8, Figs. J-33 to J-38).

The LAMP data for most elements are masked by the relatively high background variation in the host rock which masks patterns in the altered fracture wallrock (Appendix J; Table J-9, Figs. J-39 to J-41). However, the datum point in the centre of the zoned area which has the highest Al level is distinct in many trace elements. Out of the 28 data points analysed it has the lowest levels of Cr, Se, Mo, Th and U. These elements are present at very depleted levels in a band 2 mm wide, lying approximately in the centre of the most intense wallrock alteration bands. The elements therefore appear to have been removed from the altered wallrock as they are present at significantly lower levels than in the host rock further from the fracture. These three data points also have particularly high Zr and Sr.

The bulk geochemistry data confirm these findings, and the low levels in the altered zone determined by LAMP are confirmed particularly for Cr, Mo and U bulk analysis.

5.3.5 Sample C359

Sample C359 (Appendix J; Fig. J-43) is from the M2 groundwater sampling site. It is an active fracture mineralised by ettringite with thaumasite, jennite and calcite. The wallrock has a hard and brittle dark alteration zone at 0–2 mm distance within a broad rusty orange-brown coloured alteration zone which persists for up to 10 mm from the fracture edge. The rest of the host rock away from the fracture is a dark-grey coloured clay biomicrite. Bedding is well defined in the host rock and aligned at approx. 45° to the fracture.

Thin microfractures (<0.5 mm) mineralised by ettringite are common in the host rock up to 17 mm from the fracture. Less common ettringite veins are also present throughout the entire host rock profile examined (i.e. up to 100 mm).

In detail the fracture is dominated by ettringite containing poorly formed central spongy masses of CSH. The wallrock edge is altered in a zone 1.2 mm wide which appears to be calcified. The outer edge of this alteration zone is defined by a series of interconnected braided microfractures <10 microns thick, subparallel to the main vein, some open and porous with others filled by ettringite. Elongate wallrock inclusions typically several millimetres thick are present within the vein and are similarly altered. Ettringite replacement of clay biomicrite has occurred with interfingering of interfaces and patchy replacement within the wallrock inclusion.

The geochemical data clearly show some disturbance of elements in the altered wallrock up to 17 mm distance from the fracture (Appendix J; Table J-11, Figs. J-44 to J-49). There appears to be enhancement of Si, Al, Fe and possibly S close to the fracture edge, and depletion of Ca, P and LOI. Trace elements show enhanced Se and Mo, possible loss of Cr, Ni and Sr, and also U.

Aluminium is enriched in the vein and at the vein edge, with a broad zone of enhancement and disturbance extending perhaps for approx. 25 mm into the wallrock. Both vein phases have similar levels to the wallrock edge, and these are the highest values of the profile with the exception of the included wallrock fragment which has very high Al. The inner part of the altered wallrock zone is complex with apparent depletion from 1–5 mm and 8–10 mm and enhanced zones (mineralisation fronts?) at 6–7 mm and 12–22 mm. This pattern of wallrock enrichment is confirmed by the bulk geochemical data.

Molybdenum is highly enriched in the wallrock inclusion and high at the immediate wallrock edge. The CSH vein phase also has high levels, whilst ettringite is very low. There appears to be a zone of depletion in the wallrock at 0.5–5 mm distance, but overall Mo enrichment is present over a wider distance. The geochemical data show similar levels of Mo with some enrichment near the vein.

Selenium also shows very high enrichment in both vein phases and in the wallrock inclusion. The wallrock itself has levels similar to the background host rock. Levels are very similar to the geochemical data which also show slight enhancement at the vein, though bulking the sample (0–10 mm subsample) has reduced this.

Barium levels show a high variation through the LAMP profile, but particularly so in the wallrock zone; it is difficult to determine if this is a primary lithological variation, or fracture induced. Barium is particularly low at the wallrock edge and in the vein. Variable levels are also seen in the geochemical data.

Chromium shows very low levels in both vein phases, and highly variable levels in the wallrock which are not readily distinguished from the overall "background" variation in the host rock. Although of similar magnitude to the geochemical data, the LAMP data do not show any enhancement or depletion of Cr from the wallrock edge.

LAMP data for U show very low levels in the vein and erratic high levels in the wallrock (Appendix J; Table J-12, Figs. J-50 to J-52). The immediate wallrock (0–0.5 mm) has levels of approx. 11 ppm which are similar to the background host rock. But higher levels of 17–18 ppm U are present in a zone 0.5 to 2 mm (one low analysis at 2 mm is in contact with an ettringite-bearing microvein with low U). However, the relatively high background variation makes it uncertain whether this enrichment continues further into the host rock. This appears to be a complex situation with low U

in vein phases and possible removal from the immediate wallrock edge, but with an enhanced zone in from this area. FTR analysis also shows varying levels at the wallrock edge. It also shows a series of low U bands throughout the profile which correlate with ettringite-bearing microveins with depleted U levels in the surrounding wallrocks. Most of these microveins have visible altered zones for up to 1 mm at either side of the veins. The geochemical profile for U shows depletion at the wallrock edge, though the variation across the entire profile is <1 ppm.

Thorium shows a broadly similar distribution to U. The ettringite contains negligible Th, whilst the CSH vein phase has Th levels only slightly lower than the host rock, and identical to the altered fringe at the wallrock margin. As with U, the wallrock further in has relatively high Th levels, but these are not particularly distinct above background variation in the host rock. The geochemistry data show low Th at the edge increasing away from the fracture, similar to the LAMP profile.

Zirconium shows a very similar pattern with very low levels in the vein, depleted levels at the wallrock edge, and possible enhancement in the wallrock for a few millimetres.

Strontium has low levels in the vein phases and is depleted in the included wallrock fragment. Any variation at the wallrock margin cannot be resolved from background variation in the host rock. The geochemical data are also dominated by the host rock variation which is similar in scale to the LAMP data (approx. 200 ppm).

Cobalt concentrations are also low at the vein edge. The included wallrock fragment and the wallrock zone from 0–0.5 mm distance have identical depleted levels. The vein phases have higher levels in CSH, and very low in ettringite (like Th). There is possible enhancement in the wallrock, but as with other elements (i.e. U, Th, Zr, Sr) it is hard to distinguish above the host rock variation. The geochemical data are also dominated by the host rock variation, although the lowest value is at the wallrock edge (0–10 mm). Note that the entire variation is <0.5 ppm.

Lead shows highly variable levels in the vein and wallrock. The included wallrock fragment and the wallrock at 0.5 mm have enhanced Pb which is significantly above the background variation in the host rock. Ettringite has very low levels, whilst CSH has levels similar to the wallrock edge.

Caesium shows a complex pattern but the overall variation across the profile is <1.5 ppm. There is possible depletion near the vein, similar to the geochemical data. The highest variation is present in the wallrock.

The data for C359 are difficult to interpret since there are highly variable element levels in a broad zone up to approx. 25 mm from the fracture edge. It is unclear whether this represents primary host rock compositional variation, or if it is fracture induced wallrock alteration.

5.3.6 Uranium Series Disequilibrium Observations

All four fracture wallrock profiles described above were analysed for U-decay series disequilibrium; Ra analysis was only measured in C353 and C359. The data are presented in Table 5-9 and the isotope ratios are plotted for each sample as a series of

profiles in Appendix J (Figs. J-14, J-30, J-42 and J-53); the plots show 1 sigma uncertainties.

For all four samples, the plots of $^{234}U/^{238}U$ and $^{230}Th/^{234}U$ show little or no deviation from unity, indicating no significant disturbance of these isotopes over the last 1 Ma.

Plots of $^{228}Th/^{232}Th$ show varying levels, some of which appear to deviate from unity. These indicate possible disturbance, with a suggestion of leaching of ^{228}Ra implying very recent (or continuous) activity. However, the patterns disappear if the more usual 2 sigma uncertainty is used.

The clearest indication of isotopic disturbance is in samples C353 and C359 where $^{226}Ra/^{238}U$ values lie significantly below unity in parts of the profiles. Even increasing the quotted errors to a more realistic 2σ rather than the 1σ quoted does not remove the signal. This indicates that Ra has been leached from the system within the last 8 000 a (assuming continuous leaching) or very recently (assuming sudden events). Interaction has been estimated to be up to 4 cm depth in C353 and 7 cm in C359.

5.3.7 Conclusions

Geochemical evidence for rock matrix diffusion around groundwater-conducting fractures in Adit A-6 is influenced by the presence of microfracture networks close to the major fractures, typically extending for several tens of millimetres into the host rock. Limitations in assessing the depth of geochemical alteration were encountered by the pre-existing lithological (and therefore geochemical) variation in the host rocks, and the short wallrock profiles investigated (maximum 100 mm).

The depth of geochemical changes in the fracture wallrock corresponds to macro-scale observations of alteration around fractures. Levels of Cr, Ni, Se, S, Mo, Cs and Ba are commonly enhanced or disturbed for up to 30–40 mm distance from fracture surfaces, and particularly enriched over several millimetres at the immediate wallrock edge. These same elements are concentrated in the dominant fracture infill mineralisation (mainly ettringite, thaumasite, jennite and barite). Geochemical enhancement in the host rock around fractures is most likely explained by the presence of these minerals within microfractures, and by the dissolution and replacement of matrix calcite in the host rock, particularly at the immediate wallrock edge. At greater distances from the major fractures (>40 mm) the geochemical composition of the host rock is indistinguishable from the background lithological variation, indicating no alteration effect.

Uranium series disequilibria (USD) data indicate that recent or continuous leaching of ^{228}Ra has occurred at distances of up to approx. 70 mm from the fracture surface (the maximum distance investigated for USD in these samples.) This indicates that potentially the entire investigated wallrock profile has been accessible to groundwater. However, because of the limited number of samples the maximum distance of penetration could not be determined.

5.4 POROSITY CHARACTERISTICS

The porosity measurements performed are outlined in Table 5-10.

5.4.1 Fractured Clay Biomicrite Wallrock

The results of the fourteen liquid resaturation porosimetry measurements, along a profile away from the fracture surface, for four samples of fractured clay biomicrite wallrock from Adit A-6, are presented in Table 5-11. Porosity determinations by image analysis of fractured marl altered wallrocks and background marl samples are given in Table 5-12. In all four samples, both BSEM and UV-epifluorescence petrography indicates enhancement of microporosity in very narrow zones immediately adjacent to the fracture surface in altered marl wallrock (Appendix I; Plates I-23 and I-24). These observations confirm the observations previously reported by Milodowski et al. (1998) and Linklater (1998).

In sample C359 the total pore volumes determined by liquid resaturation indicate that with increasing distance from the fracture the porosity remains approximately constant between 28.6% and 31.1% except the 10–17 mm interval where porosity decreases to 25.1% (Table 5-11; Fig. 5-6). This interval coincides with a zone of calcite cementation indicated by BSEM (see Milodowski et al., 1998 and Linklater, 1998). Comparisons of pore size distributions indicate that the pore throat diameter adjacent to the fracture (0–10 mm) is larger than at greater distances (48–63 mm) (Appendix J; Fig. J-54). This is probably due to calcite dissolution adjacent to the fracture. Approximately 50% of pore throats have diameters less than 0.1 μm adjacent to the fracture with approximately 95% of pore throat diameters less than 0.3 μm. At 48–63 mm more than 95% of the pore throats are less than 0.1 μm. For comparison the pore area distributions as determined by IA are also plotted (Appendix J; Fig. J-54). The IA technique measures pore areas down to a minimum area of 0.58 μm^2. Pore throats smaller than this are not measured. Note however, that the IA technique can measure pore areas up to three orders of magnitude greater than the liquid resaturation technique. It would be expected that these larger voids would dominate the permeability characteristics of the biomicrite.

The variation in total porosity with distance from the fracture wall for sample C353 is presented in Table 5-11 and Figure 5-6. The porosity increases slightly with increasing distance from 40.3% over 0–15 mm to 42.2% at 15–30 mm to 44.8% at 45–60 mm. The increase may be due to some of the porosity being infilled by secondary hyperalkaline alteration products, as described above, closer to the fracture. The porosities obtained from this sample are the highest determined in this study. MICP tests indicate that the pore throats are slightly smaller adjacent to the fracture, 0–15 mm, compared to those at 45–60 mm (Appendix J; Fig. J-15). This is again due to the presence of fine-grained alteration products within some of the porosity close to the fracture. 90% of the pore throats are less than 0.05 μm in diameter. This pore size is well below the resolution limits of both UV-epifluorescence microscopy and BSEM (image analysis can only determine pore sizes greater than 0.58 μm^2). Fracture pores are typically slightly coarser than in the wallrock. However differences are minimal. Hence MICP and image analysis techniques are predominantly measuring different pore sizes.

In samples C357 and C358 the porosity increases from 23% adjacent to the fracture to 33% at 50–74 mm (Fig. 5-6). This is probably due to the fact that much of the porosity adjacent to the fracture is infilled by secondary minerals as a result of hyperalkaline fluid interaction. Porosity in C358 follows a similar trend with increasing porosity away from the fracture. This may help to explain why resin impregnation in these fracture samples is restricted to the areas immediately adjacent to the fractures. Because of the very fine-grained secondary hyperalkaline mineralisation, and concommittant very small pore throat sizes, the porosity further into the wallrock (away from the mineralisation/ alteration) zone is probably not accessible to the viscous impregnating epoxy-resin.

5.4.2 Western Springs Colluvium

UV-epifluoresence microscope observations of resin impregnated thin sections revealed that the sandy and silty matrix of the Quaternary colluvium and fluvial boulder gravels contains significant but very fine interconnected microporosity. This porosity is hosted largely within the secondary CASH and CSH gel phases. However, most of the porosity is so fine-grained that the individual pores could not be resolved by UV-epifluoresence microscopy and consequently, it was not possible to quantify the porosity characteristics using image analysis techniques. Nevertheless, UV-epifluorescence quite clearly shows an enhancement of the microporosity in the margins of clasts (evident as brightly-luminescent rims; Appendix I; Plate I-20), particularly of dolomicrite and micrite clasts, similar to that seen in the marl fracture wallrock in Adit A-6.

5.5 SUMMARY AND CONCLUSIONS

Mineralogical and geochemical were carried out to study the interaction of discharging high pH groundwaters from the Western Springs locality with unmetamorphosed country rocks (basalt; chert; clay biomicrite limestone) contained as fragments, clasts and blocks within the Quaternary colluvium deposits which characterise the Yarmouk River Valley sides above the river bed. In addition, supplementary studies were made on high pH alteration reactions on material from the Eastern Springs locality, in particular Adit A-6. These were carried out to confirm Phase II observations and conclusions.

The colluvium deposits comprise a lower fluvial boulder/gravel unit, an overlying upper colluvium unit, and a thin soil cover with a poorly defined transitional zone of thinly weathered, weakly cemented colluvium. Since the high pH groundwaters mostly discharge through the lower fluvial unit, the samples for study were selected from this horizon.

Hyperalkaline Groundwater Reactions

Basalt, of local derivation, is mostly alkali olivine in type and alteration (due probably to weathering) is seen as alteration rims of secondary Fe oxides/oxyhydroxides around the clasts, as Fe-oxides distributed along the cleavage planes of, for example, augite, as

a weak pervasive alteration of feldspar to a white mica, and alteration of interstitial glass to clay minerals and haematite. Of the investigated rock types, the basalt clasts show most reaction, being characterised by significant reaction rims comprising major secondary CSH and CASH alteration products. The most reactive phase is the matrix glass, followed by plagioclase and K-feldspar. In contrast, augite, hypersthene and olivine are comparatively unaltered.

The chert clasts are composed of fine-grained or cryptocrystalline quartz, although this may include poorly crystalline or amorphous silica. These show variable reaction with the hyperalkaline groundwaters seen as: a) replacement by fine-grained calcite or aragonite around clast margins, and b) totally dissolved and replaced by amorphous (isotropic) gel-like CSH minerals. Most chert reaction products appear to be Al-substituted CSH gels, although some Mg-rich CSH gels were also observed. The incorporation of Al (and also Mg) is not predicted by modelling calculations, and is due to the presence of local Al/Mg sources such as the basalt clasts and clay matrix phases in the colluvium.

The clay biomicrite limestone (or "marl") clasts are identical to the Eastern Springs marls investigated during Phases I and II of the Maqarin project. The biomicrite clasts show only minor leaching in contact with the hyperalkaline groundwaters. However, those dolomicritic clasts (with an estimated enhanced porosity (~ 20%) are associated with the dissolution of the matrix dolomite typically infilled by a structureless, microporous Ca-Si-S-Al-rich material, unfortunately too fine-grained for positive identification. By comparison with the Eastern Springs material, these alteration phases may be largely ettringite-thaumasite dominated.

Similar reactivity is observed in the sand-silt matrix which characterises the colluvium. Plagioclase is highly corroded, being present only as trace relicts within a groundmass of fine CASH gel. Detrital quartz and chert grains may also be highly corroded and replaced by CASH minerals.

As a general conclusion, quartz, chert, K-feldspar, glass and plagioclase are the most reactive phases with the hyperalkaline groundwaters, dolomite is moderately reactive, augite, hypersthene (orthopyroxene) and olivine are weakly reactive, and apatite and Ti-Fe oxides appear to be largely unreactive.

Mineral paragenesis of the secondary alteration phases indicates the following sequence: a) a very hydrous Ca-K-Na-Al "zeolite-type" phase, b) a CSH gel with a variable Ca:Si ratio covering the range CSH(I) to CSH(II) (i.e. suolinite-afwillite), c) a more Si-rich CSH gel (i.e. okenite-type), and d) a low Ca-Si ratio CSH phase (i.e. truscottite-type). The latest stage of alteration is the replacement of the CSH and CASH phases by calcite or aragonite.

The new data presented in this report indicate that there is a much wider range of phases and compositions than previously expected, and that, despite the marked difference in primary mineralogical assemblage, the alteration products of the basalt-rich gravels and colluvium are broadly similar to those encountered during the alteration of clay biomicrite in Adit A-6. The alteration products typically exhibit the complete range of compositions within a small area (typically a few tens of microns of the same sample).

Trace Element Matrix Diffusion Studies

Studies showed that geochemical evidence for rock matrix diffusion adjacent of water-conducting fracture zones is influenced by the presence of microfracture networks close to the major fractures, typically extending for several tens of millimetres into the host rock. Accordingly, levels of Cr, Ni, Se, S, Mo, Cs and Ba are commonly enhanced or disturbed for up to 30–40 mm distance from the fracture surfaces, and particularly enriched at the immediate wallrock edge. These same elements are concentrated in the dominant fracture infill mineralisation (mainly ettringite, thaumasite, jennite and barite). Geochemical enhancement is most likely explained by the presence of the microfracture infill minerals, and by the dissolution and replacement of matrix calcite in the host rock, particularly at the immediate wallrock edge. At greater distances from the major fractures (>40 mm) the geochemical composition of the host rock is indistinguishable from the background lithological variation, indicating no alteration effect.

Uranium-decay Series Observations

All four profiles were measured for U-decay series disequilibrium; Ra analysis was only measured for two profiles. All four profiles show little or no deviation from unity for $^{234}U/^{238}U$ and $^{230}Th/^{234}U$ indicating no significant disturbance of these isotopes within the last 1 to 0.3 Ma. In contrast, $^{228}Ra/^{232}Th$ show varying deviation possibly resulting from the leaching of ^{228}Ra. This would imply very recent (or continuous) activity within the last 8 000 a, with interaction up to 3–7 cm depth.

5.6 ACKNOWLEDGEMENTS

The authors thank Dr. Rob Ellam at SURRC for undertaking the strontium isotope measurements reported in this work. Dr. S.R.N. Chenery (BGS) carried out the LAMP-ICP-MS analysis. Mr. Mark Ingham, Dr. Mark Cave and Mr. Shaun Reeder, and colleagues in the Analytical Geochemistry Group (BGS) are thanked for provision of the whole-rock and groundwater analyses undertaken for this study. Mr. John Bloomfield is thanked for undertaking the liquid resaturation porosimetry measurements. Finally, Mr. David Oates (BGS) is acknowledged for his painstaking efforts in successfully preparing high-quality polished thin sections from extremely difficult materials used in this study.

5.7 REFERENCES

Alexander, W.R. (Ed.), 1992. A natural analogue study of the Maqarin, hyperalkaline groundwaters. I: Source term description and thermodynamic database testing. Nagra, Tech. Rep. (NTB 91-10), Nagra, Wettingen, Switzerland.

Arakel, A.V. and McConchie, D., 1982. Classification and genesis of calcrete and gypsite lithofacies in palaeodrainage systems of inland Australia and their relationship to carnotite mineralization. J. Sed. Pet., 52, 1149–1170.

Linklater. C.M. (Ed.), 1998. A natural analogue study of cement-buffered, hyperalkaline groundwaters and their interaction with a repository host rock: Phase II. Nirex Science Report, S/98/003, Nirex, Harwell, U.K.

Lea, F.M., 1970. The Chemistry of Cement and Concrete. 3rd Edition. Edward Arnold, London.

Milodowski, A.E., Khoury, H.N., Pearce, J.M. and Hyslop, E.K., 1992. Results: Source/sink terms. In: W.R. Alexander (Ed.), A natural analogue study of the Maqarin hyperalkaline groundwaters. I: Source term description and thermodynamic database testing. Nagra, Tech. Rep. (NTB 91-10), Nagra, Wettingen, Switzerland, p. 41–51 and C1–C53.

Milodowski, A.E., Pearce, J.M., Hyslop, E.K., Hughes, C.R., Inglethorpe, S.D.J., Strong, G.E., Wheal, N., MacKenzie, A.B., Karnland, O. and Khoury, H.N., 1998. Mineralogy and petrology. In: C.M. Linklater (Ed.), A natural analogue study of cement-buffered, hyperalkaline groundwaters and their interaction with a repository host rock: Phase II. Nirex Science Report, S/98/003, Nirex, Harwell, U.K., p. 70–145.

Strong, G.E. and Milodowski, A.E., 1987. Aspects of the diagenesis of the Sherwood Sandstones of the Wessex Basin and their influence on reservoir characteristics. In: J.D. Marshall (Ed.), Diagenesis of Sedimentary Sequences. Geol. Soc. Lon. Spec. Pub., 36, 325–337.

TABLES

Table 5-1. Summary of sample numbers, localities and method of XRD analysis.

Sample No.	Locality	Method of XRD analysis			
		Whole-rock	Acid leach Whole-rock	<2 μm oriented	Acid leach <2 μm oriented
C364	Western Springs	√	√	–	√
C365	Western Springs	√	√	–	√
C369	Western Springs	√	√	–	√
C370	Western Springs	√	√	–	√
C372	Western Springs	√	√	–	√
C390	Central Jordan S3	√	–	–	–
C391	Central Jordan S3	√	–	√	–
C392	Central Jordan S3	√	–	–	–
C393	Central Jordan S3	√	–	√	–
C394	Central Jordan S3	√	–	–	–
C711	Central Jordan S3	√	–	–	–
C395	Central Jordan S3	√	–	√	–
C396	Central Jordan S3	√	–	√	–
C378	Sweileh road cut	√		√	–
C379	Sweileh road cut	√		√	–
C380	Sweileh rod cut	√		√	–
C381	Sweileh road cut	√		√	–
C382	Sweileh road cut	√		√	–
C383	Sweileh road cut	√		√	–

Table 5-2. Summary of whole-rock mineralogy XRD.

Sample	Treatment	Mineralogy (decreasing order of abundance)
C364	Tema	Calcite, quartz, ettringite
C365	Tema	Calcite, quartz, augite, hematite
C369	Tema	Calcite, ankerite, ettringite, quartz
C370	Tema	Calcite, quartz, gypsum, ankerite, fluorapatite, ?mica
C372	Tema	Calcite, thaumasite, bentorite, ?ettringite, ?epistilbite
C364	Tema (acid leach)	Calcite, quartz, albite, K-feldspar, fluorapatite, kaolinite
C365	Tema (acid leach)	Calcite, quartz, augite, hematite
C369	Tema (acid (leach)	Calcite, ankerite, quartz, kaolinite, 'mica'
C370	Tema (acid leach)	Calcite, quartz, ankerite, fluorapatite, ?'mica'
C372	Tema (acid (leach)	Quartz, kaolinite, 'mica' + "broad" peak background
C390	Ground	Calcite, quartz, smectite
C391	Ground	Calcite, fluorapatite, halite, quartz, smectite
C392	Ground	Calcite, fluorapatite, halite, quartz, smectite
C393	Ground	Calcite, fluorapatite, halite, smectite
C394	Ground	Calcite, rhodochrosite, fluorapatite, quartz, smectite
C711	Ground	Calcite, rhodochrosite, fluorapatite, quartz, smectite
C395	Ground	Calcite, halite, rhodochrosite, fluorapatite, smectite
C396	Ground	Calcite, quartz, ankerite, rhodochrosite, smectite
C378	Ground	Calcite, fluorapatite, smectite, ?rhodochrosite
C379	Ground	Calcite, fluorapatite, smectite, ?rhodochrosite
C380	Ground	Calcite, fluorapatite, smectite, ?rhodochrosite
C381	Ground	Calcite, fluorapatite, smectite, ?rhodochrosite
C382	Ground	Calcite, fluorapatite, smectite, ?rhodochrosite
C383	Ground	Calcite, fluorapatite, smectite, ?rhodochrosite

Table 5-3. Summary of the <2μm mineralogy XRD.

Sample	Treatment	Mineralogy (decreasing order of abundance)
C364	Acid leach	Kaolinite, broad indistinct, low intensity band from ~17 to ~10Å
C365	Acid leach	Broad, indistinct, low intensity band from ~17 to ~10Å
C369	Acid leach	Kaolinite, broad indistinct, low intensity band from ~17 to ~10Å
C370	Acid leach	Kaolinite, 'mica', ?smectite
C372	Acid leach	Kaolinite, ?'mica'
C391	–	Smectite (001 basal spacing 14.82Å), ?zeolite
C393	–	Smectite (14.82Å), kaolinite
C395	–	Smectite (14.65Å), kaolinite
C396	–	Kaolinite, 'mica', ?smectite
C378	–	Smectite (14.9Å), 'mica'
C379	–	Smectite (14.65Å), ?iowaite
C380	–	Smectite (14.9Å)
C381	–	Smectite (14.9Å)
C382	–	Smectite (14.82Å), ?iowaite
C383	–	Smectite (14.82Å)

Table 5-4. Bulk geochemistry data for various lithologies from Maqarin.

MAJOR ELEMENTS (weight %)

Sample No.	Type	Site	SiO_2 %	TiO_2 %	Al_2O_3 %	Fe_2O_3t %	MnO %	MgO %	CaO %	Na_2O %	K_2O %	P_2O_5 %	LOI %	SO_3 %	Cr_2O_3 %	SrO %	BaO %	Total %	FeO** %	Total S %
	Clasts																			
C362	Basalt	**M10**	46.23	2.63	13.93	12.84	0.15	7.56	10.11	2.44	1.26	1.07	1.25	0.00	0.03	0.14	0.06	99.70	3.60	<0.02
C362	Basalt	**M10**	46.31	1.80	14.49	12.56	0.18	9.39	10.18	2.73	0.84	0.30	0.93	0.10	0.05	0.06	0.07	99.99	8.28	0.45
C375	Basalt	**M19**	46.64	2.21	15.03	13.44	0.19	8.38	9.68	2.81	0.90	0.36	0.87	0.00	0.04	0.06	0.02	100.63	6.84	<0.02
	Av. basalt clast		46.39	2.21	14.48	12.95	0.17	8.44	9.99	2.66	1.00	0.58	1.02	0.03	0.40	0.09	0.05	100.12		
	Quaternary sediment matrix																			
C364	Gravels matrix	**M11**	5.04	0.14	1.06	0.73	0.01	1.1	47.18	0.1	0.12	0.18	39.79	2.8	0.21	0.16	0.03	98.65	0.58	1.09
C365	Basal colluvium	**M11**	23.55	0.71	4.82	3.73	0.07	1.85	33.53	0.45	1.84	0.56	27.37	0.6	0.03	0.12	0.1	99.33	0.86	0.25
C369	Gravels matrix	**M14**	10.85	0.16	1.98	1.17	0.03	1.59	44.61	0.12	0.3	0.84	34.93	2.2	0.12	0.15	0.06	99.11	n.d.	0.76
C372	Gravels matrix	**M16**	7.40	0.19	2.06	1.17	0.02	1.15	45.18	0.07	0.1	0.06	30.34	10.3	0.28	0.06	0.01	98.39	n.d.	3.25
C370	Recent colluv. soil	**M14**	13.04	0.12	1.98	1.06	0.03	1.49	42.14	0.12	0.33	1.62	31.65	5.3	0.03	0.17	0.09	99.17	<0.30	2.01
	Av. Matrix		11.71	0.3	2.48	1.7	0.03	1.42	42.63	0.19	0.59	0.41	33.12	4	0.16	0.12	0.05	98.87	0.72	1.34
	Solid lithologies																			
C768	Silicified Limestone		99.35	0.00	0.00	0.21	0.00	0.00	0.22	0.11	0.01	0.05	0.51	0.00	0.02	0.00	0.00	100.46	n.d.	n.d.
C779	Chalky Limestone Formation		7.18	0.03	0.34	0.33	0.00	1.45	50.53	0.08	0.06	0.58	40.20	0.10	0.01	0.13	0.07	100.78	n.d.	n.d.
C782	Massive basalt		46.51	2.31	14.59	12.59	0.17	9.35	9.79	2.76	0.99	0.81	0.84	0.00	0.03	0.13	0.04	100.71	n.d.	n.d.

Table 5-4 (contd.). Bulk geochemistry data for various lithologies from Maqarin.

TRACE ELEMENTS (ppm)

Sample No.	Type	Site	Cr ppm	Co ppm	Ni ppm	Se ppm	Sr ppm	Zr* ppm	Mo ppm	Cs ppm	Ba ppm	Pb ppm	Th* ppm	U* ppm
	Clasts													
C362	Basalt	**M10**	163	48.8	173	<17	1221	233	1.1	0.45	582	<5	4.4	1.4
C362	Basalt	**M10**	271	60.0	288	<17	648	127	0.9	0.11	776	<5	2.7	0.42
C375	Basalt	**M19**	232	62.4	241	<17	528	125	1.4	0.78	208	<5	1.8	0.39
	Av. basalt clast		222	57.1	234	<17	799	162	1.1	0.45	522	<5	3.0	0.74
	Quaternary sediment matrix													
C364	Gravels matrix	**M11**	1266	3.7	25	109	1474	16.7	1.2	1.62	294	<5	0.8	1.57
C365	Basal colluvium	**M11**	194	17.7	92	30	1118	77.9	2.5	2.65	1143	<5	2.8	3.64
C369	Gravels matrix	**M14**	763	6.8	110	91	1502	28.7	4.6	4.53	740	<5	1.8	9.14
C372	Gravels matrix	**M16**	1703	4.8	20	104	535	27.5	2.3	1.13	56	<5	1.6	1.88
C370	Recent colluv. soil	**M14**	212	7.1	147	<17	1566	25.0	8.8	0.82	1003	<5	1.7	13.8
	Av. Matrix		982	8.3	62	84	1157	37.7	2.7	2.48	558	<5	1.3	4.1
	Solid lithologies													
C768	Silicified Limestone		n.d.	n.d.	n.d.	n.d.	n.d.	n.d.	n.d.	n.d.	n.d.	n.d.	<1	1
C779	Chalky Limestone Formation		n.d.	n.d.	n.d.	n.d.	n.d.	n.d.	n.d.	n.d.	n.d.	n.d.	<1	2
C782	Massive basalt		n.d.	n.d.	n.d.	n.d.	n.d.	n.d.	n.d.	n.d.	n.d.	n.d.	2	<1

Notes: All data by XRF except: *from ICP-MS following acid dissolution only; ** by acid dissolution and redox-titrimetric analysis.
LOI = loss on ignition.
Values [] are determined by XRF only.

Table 5-5. Modal analysis data for Quaternary fluvial boulder gravels, Western Springs, Maqarin.

a) Modal analyses of basalt clasts in Quaternary sediments (point counting of thin sections to 1500 points).

Sample	Plagioclase	Clinopyroxene	Oxide	Olivine	Orthopyroxene	?Serpentine	Voids
C368	40.5	38.8 (groundmass = 83.7%)	4.4	12.7	0 (phenocrysts = 12.7%)	0	3.5
C375	47	22 (groundmass = 74.5%)	5.5	0	8.6 (phenocrysts = 15.3%)	6.7	10.5
C362*	23.9	22.3	31.6	5.6	0	2.7	14

***Note:** oxide component in C362 includes fine-grained cryptocrystalline groundmass (groundmass = 77.8%) (phenocrysts = 8.3%)

b) Modal analyses of matrix in Quaternary fluvial boulder gravels (point counting of thin sections to 2000 points).

Sample	Basalt	Micrite	Chert	Matrix	Voids
C375	19.5	25.5 (clasts = 71.6%)	26.6	20.8	7.7 (matrix = 28.5%)
C362	31.9	11 (clasts = 45.2%)	2.3	46.6	8.2 (matrix = 54.8%)

c) Recalculation of composition of boulder gravels, Western Springs.

	Large-scale field traverse	Thin section point-count	Overall composition
Basalt (%)	47	32	58
Micrite (%)	8	11	12
Chert (%)	11	2	12
Matrix (%)	34	47	16
Porosity (%)	n.d.	8	3

Table 5-6. Summary scale of reactivity of different mineralogical components with hyperalkaline groundwater in the Western Springs Quaternary deposits.

BASALT CLASTS
Glass + K-feldspar > Plagioclase >> Augite + Orthopyroxene > Olivine + Fe-Ti oxides

LIMESTONE / CLAY BIOMICRITE CLASTS
Dolomite >> Calcite

MATRIX
Quartz + Chert + K-feldspar-plagioclase > Augite > Olivine + Calcite + Apatite + Ti-Fe oxides

OVERALL SCALE OF REACTIVITY

Quartz — Apatite

Chert ≥ Plagioclase > Dolomite >> Augite + Orthopyroxene > Olivine > Calcite

Glass — Ti-Fe Oxide

K-feldspar

Table 5-7. Strontium isotope ($^{87}Sr/^{86}Sr$) ratios for selected rocks and groundwaters from the Maqarin area.

Sample	$^{87}Sr/^{86}Sr$	±2 standard e	Sample Description
Rocks			
C768	0.707569	0.000016	Silicified Limestone (Amman F[m])
C779	0.707737	0.000017	Chalky Lmst. F[m] (central part; Chert Chalky Lmst. Member)
C782	0.704240	0.000017	Quaternary basalt
M15P	0.707866	0.000017	Cement zone, Adit A-6 (core sample)
Groundwaters			
M5	0.707820	0.000017	High pH groundwater; Site M5, Western Springs
M9	0.707680	0.000017	Bicarbonate groundwater, Amman F[m]
M17	0.707827	0.000016	Bicarbonate water, Bituminous Marl Formation

Table 5-8. Geochemical data from rock-matrix diffusion profiles of samples from Adit A-6 (sample length in millimetres).

Sample	SiO_2 %	TiO_2 %	Al_2O_3 %	Fe_2O_3t %	MnO %	MgO %	CaO %	Na_2O %	K_2O %	P_2O_5 %	LOI %	SO_3 %	Cr_2O_3 %	SrO %	Total %
C353 0–15	9.91	0.17	4.38	2.59	0	0.31	46.28	0.09	0.05	2.23	32.36	0.7	0.09	0.51	99.67
C353 15–30	9.57	0.16	4.51	2.05	0.01	0.27	46.88	0.07	0.06	2.17	32.73	0.6	0.09	0.59	99.76
C353 30–45	9.49	0.16	4.5	1.88	0.01	0.29	46.76	0.07	0.05	2.14	33.08	0.4	0.09	0.58	99.5
C353 45–60	9.64	0.17	4.62	2.03	0.01	0.29	46.78	0.07	0.04	2.16	32.99	0.3	0.08	0.64	99.82
C353 60–75	9.54	0.17	4.58	1.97	0	0.28	46.73	0.08	0.04	2.15	33.2	0.2	0.08	0.7	99.72
C353 75–90	9.29	0.16	4.37	1.92	0.01	0.27	46.81	0.07	0.07	2.12	33.43	0.3	0.08	0.76	99.66
C359 0–10	4.68	0.06	2.17	0.72	0	0.2	46.6	0.06	0.02	1.64	41.03	2.6	0.04	0.17	99.99
C359 10–17	5.48	0.06	2.22	0.67	0	0.18	46.59	0.07	0.02	1.61	40.31	2.4	0.03	0.18	99.82
C359 17–32	4.21	0.06	1.29	0.69	0	0.2	46.94	0.06	0.01	1.74	42.04	2.3	0.04	0.18	99.76
C359 32–48	5.04	0.06	1.15	0.67	0	0.19	46.67	0.07	0.02	1.7	41.17	2.7	0.04	0.18	99.66
C359 48–63	4.64	0.05	1.2	0.65	0	0.19	46.69	0.07	0.02	1.69	41.68	2.6	0.03	0.18	99.7
C359 63–77	3.85	0.06	1.13	0.68	0	0.2	46.88	0.06	0.01	1.72	42.17	2.6	0.04	0.17	99.57
C357 0–10	7.76	0.06	1.89	0.9	0	0.18	43	0.08	0.13	1.65	40.23	3.3	0.04	0.2	99.42
C357 50–75	4.88	0.07	2.01	1.04	0	0.22	42.54	0.11	0.1	1.83	43.33	3.1	0.05	0.26	99.54
C358 0–15	9.02	0.06	3.29	0.95	0	0.2	42.47	0.09	0.12	1.35	40.02	1.8	0.04	0.21	99.62
C358 40–55	5.28	0.07	1.79	1.05	0	0.24	42.52	0.1	0.12	1.51	43.69	2.9	0.05	0.21	99.53

Table 5-8 (contd.). Geochemical data from rock-matrix diffusion profiles of samples from Adit A-6 (sample length in millimetres).

Sample	Chromium ppm	Cobalt ppm	Nickel ppm	Selenium ppm	Strontium ppm	Zirconium ppm	Molybdenum ppm	Caesium ppm	Barium ppm	Lead ppm	Thorium ppm	Uranium ppm
C353 (0–15)	564	4.0	264	50	4644	33.5	17.2	1.40	102	<5	2.82	23.4
C353 (15–30)	480	6.7	224	49	5309	27.0	5.4	1.83	118	<5	2.65	23.8
C353 (30–45)	408	7.5	208	42	5516	26.3	5.2	2.10	113	<5	2.51	22.7
C353 (45–60)	437	6.7	194	42	5646	26.2	4.9	2.23	102	<5	2.57	23.0
C353 (60–75)	454	6.7	196	45	6296	28.0	4.8	2.44	95	<5	2.52	22.4
C353 (75–90)	471	6.7	203	43	7208	27.4	5.4	3.00	93	<5	2.48	22.3
C359 (0–10)	250	3.6	127	53	1475	13.1	10.2	0.74	87	<5	0.93	13.0
C359 (10–17)	246	4.0	126	51	1515	13.7	10.5	1.05	109	<5	0.93	13.1
C359 (17–32)	268	3.9	137	49	1532	13.4	9.4	0.95	92	<5	0.95	13.7
C359 (32–48)	253	3.7	138	50	1628	13.2	8.7	1.27	121	<5	0.99	13.5
C359 (48–65)	254	3.9	139	41	1630	13.2	9.2	1.13	122	<5	0.96	13.4
C359 (63–77)	270	4.1	142	47	1529	13.6	10.1	0.89	97	<5	1.07	13.7
C357 (0–10)	318	4.7	162	63	1907	16.3	15.2	1.61	396	<5	1.12	20.1
C357 (50–75)	329	4.5	170	33	2256	16.1	13.8	1.11	106	<5	1.30	22.5
C358 (0–15)	289	2.6	90	33	1794	13.8	10.4	1.33	521	<5	1.03	16.3
C358 (40–55)	325	3.9	151	30	1855	15	13.1	1.17	135	<5	1.17	19.9

Table 5-9. U-decay series measurements on the matrix diffusion profiles.

Sample	U (ppm)	Th (ppm)	^{226}Ra (mBq/g)	^{234}U/^{238}U	^{230}Th/^{234}U	^{228}Th/^{232}Th	^{226}Ra/^{238}U
C353							
0–15 mm	18.7(6)	2.4(2)	224(3)	0.97(3)	1.11(4)	1.0(1)	0.96(3)
15–30 mm	19.8(6)	2.7(2)	–	0.88(3)	1.18(5)	0.7(1)	–
30–45 mm	19.0(6)	2.3(2)	173(2)	0.98(3)	0.98(4)	1.0(1)	0.73(2)
45–60 mm	18.6(5)	2.3(2)	–	0.91(2)	1.06(4)	0.7(1)	–
60–75 mm	18.7(6)	1.8(2)	–	0.89(3)	1.08(4)	1.1(2)	–
75–90 mm	18.5(5)	2.0(2)	236(3)	0.94(3)	1.09(4)	1.1(2)	1.03(3)
C359							
0–10 mm	13.2(4)	3.1(2)	122(2)	0.96(4)	0.96(4)	1.3(1)	0.74(3)
10–17 mm	12.0(3)	2.4(2)	–	0.98(3)	0.97(4)	1.1(2)	–
17–32 mm	12.7(3)	*	137(2)	0.99(3)	1.15(4)	–	0.87(2)
32–48 mm	13.8(4)	*	–	0.94(3)	1.04(5)	–	–
48–63 mm	11.9(4)	2.7(2)	–	0.99(4)	1.08(5)	1.1(1)	–
63–77 mm	12.2(5)	1.3(1)	112(2)	1.02(5)	0.99(5)	0.8(1)	0.74(3)
C357							
0–10 mm	18.6(5)	2.3(2)	–	0.95(3)	0.99(4)	1.1(2)	–
50–75 mm	19.7(7)	0.9(1)	–	1.02(4)	0.97(4)	1.4(3)	–
C358							
0–15 mm	14.7(5)	1.1(1)	–	1.00(4)	1.06(5)	1.2(2)	–
40–55 mm	17.7(6)	1.0(1)	–	0.96(4)	0.96(4)	1.3(2)	–

All errors in parentheses are at the least significant place and represent 1 sigma uncertainties due to counting statistics alone.

* Results for ^{232}Th for C359 17–32 and 32–48 mm failed laboratory QA.

Average chemical recoveries are C353 (80% U and 77% Th) and C359 (70% U and 71% Th).

Table 5-10. Porosity measurements performed during analysis.

Field Measurements (Derived from the whole image area)	**Object Specific Measurements** (Derived from individual pores)
Percentage porosity	Pore area
Actual area of porosity (μm^2)	Pore perimeter
	Pore aspect ratio:
	= Maximum pore diameter/ Minimum pore diameter
	Pore circularity
	= 4^1 pore area/ pore perimeter

Table 5-11. Results of liquid resaturation porosimetry measurements on fractured biomicrite wallrock from Adit A-6.

Sample Number		**C353** 0–15	**C353** 15–30	**C353** 30–45	**C353** 45–60	**C357** 0–10	**C357** 50–74	**C358** 0–15	**C358** 40–55	**C359** 0–10	**C359** 10–17	**C359** 17–32	**C359** 32–48	**C359** 48–63	**C359** 63–77
Dry weight	(g)	5.4	2.6	3.2	3.9	11.2	29.1	9.8	7.0	8.6	10.1	4.3	5.9	4.7	3.5
Sat. weight in fluid	(g)	3.6	1.7	2.2	2.7	7.3	18.9	6.4	4.6	5.7	6.7	2.9	3.9	3.1	2.3
Sat. weight in air	(g)	6.6	3.2	4.0	4.8	12.4	34.0	10.7	8.2	9.8	11.3	5.0	6.7	5.3	4.1
Fluid density	(g)	0.8	0.8	0.8	0.8	0.8	0.8	0.8	0.8	0.8	0.8	0.8	0.8	0.8	0.8
Dry bulk density	(g/cm^3)	1.4	1.4	1.4	1.4	1.7	1.5	1.8	1.5	1.7	1.8	1.6	1.7	1.7	1.6
Sat. bulk density	(g/cm^3)	1.8	1.8	1.9	1.9	2.0	1.9	2.0	1.9	1.9	2.0	1.9	2.0	2.0	1.9
Grain density	(g/cm^3)	2.4	2.4	2.6	2.6	2.3	2.3	2.3	2.3	2.3	2.4	2.3	2.3	2.3	2.3
Porosity	(%)	40.3	42.2	45.3	44.8	23.4	32.9	21.8	31.4	29.2	25.1	29.8	29.3	28.6	31.1

Table 5-12. Results of image porosity determinations for fractured biomicrite.

Sample		Fracture porosity (%)		Wallrock porosity (%)	
		Mean	St. Dev.	Mean	St. Dev.
C353	Fracture from Adit A-6	25.07	7.65	39.25	14.81
C359	Fracture from Adit A-6	31.46	4.96	0.886	0.289
C767	"Unaltered" biomicrite	N/A	N/A	10.58	2.55
C776	Secondary fillings (green) on top of biomicrite Wadi Sijin	N/A	N/A	8.83	2.44
C779	Chert Chalky Limestone Member with secondary fillings	N/A	N/A	17.54	4.67
C780	Upper Chalky Limestone Member with secondary fillings	N/A	N/A	15.42	6.44

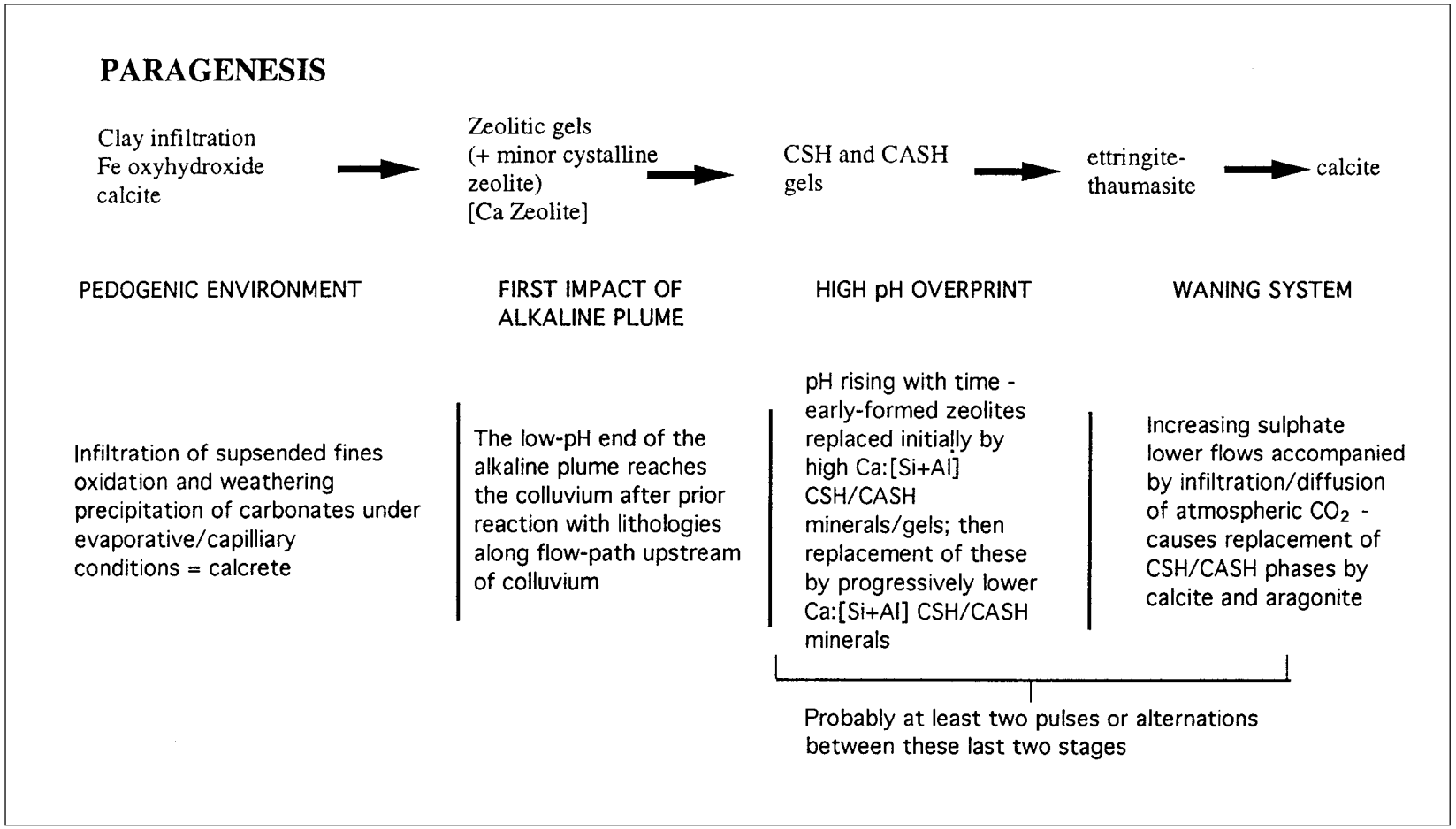

Figure 5-1. *Summary of the mineral paragenesis and alteration processes at the Western Springs area, Maqarin.*

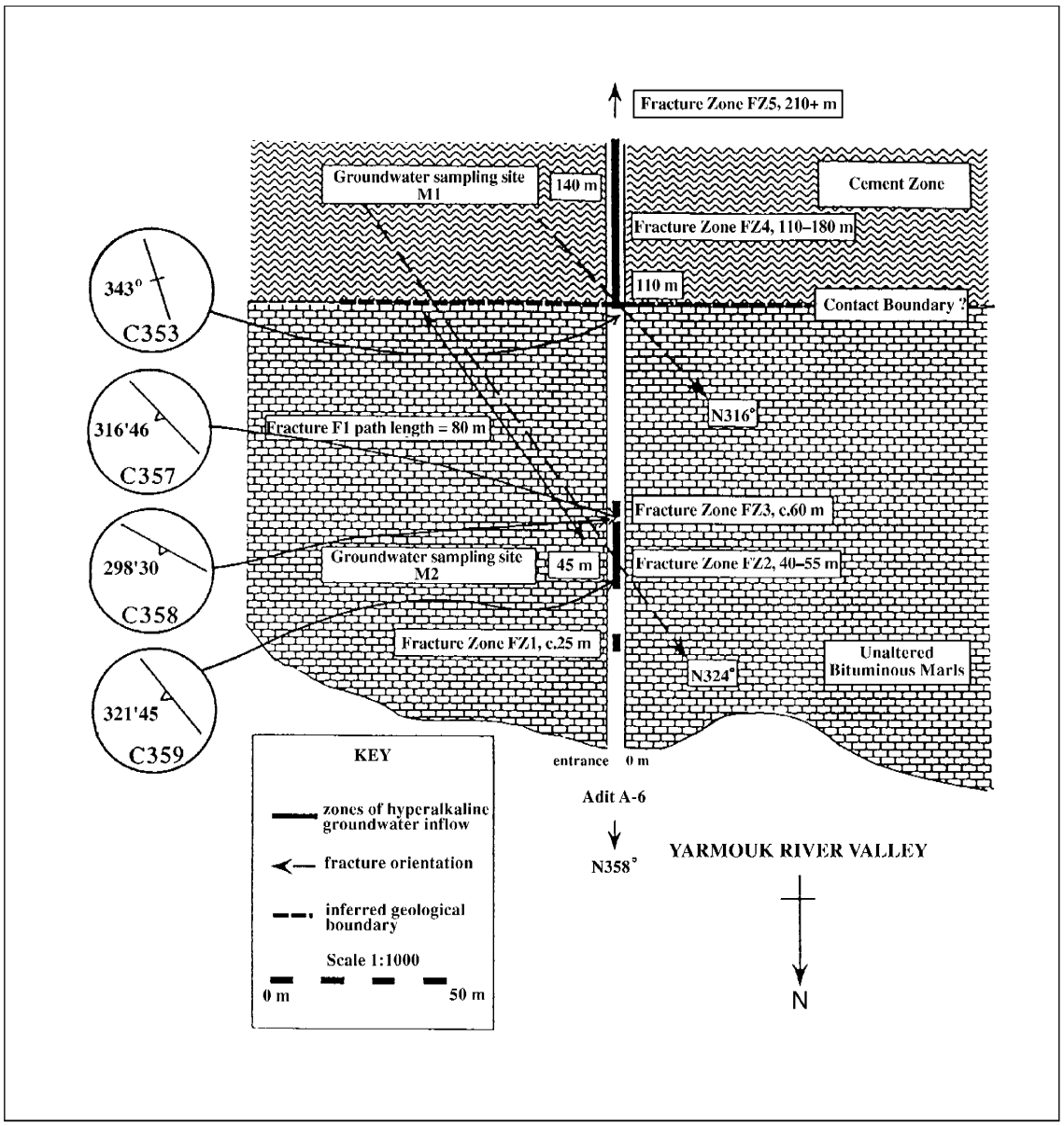

Figure 5-2. *Plan diagram showing the local geology, and location and geometrical relationships of the principle hydrogeological features and sampling sites in Adit A-6, Maqarin.*

Figure 5-3. *Photographs showing sampled vein and wallrock [C357 (top) and C353 (bottom)].*

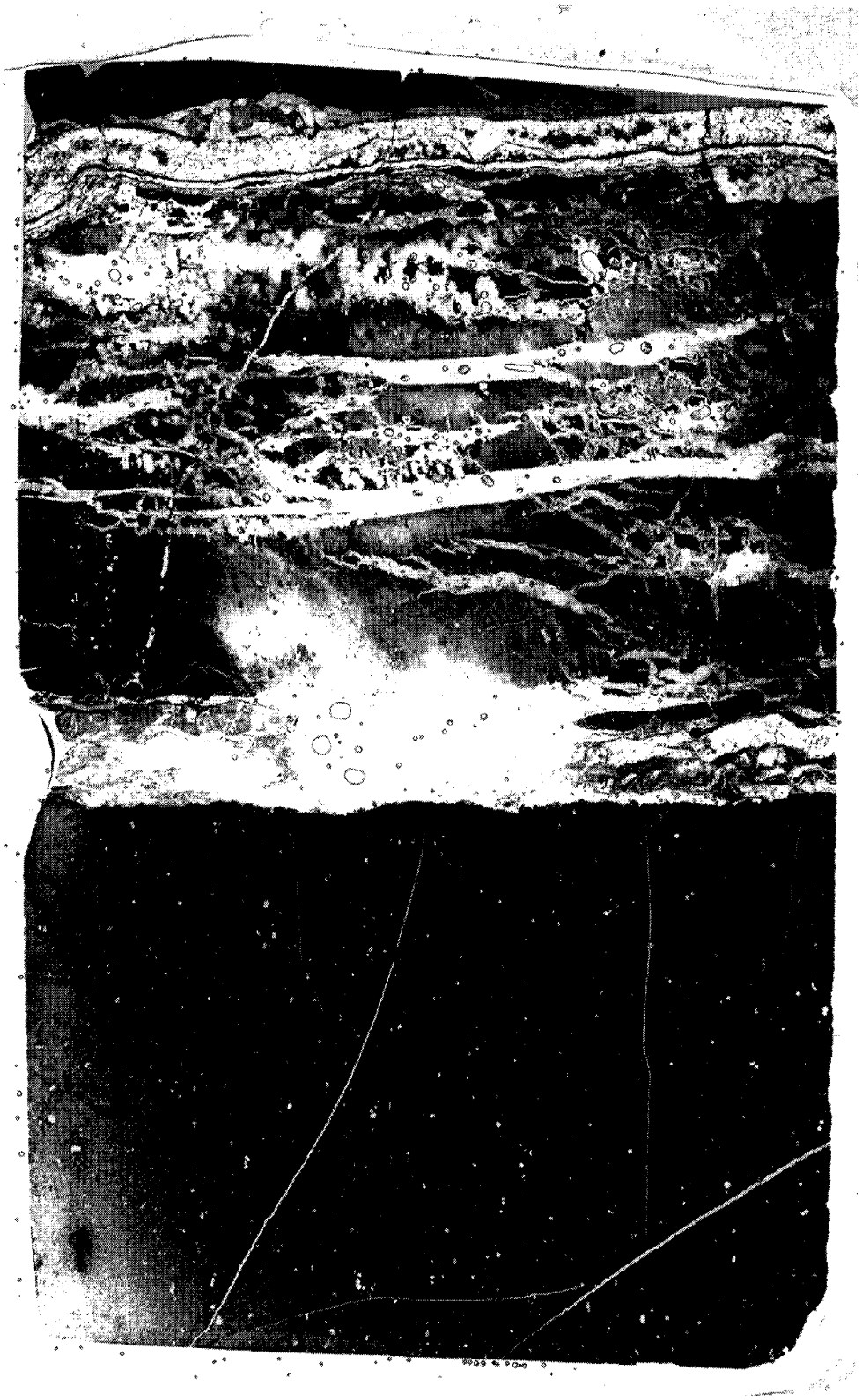

Figure 5-4. *Contact print of polished thin section of sample C353 showing complex vein structure (upper half) and relatively uniform biomicrite host rock (lower half). Note presence of microveining in host rock. Length of polished section is 35 mm.*

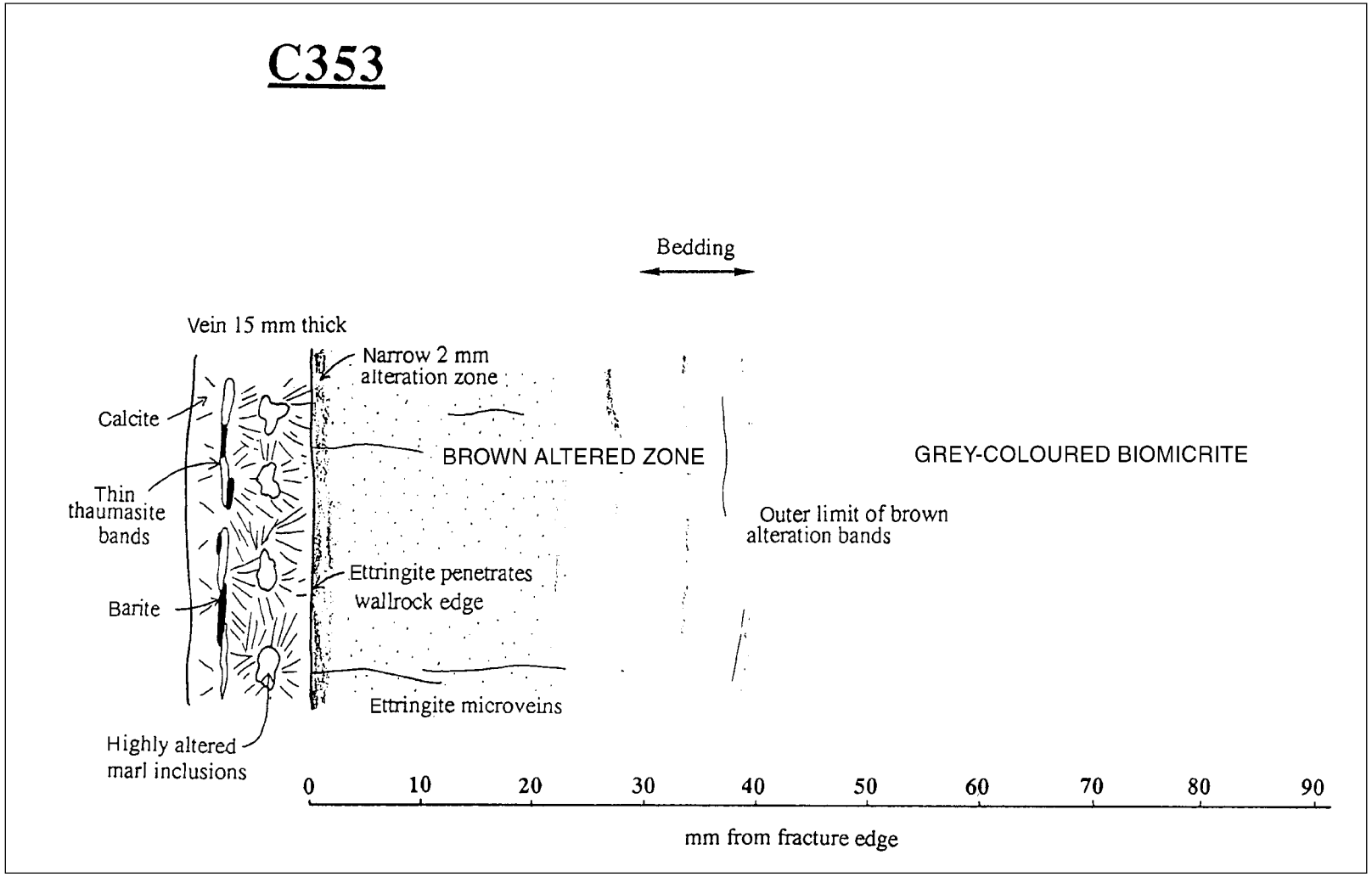

Figure 5-5. *Diagrammatic sketch of vein and wallrock profile in sample C353.*

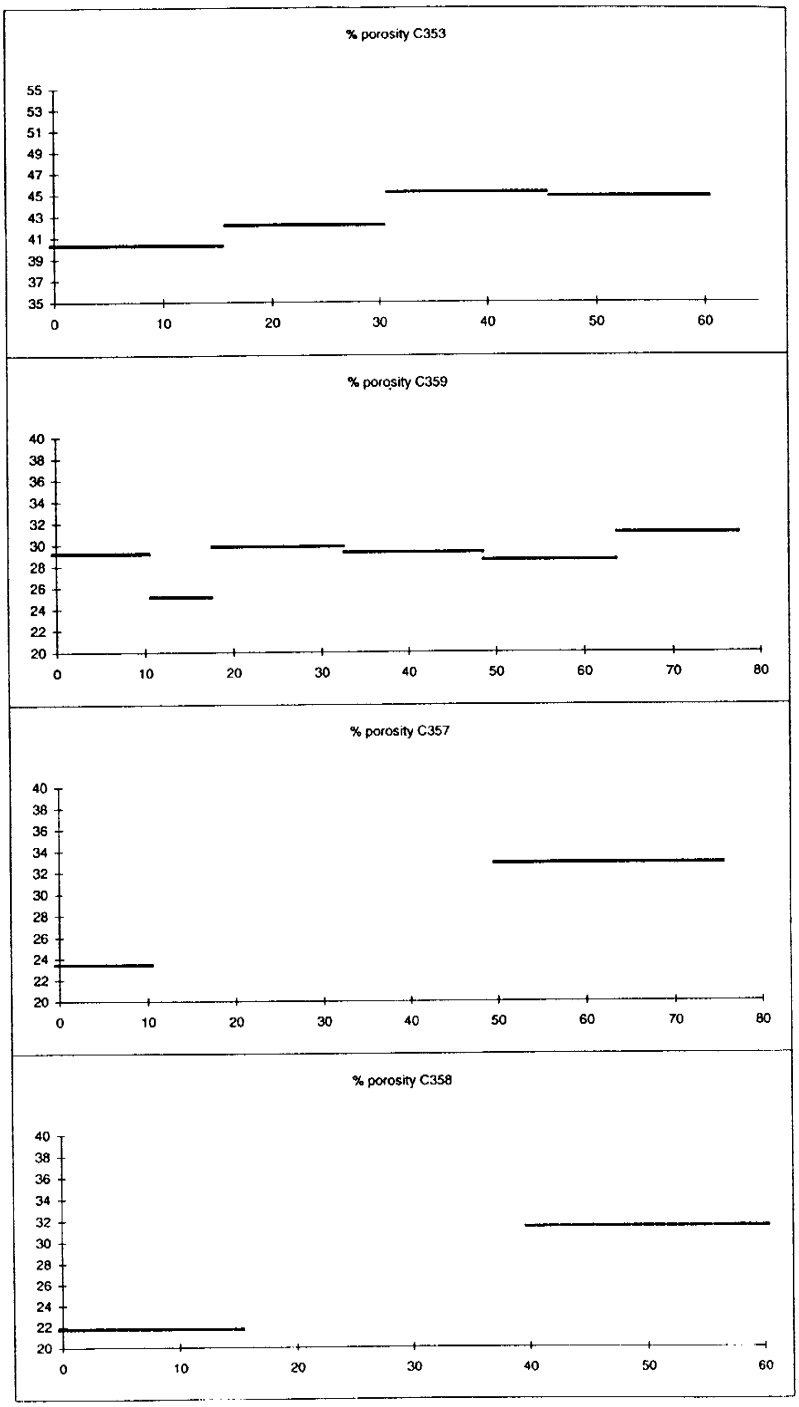

Figure 5-6. *Porosity data plotted as profiles across the biomicrite wallrock with increasing distance from fracture edge for samples C353, C359, C357 and C358. (Vertical axis represents percent porosity from liquid resaturation analysis; horizontal axis represents distance from fracture edge in millimetres).*

6 HYDROGEOCHEMISTRY OF THE MAQARIN AREA

(H.N. Waber, I.D. Clark, E. Salameh and D. Savage)

6.1 BACKGROUND AND OBJECTIVES

Hydrogeochemical interpretation of the Maqarin region has been largely focussed on providing specific input to address the various objectives of the different phases of the Maqarin study. The emphasis in Phase I (Alexander, 1992) was to generally characterise the Eastern and Western Springs groundwaters using major element and isotopic parameters, and to provide suitable major and trace element data to test thermodynamic databases and geochemical codes used to predict safety-related heavy element solubility and mobility under highly alkaline conditions. Phase II (Linklater, 1998) expanded the area of study by looking at geochemical modifications and transport phenomena in the Eastern Springs localities at the zone of interaction between the near-field leachates and the far-field unaltered Bituminous Marl Formation. This necessitated additional groundwater sampling and the analysis of a greater suite of trace elements, together with selected environmental isotopes. Whilst Phase I database testing examined essentially pure end-member mineral species, in the Phase II study more effort was given to the provision of relevant field data for testing the model predictions (aqueous speciation data was improved; more details regarding trace element sources/sinks etc.). Modelling was also extended to test coupled flow-transport codes in the hyperalkaline environment.

Following the Phase I and II studies, some doubts persisted as to the origin of the Eastern and Western Springs groundwaters, in particular the distinct difference in composition. The Western Springs groundwaters, when compared with the Eastern Springs varieties, are more mineralised, particularly in conservative species (SO_4^{2-}, Na^+), and contain unusually high concentrations of K^+ and Cr. It was thought that these variations reflected the nature of the reacting cement zones, i.e. different ages, different retrograde alteration sequences etc., or variations in groundwater circulation rates. The Western Springs localities (NaOH and KOH leachates in addition to $Ca(OH)_2$ leachate) might then be considered as representing a more recent event than the Eastern Springs localities (mainly dominated by $Ca(OH)_2$ leachate), conveniently analogous to the sequence of events expected to characterise the evolution of leachate release from a cementitious repository environment.

Accordingly, the major objectives of Phase III were to confirm the presence of Na/K-hydroxide groundwaters at the Western Springs locality, establish their origin and chemistry, and study the water/rock interactions. It was hoped that by comparing and integrating these data with existing data from the eastern localities, and generally providing a more regional context for hydrogeochemical interpretation (i.e. greater integration of hydrogeology and geomorphology), would help to fill the current gap concerning present knowledge on the very earliest stage of the cement leachate/host rock interaction and allow some form of validation of the current conceptual models of

the repository/host rock evolution. In addition, the data could be used to test those coupled codes employed in assessing the long-term evolution of the repository as part of a repository safety assessment, indicating both the applicability of the codes in a repository analogous environment and identifying those areas where further code development may be necessary.

To put Maqarin in perspective, a hydrochemical survey of the regional groundwaters in northern Jordan has been conducted to obtain detailed information about the general hydrochemical evolution in the area. Furthermore, it was aimed to obtain specific geochemical information about the recharge conditions in the Maqarin area and to define an inlet composition of normal pH groundwater infiltrating into the cement zone and subsequently evolving to high-pH groundwater. This inlet composition provided the source term for modelling the rock/water interaction in the Western Springs area, both in this Chapter and in Chapter 7.

6.2 GENERAL FEATURES OF THE REGIONAL GROUNDWATERS

The survey is focussed on the drainage system of the Yarmouk River in northern Jordan covering an area of approximately 3600 km^2 (Fig. 6-1). A total of 454 groundwater analysis from local and regional studies in northern Jordan, involving seven major groundwater systems in the area, have been compiled (Appendix K), reviewed, classified and investigated for their geochemical evolution. Based on a rigorous quality check of the analyses at hand, a set of 358 groundwater analyses, including the Maqarin Project groundwater samples, was selected and used for further investigations. These groundwaters have been related to data from local regional rock geochemical and mineralogical studies in northern and central Jordan (Appendix L). Thermodynamic calculations were performed with PHREEQC (Parkhurst, 1995) using the Nagra thermodynamic database tested in Phase II (Pearson and Berner, 1991; Pearson et al., 1992, Alexander et al., 1998). The input groundwater compositions and results of the thermodynamic calculations are presented in Appendix M.

For most of the regional groundwaters, only major element analyses are available and many of them have only semi-quantitative pH-measurements, both restricting the interpretation of the geochemical evolution of these groundwaters. Also, the majority of these groundwaters were sampled from open boreholes and wells and thus many of the groundwaters underwent degassing during sampling and/or may also represent mixtures of waters from different groundwater systems. Groundwater mixing is very much dependent on borehole depth (i.e. number of aquifers intercepted) and the hydraulic properties of the boreholes (i. e. open-hole effects); borehole data are limited to open boreholes.

In the following sections the chemistry, origin and age of the main regional aquifers are described, and their importance in conceptualising the Maqarin local scale groundwater flow system, in particular the Western Springs locality, is emphasised.

6.2.1 Hydrogeological Setting

The origin of groundwaters in the Maqarin area must be examined in view of the regional flow systems of northern Jordan. The geology of northern Jordan consists of a succession from Triassic through Quaternary sediments, partly overlain by basalt flows of Oligocene to Holocene age (Bender, 1968; 1974). Table 6-1 shows the stratigraphic sequence as observed in northern Jordan and its nomenclature according to different authors; the local Maqarin nomenclature (cf Chapter 2, Fig. 2-3) is also given for reference. The different stratigraphic units generally dip towards the north-northwest, towards the Yarmouk and Jordan River Valleys. The stratigraphically oldest units outcrop in the area of the Zarqa River Valley, whereas in the Maqarin area the sequence includes younger, late Cretaceous to Tertiary formations.

Structurally, Northern Jordan is dominated by a synclinal structure between the Ajlun Highlands and the Golan Heights, the base of which forms the Yarmouk Valley (Bender, 1974). The Ajlun Highlands further act as a groundwater divide for groundwaters discharging through the Side Wadis directly into the Jordan Rift Valley and groundwaters that discharge towards the east into the SE-NW oriented flow system of the Ramtha-Irbid-Yarmouk area (Fig. 6-1). Thus, three regional hydrostratigraphic units dominate (Figs. 6-2; 6-3):

1. The deep Ajlun Group (A_1-A_6) is a low-yield artesian aquifer system consisting mainly of dolomitic limestone with intercalated marl and marl sequences; there is geochemical evidence for subsurface gypsum.

2. The overlying Wadi es Sir Formation (A_7) is a marly dolomitic limestone, outcropping in the Ajlun Highlands and in deeply incised wadi channels on the East Bank of the rift valley (Fig. 6-1). Groundwaters (A_7-aquifer) are mainly developed by wells along the eastern boundary of the northern Jordan Rift Valley.

3. The overlying Amman Formation marly limestone hosts a highly productive artesian aquifer in the upper B_2 stratigraphical unit (B_2-aquifer). This B_2 unit outcrops south of Irbid towards the Zarqa River valley. In the Mukheiba area, 25 kilometres to the west of Maqarin (Fig. 6-1), the B_2 aquifer hosts thermal waters with temperatures up to 52°C (Bajjali et al., 1997).

The Amman Formation hosts groundwaters that are under artesian pressure throughout most of the lower Yarmouk River basin, and which can recharge overlying strata in this area. The deeper Ajlun Group (A_1 to A_7) also hosts regional confined aquifers that discharge to the surface through seepages in the lower Yarmouk Valley.

The Amman Formation is overlain by the bituminous rich marls and chalks of the Muwaqqar (B_3) Formation (at Maqarin referred to as the Bituminous Marl Formation; Table 6-1) which generally acts as an aquitard. On top of the Muwaqqar Formation the Tertiary limestone sequences of the Rijan and Shallala Formations form local aquifers in northern Jordan (B_4 and B_5 aquifers). At Maqarin these sediments comprise the Chalky Limestone Formation (Table 6-1) and are partly overlain by basalt flows of Oligocene and Holocene age. A detailed description of the regional hydrogeology of northern Jordan is given by El-Nasser (1991) and Salameh (1996).

6.2.2 Chemistry of the Groundwaters

Prior to a systematic hydrochemical evaluation, the regional chemical database was first evaluated using a Principle Component Analysis (PCA) to determine any broad regional grouping of data which might facilitate further interpretation; the first and second principal components chosen described 68% of the variability (i.e. information) of the data. This exercise revealed three major groundwater types (Laaksoharju and Skårman, written comm., 1996): a) a bicarbonate-rich type (i.e. thermal waters) with a generally low ^{18}O and a positive correlation with F and Li, b) a chloride-rich type (i.e. Amman Formation B_2/A_7 aquifer) with a generally high ^{18}O and a suggested correlation with Mg and Na, and c) a sulphate-rich type (i.e. Western Springs locality) with a suggested correlation with K and Cr.

Kurnub-Sandstone (Lower Cretaceous, Kurnub-Aquifer)

Overlying a thick sequence of Jurassic sediments, the Kurnub-Sandstone forms the lowest aquifer system in northern Jordan (Fig. 6-3) and has an increasing thickness from about 200m in the south to more than 300 m in the north at the Jordan Rift Valley (El-Nasser, 1991). The formation consists of conglomeratic layers at the bottom that are overlain by a sequence of alternating silty and marly sandstone units with some intercalated shale and marl layers. The top of the formation is made of medium- to coarse-grained sandstone units alternating with limey sandstones and dolomites.

Indirect recharge into the Kurnub-Aquifer occurs from north-northeast (Syria) and the east by subsurface flow and by downward leakage from the overlying aquifers (El-Nasser, 1991). Discharge of the Kurnub-Aquifer occurs towards the south along the Zarqa River Valley (Fig. 6-1) in the form of springs and towards the Jordan Rift Valley in the northwest. In the Mukheiba – Wadi Al Arab area (Fig. 6-1), the potentiometric surface of the Kurnub-Aquifer is higher than the one of the overlying Wadi Sir – Amman Aquifer System (A_7/B_2) invoking an upward leakage of Kurnub groundwater into the overlying groundwater system.

Analyses of Kurnub groundwater are available from the southern discharge area, the El-Hamma spring in the Zarqa River Valley, and from a depth of 2190 m below the surface in borehole S-90 near the city of Ramtha (Fig. 6-1). Both groundwaters are strongly mineralised with total dissolved solid contents of more than 2000 mg/L indicating a long residence time. The slightly less mineralised groundwater of the El-Hamma spring, to the immediate SW of Mukheiba, is a Na-Ca-SO_4-Cl-HCO_3 type whereas the one from borehole S-90 is of Ca-Na-SO_4-HCO_3-type. The Kurnub groundwater of the Ramtha area (Fig. 6-1) displays much higher concentrations of calcium, sulphate and potassium, but lower chloride than the El-Hamma spring water (Appendix M; Table M-1). The different chemical compositions indicate a different geochemical evolution for the two Kurnub groundwaters. Different flow regimes in the Kurnub aquifer for the Ramtha area and the Zarqa River area, to the south of the Ajlun Heights (Fig. 6-1), are in agreement with the extrapolated topography of the Kurnub sandstone in northern Jordan displaying an anticlinal structure between these two areas (Fig. 6-3). Consistent with the high mineralisation, the O- and H-isotopic compositions of the Kurnub groundwater from borehole S-90 indicate infiltration during cooler climatic conditions of the late Pleistocene.

Saturation state calculations using the measured data indicate that within the analytical uncertainties the groundwaters are saturated with respect to calcite ($Si_{calcite}$ = -0.27 to 0.00). This is consistent with the long residence time of these groundwaters in a carbonate-bearing aquifer system. In equilibrium with calcite the groundwaters display high pCO_2-values between $10^{-0.76}$ to $10^{-0.51}$ bars, and are undersaturated with respect to dolomite, gypsum and fluorite, but about in equilibrium with chalcedony (Appendix M; Table M-2).

Wadi es Sir Formation (Middle Cretaceous, A_7-Aquifer)

The Wadi es Sir Formation (Figs. 2-3 and 6-1) forms the uppermost part of the approx. 270–570 m thick Ajlun Group which consists of intercalated limestones, marls and dolomites. The thickness of all the Ajlun Group units generally increases towards the Yarmouk River Valley and the Jordan Rift Valley. The Wadi es Sir Formation is made of massive limestones that increase from 80–90 m in the central part of Jordan to about 200 m in the northern part of the country. The Wadi es Sir Formation forms together with the overlying Amman Formation one of the most important aquifer systems (A_7/B_2 Aquifer system, see below) in northern Jordan. In the north, these two formations are separated by the Wadi Al Ghudran Formation (B_1-Aquifer) which consists of about 35 m of intercalated limestones, chalky marls, and dark coloured marls, and which thins out towards the south. The Wadi es Sir Formation is directly recharged in the east (NE-Desert, Figs. 6-1 and 6-4) from where the groundwater flows towards the northwest. Additional subsurface recharge into this flow system occurs through basaltic rocks from the Syrian side. The major recharge area of the flow system towards the west of the Ajlun Highlands is formed by these highlands themselves. From there the groundwater flows towards the west-northwest and discharges in the Side Wadis (i.e. a collective term for all the wadis discharging west into the Jordan River Valley) along the Jordan Rift Valley (Fig. 6-1).

Analyses of groundwaters assigned to be pure A_7-Aquifer groundwaters are available from wells within the NE-Desert recharge area and from springs and wells of the Side Wadis discharge area. Comparison of the total dissolved solids (TDS) concentrations and tritium contents of these groundwaters shows that the A_7-Aquifer groundwaters from the NE-Desert recharge area (Fig. 6-1) are geochemically more evolved and have longer residence times than the A_7-Aquifer groundwaters from the Side Wadis discharge area (Appendix M; Table M-3). Tritium values indicate a residence time in the range of a few years for the Side Wadis A_7-groundwaters and in the range of a few tens of years for the NE-Desert A_7-groundwaters.

According to their chemical and isotopic composition, the A_7-groundwaters discharging in the Side Wadis must recharge in the near-by Ajlun Highlands, whereas discharge of the groundwaters sampled in the NE-Desert takes place close to the junction of the Yarmouk River and the Jordan River. Possible discharge waters are the thermal groundwaters found along the Yarmouk River Valley in the northwest of Jordan (for a detailed description of the thermal waters in northern Jordan see the studies by El-Nasser, 1991; Bajjali, 1994; Clark et al., 1995). The observed geochemistry of the A_7-groundwaters is therefore in agreement with the flow pattern as derived from groundwater isotopic data (cf sub-section 6.2.3) and hydrological data (El-Nasser, 1991).

The more evolved A_7-groundwaters from the NE-Desert are in equilibrium with calcite, as are the less evolved A_7-groundwaters from the Side Wadis, and undersaturated with respect to all other minerals (Appendix M; Table M-4). In the latter groundwaters, the apparent calcite oversaturation in some of the samples has to be attributed to sampling and/or analytical artefacts. Based on the available major cation and anion data, the major processes in the A_7-groundwaters of the NE-Desert are carbonate dissolution until calcite equilibrium is achieved accompanied by minor sulphide dissolution. The elevated Na/Cl ratios and the low Ca/HCO_3 ratios in these groundwaters compared to evaporated precipitation could be explained by cation exchange processes. Calcite dissolution would then be initially triggered by soil CO_2 and later on by Ca-Na cation exchange in the marly units. To what degree mixing with evolved basaltic waters might occur in these groundwaters cannot be further evaluated based on the available data. In the A_7-groundwaters of the Side Wadis carbonate dissolution through soil CO_2 is by far the dominant process. In these groundwaters the Na/Cl ratio is equivalent to precipitation evaporated to 40%.

Amman Formation (Upper Cretaceous, B_2-Aquifer)

The thickness of the Amman Formation or B_2-Aquifer increases from about 50 m in the central part to about 130 m towards the Jordan Rift Valley in the northwest. The lower part consists of dark-coloured cherts with siliceous limestone bands and nodules and intercalated bituminous marls and fossiliferous limestones (Abdul-Jaber, 1989). This lower part is highly fractured with abundant calcite and bituminous material as fracture coatings. The upper part of the Amman Formation is characterised by its abundant fossil fragments which can make up to more than 50% of the whole rock. The groundmass of the heavily fractured rock is either a fine-grained, dark-coloured marl, or a sandy limestone.

The Amman Formation forms together with the Wadi es Sir Formation (Fig. 2-3) one of the most important aquifer systems in northern Jordan, the A_7/B_2-Aquifer, reaching a thickness of up to 400 m towards the Jordan Rift Valley. The hydrologic properties are anisotropic and heterogeneous in both these formations, and transmissivities increase from southeast to northwest to values of 10^{-7} to 10^{-5} m^2/s (El-Nasser, 1991). The hydrologic communication between the Wadi es Sir Formation and the Amman Formation appears to be good, especially in places where the Wadi Ghudrun Formation is missing, so that most groundwaters sampled within the Amman Formation are probably mixtures of groundwaters from the two geological formations. In the Maqarin area strong artesian conditions prevail in the A_7/B_2-Aquifer. As for the A_7-Aquifer system, the major direct recharge areas are in the NE-Desert area and the Ajlun Highlands where the rocks of the Amman Formation are directly exposed. In addition, sub-surface recharge occurs from the Jabel Al Arab in Syria through basaltic aquifers.

Wadi es Sir-Amman Formation (A_7/B_2) groundwaters from the NE Desert area

- In the NE-Desert area, three different groups of A_7/B_2-groundwaters can be discerned based on their chemical composition. These are from east to west (Figs. 6-1 and 6-4):

- NE-Desert I: Na-Mg-Cl-HCO_3 groundwaters;
- NE-Desert II: Ca-Na-Mg-HCO_3-Cl groundwaters;
- NE-Desert III: Ca-Mg-HCO_3 groundwaters.

Groundwaters of the most eastern group, the NE-Desert I group, have pH-values around 8 and TDS-contents between 445–653 mg/L. The stable isotope compositions of these groundwater samples indicate an infiltration under present-day climatic conditions. The ^{3}H-content is below detection limit in most of the samples and therefore groundwater infiltration took place more than 40 years ago. The typically high Na^+-, Mg^{2+}- and K^+-concentrations together with the low Ca^{2+} and HCO_3^- (Appendix M; Table M-5) indicate that these groundwaters derived most of their mineralisation in rocks different from the ones in the Wadi es Sir and Amman Formations. Their chemical composition is closely similar to the one of evolved groundwater sampled in basaltic rocks (see below). The sampled groundwaters therefore represent mixtures of sub-surface recharge from the Syrian basalt aquifers into these formations, with only very minor amounts of ^{3}H-free A_7/B_2-groundwater. Worth mentioning is the high SO_4^{2-}-concentration (Appendix M; Table M-5) in these mainly basaltic groundwaters which derives from sulphide oxidation within the basaltic rocks.

Groundwater from the NE-Desert I group is in equilibrium with calcite and very close to equilibrium with dolomite and magnesite due to the elevated Mg^{2+}-concentrations (Appendix M; Table M-6). This is of importance because for any further interaction with the rocks of the Wadi es Sir and Amman Formations, a driving force different from that of the carbonate system would be required. Unfortunately, there are no data available about the redox conditions of these groundwaters.

Groundwaters from the NE-Desert II group (Fig. 6-1) have TDS contents between 408–539 mg/L, and, except for HCO_3^-, major cation and anion concentrations are intermediate between the NE-Desert I group and the NE-Desert III group (Appendix M; Table M-5). The groundwaters infiltrated under present-day climatic conditions more than 40 years ago as shown by their stable isotopic composition and ^{3}H contents (Appendix M; Table M-5). These groundwaters are also in equilibrium with calcite, but slightly undersaturated with respect to dolomite and magnesite (Appendix M; Table M-6). Chemical and isotopic composition of these groundwaters indicate for the NE-Desert II groundwaters a mixture of basaltic groundwater with a larger component of ^{3}H-free A_7/B_2-groundwater compared to the NE-Desert I groundwaters. This A_7/B_2-groundwater component must be a largely evolved carbonate groundwater as shown by the low ^{14}C activities and the less negative δ^{13}C-values; both are a result of increased carbonate dissolution, compared to the young NE-Desert III groundwaters (see below).

NE-Desert III groundwaters (Fig. 6-1) are typical direct recharge groundwaters of the A_7/B_2-Aquifer system. From the chemical point of view, these waters are the type of groundwater that acts as recharge for the A_7/B_2-groundwaters in the Maqarin area (cf sub-section 6.3.1). They are of Ca-Mg-HCO_3-type groundwaters with TDS contents of 352–402 mg/L, pH-values around 7.3, and a chemical composition typical for young carbonate groundwaters (Appendix M; Table M-5). Their Na^+- and Cl^- concentrations are that of local evaporated precipitation. Ca^{2+}-, Mg^{2+}- and HCO_3^- - concentrations derive mainly from calcite and dolomite dissolution induced by soil CO_2. The NE-Desert III groundwaters have average ^{3}H-contents only slightly lower than average precipitation, indicating a very short underground residence time of only a few years. This is consistent with the high ^{14}C-activities and low δ^{13}C-values. The slight calcite

oversaturation computed from the measured values is attributed to analytical artefacts. At calcite equilibrium, these groundwaters are undersaturated with respect to dolomite (Appendix M; Table M-6).

Amman Formation (B_2) – groundwaters from the Ramtha area

B_2-groundwaters of the Ramtha area (Fig 6-1) can be subdivided into two groups according to their mineralisation and pH-values (Appendix M; Table M-7). Lower mineralised groundwaters with TDS contents between 400-590 mg/L and pH-values at calcite saturation of 7.34 ± 0.12 belong to the Ca-Mg-(Na)-HCO_3-Cl-type waters. Higher mineralised groundwaters with TDS contents between 635–786 mg/L and pH-values at calcite saturation of 6.96 ± 0.04 belong to the Ca-Mg-Na-HCO_3-SO_4-Cl-type waters.

The lower mineralised groundwaters represent typical carbonate groundwaters that are chemically only slightly more evolved than the recent recharge waters of the NE-Desert III area. According to their ^3H-contents these waters infiltrated into the Amman Formation certainly more than 40 years ago. Low ^{14}C-contents associated with low $\delta^{13}C$-values (due to only a moderate calcite/dolomite dissolution or sulphate reduction) in some of these waters indicate a very long residence time in the range of several hundreds or more years. They have Na/Cl equivalent to that of evaporated precipitation and their low mineralisation is mainly derived from calcite and dolomite dissolution along the flow path. Sulphate cannot be derived from pyrite oxidation as the $\delta^{34}S$ is too enriched and the concentrations are too high. Dissolution of subsurface gypsum must be the source. The groundwaters are in equilibrium with calcite, undersaturated with respect to dolomite and gypsum, and in equilibrium with chalcedony (Appendix M; Table M-8; only one SiO_2 analysis available).

The higher mineralised B_2-groundwaters from the Ramtha area have elevated Na^+-, Mg^{2+}-, Ca^{2+}-, HCO_3^-- and especially SO_4^{2-}-concentrations compared to the lower mineralised groundwaters from the same area. These groundwaters also infiltrated certainly more than 40 years ago according to their ^3H-contents. However, their stable isotopic composition (Appendix M; Table M-7) indicates that the infiltration area of these groundwaters was, however, different (probably at higher elevation) from the one of the low mineralised groundwaters of the area. As for the low mineralised waters, the low ^{14}C-contents suggest old waters. However, their depleted $\delta^{13}C$ values indicate the oxidation of bitumen present in the bituminous marl. Stable isotope data suggest that these waters are late Holocene in age (Bajjali et al., 1997).

The chemical composition of these groundwaters suggest a mixture of mainly carbonate water with groundwater derived from basaltic rocks. However, the incomplete analytical data set available does not allow further interpretation. The higher mineralised groundwaters are saturated with respect to calcite and more undersaturated with respect to dolomite, but less undersaturated with respect to gypsum compared to the less mineralised groundwaters of the area.

Wadi es Sir – Amman Formations (A_7/B_2) – groundwaters from the Side Wadis

A_7/B_2 groundwater analyses from Side Wadis discharging into the Jordan Rift Valley are available from Wadi Al Arab, Wadi Jurum, and Wadi Yabis (Fig. 6-1). In Wadi Al Arab, groundwaters were analysed from boreholes that were drilled into the Wadi es Sir Formation and produced water from the A_7/B_2-Aquifer. Other boreholes were drilled only into the Amman Formation and produced mainly water of the B_2- Aquifer (El-Nasser, 1991). Groundwater from the A_7/B_2-Aquifer in Wadi Al Arab belongs to the Ca-Mg-HCO_3-SO_4-type, whereas the B_2-Aquifer water represents typical carbonate groundwater of the Ca-Mg-HCO_3-type. The groundwaters of both these groups are closely similar, except for the elevated Na^+- (factor of 1.5) and SO_4^{2-}- (factor of 2) contents in the A_7/B_2-groundwaters (Appendix M; Table M-9). All the groundwaters have ^3H-contents around detection limit indicating an infiltration of more than 40 years ago. The ^{14}C-activities in the A_7/B_2-groundwaters of Wadi Al Arab are less than half the ones in the B_2-Aquifer waters which can be either interpreted as a longer residence time or dilution by ^{14}C-free water. El-Nasser (op.cit.) attributed the chemical and isotopic differences in these groundwaters to a mixture of 97% pure carbonate groundwater with 3% upward leaking of old Kurnub groundwater towards the Jordan Rift Valley. Rock mineralogy along the flow path and residence time of these groundwaters suggest that they are in equilibrium with calcite. The measured values yield a slight computed calcite oversaturation in these groundwaters (Appendix M; Table M-10). This is attributed to degassing of CO_2 during sampling. At calcite equilibrium the groundwaters are undersaturated with respect to dolomite and gypsum.

Young A_7/B_2-groundwater from the Wadi Jurum and Wadi Yabis is chemically very similar to the B_2-groundwater of Wadi Al Arab except for their higher NO_3^--concentrations (Appendix M; Table M-9). These higher NO_3^--concentrations have to be attributed to stronger anthropogenic influences. The A_7/B_2-groundwaters have ^3H-activities that are about half of the local precipitation. This indicates a residence time for these groundwaters of only a few years. These groundwaters are also oversaturated with respect to calcite when calculating calcite saturation with the measured values. At calcite equilibrium, the A_7/B_2-groundwaters of these two side wadis are more undersaturated with respect to dolomite and gypsum compared to the Wadi Al Arab B_2-groundwaters.

The close chemical similarity of the young A_7/B_2-groundwaters of Wadi Jurum and Wadi Yabis with the B_2-groundwaters of Wadi Al Arab clearly shows that the mineralisation in these Aquifers occurs very rapidly. This is characteristic for carbonate aquifers. Additional mineralisation can only occur if there are other driving forces than the carbonate system for further reactions. Such driving forces may include the oxidation of organic material or cation exchange, both of which, however, would require rock compositional changes along the flow path.

Rijam Formation (Lower Tertiary, B_4-Aquifer)

The Rijam Formation consists of three lithologically different limestone units which in the Maqarin Area are partly equivalent to the lower part of the Lower Chalky Limestone Member of the Chalky Limestone Formation (Fig. 2-3; Table 6-1). Calcite is by far the most abundant mineral component in all units (40–88 wt%; data from Abed and Amireh, 1983). Apatite and clay minerals average around 5 wt%. Pyrite is always

present between 1.2–4.1 wt%, whereas dolomite and quartz may be absent or present up to 12 wt% and 37 wt%, respectively. The limestones and intercalated cherts of the Rijam Formation are affected by a high degree of karstic weathering. The Rjiam Formation is only partly saturated and infiltration and groundwater flow in the aquifer occur mainly along the karst structures. Compared to the underlying marls of the Muwaqqar-Formation (B_3-Aquitard, see below), equivalent to the Bituminous Marl Formation at Maqarin (Table 6-1), the Rijam Formation or B_4-Aquifer is highly permeable with a fracture flow dominated groundwater system.

B_4-groundwater analyses are available from the Ramtha area, and indicate a mixture of B_4/B_5 groundwaters from Wadi Shallala (Fig. 6-1) to the east of the Maqarin area (Appendix M; Table M-11; see below). B_4-groundwaters of the Ramtha area are of the Na-Ca-HCO_3-Cl-type with TDS contents between 435–931 mg/L. ^{3}H-content of these groundwaters range from 1–9 TU indicating a residence time of less than 40 years with a groundwater component of only a few months to years old. Besides the unusually high Na^+- and Cl^-concentrations, the groundwaters also have high SO_4^{2-}- and NO_3^--concentrations (Appendix M; Table M-11).

The chemistry of these groundwaters cannot be explained by simple water-rock interaction within the rocks of the Rijam Formation (at least not with the available rock data). The high Na^+ and Cl^- concentrations could indicate a large degree of evaporation (e.g. in the sampling well) which also could explain the high $\delta^{18}O$- and δ^2H-values. Such an explanation would be supported by the Na/Cl ratio being similar to the Project M4 groundwater, the latter, however, having three times lower absolute contents (Appendix M; Table M-11). The high NO_3^--concentrations are most probably due to anthropogenic contamination. All the B_4-aquifer groundwaters from the Ramtha area appear to be in calcite equilibrium (Appendix M; Table M-12).

Wadi Shallala Formation (Lower Tertiary, B_5-Aquifer)

The Wadi Shallala Formation (at Maqarin equivalent to most of the Chalky Limestone Formation; Fig. 2-3 and Table 6-1) overlies the Rijam Formation (~ lower part of the Lower Chalky Limestone Member). The Wadi Shallala Formation is described to be mineralogically similar to the Rijam Formation, but with more abundant chalky limestone layers and thus even less resistant to weathering. Karstic weathering is also pronounced and groundwater infiltration and flow occurs rapidly and mainly along karstic structures.

It was found important to keep the distinction between Rijam Formation and Wadi Shallala Formation as made by Quennel (1951) and UNDP/FAO (1970) because of the clearly different groundwater types reported in the literature for these Formations. This is also evidenced by the different chemistry of the two Project samples (M4 and M6; Appendix M; Tables M-11 and M-13) sampled within these formations.

B_5-groundwaters are of dilute Ca-HCO_3-type waters with TDS contents between 219–477 mg/L. Except for Ca^{2+} and HCO_3^-, all elements are present in low concentrations (Appendix M; Table M-13). The Na/Cl ratio is equivalent to the one of evaporated precipitation, and the average Na^+- and Cl^-concentrations match the waters representing precipitation evaporated to 40%.

Even though they have a low total mineralisation and appear to be very young, the B_5-groundwaters are already at equilibrium with calcite (Appendix M; Table M-14). Their chemical composition is mainly derived from calcite dissolution. The small amounts of SO_4^{2-} may be partly derived from the overlying basalts and from oxidation of organic matter. Oxidation of organic matter could also be a source for NO_3^- that occurs in elevated concentrations in these groundwaters. However, the possibility that NO_3^- might also be of anthropogenic origin, or due to oxidation of N_2, cannot be further defined with the available data.

Basalt Flows (Lower Tertiary to Quaternary; B_a-Aquifer)

A sequence of young basalt flows cover a large area of northern Jordan and southern Syria and precipitation infiltrates through these rock types into the underlying sedimentary rock formations. The basalts are described as being mainly of alkali basalt and basanite type separated with tuff horizons (e.g. Van Den Boom, 1968). Pyroxenes, olivine and basic plagioclase are the most abundant minerals in these rocks. The hydrological properties of the basalt flows are largely unknown. A detailed study of basalt groundwaters from southern Syria has been presented by Kattan (1995).

Young, tritiated basalt groundwaters from the Jordanian-Syrian border region belong to the Ca-Na-Mg-HCO_3-Cl-type groundwaters with TDS contents ranging between 117–242 mg/L. More evolved, low-tritium to tritium-free basalt groundwaters belong to the Na-Mg-Ca-HCO_3-SO_4-Cl-type groundwaters and have TDS contents between 448–483 mg/L. Generally, basalt groundwaters are characterised by their high Na/Cl ratio (greater than unity in evolved groundwaters), their high Mg/Ca-ratios, and their low HCO_3^--concentration (Appendix M; Table M-15). Important to note are the relatively high concentrations of SO_4^{2-}, Na^+, and Cl^- in the evolved groundwaters which during mixing can significantly contribute to the observed concentrations of these elements in groundwaters from the sedimentary rock formations.

Young basaltic groundwaters are undersaturated with respect to calcite, dolomite, fluorite, and gypsum, but slightly oversaturated with respect to chalcedony (Appendix M; Table M-16). Evolved basalt groundwaters are near saturation or in equilibrium with respect to calcite but undersaturated with respect to dolomite and gypsum. The mineralisation of these groundwaters is mainly derived from the weathering of silicates such as olivine, pyroxene, and basic plagioclase, as can be seen by the high SiO_2-concentrations in the young basalt groundwaters.

6.2.3 Recharge Origin and Age of the A_1-A_6 and A_7/B_2 Groundwaters

Stable isotopes have been monitored in groundwaters from thermal wells and from wells in the recharge areas near Irbid and Ajlun (Fig. 6-1) over a six year period (Bajjali et al., 1990, 1997). Monitoring has also included wells completed in the Amman Formation, i.e. A_1-A_6 aquifers (Jordan River Valley [JRV1] and the Maqla spring); A_7 aquifer (principally the JRV wells), and in the Baqla Formation, i.e. B_2 aquifer (the Mukheiba field).

The isotopic composition of modern precipitation has been monitored at three stations in northern Jordan; Irbid, Ajlun and Deir Alla (Fig. 6-2) (Bajjali, 1994), which are plotted together in Figure 6-5 with limited precipitation data from the Golan region in Syria (Kattan, 1991). Precipitation in this region is similar to that which defines the Eastern Mediterranean meteoric water line (EMWL; Gat and Carmi, 1970), which differs from the global meteoric water line (GMWL) by a strong deuterium excess (+22 ‰) due to strong primary evaporation. The local meteoric water line (LMWL) in this study was calculated from the long-term monitoring of precipitation at these three stations, excluding rain events of less than 10 mm, and is defined by the equation $\delta^2H = 7.0\ \delta^{18}O + 16$ ‰.

Shallow tritiated ($^3H > 1$ TU) groundwaters in the aquifer outcrop regions plot on the local meteoric water line defined by precipitation data from Ajlun and Irbid (Fig. 6-5) and are used to define recharge regions for the thermal waters in the B_2 and A_7 aquifers (Fig. 6-6). By contrast, the regional thermal groundwaters are tritium free, and older than at least four decades. However, like the recharge area groundwaters, the thermal groundwaters plot close to the local meteoric water line, which constrains their age to the Holocene. Pleistocene groundwaters from the Lower Cretaceous Kurnub aquifer can be distinguished by a depletion in their isotopic composition due to cooler conditions of the late Pleistocene.

Although their stable isotopes indicate modern recharge, these regional groundwaters have low ^{14}C activities that suggest pre-Holocene recharge. However, the evolution of DIC and hence $^{14}C_{DIC}$ in these groundwaters is complicated by carbonate dissolution, sulphate reduction and incorporation of a third source of carbon from either mantle or volcanic CO_2 or matrix exchange (Clark et al., 1995). Application of a series of corrections for these processes indicates that these regional groundwaters were recharged during the mid-Holocene (Fig. 6-7). This is after the Lake Lisan period when climate patterns were still dominated by a southward-displaced jet stream due to glacial conditions in Eurasia. These groundwater ages are consistent with the stable isotope data (Fig. 6-5) which indicate Holocene recharge under a climate similar to that which prevails today.

The thermal waters from the B_2, the A_7 and the deeper $A_{1\text{-}6}$ aquifers are characterised by isotopic variations that reflect differences in recharge elevation, correlating with the outcrop region of their respective strata (Figs. 6-2 and 6-6). The depleted isotopic composition of the JRV1/Maqla thermal groundwaters indicate a recharge elevation higher than the catchment area in northern Jordan, suggesting that these deep A_1/A_6 groundwaters may receive a component of recharge from the Golan heights to the north in Syria.

The high-yield artesian groundwaters of the Amman (B_2) Formation are recharged in the NE Desert or Ajlun Highlands where the upper B_2 stratigraphic unit outcrops (Fig. 6-1). The isotopic composition of these groundwaters corresponds to precipitation within the higher elevations of the Side Wadis catchment. The karstic nature of this recharge region, combined with the considerable drop in elevation along the Yarmouk Valley has created the high artesian pressure in this aquifer.

6.3 GENERAL FEATURES OF THE MAQARIN GROUNDWATERS

6.3.1 Chemistry

Amman Formation (B_2) Groundwaters

In the Maqarin area, groundwater from the Amman Formation B_2-Aquifer was mainly sampled from open boreholes during the investigations for the Jordanian-Syrian Yarmouk River Dam Project (Harza, 1978). Groundwater samples from this period were mainly analysed for major elements and only semi-quantitative pH-measurement are available (Appendix M; Table M-17). These groundwater data have to be regarded with some caution since the sampling procedures used in open boreholes were not designed to distinguish between individual flow paths in the complex hydraulic system represented by the Yarmouk River Valley. Within the scope of Phase II, one groundwater from the Amman Formation (sample M9) has been analysed in more detail and is shown in Appendix M (Table M-17) for comparison.

B_2-groundwaters from the Maqarin area were sampled under artesian conditions and show a considerable spread in their chemical composition with TDS contents between 340–658 mg/L. Characteristic for the B_2-groundwaters is the presence of H_2S indicating that reducing conditions prevail in the B_2-Aquifer in the Maqarin area. They have similar Na^+, K^+ and Mg^{2+} concentrations to the low mineralised B_2-groundwaters from the Ramtha area (Fig. 6-1). However, the B_2-groundwaters from the Maqarin area have higher Ca^{2+}, SO_4^{2-} and HCO_3^- concentrations, and most of them lower Cl^- concentrations, compared to the Ramtha groundwaters. There exists a weak trend from lower mineralised, Ca-Mg-Na-HCO_3-Cl-type groundwaters at the Eastern Springs locality, to higher mineralised Ca-Mg-Na-HCO_3-Cl-SO_4-type groundwaters at the Western Springs locality. From the existing groundwater data, however, it cannot be discerned if this is due to a different geochemical evolution of these groundwaters (e.g. mixing with deep Kurnub-groundwater at the western site) or if it is due to dilution by shallow groundwaters in the open borehole by some of these B_2-groundwaters.

Sample M9, collected from the Eastern Springs locality, resembles chemically the higher mineralised Ca-Mg-Na-HCO_3-Cl-SO_4-type B_2-groundwaters of this area. It has, however, a lower SO_4^{2-} and Cl^--concentration but higher HCO_3^--concentration. This groundwater, too, must be more considered as a mixture of different groundwaters because its composition cannot be explained by water-rock interaction within the Amman Formation itself.

Calculated for calcite equilibrium, the B_2-groundwaters would be undersaturated with respect to dolomite and gypsum at pH-values in the range of 6.94–7.89 (Appendix M; Table M-18). The M9-sample further indicates undersaturation with respect to fluorite, and the Sr-minerals celestite and strontianite, and oversaturation with respect to chalcedony and barite at a reliable pH of 7.6.

Muwaqqar/Bituminous Marl Formation (B_3) Groundwaters

The Muwaqqar Formation in the Maqarin area is represented by the Bituminous Marl Formation (Table 6-1), and is divided into a sequence of unmetamorphosed Bituminous

Marls rich in organic material and the cement zone where high-pH groundwaters prevail. The geology and mineralogy of these zones has been described already in detail (Alexander, 1992; Linklater, 1998). Hydrologically, the Muwaqqar/Bituminous Marl Formation forms an aquitard with transmissivities lower than 10^{-8} m^2s^{-1}. Fracturing of the rock sequence, however, allows groundwater from the overlying formations to infiltrate into the Muwaqqar/Bituminous Marl Formation along discrete flow paths. The intensity of fracturing increases towards the cement zone in the Maqarin area.

B_3 Groundwaters from the unmetamorphosed Bituminous Marls (Neutral pH)

Neutral-pH groundwater from the B_3-Aquitard was mainly sampled from open boreholes as part of the investigations for the Jordanian-Syrian Yarmouk River Dam Project (Harza, 1978). An extensive set of analyses is reported by Abdul-Jaber (1982 and 1989).

B_3-groundwaters cover a wide range in composition and vary from dilute Ca-Mg-(Na)-HCO_3-(Cl)-type groundwaters with TDS contents of 348–545 mg/L to strongly mineralised Na-Ca-SO_4-Cl-type groundwaters with TDS contents between 1077–2161 mg/L. Unfortunately, no isotopic data are available for these groundwaters and most of the pH-measurements are only semi-quantitative. B_3-groundwaters with accurate pH-measurements are in equilibrium with calcite which is geochemically meaningful since the groundwaters in the overlying formation have also reached calcite equilibrium. Under certain circumstances, mixing of two calcite saturated groundwaters with strongly different ionic strengths might result in a calcite undersaturation of the mixture. If such a process takes place between infiltrating dilute groundwaters from the overlying Rijam Formation/lower part of the Lower Chalky Limestone Member (B_4-Aquifer), and strongly mineralised formation water of the Muwaqqar/Bituminous Marl Formation, remains a matter of speculation due to the limited quality of the groundwater analyses.

Low mineralised B_3-groundwaters have Na/Cl ratios higher than evaporated precipitation indicating a different source for Na. Such a source might be Ca-Na cation exchange on clay minerals in the marls. This could also explain the slightly elevated K^+- and, in parts, the Mg^{2+}-concentrations (Appendix M; Table M-19). Such a process would be consistent with the low NO_3-concentrations (no anthropogenic input of fertilizers), the different ion/ion ratios which exclude an admixture of known B_2- or deeper groundwaters, and the high pCO_2 which would then be a result from further calcite dissolution triggered by cation exchange. Furthermore, the oxidation of organic matter will also contribute to a high pCO_2. Carbonate and pyrite dissolution are responsible for the Ca^{2+}, HCO_3^-, SO_4^{2-} and, in parts, Mg^{2+}-concentrations. At calcite equilibrium, these groundwaters are undersaturated with respect to dolomite and gypsum (Appendix M; Table M-20).

Similar processes are thought to account for the mineralisation in the highly mineralised B_3-groundwaters. Again, a simple mixing with known deep groundwaters can be excluded, based on the observed ion/ion ratios, and also mixing with known high-pH groundwaters. Such high mineralised groundwaters might, however, represent mixtures of young carbonate groundwater with very old formation water of the Muwaqqar/Bituminous Marl Formation. Measured pH- and alkalinity values indicate that these

highly mineralised groundwaters are in equilibrium with calcite, but undersaturated with respect to dolomite and gypsum (Appendix M; Table M-20).

B_3 Groundwaters from the cement zone (High pH)

During Phases I and II, high-pH groundwaters of Ca-(Na,K)-OH-type were sampled from the cement zone in the Muwaqqar/Bituminous Marl Formation at the Eastern Springs locality, and high-pH groundwaters of Ca-K-(Na)-OH-SO_4-type were sampled at the Western Springs locality, although samples M8 and M10 would be better described as Ca-Na-OH-SO_4 groundwaters having less potassium than the other groundwaters of this group. The chemical and isotopic composition of these groundwaters have been described earlier in detail (Khoury et al., 1992; Alexander et al., 1992; Clark et al., 1992a, b; Fritz et al., 1992; Milodowski et al., 1998a). For completeness, and as reference for this present section, the average chemical composition of these groundwaters is shown in Tables 6-2 and 6-4. In Table 6-2 the average of the high-pH samples (Phases I-III) are compared to the average of high-pH groundwaters sampled previously by Abdul-Jaber (1989). Tables 6-3 and 6-5 show the average saturation state of these high-pH groundwaters. In all these calculations the pH was calculated from the titrated hydroxide alkalinity measurements and, for the Phase I samples, the vacuum extracted CO_3 concentrations (see Clark et al., 1992c).

Rijam Formation/lower part of the Lower Chalky Limestone Member (B_4) Groundwater

No published data of B_4-groundwaters (or basaltic groundwaters) from the near-vicinity of the cement zone in the Maqarin area exist. During Phase I a single sample of B_4-groundwater was sampled from Adit A-7 (sample M4). In general, this groundwater represents a typical young Ca-HCO_3 similar to that observed in Wadi Shallala. Although probably contaminated by wildlife resident in the tunnel, this sample is less mineralised than B_4-groundwaters from the Ramtha area, and has considerably lower Na^+-, Mg^{2+}-, Cl^--, and HCO_3^- concentrations (Appendix M; Table M-11). Elevated NO_3^--and K^+-concentration might at least be due partly to contamination. The groundwater is slightly undersaturated with respect to calcite and undersaturated with respect to all other mineral phases, except for chalcedony (Appendix M; Table M-12).

6.3.2 Isotope Geochemistry

At the outset of the Maqarin natural analogue project, the origin and age of the high pH groundwaters were questioned. The hyperalkaline groundwaters issue from fractured, brecciated material at relatively shallow depths in the Yarmouk River Valley. While their unusual geochemical facies suggested an evolved groundwater of uncertain origin and perhaps great age, their geological setting suggests a shallow, locally recharged flow system. This section summarises the environmental isotope studies carried out in Phase III and in previous studies, that have attempted to constrain the recharge origin.

Groundwater sampling sites for the isotope geochemistry carried out in Phase III are described elsewhere in this report (see Chapter 4), and summarised in Table 6-6.

Samples and analyses undertaken during Phases I and II are also presented in this section for comparison purposes, and summarised with the Phase III results.

Stable Isotope Studies

Additional data from Phase III samples supports earlier measurements of $\delta^{18}O$ and $\delta^{2}H$ for the high pH groundwaters (Fritz et al., 1992; Clark and Fritz, 1998). Both the Eastern and Western Spring groundwaters are enriched in ^{18}O and ^{2}H with respect to the regional groundwaters in the B_2 aquifer. These data suggest that the high pH groundwaters have been recharged at a low elevation, and are unlikely to receive recharge from the underlying artesian groundwaters. Further, the $\delta^{18}O$-$\delta^{2}H$ signal appears to have been modified. Comparison with neutral pH groundwaters from the Maqarin site is useful (Fig. 6-8), and provides the following observations:

- The Eastern Springs high pH groundwaters (Adit A-6; M10) show considerable variability in $\delta^{18}O$, with one value being as enriched as -3.2‰.
- The Maqarin Station Railway Cutting waters show a similar spread, although tend to be more isotopically depleted than the Adit A-6 samples.
- Compared to the Eastern Springs, the Western Springs high pH groundwaters are similarly enriched in ^{18}O but with a deuterium excess of some 3 to 5‰.
- The sample from the Amman Formation at Maqarin has an isotopic composition close to, but enriched above, the range of regional samples from the Amman Formation (i.e. above both the thermal waters and recharge waters).
- By contrast, the Ain Quelba (B_4; Chalky Limestone Formation), and Diversion Tunnel samples (artesian waters collected from the Bituminous Marl Formation at the site of Jordanian-Syrian Yarmouk River Dam construction in Syria) are more enriched, consistent with local, low elevation recharge to the B_4 aquifer. These samples also demonstrate the non-homogeneous isotopic composition of local bicarbonate groundwaters.
- The three borehole samples from the Eastern (M9; Borehole M-13: M18; Borehole RW1) and Western (M17; Borehole WS1) Spring areas appear to be mixtures between the eastern and western high pH groundwaters and a more depleted end-member similar to the Amman Formation (B_2) groundwater.
- Yarmouk River water is the most isotopically depleted group in the area, and integrates recharge over the range of elevations found in the catchment.

A distinction can be made between the isotopically-enriched high pH groundwater and a more depleted bicarbonate groundwater of regional origin as represented by the Amman Formation (B_2) groundwater. From the previous section, the B_2 groundwaters have been shown to be recharged at higher elevations south of Irbid. However, the Ain Quelba (B_4) bicarbonate groundwaters discharge from a shallow lower elevation flow system, and are by consequence more enriched. The single sample collected from a small puddle in Adit A-7 (also from the Chalky Limestone Formation) is strongly enriched. This can be attributed to evaporation along a line with slope ~5, and is not useful in defining the local bicarbonate groundwaters.

The isotopic composition of the high pH groundwaters from both the Eastern and Western Spring areas can be accounted for by two possible processes; a) local, low-elevation recharge in the Maqarin area, or b) modification of bicarbonate groundwaters through reaction with hydroxide and hydration of ettringite and thaumasite in the cement zones.

In Phase II of the Maqarin study (Clark and Fritz, 1998), the δ^2H contents of the hydrated mineral phases collected from Adit A-6 were measured and found to be depleted by up to 60‰ with respect to the Western Springs high pH groundwaters. It was concluded from that work that the hydration process was strongly fractionating and may have imparted an enrichment on the residual high pH pore waters draining from the alteration zone. If so, this would account for the enrichments in ^2H observed for the Western Springs high pH waters in Figure 6-8. A similar enrichment in $\delta^{18}O$ can be anticipated in residual pore waters following the hydration of cementitious minerals, which has been observed by Dakin et al. (1985). This evidence suggested that the enrichments in ^2H and ^{18}O were then a result of hydration reactions in the zone of alteration, rather than a primary signature of the infiltrating groundwaters. Accordingly, the groundwater precursor would be a more depleted end member, similar to the local bicarbonate groundwaters.

Laboratory Support Studies

Experimental hydration of cement zone clinker was undertaken in Phase III in an attempt to demonstrate whether or not this process could alter the isotopic composition of the water. Samples of Bituminous Marl were calcined by firing in a Muffle furnace at 1050°C for 48 hours. The resulting clinker was then ground for use in the rehydration experiments. One and three gramme aliquots of two samples were divided and weighed into plastic reaction tubes, to which 10 cm^3 of deionized water was added. These were left to react over 48 hours, with periodic agitation. The samples were then centrifuged and submitted for analysis of $\delta^{18}O$ and δ^2H. Experimental details and analytical results are presented in Table 6-7 and in Figure 6-9.

From Figure 6-9, these results suggest that there is no measureable effect on δ^2H during these hydroxide reactions, for the water/clinker ratios used. This is contrary to the depletions observed in the hydrated minerals (mainly thaumasite and ettringite) analysed in Phase II, which suggested that residual waters would experience a reciprocal enrichment.

By contrast, the ^{18}O contents of these waters show an evolution with decreasing water-rock ratios. Mixtures of 1 g clinker to 10 mls water produced about a 0.3‰ increase in $\delta^{18}O$, while mixtures of 3 g clinker with 10 mls water increased the $\delta^{18}O$ content of the water by 0.15‰. Although these measured enrichments are minor, they demonstrate that water-rock ratios of less than 1 may result in enrichments in $\delta^{18}O$ that are greater than 1‰. These results are consistent with the experimental work of Dakin (1985) using portland cement.

To conclude, this laboratory approach looks very promising and, while it was decided to err on the conservative side, it is recommended that further work be carried out. Guarded indications from these experimental data are that the enriched oxygen isotopic

signature of the high pH groundwaters is an evolved signature, modified during mineral hydration and hydroxylation of the primary cement minerals.

In summary, with respect to the stable isotope data, the following observations and conclusions can be made:

- Hydroxide reactions involving meteoric waters and the high-temperature cement minerals (mainly CaO) producing portlandite has likely imparted an enrichment to the ^{18}O content of the high pH groundwaters.
- An enrichment in ^{2}H for the high pH groundwater is not demonstrated by the experimental data possibly due to the high water/clinker ratio used in the experiment. However, the depletion in ^{2}H in the hydration waters of thaumasite and ettringite suggests that a minor enrichment of the ^{2}H in the high pH groundwaters is likely.
- The meteoric water precursor to the Western Springs high pH groundwaters probably has an isotopic signature close to the locally sampled bicarbonate waters at Maqarin, including the Ain Quelba Spring, M9 and M18 (Table 6-6). All of these bicarbonate groundwaters are tritiated (3.9 ±1.2 TU, 1.3 ±0.2 TU and 3.7 ±0.3 TU, respectively), and must be locally recharged. This is confirmed by their stable isotope contents, which are enriched above regional groundwaters (i.e. those in the Amman Formation recharged within the Irbid area), signifying low elevation recharge. Recharge waters at low elevation, typified by precipitation at the low elevation meteorological station at Deir Alla (Fig. 6-5), are enriched in ^{18}O and ^{2}H.
- The high pH groundwaters are then probably derived from locally recharged bicarbonate groundwaters that have been modified by hydroxide reactions in the metamorphic zone.
- The observed heterogeneities in the stable isotope values for the high pH groundwaters, even though the effect (outside error) is very small, are likely due to heterogeneities in the isotopic composition of the local bicarbonate groundwaters, differences in water/rock ratios, and secondary mixing between the high pH groundwaters and bicarbonate groundwaters in the discharge area. Heterogeneities in the isotopic composition of all Maqarin groundwaters is indicated in Figure 6-10, where their $\delta^{18}O$ composition is plotted with pH. The strong variations in $\delta^{18}O$ of the bicarbonate groundwaters does not permit observation of any secondary mixing. Nonetheless, ^{3}H data, discussed below, provide evidence that the high pH groundwaters are mixed with up to ~30% bicarbonate groundwaters.

Tritium Contents

Tritium has been analysed in most high pH samples collected over the course of Phases I, II and III, in an effort to constrain groundwater age and mixing. The Phase III data are summarised in Table 6-6, and all data are presented in Figure 6-11. Note that during Phase III sampling, some waters may be contaminated with recent precipitation (see sub-section 4.3.5).

Measurements of the high pH groundwaters in Phase I showed that for most samples, tritium was less than the analytical detection limit. Subsequent analyses have shown that tritium contents in these waters are generally close to but often above detection

(Table 6-6). This suggests that the high pH groundwaters may have a component recharged within the past few decades. Mixing with local bicarbonate groundwaters may contribute to these low tritium contents.

Figure 6-11A shows the pH-^{3}H relationship for all groundwaters sampled at Maqarin. A mixing line is plotted between a bicarbonate end member with 4 TU of ^{3}H, and a high pH groundwater with 0 TU. Figure 6-11B presents these data on an expanded scale in the high pH range. Although the analytical error associated with each analysis increases the uncertainty of such a mixing relationship, a trend is suggested. From Figure 6-11A, the high pH groundwaters may have been diluted with up to 30% tritiated, bicarbonate groundwaters.

There are at least 3 outlying data points that do not follow this mixing trend. Variations in the ^{3}H content of the bicarbonate groundwater end member could be responsible for these outliers. If substantiated, this mixing relationship would indicate that the high pH groundwaters are ^{3}H-free and recharged prior to about 1950. At the moment, however, the data only tentatively support this premiss.

6.3.3 Geochemical Evolution

As described above, at Maqarin two groundwater sources occur: a) from the deep Amman Formation B_2-aquifer, and b) from the overlying Muwaqqar/Bituminous Marl Formation B_3-aquitard.

Origin of the Amman Formation Groundwaters (B_2-Aquifer)

In the Maqarin area most of the deep Amman Formation B_2-groundwaters represent mixtures of different groundwaters. Mixing becomes obvious when comparing the chemical composition of B_2-groundwaters from along the major flow lines derived from hydrological modelling (Figs. 6-2 and 6-4; see also Chapter 2). The main component of the B_2-groundwaters at Maqarin is a carbonate groundwater that evolves from evaporated precipitation in an aquifer system dominated by carbonate rocks containing minor sulphides. TDS-contents and ion/ion ratios of the B_2-groundwaters at Maqarin indicate that the probable recharge area for this component would be in the NE-Desert III area (Figs. 6-1, 6-12 and 6-13).

After infiltration, carbonate and sulphide dissolution are the dominant processes that occur in these groundwaters. Once equilibrium with calcite is reached, compositional changes will be very limited in the groundwater except for possible on-going dolomite and pyrite dissolution. Major compositional changes would have to be triggered by new processes such as, for example, cation exchange and groundwater mixing. Both such processes could lead to further mineral dissolution reactions and so to a further increase in the mineralisation of the groundwater. Whereas cation exchange in the Amman Formation is limited by the low clay mineral content of the rocks, groundwater mixing is observed as evidenced by the scatter of chemical compositions in this Aquifer. If no such other processes affect the groundwater during their flow from the NE-Desert to the Maqarin area, then the groundwaters within the Amman Formation would arrive at Maqarin with a dominant recharge signature.

It is probable, however, that this is not a pure mixing/non-mixing issue. The B_2-groundwaters at Maqarin are oxygen-free and the nitrate content is low; oxidation of organic matter and reduction of nitrates must have played a role in the groundwater composition.

Some of the low mineralised B_2-groundwaters sampled in the Maqarin area appear to have evolved without being influenced by mixing processes. These groundwaters show ion/ion ratios similar to the NE-Desert III recharge waters but increased absolute concentrations. The chemical composition of low mineralised B_2-groundwater samples from the Ramtha area, situated approximately in the middle of the flow path, fit well into such an evolution (Figs. 6-12 and 6-13). Very low mineralised groundwater samples from the Maqarin area most probably became diluted during sampling in the open boreholes.

Natural mixing of groundwater in the B_2-aquifer also occurs in the Maqarin area itself as exemplified by some highly mineralised groundwater samples with chemical similarities to the underlying deep groundwaters. Based on the available data, however, these mixing processes cannot be further quantified.

Origin of the Muwaqqar/Bituminous Marl Formation Groundwaters (B_3 Aquitard) – The Neutral-pH Waters

Most of the neutral-pH groundwaters sampled within the Muwaqqar/Bituminous Marl Formation; (Table 6-1) B_3-Aquitard, are rather dilute carbonate groundwaters that must have recharged locally along fractures from the overlying Rijam Formation/lower part of the Lower Chalky Limestone Member. The total mineralisation and Na^+-and Cl^--concentrations are considerably lower in these low mineralised B_3-groundwaters than in ^3H-bearing groundwaters of the overlying Rijam Formation/lower part of the Lower Chalky Limestone Member (B_4-Aquifer) sampled in the Ramtha area and in Wadi Shallala. This implies that in the Maqarin area the infiltration into the Muwaqqar/Bituminous Marl Formation must occur very locally with dilute B_4-groundwater, i.e. groundwaters that have short transport pathways within the B_4-Aquifer. This also limits the recharge conditions into the cement zone to groundwaters of mainly very local origin (see Chapter 2).

Calcite, dolomite and pyrite dissolution are the predominant water/rock interactions experienced by the low mineralised B_3-groundwaters. Most of these reactions might already take place during infiltration through the Rijam Formation/lower part of the Lower Chalky Limestone Member. Once infiltrated into the rocks of the Muwaqqar/Bituminous Marl Formation, the groundwater composition is further changed by cation exchange reactions and probably also by oxidation of organic matter. In certain parts of this Formation, mixing with highly mineralised groundwater occurs as evidenced by the mineralised groundwaters sampled within the B_3-Aquitard. Based on ion/ion ratios this must be old formation water and cannot be groundwater derived from underlying aquifers.

The geochemical evolution of the more highly mineralised B_3-groundwaters sampled in the Maqarin area cannot be described in detail based on the available data. What can be excluded, however, for these groundwaters, can be mixing with any known high mineralised groundwater type (including high-pH groundwaters) from the Maqarin area

with dilute Ca-HCO_3^- groundwater from the overlying Rijam Formation/lower part of the Lower Chalky Limestone Member. They might in fact represent more the mixing of dilute HCO_3^- groundwater with old Muwaqqar/Bituminous Marl Formation water of unknown evolution.

Origin of the Muwaqqar/Bituminous Marl Formation Groundwaters (B_3 Aquitard) – The High-pH Waters

The Muwaqqar/Bituminous Marl Formation comprises the unmetamorphosed and metamorphosed (i.e. cement zone) Bituminous Marls, the latter providing the source of the high pH groundwaters through interaction with the normal pH waters (Khoury et al., 1985, 1992). Present studies suggest that the geochemical composition of high pH-groundwaters of the Eastern and the Western Springs locations can be derived by water/rock interaction of a typical dilute carbonate groundwater (i.e. B_3-aquitard) with the rocks of the cement zone. The different state of mineralisation between Ca-(Na,K)-OH-type high-pH groundwaters from the Eastern Springs and the Ca-K-(Na)-OH-SO_4-type high-pH groundwaters from the Western Springs can therefore be attributed to a different stage of water/rock interaction of these waters. Ca^{2+}-concentrations are derived in both types mainly from portlandite dissolution which is also responsible for the high-pH values observed in these groundwaters. There are no convincing arguments that the comparably high Na^+, K^+ and SO_4^{2-} concentrations in the Western Springs waters would be due to different infiltration conditions or anthropogenic contamination (see sub-section 2.2.3). Thus, the contents of these components must be due to interaction with a cement rock that differs in its mineralogical composition from the one in the Eastern Springs area. The high sulphate abundances are most likely derived from the hydration of the products of combustion of sulphur in organic materials within the Bituminous Marl Formation (Clark et al., 1992b). All these groundwaters have potassium > sodium, which is an unusual feature. The concentrations of nitrogen species are relatively high, suggesting possible leaching from the organic component. Inorganic carbon and dissolved silica are both uniformly low. Chromium and selenium concentrations are both high due (presumably) to the dissolution of Cr-rich clay (volkonskite), hashemite (barium chromate-sulphate solid-solution) and Cu-Na-K-selenides in the mineral assemblage (e.g. oldhamite; see Milodowski et al. (1992a, b) and Appendix L: Table L-6). There is no obvious petrographic reason why such a mineralogical difference should have been established during the metamorphic overprint of the Bituminous Marl, and therefore the mineralogical composition of the cement zone has to be regarded as being initially equal in both areas. The only way to explain the different chemistry of the high-pH groundwaters of the different areas would then be a time (or amount of flow) difference in the groundwater circulation at the two sites. A difference in timescale was also suggested from the Phase II studies by Milodowski et al. (1998a).

A possible scenario is that in the Eastern Springs area groundwater circulation has occurred over a much longer timespan and readily soluble mineral phases are already completely dissolved. This compares with the Western Springs area where younger groundwater flowpaths circulate and therefore the system is less evolved geochemically. In this context it is important to note that within the Jordanian-Syrian Yarmouk River Dam Project, high-pH groundwaters were sampled from boreholes in the Eastern Springs area (Abdul-Jaber, 1989) that resemble closely the chemical

character of the high-pH groundwaters from the Western Springs area (Figs. 6-17 and 6-18).

To test such a scenario, high-pH groundwater evolution was simulated for the two areas. Evaporated precipitation values were chosen and allowed to infiltrate into the Rijam Formation/lower part of the Lower Chalky Limestone Member (Table 6-1) where it was assumed they would react until calcite equilibrium was established. The groundwater was then allowed to infiltrate into the Muwaqqar/Bituminous Marl Formation, first into the unmetamorphosed marls and from there into the cement zone. Cement mineral reactions were considered to be rapid so that the groundwater at each step would reach equilibrium with the major reacting cement phases. In addition to portlandite, hypothetical alkali-sulphide phases with a 1:1 stoichiometry where assumed to occur in the cement zone unaltered by meteoric groundwaters. Such alkali-sulphide phases were actually observed in the Eastern Springs area (Alexander, 1992). The objective of the simulations was to derive the mass transfer of all mineral phases involved, the relation of this calculated mass transfer to the natural occurrence, and whether major variables such as pH, pCO_2 etc of the calculated groundwater composition are in agreement with the measured values.

The simulations of the high pH groundwater evolution were performed with PHREEQC (Parkhurst, 1995) using the Nagra thermodynamic database (Pearson and Berner, 1991; Pearson et al., 1992; Alexander et al., 1998). Not included in these initial calculations were secondary alteration products like zeolites and CSH-phases, the calculated saturation state of which could serve as a check for the accuracy of the simulations. The results of these initial simulations are shown in Figures 6-14 to 6-18 where the calculated pH, pCO_2 and major element composition, are compared to the measured compositions of the high-pH groundwaters from the Eastern and Western Springs area. As can be seen from these figures, the model calculations can reproduce the measured data for both Eastern and Western Springs high-pH groundwaters. For the Western Springs area the calculation yielded saturation with gypsum in the final composition (Fig. 6-17) which is also in agreement with the gypsum saturation state calculated from the measured data and the observation of secondary gypsum in this area.

The required mineral mass transfer to derive the high-pH groundwater compositions is given in Table 6-8. Portlandite dissolution is the dominant mineral reaction that is required to derive the composition of the Eastern Springs high-pH groundwaters. To derive the composition of the Western Springs high-pH groundwaters, relatively large amounts of alkali-sulphide phases would have also to be dissolved. Such dissolution would have to be confirmed by further mineralogical investigations. In both cases similar amounts of calcite (and small amounts of dolomite) will be precipitated during the groundwater evolution, which is in agreement with mineralogical observations.

Laboratory Support Studies

Experimental hydration of clinker was undertaken to determine the concentration of readily leached K and Na solutes. Samples of the clinker produced for isotopic studies (Table 6-9) were used in this leach experiment. The marl samples sampled from the vicinity of the Yarmouk River Diversion Tunnel were calcined by firing in a Muffle furnace at 1050°C for 48 hours. Four 3-g clinker subsamples were ground and weighed into plastic reaction tubes, to which 40 cm^3 of deionized water was added. These were

left to react over 48 hours, with periodic agitation. The samples were then centrifuged and submitted for analysis of Ca, K and Na. Experimental details and analytical results are presented in Table 6-10. Measurements of pH were made within 5 minutes of hydration, using a Hannah Instruments field pH meter calibrated with pH 7 and 11 buffers. As pH measurements are almost 2 pH units beyond the calibration end point, their reliability is not high.

These data were then corrected to a volume ratio of 1:1, assuming a high initial porosity in the metamorphic zone. The calculation was not made for Ca, which was assumed to be limited by portlandite solubility.

In these tests, chromium concentrations were found to be less than the analytical detection, which when corrected to a water:rock ratio of 1:1 is 0.012 meq/L. Chloride concentrations were also close to detection, suggesting an external source for Cl^- in the Western and Eastern Springs groundwaters.

These leach test results are based on marl sampled from a single location; the lower part of the Chalky Limestone Formation (B_3) in the vicinity of the Diversion Tunnel excavation (Syrian side). Hence, heterogeneities in Na and K in the marl has not been examined. Nonetheless, the results in Table 6-10 show that all of the K and Na measured in the Western Springs seeps can be attributed to the dissolution of soluble alkali minerals, such as alkali hydroxides and sulphides, in the metamorphic zone. This supports the above hypothesis that the differences in groundwater composition in the Eastern and Western Springs areas is more a function of rock/water reaction time, rather than initial differences in mineralogy or artefacts of anthropogenic contamination.

Aqueous Speciation

The aqueous speciation of the high pH groundwaters, studied during Phase II of the project (Milodowski et al., 1998a; Short, 1998), has been reappraised using the Phase III data; calculations were carried out using the computer code EQ3 (Wolery, 1992; Version 7.2A, database R161). Groundwater analyses in Tables 6-11 and 6-12 were used as input to EQ3 and distribution of species calculations performed at a temperature of 25°C. The results of these calculations for the hyperalkaline groundwaters are presented in Table 6-13.

The activity of dissolved silica and the fugacity of carbon dioxide in the hyperalkaline groundwaters (Table 6-13) are both exceptionally low for groundwaters. The log activity of dissolved silica buffered by quartz solubility at 25°C is approximately -4, some 7–8 orders of magnitude greater than that observed in the Maqarin hyperalkaline groundwaters. The low carbon dioxide fugacities of the Maqarin hyperalkaline groundwaters were also noted by Clark et al. (1992b).

In analogy to cement pore waters, the Maqarin hyperalkaline groundwaters are strongly undersaturated with silicate minerals. There will thus be a tendency for the hyperalkaline groundwaters to dissolve silicate and aluminosilicate minerals upon contact with these mineral types. The log fugacity of carbon dioxide pressure of groundwaters equilibrated with the atmosphere is approximately -3.5, some 8 orders of magnitude higher than values calculated for the Maqarin hyperalkaline groundwaters. Such low values of carbon dioxide fugacity are typical of pore fluids equilibrated with

calcium silicate hydrate minerals and gels, such as those in cements. There will be a strong tendency for the Maqarin hyperalkaline groundwaters to absorb carbon dioxide from the atmosphere upon exposure to air. This tendency is demonstrated by the abundance of calcite/aragonite/vaterite ($CaCO_3$) tufa precipitates at sites of groundwater seepage in adits and springs at Maqarin (Milodowski et al., 1998b,c; this report Chapter 4).

The Maqarin hyperalkaline groundwaters are saturated with barite, gypsum and portlandite, supersaturated with respect to carbonates (aragonite, calcite, strontianite and witherite), but undersaturated with respect to celestite, fluorite, calcium silicate hydrate minerals and the entire range of silicates contained in the EQ3 database. Hillebrandite has been included in Table 6-13, as the least undersaturated representative of the range of the calcium silicate hydrate minerals available in the database. Only data for crystalline CSH phases, which are less soluble than amorphous or gel varieties, are included in the EQ3/6 database. Although some differences exist between databases used for the EQ5/6 (Table 6-13) and PHREEQC calculations (Table 6-3), the conclusions from the modelling studies are in broad agreement with each other.

These conclusions concerning mineral solubilities are similar to those of Clark et al. (1992b) who also noted that the groundwaters from the Western Springs area are more mineralised and have a higher pH than those of the Eastern Springs area (Adit A-6 and Wadi Sijin). Groundwaters from the Eastern Springs area are generally undersaturated with respect to solid sulphate minerals (Clark et al., 1992b).

Although the hyperalkaline groundwaters have some similarities with cement pore fluids, there are also marked differences. Comparison of the chemical composition of sample M5 (as an example) of the Maqarin groundwaters with a typical cement pore fluid (Table 6-14) shows that the groundwaters have considerably lower contents of alkali metals, lower pH and much higher sulphate contents. These differences should not be ignored when attempting to apply information from the Maqarin system to radioactive waste applications.

The silica-controlling phase in the hyperalkaline groundwaters is probably thaumasite. Mineral species of the thaumasite-ettringite solid-solution series have been observed at Maqarin (Alexander, 1992) and are the most likely candidates for controlling the abundances of both dissolved silica and sulphate in the hyperalkaline groundwaters. Although EQ3 contains thermodynamic data for ettringite, there are no data for thaumasite so these hypotheses could not be tested further.

6.4 SUMMARY AND CONCLUSIONS

Some doubt has persisted over the course of the Phase I and Phase II Maqarin studies as to the origin of the high K^+, and Na^+ observed in the Western Springs high pH groundwaters, which contrasts with the Eastern Springs variety. These alkali metals occur in soluble mineral phases (e.g. oldhamite) observed by petrological analysis (Milodowski et al., 1992a, b; 1998a), although their percent representation in the cement zone was not known. Other possible sources of these alkali metals might include leaching from basalt clasts in the river alluvium, fertilizers applied in fields in the

recharge areas (K^+) and salts accumulated in the recharge areas from marine aerosols. The occurrence of high K^+ and Na^+ concentrations in the Western Springs seeps, with lower concentrations in the Eastern Springs groundwaters, is significant to the repository analogue. If they are shown to originate in the cement zone, it follows that the Western Springs groundwaters represent the first pore volume of water leaving the cement zone (somewhat analogous to Region 1 in cement terminology), and that the Eastern Springs groundwaters represent subsequent pore volumes (somewhat analogous to Region 2) from a more highly leached cement zone.

Additional studies carried out in Phase III have expanded the data base of groundwater chemistry and environmental isotopes. These data, together with a better regional understanding of the hydrogeochemistry, have greatly helped to improve understanding the groundwater provenance and age at the Maqarin site. Hydrogeochemical modelling of the data, supported by new experimental data, have helped constrain interpretations of the origin of these high pH groundwaters, and of their high concentrations of K^+ and Na^+.

The main hydrogeochemical conclusions from the Phase III study are:

- Most of the normal pH groundwaters which interact with the cement zones at Maqarin have recharged locally, via short transport pathways, along fractures from the overlying Chalky Limestone Formation (regionally known as the Wadi Shallala and Rijam Formations) into the Bituminous Marl Formation (regionally known as the Muwaqqar Formation). The recharged dilute bicarbonate groundwaters, represented by samples from Ain Quelba Spring (Chalky Limestone Formation), and site M18 (Bituminous Marl Formation) is therefore the probable precursor to the high pH groundwaters. These are modern (tritiated) groundwaters from local flow systems in the carbonate bedrock. No significant mixing of groundwaters from the underlying, confined Amman Formation B_2-aquifer has occurred.

- Interaction of normal pH groundwaters with the cement zone has produced two chemically distinct high pH groundwaters: The Eastern Springs waters of Ca-(Na,K)-OH-type and the Western Springs waters of Ca-K-(Na)-OH-SO_4-type.

- The minor amounts of tritium measured in the Western Springs high pH groundwaters are attributable to mixing with local bicarbonate groundwaters (^3H currently ~4 TU); some minor contamination due to precipitation may have influenced some of the samples. Mixing with up to 50% bicarbonate waters has a minor influence on pH. Accordingly, unmixed high pH groundwaters are considered to be ^3H-free and older than at least 40 years.

- Analysis of residual waters following the experimental hydration of calcined marls from Maqarin suggests that hydration and hydroxylation reactions may have an effect on the $\delta^{18}O$ composition of the effluent water, although no effect for δ^2H was observed. However, earlier (Phase II) studies of the Eastern Springs locality show that hydration waters from minerals in the reaction zone are depleted in ^2H. Accordingly, the $\delta^{18}O$ and δ^2H composition of the high pH groundwaters from the higher pH Western Springs is considered to have an evolved signature from a more depleted meteoric water precursor. Secondary mixing with up to 30% bicarbonate groundwaters may have taken place in the discharge area.

- Measurement of ^{36}Cl in the high pH groundwaters from Phase II studies demonstrated that there was no thermonuclear ^{36}Cl in these waters. This is consistent with the interpretation of the ^{3}H data, indicating recharge prior to 1950. The age of the high pH groundwaters cannot, with the currently available data, be constrained to better than >40 years.

- Hydrogeochemical modelling suggests that the observed differences in groundwater composition between the Eastern and Western Springs localities can be attributed to different stages of water/rock interaction. There is no convincing evidence that the higher Na^+, K^+ and SO_4^{2-} concentrations at the Western Springs locality are due to initial differences in the clinker compositions of the Eastern and Western Springs cement zones, variable infiltration conditions or anthropogenic contamination.

- A reappraisal of aqueous speciation calculations show that the high pH groundwaters are strongly undersaturated with respect to silicate minerals. There will thus be a tendency for these waters to dissolve silicate and aluminosilicate minerals upon contact. Low carbon dioxide fugacity values result in a strong tendency to absorb atmospheric carbon dioxide when in contact with the air resulting in the observed widespread precipitation of, for example, calcite, aragonite and vaterite associated with the Eastern and Western Springs seepages. The observed mineral species of the thaumasite-ettringite solid-solution series are the most likely candidates for controlling the abundances of both dissolved silica and sulphate in the high pH groundwaters. These calculations are in accordance with Phases I and II studies.

- Laboratory support studies show that high concentrations of K and Na can be leached from samples of calcined marl. Corrected to a volumetric water to rock ratio of 1:1, their concentrations correspond with the concentrations measured in the Western Springs groundwaters. Accordingly, this supports the concept that the Western Springs groundwaters represent the first pore volume discharging from the metamorphic zone, and that the Eastern Springs groundwaters represent late, more dilute, discharge.

The most probable scenario is that groundwater circulation has occurred at the Eastern Springs area over a much longer timespan and readily soluble mineral phases (e.g. oldhamite, a potential source of Na and K) are already completely dissolved. This compares with the Western Springs area where younger flowpaths circulate and therefore the system is less evolved geochemically. This may be supported by the geomorphological evidence discussed above which recognises two potential phases of landslides in the Maqarin area; an earlier evolved phase (Eastern Springs?), and a later, less evolved phase (Western Springs?).

6.5 ACKNOWLEDGEMENTS

The isotope analyses presented in Table 6-6 were undertaken at the GSF Institute for Hydrology in Munich, under the direction of Dr. Manfred Wolf.

6.6 REFERENCES

Alexander, W.R. (Ed.), 1992. A natural analogue study of hyperalkaline groundwaters. I: Source term description and thermodynamic database testing. Nagra Tech. Rep. (NTB 91-10), Nagra, Wettingen, Switzerland.

Alexander, W.R., McKinley, I.G., Linklater, C.M., Tweed, C.J., Casas, I., Börjesson, S. and Sellin, P., 1998. Testing the limits of applicability of thermodynamic databases. In: C.M. Linklater (Ed.), A natural analogue study of cement-buffered, hyperalkaline groundwaters and their interaction with a repository host rock: Phase II. Nirex Science Report, S/98/003, Nirex, Harwell, U.K., p. 242–277.

Abdul-Jaber, Q., 1989. Hydrochemische, geochemische und petrographische untersuchungen im Maqarin-Gebiet Nord-Jordanien. Ph.D. Thesis, Westfälische Wilhelms Universität, Münster, Germany.

Abdul-Jaber, O., 1982. Hydrochemistry and hydrology of the Maqarin area. M. Sc. Thesis, University of Amman, Jordan.

Abed A. and Amireh, B., 1983. Petrography and geochemistry of some Jordanian oil shales from North Jordan. J. Petrol. Geol., 5, 261–247.

Bajjali, W.T., 1990. Isotopic and hydrochemical characteristics of precipitation in Jordan, M.Sc. Thesis, University of Amman, Jordan.

Bajjali, W.T., 1994. Recharge and regional circulation of thermal groundwater in northern Jordan using isotope geochemistry. Ph.D. Thesis, University of Ottawa, Canada.

Bajjali, W.T., Clark, I.D. and Fritz, P., 1997. The artesian thermal groundwater of northern Jordan: Insights to their recharge history and age. J. Hydrol., 187, 355–382.

Bender, F., 1968. Geologic von Jordanien, Beitrage zur regionalen Geologie der Erde. Gebrüder Bornträger, Berlin, Germany.

Bender, F., 1974. Geology of Jordan, Gebrüder Bornträger, Berlin, Germany.

Clark, I.D., Milodowski, A.E., Fritz, P., Khoury, H.N., Hall, G., Cave, M., Smith, B. and Cook, J.M., 1992a. Aqueous geochemistry. In: W.R. Alexander (Ed.), A natural analogue study of hyperalkaline groundwaters. I: Source term description and thermodynamic database testing. Nagra Tech. Rep. (NTB 91-10), Nagra, Wettingen, Switzerland, p. 51–57.

Clark, I.D., Khoury, H.N., Salameh, E., Fritz, P., Seidlitz, H.Y. and Milodowski, T.E., 1992b. Origin of the Maqarin, Jordan hyperalkaline groundwaters: isotopic and geochemical evidence for *in situ* combustion, calcination and recarbonation of bituminous marls. In: Y.K. Kharaka and M.S. Maest (Eds.), Water-Rock Interaction, Balkema, Rotterdam, 1485–1489.

Clark, I.D., Fritz, P., Milodowski, A.E. and Khoury, H.N., 1992c. Sampling and analytical methods. In: W.R. Alexander (Ed.), A natural analogue study of hyperalkaline groundwaters. I: Source term description and thermodynamic database testing. Nagra Tech. Rep. (NTB 91-10), Nagra, Wettingen, Switzerland, p. 19–40.

Clark, I.D., Bajjali, W.T. and Phipps, G.Ch., 1995. Constraining ^{14}C ages in sulphate reducing groundwaters: two case studies from arid regions. Intern. Symp. on Isotopes in Water Resources Management, IAEA-SM/336/10, Vienna, Austria.

Clark, I.D. and Fritz, P., 1998. Isotope hydrogeology of the Maqarin hyperalkaline groundwaters. In: C.M. Linklater (Ed.), A natural analogue study of cement-buffered, hyperalkaline groundwaters and their interaction with a repository host rock: Phase II. Nirex Science Report, S/98/003, Nirex, Harwell, U.K., p. 198–210.

Dakin, R.A., Farvolden, R.N., Cherry, J.A. and Fritz, P., 1985. Origin of dissolved solids in groundwaters of Mayne Island, British Columbia, Canada. J. Hydrol., 63: 233–270.

El-Nasser, H., 1991. Groundwater resources of the deep aquifer systems in NW-Jordan: Hydrology and hydrochemical quasi 3-dimensional modelling. Ph.D. Thesis, University of Würzburg, Germany.

Fritz, P., Clark, I.D., Bajjali, W. and Khoury, H.N., 1992. Isotopic composition of the hyperalkaline waters. In: W.R. Alexander (Ed.) A natural analogue study of hyperalkaline groundwaters. I: Source term description and thermodynamic database testing. Nagra Tech. Rep. (NTB 91-10), Nagra, Wettingen, Switzerland, p. 58–69.

Gat, J.R., and Carmi, L., 1970. Evolution of the isotopic composition of atmospheric waters in the Mediterranean Sea area. J.Geophys. Res., 75: 3039–3048.

German Geological Mission, 1966. Geologie und hydrogeologie von Irbid district/Jordanien. Rep. No. 13.

Harza, 1978. Hydrogeological investigations at Maqarin Dam Site. Harza Engineering Company. Unpbl. Int. Rep. Jordan Valley Authorities.

Kattan, Z., 1991. Environmental isotope study of the major karst springs in Damascus limestone aquifer system: case of the Figeh and Barada springs. Ankara, IAEA workshop.

Kattan, Z., 1995. Chemical and environmental isotope study of the fissured basaltic aquifer systems of Yarmouk Basin (Syria). Intern. Symp. on Isotopes in Water Resources Management, IAEA-SM/336/28, Vienna, Austria.

Khoury, H.N., Salameh, E. and Abdul-Jaber, Q., 1985. Characteritstics of an unusual highly alkaline water from the Maqarin area, northern Jordan. J. Hydrol., 81, 79–91.

Khoury, H.N., Salameh, E., Clark, I.D., Fritz, P., Bajjali, W., Milodowski, A.E., Cave, M.R. and Alexander, W.R., 1992. A natural analogue of high pH waters from the Maqarin area of northern Jordan. I: Introduction to the site. J. Geochem. Explor., 46, 117–132.

Linklater, C.M. (Ed.), 1998. A natural analogue study of cement-buffered, hyperalkaline groundwaters and their interaction with a repository host rock: Phase II. Nirex Science Report, S/98/003, Nirex, Harwell, U.K.

Lunden, I. and Andersson, K., 1989. Modeling of the mixing of cement pore water and groundwater using the PHREEQE code. In: Scientific Basis for Nuclear Waste Management, 949–956.

Milodowski, A.E., Khoury, H.N., Pearce, J.M. and Hyslop, E.K., 1992a. Results: Source and sinks. In: W.R. Alexander (Ed.), A natural analogue study of hyperalkaline groundwaters. I: Source term description and thermodynamic database testing. Nagra Tech. Rep. (NTB 91-10), Nagra, Wettingen, Switzerland, p. 48–69.

Milodowski, A.E., Khoury, H.N., Pearce, J.M., Hyslop, E.K. and Clark, I.D., 1992b. Description of the mineralogy, petrography and geochemistry of the Maqarin source-term rocks and their secondary alteration products. In: W.R. Alexander (Ed.), A natural analogue study of hyperalkaline groundwaters. I: Source term description and thermodynamic database testing. Nagra Tech. Rep. (NTB 91-10), Nagra, Wettingen, Switzerland, p. C-1 to C-53.

Milodowski, A.E., Cave, M.R., Reeder, S., Smith, B., Chenery, S.R.N. and Cook, J.M., 1998a. Aqueous geochemistry at Maqarin. In C.M. Linklater (Ed.), A natural analogue study of cement-buffered, hyperalkaline groundwaters and their interaction with a repository host rock: Phase II. Nirex Science Report, S/98/003, Nirex, Harwell, U.K., p. 48–63.

Milodowski, A.E., Pearce, J.M., Hyslop, E.K., Hughes, C.R., Inglethorp, S.D.J., Strong, G.E., Wheal, N., MacKenzie, A.B., Karnland, O. and Khoury, H.N., 1998b. Mineralogy and Petrology. In: C.M. Linklater (Ed.), A natural analogue study of cement-buffered, hyperalkaline groundwaters and their interaction with a repository host rock: Phase II. Nirex Science Report, S/98/003, Nirex, Harwell, U.K., p. 70-145.

Milodowski, A.E., Hyslop, E.K., Khoury, H.N. and Salameh, E., 1998c. Site description and field sampling programme. In: C.M. Linklater (Ed.), A natural analogue study of cement-buffered, hyperalkaline groundwaters and their interaction with a repository host rock: Phase II. Nirex Science Report, S/98/003, Nirex, Harwell, U.K., p. 10–47.

Parkhurst, D.L., 1995. User's guide to PHREEQC – A computer program for speciation, reaction-path, advective-transport, and inverse geochemical calculations. USGS, Water Resources Investigation Report 95–4227.

Pearson, F.J.Jr. and Berner, U., 1991. Nagra Thermochemical Data Base. I Core Data. Nagra Tech. Rep. (NTB 91-17), Nagra, Wettingen, Switzerland.

Pearson, F.J.Jr., Berner, U. and Hummel, W., 1992. Nagra Thermochemical Data Base. II Supplemental Data 05/92. Nagra Tech. Rep. (NTB 91-18), Nagra, Wettingen, Switzerland.

Plummer, L. N., Prestemon, E. C., and Parkhurst, D. L., 1991. An Interactive Code (Netpath) for modeling Net geochemical Reactions along a flow Path: U. S. Geol. Surv. Water Res. Invest. Rep. 91–4078.

Quennel, A.M., 1951. The Geology and Mineral Resources of (former) Transjordan. Geol. Min. Resour. 2, 2, London.

Salameh, E., 1996. Water Quality Degradation in Jordan. Royal Society for the Conservation of Nature, Amman, Jordan.

Short, S.A., 1998. Ion exchange resin studies of speciation in Maqarin groundwaters. In: C.M. Linklater (Ed.), A natural analogue study of cement-buffered, hyperalkaline groundwaters and their interaction with a repository host rock: Phase II. Nirex Science Report, S/98/003, Nirex, Harwell, U.K., p. 64–69.

UNDP/FAO, 1970. The hydrogeology of the Mesozoic-Camozoic aquifers of the Western highlands and plateau of east Jordan. UNDP/FAO 212, Rome.

van Den Boom, G., 1968. Zur petrogenese der plateau basalte nordost Jordanien. Geol. Jb., 85, 489–496.

Wolery, T.J., 1992. The EQ3/6 package overview and installation guide (version 7.0). Lawrence Livermore Nat. Lab. Rep. (UCRL-MA-110662PT-I.)

Table 6-1. Regional stratigraphy in northern Jordan clarifying the terminology used by different authors. The stratigraphic units discussed in this report are in bold typeface (based on El-Nasser, 1991 and Milodowski et al., 1998c; Chapter 2, this report).

Time Scale		Quennel (1951)		German Geol. Mission (1966)	UNDP/FAO (1970) (1970)	Phase III Report (1998)
Period	Epoch	Group	Symbol			
Quaternary	Holocene					
	Pleistocene			**Basalt Flows**		**Basalt Flows**
Tertiary	Oligocene	Belqa Group	**B_a**			
	Eocene		**B_5**	**Chert Lime-**	**Shallala**	**Chalky Limestone**
	Paleocene		**B_4**	**stone**	**Rijam**	**Formation**
Cretaceous	Maastrichtian		**B_3**	**Chalk-Marl Phospor. Limestone**	**Muwaqqar**	**Bituminous Marl Formation**
	Campanian		**B_2**	**Silicified Limestone**	**Amman**	**Amman Formation**
	Santonian		B_1	**Massive**	Wadi Ghudrun	
	Turonian	Ajlun Group	A_7	**Limestone**	**Wadi es Sir**	
			A_6	Echinoidal		
			A_5	Lime-	Shueib	
			A_4	stone	Humar	
			A_3	Nodular	Fuheis	
			A_2	Lime-		
	Cenomanian		A_1	stone	Na'ur	
	Albian	Kurnub	**K_2**	**Kurnub Sand-**		
	Aptian	Group	**K_1**	**stone**		
Jurassic		Zarqa	Z_2	Zarqa Sand-		
Triassic		Group	Z_1	stone		

Table 6-2. Average chemical composition of high-pH groundwaters from the Eastern Springs area at Maqarin (B_3-Aquitard; data of non-Project samples from Abdul Jaber, 1989).

		Adit A-6 pre-Project Samples			Adit A-6 Project Samples			Railway Cutting Samples		
		Average	*Stdev*	*n*	*Average*	*Stdev*	*n*	*Average*	*Stdev*	*n*
pH		12.34	0.23	11	12.56	0.09	5	12.7	0.1	3
Eh	mV	–	–	–	239	63	4	197	66	2
T(Wa)	°C	25.0	0.0	11	23.94	1.8	5	24.9	1.7	3
Cond	µS/cm	5156.7	618.5	6	5165.0	1081.9	2	7220.0	–	1
TDS (calc.)	mg/L	1341.1	145.5	11	1474.8	193.5	5	1687.4	106.1	3
Li	mg/L	–	–	–	0.394	0.332	5	–	–	–
Na	mg/L	61.1	8.6	11	47.1	3.5	5	38.6	6.9	3
K	mg/L	20.2	3.9	11	13.4	3.0	5	18.3	1.7	3
Mg	mg/L	3.7	–	1	0.1	0.0	5	0.1	0.1	3
Ca	mg/L	527.4	80.4	11	603.4	104.4	5	683.3	104.5	3
Sr	mg/L	–	–	–	7.0	1.7	5	10.6	0.3	3
Mn	mg/L	0.001	0.000	3	–	–	–	–	–	–
Fe_{tot}	mg/L	0.010	0.004	4	–	–	–	–	–	–
NH_4	mg/L	–	–	–	0.200	–	1	0.130	–	1
Ba	mg/L	–	–	–	0.033	0.008	5	0.047	0.006	3
Zn	mg/L	0.027	0.015	6	0.047	0.017	4	0.043	0.023	3
Cu	mg/L	0.004	0.003	6	–	–	–	–	–	–
Ni	mg/L	0.0	0.0	6	–	–	–	–	–	–
F	mg/L	–	–	–	0.323	0.055	5	0.329	0.023	3
Cl	mg/L	79.3	7.1	11	58.9	6.3	5	70.7	2.0	3
Br	mg/L	–	–	–	0.258	0.081	4	0.313	0.051	3
SO_4	mg/L	253.8	32.5	11	285.4	13.0	5	288.0	3.6	3
NO_3	mg/L	6.9	6.3	10	7.3	9.2	5	7.6	0.1	3
HCO_3	mg/L	–	–	–	–	–	–	–	–	–
CO_3	mg/L	35.3	27.4	11	1.98	0.0	5	1.98	0.0	3
OH	mg/L	357.5	75.7	11	435.0	111.9	5	551.0	22.3	3
Al	mg/L	–	–	–	0.160	0.028	2	0.150	–	1
P	mg/L	–	–	–	0.003	–	1	0.006	–	1
Si	mg/L	–	–	–	1.14	–	1	0.19	0.06	3
O_2	mg/L	–	–	–	4.0	0.0	2	11.0	–	1
TOC	mg/L	–	–	–	3.9	1.0	2	1.6	0.2	3
^{18}O	‰	–	–	–	-4.5	0.3	5	-4.9	0.8	3
^{2}H	‰	–	–	–	-23.0	1.7	5	-24.2	4.4	3
^{3}H	TU	–	–	–	1.2	0.4	2	1.5	–	1
^{34}S	‰	–	–	–	-0.5	1.0	4	-1.1	–	1
$^{18}O(SO_4)$	‰	–	–	–	12.2	0.6	4	9.8	–	1

* CO_3- from vacuum extraction of sample MQ1 (Adit A-6, 06/04/90).

Table 6-3. Average saturation state of high-pH groundwaters from the Eastern Springs area at Maqarin (B_3-Aquitard; data of non-Project samples from Abdul-Jaber, 1989).

		Adit A-6 pre-Project Samples			Adit A-6 Project Samples			Railway Cutting Samples		
		Average	*Stdev*	*n*	*Average*	*Stdev*	*n*	*Average*	*Stdev*	*n*
Measured:										
pH		12.34	0.23	11	12.56	0.09	5	12.7	0.1	3
pH from OH-activities:										
pH		12.22	0.09	11	12.30	0.13	5	12.39	0.03	3
ionic strength		3.72E-02	4.90E-03	11	4.22E-02	6.05E-03	5	4.83E-02	3.67E-03	3
total C*	mol/L	5.90E-04	4.58E-04	11	3.31E-05	1.61E-08	5	3.31E-05	1.71E-09	3
log pCO_2	bar	-10.62	0.40	11	-11.98	0.29	5	-12.20	0.05	3
Calcite	SI	1.84	0.28	11	0.69	0.01	5	0.69	0.01	3
Dolomite disord.	SI	1.24	–	1	-3.64	0.46	5	-3.67	0.62	3
Dolomite ord.	SI	1.79	–	1	-3.09	0.46	5	-3.12	0.62	3
Fluorite	SI	–	–	–	-1.40	0.15	5	-1.37	0.04	3
Gypsum	SI	-0.78	0.05	11	-0.70	0.04	5	-0.69	0.03	3
Portlandite	SI	-0.67	0.22	11	-0.47	0.29	5	-0.21	0.01	3
Chalcedony	SI	–	–	–	-3.56	–	1	-4.72	0.16	3
Quartz	SI	–	–	–	-3.13	–	1	-4.30	0.16	3
Barite	SI	–	–	–	-0.11	0.08	5	0.01	0.08	3
Celestite	SI	–	–	–	-0.87	0.08	5	-0.72	0.04	3
Strontianite	SI	–	–	–	-0.74	0.10	5	-0.60	0.06	3
Magnesite	SI	-0.96		1	-4.35	0.46	5	-4.38	0.63	3
$Al(OH)_3$ am.	SI	–	–	–	-5.65	0.23	2	-5.88	–	1
Gibbsite mc.	SI	–	–	–	-4.20	0.23	2	-4.43	–	1
Kaolinite	SI	–	–	–	-11.04	–	1	-13.81	–	1
$Fe(OH)_3$ am.	SI	-0.51	0.15	4	–	–		–	–	
Goethite	SI	3.49	0.15	4	–	–		–	–	

* = CO_3- from vacuum extraction of sample MQ1 (Adit A-6, 06/04/90).
SI = Saturation Index.

Table 6-4. Average chemical composition of high-pH groundwaters from the Western Springs area at Maqarin.

		Western Springs Project-Samples		
		Average	*Stdev*	*n*
pH		12.66	0.16	11
Eh	mV	173	59	4
T(Wa)	℃	24.1	2.1	11
Cond	µS/cm	10210.0	–	1
TDS (calc.)	mg/L	3590.1	1029.0	11
Li	mg/L	0.3	0.3	10
Na	mg/L	122.6	47.2	11
K	mg/L	474.8	253.4	11
Mg	mg/L	0.1	0.0	5
Ca	mg/L	995.2	158.1	11
Sr	mg/L	14.1	4.1	11
Mn	mg/L	–	–	–
Fe_{tot}	mg/L	–	–	–
NH_4	mg/L	3.6	2.4	11
Ba	mg/L	0.028	0.009	11
Zn	mg/L	0.023	0.013	10
Cu	mg/L	0.080	0.014	2
Ni	mg/L	–	–	–
F	mg/L	0.764	0.248	11
Cl	mg/L	47.1	13.0	11
Br	mg/L	–	–	–
SO_4	mg/L	1283.8	491.7	11
NO3	mg/L	28.3	13.1	11
CO_3*	mg/L	1.2	0.0	11
OH	mg/L	600.5	110.7	11
Al	mg/L	0.1	–	1
P	mg/L	0.1	0.1	6
Si	mg/L	0.4	0.3	8
O_2	mg/L	0.4	0.3	7
TOC	mg/L	6.6	3.2	10
^{18}O	‰	-4.1	0.5	6
^{2}H	‰	-19.1	2.5	6
^{3}H	TU	0.5	0.5	3
^{34}S	‰	-2.6	0.1	2

Table 6-5. Average saturation state of high pH groundwaters from the Western Springs area at Maqarin.

		Western Springs Project-Samples		
		Average	*Stdev*	*n*
Measured:				
pH		12.66	0.16	11
pH from OH-activities:				
pH		12.41	0.08	11
ionic strength		7.76E-02	1.63E-02	11
total C	mol/L	2.01E-05	2.59E-08	11
log pCO_2	bar	-12.51	0.18	11
Calcite	SI	0.47	0.01	11
Dolomite disord.	SI	-4.36	0.59	5
Dolomite ord.	SI	-3.81	0.58	5
Fluorite	SI	-0.68	0.36	11
Gypsum	SI	-0.11	0.25	11
Portlandite	SI	-0.15	0.19	11
Chalcedony	SI	-4.48	0.40	8
Quartz	SI	-4.05	0.40	8
Barite	SI	0.12	0.09	11
Celestite	SI	-0.21	0.35	11
Strontianite	SI	-0.89	0.15	11
Magnesite	SI	-4.85	0.59	5
$Al(OH)_3$ am.	SI	-6.03	–	1
Gibbsite mc.	SI	-4.58	–	1
Kaolinite	SI	-14.84	–	1
$Fe(OH)_3$ am.	SI	–	–	–
Goethite	SI	–	–	–

SI = Saturation Index.

Table 6-6. Environmental isotope data and field measurements for samples collected in the Maqarin Phase III study.

Sample ID	Site	pH	$\delta^{18}O$ (‰)	$\delta^{2}H$ (‰)	^{3}H (TU)
M9	Artesian borehole in the Amman Fm.	7.61	-5.10	-23,9	1.3±0.20
M10	Eastern Springs seepages at Yarmouk River	12.4	-3.21	-16.7	1.1 ±0.20
M11	Western Springs seepages at Yarmouk River	12.7	-4.00	-18.4	0.21±0.19
M15	Western Springs seepages at Yarmouk River	12.7	-4.03	-18.1	0.11±0.21
M17(1)	Borehole (WS1) in Bituminous Marls (Western Springs)	7.24	-4.62	-21.6	0.34±0.21
M18	Borehole (RW1) at Railway Cutting (Eastern Springs)	8.81	-5.09	-26.6	3.7 ±0.30
M8	Railway Cutting (Eastern Springs) (95-5-1)	–	-4.41	-21.6	0.08 ±0.2
M17(2)	Borehole (WS1) in Bituminous Marls (Western Springs) (95-5-1)	–	-4.81	-24.3	3.5 ±0.4
M5	Western Springs seepages at Yarmouk River (95-5-1)	–	-4.25	-19.9	0.10±0.19
M1	Adit A-6 (Eastern Springs), 140 m from entrance (95-5-1)	–	-4.41	-21.6	0.08 ±0.2

Table 6-7. Experimental rehydration of calcined Bituminous Marl.

Sample	LOI (%)	Clinker (g)	Water (cm^3)	pH (‰)	$\delta^{18}O$ (‰)	$\delta^{2}H$ /repeat (‰)
Deionized	–	0	10	7.0	-13.28	-90.8
1a	31.4	1	10	12.80	-13.12	-92.4 /-90.9
1b	31.4	3	10	12.80	-12.99	-91.0 /-89.7
9a	37.8	1	10	12.78	-13.13	-91.4 /-92.2
9b	37.8	3	10	12.78	-13.00	-89.5 /-92.6

Table 6-8. Preliminary calculated mass transfer required to derive the high-pH groundwater compositions of the Eastern and Western Springs areas from local recharge water; negative numbers indicate precipitation, positive numbers indicate dissolution.

Path	**Western Springs area** *Precipitation – M14* (mmol/kg H_2O)	**Eastern Springs area** *Precipitation – M3* (mmol/kg/H_2O)
Calcite	-5.0	-5.1
Brucite	-1.2	-0.55
Portlandite	30.7	23.9
K-S-phases	13.4	0.33
Na-S-phases	3.7	0.03
Pyrite	7.2	1.7
Fe-hydroxides	-7.2	-1.7

Table 6-9. Geochemical data for clinker leaching experiment (data as mg/L).

Sample	**Rock:water**	**pH**	**Ca**	**K**	**Na**
ML 1	3g:40 mls	12.78	495	13	4.1
ML 2	3g:40 mls	12.80	926	18	24.6
ML 3	3g:40 mls	12.82	856	34	9.4
ML 4	3g:40 mls	12.84	–	22	9.9

* These data were then corrected to a volume ratio of 1:1, assuming a high initial porosity in the cement zone. The calculation was not made for Ca, which was assumed to be limited by portlandite solubility.

Table 6-10. Geochemical leaching data corrected to water/rock volume ratio of 1:1.

Sample	K *(meq/L)*	Na *(meq/L)*
ML 1	11.1	5.96
ML 2	15.3	35.6
ML 3	29.0	13.6
ML 4	18.7	14.3
Average	***18.5***	***17.4***
Western seeps (M45)	13.5	5.9
Eastern seeps (M10)	0.52	2.33

Table 6-11. The chemical compositions of hyperalkaline groundwaters (samples M5, M8, M9, M10, M11, M12, M14 and M15 collected during Phase III) from the Western Springs locality at Maqarin. Concentrations are in mg/L, unless otherwise stated.

	M5	M8	M9	M10	M1l	M12	M14	M15
pH (lab)	12.70	12.50	7.61	12.40	12.70	12.50	12.70	12.77
pH (calc.)	12.45	12.37	–	12.36	12.44	12.27	12.45	12.46
Na	129.0	25.3	64.1	53.6	124.0	118.0	130.0	135.0
K	491.0	3.1	4.5	20.6	502.0	452.0	531.0	528.0
Ca	1067	786	93	729	1033	747	1072	1113
Mg	<0.1	<0.1	28.7	<0.1	<0.1	<0.1	<0.1	<0.1
Al	<0.20	<0.20	0.03	<0.20	<0.20	<0.20	<0.20	<0.20
Ba	0.024	0.036	0.197	0.051	0.024	0.032	0.026	0.025
Sr	15.50	3.81	0.87	11.90	14.32	12.02	14.90	15.30
Li	0.46	<0.01	<0.01	0.05	0.43	0.38	0.47	0.50
Mn	<0.001	<0.001	0.004	<0.001	<0.001	<0.001	<0.001	<0.001
Fe	<0.01	<0.01	<0.01	<0.01	<0.01	<0.01	<0.01	<0.01
Zn	0.028	0.015	0.034	0.012	0.018	<0.005	0.005	0.022
Cr	5.24	0.95	<0.01	0.36	5.14	4.38	5.36	5.46
U (µg/L)	0.082	0.041	2.520	<0.022	0.023	<0.022	<0.022	<0.022
Cl	34.9	40.3	108.0	83.2	39.9	39.7	39.3	50.2
SO_4	1410.00	3.52	68.80	290.00	1390.00	1270.00	1470.00	1510.00
S^{2-}	0.030	<0.005	<0.005	<0.005	0.023	<0.005	0.017	0.028
ΣCO_2	14.75	6.90	301.00	6.45	14.35	6.85	9.25	6.60
SiO_2	0.15	0.09	22.90	0.56	0.39	0.79	0.30	0.28
F	0.92	0.43	0.62	0.26	0.95	0.74	0.96	0.97
NO_3	34.80	7.13	11.60	3.09	29.10	18.00	30.20	32.60
NO_2	1.47	<0.40	0.07	0.51	2.88	9.89	2.94	3.19
NH_4	2.81	0.16	<0.05	0.23	2.68	1.89	3.20	3.14
HPO_4	0.55	0.10	<0.05	<0.05	0.54	0.44	0.57	0.60
B	0.14	0.03	0.11	<0.02	0.12	0.07	0.12	0.12
Sc (µg/L)	1070.0	55.5	4.5	52.0	1070.0	1030.0	1140.0	1310.0

Table 6-12. The chemical compositions of other groundwaters (samples M17 and M18 collected during Phase III) from the Western Springs locality at Maqarin. Concentrations are in mg/L, unless otherwise stated.

	M17	M18
pH	7.24	8.81
Na	56.50	38.10
K	57.0	13.6
Ca	87	113
Mg	38.20	2.26
Al	<0.20	0.09
Ba	0.040	0.031
Sr	3.47	3.39
Li	0.04	0.01
Mn	0.010	0.001
Fe	<0.01	0.02
Zn	<0.005	<0.005
Cr	<0.01	<0.01
U (µgl)	0.079	0.834
Cl	46.0	47.30
SO_4	449	280
S	0.894	0.072
CO_2	77.50	21.40
SiO_2	32.10	6.55
F	2.44	0.63
NO_3	<0.20	0.80
NO_2	<0.04	0.16
NH_4	5.84	0.81
HPO_4	<0.05	<0.05
B	0.09	0.02
Se (µgl)	<0.50	0.60

Table 6-13. Ion activity ratios and some mineral saturation indices (+ve = saturated-supersaturated; -ve = saturated-undersaturated) for the Western Springs hyperalkaline groundwaters.

	M5	M8	M9	M10	M11	M12	M14	M15	M17	M18
Activity ratios:										
log Na^+/H^+	10.1	9.3	5.0	9.6	10.0	9.9	10.1	10.1	4.6	6.0
log K^+/H^+	10.4	8.2	3.6	9.0	10.4	10.2	10.4	10.5	4.3	5.3
log $Ca^{2+}/(H)^2$	22.8	22.6	12.3	22.5	22.7	22.3	22.8	22.8	11.5	14.8
log $A1^3+/(H)^3$	<3.50	<4.60	8.50	<4.60	<4.50	<4.70	<4.47	<4.46	<9.70	7.80
log $SO_4^{2-}/(H^+)^2$	-27.3	-27.7	-18.7	-27.7	-27.3	-26.9	-27.3	-27.3	-17.1	-20.4
log H_4SiO_4	-11.4	-11.4	-3.3	-10.6	-10.9	-10.2	-11.1	-11.1	-3.2	-4.0
log f_{CO2}, bars	-11.5	-11.63	-2.0	-11.6	-11.5	-11.4	-11.7	-11.9	-2.3	-4.4
Saturation indices:										
anhydrite, $CaSO_4$	-0.22	-0.78	-2.00	-0.88	-0.23	-0.32	-0.21	-0.19	-1.29	-1.28
aragonite, $CaCO_3$	+1.47	+1.15	+0.50	+1.12	+1.46	+1.13	+1.27	+1.12	-0.57	-0.60
barite, $BaSO_4$	+0.37	+0.08	+0.48	+0.16	+0.37	+0.54	+0.42	–	+0.57	+0.34
calcite, $CaCO_3$	+1.62	+1.29	+0.64	+1.26	+1.60	+1.27	+1.41	+1.27	-0.43	+0.74
celestite, $SrSO_4$	-1.04	-2.04	-3.00	-1.61	-1.07	-1.11	-1.04	-1.03	-1.70	-1.80
fluorite, CaF_2	-0.95	-1.59	-1.93	-2.05	-0.93	-1.22	-0.91	-0.89	-0.83	-1.82
gypsum, $CaSO_4.2H_2O$	-0.05	-0.60	-1.83	-0.70	-0.06	-0.15	-0.03	-0.02	-1.12	-1.11
hillebrandite, $Ca_2SiO_2(OH)_2$	-2.64	-3.06	–	-2.30	-2.27	-2.38	-2.34	-2.34	–	–
portlandite, $Ca(OH)_2$	+0.22	+0.03	–	-0.01	+0.18	-0.24	+0.22	+0.25	–	–
strontianite, $SrCO_3$	+1.59	+0.82	+0.45	+1.32	+1.56	+1.28	+1.37	+1.22	-0.04	+1.01
witherite, $BaCO_3$	+1.39	+1.33	+2.31	+1.48	+1.39	+1.32	+1.22	–	+0.61	+1.55

Table 6-14. The chemical compositions of a hyperalkaline groundwater (sample M5) in comparison with a typical cement pore fluid (data from Lunden and Andersson (1989) and R. Quillin, unpublished data). Concentrations are in mg/L, unless otherwise stated.

	M5	Cement
pH	12.70	13.40
Na	129	1500
K	491	6300
Ca	1067	90
Mg	<0.10	0.20
Al	<0.20	0.40
Cl	34.9	<5.00
SO_4	1410	<2
ΣCO_2	14.75	<10.00
SiO_2	0.15	0.10

FIGURES

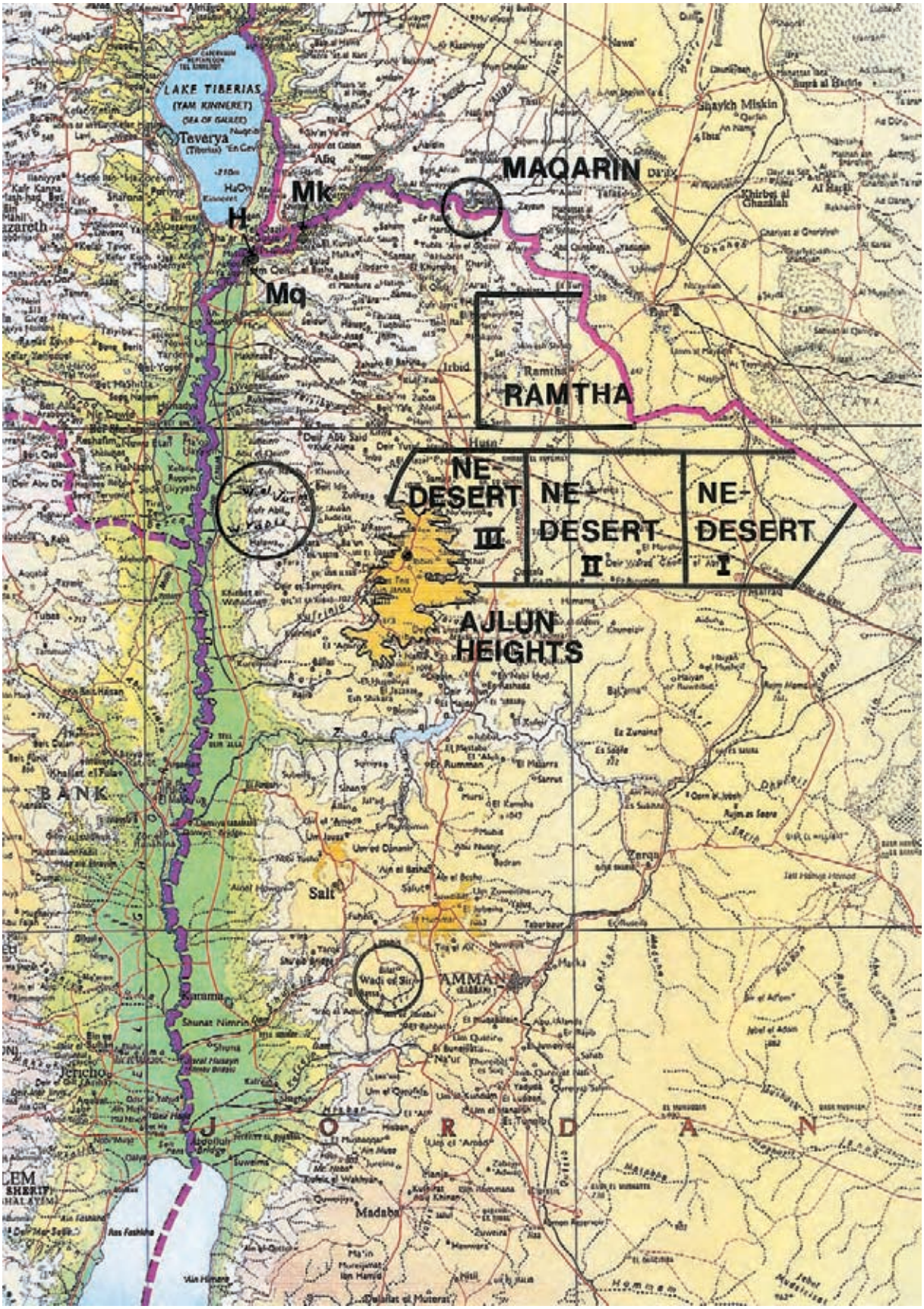

Figure 6-1. *Regional topographic setting of the Maqarin Project area. Marked are key regions and some place names referred to in the text (H = El Hamma; Mq = Maqla; Mk = Mukheiba).*

(© Bartholomew 1995. Reproduced with kind permission).

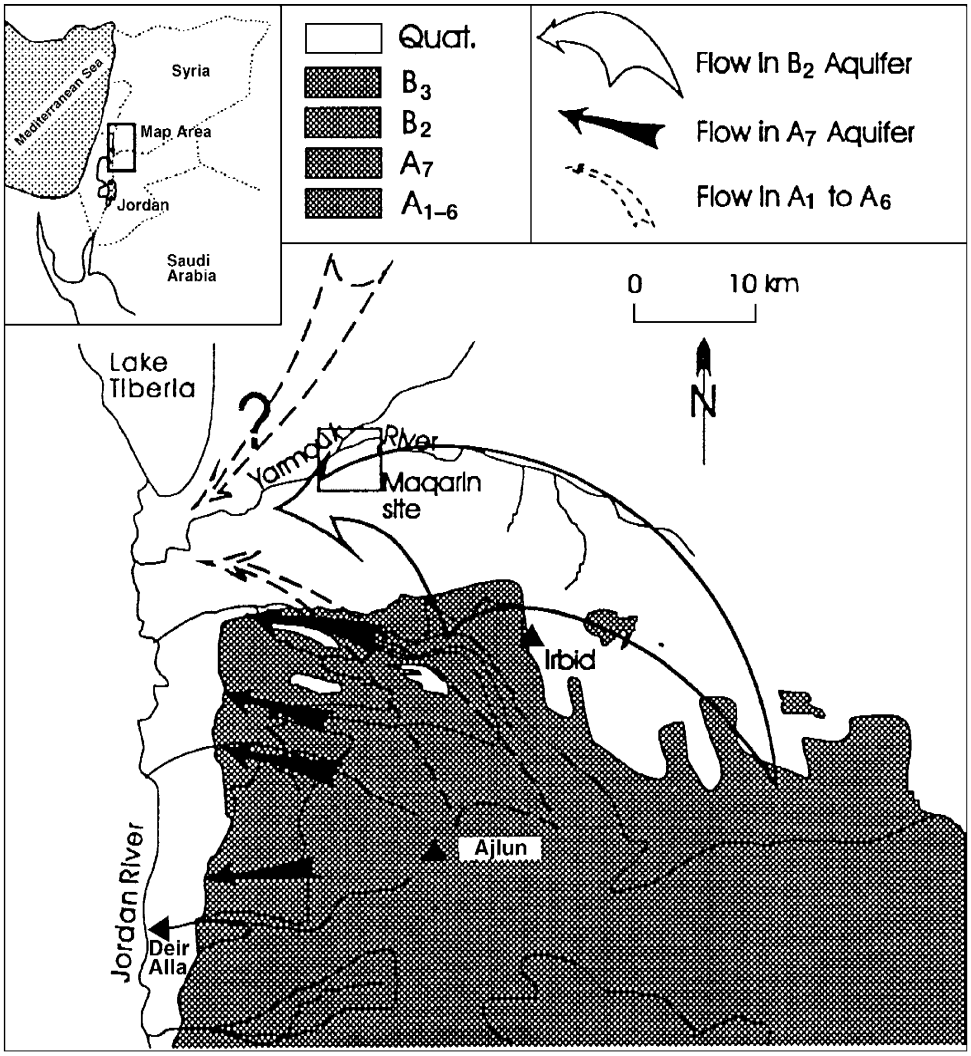

Figure 6-2. *Regional geology and groundwater flowpaths in northern Jordan.*

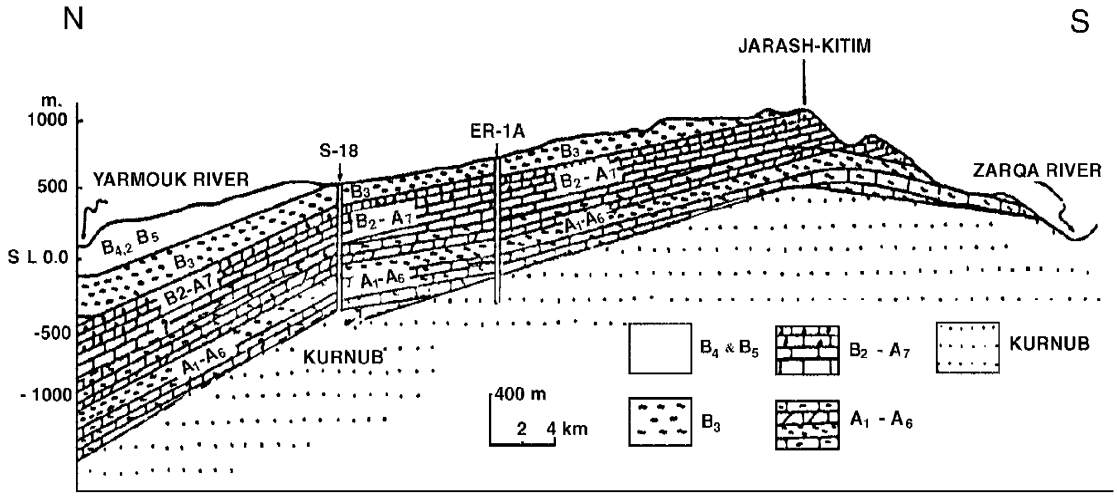

Figure 6-3. *Schematic geological cross-section from the Yarmouk River in the north to the Zarqa River to the south, showing the general inclination of the stratigraphic units towards the northwest (after El-Nasser, 1991). See Figure 6-1 for general location.*

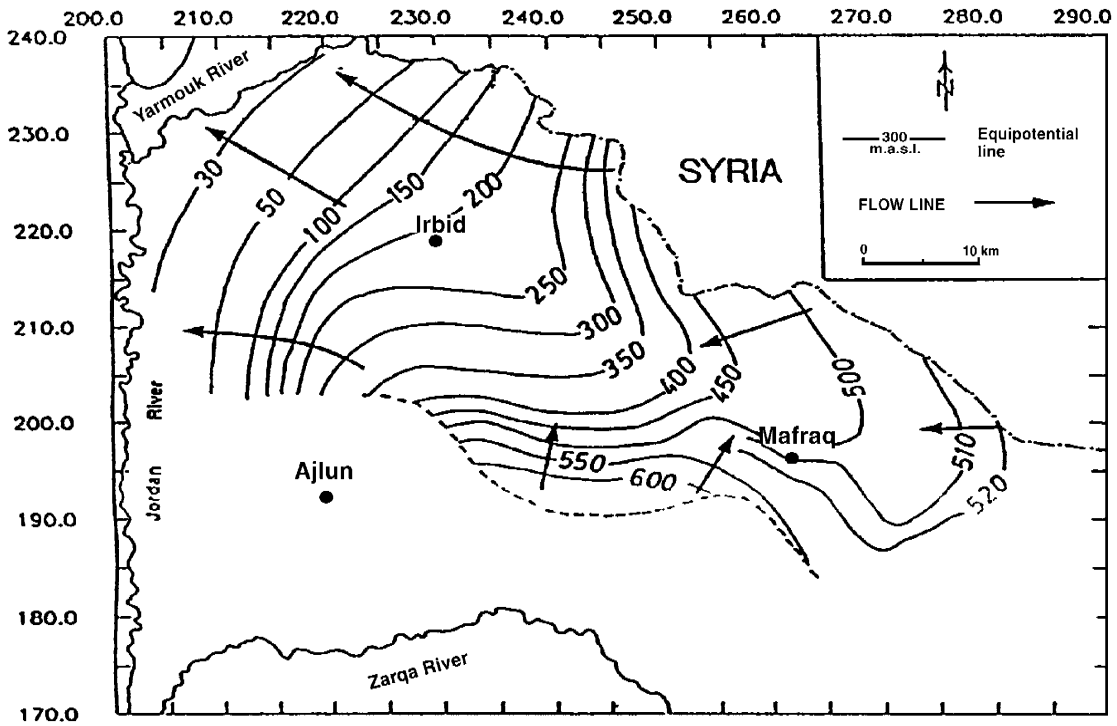

Figure 6-4. *Potentiometric map of the A_7/B_2 aquifer system and its major flow lines (after El-Nasser, 1991).*

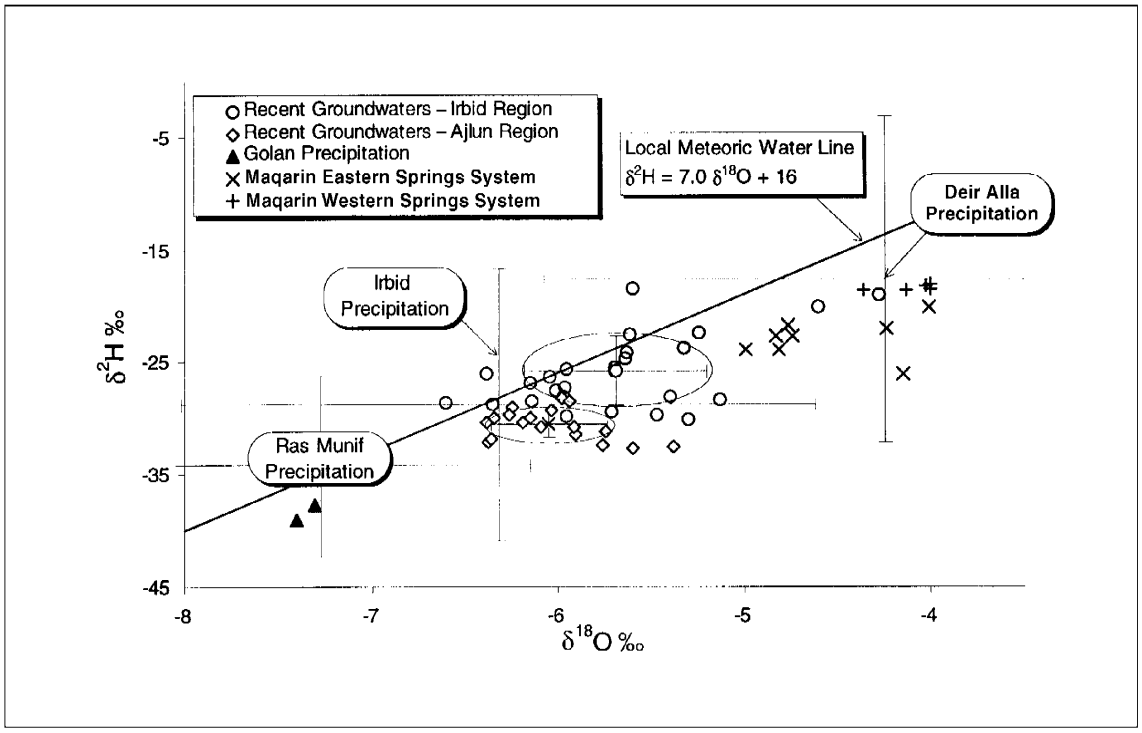

Figure 6-5. *Stable isotope content of precipitation and modern (^3H) groundwaters in northern Jordan. Precipitation shown as mean value and 95% confidence limits for samples collected at Irbid, Ras Munif (Ajlun highlands) and Deir Alla in the Jordan Rift Valley. Hyperalkaline groundwaters from Maqarin also shown.*

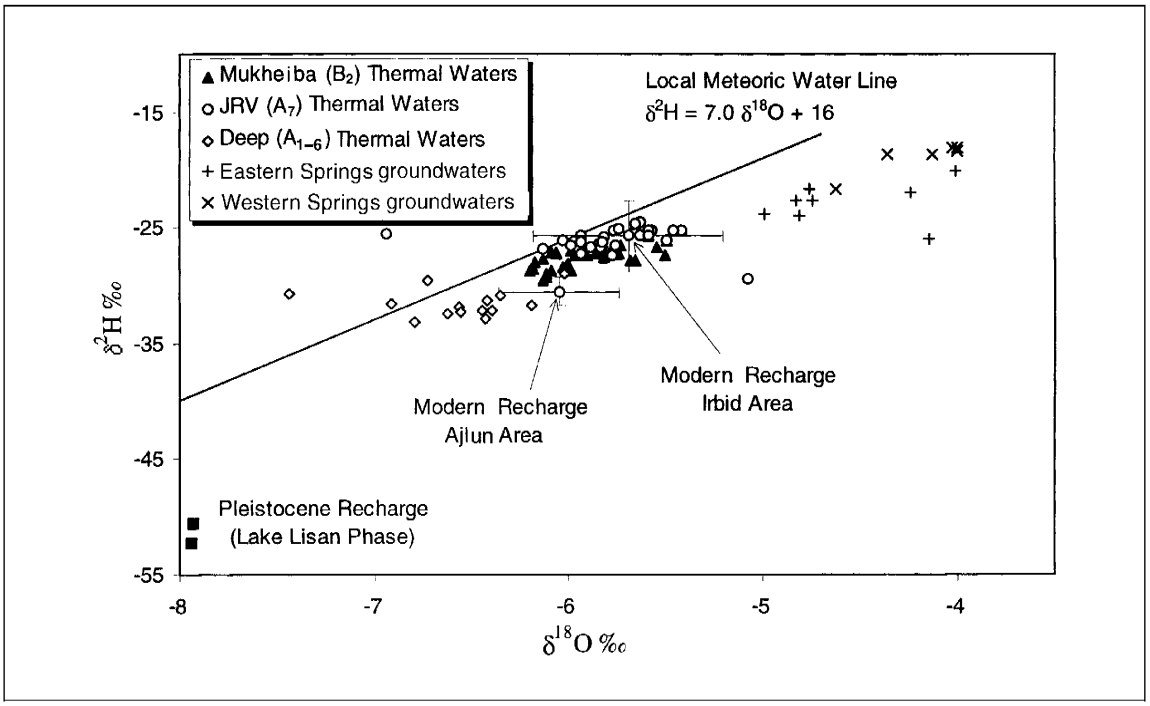

Figure 6-6. *Stable isotope content of regional artesian groundwaters in northern Jordan, sampled from wells at Maqarin (B_2 groundwaters) and in the northern Jordan Rift Valley (A_7 groundwaters). The A_1 to A_6 groundwaters occur in deep wells and the Maqla spring at Maqarin. The Maqarin high pH groundwaters (B_3 groundwaters) are enriched above the range of values for these regional groundwaters.*

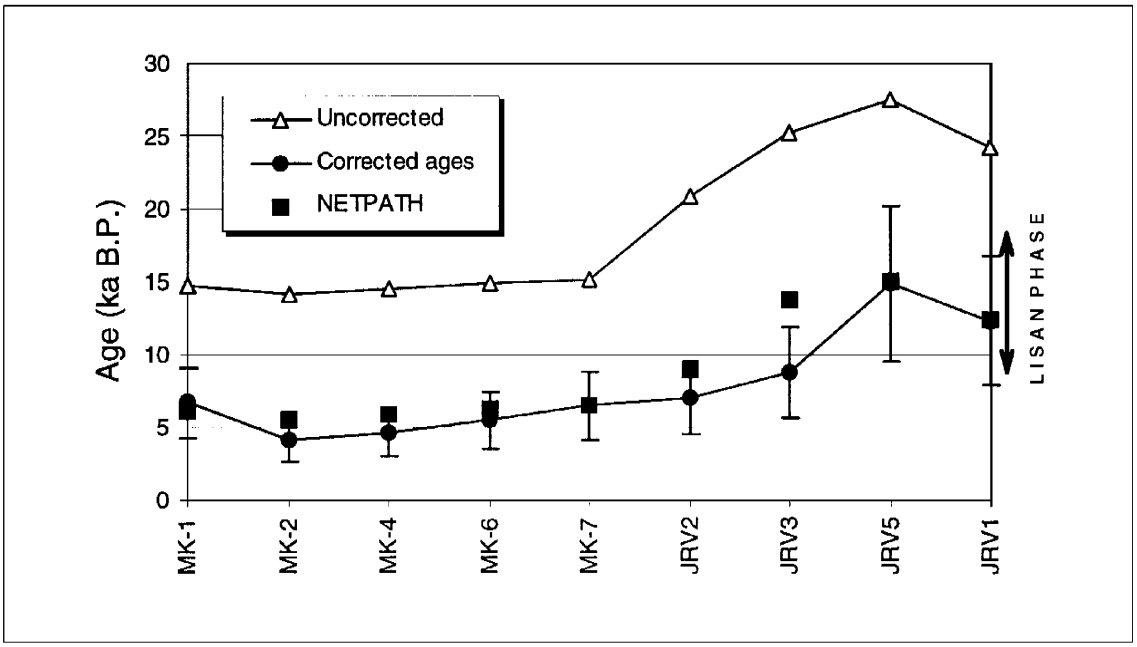

Figure 6-7. *Corrected ages for regional groundwaters in the B_2 and A_7 aquifer. MK wells are found at Mukheiba, some 10 km to the west of Maqarin in the Yarmouk River Valley (Fig. 6-1), and tap artesian groundwaters mainly in the B_2 regional aquifer. JRV wells are found in the northern Jordan Rift Valley, and tap mainly A_7 groundwaters. Groundwater ages produced through geochemical modelling with NETPATH (Plummer et al., 1991) correspond well with the correction algorithms developed for these groundwaters.*

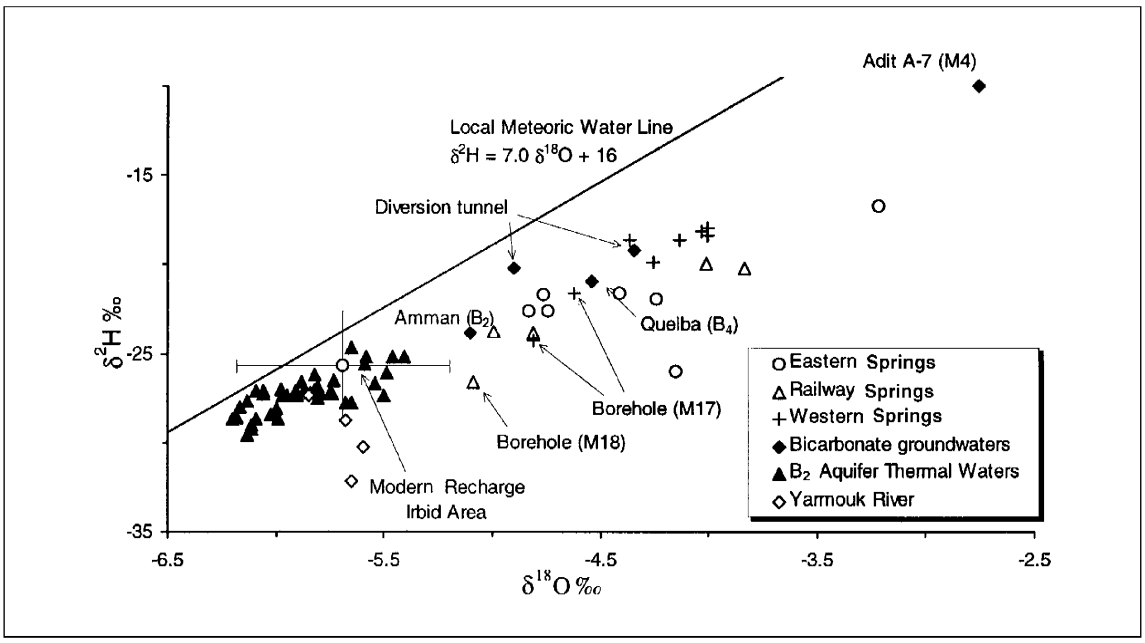

Figure 6-8. *Stable isotopes in high pH and bicarbonate groundwaters from the Maqarin study area.*

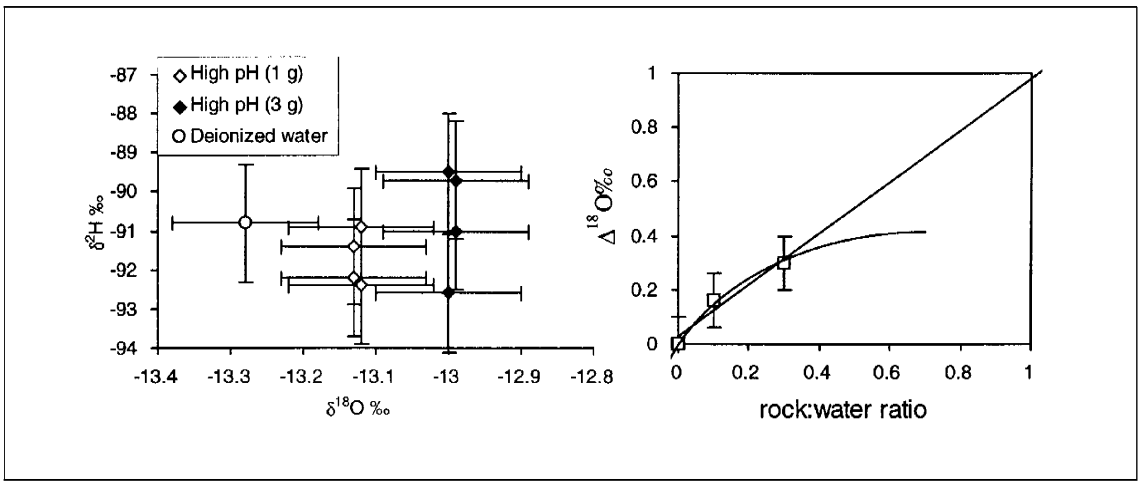

Figure 6-9. *Stable isotopes in waters from rehydration experiment. Shown are the deionised water used, samples with 1 g clinker in 10 mls water and samples with 3 g clinker in 10 mls water ratios. Analytical error shown for each sample. Variations in δ^2H have no significant difference between reacted waters and deionised water. Values for $\delta^{18}O$ show a clear increase with the amount of clinker used.*

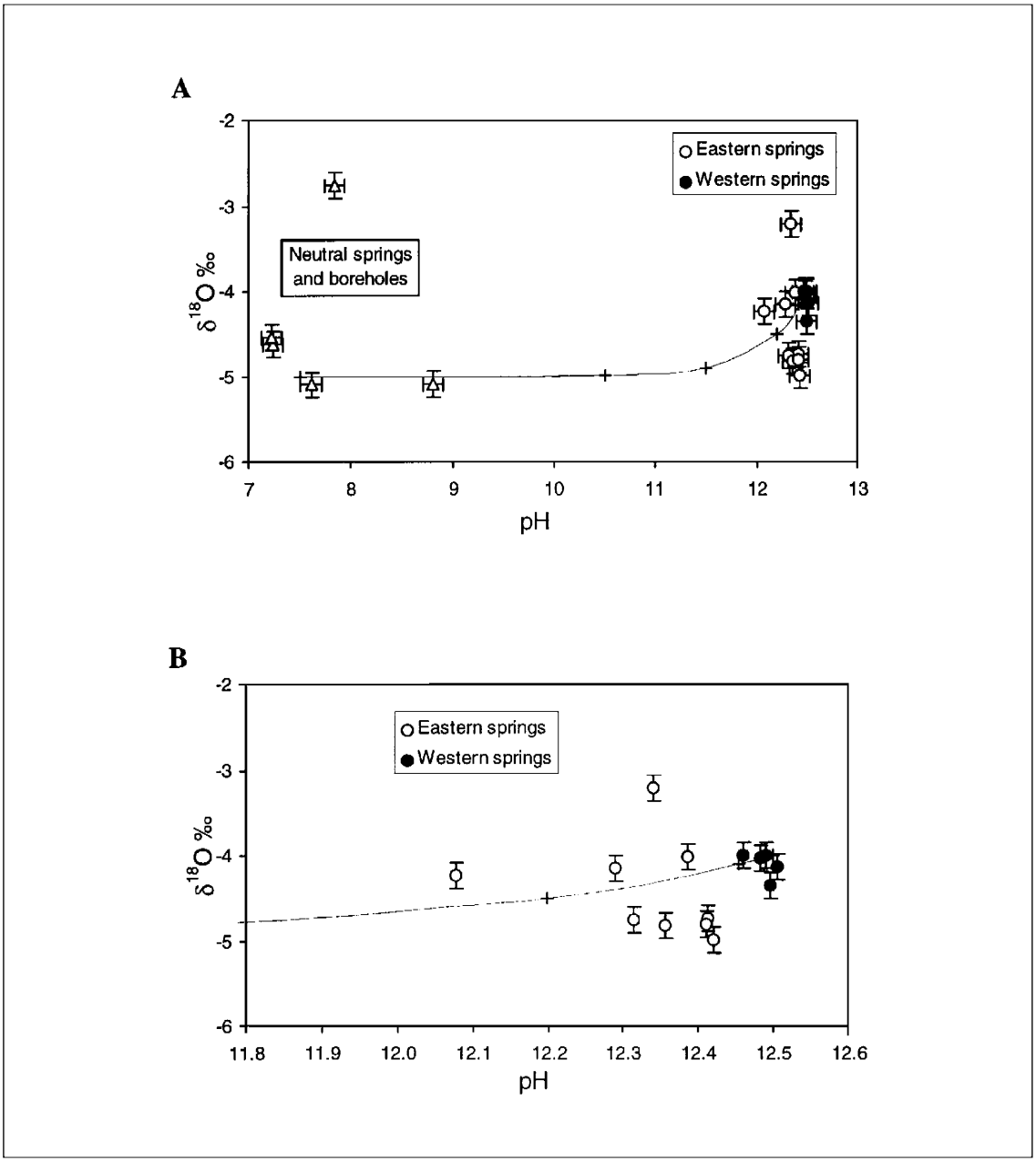

Figure 6-10. *pH vs $\delta^{18}O$ diagram for high pH and neutral pH groundwaters from Maqarin (A) and expanded scale for the high pH groundwaters (B). The line represents a theoretical mixing between a neutral pH ($\delta^{18}O$ set at -5%) and high pH endmembers ($\delta^{18}O$ set at -4%). pH values are based on titrated hydroxide alkalinities for high pH groundwaters.*

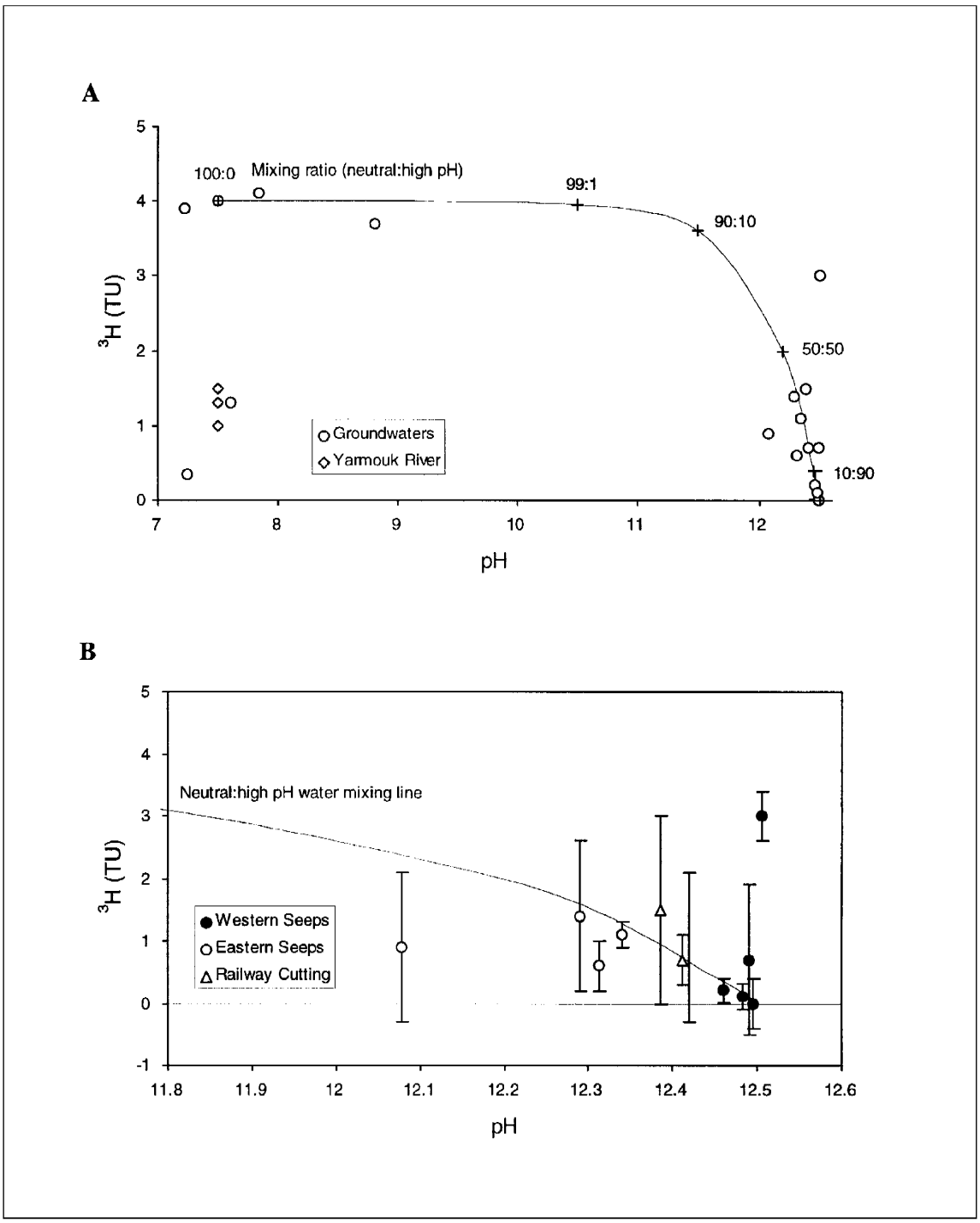

Figure 6-11. *Tritium content of high and neutral pH groundwaters sampled from the Maqarin area (A), and expanded scale for high pH groundwaters (B). The mixing line was produced from a neutral pH bicarbonate groundwater with ^3H = 4 TU and a Ca-OH groundwater with pH 12.5 and ^3H = 0 TU.*

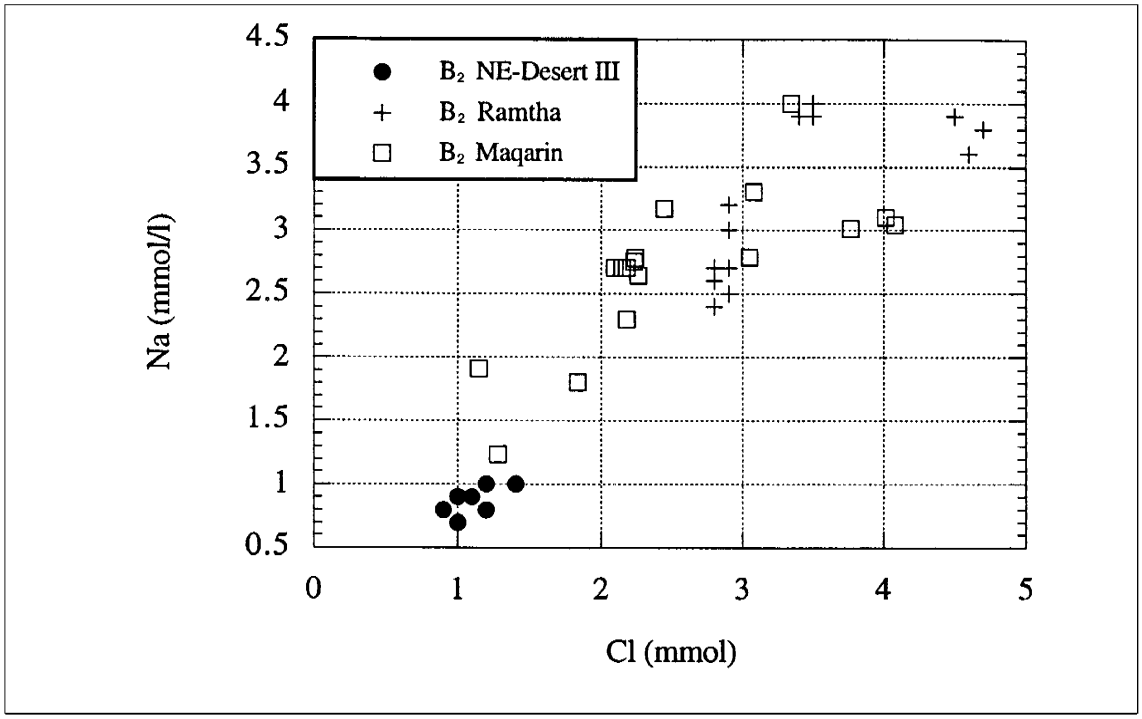

Figure 6-12. *Na^+ vs. Cl^- concentrations in groundwaters from the B_2 aquifer, i.e. NE Desert III recharge area to the Maqarin area.*

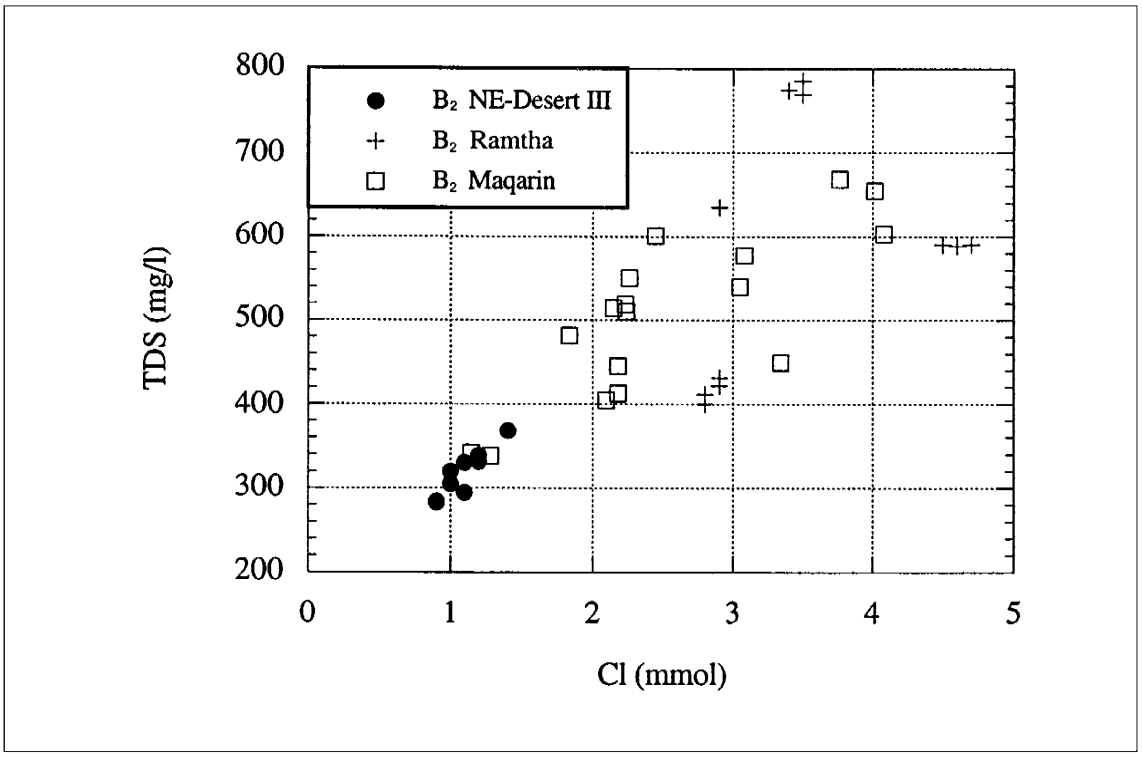

Figure 6-13. *TDS vs. Cl^- concentrations in the groundwaters from the B_2 aquifer, i.e. the NE Desert area to the Maqarin area.*

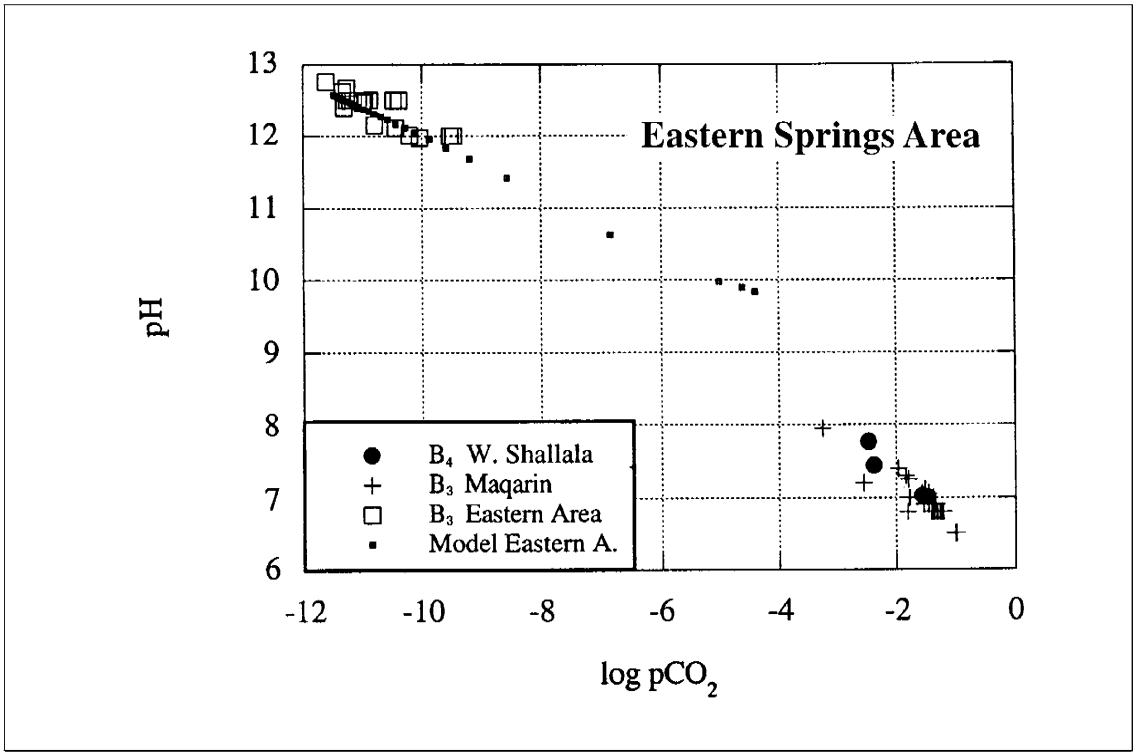

Figure 6-14. *Calculated evolution of pH and pCO_2 compared with measured data of high-pH groundwaters from the Eastern Springs area.*

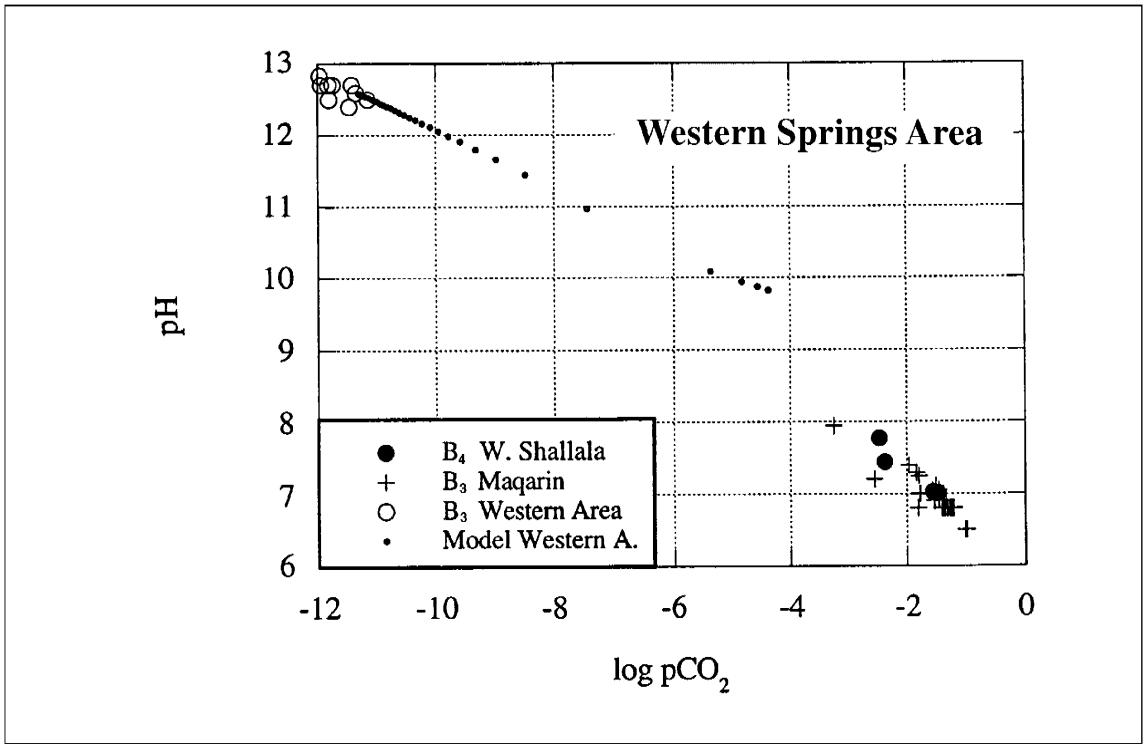

Figure 6-15. *Calculated evolution of pH and pCO_2 compared with measured data of high-pH groundwaters from the Western Springs area.*

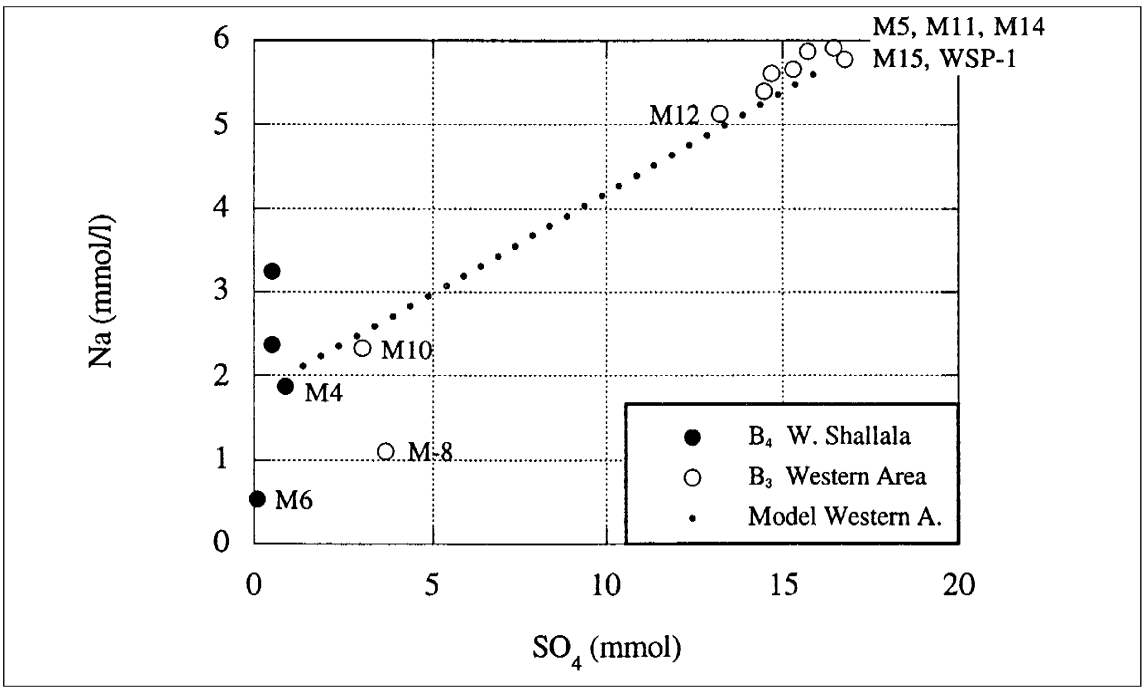

Figure 6-16. *Calculated evolution of Na^+ and SO_4^{2-} concentrations compared with measured data of high-pH groundwaters from the Western Springs area.*

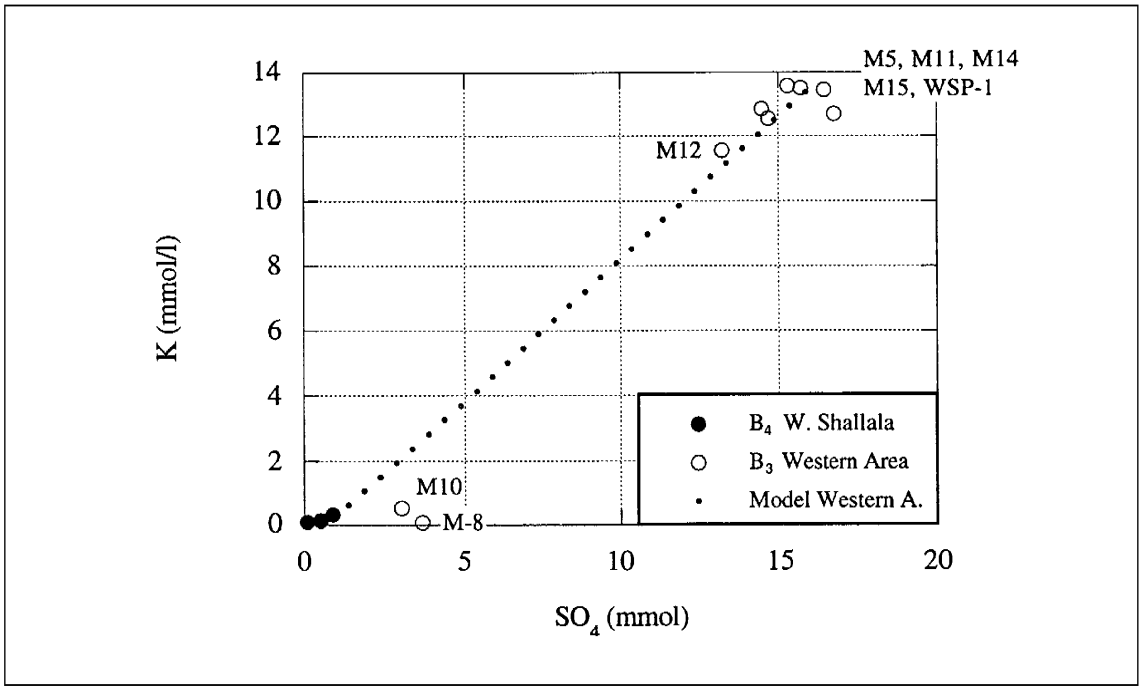

Figure 6-17. *Calculated evolution of K^+ and SO_4^{2-} concentrations compared with measured data of high-pH groundwaters from the Western Springs area.*

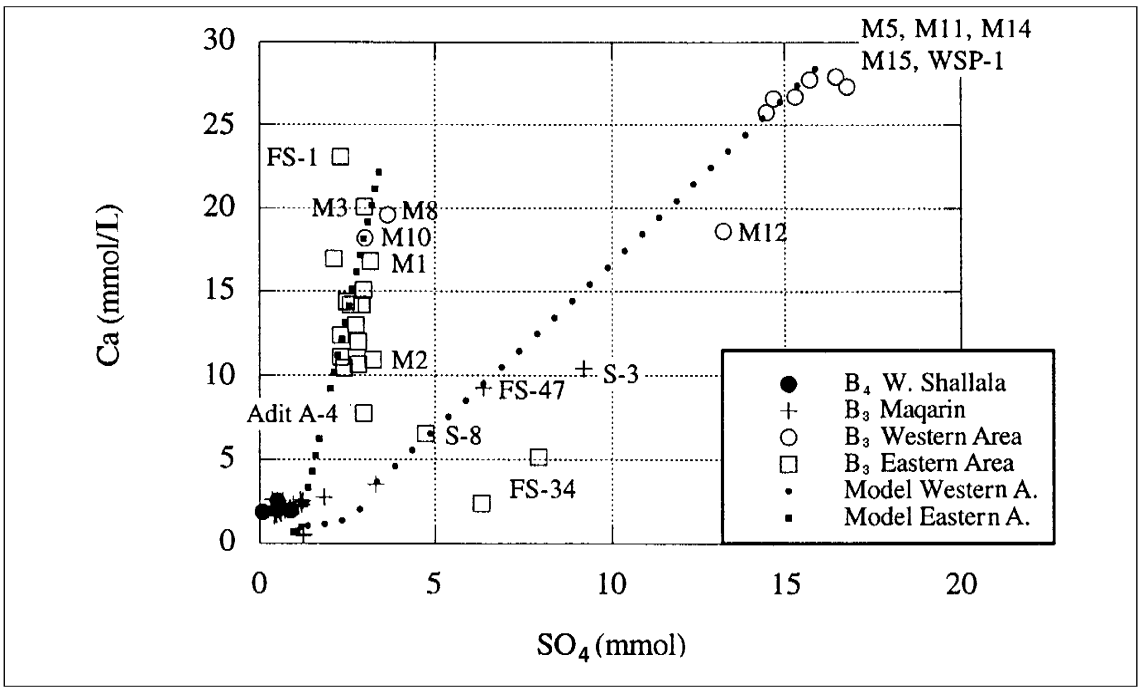

Figure 6-18. *Calculated evolution of Ca^{2+} and SO_4^{2-} concentrations compared with measured data of high-pH groundwaters from the Eastern and Western Springs areas.*

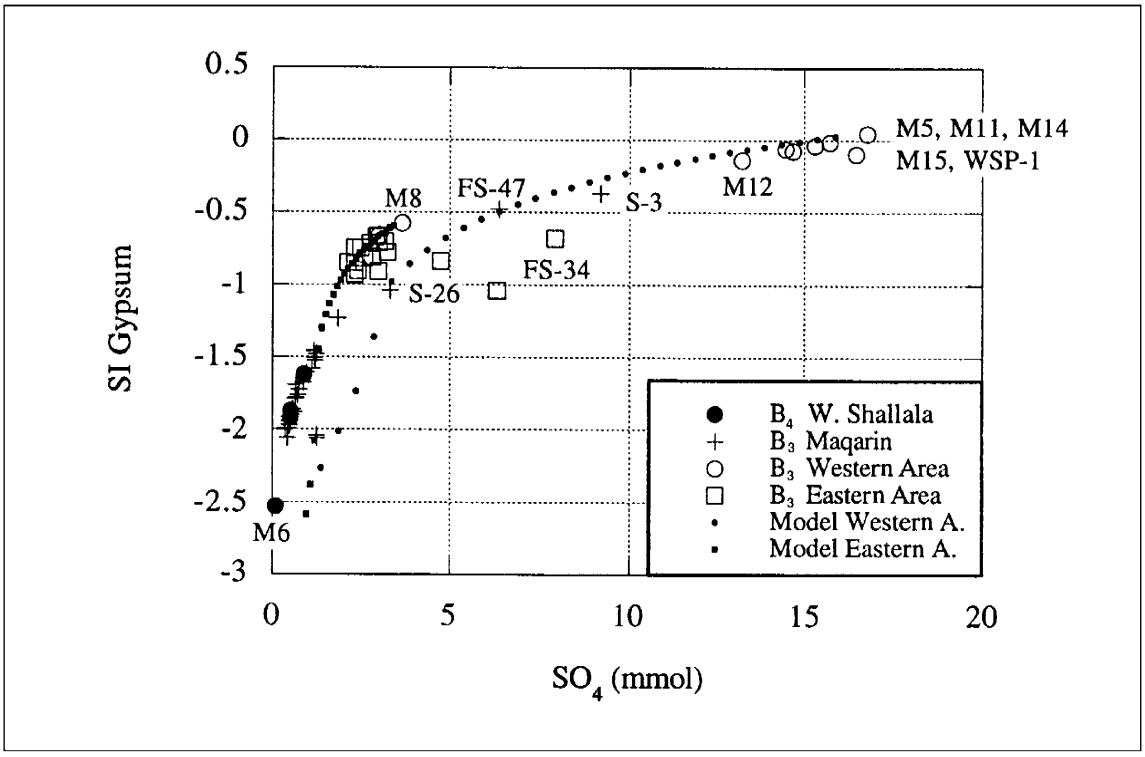

Figure 6-19. *Calculated evolution of the saturation index of gypsum and the SO_4^{2-}-concentrations compared with measured data of high-pH groundwaters from the Western Springs area.*

7 GEOCHEMICAL MODELLING OF HYPERALKALINE WATER/ROCK INTERACTIONS

(A.V. Chambers, A. Haworth, D. Ilett, C.M. Linklater and C.J. Tweed)

7.1 INTRODUCTION

The Western Springs study area consists of a colluvium deposit containing clasts of different rock types, mainly basalt, clay biomicrite ("marl") and chert (see Chapter 4). High pH, high Na and K groundwater is flowing through this colluvium and there is evidence that alkaline water/rock interaction has occurred. The aim of the modelling was to predict the nature of reaction rims around the different clasts and to compare these predictions with characterisation of the clasts. Both an equilibrium and a kinetic modelling approach have been used. The calculations are preliminary and intended only to indicate whether the rates of mineral precipitation or dissolution might need to be taken into account when considering the mineralogical evolution of the system. The kinetic modelling considered a system where dissolution of the primary minerals was kinetically controlled, and examined the consequences with regard to the suite of secondary minerals predicted to precipitate (also kinetically controlled, or assumed instanteous equilibrium).

The high pH (>12), and high Na and K concentration in the Western Springs waters shows some similarities to that in an early stage in the development of cement porewater chemistry. The Western Springs groundwaters therefore form an approximate analogue for the young near-field waters in a cementitious radioactive waste repository, which contain significant quantities of soluble alkali leached from the cement formulation. By studying the interaction of the Western Springs groundwaters with a number of different lithologies it is possible to scope the effects of mineralogy on alkaline water-rock interaction. An increased understanding of the effect of different primary mineralogies has been developed, building confidence in models of the long-term evolution of alkaline disturbed zones in different geological environments.

The Phase III modelling is complementary to modelling carried out during Phase II which concerned interaction of the Eastern Springs waters with the Bituminous Marl Formation lithology (Chambers and Haworth, 1998). Groundwaters in the Eastern Springs area have a composition similar to an evolved near-field groundwater. Comparison of results from the Phase II and III modelling studies scopes the effect of near-field porewater chemistry on the nature of alkaline water-rock interaction.

7.2 MODELS OF THE SYSTEM

7.2.1 Coupled Chemistry and Transport

The System

The system of interest comprises high pH groundwater flowing through a colluvium deposit containing clasts of varying lithologies. As the groundwater flows through the deposit, alkaline water-rock interaction has occurred involving dissolution of primary minerals and subsequent precipitation of secondary minerals. The secondary minerals have precipitated both within the clasts and in the matrix surrounding the clasts. Two aspects of the system have been modelled as part of this study:

- The diffusion of high pH groundwater into individual clasts. Calculations have been carried out to predict the nature of reaction rims around the clasts, e.g. the width of the rims, the distribution of secondary minerals. Three types of clasts were selected for study, basalt, chert and clay biomicrite;
- The diffusion/advection of groundwater through the colluvium deposit. Calculations have been carried out to predict the position and nature of reaction fronts.

The Models

In the coupled chemistry and transport calculations, changes in the rock are related to a one-dimensional grid. High pH groundwater is input at one end and allowed to diffuse/advect along the grid. The high pH solution therefore provides the boundary condition at one end of the grid and its composition is considered to be constant. The rate at which the high pH groundwater travels through the grid is dependent on the transport properties of the rock. As the high pH groundwater moves through, chemical reactions will occur where disequilibrium exists between the solution and the contacting minerals. These reactions will involve dissolution of the primary minerals and precipitation of secondary minerals. The chemical reactions were treated using two different approaches:

- An equilibrium approach where it is assumed that mineral reactions progress to completion instantaneously;
- A preliminary examination of the possible impact of the rates of precipitation and dissolution reactions on mineral alteration.

A key difference in the two modelling approaches is related to the controls on movement of the high pH front through the system. Using an equilibrium approach such as that represented in CHEQMATE, it is assumed that mineral reactions progress to completion instantaneously. Therefore, following equilibration with the minerals present in cell n of the CHEQMATE grid, water moving into cell n+1 will already be close to equilibrium with the minerals present in cell n+1 (assuming the minerals present in cell n+1 are similar to those present in cell n). Further reaction is minimal

and the water continues to move into the grid at a rate controlled principally by the transport properties of the system.

Using a kinetic approach such as that represented in MARQUISS, reaction within cell n is incomplete. Water leaving cell n and entering cell n+1 is therefore still significantly out of equilibrium with the mineral present in cell n+1. Further (incomplete) reaction will occur. As the water moves through the MARQUISS grid the water chemistry continues to change in this stepwise fashion. The controls on the movement of the high pH front in the MARQUISS system are therefore a complex interplay of the transport rates versus the rate at which aqueous components are removed/added to solution as a consequence of mineral reaction.

This difference in the control of movement of the hyperalkaline water through the system may affect the development of the reactions front by altering the sequences of secondary minerals, as well as the length scales of reaction. The kinetic approach was only applied to simulations of the diffusion of high pH groundwater into the basalt and chert clasts, and employed a number of simplifications as discussed below. It was of interest to investigate the potential of a kinetic treatment, even if simplifications were necessary.

Sources of Uncertainty

At this point, it is worth identifying the main sources of uncertainty in the model predictions. The input data used to define the system are described in some detail below, and the uncertainties associated with selection of these data are discussed. These data are used to describe the physical and chemical properties of the system prior to the influx of hyperalkaline water, and to calculate the evolution of the system over time. The length scales over which reaction fronts have travelled in a specified time will be a function of both the transport properties of the system, and the amount of reaction between the primary minerals and the hyperalkaline water (i.e. are the reactions kinetically inhibited?). Uncertainty in input data can therefore be expected to affect the behaviour of the reaction fronts.

A key uncertainty is exactly how long hyperalkaline water/rock interaction has been active at the Western Springs. The calculations are carried out over a specified period of time, and this obviously influences the model results. Previous studies (Chambers and Haworth, 1998) have suggested the Maqarin alkaline water/rock system has undergone more than one period of reaction, leading to estimates of age ranging from a few hundred years, to 100 000 years. Stable isotope evidence and hydrochemical simulation of the groundwater system (Clark and Fritz, 1998; Chapter 6, this report) has suggested that the waters discharging at the Western Springs represent early waters leaving the cement zone; this could suggest that the Western Springs hyperalkaline alteration system has not been operative for very long. For this present study, in the first instance, the calculations were run for a timescale of 100 years. Following this time, as will be seen in later sections, the predicted reaction rims around the clast were already significantly wider than those observed in the field. No longer runs were therefore carried out.

Supporting Chemical Calculations

It is possible that certain secondary phases might precipitate, not as a result of alkaline water-rock interaction, but as a consequence of mixing the high pH waters with water already resident in the rocks of interest, e.g. water occupying porespace within clasts, or within the colluvium itself. Furthermore, alkaline water/rock interaction at the Western Springs is occurring at or close to the ground surface and may therefore be influenced by equilibration with atmospheric carbon dioxide. Supporting chemical calculations were carried out to ascertain whether these aspects of the system were likely to play an important role in controlling the precipitation of secondary minerals at the Western Springs.

7.3 DESCRIPTION OF PROGRAMS

The following sections are brief descriptions of the computer programs used for the calculations carried out during this study. There were two types of calculations:

- calculations where both chemical changes and transport of species through the system are represented, and;
- calculations where only the chemistry is described.

Chemistry

The thermodynamic equilibrium program HARPHRQ, version 1.41 (Brown et al., 1990), developed by AEA Technology, was used for the modelling. HARPHRQ is based on the U.S. Geological Survey code PHREEQE (Parkhurst et al., 1980). HARPHRQ can be used to model various aspects of a system of interest such as chemical speciation in groundwaters, mineral solubility and sorption of aqueous species onto mineral surfaces.

Thermodynamic Data

The thermodynamic database HATCHES was used for all calculations. HATCHES version 7.1 was used for CHEQMATE calculations; version 8.0 was used for the later MARQUISS calculations. For the species and minerals of interest in this study, there were no major changes in the thermodynamic data between these two versions of HATCHES. As part of the Phase III project, a literature review of thermodynamic data for the formation of zeolites was performed (see Chapter 8). For all the calculations carried out during this modelling study, the zeolite dataset in HATCHES was up-dated and extended to include zeolite data compiled during the literature review.

7.3.1 Coupled Chemistry and Transport

CHEQMATE

The CHEQMATE program has been developed at AEA Technology and models chemical changes in a system due to coupled chemical and transport processes (Haworth et al., 1988). It is an iteratively coupled program; it employs a two-step solution to simulate coupled ionic transport and chemical equilibrium. The simulations are carried out for a one-dimensional section of the material of interest divided into a number of different cells. The flux of each species over the cell boundaries is calculated using a finite difference representation of the transport equations. The transport is in one dimension and can include advection, dispersion, diffusion and electromigration. The change in concentration in each cell is then calculated and passed to the program HARPHRQ which equilibrates the aqueous solution. The CHEQMATE program uses an equilibrium approach and assumes that the mineral reactions progress to completion instantaneously. The use of the two-step solution allows complex chemistry to be considered. However, there may be numerical problems associated with solving the transport equations where sharp reaction fronts occur (such as in the case of mineral precipitation/dissolution). The MARQUISS code is, therefore, under development to complement the use of CHEQMATE for these types of problems.

MARQUISS

The MARQUISS (Mineral Alteration Reactions using the QuasI-Stationary State approximation) is under development by AEA Technology to simulate the migration of sharp chemical fronts through geological systems over geological timescales (Chambers, 1994). It includes treatment of the effect of the chemical kinetics of mineral reactions using pseudo-kinetic rate laws (Steefel and von Cappellen, 1990). At its current stage of development, the program employs a number of simplifications which must be recognised in the current context:

- it simulates the transport of material in one spatial dimension and therefore the process of dilution is ignored. No representation of dispersion is included;
- aqueous speciation is not included, and so the choice of a single aqueous species for each element included in the simulations is required. This is an important limitation in the applicability of the current version of the program, especially as there are large variations in the pH at different points in the system. Nonetheless, previous applications, including interpretation of data from the Maqarin site obtained during Phase II (Chambers, 1994; Chambers and Haworth, 1998) had suggested that this might not be a significant constraint here.

  For the calculations reported here, HARPHRQ was used to determine the dominant aqueous species for each element of interest. Where differences occurred in the dominant species predicted for the high pH water and the near-neutral groundwater, the species of the former were used because mixing of the waters results in high pH solutions even with low ratios of high pH water;

- MARQUISS can consider only the precipitation and dissolution of a small number of minerals (typically of the order of ten) in any calculation. It is important, therefore, that careful consideration is given to the selection of minerals such that the most significant mineral alteration processes are represented;

- data for the kinetics of the dissolution and precipitation of minerals are limited, particularly at the high pH values required for this work. The kinetics of the dissolution of key primary silicates and carbonates have been studied (Rochelle et al., 1992; Savage et al., 1992). The question of data availability is discussed further in Section 7.4.

It should be noted that MARQUISS is the latest in a number of programs designed to predict long-term changes in mineralogy; other examples include PRECIP (Noy, 1990), the work of Lichtner (1992), Lichtner and Biino (1992) and of Ortoleva et al. (1987 a,b). As MARQUISS has been designed to provide qualitative predictions of the long-term changes in the main geochemical features of the system, it cannot necessarily be expected to provide information on the details of geochemical change at shorter timescales, because it must apply some simplifications in order for the problems it addresses to be tractable computationally. This is also true, to differing extents, for the other software cited, and is typified by the general use of pseudo-kinetic rate laws which do not require a detailed mechanistic understanding of the underlying chemical processes. The current application is therefore challenging, but nonetheless, given the outcome of previous studies (Chambers, 1994) MARQUISS may provide indications as to whether the rates of chemical change lead to a deviation in the predicted behaviour of the system, from that predicted by models based on the assumption of thermodynamic equilibrium having been attained.

7.4 INPUT PARAMETERS

7.4.1 Solution Compositions

The solution compositions used in the modelling study are shown in Table 7-1. The M5 hyperalkaline water was collected at the base of the colluvium and had already passed through the sedimentary sequence prior to collection. It is not known to what extent reaction with colluvium components (clasts, matrix) may have conditioned the M5 composition. A groundwater sample collected at the top of the colluvium would have been preferable as it would have been more representative of an 'input' solution for the modelling calculations, i.e. prior to reaction with colluvium components. However, as this was not possible, the M5 composition was used.

The measured M5 composition was oversaturated with respect to certain minerals (discussed below). For the equilibrium calculations using CHEQMATE this oversaturation was ignored and the M5 solution was used as measured (given in Table 7-1). For CHEQMATE calculations, therefore, some of the minerals precipitating at the first point along the grid were precipitating simply as a consequence of oversaturation in the high pH input solution. One of the assumptions implicit in the approach used by MARQUISS is that either side of the chemical front the system is in local

thermodynamic equilibrium (Chambers, 1994). For MARQUISS, therefore, it was necessary that the M5 solution was equilibrated before use in the calculations.

It was necessary to define a water composition that might be representative of water occupying the clasts prior to infiltration by the alkaline water. It was assumed that all the clast types were saturated with the same, 'typical non-alkaline groundwater', prior to the hyperalkaline interaction. The M17 water composition was selected as a typical shallow non-alkaline groundwater in the area. A more rigorous approach requires individual water compositions for each clast type studied. However, there are no direct measured data for clast porewaters and the indirect dataset (i.e. water compositions from the rock formations where the clasts originate) is incomplete. Furthermore, it is also possible that the clasts were unsaturated prior to introduction of the hyperalkaline waters. Models of transport through an unsaturated medium are much more complex and lie outside the scope of this study.

For the coupled chemistry and transport calculations, the neutral M17 water was equilibrated with the primary clast minerals prior to infiltration of the high pH water. In the CHEQMATE calculations, this equilibration is carried out implicitly as a preliminary call to HARPHRQ before the first timestep involving solution of transport equations. This equilibration results in the precipitation of small amounts of silicates all along the grid as a consequence of initial oversaturation in the M17 water (Section 7.5). For MARQUISS, preliminary HARPHRQ equilibrations were carried out separately, and the results used to indicate the solution composition to use in the coupled chemistry and transport calculations. Changes to the clast porewater composition as a consequence of this equilibration are minor.

7.4.2 Rock Mineralogy

The rock types considered were clay biomicrite ("marl"), chert, basalt and colluvium. The representative mineralogies used for the calculations are shown in Table 7-2. These mineralogies were based on available data regarding the major components of the different rock types. At this stage, minor components (e.g. pyrite, organic material) were not included in order to limit the complexity of the problem and concentrate on the main processes occurring.

The mineralogy of the Western Springs biomicrite is not significantly different to the Eastern Springs biomicrite and therefore the marl composition selected is that used in the Phase II modelling (Chambers and Haworth, 1998) consisting of calcite, illite, kaolinite and chalcedony. Chert clasts consist of very fine-grained granular silica and in the calculations are taken to be pure chalcedony. The main components of the basalt are feldspar, olivines, pyroxenes and magnetite. Mineralogical observations on Maqarin samples (see Chapter 5) have suggested that the alkaline water-rock reaction is confined mainly to feldspar and any glassy matrix that might be present. The composition of the glass matrix is quite evolved (silicic) and feldspathic in character. Other minerals present, such as olivine and pyroxene, show less evidence of reaction. The lack of reaction with respect to the latter minerals is thought due to the presence of a coating of unreactive Fe/Mg hydroxide. It is not clear whether this hydroxide coating formed as a consequence of some limited reaction with high pH water, or was a result of weathering processes predating the inclusion of basalt within the colluvium deposit. To keep the models as simple as possible, olivine and pyroxene were considered to be unreactive

and the 'basalt' is represented by feldspar alone. Plagioclase end-member compositions were used, based on normative analyses of the basalt clasts (see Chapter 5). The colluvium composition is variable within the deposit dependent on the proportions of different rock clasts present. The composition used for the calculations is based on a representative modal mineralogy calculated from both a field traverse and point counting of thin sections (see Chapter 5).

7.4.3 Physical Properties of the Rocks

The transport parameters used in the calculations are given in Table 7-3; those values for the marl were taken from Phase II and correspond to experimental measurements on similar samples (Chambers and Haworth, 1998). Data are available regarding the matrix porosity of the other rock types (see Chapter 5) but measurements were not made concerning the matrix diffusion properties. It was necessary, therefore, to use estimated values of diffusion coefficient. Diffusion coefficients measured in geological materials typically range from 10^{-14} to 10^{-10} m^2s^{-1} (Bradbury and Green, 1986; Lever and Woodwark, 1989). For the chert and basalt, a diffusion coefficient central to this range was used (10^{-12} m^2s^{-1}). For the colluvium calculations, as advection is very rapid, diffusion becomes an insignificant influence; a diffusion coefficient of $2 \cdot 10^{-11}$ m^2s^{-1} was used in the calculations.

Groundwater flow through the colluvium is extremely rapid. A specific discharge of 10^{-2} m sec^{-1} has been estimated. Such rapid advection could not be represented in the calculations due to numerical problems. The highest value that could be used was 10^{-6} m sec^{-1}. Although this value is considerably lower than in the real system, the calculations will at least give an insight as to the effect that rapid advection may have on the predicted reaction zones and length scales of reaction.

It was originally intended to include representation of changes in the transport properties of the rock as alkaline water/rock interaction progressed. This would be achieved by calculating porosity changes along the grid based on the volumes of mineral dissolved and precipitated. However, as will be discussed in later sections:

- in the calculations using an equilibrium approach, the volume of secondary mineral precipitation close to the clast edge is such that the porosity is effectively blocked after only a short time, thus preventing further reaction;
- in the calculations using a kinetic approach, the amount of mineral reaction was so limited that the volume changes were insignificant.

Changes in the transport properties of the system are not, therefore, included in the results presented in the following sections.

7.4.4 Rates of Reaction

As alluded to above, there are only limited data on the rates of precipitation and dissolution of minerals under high pH conditions. Therefore, although there are data on the dissolution behaviour of some key silicates and carbonates (Savage et al., 1992; Rochelle et al., 1994), there are no data available for the kinetics of CSH, ettringite or

zeolite dissolution. No data are available for kinetics of precipitation of the phases of interest. In the current study, minerals of similar type were grouped and assigned rate constants based on their expected behaviour in alkaline environments (Table 7-4). As the calculations involving MARQUISS are preliminary and intended only to indicate whether the rates of mineral precipitation or dissolution might need to be taken into account when considering the mineralogical evolution of the system, this approach is acceptable. However, a more detailed, quantitative approach would require more accurate kinetic data.

Note, pseudo-kinetic rate laws express the rate of chemical reaction as a product of the surface area of the mineral precipitating or dissolving in the reaction, and the rate constant for the reaction. It was found in applying the rate constant data in Table 7-4, that calculations using MARQUISS converged only when values for the surface area, typically of the order of 10^{-5} m^2g^{-1}, were assigned. These are unrealistically low values for the minerals in question; in assigning these low values, the rates of mineral reactions have effectively been scaled down in order to achieve convergence.

Refinement of the numerical integrator used in MARQUISS would enable more representative surface areas to be specified. The cause of the convergence problem appears to be large and rapid changes in the quantities of minerals when the M5 high pH water comes in contact with the primary silicates. MARQUISS was not originally designed to represent such fast processes, and further development is beyond the scope of the present study. Nonetheless, the results of considering the rates of chemical reactions, where the fluxes of dissolving/precipitating minerals have been reduced by scaling down the reactive surface area, are still of interest.

7.5 RESULTS OF CHEMICAL MODELLING

HARPHRQ calculations were carried out to ascertain whether significant precipitation of secondary phases could occur as a consequence of mixing the high pH waters with water already resident in the rocks of interest. In this way it would be possible to determine the relative importance of water/water reaction, and water/rock reaction in the coupled calculations. The M5 and M17 solution compositions were used as the basis for the HARPHRQ mixing calculations. The results of calculations concerning the two end-member waters are first discussed and then the results of the mixing calculations described.

7.5.1 M5 and M17 Water Compositions

M17 Water

The results (Table 7-5) indicate a degree of oversaturation (positive saturation indices) with respect to many silicate minerals in the measured M17 groundwater. The suite of oversaturated minerals includes quartz, feldspar, clays and zeolites. This oversaturation may indicate one or more of the following:

- although thermodynamically stable, the mineral concerned has not precipitated due to kinetic factors, e.g. lack of nucleation sites, failure to exceed some finite activation energy required to initiate precipitation, etc;
- uncertainty in the field data with respect to Si and Al. These elements are present at low levels and are close to detection limits;
- uncertainty in the thermodynamic data used in the calculations. Data for complex silicates are often sourced to experimental data collected at higher temperatures and extrapolated down to 25°C.

M5 Water

The high pH M5 groundwater is oversaturated with respect to a different suite of minerals: ettringite, calcite, $Ca(OH)_2$ and $Mg(OH)_2$ (Table 7-5; see also discussion in sub-section 6.3.3). Oversaturation of these minerals is unusual, as they are generally assumed to precipitate freely, even in low temperature systems such as the Western Springs. These phases are observed within the colluvium matrix in the Western Springs. It might be expected that the M5 water composition should be close to equilibrium with this suite of minerals, i.e. the saturation indices (Table 7-5) of these minerals should be close to zero.

As mentioned above, uncertainty in thermodynamic data used may lead to calculation of an apparent over- or undersaturation of minerals in a water.

Uncertainty in the measured concentrations of key elements may also lead to an erroneous calculation of saturation of a particular phase. Oversaturation in ettringite and $Mg(OH)_2$ may reflect uncertainty in the Al and Mg analyses, as both of these elements are present at very low concentrations. Ca is present in relatively high concentrations in the M5 groundwater and should not be subject to significant uncertainty. The oversaturation with respect to calcite and $Ca(OH)_2$ is therefore unlikely to reflect uncertainty in Ca concentration.

It is possible that the groundwater chemistry has been affected by contamination of the groundwater due to adsorption of atmospheric CO_2 during sampling. Such contamination will result in an increase in aqueous carbonate and a reduction in the pH. Equilibration of the M5 water composition with atmospheric CO_2 (Table 7-5) results in a reduction of the solution pH to 9.7. The aqueous carbonate concentration rises to 10^{-2}M, calcite remains oversaturated and dolomite becomes oversaturated in the resultant water composition. Ettringite, $Ca(OH)_2$ and $Mg(OH)_2$ are undersaturated. The fact that the measured pH of the M5 water remains at a high value (pH >12) suggests that only limited interaction with atmospheric CO_2 can have occurred, unless the initial water was >pH 13.3.

Geochemical modelling techniques can be used to correct for groundwater perturbation during sampling (e.g. Bond et al., 1995). Based on these techniques, scoping calculations were carried out to ascertain at what aqueous carbonate and pH value, calcite and $Ca(OH)_2$ would be at equilibrium in the M5 water. The resultant values could be considered representative of the unperturbed, *'in-situ'* groundwater. It was

shown that with an aqueous carbonate concentration of ~10^{-5}M, and a pH value of 12.5, then both calcite and $Ca(OH)_2$ are close to equilibrium.

It could be considered that a field pH value should be closer to the true *'in-situ'* value than a laboratory pH value, as there has been less opportunity for sample perturbation. The pH value measured in the field for M5 was 12.2. This was considered to be an underestimate due to possible dilution during the measurement as a consequence of adverse weather conditions. A predicted *'in-situ'* pH value of 12.5 would therefore be consistent with a slightly lower field pH measurement.

These calculations suggest that sample contamination could have occurred in the period between field sampling and measurement of pH and total inorganic carbon in the laboratory. This contamination has lead to an increase in the carbonate concentration of the M5 water. The change in pH, however, is inconsistent with this explanation: contamination with atmospheric CO_2 should have resulted in a lower laboratory pH when compared to the *'in-situ'* pH. Uncertainty on a pH measurement is typically between 0.2 and 0.5 of a pH unit. The true laboratory pH value could therefore lie between 12.2 and 13.2. The modelling predictions suggest that the true pH should be at the lower end of this range. In fact, a pH value of 12.45 is calculated for the M5 water based on filtration of OH^- (Table 6-11). Thus the interpretations given here are consistent with those described in Chapter 6.

7.5.2 M5/M17 Mixing Calculations

Mixing ratios of 1:10, 1:1 and 10:1 were considered and the identities of oversaturated minerals recorded. The calculations were repeated for a system in equilibrium with atmospheric carbon dioxide. These latter calculations were carried out because the alkaline water/rock interaction at the Western Springs locations is occurring at or close to the surface and therefore may be in contact with air. The results are shown in Table 7-5.

The behaviour of the mixed groundwaters is, to a large extent, dominated by the behaviour of the high pH solution. The same suites of oversaturated minerals are indicated, but perhaps slightly less oversaturated than in the pure M5 case. In mixes with higher M17 contents, the suite of minerals contained, in addition, oversaturated silicate minerals.

CSH phases and some silicates (e.g. sepiolite and talc), although undersaturated in the end-member M5 and M17 groundwaters, are oversaturated in mixes of the two groundwater compositions. This is because a relatively Si- and Mg-rich end-member solution (M17) is being combined with a high pH end-member solution (M5), leading to oversaturation of these phases in the mixed solution.

These calculations suggest that significant mineral precipitation may occur as a result of mixing of hyperalkaline water with near-neutral water, particularly if the near-neutral water contains significant amounts of Si and Mg.

7.6 RESULTS OF COUPLED CHEMICAL AND TRANSPORT MODELLING

7.6.1 General

Calculations were carried out for:

- Diffusive transport of high pH groundwater into three different types of clasts: clay biomicrite ("marl"), 'basalt' (i.e. feldspar) and chert;
- Diffusive and advective transport of high pH groundwater through the colluvium.

Calculations using an equilibrium approach predicted that, in general, the sequence of mineral reactions was the same in all cases. As the high pH front passes through the rock, the primary silicate phases present dissolve to be replaced by secondary precipitates. Close to the input of the high pH water there is an initial zone of CSH, ettringite, carbonate and Ca and Mg hydroxide precipitation. Two types of CSH phases are predicted to form; foshagite (high Ca:Si CSH phase) precipitates closest to the input, and then tobermorite (low to moderate Ca:Si CSH phase). The phases precipitating in this initial zone are associated with high molar volumes and within this zone a reduction in the matrix porosity is predicted. Beyond this zone, the pH of the water is reduced, and there is a region of zeolite precipitation which coincides with the primary mineral dissolution front.

For the different rock types, differences are predicted in:

- The amounts/volumes of mineral precipitating;
- The length scale of interaction.

Additional calculations using a kinetic approach were carried out in the case of the silicate-dominated basalt and chert clasts; silicates are known to dissolve slowly, so it was of interest to scope the effects of kinetics on the alkaline water-rock interaction for these clasts. These calculations showed that there were broad similarities, with respect to the reaction zones and the length scale of interaction, to those predicted using the equilibrium approach. Smaller amounts of secondary phase minerals were predicted to form, and the dissolution of the primary minerals was also predicted to be less extensive. This at least in part must result from the assumptions of the model where scaling down of the reactive surface area was required to achieve convergence.

In the following sections, the results of the calculations are presented in detail.

7.6.2 Equilibrium Modelling of Diffusion into Biomicrite Clasts (CHEQMATE)

Using Phase II Transport Parameters

The predicted zone of alteration extends to over 5 cm (Fig. 7-1). There is a large, narrow peak of $Ca(OH)_2$ precipitation close to the clast edge (not shown in Fig. 7-1) and wider zones of CSH and ettringite precipitation, also located close to the clast edge. There is also a zone of ashcroftine precipitation at greater distances into the marl. The predicted evolution of the primary marl minerals is shown in Figure 7-2. Illite and silica are predicted to become exhausted on timescales of less than 50 years. The kaolinite is

exhausted on a timescale of less than 100 years. The calcite is predicted to precipitate close to the edge in a narrow zone. Figure 7-3 shows the evolution of the CSH phases and the zeolites in the biomicrite. There are three peaks of mineral precipitation. Close to the edge foshagite is predicted to precipitate, then tobermorite and, closest to the centre, ashcroftine. At 100 years, the foshagite precipitation peak has broadened and the other minerals have moved further into the biomicrite, maintaining their relative positions. At a point in the biomicrite, therefore, there is a sequence of mineral precipitation and redissolution events. This sequence is predicted to be ashcroftine, then tobermorite which is replaced by foshagite.

Using Reduced Transport Parameters

The porosity and diffusion coefficient in the biomicrite marl are higher than those used for the 'basalt' and the chert calculations (Table 7-4). So that the influence of primary mineralogy could be assessed in isolation, it was of interest to carry out a set of calculations for the marl using the same transport properties as for the other two rock types.

The predicted secondary minerals for the biomicrite with lower diffusion coefficient and porosity are shown in Figure 7-4. The predicted alteration zones are narrower than those shown in Figure 7-1 with significant alteration only predicted to occur up to a distance of 5 mm. The sequence and type of mineral precipitation is similar to that predicted for the calculations using a higher diffusion coefficient except for small zeolite peaks which were probably present at earlier times in the higher diffusion predictions.

7.6.3 Equilibrium Modelling of Diffusion into Silicate-dominated Clasts (CHEQMATE)

'Basalt'

As outlined above, the basalt mineralogy is represented by feldspar alone. Figure 7-5 shows the predicted profiles of the secondary minerals in the 'basalt' at 100 years. The minerals predicted to precipitate include CSH phases, zeolites, prehnite, calcite and ettringite. Talc (not shown in Fig. 7-5) and brucite are also predicted in small amounts. The main precipitation zone is confined to a distance of 1–2 mm from the input, although there is a small amount of alteration up to 8 mm. The albite dissolves up to 7 mm (Fig. 7-6). The evolution of the secondary minerals is shown in Figures 7-7 and 7-8. The positions of the zeolite precipitation at 50 and 100 years are shown in Figure 7-7. The phillipsite and analcime peaks move into the 'basalt' following the albite dissolution front. These zeolites precipitate and then re-dissolve. In the CSH phase precipitation zone (Fig. 7-8) foshagite precipitates closest to the surface with a tobermorite peak positioned further into the clast.

Chert

The predicted profiles for the minerals precipitated in the chert are shown in Figure 7-9. The zone of precipitation is smaller than in the case of the 'basalt' and is confined to 3 mm from the clast surface. The classes of minerals predicted to be precipitated are similar to those for the 'basalt', but the composition of the zeolites is different. The precipitated $Ca(OH)_2$ peak is smaller than for the 'basalt' but the amount of precipitation of foshagite is predicted to be greater. The chalcedony has dissolved up to a distance of 2 mm into the clast after 100 years (Fig. 7-10). The evolution of the zeolite profiles is different from that predicted for the 'basalt' and is shown in Figure 7-11. In the chert, the zeolite peaks do not appear to move with the dissolution front but remain at one position. However, the composition of the zeolite evolves. At 50 years, the predicted phase is mordenite-K. The concentration of this reduces with time and is replaced by wairakite and the clay mineral, saponite-K. The behaviour of the CSH phases is similar to that in the 'basalt' as there is an initial foshagite peak, with a smaller tobermorite peak positioned further into the clast (Fig. 7-12). The predicted concentrations of foshagite are, however, much higher for the chert.

7.6.4 Kinetic Modelling of Diffusion into Silicate-dominated Clasts (MARQUISS)

'Basalt'

The predicted profiles for mineral alteration within 'basalt' are shown in Figures 7-13 to 7-16. The zone of alteration extends to around 4 mm at 100 years. The primary minerals, anorthite and albite, show a sloped dissolution front with larger amounts of dissolution closest to the input of the high pH water (Figs. 7-13 and 7-14). The amounts of dissolution predicted after 100 years (<0.3% of initial volume) are much smaller than that predicted using thermodynamic assumptions (100% of initial volume). This is a reflection of the scaling down of the reactive surface area employed in the MARQUISS calculations as discussed in subsection 7.4.3. The secondary mineral profiles are shown in Figures 7-15 and 7-16. Close to the input of the high pH water there is a zone of ettringite precipitation, extending to 1.5 mm at 100 years. Further into the clast there is a zone of prehnite precipitation (1–4 mm at 100 years).

Chert

The predicted profiles for mineral alteration within chert are shown in Figures 7-17 and 7-18. The zone of alteration extends to around 4 mm at 100 years. A sloped chalcedony dissolution profile is predicted with larger amounts of dissolution closest to the input of the high pH water (Fig. 7-17). The amounts of dissolution predicted after 100 years (<0.3% of initial volume) are much smaller than that predicted using thermodynamic assumptions (100% of initial volume). This is a reflection of the scaling down of the reactive surface area employed in the MARQUISS calculations as discussed above in subsection 7.4.3.

Talc is the only secondary mineral predicted to form and precipitates in extremely small amounts (Fig. 7-18). The talc precipitation zone forms a narrow band. At the surface of the clast, talc is absent; this may be due to instability at high pH, although the

limitations of the modelling approach must be taken into account. If there is instability at high pH, then in the first instance of talc precipitation the band would lie at a finite distance into the clast. The other end of the precipitation band lies slightly beyond the chalcedony dissolution front. This suggests that talc precipitation may not exclusively be due to the increased Si levels in solution as a consequence of the dissolution reaction. In fact this end of the precipitation zone lies at a position coincident with the limit to which the high pH water has extended into the clast (Fig. 7-19) and suggests that some talc precipitation is occurring due to mixing of the high pH water with the water already resident in the clasts.

7.6.5 Equilibrium Modelling of Diffusion/Advection Through Colluvium (CHEQMATE)

CHEQMATE calculations were carried out for the colluvium including an advection component. In terms of the identities of secondary minerals and the spatial arrangement of the reaction zones, the results obtained were very similar to those of the marl calculations (see subsection 7.6.2). This is because, like biomicrite, carbonate was an important component of the mineral representation of the colluvium (see subsection 7.4.2). In the case of the colluvium calculations, due to the rapid advection, the reactions fronts travelled over longer distances, metres as opposed to a few centimetres in the case of the biomicrite.

The model predicted that CSH would precipitate near the input of the high pH water where the pH is high. Zeolites precipitate further away corresponding to a region where the pH is slightly reduced relative to the input value. As the system develops with time, the CSH front widens and moves further into the grid. Zeolite is always positioned at greater distances into the grid, i.e. preceding the CSH front.

7.7 DISCUSSION OF RESULTS

This section compares the key outputs as predicted by the different modelling calculations described in previous sections. The sensitivity of predictions of the models to various key input parameters and assumptions is discussed. Section 7.8 is a comparison of model predictions with available field data. The quality of the comparison will be discussed on the basis of our understanding of the way the models respond to these key input variables and assumptions.

7.7.1 Secondary Minerals

Suite of Minerals Precipitating

The suite of secondary minerals predicted to form using an equilibrium modelling approach was very large when compared to the suite of secondary minerals predicted using a kinetic modelling approach. The reduced suite of secondary minerals in the case of the calculations using a kinetic approach are largely due to the combined effect of (i) limited dissolution of the primary minerals, and (ii) the fact that the high pH water had been pre-equilibrated (thus removing oversaturation of phases such as calcite and

$Ca(OH)_2$ in the input water). As discussed above, the total number of minerals that could be considered in the calculations was also constrained by the numerical approach applied in the MARQUISS program.

Two processes influence the suite of secondary minerals predicted to precipitate within clast reaction rims. These are:

- Disequilibrium within the solutions (without any contact with solid phases) can result in precipitation of oversaturated phases. This disequilibrium may already be present in the starting solutions, or could be created later due to mixing of the solutions;
- Ingress of high pH water results in dissolution of the primary minerals. Large concentrations of elements such as Al and Si are released to solution which, coupled with the high pH, results in precipitation of minerals such as ettringite, CSH and CASH (zeolite) phases.

The chemical modelling described in Section 7.5 provided a guide to which minerals might precipitate due to disequilibrium in the solutions (both the end-member input solutions and various mixes of the solutions). Likely precipitated phases were silicates in the case of the near-neutral M17 water, and carbonates, hydroxides and ettringite in the case of the high pH M5 water. In addition to some of the aforementioned minerals, CSH phases and some silicates (e.g. sepiolite, talc) can be oversaturated in mixes of the M5 and M17 waters.

Mineral Amounts

Table 7-6 summarises the amounts of particular minerals which precipitate within clast rims. The following observations can be made regarding the results:

- Using an equilibrium approach, large amounts of CSH phases (foshagite and tobermorite) precipitate in all cases. The amounts increase according to the order:

  Biomicrite < 'Basalt' < Chert;

- CSH phases did not precipitate using a kinetic approach (over the timescales studied);
- Ettringite precipitation is much reduced in the case of chert clasts (using both an equilibrium and a kinetic approach);
- In the 'basalt' calculations using a kinetic approach, the amount of ettringite precipitation (up to 10 mol dm^{-3}) is large when compared to the amount of primary mineral dissolution;
- Using an equilibrium approach, large amounts of calcite and $Ca(OH)_2$ precipitate in all cases. The amounts of $Ca(OH)_2$ precipitation (equilibrium approach) show the opposite trend to that shown by CSH phases, increasing according to the order:

  Chert < 'Basalt' < Biomicrite;

- Calcite and $Ca(OH)_2$ precipitation were absent in the calculations using a kinetic approach;
- Pronounced zeolite precipitation is associated with 'basalt' clasts (equilibrium approach).

Figure 7-20 shows pH profiles at 100 years for the biomicrite, 'basalt' and chert calculations using an equilibrium approach. Close to the edge of the clasts there is a region where the pH remains high (>12.5). The width of this region varied according to which clast is under consideration. Further into the clasts, the pH decreases from the initial high value towards a lower value (between 11.5 and 12 dependent on the clast concerned). This lower value is reached at a distance corresponding roughly to the primary mineral dissolution front. The pH of the water then remains constant beyond the dissolution front, only decreasing to the near-neutral value of the original porewater at great distances into the clast (often beyond the end of the grid studied).

The highest pH is maintained for longer distances in the case of the biomicrite clasts, and corresponds to decreased CSH precipitation and increased $Ca(OH)_2$ precipitation. This is consistent with the pH-dependent solubility of $Ca(OH)_2$ (see also the saturation indices given in Table 7-5 for M5:M17 mixes of differing pH). CSH phases are more complex as they are also influenced by the availability of Si through dissolution of primary minerals.

Figure 7-21 shows the pH profiles at 100 years for the 'basalt' and chert calculations using a kinetic approach. The profiles show a gradual decrease from pH 12.5 to the near-neutral value of the original porewater. The pH remains constant at the near-neutral value for the remainder of the grid. The near-neutral value is reached at a distance just beyond the primary mineral dissolution front. Unlike the calculations using an equilibrium approach, high pH values are only present for a very narrow region (<1 mm) close to the edge of the clast. The different distances of penetration of the high pH water are a reflection of different controls on the movement of the high pH water in the kinetic vs. equilibrium model representations.

The very small amount of secondary precipitation in the calculations using a kinetic approach is principally related to the extremely limited dissolution of the primary minerals. However, the identity of the secondary precipitates is probably influenced by the lack of an extended region of elevated pH (pH >11). This may explain formation of the minerals, prehnite and talc but not CSH phases and zeolites, as seen in the calculations using an equilibrium approach, although the assumptions employed in the kinetic approach, as discussed above, and the form of the data employed must also be borne in mind (see subsections 7.4.1 and 7.4.2).

From the observations described above it is clear that the availability of Al in the primary mineral assemblage exerts a strong control on the precipitation of zeolite and ettringite. Chert dissolution provides no Al and this is reflected in reduced precipitation of ettringite and zeolites within chert reaction rims. In contrast, dissolution of feldspar contained within 'basalt' clasts provides a source of Al and is associated with the precipitation of large amounts of ettringite and zeolite.

The lack of calcite and $Ca(OH)_2$ precipitation in calculations using a kinetic approach is due to the fact that the high pH M5 input water had been pre-equilibrated and was therefore no longer oversaturated with respect to these phases. This pre-equilibration was discussed subsection 7.4.1.

7.7.2 Mineral Reaction Zones

Using an equilibrium model the following reaction zones are indicated as a function of increasing distance from the source of the high pH water:

ZONE 1	ZONE 2	ZONE 3
High Ca:Si CSH phases (foshagite) Ettringite Calcite $Ca(OH)_2$ and $Mg(OH)_2$	Low Ca:Si CSH phases (tobermorite)	Zeolites (various)

The width of the zones vary according to the system concerned. The positions of the reaction fronts move to greater distances at longer times. This suggests that at a particular point within the system, different minerals will be precipitating as a function of time. In an equilibrium system evidence of this would not be seen. The first minerals would dissolve away completely prior to precipitation of subsequent minerals. In natural systems, early mineral phases are often overprinted by later minerals before complete dissolution can occur. Such a situation results due to:

- Slow kinetics of mineral dissolution reactions;
- Coating of the initial precipitates by subsequent precipitates, thus isolating them from further reaction with the solution.

For the silicate-dominated clasts, calculations using a kinetic model indicated the following sequence of reaction zones:

ZONE 1	ZONE 2
Ettringite	Prehnite ('basalt' clasts) Talc (chert clasts)

Reasons for the reduced suite of minerals when using a kinetic modelling approach were discussed above. As with the equilibrium modelling approach, the mineral fronts move to greater distances with time.

7.7.3 Evolution of Porosity

Figure 7-22 shows the porosity profiles at 100 years for the bituminous marl, 'basalt' and chert calculations using an equilibrium model. In all cases there is an initial decrease in porosity close to the edge of the clast. This region corresponds to the zone where large volumes of secondary minerals are predicted to precipitate. Beyond this region the porosity is maintained close to its original value, or is slightly increased (biomicrite calculations). In this latter region the volume of minerals dissolving either equals or slightly exceeds the volume of minerals precipitating. In these regions, uncertainty regarding the molar volumes of key mineral phases may influence the results.

Figure 7-23 shows the porosity profiles at 100 years for the 'basalt' calculations using a kinetic model. The volume of the ettringite predicted to precipitate was enough to completely block the porosity of the 'basalt' within the first millimetre after 10 years, even with the reduced mineral reaction fluxes used. The large quantities of ettringite predicted to form appear to be an artefact of the modelling approach. In particular, the lack of aqueous speciation in the modelling approach may be a key factor; however, it should be noted that in qualitative terms both the equilibrium and kinetic approaches are in agreement, in that close to the edges of the clast a reduction in porosity is predicted due at least in part to ettringite formation.

A porosity profile for the chert calculations using a kinetic model are not shown in Figure 7-23 because the volumes of mineral alteration produced a negligible variation in the chert porosity.

7.7.4 Length Scales of Interaction

For the systems studied, the predicted widths of reaction zones are summarised in Tables 7-7 and 7-8. The shortest widths were predicted in the case of silicate-dominated clasts ('basalt' and chert). Reaction rims around silicate-dominated clasts were predicted to reach a width of only a few millimetres after 100 years. Reaction rims around carbonate-dominated clasts were wider, reaching a width of a few centimetres after 100 years. The width of the biomicrite reaction rim was narrower when the biomicrite transport properties were reduced to those of the silicate-dominated clast, but still exceeded the width of rims around silicate-dominated clasts. Inclusion of advective flow for the colluvium calculations resulted in much wider reaction zones, reaching a scale of metres after 100 years.

In summary, within the timescale considered, both the mineralogy and the transport properties of the system influenced the width of the reaction zones, within the timescale studied. The length scales were very similar using the equilibrium and kinetic modelling approaches. Had it been possible to represent greater amounts of mineral reaction in the MARQUISS calculations, this might not have been the case.

7.7.5 Influence of High pH Groundwater Chemistry

Comparison of the results from the Phase II modelling study (Chambers and Haworth, 1998) and the present study allows scoping of the effect of high pH porewater chemistry on the nature of alkaline water-rock interaction. The high pH, and high Na and K concentration in the Western Springs waters is similar to that in an early stage in the development of cement porewater chemistry. Groundwaters in the Eastern Springs area have a composition similar to that expected late in the development of cement porefluid.

Complete comparison is difficult as, during Phase II, variable sized grids were used in the calculations. This difference in the discretization of the grid allowed greater confidence in the positions of reaction fronts at short distances. However, due to the more complex grid, shorter timesteps were required and therefore calculations were restricted to shorter timescales of one or two years. Phase III calculations were carried out to timescales of 100 years.

However, even allowing for the differences in mathematical grids used and the timescales to which the calculations were carried out, the predicted trends in the distribution of secondary minerals, the pH profiles and the changes in porosity are similar in both the Phase II and Phase III modelling studies. The models therefore suggest that the near-field porewater chemistry would not have a great effect on at least these aspects of the alkaline water-rock interaction for the biomicrite. This is borne out to some degree by field observations which also suggest that similar secondary phases[1] are formed in the two areas studied even though the water chemistry varies. However, other aspects of the areas vary, e.g. the mineral paragenesis (see subsection 7.8.3).

7.8 COMPARISON WITH FIELD OBSERVATIONS

7.8.1 Summary of Field Observations

The compositional ranges shown by the field CSH and zeolite-type phases are shown in Figure 7-24. Three principle groups of phases are observed:

- Tobermorite-type CSH phases with Ca:Si ratios lying in the range 0.3 to 0.5;
- Unusual CSH phases with a very high Al content, not previously described in natural systems;
- Zeolite-type phases (non-crystalline but with the composition of zeolites) with compositions corresponding to the zeolites, laumontite (or wairakite) and epistilbite. These are less Si-rich than zeolites identified at the Eastern Springs site during Phase II, e.g. mordenite and dachiardite.

---

[1] (Western Springs minerals tend to be Na/K analogues of Ca-dominated minerals seen at the Eastern Springs area).

The above analyses all correspond to measurements on phases present within the colluvium matrix. The observed reaction rims around clasts are very narrow (μm to mm) making analyses of the secondary phases difficult. Available analyses suggest that the phases present within the individual clasts are similar to those seen in the colluvium matrix. Other phases observed within the colluvium matrix include calcite, ettringite, $Ca(OH)_2$, and $Mg(OH)_2$.

7.8.2 Secondary Phases Predicted by the Models

Figure 7-25 summarises the compositions of CSH phases and zeolites predicted to form during the CHEQMATE (equilibrium) calculations. It should be noted that during the calculations some phases were not represented in the thermodynamic database used. Due to numerical problems, only a subset of the complete zeolite dataset could be used. The subset however included zeolites representative of the full range of compositions and so should allow at least qualitative comparison with field data. Thermodynamic data are not available for Al-rich CSH phases and so these phases could not be represented in the calculations.

There is good agreement between the compositional ranges of the predicted zeolites and those observed in the field. For the 'basalt', analcime and phillipsite are predicted to form. The more Al-rich mineral, prehnite, is also predicted to form although this mineral has not been recorded in the field. Prehnite, although not a zeolite, was included in the calculations because it is often associated with zeolites in natural systems. In the chert calculations mordenite is predicted to form at early times but is replaced by wairakite at longer times. For the biomicrite, ashcroftine is predicted to form. All of these zeolites have Al:Si ratios close to those observed in the field. The only more Si-rich zeolite predicted to form was mordenite (chert calculations at early times), however it was replaced by the more Al-rich zeolite, wairakite, at longer times.

Zeolite compositions were apparently dependent on the rock type being considered and the evolution of the system in time. It is known that the composition of zeolites can be controlled by the following properties of the system:

- The Al and Si concentrations in the water;
- The pH of the water;
- The Al:Si ratio of the primary mineral dissolving.

7.8.3 Mineral Paragenesis

Definitions

In the following text the spatial distribution of minerals is defined as 'zoning' and the temporal order in which minerals precipitated is defined as the 'mineral sequence'.

Clast Reaction Rims

The calculations generally predicted that large amounts of calcite, portlandite, ettringite and CSH would precipitate in a zone very close to the outside edge of the clast, whereas

zeolites would precipitate further in. Unfortunately the observed reaction rims were very narrow, and the secondary phases too fine-grained to permit study of either the distribution of zones, or mineral sequences within the reaction rim.

Colluvium

Field studies of the colluvium deposit have suggested zoning with respect to the distribution of different types of clasts (see Chapter 5). For example, the base of the colluvium is particularly rich in basalt clasts. It was not possible, however, to discern whether there was large-scale (metres) zoning of secondary reaction products with respect to the input of high pH water. In fact, the point at which high pH water enters the system has not been unequivocally established. Small-scale zoning (centimetres) was found in that certain secondary products were more abundant in association with particular types of clasts. Zeolite and ettringite were found to be abundant close to basalt clasts, which is consistent with the predictions of the models. Ettringite was observed to be absent around chert clasts, which is again consistent with the predictions of the models.

Field observations regarding the mineral sequence within the colluvium reaction products suggest that zeolites form before CSH phases. Modelling predictions suggest that CSH phases and zeolites do not generally coexist within the same reaction zone. CSH phases are at equilibrium with a solution of pH >12.5, whereas zeolites are stable at lower pH, pH 11–12.

An important control on mineral paragenesis is whether the system is 'waxing' or 'waning':

- In a 'waxing' system, the chemistry of the high pH input water remains constant, and with time, the high pH front moves to greater distances and the reaction zones widen.
- In a 'waning' system, the chemistry of the high pH input water changes with time (due to progressive reaction with the rock). As the pH decreases the nature of the alkaline water/rock interaction would also change. In this case it is possible that the reaction zones would shrink.

It is possible that the situation observed at the Western Springs is a result of a waxing system, with a high pH reaction front migrating outwards through the system. At short times, the front is positioned at small distances into the colluvium. There is a zone of precipitation of CSH phases closest to the high pH input and then, at a greater distance from the source, a zone of zeolite precipitation where the pH has dropped slightly. At longer times, the high pH front moves to greater distances and the reaction zones widen. As the chemistry of the water at a particular point changes, initial mineral precipitates will become unstable and dissolve to be replaced by more stable reaction products, i.e. zeolites will be overprinted by CSH phases. The observed mineral sequence is consistent with the behaviour of a waxing system and is probably a consequence of the slow dissolution of zeolites such that older zeolites are overprinted by CSH phases before they have had sufficient time to dissolve completely.

7.8.4 Width of Reaction Rims

The observed reaction rims on the colluvium clasts were irregular. In the biomicrite, preferential alteration was observed along particular bedding planes. In the basalt clasts, extended alteration could be observed corresponding to the position of feldspar laths. In general, the reaction rims were very narrow, less than 1 mm. This is somewhat narrower than the predicted reaction rims which were up to a few centimetres in the case of biomicrite, and millimetres in the case of the 'basalt' and chert respectively. One of the key uncertainties underlying the model predictions, as mentioned in Section 7.2.1, is that the timescale over which the system has been active is unknown. It is also possible that the system behaved in an episodic way. Therefore, although the system as a whole might have an age of tens of thousands of years or more, an individual event might be significantly shorter. If the actual timescale of one episode is very short (less than the 100 years over which the calculations were carried out) then it is not suprising that calculations overpredict the length scales of interaction. Overprediction by the models could also be related to uncertainty regarding the physical properties of the system.

- The diffusion coefficient and porosity of the rocks in most cases was estimated. A scoping calculation carried out in the case of the biomicrite showed that reducing these parameters resulted in a significant reduction in the width of the reaction rim;
- Changes in the transport properties of the system as a result of dissolution/ precipitation reactions will affect the transport of species through the rock. If such changes were incorporated in the calculations then it is possible that the predicted width of reaction rims would decrease due to pore-blocking by the newly-precipitated secondary phases;
- It is possible that, prior to input of the alkaline waters, the clasts were unsaturated. Infiltration of a solution into an unsaturated medium is subject to parameters such as capillarity, surface tension, and many more. This subject is outwith the scope of the present study. However, it is likely that if some areas within the clast were unsaturated that infiltration of the alkaline water would be impeded, resulting in narrower alteration rims than those that would be predicted based on diffusion into a saturated medium.

Quantitative estimates of the width of reaction rims are therefore subject to uncertainty regarding the physical representation of the rocks. However, it was noted in subsection 7.7.4 that both the mineralogy and the transport properties of the system play an important role in determining the width of reaction rims. In the field, it was observed that reaction rims on biomicrite clasts were widest, followed by chert, and the narrowest rims were observed in the case of basalt clasts. The models suggested that the width of reaction rims in the different rock types studied should follow the order:

biomicrite > 'basalt' > chert

However, as pointed out in sub-section 5.2.2 (p. 108), limited rim alteration on the chert and basalt clasts does not necessarily preclude that individual mineral components may be more reactive than the biomicrite minerals.

In a qualitative comparison the models correctly predict that alkaline water-rock interaction affects the marl over greater distances than the silicate-dominated rock types.

7.9 CONCLUSIONS

Equilibrium (HARPHRQ and CHEQMATE) and kinetic (MARQUISS) modelling approaches were used to model the alkaline water-rock interaction within the colluvium at the Western Springs. The following conclusions can be made:

- two processes influence the suite of secondary minerals precipitating within clast reaction rims: disequilibrium within the solutions (without any contact with solid phases) and dissolution of primary minerals as a consequence of alkaline water-rock interaction;
- the secondary minerals predicted to form using an equilibrium model were in reasonable agreement with those observed in the field;
- the observed mineral paragenesis could be explained in terms of the evolution of the high pH front in a waxing system;
- modelling showed that there were broad similarities between the kinetic and equilibrium modelling approaches with respect to the reaction zones and the length scale of interaction. Using the kinetic approach, smaller amounts of secondary phase minerals were predicted to form, and the dissolution of the primary minerals was also predicted to be less extensive. This at least in part must result from the assumptions of the model and the scaling down of the reactive surface area (see subsection 7.4.3) that was required to achieve convergence;
- the calculations overpredicted the width of the reaction rims around clasts. As well as uncertainty regarding the timescale over which the system has been active, this could be attributed to uncertainty regarding the physical properties of the system both in terms of (i) initial diffusion coefficient and porosity of the rock, and (ii) changes in porosity occurring as the alkaline water-rock interaction progresses;
- both the mineralogy and the transport properties of the system play an important role in determining the width of reaction rims. In a qualitative comparison, an equilibrium model correctly predicted that the widest reactions rims would occur in the case of the biomicrite lithology;
- comparison of the Phase II and III modelling studies (reaction of biomicrite with analogues of evolved near-field groundwater and young near-field porewater respectively) suggested that near-field porewater chemistry would not have a great effect on many aspects (types of secondary minerals, length scale of reaction zones, porosity changes) of the alkaline water-rock interaction for the biomicrite.

7.10 REFERENCES

Bond, K.A., Moreton, A.D. and Tweed, C.J., 1995. Water compositions of relevance to a deep cement-based repository at Sellafield: Evaluation using thermodynamic modelling. Nirex Report (NSS/R310), Nirex, Harwell, U.K.

Bradbury, M.H. and Green, A., 1986. Retardation of radionuclide transport by fracture flow in granite and argillaceous rocks. CEC Rep. (EUR 10619), Luxemburg.

Brown, P.L., Haworth, A., Sharland, S.M. and Tweed, C.J., 1990. HARPHRQ: A geochemical speciation program based on PHREEQE. Nirex Report (NSS/R188), Nirex, Harwell, U.K.

Chambers, A.V., 1994. Use of the quasi-stationary state approximation to determine the migration of mineral alteration zones as a natural analogue for the disturbed zone of a cementitious waste repository. Sci. Basis Nucl. Waste Manag. XVII (Eds. A. Barkatt and R.A. von Konynenburg). MRS, Pittsburgh, 639–644.

Chambers, A.V. and Haworth, A., 1998. Coupled modelling for the Jordan natural analogue project. In: C.M. Linklater (Ed.), A natural analogue study of cement-buffered, hyperalkaline groundwaters and their interaction with a repository host rock: Phase II. Nirex Science Report, S/98/003, Nirex, Harwell, U.K., p. 277–301.

Clark, I.D. and Fritz, P., 1998. Isotope hydrogeology of the Maqarin hyperalkaline groundwaters. In: C.M. Linklater (Ed.), A natural analogue study of cement-buffered, hyperalkaline groundwaters and their interaction with a repository host rock: Phase II. Nirex Science Report, S/98/003, Nirex, Harwell, U.K., p. 198–210.

Haworth, A., Sharland, S.M., Tasker, P.W. and Tweed, C.J., 1988. A guide to the coupled chemical equilibria and migration code CHEQMATE. Nirex Report (NSS/R113), Nirex, Harwell, U.K.

Lever, D.A. and Woodwark, D.R., 1990. Radionuclide transport by groundwater flow through the geosphere: Current status 1989. Nirex Report (NSS/G113), Nirex, Harwell, U.K.

Lichtner, P.C., 1992. Time-space Continuum Description of Fluid/Rock. Interaction in Permeable Media. Water Resour. Res., vol. 28., 3135–3155.

Lichtner, P.C. and Biino, G.G., 1992. A first Principles Approach to Supergene Enrichment of a Porphyry Copper Protore, I, Cu-Fe-S-H_2O Subsystem. Geochim. Cosmochim. Acta, vol. 56, 397–4015.

Linklater, C. (Ed.), 1998. A natural analogue study of cement-buffered, hyperalkaline groundwaters and their interaction with a repository host rock: Phase II. Nirex Science Report, S/98/003, Nirex, Harwell, U.K.

Noy, D.J., 1990. PRECIP: A program for coupled groundwater flow and precipitation/dissolution reactions. Nirex Report (NSS/R275), Nirex, Harwell, U.K.

Ortoleva, P., Chadam, J., Merino, E. and Sen, A., 1987a. Geochemical Self-organization II: The Reactive-infiltration Instability. Am. J. Sci., 287, 1008–1040.

Ortoleva, P., Merino, E., Moore, C. and Chadam, J., 1987b. Geochemical Self-organization I: Reaction-transport Feedbacks and Modelling Approach. Am. J. Sci., vol. 287, 979–1007.

Parkhurst, D.L., Thorstenson, D.C. and Plummer, L.N., 1980. PHREEQE – A computer program for geochemical calculations. US Geol. Surv. Water Resource Investigations (80-96), NTIS Tech. Rep. (PB81-167801), 1980 revised 1985.

Rochelle, C.A., Bateman, K., MacGregor, R., Pearce, J.M., Savage, D. and Wetton, P., 1994. The evaluation of chemical mass transfer in the disturbed zone of a deep geological disposal facility for radioactive wastes. IV: The kinetics of dissolution of chlorite and carbonates at elevated pH. Nirex Report (NSS/R275), Nirex, Harwell, U.K.

Savage, D., Bateman, K., Hill, P., Hughes, C., Milodowski, A.E., Pearce, J., Rae, E. and Rochelle, C.A., 1992. Rate and mechanism of the reaction of silicates with cement porefluids. Appl. Clay Sci., 7, 33–45.

Steefel, C.I. and Van Cappellen, P., 1990. A New Kinetic Approach to Modelling Water-rock Interaction: The Role of Nucleation, Precursors, and Ostwald Ripening. Geochim. Cosmochim. Acta, vol. 54, 2657–2677.

TABLES

Table 7-1. Measured solution compositions / mol dm^{-3}.

	High pH solution M5	Near-neutral solution present within the clasts M17
Ca	$2.8 \cdot 10^{-2}$	$2.2 \cdot 10^{-3}$
Mg	$4.1 \cdot 10^{-7}$	$1.6 \cdot 10^{-3}$
Na	$5.9 \cdot 10^{-3}$	$2.5 \cdot 10^{-3}$
K	$1.3 \cdot 10^{-2}$	$1.5 \cdot 10^{-3}$
Si	$2.5 \cdot 10^{-6}$	$1.6 \cdot 10^{-4}$
Al	$5.2 \cdot 10^{-6}$	$7.4 \cdot 10^{-7}$
C	$6.2 \cdot 10^{-4}$	$1.3 \cdot 10^{-3}$
Cl	$1.3 \cdot 10^{-3}$	$1.3 \cdot 10^{-3}$
S	$1.7 \cdot 10^{-2}$	$4.7 \cdot 10^{-3}$
Field pH	12.2	7.7
Laboratory pH	12.7	7.2

Table 7-2. Representative rock mineralogy.

	Wt %			Vol %	
	Biomicrite*	Chert	'Basalt'*	Colluvium	
Calcite	70%			'Basalt'	58%
Illite	2%			Marl	12%
Kaolinite	5%			Chert	12%
Chalcedony	5%	100%		Matrix (=calcite)	16%
Feldspar**			50%	Void	3%

* – the remainder of the rock was considered to be unreactive solid and therefore not considered in the calculations.

** – the normative composition of basalt typically contains ~25 wt% albite, ~25 wt% anorthite, ~5 wt% K-feldspar.

In the calculations, for simplicity, only the plagioclase feldspars were used. 25 wt% albite + 25 wt% anorthite in the MARQUISS calculations, and 50 wt% albite for the CHEQMATE calculations (convergence problems were encountered when both plagioclase feldspar end-members were represented).

Table 7-3. Physical properties of the rocks.

	Biomicrite	Chert	'Basalt'	Colluvium
Intrinsic diffusion coefficient/m^2s^{-1}	$3 \cdot 10^{-11}$	$1 \cdot 10^{-12}$	$1 \cdot 10^{-12}$	$2 \cdot 10^{-11}$
Porosity	0.3	0.1	0.1	0.03
Velocity/$msec^{-1}$	–	–	–	10^{-6}

Table 7-4. Kinetic data for MARQUISS simulations of 'basalt' and chert clasts.

Mineral	log (rate constant / mol m^{-2} s^{-1}) as taken from literature* [Rochelle et al., 1994] or estimated**	log (surface area X rate constant / mol m^{-2} s^{-1}) used during the calculations#
Calcite	-7.0*	-12.0
Brucite	-8.34**	-13.34
Ettringite	-8.34**	-13.34
Foshagite	-8.34**	-13.34
Portlandite	-8.34**	-13.34
Tobermorite	-8.34**	-13.34
Chalcedony	-9.8*	-14.8
Albite	-9.8*	-14.8
Anorthite	-9.8*	-14.8
Analcime	-9.8**	-14.8
Mordenite-K	-9.8**	-14.8
Phillipsite-K	-9.8**	-14.8
Prehnite	-9.8**	-14.8
Talc	-9.8**	-14.8

– pseudo kinetic rate laws express the rate of chemical reaction as a product of the surface area of the mineral precipitating or dissolving in the reaction, and the rate constant for the reaction. Calculations using MARQUISS converged only when values for the surface area typically of the order of 10^{-5} m^2g^{-1} were assigned. These are quite low values for the minerals in question; in assigning these low values, the rates of mineral reactions have effectively been scaled down in order to achieve convergence.

N.B. A bulk density of $2.2 \cdot 10^6$ g m^{-3} was assigned in the calculations to determine the volume change of minerals.

Table 7-5. HARPHRQ calculated saturation indices* for selected minerals in mixed groundwater compositions.

MINERAL	Initial Groundwaters			M17:M5 Mixes			M17:M5 Mixes**		
	M17	M5	M5*	1:10	50:50	10:1	1:10	50:50	10:1
pH	7.2	12.7	9.7	12.7	12.5	11.8	9.7	9.5	9.1
Albite	-0.7	-18.4	-5.7	-15.8	-12.4	-7.6	-3.3	-1.3	-0.8
Anhydrite	-1.4	-0.4	-0.6	-0.5	-0.7	-1.1	-0.7	-0.8	-1.1
Anorthite	-4.7	-15.0	-6.7	-13.2	-11.3	-8.9	-5.1	-4.1	-4.3
Brewsterite-Ca	1.4	-34.0	-8.8	-28.7	-21.9	-12.3	-3.9	0.1	1.4
Clinoptilolite-K	4.0	-55.4	-12.9	-46.5	-35.1	-19.0	-4.7	1.9	3.8
$Ca(OH)_2$	-11.3	0.5	-6.0	0.4	-0.2	-2.1	-6.1	-6.4	-7.4
$Ca_2SIO_4.1.17H_2O$	-17.8	0.3	-9.2	0.4	0.4	-1.7	-8.5	-8.4	-10.1
Foshagite	-30.3	-1.8	-15.3	0.5	1.8	-0.6	-13.0	-12.0	-15.1
Calcite	-0.6	2.0	3.6	2.0	2.1	2.1	3.5	3.2	2.2
Dachiardite-Ca	4.1	-109.6	-29.5	-92.7	-70.8	-39.8	-13.9	-1.0	3.6
Dolomite	-1.3	-1.3	2.5	1.4	2.7	3.7	5.0	5.3	4.0
Erionite-Ca	6.4	-153.1	-39.5	-129.1	-98.4	-55.5	-17.5	0.6	6.2
Ettringite	-24.8	4.1	-10.0	3.7	1.4	-5.0	-10.3	-11.8	-15.7
Faujasite-Ca	1.1	-21.7	-5.0	-18.2	-13.8	-7.8	-1.8	0.8	1.3
Gismondine	0.9	-9.4	-1.2	-7.7	-5.8	-3.3	0.4	1.4	1.2
Gypsum	-1.0	-0.1	-0.3	-0.1	-0.3	-0.8	-0.3	-0.5	-0.8
Heulandite-Ca	-36.5	-78.3	-48.8	-72.0	-64.0	-52.7	-43.0	-38.3	-36.7
Illite	3.6	-23.8	-5.1	-20.1	-15.8	-9.6	-1.6	0.8	1.6
K-feldspar	2.1	-15.0	-2.3	-12.4	-9.1	-4.6	0.1	2.0	2.2
Laumontite	5.4	-17.5	-0.8	-13.9	-9.6	-3.6	2.5	5.0	5.5
Mesolite	11.2	-5.5	7.1	-2.9	0.3	4.5	9.5	11.3	11.4
$Mg(OH)_2$	-5.5	1.2	-4.8	3.7	4.1	3.3	-2.3	-1.6	-2.0
$MgCO_3$	-1.3	-3.9	-1.7	-1.3	-0.1	0.9	0.8	1.5	1.1
Montmorillonite-Ca	2.8	-26.2	-7.0	-21.7	-16.7	-9.5	-2.8	0.2	1.4
Mordenite-Na	-38.7	-69.0	-47.8	-64.6	-58.8	-50.4	-43.7	-40.3	-39.0
Muscovite	6.1	-20.6	-1.5	-17.9	-14.6	-9.2	0.9	2.6	2.9
Phillipsite-Ca	5.2	-22.8	-1.9	-18.4	-13.1	-5.8	2.1	5.2	5.6
Prehnite	-3.2	-7.9	-2.0	-5.4	-2.9	-0.6	0.3	1.8	0.9
Quartz	0.2	-6.1	-1.8	-5.2	-4.0	-2.2	-1.0	-0.3	0.1
Saponite-Ca	-1.8	-4.5	-6.8	6.3	12.1	15.8	3.8	8.3	8.6
Scolecite	14.5	-2.1	10.4	-0.6	3.7	7.9	12.8	14.6	14.8
Sepiolite	-4.6	-10.2	-9.3	-2.4	2.1	5.7	-1.8	1.7	2.1
Talc	-2.7	-7.9	-8.8	3.2	9.5	14.0	2.1	7.0	7.5
Tobermorite	-29.5	-8.0	-15.3	-3.1	1.2	2.3	-10.6	-7.7	-10.8
Yugawaralite	-2.8	-31.9	-11.0	-27.5	-21.9	-14.2	-6.9	-3.6	-2.7

* The saturation index is defined as the log (activity product of the ions in solution:solubility product). Positive values of saturation index indicate that the solution is predicted to be oversaturated with respect to a particular mineral phase and precipitation would be expected. Negative values indicate that a solution in equilibrium with a given solid would show a higher concentrations of its ions than is measured.

** Equilibrated with CO_2.

Table 7-6. Secondary mineral amounts* for biomicrite, 'basalt' and chert clasts (at 100 years) / mol dm^{-3}.

	Biomicrite**	'Basalt'		Chert	
	Eqbm	*Eqbm*	*Kinetic*	*Eqbm*	*Kinetic*
Foshagite	16	88	–	230	–
Tobermorite	3	18	–	25	–
Ettringite	7	23	10	<1	–
Calcite	45	31	–	29	–
$Ca(OH)_2$	484	277	–	60	–
Zeolite	4	35	0.17***	0.01	0.0009***

* – The maximum amount of a particular mineral precipitating at any point along the grid.

** – To allow direct comparison with 'basalt' and chert results, the values shown in the table correspond to the calculations carried out with reduced transport parameters.

*** – In the calculations using a kinetic approach no zeolites were predicted to form, instead other aluminosilicate minerals formed: prehnite ('basalt' clasts) and talc (chert clasts).

Table 7-7. Summary of predicted length scales of interaction using an equilibrium modelling approach.

	Width of Zone 1* (significant secondary mineral precipitation)	**Width of Zone 1–3***
Biomicrite	1.5 cm (3 mm)	>5 cm (>2.5 cm)
'Basalt'	2 mm	8 mm
Chert	1 mm	3 mm
Colluvium		many metres

* – Mineral zones are defined in Subsection 7.7.2.

() – Results after reducing the transport properties of the marl system.

Table 7-8. Summary of predicted length scales of interaction using an kinetic modelling approach.

	Width of Zone 1* (significant secondary mineral precipitation)	**Width of Zone 1–2***
'Basalt'	1.5 mm	4 mm
Chert	–	4 mm

* – Mineral zones are defined in sub-section 7.7.2.

FIGURES

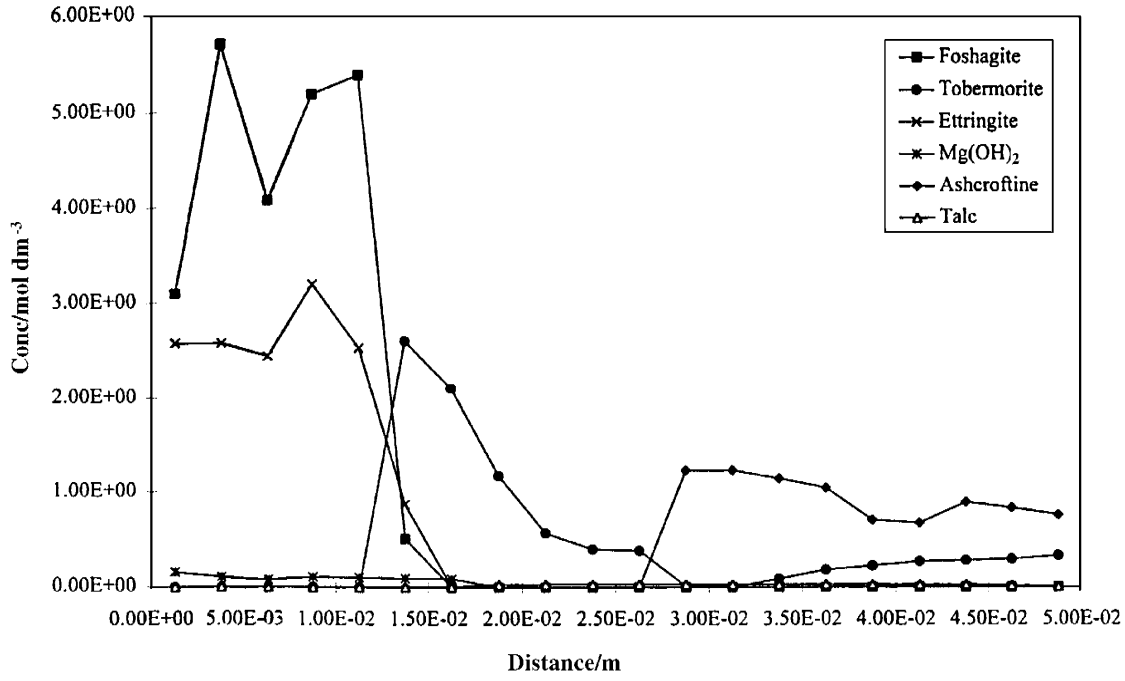

Figure 7-1. *Biomicrite secondary minerals at 100 years (CHEQMATE).*

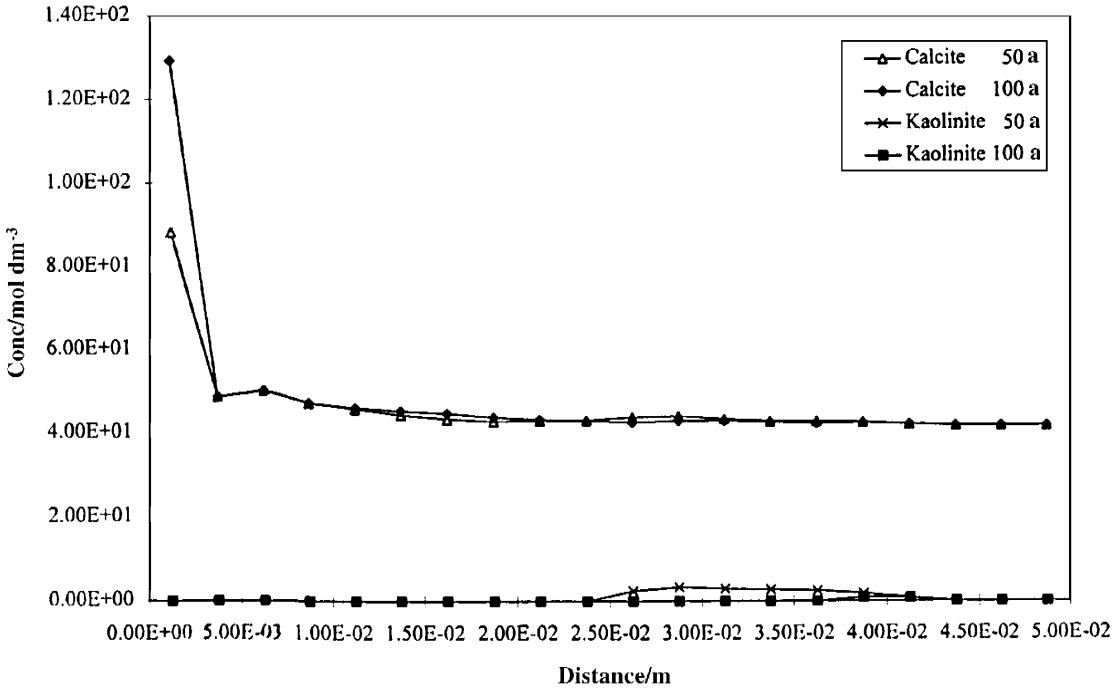

Figure 7-2. *Evolution in years of the primary biomicrite minerals (CHEQMATE).*

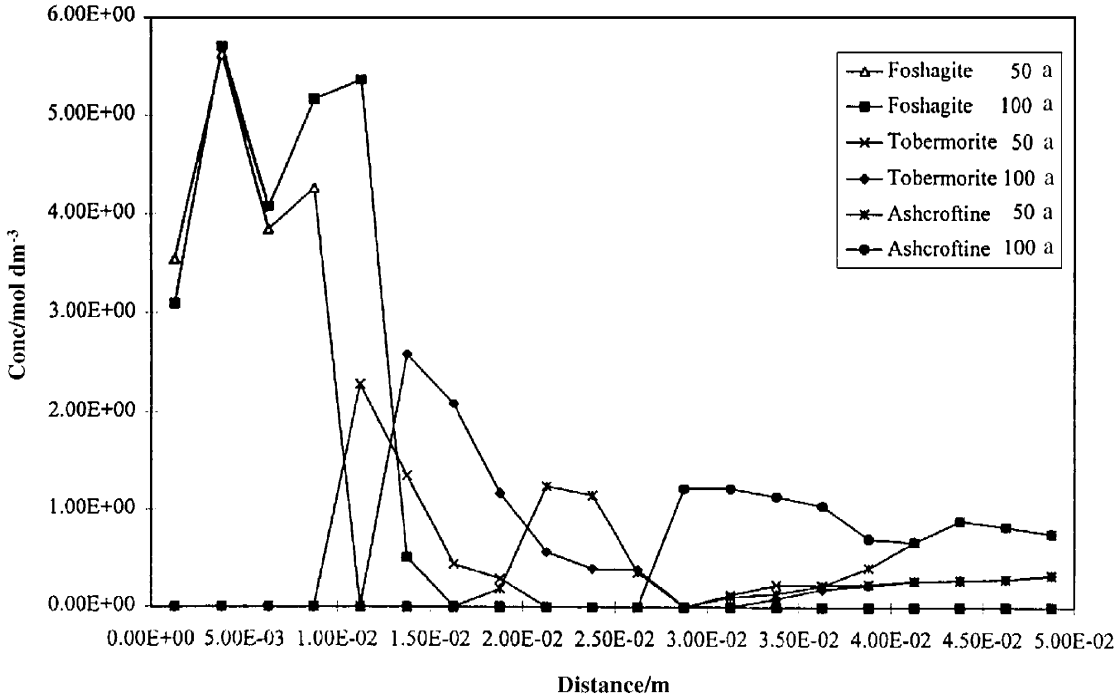

Figure 7-3. *Evolution in years of the CSH phases and zeolites in biomicrite (CHEQMATE).*

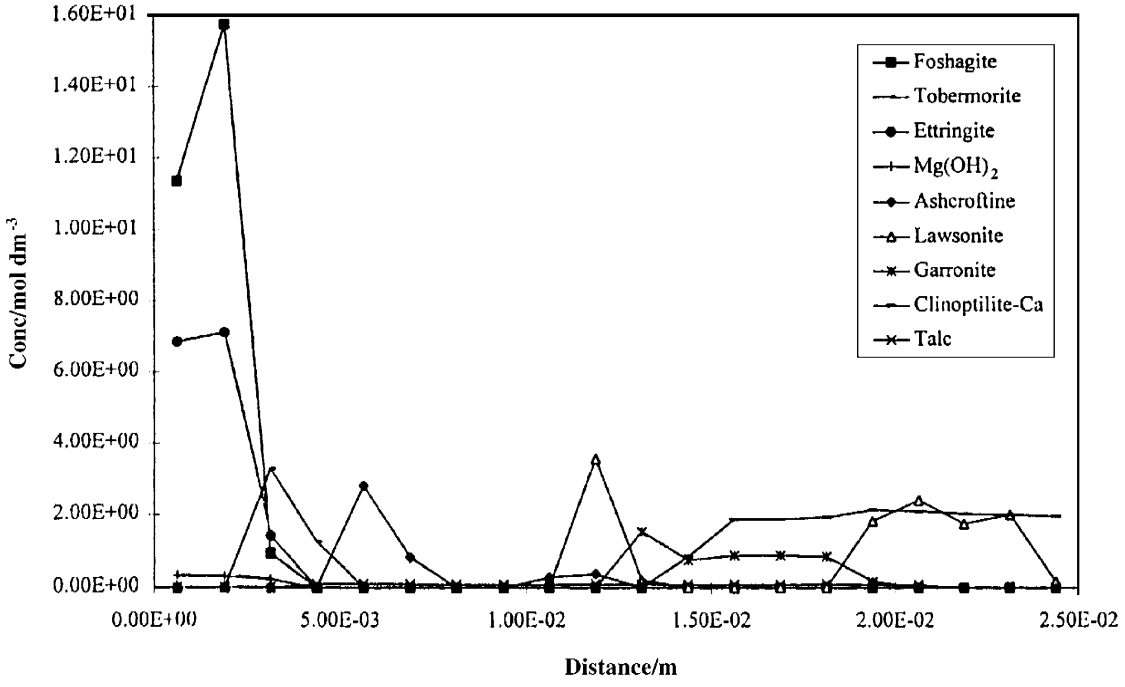

Figure 7-4. *Biomicrite secondary minerals at 100 years using low transport parameters (CHEQMATE).*

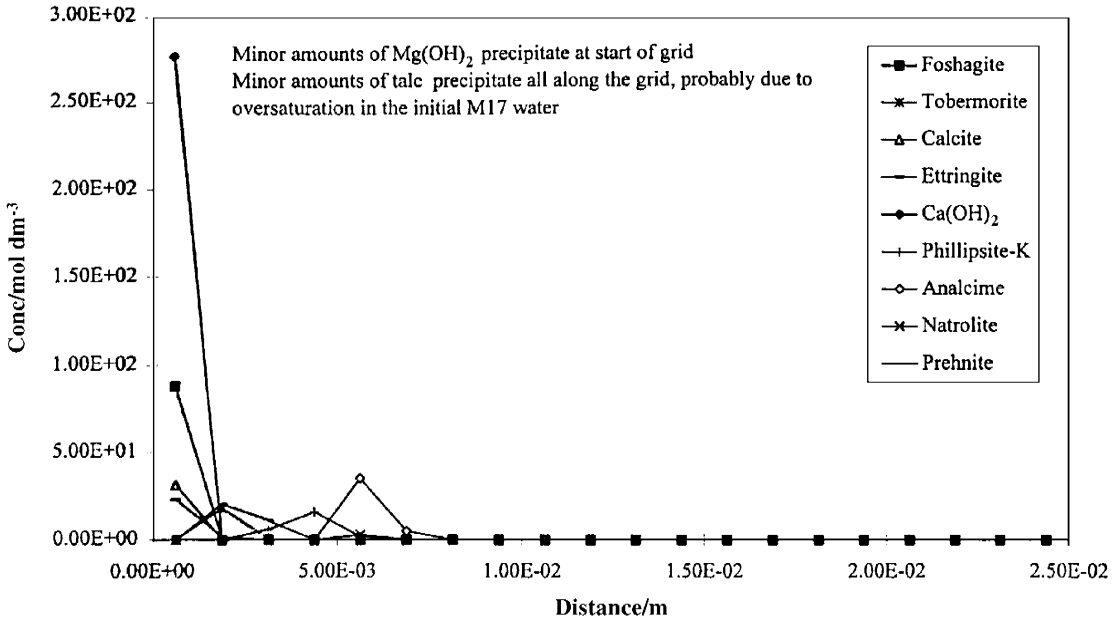

Figure 7-5. *Basalt secondary minerals at 100 years (CHEQMATE).*

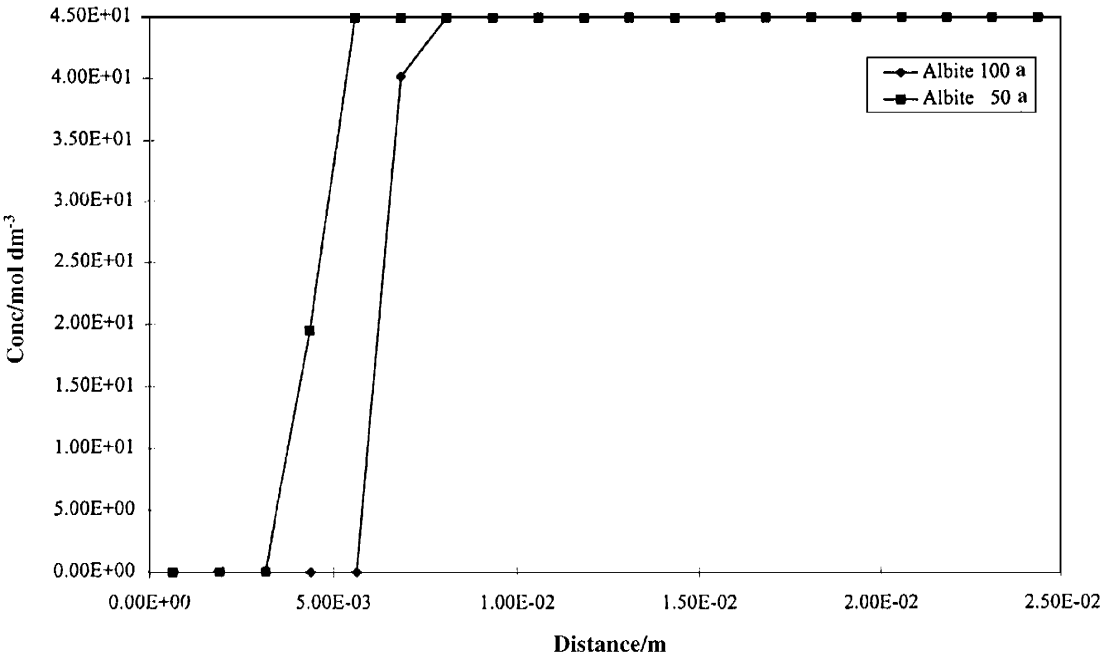

Figure 7-6. *Evolution in years of primary albite in the basalt (CHEQMATE).*

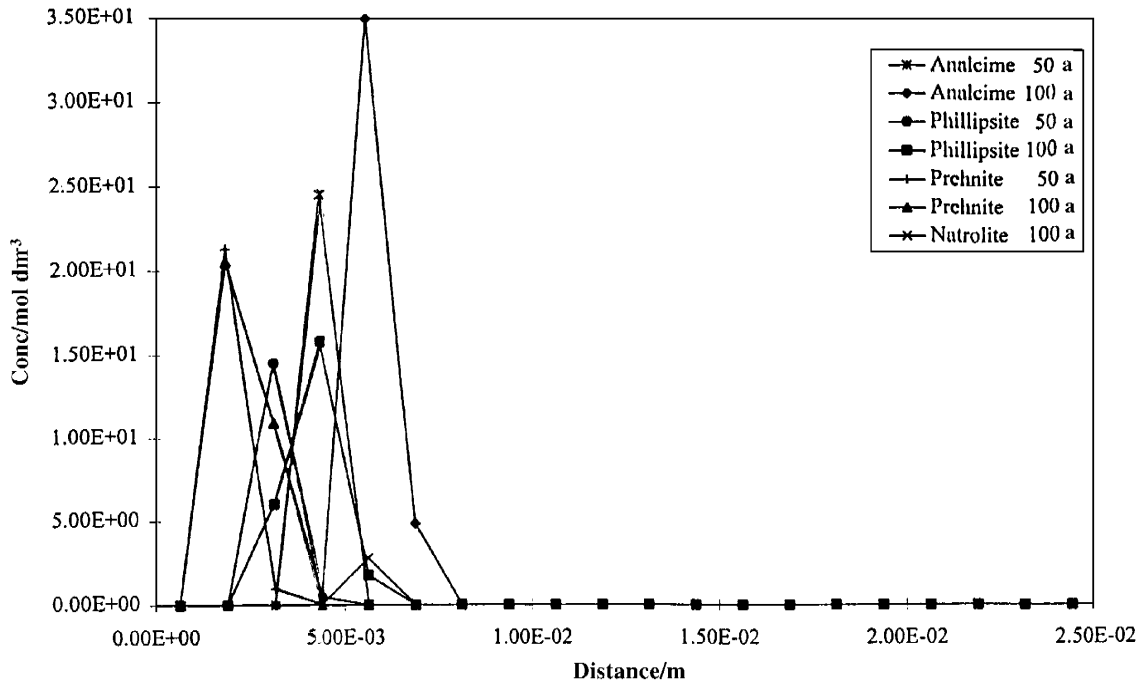

Figure 7-7. *Evolution in years of zeolites and prehnite in basalt (CHEQMATE).*

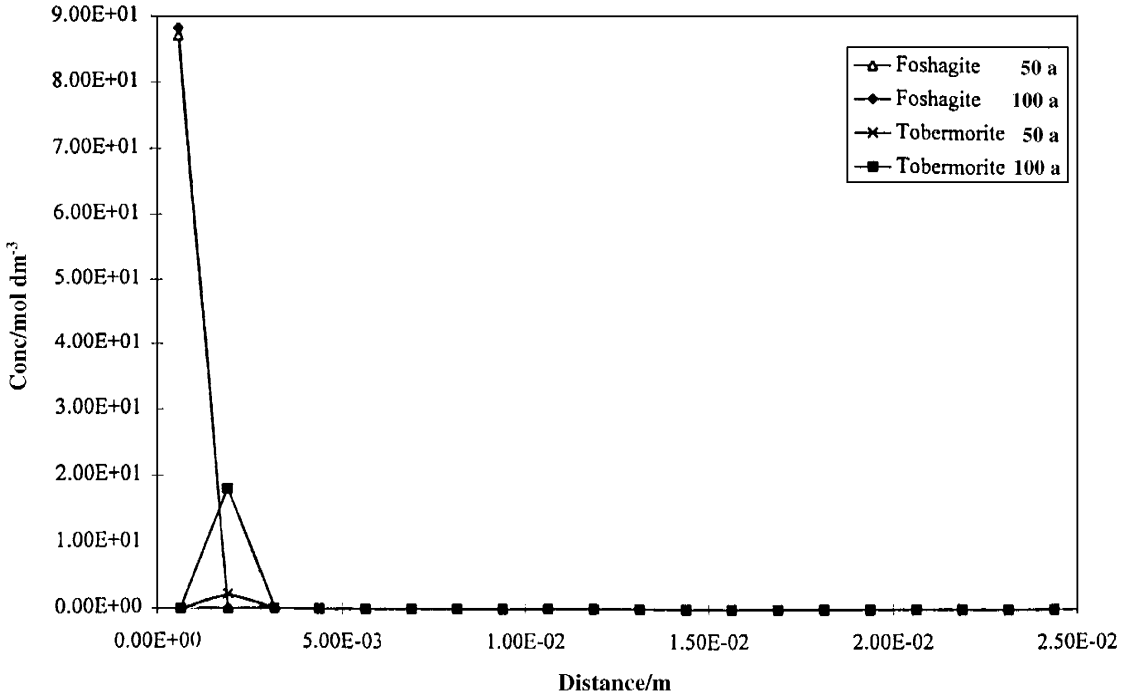

Figure 7-8. *Evolution in years of the CSH phases in basalt (CHEQMATE).*

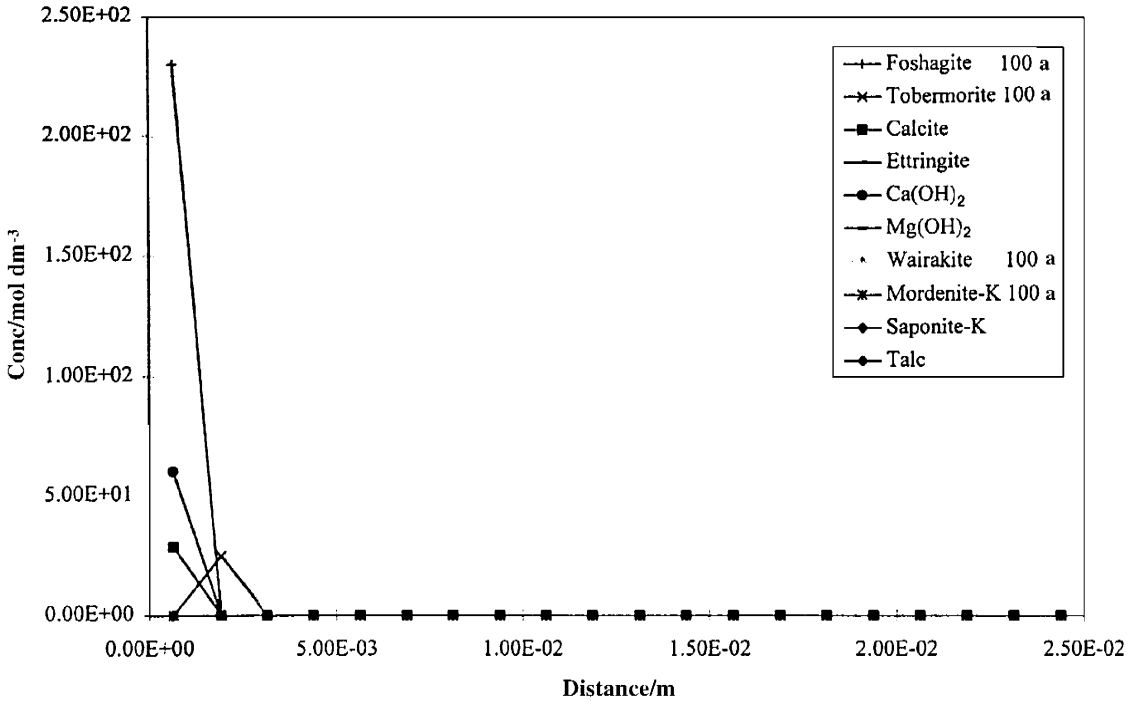

Figure 7-9. *Chert secondary minerals at 100 years (CHEQMATE).*

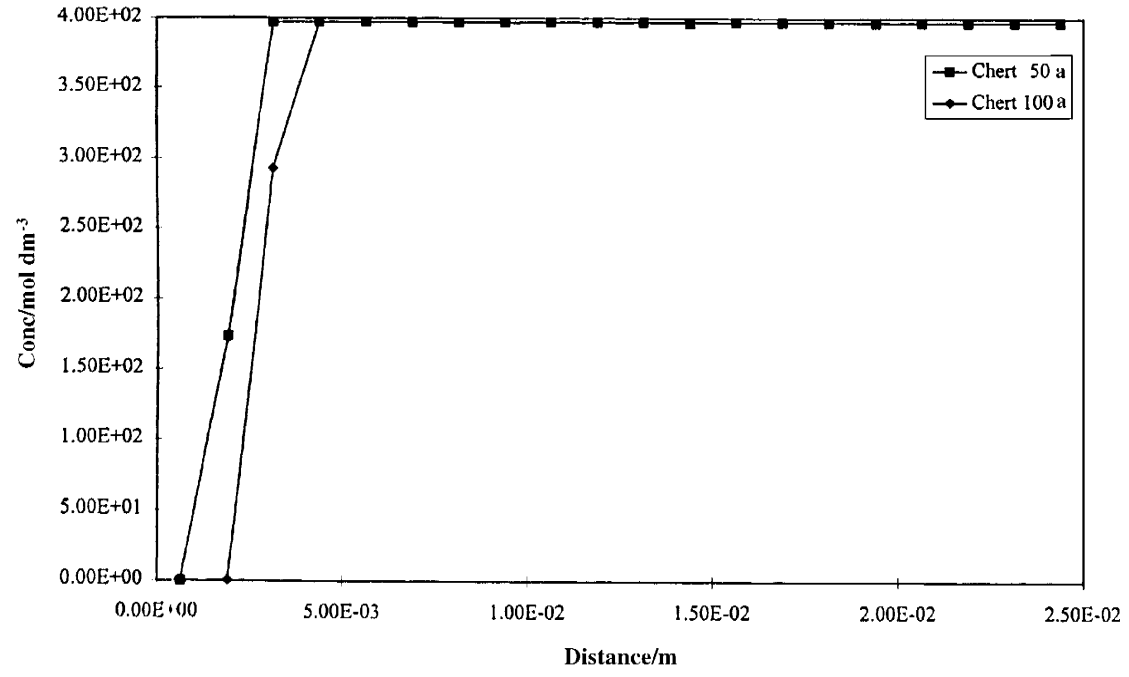

Figure 7-10. *Evolution in years of primary minerals in chert (CHEQMATE).*

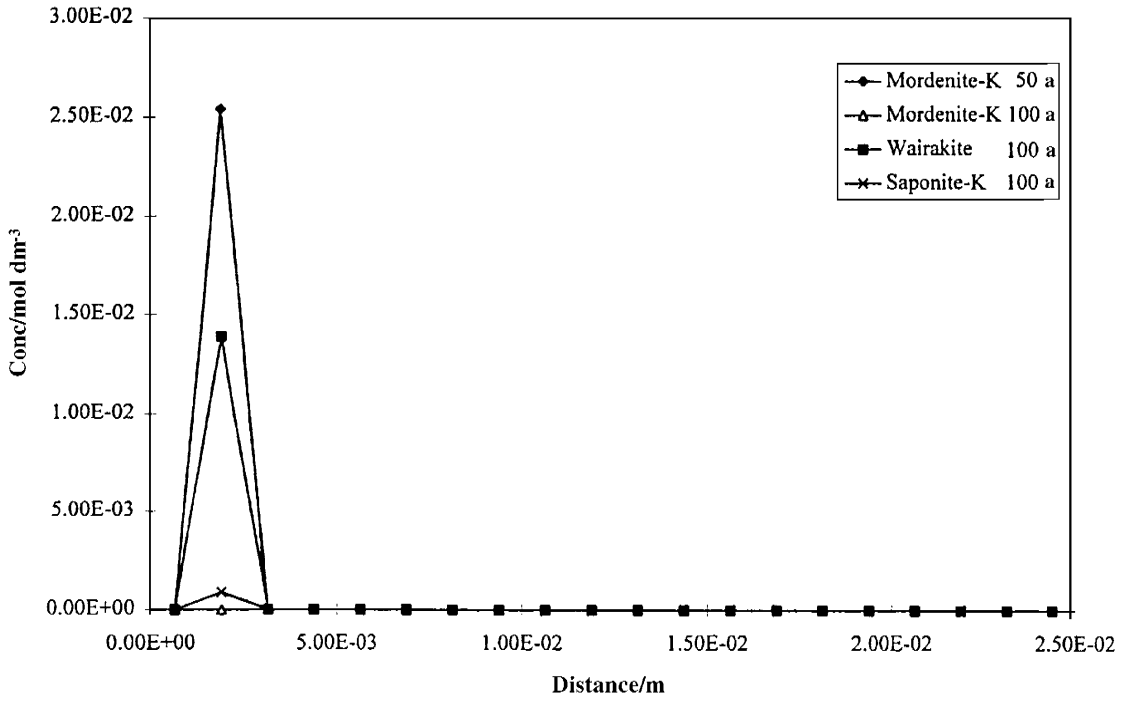

Figure 7-11. *Evolution in years of the zeolites in chert (CHEQMATE).*

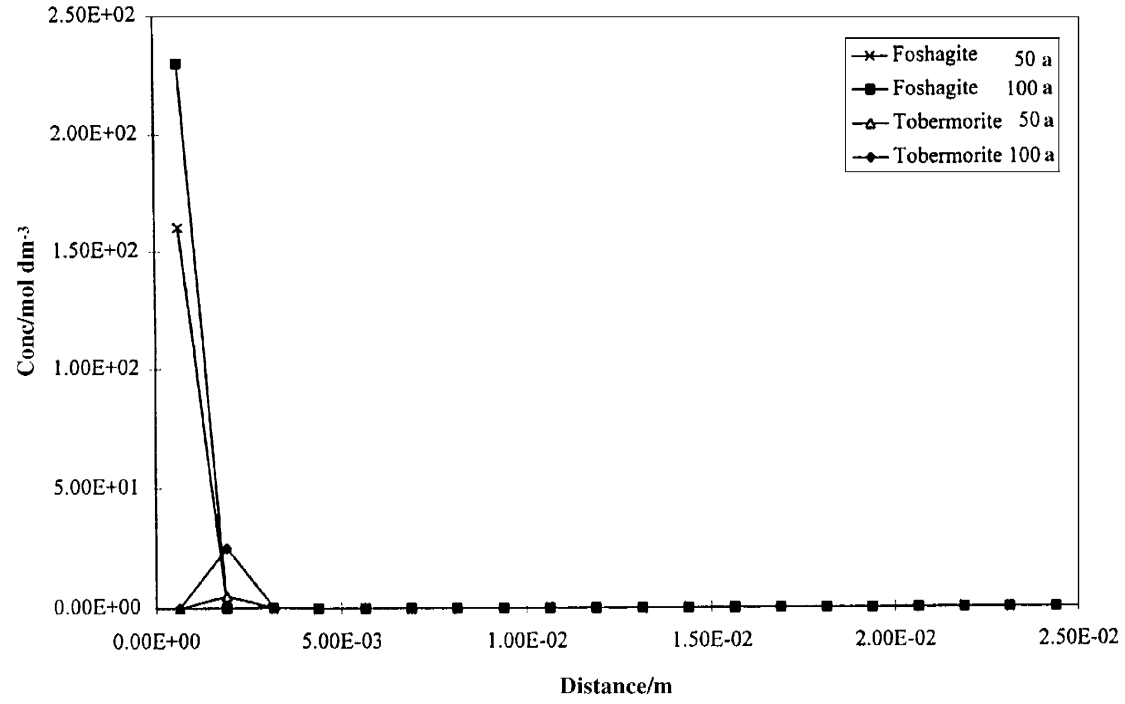

Figure 7-12. *Evolution in years of the CSH phases in chert (CHEQMATE).*

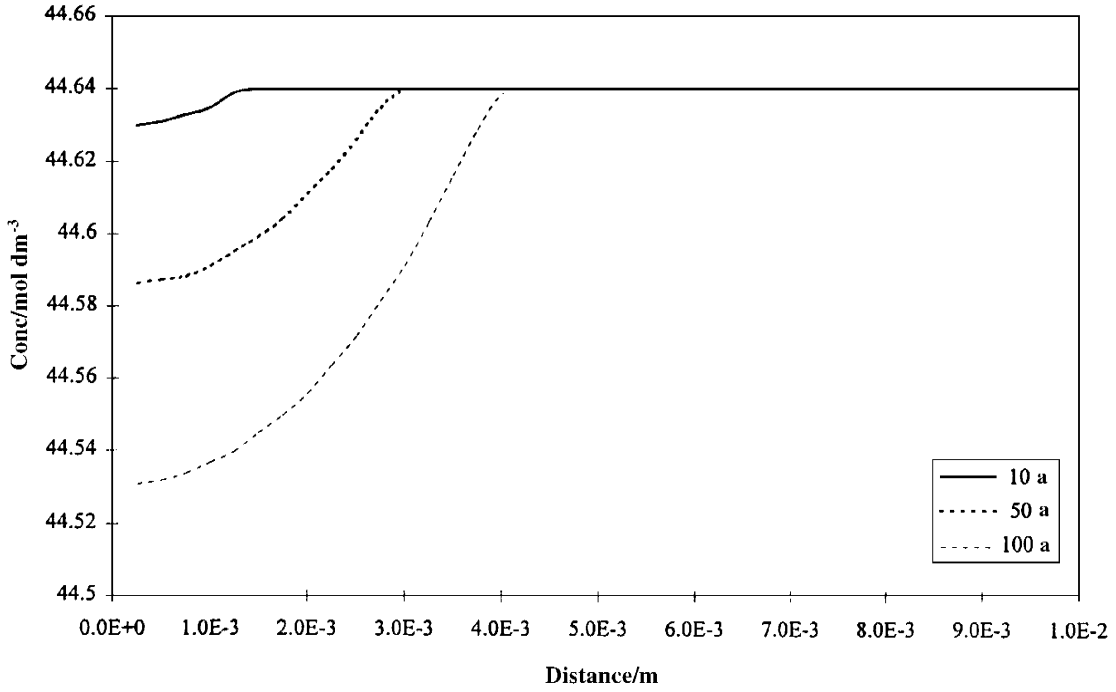

Figure 7-13. *Anorthite dissolution (in years) in basalt system (MARQUISS).*

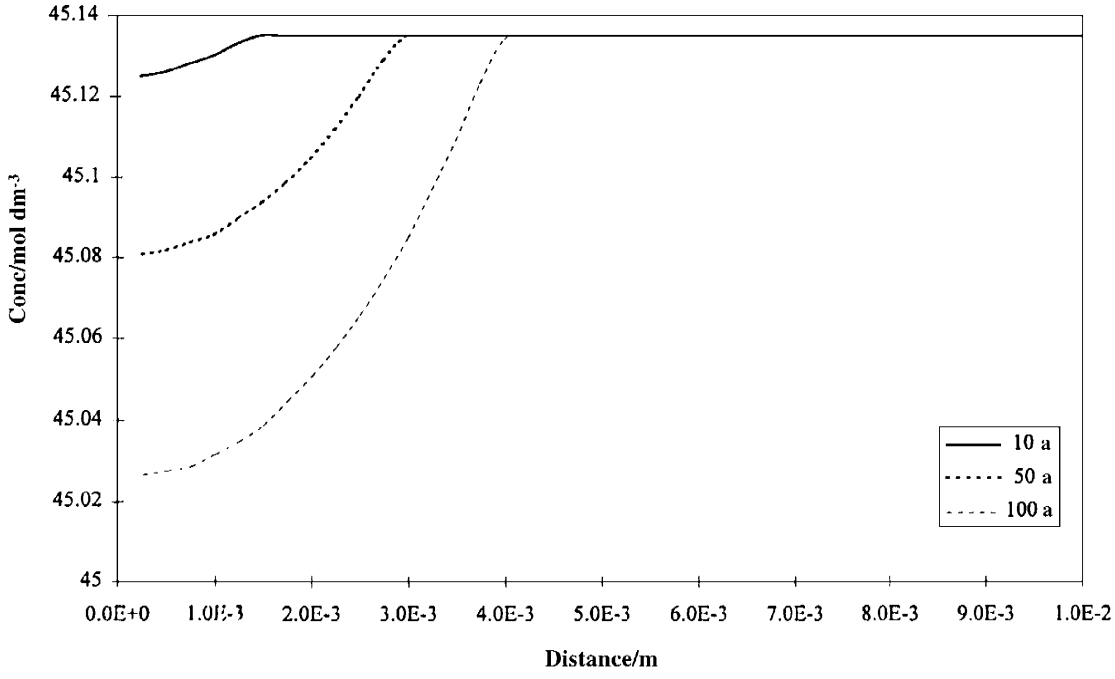

Figure 7-14. *Albite dissolution (in years) in basalt system (MARQUISS).*

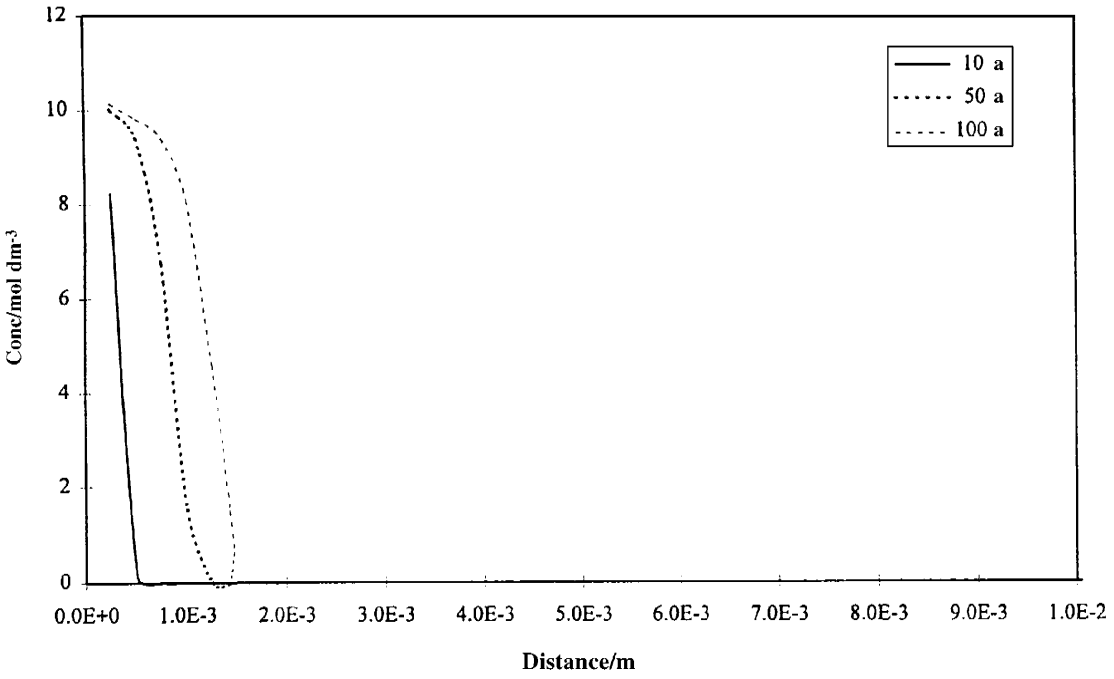

Figure 7-15. *Ettringite precipitation (in years) in basalt system (MARQUISS).*

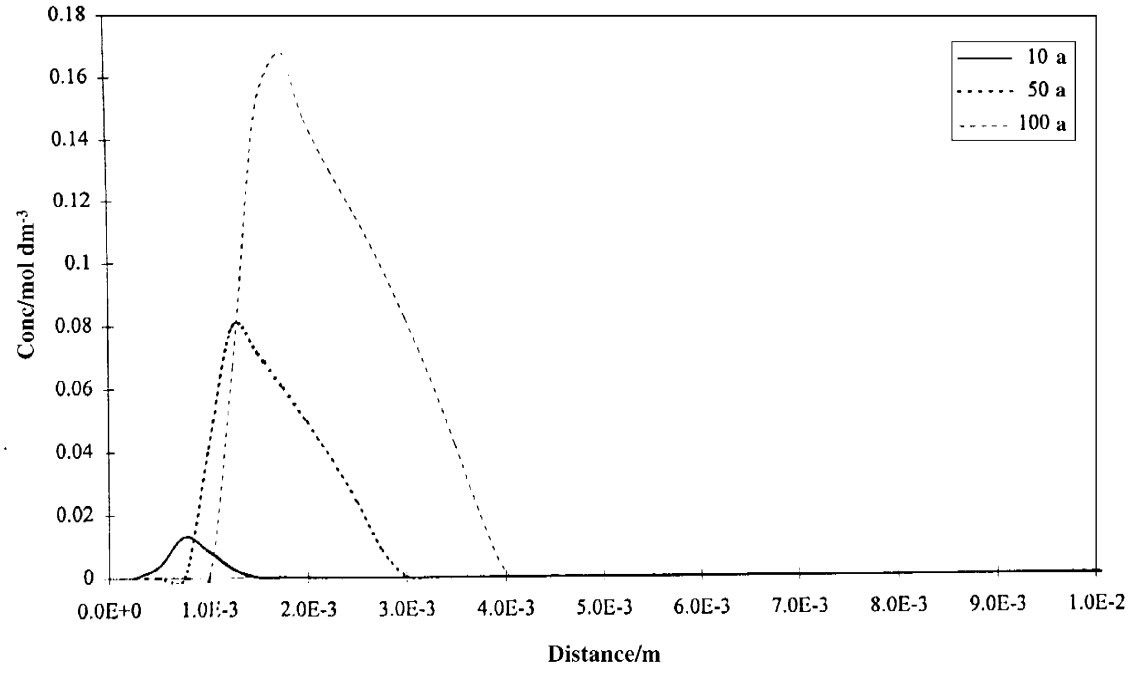

Figure 7-16. *Prehnite precipitation (in years) in basalt system (MARQUISS).*

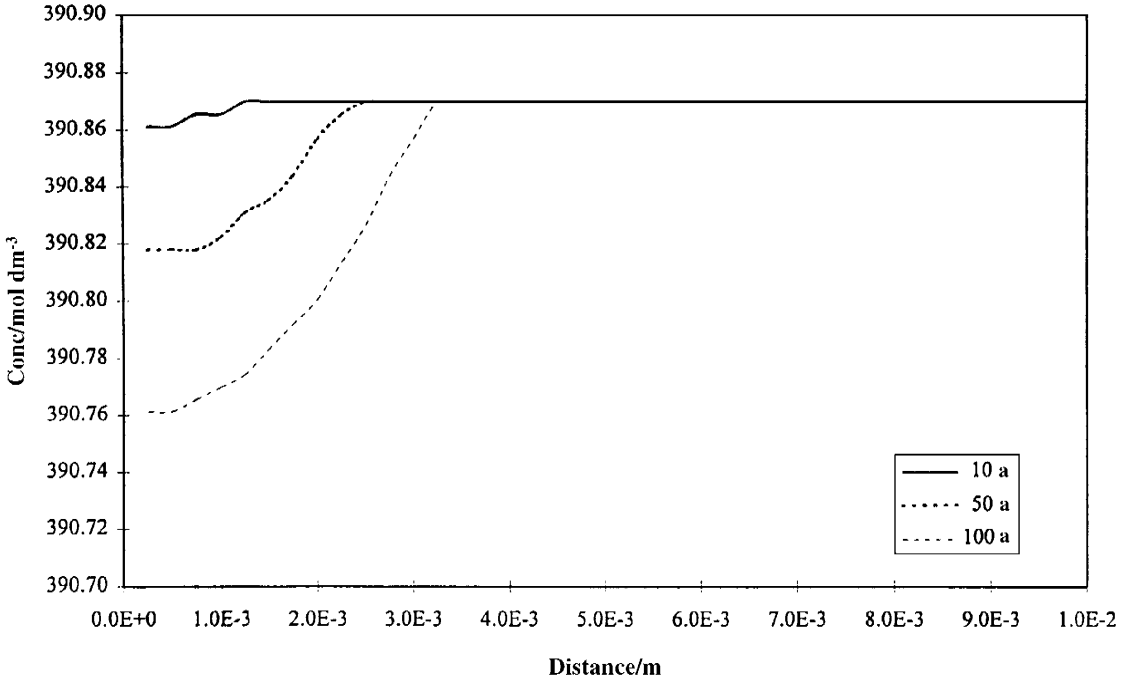

Figure 7-17. *Chalcedony dissolution (in years) in chert system (MARQUISS).*

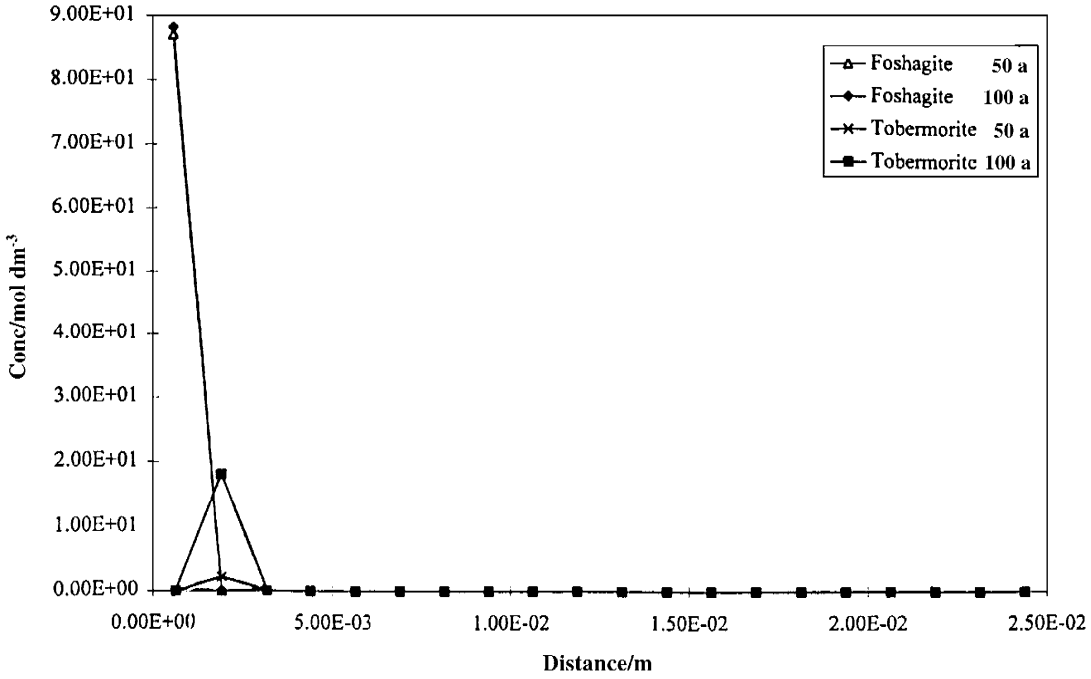

Figure 7-18. *Talc precipitation (in years) in chert system (MARQUISS).*

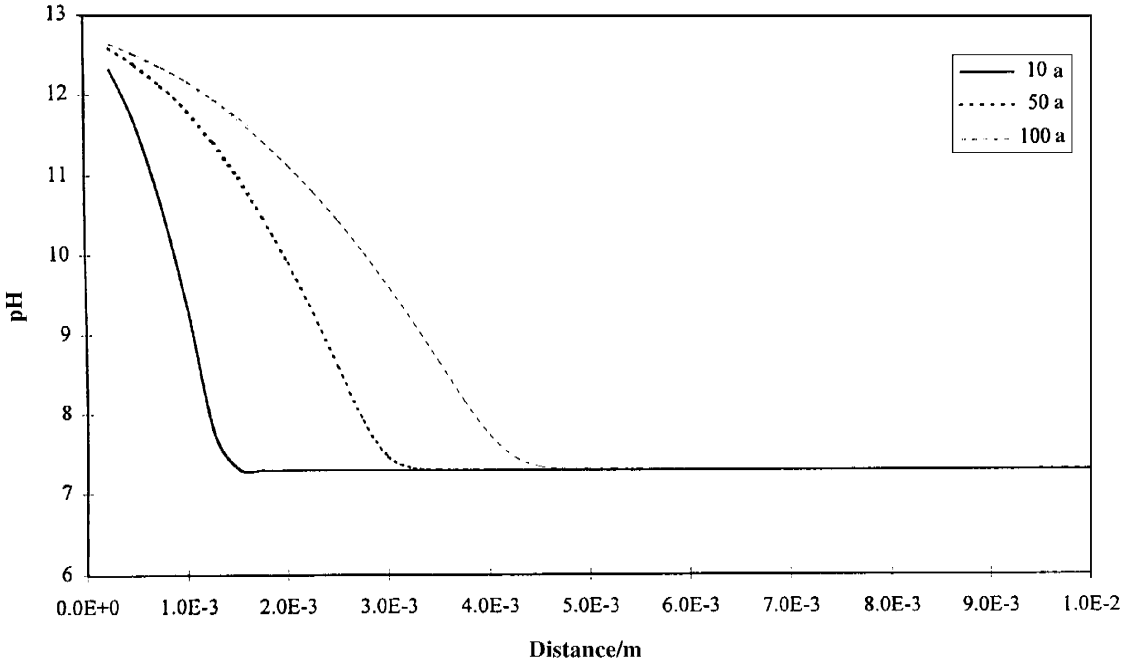

Figure 7-19. *pH (in years) in chert system (MARQUISS).*

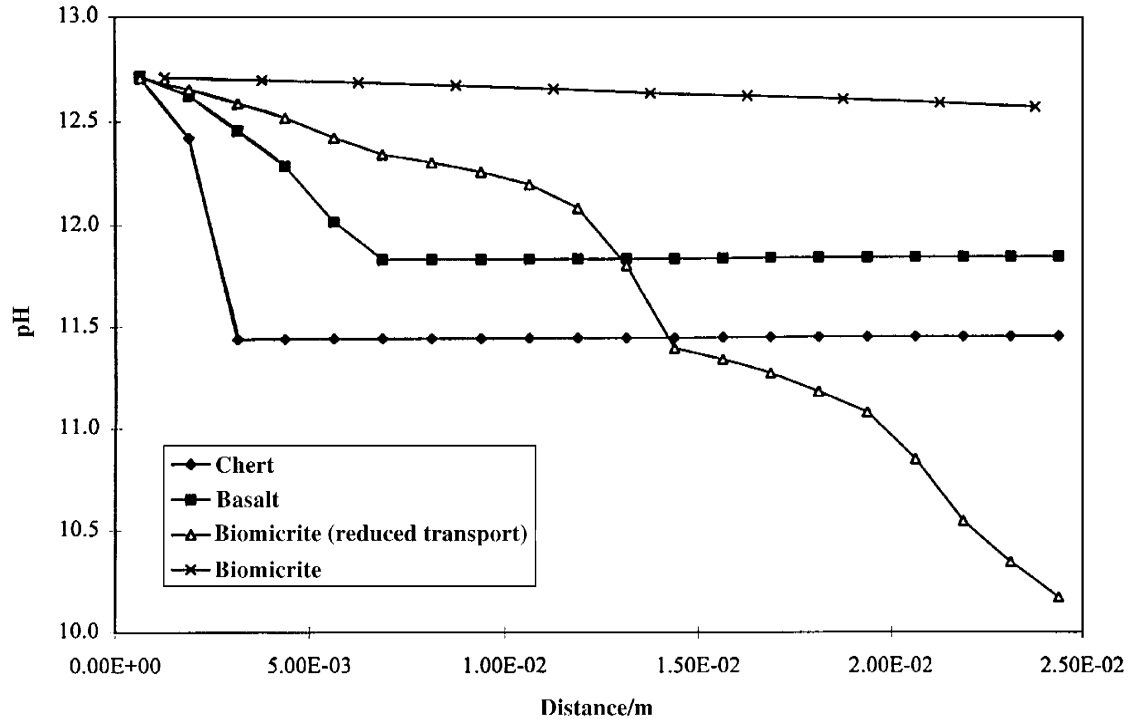

Figure 7-20. *A comparison of the pH profiles for the different rock-types at 100 years (CHEQMATE).*

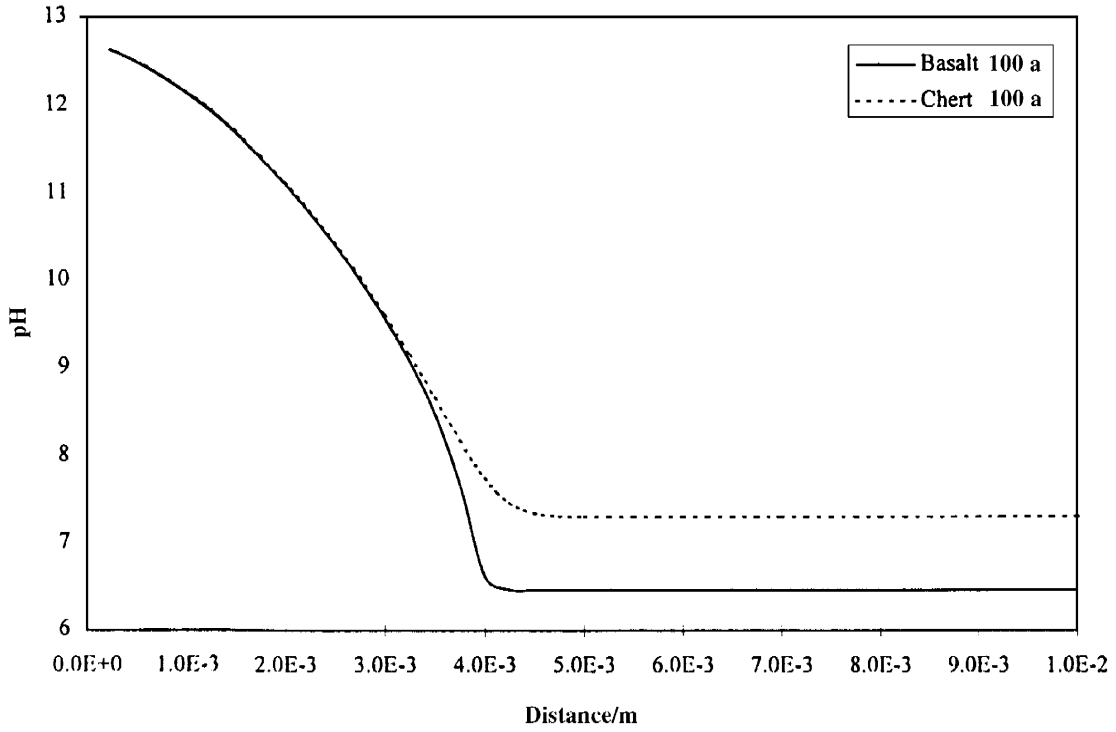

Figure 7-21. *A comparison of pH profiles for basalt and chert at 100 years (MARQUISS).*

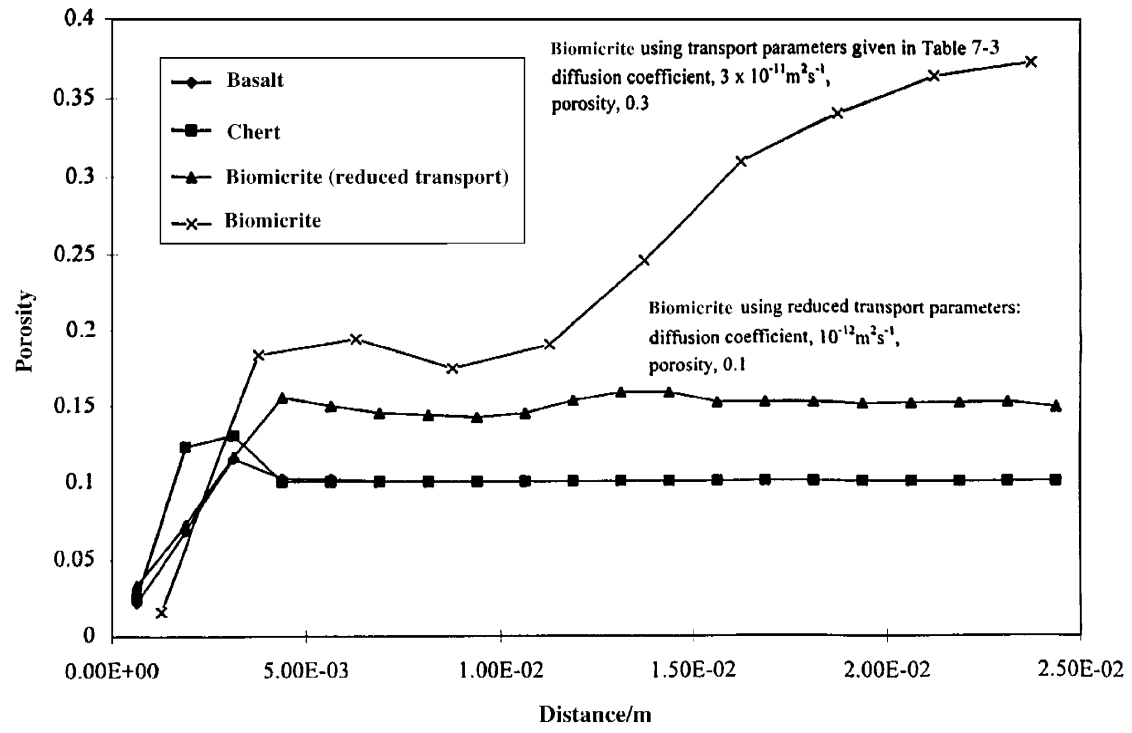

Figure 7-22. *Comparison of porosity profiles for basalt, chert and biomicrite at 100 years (CHEQMATE).*

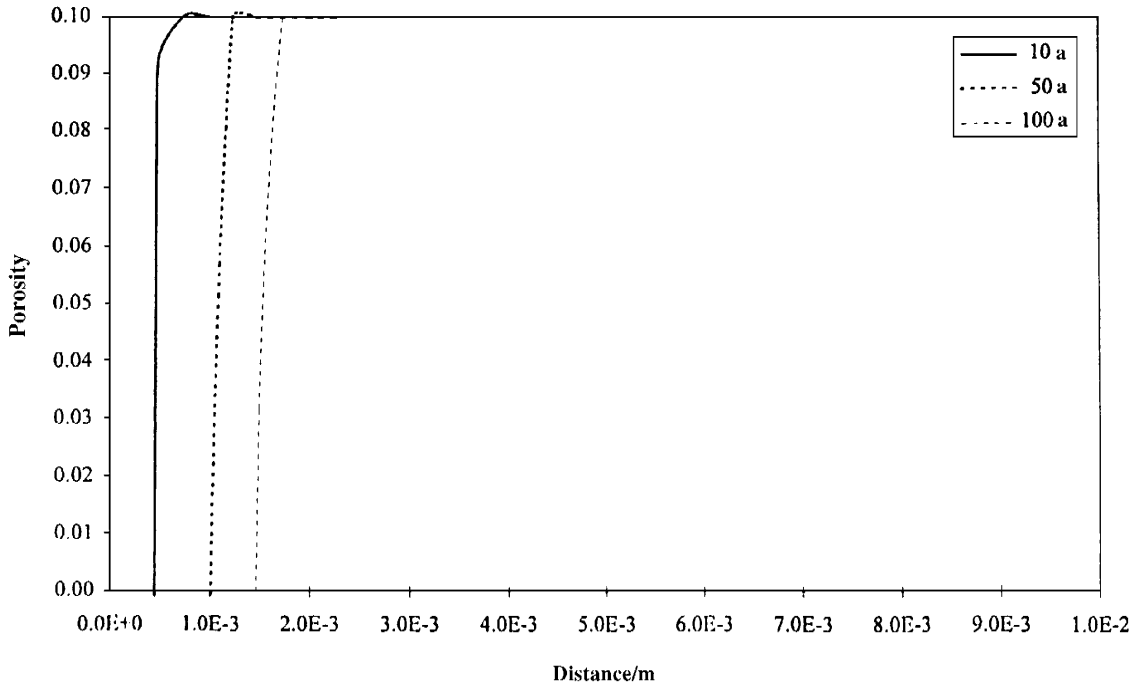

Figure 7-23. *Porosity profile in years for basalt (MARQUISS).*

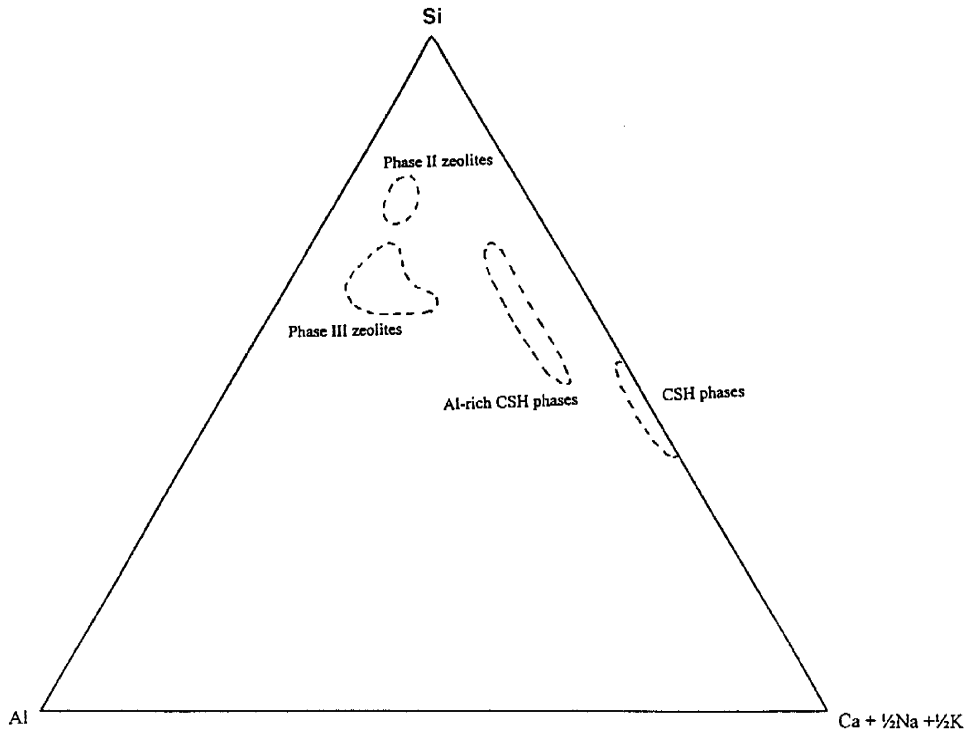

Figure 7-24. *The compositional ranges shown by field CSH- and zeolite-type phases (Phase III data, see Chapter 5; Phase II data, see Milodowski et al., 1998).*

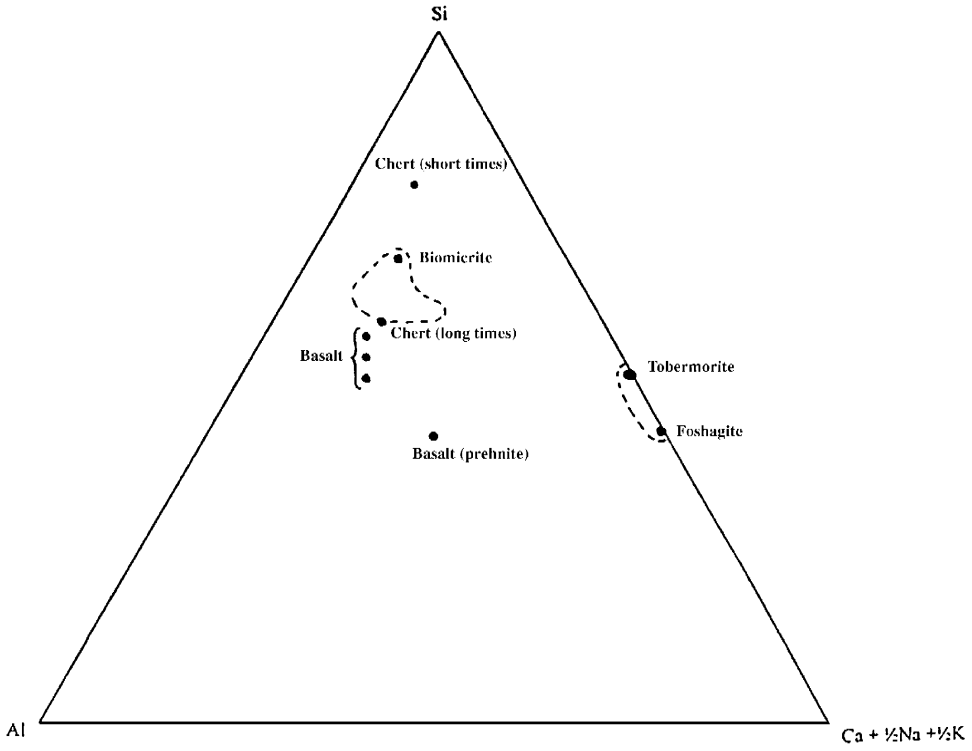

Figure 7-25. *Compositions of CSH phases and zeolites predicted to form during the CHEQMATE calculations.*

8 ZEOLITE OCCURRENCE, STABILITY AND BEHAVIOUR

(D. Savage)

8.1 INTRODUCTION

Zeolites occur as products of the interaction of hyperalkaline groundwaters and silicate/aluminosilicate minerals at Maqarin (Section 5), and are expected to precipitate as a result of the reaction of cement pore fluids with rocks surrounding a cementitious repository for radioactive wastes (Savage, 1997). Consequently, it is desirable that their conditions of formation and stability are understood.

The interaction of hyperalkaline fluids with (predominantly) aluminosilicate minerals is a complicated problem. The chemistry of silica, for example, at elevated pH is poorly understood, with the potential existence of several aqueous species (Eikenberg, 1990). The dissolution of rock minerals and the precipitation of product solids as the plume migrates means that a constant porosity boundary condition cannot be assumed for numerical simulations of such processes (Lichtner and Eikenberg, 1994). The chemical composition of the cement pore fluids will also change with time, as more soluble oxides/hydroxides of the alkali metals are dissolved before those of the alkaline-earths (Atkinson, 1985). Furthermore, the reactivity of hyperalkaline systems ensures that there are relatively few appropriate natural examples to study as analogues of repository processes (Miller et al., 1994).

Despite these many uncertainties, it is likely that zeolites will occur as products of the interaction of hyperalkaline groundwater with aluminosilicate rocks. Zeolites have been described as products of laboratory experiments (Chermak, 1992, 1993), numerical simulations (Fritz et al., 1988; Savage and Rochelle, 1993; Lichtner and Eikenberg, 1994) and natural analogues (Alexander, 1992; Linklater, 1998; this report) of hyperalkaline water-rock reaction. The precipitation of zeolites will produce significant changes to the behaviour (retardation properties, water and gas flow properties) of that portion of the far-field affected by plume migration, because of their large molar volumes and high ion exchange capacity.

This section reviews the stability and occurrence of zeolites with reference to their occurrence at Maqarin, and also as potential products of the interaction of cement pore fluids with rocks surrounding a cementitious repository for radioactive wastes.

8.2 A REVIEW OF ZEOLITE OCCURRENCE AND BEHAVIOUR

8.2.1 Zeolite Structure and Mineralogy

Zeolites are crystalline, hydrated aluminosilicates of alkali and alkaline-earth cations, having 3-D structures (Gottardi, 1977; Mumpton, 1977). They are characterised by an ability to lose and gain water molecules reversibly and to exchange cations without a major change of structure. Zeolites were discovered in 1756 by Freiherr Axel Fredrick Cronstedt, a Swedish mineralogist, who named them from the greek words meaning 'boiling stones', in reference to their frothing characteristics when heated (Gottardi, 1977; Mumpton, 1977). Zeolites are one of the largest mineral groups with 40 distinct natural species recognised and approximately 100 synthetic species.

Zeolites are tektosilicates (like quartz and feldspars) and consist of 3-D frameworks of SiO_4 tetrahedra where all four corner oxygen ions of each tetrahedron are shared with each adjacent tetrahedron. Some of the quadravalent silicon is replaced by trivalent aluminium, giving rise to a deficiency of positive charge. This charge deficiency is balanced by the presence of mono and divalent cations elsewhere in the structure. Thus the empirical formula for a zeolite is:

$$M_{2/n}O.Al_2O_3.xSiO_2.yH_2O$$

where M is any alkali or alkaline-earth cation, n is the valence of the cation, x is a number from 2 to 10, and y is a number from 2 to 7. The ratio of SiO_2 to Al_2O_3 is always equal to or greater than 2.The Si/Al ratio in natural zeolites is in the range 1–6. Trivalent cations are generally not found in the exchange sites of most zeolites. Loosely bound water is present in the structures of all natural zeolites and ranges from 10–20% of the dehydrated phase. Dehydration of a zeolite is an endothermic process.

Whereas the framework structures of quartz and feldspar are tightly packed, those of zeolites are remarkably open, such that void volumes of 50% are known (Mumpton, 1977). The channels and cavities in zeolites enable them to "screen" molecules and "sieve" cations. Most zeolite structures can be visualised as SiO_4 and $Al0_4$ tetrahedra linked together in a variety of ways, e.g. by double 4 rings or double 6 rings of oxygen (Fig. 8-1).

8.2.2 Geological Occurrences

Before the 1960s, zeolites were believed to occur only in cavities and amygdales in volcanic rocks. The discovery of zeolites in tuffaceous sedimentary rocks with the simultaneous stimulus of research into synthetic zeolites led to a growth of studies of geological occurrences of zeolites (Tsitsishvili et al., 1993). The principal geological occurrences of zeolites are:

- saline, alkaline lakes;
- deep-sea sediments;
- low-temperature open hydrogeological systems;
- burial diagenesis;
- hydrothermal-geothermal systems.

Features common to all systems are the availability of Si and Al and a pore fluid (Ca+Na+K)/H activity ratio greater than that at which sheet silicates would form. The type of zeolite forming in a geological system depends upon the nature of the source material, the chemical composition of the pore fluid, temperature, and time. A common reactant in geological systems is volcanic glass. The type of zeolite will depend upon temperature and pressure, as well as chemical parameters such as pH, and the activities (or fugacities) of species such as Si, Al, Ca, Na, K, H_2O and CO_2. Less hydrous zeolites will form in systems of high ionic strength or high Pco_2.

Coombs et al. (1959) noted that zeolites could be divided into three groups according to silica content: those forming in environments supersaturated with respect to silica; those coexisting with quartz; and those favoured by silica deficient environments (Fig. 8-2). For example, the stability of high-silica zeolites such as mordenite is extended when the silica activity is higher than that of quartz. In addition to silica activity, the importance of pH is emphasised, and in particular the carbon dioxide content, which has a direct influence on pH.

8.2.3 Saline and Alkaline Lakes

Saline and alkaline lakes are ideal environments for the development of zeolites. These lakes occur in situations typified by intra-continental rift faulting and arid and/or semi-arid climate. The tectonic setting provides abundant glassy pyroclastic volcanic rocks and closed hydrographic basins, whereas the climate helps develop evaporative saline, alkaline lake fluids. This combination of highly reactive volcanic material and saline alkaline solutions is ideal for the formation of zeolites. Reactions are relatively rapid and vitric tuffs can alter to zeolites in 1 000 years (Hay, 1977a, b). Typical of these lakes are Owens, Tecopa, Waucoba, and China Lakes (all California), Teels Marsh (Nevada), and Lake Magadi (Africa). Although 40 zeolites occur in nature, only 6 of them, analcime, clinoptilolite, phillipsite, erionite, chabazite, and mordenite, have been reported from saline, alkaline lake deposits.

A marked feature of the diagenesis of volcanic tuffs around saline, alkaline lakes is the strong zonation of zeolite minerals (Surdam, 1977; Surdam and Sheppard, 1977; Hay, 1977a, b, 1986). There is a concentric pattern of alteration of tuffs from (moving inwards) unaltered glass to alkalic, silicic zeolites, to analcime, and finally to K-feldspar. This zonation of mineral parageneses reflects the chemical zonation of lake and interstitial waters (Figs. 8-3 and 8-4). At Deep Springs Valley, California, pore waters evolve from the point of recharge to the most saline pore fluids as follows: Na from 12 000–100 000 mg/L; K from 5 000–18 000 mg/L; Ca from 40–3 mg/L (Surdam, 1977). Lake waters are generally rich in sodium and have a pH of 9.5. The mineral trona, $Na_2CO_3.NaHCO_3.2H_2O$, forms at maximum salinities. At Teels Marsh, brines are essentially Na-Cl waters with carbonate and sulphate as the next most abundant constituents, whilst Ca and Mg are near absent. pH ranges from 9.0 to 10.1 and TDS from 20 000–300 000 mg/L (Taylor and Surdam, 1981). The composition of these brines is in chemical equilibrium with K-feldspar, but mineral parageneses are dominated by phillipsite and analcime (Taylor and Surdam, 1981). This suggests that the mineral parageneses are controlled by kinetics rather than chemical equilibrium.

Silica increases in the most saline waters of saline, alkaline lakes (Table 8-1). In lake waters rich in boron, searlesite ($NaBSi_2O_6.H_2O$) precipitates, which may

buffer the silica content of the water to relatively low levels. Searlesite occurs at Teels Marsh, Nevada, but not at Lake Magadi, resulting in quite different Si contents of lake waters at these two localities (Taylor and Surdam, 1981) (Fig. 8-5).

Phillipsite is consistently an "early" zeolite; clinoptilolite and erionite are usually "late" zeolites (Surdam, 1977). Optimum conditions for phillipsite formation are pH = 9–10.5 and a Na/K ratio of 10–50 (Hay, 1964). Analcime and K-feldspar are never seen to form directly from volcanic glass, but always involve a zeolite precursor (Surdam, 1977; Surdam and Sheppard, 1977; Taylor and Surdam, 1981). In Eocene and older deposits, analcime and other zeolites are often replaced by the sodium plagioclase, albite. Erionite is the preferred initial zeolite in environments rich in Na and Si, but poor in alkaline-earths, particularly Ca. There is a general absence of heulandite in these environments, which is probably caused by the low activity of calcium (Hay, 1964).

Age relationships of sediment deposition in these lakes show that phillipsite can form on the timescale of a few hundred years and complete conversion of tuffs to zeolites ("zeolitisation") can occur over a few thousand years (Hay, 1964). Reaction rates are apparently increased by the increasing salinity of the pore fluids. At Teels Marsh, alteration of the upper ash bed (1–5 cm thick) to phillipsite was complete in 1 000 years (Taylor and Surdam, 1981). At Searles Lake, California, silicic ash layers were altered to phillipsite and merlinoite in 10 000 to 100 000 years (Hay, 1986). Ash layers 140 000 years old are altered to phillipsite and K-feldspar, and ash layers 0.5 to 1.83 Ma old are altered to K-feldspar. Searles Lake is characterised by saline, but not alkaline, pore fluids. As a consequence, alteration of the ash layers was much slower than that observed in saline, alkaline lake deposits. Alteration at Searles Lake is therefore comparable to that in deep-sea sediments (Hay, 1986). These observations emphasise the importance of pH (or, more precisely, the activity of the OH ion) in the catalysis of zeolite reactions.

Zeolites typical of saline, alkaline lakes also occur in fossil lake beds of the western USA, e.g. the Big Sandy Formation of Mohave County, Arizona (Sheppard and Gude, 1973) and the Barstow Formation, San Bernardino County, California (Sheppard and Gude, 1969).

The Big Sandy Formation of Pliocene age consists of vitric tuffs completely altered to zeolites, K-feldspar, clay minerals and silica. The zeolites are mainly analcime, clinoptilolite, erionite and chabazite; phillipsite, mordenite and harmotome are much less abundant. The distribution of diagenetic minerals is zoned, which was probably inherited from the zonation of the chemical composition of lake fluids during deposition of the tuffs.

The Barstow Formation of Miocene age is composed for the most part of zeolites, K-feldspar, clay and silica minerals, but parts contain as much as 90% relict glass. The zeolites are mainly analcime and clinoptilolite, but local concentrations of chabazite, erionite, mordenite and phillipsite exist. These zeolites, except analcime are associated with relict glass. Glass does not coexist with analcime or K-feldspar anywhere in the tuffs. Analcime has a Si/Al ratio of 2.2 to 2.8 and thus falls at the Si-rich end of the analcime series. The Si content of analcime is believed to be inherited from precursor zeolites.

Mariner and Surdam (1970) attempted to interpret the zeolite parageneses of saline, alkaline lakes by consideration of the aqueous speciation of coexisting pore fluids. Silica-rich zeolites such as mordenite and clinoptilolite are typical of the alteration of volcanic glass in marine and freshwater environments (pH 7–9), whereas silica-poor zeolites such as phillipsite and erionite are the dominant zeolites in saline, alkaline lakes (pH 9–10.5). This phenomenon occurs despite the increase of silica solubility with increasing pH. They concluded that more important than the increase in solubility of silica with increasing pH is that the activity of aluminium in the pore fluid increases more rapidly (Fig. 8-6). Consequently, zeolites forming from high pH fluids are characterised by lower Si/Al ratios than those forming at lower pH. Mariner and Surdam (1970) suggest that the reaction of volcanic glass with alkaline solutions is characterised by the formation of a gel whose Si/Al ratio is controlled by that of the pore fluid, and ultimately a zeolite of the same Si/Al ratio forms from the gel.

A different hypothesis to explain the zonation of zeolites around saline, alkaline lakes was offered by Dibble and Tiller (1981). They suggested that zeolite zonation was principally due to kinetic, rather than equilibrium thermodynamic factors. Their thesis was based upon the idea that the mineral sequence in these systems could be interpreted in terms of an Ostwald step sequence. Metastable zeolites such as phillipsite and clinoptilolite form instead of more thermodynamically stable minerals such as analcime and feldspars because the former phases lower the total free energy of the system faster than the latter. In other words, the growth of disordered zeolites and smectites is faster than that of more ordered and thermodynamically stable minerals. Eventually, after a series of steps, the most stable silicate assemblage for the bulk composition may form. However, the formation of metastable phases may delay the attainment of equilibrium by tens of millions of years (Fig. 8-7). This hypothesis is supported by the observation that feldspars never coexist with glass in these systems.

8.2.4 Deep-sea Sediments

The occurrence of zeolites in deep-sea sediments has been described by Boles (1977b), Boles and Wise (1977), Kastner and Stonecipher (1977), Iijima (1977), and Hay (1977a, b, 1986). Most of the information for the presence of zeolites in deep-sea sediments comes from deep sea drilling projects.

Deep-sea zeolites have generally formed at temperatures lower than in other environments, with temperatures of 10–34°C being typical. Zeolites occur in a wide variety of sediments and are not restricted to volcanogenic types. The salinities of interstitial fluids are essentially those of seawater; pH is generally between 7 and 8 with dissolved silica ranging from 4 to 65 mg/L. Clinoptilolite-bearing sediments have pore waters with dissolved silica of 20–40 mg/L, whilst pore waters of phillipsite-bearing sediments have silica contents less than 20 mg/L.

Zeolites are amongst the most important authigenic minerals in pelagic sediments. The type and distribution depend on: a) the composition of the presursor minerals, b) the composition of the host sediments and interstitial waters, c) pH, d) temperature, e) thermodynamic stability, f) hydrodynamics of the system, and g) time.

Phillipsite and clinoptilolite are the most abundant zeolites and may make up to 80% of a sediment. Other zeolites in decreasing order of abundance are: analcime; chabazite;

erionite; gmelinite; laumontite; thomsonite; and natrolite. Analcime and K-feldspar increase with age and are most abundant in sediments of late Jurassic age. Here, analcime and K-feldspar can be directly associated with glass, in contrast to non-marine vitric tuffs, where they form from zeolite precursors. Glass is altered slowly in deep-sea sediments and unaltered glass as old as Cretaceous has been found (Hay, 1986). Little evidence exists for the widespread alteration of non-analcimic zeolites to analcime over 100 Ma (Hay, 1977). The slow rate of alteration explains why K-feldspar can be precipitated directly in a pore fluid containing dissolving glass rather than from a metastable zeolite precursor which precipitates where glass dissolves more rapidly than feldspar can nucleate and crystallise. Zeolites progressively decrease in abundance as a function of age in Mesozoic and Palaeozoic marine rocks, probably reflecting their alteration to feldspars.

Phillipsite is more characteristic of Miocene and younger sediments, whereas clinoptilolite and analcime characterise older sediments (Fig. 8-8). This suggests that reaction kinetics are important and that phillipsite may occur metastably. It is suggested that phillipsite is eventually replaced by clinoptilolite. Phillipsite apparently nucleates at the sediment-water interface with growth periods between 150 000 and 1 million years. It is not found in great abundance below 150 m depth in the sediments. The Si/Al ratio varies between 2.4 and 2.8 and K exceeds Na and Ca. The most common precursor is basaltic glass and palagonite. Phillipsite is probably not a stable phase in the deep sea environment and kinetic factors control its nucleation and growth.

Clinoptilolite predominates in calcareous and clayey sediments of Miocene to Cretaceous age. Clinoptilolite has been reported in sediments as young as Pleistocene, but is most abundant in Eocene and Cretaceous samples. It persists below 850 m depth in the sediments. Clinoptilolites of the deep-sea floor are relatively uniform in composition with the Si/Al ratio varying between 4.2 and 5.2 and alkalis exceeding alkaline-earth cations. Compared with associated pore fluids, Na is depleted by a factor of 80, calcium by 50 and magnesium by about 55 in clinoptilolite relative to potassium.

8.2.5 Open Hydrogeological Systems

These systems consist of continental vitric tuffs which show a depth zonation of zeolites. These tephra sequences exhibit a vertical zonation of smectite and zeolites which reflect the changing chemical composition of groundwater moving through the system (Hay, 1977, 1986). Dissolution of glass to smectite in the upper part of the system increases the pH, the activity of dissolved SiO_2 and (Na+K)/H activity ratio so that glass alters to zeolites rather than smectite. In silicic ashes, zeolites are found at depths greater than 200–500 m, whereas in alkali-rich, low silica ashes, zeolites form at depths of only a few metres or tens of metres. The development of zeolites is zoned, with clinoptilolite, phillipsite and chabazite in upper zones, and analcime in lower zones.

A sequence of 3 000 m of Miocene silicic tuffs, lavas and breccias occurs at Yucca Mountain, Nevada and is being investigated as a possible repository for high-level radioactive waste (Sheppard et al., 1988). Much of the original glassy material has been altered to clay and silica minerals, zeolites and feldspars. Unaltered glass persists in the upper part of the system, but zones of clinoptilolite and mordenite, analcime, and albite follow with depth. In samples of tuff from the mordenite-clinoptilolite zone, mordenite

makes up 0–90% of the tuff and is usually associated with clinoptilolite. Mordenite forms both earlier and later than associated clinoptilolite, but there is good textural evidence that mordenite forms at the expense of clinoptilolite. This reaction may be driven by a higher temperature regime due to the presence of the Timber Mountain Caldera to the north. Smyth (1982) has reviewed the stability of clinoptilolite, mordenite and analcime in tuffs at Yucca Mountain, USA. He concludes that these minerals are unstable at elevated temperatures and low water vapour pressures and may break down either by irreversible dehydration or by irreversible mineralogical reactions.

8.2.6 Burial Diagenesis

The regional occurrence of zeolites as products of burial diagenesis (or lowgrade metamorphism) was first recognised by Coombs (1954) in southern New Zealand. On the basis of these observations Coombs et al. (1959) defined a "zeolite facies" of metamorphism to bridge the gap (as they saw it) between diagenesis and conventional metamorphism. They defined a lower grade of a heulandite-analcime-quartz assemblage and a higher grade laumontite-albite-quartz assemblage. Although the idea of a zeolite facies is a useful concept, in practice, the dependence of zeolite occurrence upon factors such as rock and fluid composition limits its widespread applicability. In general, the following comments are relevant to zeolite occurrence in burial diagenesis (Boles, 1977a):

- volcanic glass and calcic plagioclase are common precursors;
- zeolites make up less than 25% of the bulk rock;
- the distribution of individual zeolites with depth shows considerable overlap, which indicates that factors other than temperature and pressure are important;
- laumontite, analcime and heulandite are the most common zeolites, but Tertiary and younger rocks may contain a more diverse suite including mordenite, erionite, chabazite and phillipsite;
- zeolites are associated with quartz, albite, K-feldspar, calcite, sheet silicates.

In burial diagenesis, temperature is the dominant influence on zeolite type, composition and distribution. Within silicic tuffs, a typical downward sequence is:

- fresh glass with smectite;
- clinoptilolite and mordenite;
- heulandite and analcime;
- albite and laumontite.

The thickness of these zones varies according to the geothermal gradient. In areas of active diagenesis, temperatures at the top of the clinoptilolite-mordenite zone are 30–50°C, and 120–124°C at the top of the albite-laumontite zone (Hay, 1986). These temperature limits are very variable, since laumontite can form at temperatures as low as 50–60°C. Five zeolites predominate in sedimentary rocks: analcime; clinoptilolite; heulandite; laumontite and phillipsite. Next in abundance are: chabazite; erionite; mordenite; natrolite and wairakite. The main compositional features of zeolites found in sedimentary rocks are shown in Table 8-2.

Zeolites are abundant in Triassic and Jurassic marine strata of the Southland Syncline of New Zealand (Coombs, 1954; Boles and Coombs, 1975). Laumontite and heulandite are common in both the upper and lower parts of the section. In sandstones, heulandite, laumontite, prehnite, sphene, chlorite and pumpellyite are associated with rocks of andesitic parentage, whereas authigenic quartz, albite and K-feldspar characterise sandstones of rhyolitic to dacitic parentage. The following reactions summarise the paragenetic sequence (Boles and Coombs, 1975):

- glass → montmorillonite ± illite;
- glass → heulandite + chlorite;
- heulandite → laumontite or prehnite or calcite or analcime or albite.

The Si/Al ratio of the heulandite was controlled by that of the precursor. Pressure and fluid composition were more important than depth of burial for controlling the type and distribution of alteration phases.

In Japan, zeolites have been reported in sediments ranging from Quaternary to Triassic in age, but the majority occur in Miocene pyroclastic and volcanogenic sedimentary rocks (Boles, 1977a). Distinct zeolite zonations with increasing depth are recognised in these rocks: fresh glass; alkali clinoptilolite; clinoptilolite + mordenite; analcime ± heulandite; albite

There are several distinct features of this zonation in comparison with zeolites from other regions:

- mordenite is relatively common;
- opaline silica coexists with clinoptilolite and mordenite;
- a transition from alkalic clinoptilolite to calcic clinoptilolite or heulandite occurs with depth;
- laumontite is not particularly common.

From the above comments, it may be concluded that zeolite occurrences in burial diagenetic environments of Japan developed in a high temperature-pressure regime during the late Tertiary. The high thermal gradients may have produced the distinct zeolite zonation which is different from other regions of the world (Boles, 1977a). In western North America, there are important occurrences of zeolites in burial diagenetic environments at British Columbia, Canada (Surdam, 1973); Washington-Alaska (Galloway, 1974; Stewart, 1974); Oregon (Dickinson, 1962; Brown and Thayer, 1963); and California (Dickinson et al., 1969; Castano and Sparks, 1974; Merino, 1975; Helmold and van de Kamp, 1984).

8.2.7 Geothermal and Hydrothermal Systems

Zeolites are common in areas of hydrothermal alteration and often exhibit a well-defined zonation. Clinoptilolite or mordenite characterises the shallowest and coolest zones, whereas deeper zones progressively contain analcime or heulandite, laumontite,

and wairakite. Well-known examples include Yellowstone Park, USA (Honda and Muffler, 1970), Wairakei, New Zealand (Steiner, 1953), Onikobe, Japan (Seki et al., 1969), and Iceland (Kristmannsdottir and Tomasson, 1977).

Zeolitic alteration of basalts and hyaloclastites in Iceland has been documented by Kristmannsdottir and Tomasson (1977). Four distinct zones of alteration were found in so-called low-temperature (<150°C) geothermal areas (in increasing order of depth/temperature): chabazite; mesolite/scolecite; stilbite; laumontite. In the high temperature geothermal areas (>200°C), the zeolites present are mordenite, heulandite, laumontite and analcime. A summary of the zeolite zones in Iceland is shown in Figure 8-9.

Dachiardite is a rare high-silica zeolite with a cation content similar to mordenite. The type dachiardite is from a hydrothermally altered pegmatite in Italy where it occurs with tourmaline, pollucite, stilbite, heulandite and mordenite. Dachiardite from cavities in tholeiitic basalts at Altoona, Washington and Cape Lookout and Agata Beach, Oregon has been investigated (Wise and Tschernich, 1977). At Altoona, dachiardite was the last mineral to form, following siderite, iron smectite, mordenite, ferrierite and clinoptilolite. At Cape Lookout it forms in the sequence smectite, erionite, phillipsite, mordenite, dachiardite. At Agate Beach, it is associated with clinoptilolite only. Microprobe analyses reveal the following composition for the Altoona dachiardite:

$$Ca_{1.0}Na_{0.6}K_{0.3}[Al_{3.4}Si_{20.6}]O_{48}.14.2H_2O.$$

Analyses of mordenite and dachiardite suggest that fluid compositional parameters such as a_{SiO2} did not play a part in the crystallisation of one zeolite in preference to another. From considerations of crystal size, it is suggested that mordenite nucleates more easily in supersaturated fluids, whilst dachiardite forms from solutions with less supersaturation.

8.2.8 Laboratory Systems

Barth-Wirsching and Holler (Holler and Wirsching, 1977; Barth-Wirsching and Holler, 1989) investigated zeolite formation in laboratory experiments with basaltic, phonolitic and rhyolitic glass, nepheline and oligoclase starting materials. Their experiments demonstrated that solution pH controls the zeolite Si/Al ratio, although the Si/Al ratio of the starting material may also have an effect.

Donahoe and Liou (1985) investigated the effects of pH on zeolite formation. Zeolites were synthesised at 80°C from clear solutions rather than gels. At a fixed concentration of silica (3.5 M), the zeolite Si/Al ratio was a linear function of pH (Fig. 8-10). pH determines the Si/Al ratio of the solution phase and that of the zeolite. Decreasing solution pH shifts the aqueous aluminosilicate polymer distribution towards dominance by ring and cage species. They hypothesise that these ring and cage structures join by means of dehydration reactions to form zeolites, so that the Si/Al ratio of the zeolite is inherited directly from the aqueous aluminosilicate polymers. At high pH, only monomeric species will exist and these will have generally lower Si/Al ratios. For a fixed exchangeable cation composition, the zeolite Si/Al ratio is only a function of the distribution of polymeric aluminosilicate species in solution. Figure 8-11 illustrates the combined effect of pH and total dissolved silica concentration. Zeolites precipitated

with or without the presence of a precursor gel, depending upon solution composition. The compositions of gels and coexisting zeolites were determined using SEM. In general, the gel had the same Si/Al ratio as the zeolite. Zeolite growth rate was dependent upon solution pH and aluminium concentration. Higher Al concentration or lower Si/Al ratio in solution led to faster zeolite growth. This increase in rate may be accelerated by the formation of aluminosilicate polymers through the interaction of tetrahedral Al with aqueous silicate species. Zeolites which precipitate by means of a gel precursor have a higher growth rate than those which precipitate directly from solution. The presence of a gel may permit nucleation to occur more readily by providing a surface with adsorbed aluminosilicate species available for crystal growth.

As a result of experiments to investigate the crystallisation of zeolites in the system Na_2O-K_2O-Al_2O_3-SiO_2-H_2O, Donahoe et al. (1984) noted that merlinoite may be more common than previously recognised and is often mistaken for phillipsite. The crystallisation of merlinoite in preference to phillipsite is favoured by high pH (>13.6) and low Na/(Na+K) ratios (<0.5).

Hawkins and co-workers (Hawkins, 1981; Hawkins et al., 1977) investigated zeolite formation as a result of the dissolution of volcanic glass. The early formation of phillipsite, followed by clinoptilolite and then mordenite was noted. The early formation of phillipsite (which consists of 4-membered rings of SiO_4 tetrahedra) was ascribed to the dominance of tetramers of aqueous silica in alkaline hydrothermal solutions and concluded therefore that the results of hydrothermal experiments may not be completely analogous to low-temperature natural processes.

Milodowski et al. (1985) noted that clinoptilolite was removed from samples of mudrocks stored under water in contact with cements after 15 months at 25°C. This suggests that this zeolite was not stable under the pore fluid conditions in equilibrium with cement.

Ueda et al. (1980) investigated the precipitation of mordenite from aqueous solutions and concluded that the composition of the zeolite was governed by the composition of the initial gels in seeded systems.

Knauss and co-workers have investigated the formation of zeolites in tufts from Yucca Mountain at temperatures up to 250°C (Knauss et al.,1986; Knauss, 1987). Dachiardite and mordenite were synthesised at 250°C, whereas lower temperature (150°C) assemblages were characterised by clay minerals.

Chermak investigated the interaction of sodium (Chermak, 1992) and potassium (Chermak, 1993) hydroxide solutions on Opalinus Clay at temperatures in the range 150–200°C. The formation of analcime was noted, followed by vermiculite and Na-rectorite in NaOH solutions and a reaction sequence of phillipsite, followed by K-feldspar ± K-rectorite in KOH solutions. Analcime formed after only one day reaction in the NaOH experiments. Phillipsite was a metastable reaction intermediary in the KOH experiments.

There have been a few kinetic studies of the dissolution-precipitation behaviour of zeolites. Hayhurst and Sand (1977) studied the precipitation kinetics of Na, K-phillipsites in the temperature range 25°–175°C. Phillipsite synthesis was aided by low silica starting materials, and as silica increased, zeolites other than phillipsite stabilised. Phillipsite nucleation and growth were observed to be second order with respect to

hydroxide concentration with rate constants at 100°C of 0.013 1^2/hour $mole^2$ and 6.748% x 1.1^2/hour $mole^2$. Savage et al. (1986, 1993) investigated the dissolution kinetics of laumontite at 80°, 120° and 150°C in the pH range 7–10. Dissolution rates were independent of pH at 80°C, but increased slightly with decreasing pH at 120° and 150°C.

Dissolution rates were in the range $3x10^{-11}$ (80°C) to 10^{-9} mol $m^{-2}s^{-1}$ (150°C). The activation energy for dissolution was determined to be 58 kJ mol^{-1}. Ragnarsdottir (1993) studied the dissolution kinetics of heulandite at 25°C in the pH range 2–12. Dissolution behaviour was strongly pH-dependent with rates increasing with decreasing pH in the acid regime (pH 2–6) and increasing pH in the alkaline regime (pH 7–12). The dissolution rate at neutral pH was $2x10^{-12}$ mol $m^{-2}s^{-1}$. Murphy and Pabalan (1994) investigated the reaction kinetics and solubilities of analcime and clinoptilolite. Bateman et al. (1995) back-calculated the precipitation rates of erionite and analcime from the results of a column experiment investigating zeolite formation from the alteration of Ca-plagioclase at 150°C. These authors estimated the precipitation rates of erionite and analcime as $5x10^{-14}$ and $5x10^{-7}$ mol $m^{-2}s^{-1}$, respectively (at 150°C).

The ion-exchange behaviour of zeolites has been studied *inter alia* by Bray and Fullam (1971), Mercer and Ames (1977), Semmens and Seyfarth (1977), Barrer (1977) and Pabalan (1994). Bray and Fullam *(ibid.)* noted 98+% recovery of ^{137}Cs from Purex process effluent using a synthetic zeolite "Zeolon" column. The use of natural zeolites such as clinoptilolite, mordenite, erionite and chabazite to remove Cs from radioactive waste water has been described by Mercer and Ames (op. cit.). The cation exchange properties of zeolites has been reviewed by Barrer (op. cit.). Cs is preferred to K and Na in the following zeolite types: mordenite; phillipsite; gismondine; faujasite and chabazite. Table 8-3 is a synthesis of ion exchange data for zeolites.

Semmens and Semmens (1977) noted that clinoptilolite has higher selectivity for barium and lead as compared with copper, cadmium and zinc.

Pabalan (1994) carried out ion exchange experiments with clinoptilolite at 25°C and concluded that a Margules solid-soludon model successfully describes binary ion exchange between clinoptilolite and aqueous solutions.

Sorption of radionuclides on zeolites with regard to the migration of a hyperalkaline plume from a repository for low- and intermediate-level radioactive wastes has been reviewed by Valcke and Cremers (1995). They noted that simple radionuclides (mainly alkalis and alkaline-earths) would probably be retained by ion-exchange processes, whereas trivalent elements and the actinides would tend to be retained by surface adsorption-complexation reactions. The relatively high ion-exchange coefficients anticipated for mono- and divalent cations would be compromised by the high concentrations of competing Na and K ions in migrating cement pore fluids. The following K_d values were suggested: 50–100 L kg^{-1} for alkali metals; 5–50 L kg^{-1} for alkaline-earths; 5–50 L kg^{-1} for heavy metals and transition elements; and up to 10 L kg^{-1} for trivalent elements and actinides.

8.3 ZEOLITE STABILITY AT MAQARIN

8.3.1 Background

The nature and origin of the hyperalkaline groundwaters at Maqarin have been the focus of the Phase I and Phase II studies (Alexander, 1992 and Linklater, 1998) and are further discussed in this present report (see Chapters 6 and 7). Using the thermodynamic data tabulated in Appendix N, thermodynamic activity diagrams have been constructed to investigate the potential stability of zeolites in the hyperalkaline groundwaters from Maqarin. Thermodynamic activity diagrams provide a convenient means by which the thermodynamic stability of minerals and coexisting solutions can be investigated graphically (Garrels and Christ, 1965). Relationships between 4–5 variables (typically 2 metal cations, pH, aluminium and silica) can be displayed on each 2-D diagram.

8.3.2 Approach

With regard to the assessment of the stability of zeolites, key variables are pH, aluminium, silica, sodium, calcium and potassium. Consequently, a suite of diagrams (Figs. 8-12 – 8-15) employing these variables has been constructed to evaluate zeolite stability. Each diagram is similar in that each is a plot of 'Al_H' (log_{10} of the activity of aluminium divided by the activity of hydrogen ion raised to the power of three) versus 'S' (the log_{10} of the activity of aqueous silica). Such diagrams were first drafted by Giggenbach (1984, 1988) to assess the stability of aluminosilicate minerals in geothermal systems. Mineral-fluid equilibria are "balanced" using cations so that mineral stability can be assessed in terms of aluminium, silica and the pH of coexisting pore fluids. For example, the coexistence of muscovite and erionite (both potassium aluminosilicates) can be written as follows (balancing the reaction using potassium):

$$KAlSi_3O_8.3H_2O + 2Al^{3+} + H_2O = KAl_3Si_3O_{10}(OH)_2 + 6H^+ \qquad (8.1)$$

The stability line for this reaction is defined as follows:

$$K_{musc-erion} = \frac{a^2_{Al3+}}{a^6_{H+}} \qquad (8.2)$$

taking logarithms, this can be arranged as:

$$\log \frac{a_{Al3+}}{a_{(H+)3}} = \frac{logK_{musc} - logK_{erion}}{2} \qquad (8.3)$$

Consequently, a value for the intercept of this line on an axis of log a_{SiO_2} can be calculated from thermodynamic data for the hydrolysis reactions of muscovite and erionite.

Thermodynamic data from Appendix N; Table N-1) were used to construct the diagrams. Although these data are considered to be the most up to date dataset available

for zeolites, it became apparent during construction of the diagrams that inconsistencies existed because data had been derived by different methods (e.g. by experimental calorimetry in some instances, and by different calculational methods in others). Consequently, it was not possible to include data for the following zeolites in the diagrams: chabazite, epistilbite, laumontite and phillipsite.

The activity ratios of groundwaters plotted on the diagrams were taken from EQ3 calculations reported in Chapter 6 (Table 6-13). Although $Al(OH)^-_4$ and $CaH_2SiO_4(aq)$ were identified as the dominant aqueous species for Al and Si, respectively at high pH, by convention, activity diagrams were constructed and groundwaters plotted using data for Al^{3+} and $SiO_2(aq)$.

8.3.3 Results and Discussion

Figure 8-12 is an activity diagram showing stability relations in the system $CaO-Al_2O_3-SiO_2-H_2O$. Maximum Al_H values are defined by the solubilities of gibbsite $[Al(OH)_3]$, kaolinite $[Al_2Si_2O_5(OH)_4]$ and pyrophyllite $[Al_2Si_4O_{10}(OH)_{21}$, respectively (in increasing order of silica activity). Silica solubilities defined by quartz and chalcedony are shown as dotted lines. Most groundwaters have dissolved silica activities bounded by these stability lines. Stable calcium aluminosilicates identified were scolecite (covering much of the activity diagram), and heulandite at silica activities greater than that of chalcedony. The hyperalkaline groundwater data (samples M5-8 and M10–15) plot off the diagram at S <-10. 6 and Al_H <4.5. The non-hyperalkaline groundwater data plot in an area of supersaturation with respect to kaolinite.

It is implicit in Figure 8-12 that scolecite is the stable calcium aluminosilicate at all S values less than -3.5, so that it could be considered that the Western Springs hyperalkaline groundwaters are in equilibrium with this mineral. However, if calcium silicate hydrate minerals are also considered (Fig. 8-13), then it is apparent that the Western Springs groundwaters are undersaturated with respect to scolecite. Although the groundwater data plot in the field of hillebrandite, it is likely that Al_H and S are controlled by an aluminous CSH phase such as thaumasite or a thaumasite-ettringite solid-solution. Unfortunately, there are no thermodynamic data available for such phases in order to test this theory further. However, it is clear from Figures 8-12 and 8-13 that the Western Springs hyperalkaline groundwaters cannot be in equilibrium with zeolites such as scolecite and heulandite.

Activity diagrams for sodium (Fig. 8-14) and potassium (Fig. 8-15) show a similar picture to that of Figure 8-12. Stable sodium aluminosilicates are natrolite, analcime and mordenite in increasing order of silica activity. Fields of coexistence for muscovite, kalsilite, erionite and clinoptilolite are shown on Figure 8-15, but this assemblage is metastable with respect to muscovite and K-feldspar (shown as dotted phase boundaries). Mordenite is a zeolite identified at Maqarin, but is clearly not in equilibrium with the hyperalkaline groundwaters sampled, since it would require of the order of 50 mg/L SiO_2 in a coexisting pore fluid.

To take this point further, EQ3 has been used to calculate a fluid composition which would be in equilibrium with the zeolitic minerals observed at Maqarin. Milodowski (1994) has reported the following zeolites at Maqarin: mordenite, dachiardite, epistilbite, yugawaralite, laumontite and chabazite. Table 8-4 presents the results of a

EQ3 calculation using some of these minerals (all data from the existing EQ3 database) to control the chemical composition of a coexisting fluid phase. It may be seen from Table 8-4 that there are marked differences between this calculated composition and the composition of the hyperalkaline groundwaters at Maqarin (the composition of sample M5 is shown in Table 8-4 for comparison). Most notable is the greatly reduced concentration of calcium, the decreased pH, the increased concentration of sodium, and the very large increase in dissolved silica.

The range of minerals lining groundwater flowpaths at Maqarin (aragonite, gypsum, ettringite-thaumasite, calcium silicate hydrates and zeolites) may be interpreted by the reaction of a Ca-OH-SO_4 type groundwater with the marl, progressively losing Ca, OH and SO_4 ions by the precipitation of CSH, gypsum and ettringite whilst gaining Al and Si by reaction with the marl and ultimately precipitating zeolites (Fig. 8-16).

The types of zeolites observed at Maqarin are typical of those associated elsewhere with fluids which are either saturated or supersaturated with respect to quartz solubility. Specifically, yugawaralite, mordenite and dachiardite are usually associated with fluids supersaturated with respect to quartz (Coombs et al., 1959). Laumontite and epistilbite form from solutions saturated with quartz, whereas chabazite is the only zeolite at Maqarin normally associated with fluids undersaturated with respect to quartz. All this evidence suggests that the zeolites found at Maqarin coexisted with pore fluids which were much more siliceous and less alkaline than those currently sampled from groundwater seepages. Such pore fluids may develop only locally, perhaps during the final stages of the sealing of an alteration vein, whilst the bulk of the alteration fluids are of the hyperalkaline type. They may thus represent a small fraction of the pore fluids extant in the Maqarin area.

8.4 IMPLICATIONS FOR RADIOACTIVE WASTE DISPOSAL

It is clear from the above that cement pore fluids (as approximated by the Maqarin groundwaters) have low thermodynamic activities of aluminium and silica in relation to their elevated pH. Such pore fluids are incapable of precipitating zeolites without a decrease in pH and reaction with a source(s) of alumina and silica. Some cements employing PFA (pulverised fly ash) as a filler tend to develop pore fluids with lower equilibrium pH and may be capable of precipitating zeolites under suitable conditions. However, the rock surrounding a cementitious repository for radioactive waste will be the principal source of alumina and silica as a hyperalkaline plume migrates through the geosphere. It follows, therefore, that zeolites will form in that part of the plume which has reacted most with the host rock, i.e. "the distal" edges. This portion of the plume will have a considerably lower pH than that nearer the engineered barriers of the repository, and much higher dissolved silica and alumina contents. A schematic diagram of this scenario is presented in Figure 8-17. At any point "downstream" of the plume at which enough Al and Si has been dissolved from the rock to stabilise zeolites, the mineral (note that gels rather than true crystalline solids are more likely to form) alteration sequence with time will be:

- zeolites stable at low pH (high silica zeolites such as clinoptilolite, mordenite and dachiardite);
- zeolites stable at high pH (low silica zeolites such as scolecite and phillipsite);
- aluminous CSH minerals such as tacharanite;
- CSH minerals of low Ca/Si (okenite, gyrolite, tobermorite);
- CSH minerals of high Ca/Si (jennite, hillebrandite or ettringite-thaumasite if sulphate contents are high enough).

Both the above sequence, and the reverse of it, occur in alteration observed at Maqarin.

At any point in space contacted by the alkaline plume (assuming the fracture doesn't seal), zeolites will tend to form first, followed by CASH, followed by CSH etc. The whole process can be envisaged as a continuous evolution of pore fluid and solids composition. This sequence of solid phases may mean that radionuclides captured by early forming zeolites may be subsequently released as zeolites are de-stabilised and other solid phases form.

This spatial alteration sequence is emphasised in Figure 8-17. At any time after plume migration, fluids nearest the repository will tend to precipitate ettringite and CSH minerals, and those furthest away will tend to precipitate zeolites. However, in the case where a fracture remains open or is tectonically re-activated, individual fracture fillings at any particular location may show zoning perpendicular to the fracture length.

This evolving sequence of mineral composition means that if it is believed that the fractures in a particular host rock will remain open, radionuclide sorption properties will be time-dependent which may need to be considered for performance assessment. Although zeolites have favourable ion exchange and sorption properties for elements such as the alkali and alkaline-earth metals, their sorption of actinide elements is less than that of iron oxyhydroxides (Valcke and Cremers, 1995).

Alkalic zeolites, such as phillipsite, erionite, natrolite, clinoptilolite and analcime will form during the early evolution of the system when cement pore fluids are dominated by alkali hydroxides. If the fractures remain open, calcic zeolites (scolecite, chabazite, laumontite, epistilbite, heulandite) may replace early-formed alkalic zeolites when cement leachates become dominated by calcium (where early-formed zeolites are accessible to later pore fluids). This sequence of zeolites may not have significant impacts for radionuclide retardation, since calcic zeolites have similar cation exchange characteristics as alkali metal zeolites (Table 8-3).

Natural system and laboratory observations suggest that it is likely that zeolites will form at the distal edges of the hyperalkaline plume over timescales of 100 years. However, there is evidence that zeolites are de-stabilised and dissolved by cement pore fluids over timescales of only tens of months (Milodowski et al., 1985). The replacement of zeolite-forming pore fluids by those precipitating cement minerals will mean that early-formed zeolites will be quickly removed by the bulk of the hyperalkaline plume. Zeolites may thus have only a temporary existence in the body of rock contacted by the hyperalkaline plume and consequently be a minor solid phase in comparison to calcium (aluminium) silicate hydrates.

Once calcium is removed from migrating cement pore fluids by CSH precipitation, the dissolved silica content increases due to the pH-dependence of the solubility of solid silica polymorphs. This phenomenon was observed by Savage et al. (1992) in experiments involving quartz and pH13, Na-K-Ca hydroxide solutions. Similarly, groundwaters precipitating zeolites at the edge of the hyperalkaline plume may have dissolved silica concentrations in excess of 10 mg/L, depending upon the precise pH. Since pH gradients at the edge of the plume will be sharp, there is thus a tendency for large supersaturations of silica to develop in the groundwater. Fluids strongly supersaturated with silica tend to cause the formation of silica colloids (Weres et al., 1982). There is thus the possibility of the development of large amounts of silica colloids at the margins of the plume. These colloids may be of significance to performance assessment if radionuclides migrate to the advanced edge of the plume. Field samples studied to date from Maqarin (within which no significant colloid populations were found) were from either the cement zone, or the cement/water interface, where Si colloids would not be expected to form (see Chapters 10 and 12).

8.5 SUMMARY AND CONCLUSIONS

Zeolites are hydrated aluminosilicates with a wide range of composition and an open framework structure of SiO_4 tetrahedra, enabling them to incorporate and "sieve" a range of molecular and ionic species. Their principal cationic constituents are sodium, calcium and potassium. They have a relatively high molar volume (generally greater than 150 cm^3 mol^{-1}) due to a high void volume (up to 50%). Although cation exchange capacities for alkali and alkaline-earth metals are high (of the order of a few hundred meq/100 g), their selectivity for tri- and tetra- valent metals is low.

In the geological environment, the principal occurrences of zeolites are: tuffaceous rocks of saline, alkaline lakes; deep-sea sediments; low temperature open hydrological systems; during burial diagenesis; and in hydrothermal geothermal systems. They are most abundant in tuffaceous rocks of saline, alkaline lakes. Zeolite formation is encouraged by alkaline pore fluids (pH 9–10), which are often produced by the diagenetic alteration of volcanic glass. The type and amounts of zeolites formed in all systems are strongly controlled by growth kinetics. Phillipsite consistently forms early in the evolution of a diagenetic system, to be replaced by more thermodynamically stable zeolites at later stages of evolution of the system. Zeolites with relatively high Al/Si ratios (e.g. phillipsite, erionite) tend to be associated with pore fluids in the pH range 9–10.5, whereas those with lower Al/Si ratios (e.g. mordenite, clinoptilolite) are more characteristic of pore fluids in the pH range 7–9. All zeolites are generally metastable in nature, transforming over time into more ordered varieties, and ultimately, into feldspars. Zeolite formation in preference to feldspars is favoured by their higher growth rates (volcanic ash beds may be transformed completely into zeolites over a time period of 10^3a). Precipitation rates are increased with increasing hydroxyl ion activity in the fluid phase.

Laboratory studies have shown that zeolite type is dependent upon pH, which controls the aqueous speciation of aluminium and silica. Increasing pH increases the Al/Si ratio of the zeolite. There are few published experimental studies of the kinetics of reaction

of natural zeolites. There are numerous studies of the ion-exchange characteristics of zeolites. A review of sorption data for zeolites recommends the following K_d values: 50–100 L kg^{-1} for alkali metals; 5–50 L kg^{-1} for alkaline-earths; 5–50 L kg^{-1} for heavy metals and transition elements and up to 10 L kg^{-1} for trivalent elements and actinides.

A variety of thermodynamic data for zeolites of variable quality exists in the literature. A compilation of the most up to date data has been produced. No data were found for dachiardite (a high-silica zeolite) and thaumasite (two minerals occurring at Maqarin).

Hyperalkaline groundwaters at Maqarin are not in thermodynamic equilibrium with zeolites and the concentrations of major aqueous species are probably controlled by equilibrium with portlandite and an ettringite-thaumasite solid solution. Mineral alteration sequences at Maqarin confirm that the formation of zeolites is intimately linked with pore fluid composition (pH, activities of aluminium and silica). Thus zeolites may form "early" or "late" in mineral alteration sequences according to the physical dynamics of the system (open or closed system alteration). Pore fluids in equilibrium with the range of zeolites observed at Maqarin (chabazite, dachiardite, laumontite, mordenite, yugawaralite) would be expected to be in the pH range 7–9 and to have dissolved silica concentrations in excess of 10^3 mg/L. Such pore fluids may exist locally at Maqarin in alteration veins in the last stages of sealing.

Extrapolation of the above information to the understanding of the migration of a hyperalkaline plume from a cementitious repository for radioactive wastes, suggests that zeolites will form at the distal edges of any such plume, where pH will be in the range 7–10 and enough aluminium and silica has been dissolved from the host rock to stabilise aluminosilicates. Mineral formation within the plume will be zoned in space and time and locally within individual fractures. During the "early" stages of repository evolution (up to 10^4–10^5 a after closure), these zeolites will be alkalic and minerals such as phillipsite, analcime, erionite, mordenite, natrolite and clinoptilolite are likely to form. As alkali metals are removed from the cementitious materials, the more calcic leachate will encourage the growth of phases such as scolecite, laumonite, stilbite and heulandite. Since the sorptive properties of calcic zeolites are similar to those of alkalic zeolites, this transformation is expected not to be significant in terms of radionuclide retardation. The elevated pH of pore fluids associated with the precipitation of zeolites will produce large dissolved silica concentrations. The sharp pH fronts may lead to the development of large amounts of silica colloids in this zone. Early-formed zeolites will be dissolved and replaced by cement minerals as the alkaline plume continues to migrate away from the repository and over-runs the original distal edges of the plume. At all stages of repository evolution, the precise composition and amounts of zeolites forming in the system will depend as much upon the rates of growth of these minerals as upon thermodynamic stability.

8.6 ACKNOWLEDGEMENTS

Discussions with participants of the Maqarin Phase III Project helped focus the study. Valuable comments on earlier drafts were made by Susan Duerden (Environmental Agency, UK), Russell Alexander (University of Berne) and Chris Rochelle (BGS).

Staff from Nagra and the Paul Scherrer Institute (Switzerland) kindly supplied unpublished reports and data for consideration within the document review. Paul Weston drafted most of the diagrams.

8.7 REFERENCES

Alexander, W. R. (Ed.), 1992. A natural analogue study of the Maqarin hyperalkaline groundwaters. I: Source term description and thermodynamic database testing. Nagra Tech. Rep. (NTB 91-10), Nagra, Wettingen, Switzerland.

Atkinson, A., 1985. The time dependence of pH within a repository for radioactive waste disposal. U.K. At. Ener. Auth. Rep. (AERE-R12594), U.K.

Barrer, R.M., 1977. Cation-exchange equilibria in zeolites and feldspathoids. L.B. Sand and E.A. Mumpton (Eds.) In Natural Zeolites. Occurrence, Properties, Use. Pergamon Press, 385–395.

Barth-Wirsching, U. and Holler, H., 1989. Experimental studies on zeolite formation conditions. Eur. J. Min., 1, 489–506.

Bateman, Y., Noy, D.J., Pearce, J.M. and Savage, D., 1994. Coupled flow and reaction: a modelling and experimental study of zeolite diagenesis. In Extd. Abstr. V.M. Goldschmidt Conference, Edinburgh, 1994, Min. Mag., 58A, 59–60.

Boles, J.R., 1977a. Zeolites in low-grade metamorphic grades. In: Mineralogy and Geology of Natural Zeolites. Min. Soc. Am. Short Course Notes, 103–135.

Boles, J.R., 1977b. Zeolites in deep-sea sediments. In Mineralogy and Geology of Natural Zeolites. Min. Soc. Am. Short Course Notes, 137–163.

Boles, J. R. and Coombs, D. S., 1975. Mineral reactions in zeolite Triassic tuff, Hokonui Hills, New Zealand. Geol. Soc. Am. Bull., 86, 163–173.

Boles, J.R. and Wise, W.S., 1977. Nature and origin of deep-sea clinoptilolite. L.B. Sand and E. A. Mumpton (Eds.), In: Natural Zeolites: Occurrence, Properties, Use. Pergamon Press, 235–243.

Bray, L.A. and Fullam, H.T., 1971. Recovery and purification of cesium-137 from Purex waste using synthetic zeolites. R.E. Gould (Ed.). In: Molecular Sieve Zeolites, Advances in Chemistry Series 101, Am. Chem. Soc., 450–455.

Brown, C.E. and Thayer, T.P., 1963. Low-grade mineral facies in upper Triassic and lower Jurassic rocks of the Aldrich Mountains, Oregon. J. Sed. Petrol., 33, 411–425.

Castano, J.R. and Sparks, D.M., 1974. Interpretation of vitrinite reflectance measurements in sedimentary rocks and determination of burial history using vitrinite reflectance and authigenic minerals. Geol. Soc. Am. Spec. Paper 153, 31–52.

Chermak, J.A., 1992. Low temperature experimental investigation of the effect of high pH NaOH solutions on the Opalinus Shale, Switzerland. Clays and Clay Minerals, 40, 650–658.

Chermak, J.A., 1993. Low temperature experimental investigation of the effect of high pH KOH solutions on the Opalinus Shale, Switzerland. Clays and Clay Minerals, 41, 365–372.

Chermak, J.A. and Rimstidt, J.D., 1989. Estimating the thermodynamic properties (ΔGf° and ΔHf°) of silicate minerals at 298 K from the sum of polyhedral contributions. Am. Min., 74. 1023–1031.

Coombs, D.S., 1954. The nature and alteration of some Triassic sediments from Southland, New Zealand. Trans. Royal Soc. New Zealand, 82, 65–109.

Coombs, D.S., Ellis, A.J., Fyfe, W.S. and Taylor, A.M., 1959. The zeolite facies, with comments on the interpretation of hydrothermal syntheses. Geochim. Cosmochim. Acta, 17, 53–107.

Dibble, W.E. and Tiller, W.A., 1981. Kinetic model of zeolite paragenesis in tuffaceous sediments. Clays and Clay Minerals, 29, 323–330.

Dickinson, W.R., 1962. Petrology and diagenesis of Jurassic andesitic strata in central Oregon. Am. J. Sci., 260, 481–500.

Dickinson, W.R., Ojakangas, R.W. and Stewart, R. J., 1969. Burial metamorphism of the late Mesozoic Great Valley sequence, Cache Creek, California. Geol. Soc. Am. Bull., 80, 519–526.

Donahoe, R.J., Liou, J.G. and Guldman, S., 1984. Synthesis and characterization of zeolites in the system Na_2O-K_2O-$A1_2O_2$-SiO_2-H_2O. Clays and Clay Minerals, 32, 433–443.

Donahoe, R.J. and Liou, J.G., 1985. An experimental study on the process of zeolite formation. Geochim. Cosmochim. Acta, 49, 2349–2360.

Eikenberg, J., 1990. On the problem of silica solubility at high pH. Nagra Tech. Rep. (NTB 90-36), Nagra, Wettingen, Switzerland.

Fritz, B., Made, B. and Tardy, Y., 1988. Geochemical modelling of the evolution of a granite-concrete-water system around a repository for spent nuclear fuel. SKB Tech. Rep. (TR 88-18), SKB, Stockholm, Sweden.

Galloway, W.E., 1974. Depositional and diagenetic alteration of sandstone in northeast Pacific arc-related basins: implications for greywacke genesis. Geol. Soc. Am. Bull., 85, 379–390.

Garrels, R.M. and Christ, C.L., 1965. Solutions, Minerals and Equilibtia. Harper & Row, New York.

Giggenbach, W.F., 1984. Mass transfer in hydrothermal alteration systems. Geochim. Cosmochim. Acta, 48, 2693–2711.

Giggenbach, W.E., 1988. Geothermal solute equilibria. Derivation of Na-K-Mg-Ca geoindicators. Geochim. Cosmochim. Acta, 52, 2749–2765.

Gottardi, G., 1977. Mineralogy and crystal chemistry of zeolites. L.B. Sand and E.A. Mumpton (Eds.), In Natural Zeolites: Occurrence, Properties, Use. Pergamon Press, 31–44.

Hawkins, D.B.,1981. Kinetics of glass dissolution and zeolite formation under hydrothermal conditions. Clays and Clay Minerals, 29, 331–340.

Hawkins, D.B., Sheppard, R.A. and Gude, A. J., 1977. Hydrothermal synthesis of clinoptilolite and comments on the assemblage phillipsite-clinoptilolite-mordenite. L.B. Sand and E.A. Mumpton (Eds.), In Natural Zeolites: Occurrence, Properties, Use. Pergamon Press, 337–343.

Hay, R.L., 1964. Phillipsite of saline lakes and soils. Am. Min., 49, 1366–1387.

Hay, R.L., 1977a. Geology of zeolites in sedimentary rocks. In Mineralogy and Geology of Natural Zeolites. Min. Soc. Am. Short Course Notes, 53–64.

Hay, R.L., 1977b. Geologic occurrence of zeolites. L.B. Sand and E.A. Mumpton (Eds.), In Natural Zeolites: Occurrence, Properties, Use. Pergamon Press, 135–3143.

Hay, R.L., 1986. Geologic occurrence of zeolites and some associated minerals. Pure and Appl. Chem., 58, 1339–1342.

Hayhurst, D.T. and Sand, L.B., 1977. Crystallization kinetics and properties of Na, K-phillipsites. J.R. Katzer (Ed.), In: Molecular Sieves II, Am. Chem. Soc. Symp. Ser., 40, 219–232.

Helmold, K. P. and van de Kamp, P.C., 1984. Diagenetic mineralogy and controls on albitization and laumontite formation in Paleogene arkoses, Santa Ynez Mountains, California. D.A. McDonald and R.C. Surdam, In: Clastic Diagenesis, Am. Assoc. Pet. Geol. Mem., 37, 239–276.

Holler, H. and Wirsching, U., 1977. Experiments on the formation of zeolites by hydrothermal alteration of volcanic glasses. L.B. Sand and E.A. Mumpton (Eds.), In Natural Zeolites: Occurrence, Properties, Use. Pergamon Press, 329–336.

Honda, S. and Muffler, L.J.P., 1970. Hydrothermal alteration in core from research drill hole Y-1, Upper Geyser Basin, Yellowstone National Park, Wyoming. Am. Min., 55, 1714–1737.

Iijima, A., 1977. Geological occurrences of zeolite in marine environments. L.B. Sand and E.A. Mumpton (Eds.), In Natural Zeolites: Occurrence, Properties, Use. Pergamon Press, 175–198.

Kastner, M. and Stonecipher, S.P., 1977. Zeolites in pelagic sediments of the Atlantic, Pacific and Indian Oceans. L.B. Sand and E.A. Mumpton (Eds.), In Natural Zeolites: Occurrence, Properties, Use. Pergamon Press, 199–220.

Knauss, K.G., Delany, J.M., Beiriger, W.J. and Peifer, D.W., 1986. Hydrothermal interaction of Topopah Spring Tuff with J-13 water as a function of temperature. In: Scientific Basis for Nuclear Waste Management, M.R.S., 539–546.

Knauss, K.G., 1987. Zeolitization of glassy Topopah Spring Tuff under hydrothermal conditions. In Scientific Basis for Nuclear Waste Management, M.R.S., 737–745.

Kristmannsdottir, H. and Tomasson, J., 1977. Zeolite zones in geothermal areas in Iceland. L.B. Sand and E.A. Mumpton (Eds.), In: Natural Zeolites: Occurrence, Properties, Use. Pergamon Press, 277–284.

Lichtner, P.C. and Eikenberg, J., 1994. Propagation of a hyperalkaline plume into the geological barrier surrounding a radioactive waste repository. Nagra Tech. Rep. (NTB 93-16), Nagra, Wettingen, Switzerland.

Linklater, C.M. (Ed.), 1998. A natural analogue study of cement-buffered, hyperalkaline groundwaters and their interaction with a repository host rock: Phase II. Nirex Science Report, S/98/003, Nirex, Harwell, U.K.

Mariner, R.H. and Surdam, R.C., 1970. Alkalinity and formation of zeolites in saline, alkaline lakes. Science, 170, 977–980.

Mercer, B.W and Ames, L.L., 1977. Zeolite ion exchange in radioactive and municipal wastewater treatment. L.B. Sand and E.A. Mumpton (Eds.), In: Natural Zeolites: Occurrence, Properties, Use. Pergamon Press, 451–462.

Merino, E. (1975) Diagenesis in Tertiary sandstones from Kettleman North Dome, California. I. Diagenetic mineralogy Petrol. Journal of Sedimentary Petrology 45, 320–336.

Miller, W.M., Alexander, W.R., Chapman, N.A., McKinley, I.G. and Smellie, J.A.T., 1994. Natural Analogue Studies in the Geological Disposal of Radioactive Wastes. Elsevier.

Milodowski, A.E., George, I.A., Bloodworth, A.J. and Robins, N.S., 1985. Reactivity of Ordinary Portland Cement (OPC) grout and various lithologies from the Harwell Research Site. British Geological Survey Report (FLPU 85- 15), Keyworth, U.K.

Mumpton, F.A., 1977. Natural zeolites. In: Mineralogy and Geology of Natural Zeolites. Min. Soc. Amer. Short Course Notes, 1-17.

Murphy, W.M. and Pabalan, R.T., 1994. Geochemical investigations related to the Yucca Mountain environment and potential nuclear waste repository. U.S. N.R.C. Rep. (NUREG/CR-6288), Washington, USA.

Pabalan, R.T., 1994. Thermodynamics of ion exchange between clinoptilolite and aqueous solutions of Na/K and Na/Ca. Geochim. Cosmochim. Acta., 58, 4573-4590.

Ragnarsdottir, K.V., 1993. Dissolution kinetics of heulandite at pH 2-12 and 25°C. Geochim. Cosmochim. Acta, 57, 2439-2449.

Savage, D., Cave, M.R., Haigh, D. and George, I.A., 1986. Dissolution kinetics of laumontite at 150 C, 50 MPa and the relevance to models of mass transfer during diagenesis and low-grade metamorphism. Pro. Fifth Int. Symp. on Water-Rock Interaction, Reykjavik, Iceland, 485-488.

Savage, D., Cave, M.R., Haigh, D., Milodowski, A.E. and Young, M.E.,1993. The reaction kinetics of laumontite under hydrothermal conditions. Euro. J. Min., 5, 523–535.

Savage, D. and Rochelle, C.A., 1993. Modelling reactions between cement pore fluids and rock: Implications for porosity change. J. Contam. Hydrol., 13, 365–378.

Savage, D., 1997. Review of the potential effects of alkaline plume migration from a cementitious repository for radioactive waste. Implications for performance assessment. UK Environment Agency R&D Technical Report P60, London, U.K.

Seki, Y., Onuki, H., Okumara, K. and Takashima, I., 1969. Zeolite distribution in the Katayama geothermal area, Onikobe, Japan. Jap. J. Geol. Geog., 40, 63–79.

Semmens, M.J. and Seyfarth, M., 1977. The selectivity of clinoptilolite for certain heavy metals. In: Natural Zeolites. Occurrence, Proper-ties, Use. L.B. Sand and E.A. Mumpton (Eds.), In: Natural Zeolites: Occurrence, Properties, Use. Pergamon Press, 517–526.

Sheppard, R.A. and Gude, A.J., 1969. Diagenesis of tuffs in the Barstow Formation, Mud Hills, San Bernardino County, California. U.S. Geol. Surv. Prof. Paper 634.

Sheppard, R.A. and Gude, A.J., 1973. Zeolites and associated authigenic silicate minerals in tuffaceous rocks of the Big Sandy Formation, Mohave County, Arizona. U.S. Geol. Surv. Prof. Paper 830.

Sheppard, R.A., Gude, A.J. and Fitzpatrick, J.J., 1988. Distribution, characterization, and genesis of mordenite in Miocene silicic tuffs at Yucca Mountain, Nye County, Nevada. U. S. Geol. Surv. Bull. 1777.

Steiner, A., 1953. Hydrothermal rock alteration at Wairakei, New Zealand. Econ. Geol., 48, 1–13.

Stewart, R.J., 1974. Zeolite facies metamorphism of sandstone in the western Olympic Peninsula, Washington. Geol. Soc. Amer. Bull., 85, 1139–1142.

Surdam, R.C., 1973. Low-grade metamorphism of tuffaceous rocks in the Karmutsen Group, Vancouver Island, British Columbia. Geol. Soc. Amer. Bull., 84, 1911–1922.

Surdam, R.C., 1977. Zeolites in closed hydrologic systems. In: Mineralogy and Geology of Natural Zeolites. Min. Soc. Amer. Short Course Notes, 65–91.

Surdam, R.C. and Sheppard, R.A., 1977. Zeolites in saline, alkaline-lake deposits. L.B. Sand and E.A. Mumpton (Eds.), In: Natural Zeolites: Occurrence, Properties, Use. Pergamon Press, 145–174.

Taylor, M.W. and Surdam, R.C., 1981. Zeolite reactions in the tuffaceous sediments at Teels Marsh, Nevada. Clays and Clay Minerals, 29, 341-352.

Tsitsishvili, G.V, Andronikashvili, TG., Kirov, G.N. and Filizova, L.D., 1993. Natural Zeolites. Ellis Horwood, New York.

Ueda, S., Murata, H., Koizumi, M. and Nishimura, H., 1980. Crystallization of mordenite from aqueous solutions. Amer. Min., 65, 1012–1019.

Valcke, E. and Cremers, A., 1995. Sorption of radionuclides by natural zeolites: A critical literature survey on the sorption properties of seven selected zeolites. Unpubl. Nagra Int. Rep., Nagra, Wettingen, Switzerland.

Weres, O., Yee, A. and Tsao, L., 1982. Equations and type curves for predicting the polymerization of amorphous silica in geothermal brines. Soc. Petrol. Eng. J., 3, 9–16.

Wise, W.S. and Tschernich, R.W., 1977. Dachiardite-bearing zeolite assemblages in the Pacific Northwest. L.B. Sand and E.A. Mumpton (Eds.), In: Natural Zeolites: Occurrence, Properties, Use. Pergamon Press, 105–111.

Wolery, T.J., 1992. The EQ3/6 package overview and installation guide (version 7.0). Lawrence Livermore Nat. Lab. Rep. (UCRL-MA-110662PT-I.)

TABLES

Table 8-1. Compositions of brines at Deep Springs Valley, California and Lake Magadi, Kenya (concentrations in mg/L). From Surdam (1977).

	Deep Springs	Lake Magadi
pH	9.6	10.3
SiO_2	301	661
Na	99 650	83 109
K	17 550	1 167
HCO_3	9 000	8 876
CO_3	18 950	64 100
SO_4	47 350	1 925
Cl	11 000	49 772
TDS	300 000	210 000

Table 8-2. The main compositional features of zeolites in sedimentary rocks. From Hay (1977a).

Zeolite	$Si/(Al + Fe^{3+})$	Dominant Cations
clinoptilolite	4.0–5.1	K > Na
mordenite	4.3–5.3	Na > K
heulandite	2.9–4.0	Ca, Na
erionite	3.0–3.6	Na, K
chabazite	1.7–3.8	Ca, Na
phillipsite	1.3–3.4	K, Na, Ca
analcime	1.7–2.9	Na
laumontite	2.0	Ca
warakite	2.0	Ca
natrolite	1.5	Na

Table 8-3. Exchange capacities of some zeolites. From Barrer (1977) and Valcke and Cremers (1995).

	Formula	Exchange Capacity meq/100 g
analcime	$Na[AlSi_2O_6].H_2O$	450
chabazite	$(Ca_{0.5}, Na)[AlSi_2O_6].3H_2O$	400
clinoptilolite	$Na_6[Al_6Si_{30}O_{72}].24H_2O$	230–330
dachiardite	$Na_5[Al_5Si_{19}O_{48}].12H_2O$	450
edingtonite	$Ba[Al_2Si_3O_{10}].4H_2O$	390
faujasite	$(Ca, Na_2)[Al_2Si_5O_{14}].6.6H_2O$	390
gmelinite	$(Ca_{0.5}, Na)[AlSi_2O_6].3H_2O$	400
harmotome	$(K_2, Ba)[Al_2Si_5O_{14}].5H_2O$	390
heulandite	$Ca[Al_2Si_6O_{16}].5H_2O$	330
levynite	$Ca[Al_2Si_4O_{12}].6H_2O$	400
mordenite	$(Ca_{0.5}, Na)[AlSi_5O_{12}].3.3H_2O$	230
natrolite	$Na_2[Al_2Si_3O_{10}].2H_2O$	530
phillipsite	$(Ca_{0.5}, Na, K)_6[Al_6Si_{10}O_{32}].12H_2O$	340–510
scolecite	$Ca[Al_2Si_3O_{10}].3H_2O$	500
stilbite	$(Na, Ca_{0.5})[AlSi_3O_8].3H_2O$	320
thomsonite	$NaCa_2[Al_5Si_5O_{20}] .6H_2O$	620

Table 8-4. Estimate of pore fluid composition in equilibrium with zeolites calculated with the program EQ3, as compared with sample M5 of the Western Springs hyperalkaline groundwaters.

	M5	EQ3 Simulation	
	mg/L	Mineral controls	mg/L
pH	12.7	charge balance	9.5
Na	129	mordenite	524
Ca	1067	laumontite	1.7
Al	<0.2	kaolinite	0.01
SiO_2	0.15	chalcedony	2476
HCO_3	20.1	calcite	108

FIGURES

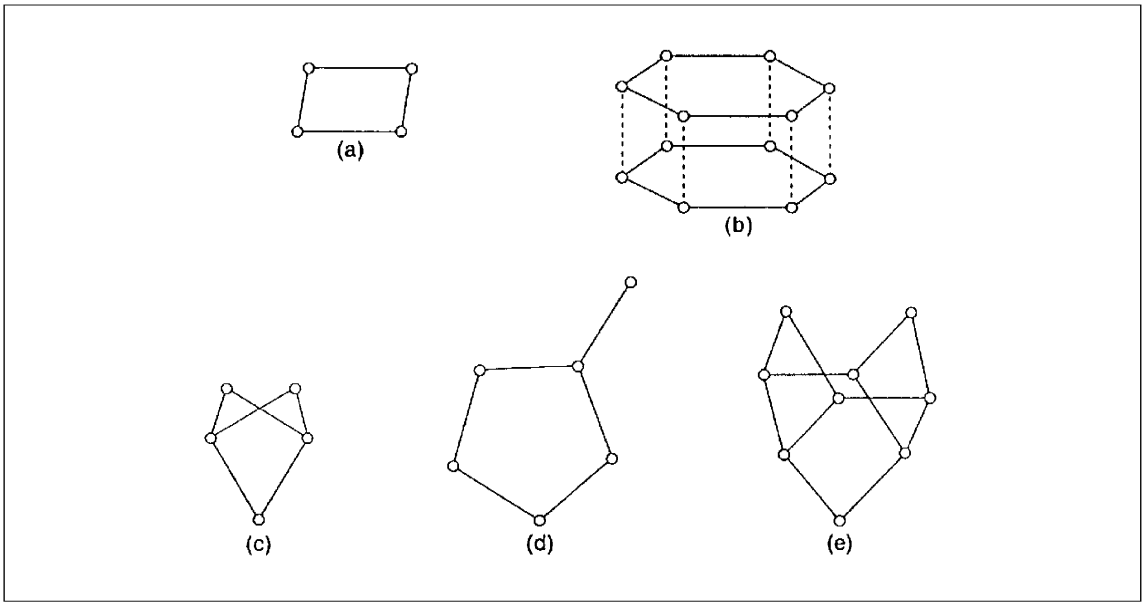

Figure 8-1. *The secondary building units ('SBU's') of zeolites. a is the single 4 ring; b the 6 ring (single or double); c the natrolite unit; d the mordenite unit; and e the stilbite unit. From Gottardi (1977).*

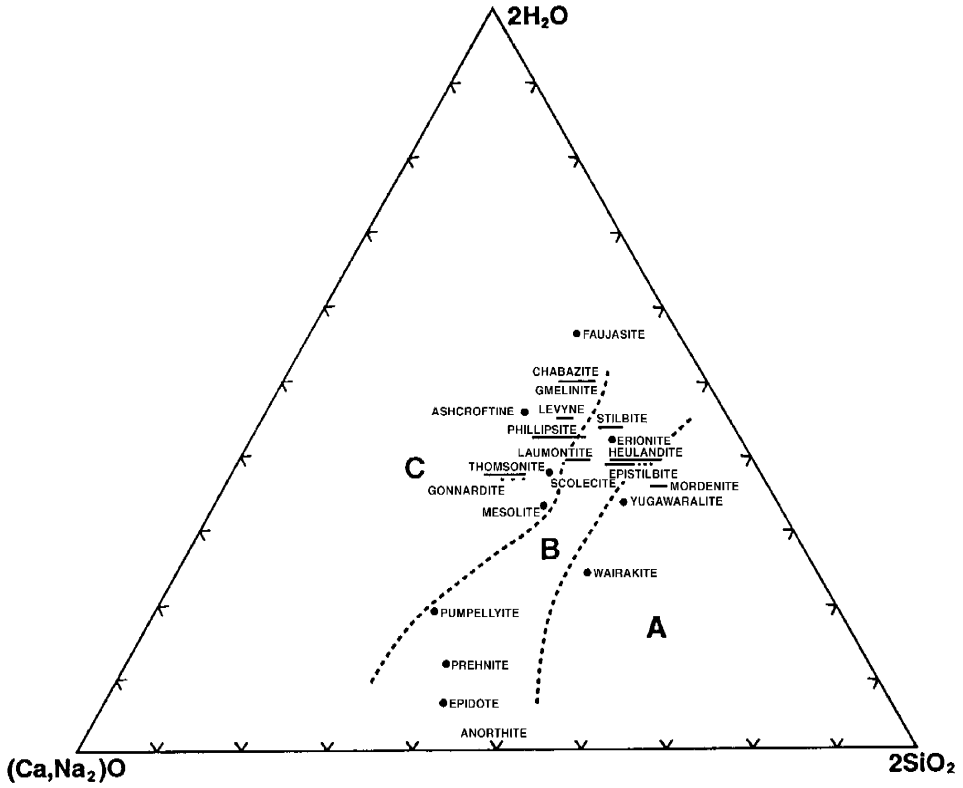

Figure 8-2. *Composition of zeolites [from Booms et al., 1959]. A: zeolites favoured by silica supersaturation. B: zeolites which commonly coexist with quartz. C: zeolites favoured by silica undersaturation.*

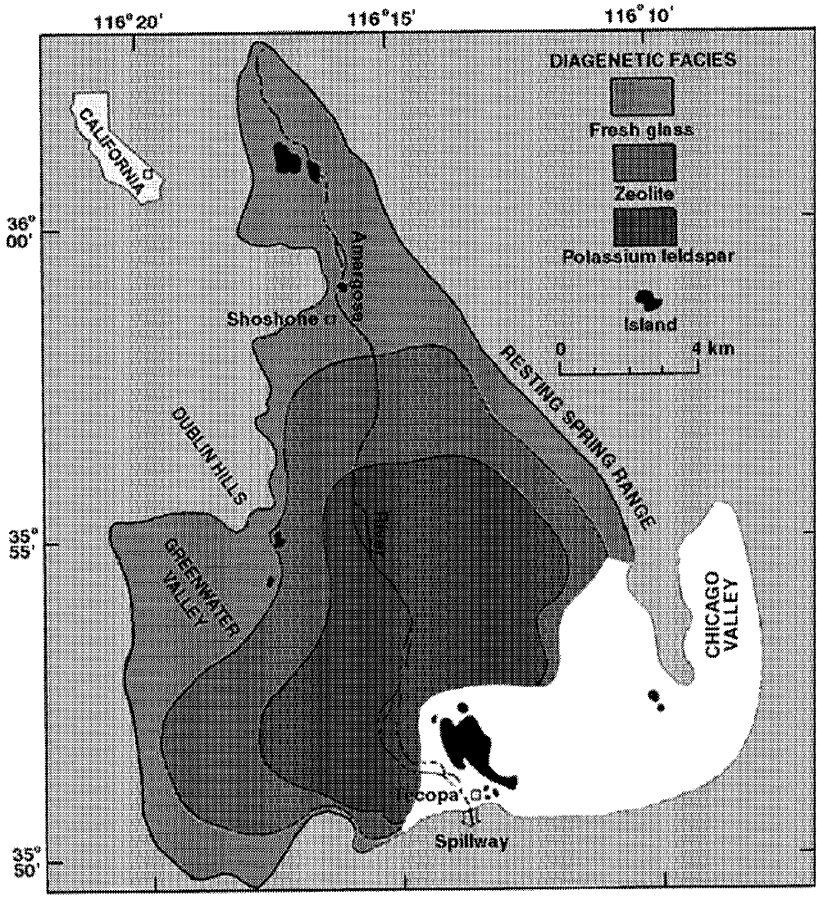

Figure 8-3. *Map of ancient Lake Tecopa near Shoshone, California, showing diagenetic facies for a composite of all the tuff beds in the deposit. From Surdam and Sheppard (1977).*

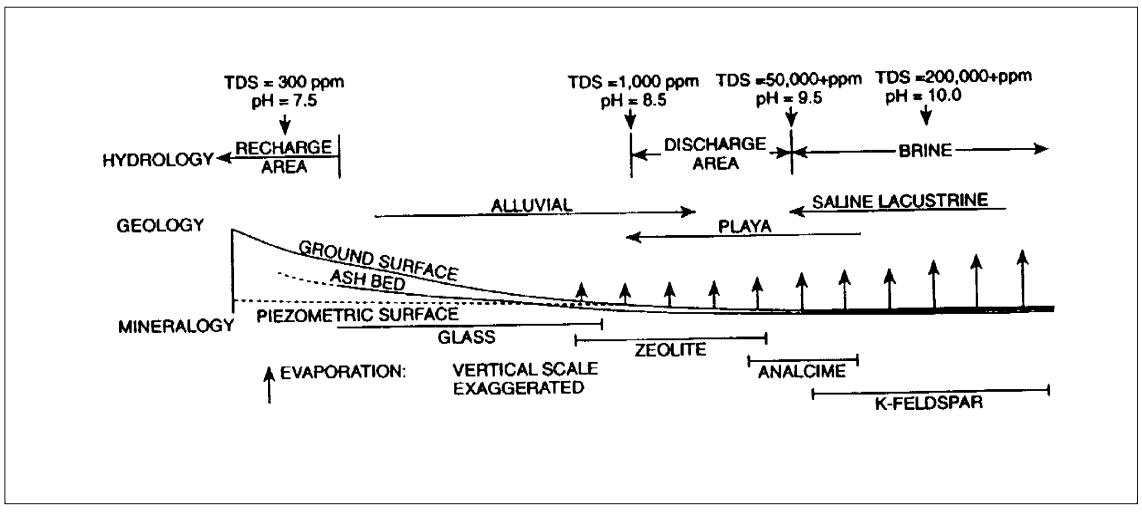

Figure 8-4. *Schematic cross-section of a saline, alkaline lake, showing the zonation of pore fluid composition and diagenetic mineralogy. From Surdam and Sheppard (1977).*

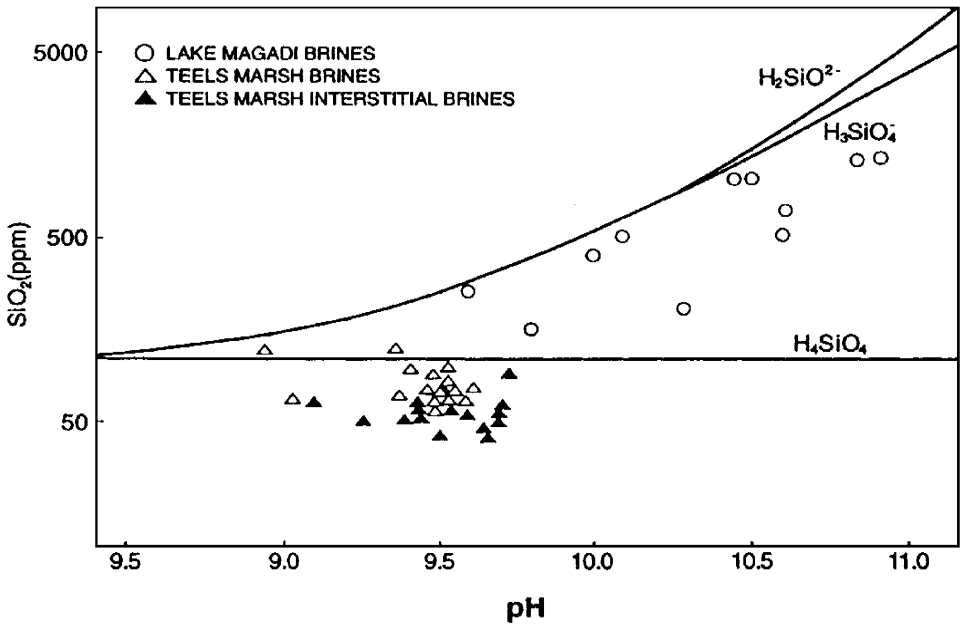

Figure 8-5. *Relationship between pH and silica for brines from Teels Marsh, Nevada and Lake Magadi, Kenya. From Taylor and Surdam (1981).*

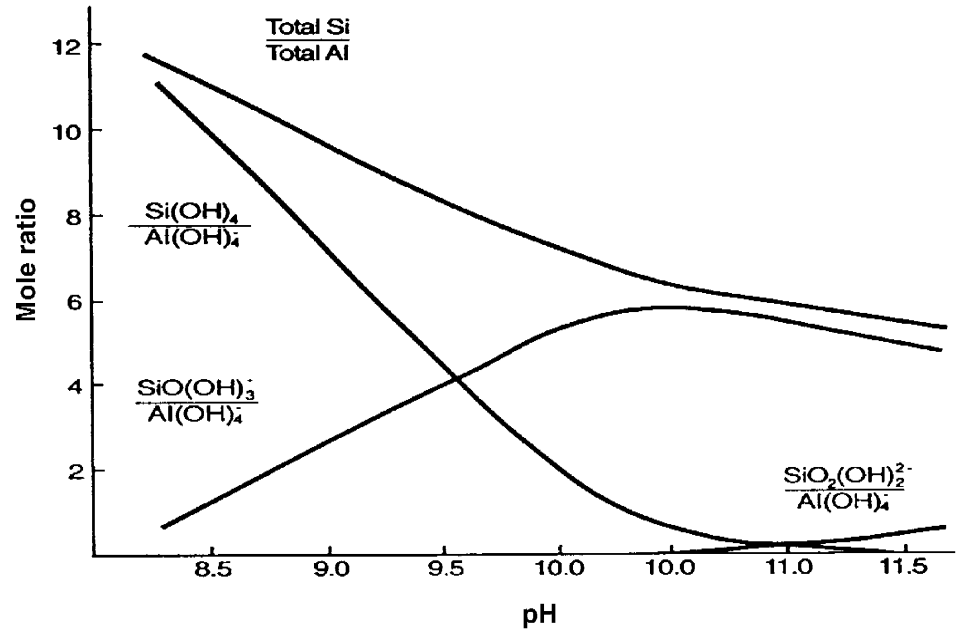

Figure 8-6. *Mole ratio of total silica to total alumina, and of various silica species in solution to the alumina species in solution as a function of pH. From Mariner and Surdam (1970).*

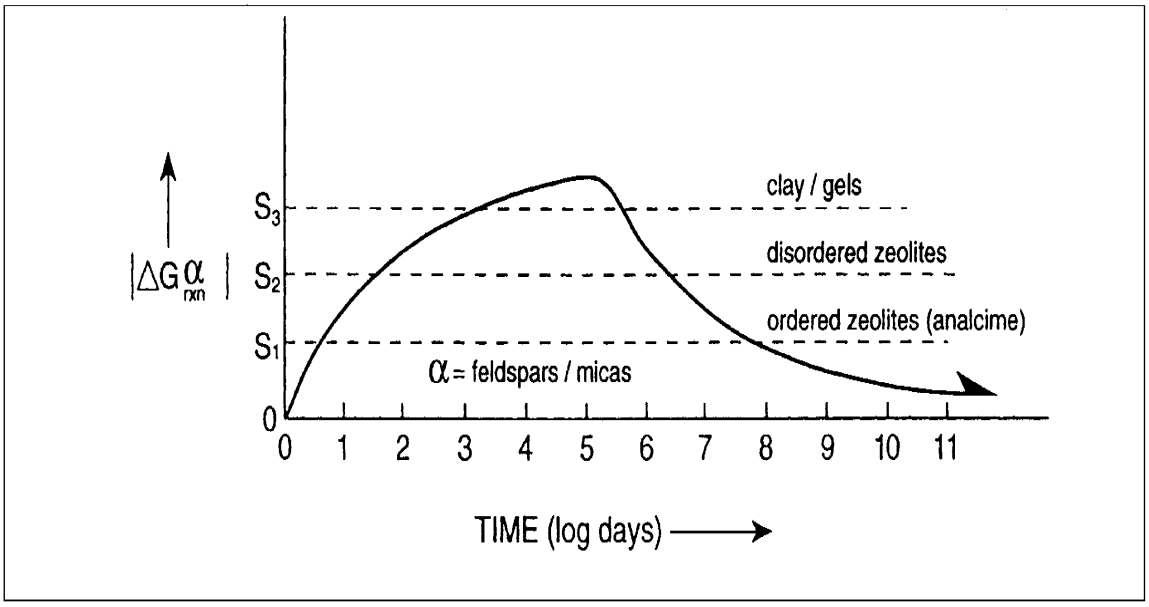

Figure 8-7. *Absolute value of the departure from equilibrium versus the time of reaction forming the stable phase α in tuffaceous rocks. Phase α may be a fully ordered feldspar, mica or quartz. The duration of the crystallisation of authigenic assemblages is determined by the intersection of supersaturation levels (S_1, S_2, S_3) indicated below each assemblage with the curve representing the time-dependence of the reaction driving force. From Dibble and Tiller (1981).*

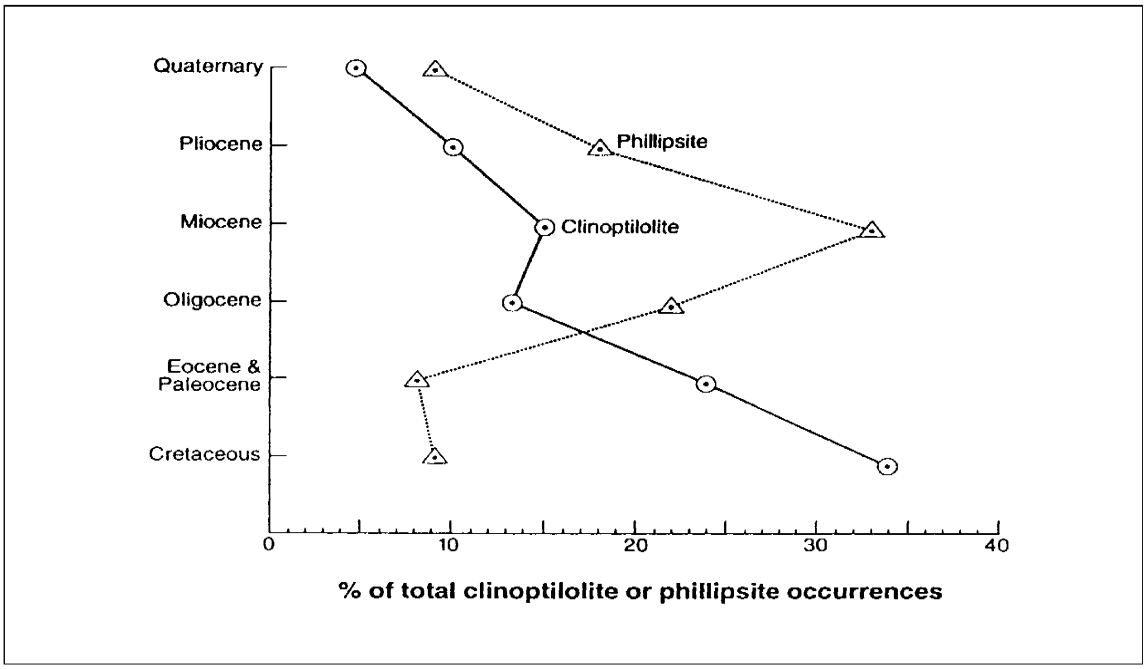

Figure 8-8. *Distribution of deep-sea phillipsite and clinoptilolite samples with respect to the age of the sediment. From Boles (1977b).*

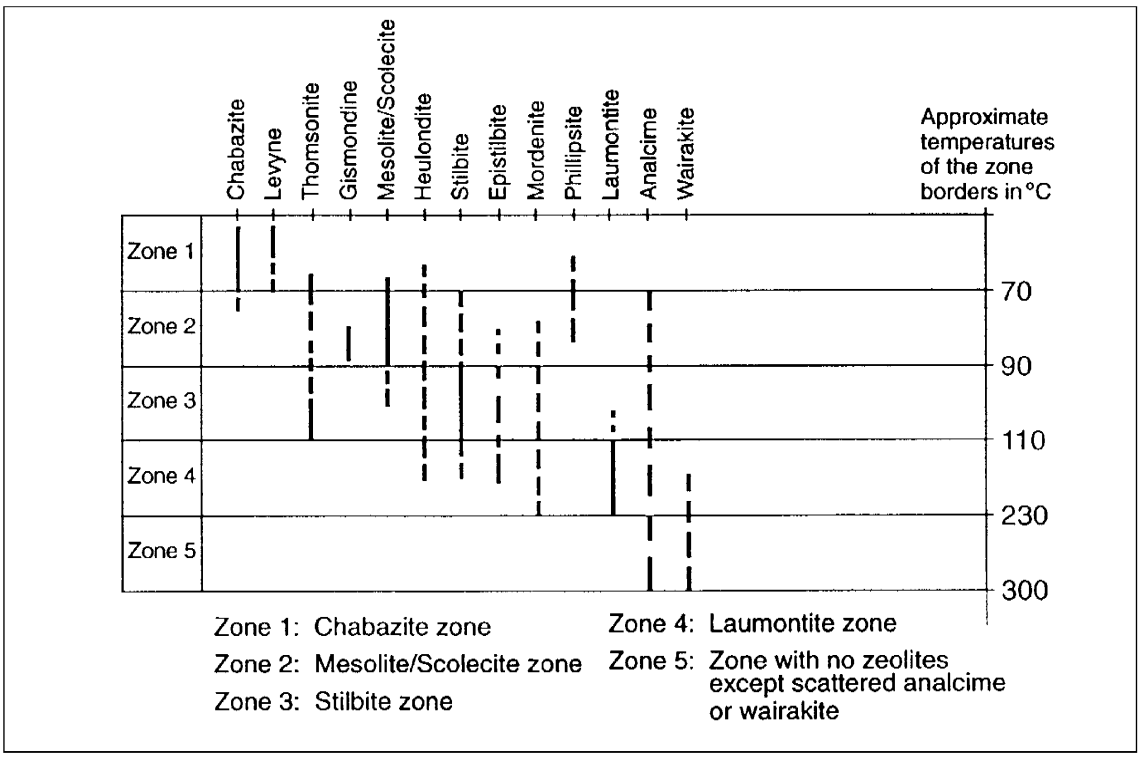

Figure 8-9. *Zeolite zones found in Icelandic geothermal areas. From Kristmannsdottir and Tomasson (1977).*

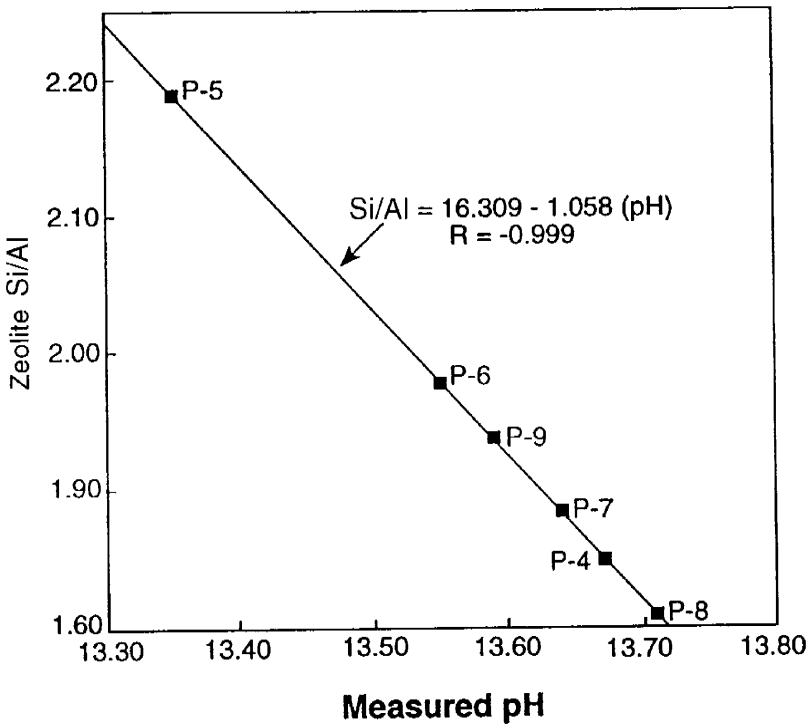

Figure 8-10. *Plot of zeolite Si/Al ratio as a function of measured solution pH. From Donahoe and Liou (1985).*

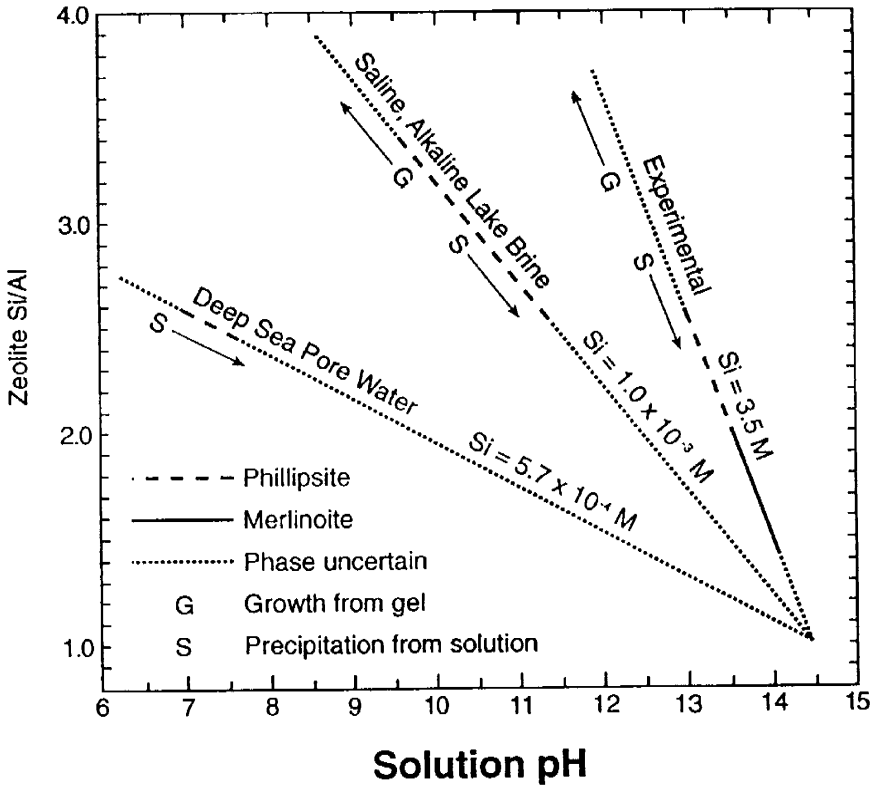

Figure 8-11. *Control of solution pH and total dissolved silica concentration on zeolite Si/Al ratio. From Donahoe and Liou (1985).*

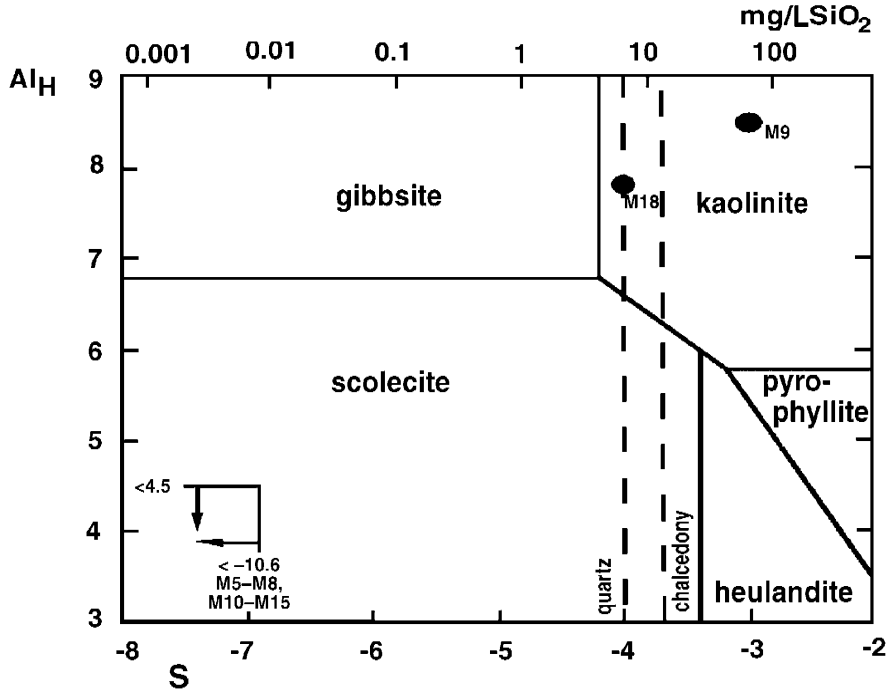

Figure 8-12. *The stability of calcium aluminosilicates as a function of* Al_H *(= log* $a_{Al^{3+}/(H^+)^3}$ *and S(= log* a_{SiO_2}*) at 25°C. Maqarin Western Springs groundwaters are indicated. Samples M5-M8 and M10-M15 have* Al_H *<4.5 and S <-10.6.*

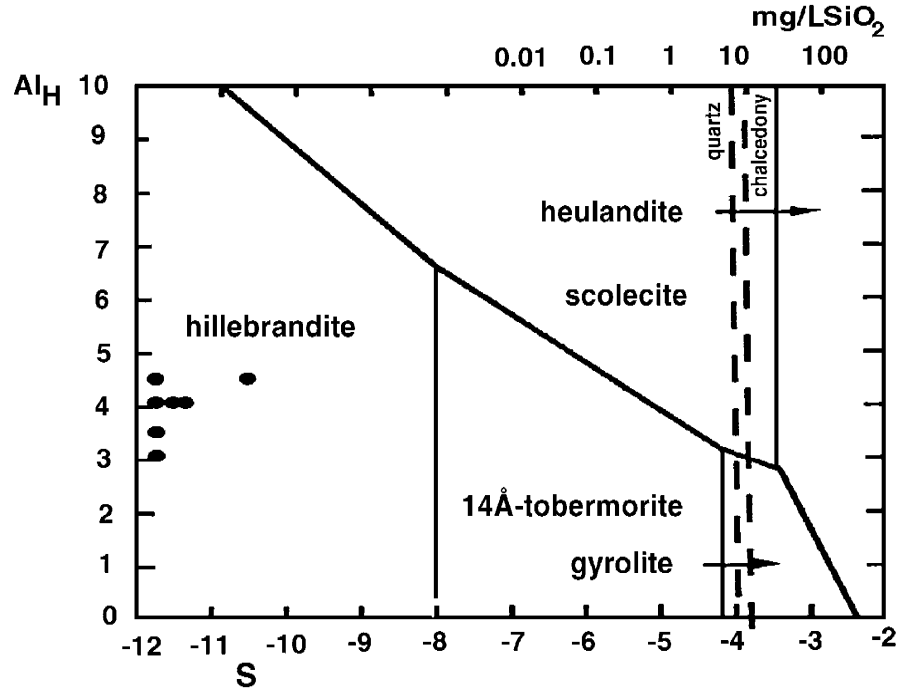

Figure 8-13. *The stability of calcium silicate hydrates and calcium aluminosilicates as a function of* Al_H *(= log* $a_{Al^{3+}/(H^+)^3}$ *and S(= log* a_{SiO_2}*) at 25°C. Maqarin Western Springs groundwaters are indicated. Samples M5-M8 and M10-M15 have* Al_H *<4.5 and S <-10.6.*

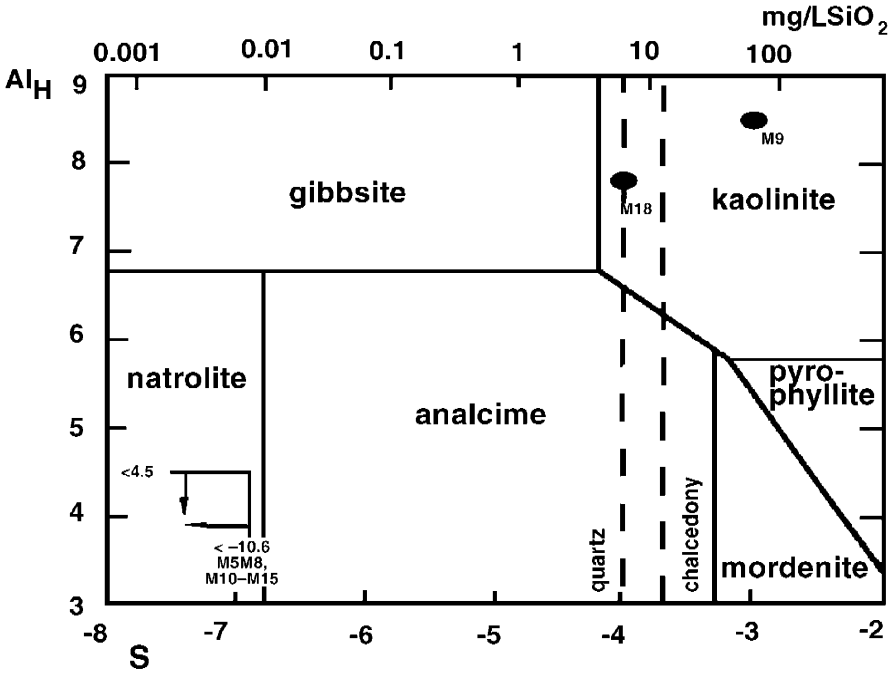

Figure 8-14. *The stability of sodium aluminosilicates as a function of* Al_H *(= log* $a_{Al^{3+}/(H^+)^3}$ *and S(= log* a_{SiO_2}*) at 25°C. Maqarin Western Springs groundwaters are indicated. Samples M5-M8 and M10-M15 have* Al_H *<4.5 and S <-10.6.*

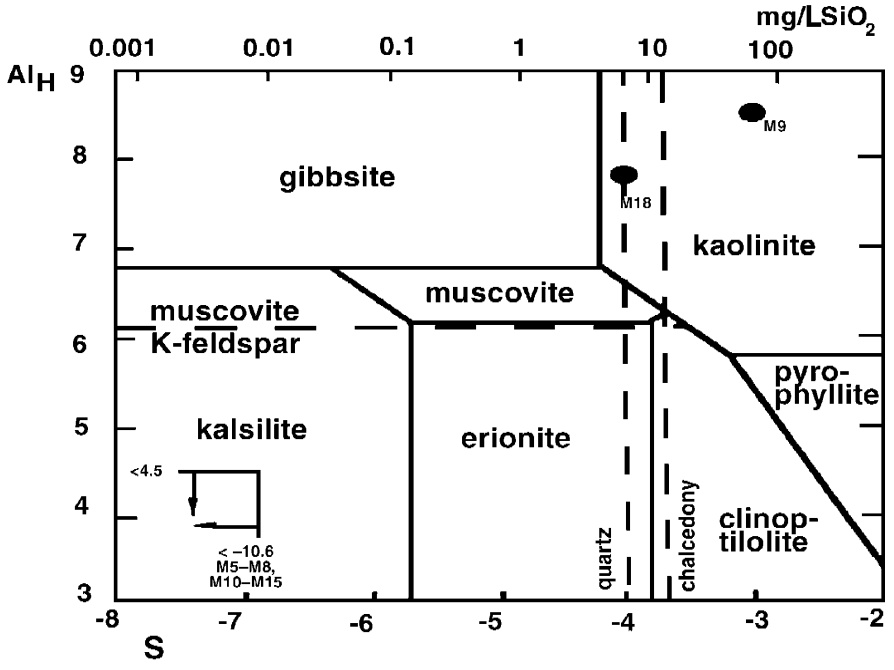

Figure 8-15. *The stability of potassium aluminosilicates as a function of* Al_H *(= log* $a_{Al^{3+}/(H^+)^3}$ *and S(= log* a_{SiO_2}*) at 25°C. Kalsilite, erionite and clinoptilolite are metastable relative to muscovite and K-feldspar (dashed stability fields). Maqarin Western Springs groundwaters are indicated. Samples M5-M8 and M10-M15 have* Al_H *<4.5 and S <-10.6.*

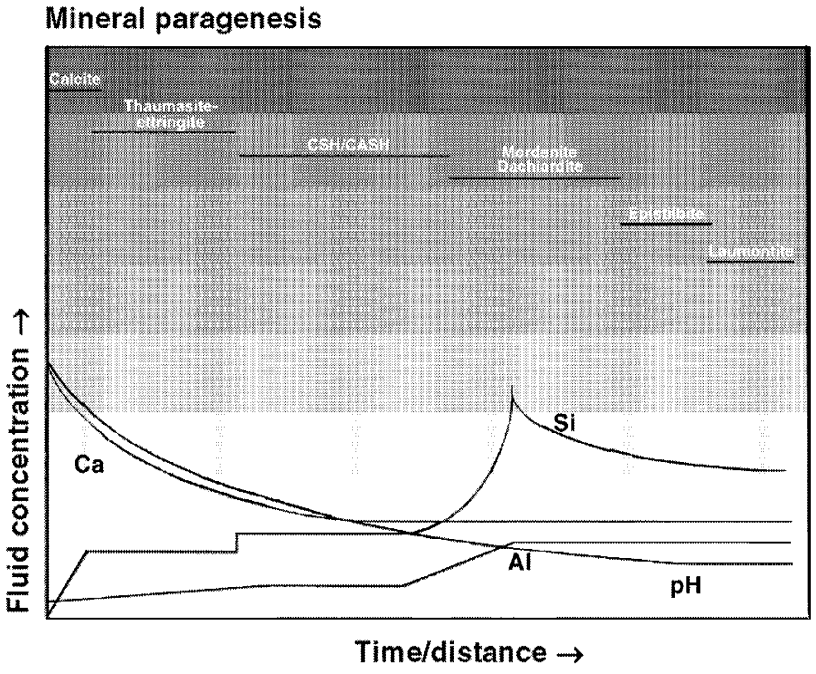

Figure 8-16. *Schematic diagram of mineral paragenesis and fluid composition evolution within a single fracture in the Maqarin alteration system.*

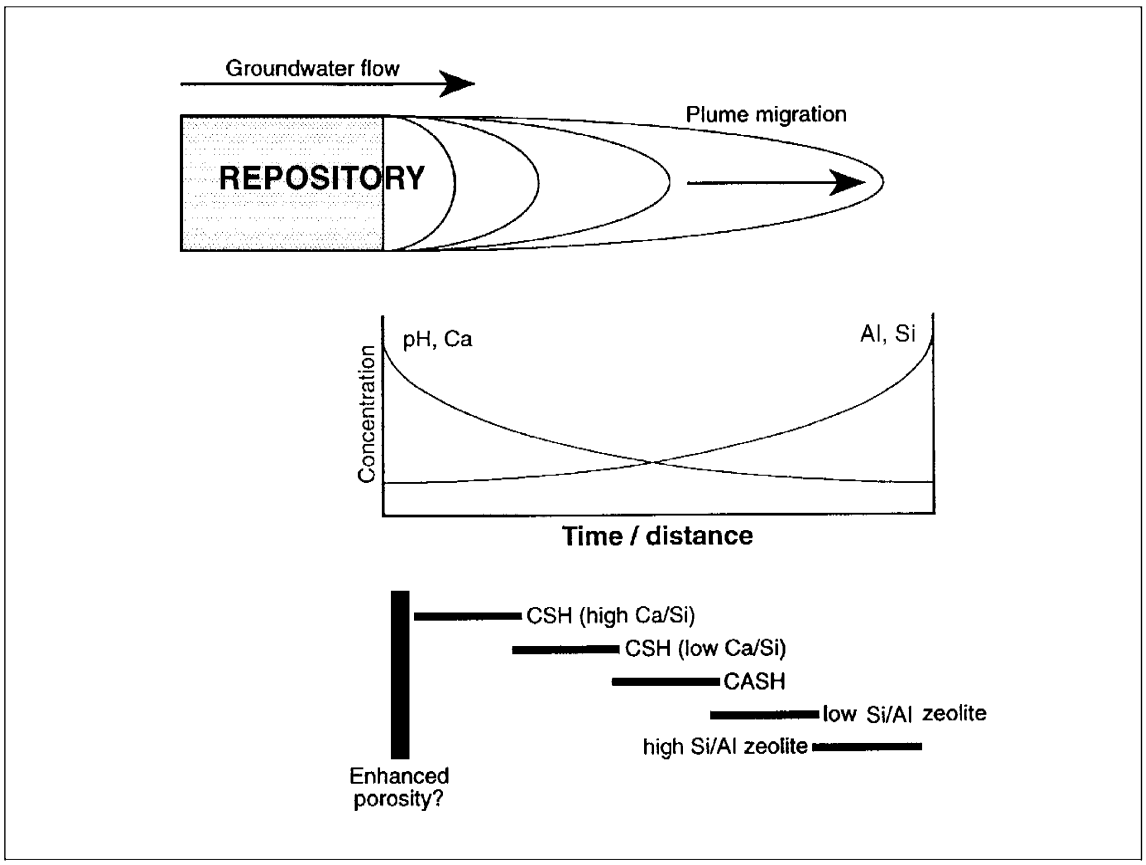

Figure 8-17. *Schematic diagram of hyperalkaline plume migration from a cementitious repository for radioactive wastes, showing hypothesised variations in fluid composition and alteration mineralogy in space and time.*

9 ORGANIC CHEMISTRY OF THE BITUMINOUS MARLS

(S. Geyer, J.Pörschmann, G. Hanschman, W. Geyer, F-D. Kopinke, W. Boehlmann and P. Fritz)

9.1 ORGANIC COMPOSITION OF THE BITUMINOUS MARLS

9.1.1 Sample Description

Two different rock specimens from the Bituminous Marl Formation were investigated. The first specimen, an unaltered marl (sample no. C355; A.E. Milodowski, per. comm., 1996; see Appendix E), was collected in the Adit A-6 close to the entrance. The second specimen, an altered marl, derives also from Adit A-6, close to a thermally altered shear zone.

9.1.2 Methods

The chemistry of the specimens was characterised using the following methods:

Thermoanalytical Measurements:

- Thermogravimetry;
- In-Source-Pyrolysis-Mass Spectrometry.

Chemical Characterisation:

- Elemental analysis;
- ICP analysis;
- IR spectroscopy;
- ^{13}C-NMR-Spectroscopy;
- Accelerated solvent extraction using:
  – an methylated extract,
  – a non-methylated extract.

9.1.3 Results

Thermogravimetric Measurements (TGA)

The loss of weight with increasing temperature versus burning time for the altered and unaltered Bituminous Marl samples is shown in Figures 9-1 and 9-2; the experimental parameters are listed within the figures. The weight loss up to 120°C (0.68–0.81 wt%) is mainly attributed to the evaporation of water, but volatile hydrocarbons cannot be excluded completely, The unaltered marl sample contains about 10 wt% of volatile components (10 wt%; T_{max} = 438°C). The temperature range and the peak shape are characteristic of cracking reactions of non-volatile hydrocarbon polymers. The high temperature peak at 700°C can be attributed to the decomposition of carbonate. Only a small organic residue (0.82 wt%) was left after pyrolysis, which is burnt off at 750°C with air. This indicates highly aliphatic hydrocarbon polymers since otherwise a major portion of the pyrolysis residue would have formed. The altered marl sample has no cracking peak, which would be expected from its geologic history. The carbonate peak is slightly smaller than in the unaltered sample (22.25 wt% vs. 26.59 wt%), but of the same order of magnitude.

In-Source-Pyrolysis-Mass Spectrometry (ISP-MS)

Based on the results of the thermogravimetric experiments, only the unaltered marl sample was used in the present analysis. This technique applies the pyrolysis of the sample directly in front of the ion source of the mass spectrometer. In this way high boiling point components evaporate under high vacuum conditions (10^{-5} torr) thus avoiding transport limitations and surface losses, which would otherwise affect the detection of products in ordinary pyrolysis devices using carrier gas flow.

Figure 9-3 shows the total ion current (TIC) of the mass spectrometer versus the scan number and the reaction time (minutes), which are linearly correlated with the sample temperature. The graph shows three distinct peaks: an evaporation peak (<150°C), the cracking peak (446°C), and the carbonate decomposition peak (631°C). The cracking peak has the same maximum temperature as under atmospheric pressure (compare Fig. 9-1). This means that cracking reactions (but not evaporation of the cracking products) are rate controlling. The shift of the carbonate peak towards lower temperatures under vacuum conditions is plausible taking into account the pressure dependence of the reaction equilibrium ($CaCO_3 = CaO + CO_2$). It is remarkable that the evaporation peak was not observed in the TGA experiments. Apparently the high vacuum enables some high boiling point, volatile components to evolve from the sample already at relatively low temperatures, whereas these components do not evaporate in the carrier gas flow.

The pyrolysis products can be further characterised in the mass spectrometer by their mass to charge ratio (m/z). The first peak in Figure 9-3 contains mainly water (m/z = 17, 18) and paraffins (m/z = 43, 57, 71, 85). The signal at m/z = 149 is characteristic of the phthalate compound, which is a widespread component of plasticizers. The second peak (cracking peak at 446°C) shows a rather complex composition with many high molecular weight components (m/z up 350 AMU at least is covered). Characteristic markers of olefins (m/z = 41, 55, 69) and paraffin-type chains (m/z = 43, 57, 71, 85) are evident. A signal at m/z = 91 indicates the presence of alkylbenzenes. The homologous

series of signals at m/z = 97, 111, 125 and 139 could possibly be attributed to alkylnaphthenes.

Altogether, the complex mass spectrum is in conformity with cracking products of highly aliphatic hydrocarbon polymers. The carbonate decomposition peak consists of carbon dioxide (m/z = 44, 28, 16, 12) exclusively.

Elemental Analysis

The unaltered marl sample was ground in a mortar. One split of the sample was treated with 3N HCl to eliminate carbonates, washed with distilled water and freeze dried; the other split was measured directly using an elemental analyser. The results are shown in Table 9-1. Assuming that the hydrogen, nitrogen and sulphur contents remain stable in the HCl treated sample, an organic carbon content of the sample around 12 to 15 wt% can be calculated, which is in a good agreement with the thermocatalytic measurements.

ICP-AES Analysis

The ICP analysis of the unaltered marl sample are tabulated in Table 9-2.

IR Spectra

The pre-treatment was similar to that carried out for the elemental analysis measurements. Only the unaltered marl sample was analysed. Bands of carbonates (Ca, Ba) were dominant in addition to the aluminosilicate bands. The carbonate bands disappeared following treatment with HCl; additional new bands appeared which can be probably attributed to different modifications of alumina oxides.

^{13}C-NMR-Spectra

The ^{13}C-NMR-(CP-MAS)-spectra provide quantitative information concerning the chemical environment of carbon in organic molecules and therefore allow differentiation of aromatic, aliphatic and other molecular structures in the sample. The spectrum taken from the sample (Fig. 9-4) is dominated by a high content of paraffinic chains (about 55%). Around 30% can be attributed to O- and N-substituted carbons, whereas the aromatic part of the molecular structure contains only around 8 to 9%. The sum of carbonyl and carbonyl carbons amounts to approximately 6%.

The structural composition identified by NMR is not characteristic of water soluble compounds such as humic substances. Nevertheless, it cannot be ruled out that a portion of the organic matter may be soluble in a high pH environment and contribute to DOC or organic colloids in groundwater. This assumption still has to be checked experimentally. Earlier studies at Maqarin (Pettersson et al., 1993) indicated that humic substances were not present in the groundwaters, and it was considered doubtful as to whether they could exist in such a hyperalkaline environment.

Accelerated Solvent Extraction and GC/MS Detection

To investigate the type of organics that could be dissolved from the sample by alkaline water, an accelerated solvent extraction was carried out followed by GC/MS analysis after acidification and reextraction of the organics with benzene. As a result, less that 1 ppm of organics were detectable, mostly hydrocarbons (long chain alkanes) and some fatty acids. It seems to be obvious that only a very small part of the organic content of the rock can dissolve in the percolating high pH groundwaters at Maqarin.

An accelerated solvent extraction was then carried out using Toluene as a solvent at a pressure of 100 bar and a temperature of 150°C with an extraction time of 15 minutes. To quantify the dissolved organics, deuterated standards were added. Using this extraction mainly alkanes (n-C10 to n-C33) with about 60 ppm could be detected, whereas the amount of alkylbenzenes was below 1 ppm (see Table 9-3).

Among the alkanes, pristane and phytane were identified. They are typical markers of crude oil sources. The extract yields almost a pure alkane spectrum with no aromatic compounds.

A second toluene extract was derivatised (methylated) by BF_3/CH_3OH treatment to analyse fatty acids. The results are shown in Table 9-4; detected fatty acids account for about 1 400 ppm.

The fatty acid pattern shows a typical even-over-odd discrimination, meaning that the chain length of the fatty acids have only the even numbers of carbon. This is typical of a marine biological origin for the organics in the unaltered bituminous marl.

9.1.4 Summary

As can be seen from the ^{13}C-NMR spectra, non-aromatics are predominant in the Bituminous Marl samples; the aromatic amount is small (8–9%). TGA and ISP-MS experiments show a very small amount of volatile hydrocarbons (<0.5%) and around 12% of mostly aliphatic hydrocarbons with components like paraffins, olefins, alkylbenzenes and alkylnaphthenes, as well as and highly aliphatic hydrocarbon polymers. Only a small part (1–2 wt%) of organic compounds could be identified by the accelerated solvent extraction methods. Only a negligible portion (<<1 ppm) of low molecular weight organic compounds was extracted under strong alkaline conditions.

9.2 RESULTS OF THE CHARACTERISATION OF A WATER SAMPLE (WESTERN SPRINGS LOCATION M5)

9.2.1 General

The water sample was collected at the Western Springs location, M5, on November 24, 1996.

9.2.2 Inorganic Chemistry of the Water Sample

The physico-chemical parameters were measured in the laboratory about one week after sampling; chemical parameters were determined by IC, ICP-MS, and AAS. The results are summarised in Tables 9-5 and 9-6. The high alkaline (pH 12.35) M5 sample is dominated by an Ca-K-Na-CO_3-SO_4- chemistry; TDS is around 3 g/L. Remarkable is the high DOC content of around 8 mg/L which is a much higher concentration than can be found in the Adit A-6 sample sites.

The nature of DOC was characterised using the measurements described below.

9.2.3 Organic Chemistry of the Water Sample

Spectroscopic Measurements

To determine the amount of dissolved humics in the sample a rough test was carried out based on Habschmann (1991). The dissolved humics are shaken out into chloroform from the acidified, NaCl-saturated water sample using a small quantity of solid cetyl-pyridinium chloride. The result gave no indication of humic-like structures in the sample.

UV/VIS spectra of the sample (Fig. 9-5) show two distinct maxima which probably result from inorganic hydrate complexes. Figure 9-5 shows, for comparison, a fulvic acid from a shallow German groundwater with a comparable DOC content, and a sample of distilled water.

Furthermore, the fluorescent spectrum (Fig. 9-6) of the M5 water sample is not typical of dissolved humics in groundwater. The presence of small amounts of olefins or aromatics could be the reason for the type of spectrum obtained.

GC/MS Measurements

Dissolved organics were extracted with benzene from 25 ml of Western Springs (M5) water and analysed with the GC/MS. The results are listed in Table 9-7.

Around 10% of DOC compounds could be detected with this method. The remaining DOC should consist of higher molecular weight organic compounds. One common aspect between the bituminous marl and the M5 groundwater sample is the so-called even-over-odd discrimination of aliphatic chains which is, in both cases, a hint for the natural origin and evolution for these organics.

9.2.4 Summary

The relatively high DOC content in the groundwater sample from the Western Springs M5 site can hardly be explained alone by dissolution of organic matter from the marl material by the percolation of high alkaline waters because:

- solution experiments show that only a minor part of the organics in the host rock could dissolve in water, and
- aromatics are found in the DOC content of the water sample whereas the organic material is predominantly non-aromatic in the unaltered bituminous marl sample.

The DOC in the M5 water sample has no dissolved humics; this essentially confirms earlier studies reported by Pettersson et al., (1993). One possible explanation is that the main part of the high DOC content derives from dissolution of organics in the soil zone, which are then strongly altered during their passage through the high alkaline milieu in the aquifer.

The source of DOC could be defined by determining the ^{14}C age of the DOC in the water sample. DOC originating from the soil zone would have a measurable radiocarbon content, in contrast to DOC originating from the Bituminous Marl which is free of radiocarbon.

9.3 REFERENCES

Hanschmann, G., 1991. A simple extraction-spectrophotometric method for the estimation of dissolved humic substances in water. Acta Hydrochim. Hydrobiol., 19, 265–266.

Linklater, C.M. (Ed.), 1998. A natural analogue study of cement-buffered, hyperalkaline groundwaters and their interaction with a repository host rock: Phase II. Nirex Science Report, S/98/003, Nirex, Harwell, U.K.

Pettersson, C. and Allard, B., 1993. Humic substances in high-pH groundwaters from Maqarin, Jordan. Linköping Univ. Int. Rep.

TABLES

Table 9-1. Elemental analysis of the unaltered Bituminous Marl sample [wt%].

Sample	Carbon	Hydrogen	Nitrogen	Sulphur
Unaltered marl	24.75	2.04	0.50	2.49
Unaltered marl, HCl treated	56.85	5.97	1.62	9.67

Table 9-2. Trace metals analysed with ICP-AES from the unaltered Bituminous Marl sample [µg/g].

B	Al	Cr	Ni	Cu	Zn	As	Cd	Pb	Th	U
25	3900	530	200	65	500	15	50	2.5	0.6	23

Table 9-3. Toluene accelerated solvent extraction* of an unaltered Bituminous Marl.

Organic compound	Amount [ppm]	Organic compound	Amount [ppm]
nC10	0.22	nC22	1.71
nC12	.055	nC23	1.96
nC13	0.41	nC24	1.74
nC14	2.03	nC25	1.96
nC15	1.37	nC26	2.16
nC16	2.82	nC27	5.34
nC17	1.93	nC28	4.35
Pristane $C_{19}H_{50}$	1.53	nC29	7.03
nC18	2.39	nC30	6.50
Phytane $C_{20}H_{42}$	2.10	nC31	4.85
nC19	1.18	nC32	3.16
nC20	1.64	nC33	1.99
nC21	2.78	**Sum of alkanes**	**60.07**
		Sum of alkylbenzenes	**< 1**

* Solvent: Toluene, 150°C, extraction time 15 min.; Identification: GC/MS MSD HP5970B, ULTRA2, SCAN, 2 µl spitless, Inj. 280°C.

Table 9-4. Accelerated solvent extraction* of an unaltered Bituminous Marl – detection of fatty acids.

Organic compound	Amount [ppm]	Organic compound	Amount [ppm]
nC6 caproic acid	89.3	palmitoleic acid	42.4
nC7 heptanoic acid	56.7	nC16 palmitinic acid	281.2
nC8 caprylic acid	146.1	oelic acid	52.2
nC9 pelargonic acid	182.9	nC18 stearinic acid	147.4
nC10 capric acid	76.3	nC20	13.1
nC11 undecylic acid	15.3	nC22	13.0
nC12 lauric acid	89.4	nC24	36.8
nC14 myristic acid	193.4	n26	37.3
nC15 pentadecanoic acid	68.2	nC28	31.0
		Sum of fatty acids	**1407**

* Purification of the toluene extract by solid phase extraction florisil, derivatisation: BF_3/CH_3OH; identification: GC/MS MSD HP5970B; column: 40(3)-8-290(5), ULTRA2, SCAN, on column injection, 2 µl, inj. 60°C; internal standard: deut. palmitic acid (10 ppm referred to solid sample), quantification by ion ratio 74/76.

Table 9-5. Physico-chemical parameters (laboratory) of the Western Springs (M5) groundwater sample (11/96).

pH (Lab. at 8°C)	eH [mV] (Lab.) / pe (Lab.)	Cond. [mS/cm]	Total Carbon [mg/L]	Inorg. Carbon [mg/L]	DOC, org. C [mg/L]	pkb (pH8.2)	pkb (pH4.3)	alkalinity [mmol/L]
12.35	225 / 4.15	10.26	9.7	1.7	8.0	37	37.2	37.14

Table 9-6. Chemistry of the Western Springs (M5) groundwater sample (11/96).

Water-type	: Ca-K-Na-CO_3-SO_4
Total dissolved solids (TDS)	: 3959 mg/L / 126.88 meq/L
Sum of anions [meq/L]	: 61.20
Sum of cations [meq/L]	: 65.67
Balance	: 3.52

Major and Minor Ion Composition

Element	Content (mg/L)	(mmol/L)	(meq/L)	(meq%)
Na	121.4	5.28	5.28	4.17
K	477.8	12.22	12.22	9.65
Ca	965.5	24.09	48.17	37.7
Mg	<0.5	–	–	–
Fe	0.057	0.001	0.002	0.002
Sum of cations	**1565.2**	**41.59**	**65.67**	
Cl	40.9	1.15	1.15	0.91
F	4.4	0.23	0.23	0.002
Br	0.14	0.002	0.002	0.001
SO_4	1420.1	14.78	29.57	23.35
NO_3	34.8	0.56	0.56	0.44
NO_2	0.85	0.018	0.018	0.015
HCO_3	5.5	0.09	0.09	0.07
CO_3	887.2	14.79	29.58	23.36
Sum of anions	**2393.9**	**14.79**	**61.20**	

Trace Elements [mg/L]

Mn	Al	Cu	Zn	As	Cd	Pb	Hg
<0.005	<0.1	<0.02	0.045	0.00017	<0.00002	0.0018	<0.00005

Table 9-7. Organic compounds of the Western Springs (M5) groundwater (11/1996) detected by benzene extraction with GC/MS* [ppm].

Organic compound	Content [ppm]	Organic compound	Content [ppm]
biphenyl	0.27	phenol	0.05
buthyl-4-hydoxyanisole	0.08	benzoic acid	0.08
benzophenone	0.06	benzene-tetramethyl	0.11
unidentified (m/z = 167, 210)	0,06	aliphatic hydrocarbons	0.09
thiophen-2.5-diphenyl	0.09	squalen	0.03
		Sum	**0.92**

* 25 ml sample at pH 3 + 1 ppm deut. palmitic acid as internal standard extracted with 200 µl benzene; measured with HP MSD5973, FFAP-Kap. 20mx0.25mmx0.25 µmFD, 40°C(3min.)-8°C/min-250°C (5min.), Inj. 280°C.

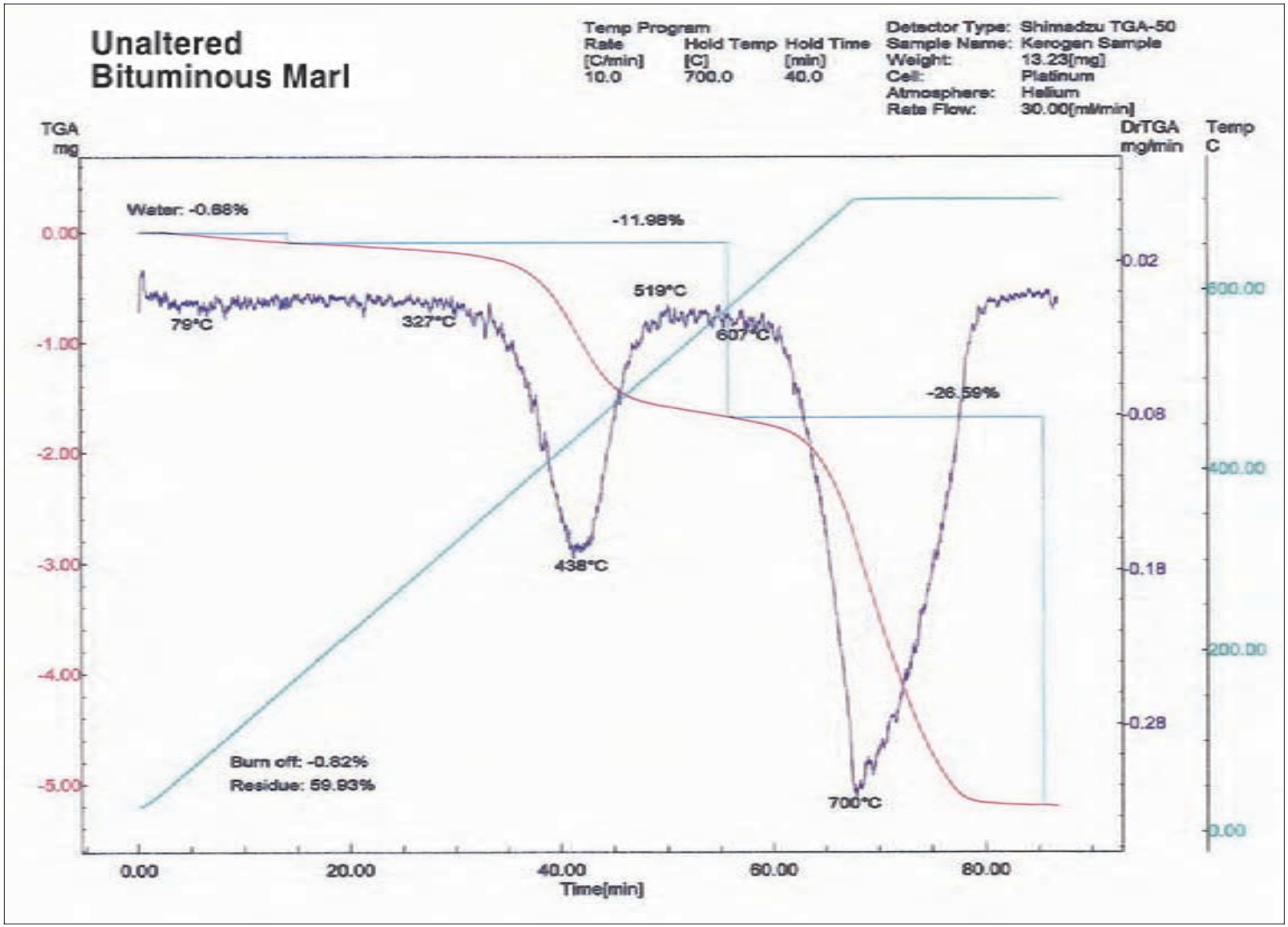

Figure 9-1. *Thermogravimetric measurement of an unaltered Bituminous Marl sample. (See text for further explanation).*

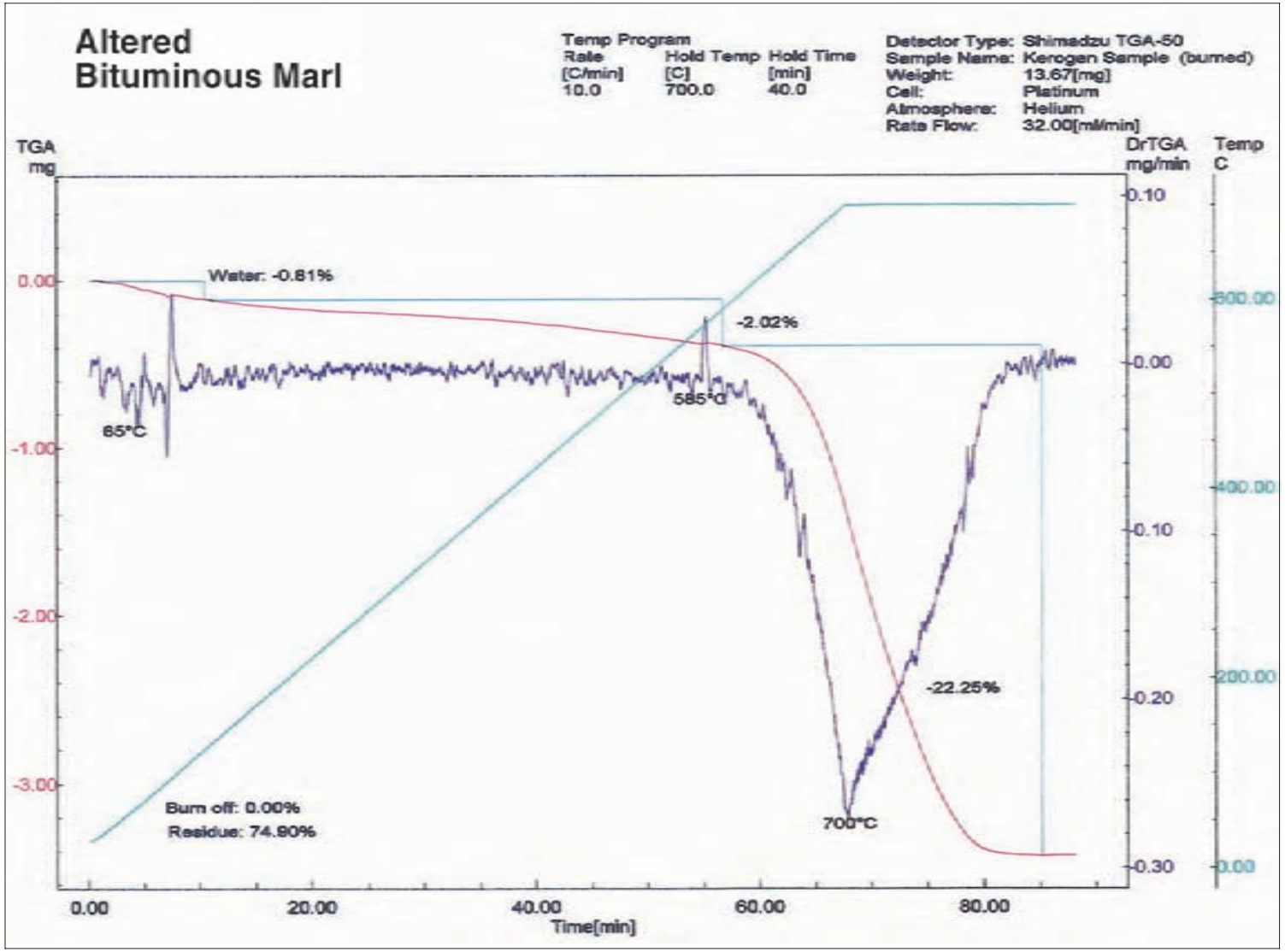

Figure 9-2. *Thermogravimetric measurement of an altered Bituminous Marl sample. (See text for further explanation)*

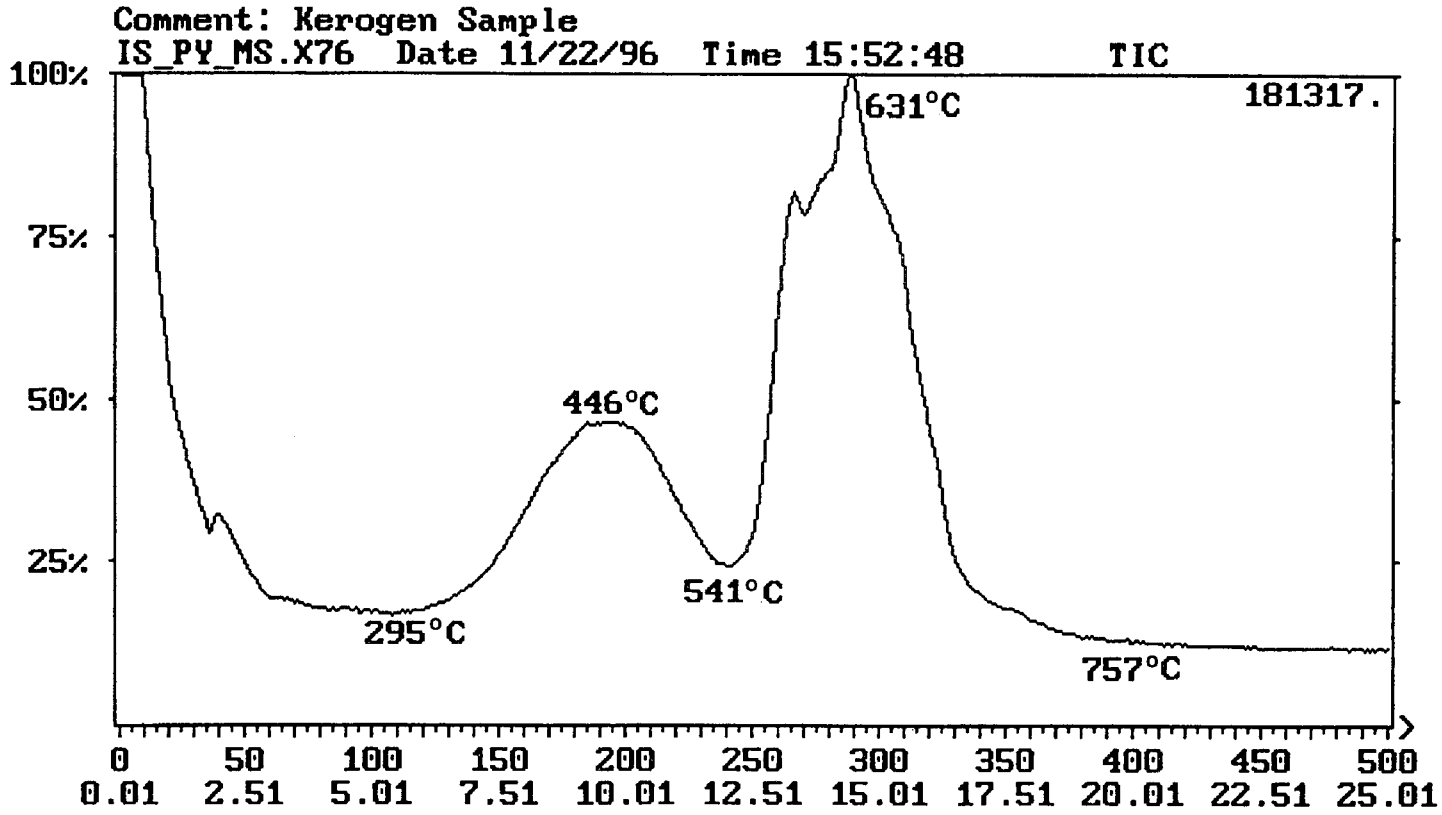

Figure 9-3. *In-Source-Pyrolysis-Mass Spectrometry; measurement of an unaltered Bituminous Marl sample. Total ion current (TIC) of the mass spectrometer is graphed versus the scan number and the reaction time, which are linearly correlated with the sample temperature. Three peaks can be distinguished: An evaporation peak, a cracking peak and a carbonate peak.*

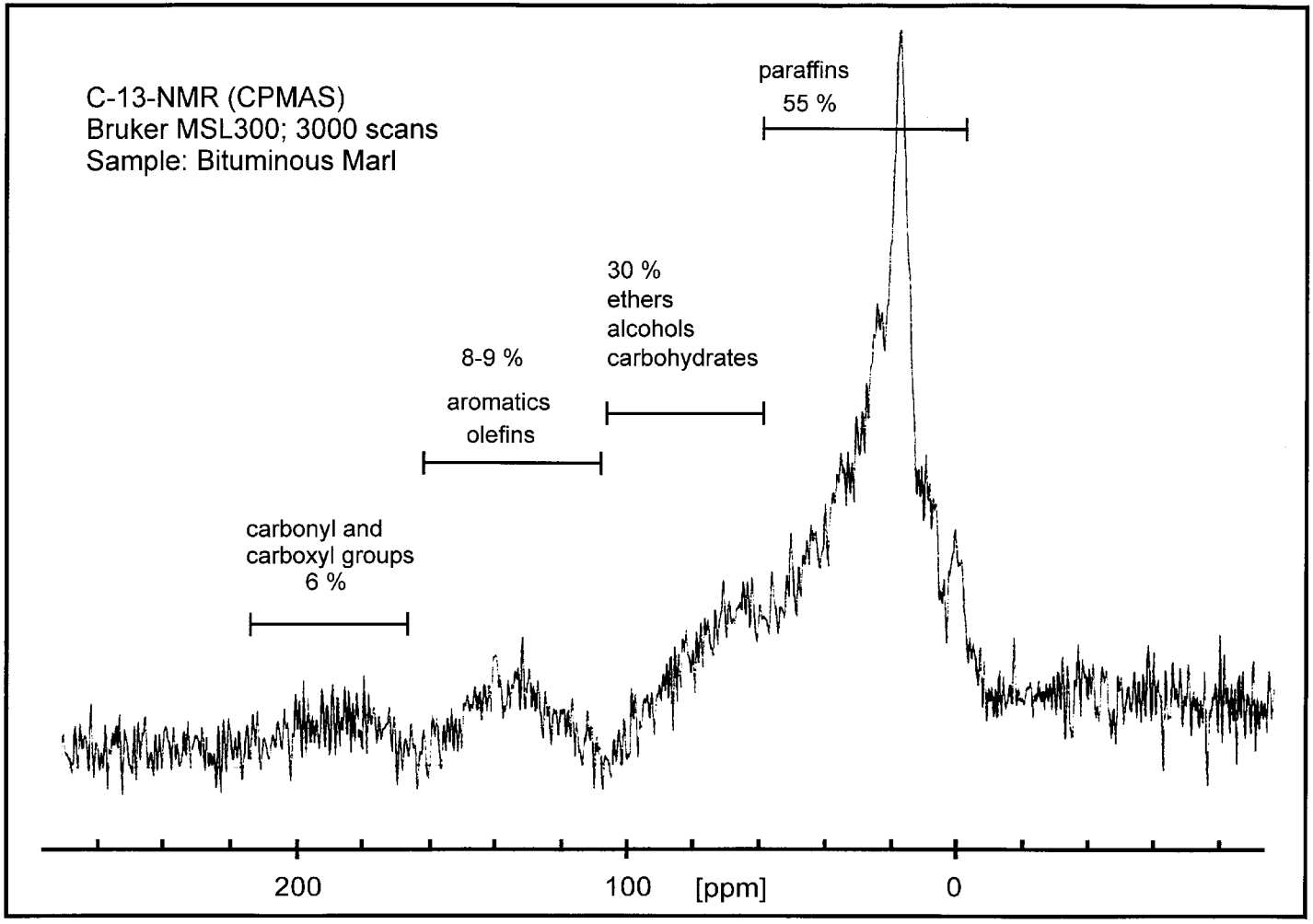

Figure 9-4. *^{13}C-NMR Spectra of an unaltered Bituminous Marl sample. Remarkable is the small amount of aromatics.*

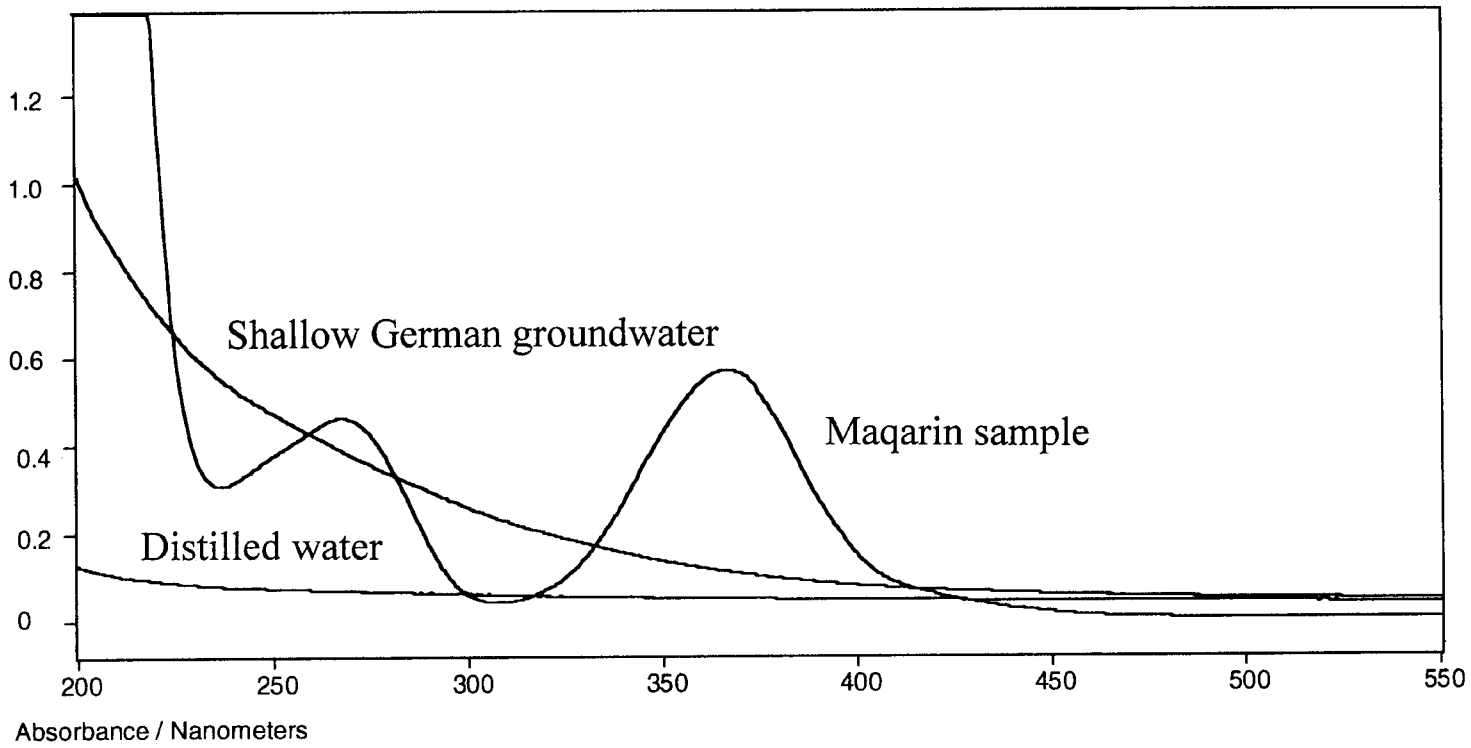

Figure 9-5. *Spectra of UV/VIS adsorption of the Western Springs (M5) groundwater sample in comparison to a typical shallow German groundwater with a comparable DOC concentration.*

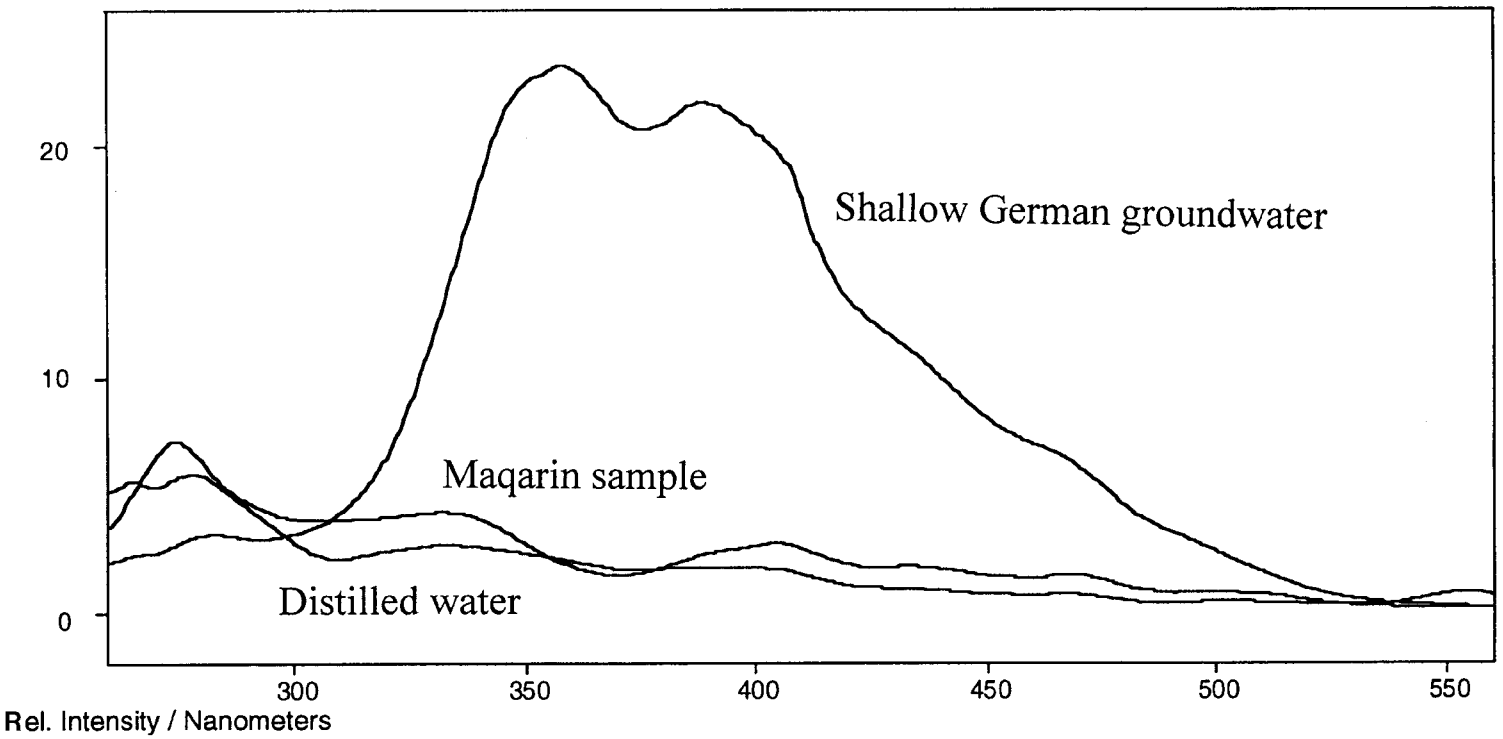

Figure 9-6. *Synchronous fluorescence spectra of the Western Springs (M5) groundwater sample in comparison to a typical shallow German groundwater with a comparable DOC concentration.*

10 THE PRODUCTION OF COLLOIDS AT THE CEMENT/HOST ROCK INTERFACE

(P.D. Wetton, J.M. Pearce, W.R. Alexander, A.E. Milodowski, S. Reeder, J. Wragg and E. Salameh)

10.1 INTRODUCTION

Modelling studies (e.g. Smith and Degueldre, 1993) have suggested that colloid transport through fractured rock systems could play a significant role in radionuclide migration. In addition, colloids have been shown to be responsible for the rapid transport of radioactive material in shallow groundwaters at two Los Alamos National Laboratory sites in the U.S. (Nuttall and Long, 1993). However, other studies, for example at the Cigar Lake uranium deposit in Canada (Vilks, et al., 1991,1993), have shown that if sorption of radionuclides onto colloids is reversible, then this transport mechanism will not be significant for the levels of colloids present in these groundwaters. If sorption is irreversible then transport of radionuclides via a colloidal medium could be important.

In the case of a cementitious repository, degradation of the cement may provide a significant source of colloids at both the near-field/far-field interface and at the margins of the hyperalkaline plume (which may extend downstream of the repository). To date, however, the full significance of the problem has been difficult to assess due to a lack of analytical data; only three laboratory experiments examining colloid production during cement degradation has been reported (Pearce, 1991; Gardiner et al., 1998; E. Wieland, per. comm., 1998), although others are currently ongoing in Switzerland and the UK. In all laboratory experiments, the production of colloids by experimental artefacts (such as CO_2 contamination) is difficult to overcome and it is not possible to recreate the *in situ* conditions of the near-field/far-field interface in a realistic manner (see further comments below).

Additional, supporting, data are therefore required to put the laboratory results in a more realistic perspective and these can be supplied by natural analogue studies. At Maqarin the exposed natural cement zone/Bituminous Marl interface in Adit A-6, analogous to a cementitious repository near-field/far-field interface, has been well characterised in previous studies (Alexander, 1992; Linklater, 1998), and offers the opportunity to collect colloids directly at the analogous near-field/far-field interface. Clearly this is also not without potential artefacts (as has already been shown by a previous attempt to sample colloids here (West et al., 1992) but the data from the Maqarin site should provide independent back-up for the data from the more controlled laboratory experiments.

To date, it has not proved possible to access a zone at Maqarin analogous to the distal portion of the hyperalkaline plume to examine potential silica colloid production at a well defined pH boundary. For example, since pH gradients at the edge of the plume

will be sharp, there is thus a tendency for large supersaturations of silica to develop in the groundwater. Fluids strongly supersaturated with silica tend to cause the formation of silica colloids (Weres et al., 1982; this report, Section 8.4). There is thus the likelihood of the development of large amounts of silica colloids at the margins of the plume. These colloids may be of significance to performance assessment if radionuclides migrate to the advanced edge of the plume.

10.2 SAMPLING AND ANALYTICAL METHODOLOGY

10.2.1 Site description

For this study, site M1 in the tunnel Adit A-6 was sampled (Fig. 10-1). This represents the natural cement/unaltered marl host rock interface and several seepages discharge through the tunnel roof from the cement zone (Milodowski et al., 1992; Milodowski et al., 1998a).

10.2.2 Equipment

The filters used were chosen for their reported stability in high pH solutions; 30 nm and 50 nm filters (Amicon), and 0.1 μm and the 1 μm Fluoropore filters (Millipore). It has been reported that the Amicon hyperalkaline resistant filters may be hydrophobic and therefore may repel colloids in the groundwaters being filtered (C. Degueldre, pers. comm., 1996). This has been checked in the laboratory by filtering standard colloid solutions through standard Amicon and Durapore filters followed by colloid enumeration of both filter types to assess any inter-filter differences. No evidence was found for colloid repulsion (or preferential retention) of the standard colloids by either filter type (detailed in Appendix O).

To minimise trace element contamination, all tubing, valves, sample bottles, connections etc. were made from Teflon®. The water was collected in a standard Millipore 50 mL capacity filtration cell. All the apparatus used, including the filters, was acid washed, rinsed in distilled water, dried in a laminar flow hood and finally packed in polythene bags in the laboratory to minimise contamination.

10.2.3 Field Sampling

Following the first unsuccessful attempt to assess artefact-free colloid populations in the Maqarin hyperalkaline groundwaters (Milodowski et al., 1992; this report, Section 10.4), a second campaign was carried out in 1994. In this case, filtration of 10 to 20 mL water samples was carried out on site. Unfortunately, this did not provide enough colloidal material to allow population enumeration or chemical analysis of the colloids (C. Degueldre, pers. comm., 1994).

The major problem during sampling of the hyperalkaline groundwaters is potential contamination from atmospheric CO_2. As noted by Milodowski et al. (1998b), the

ingress of CO_2 causes an immediate drop in the solution pH and the precipitation of a mixed carbonate/portlandite phase (seen clearly on the tunnel walls in Fig. 10-2). Indeed, this was the main problem during the first sampling campaign where carbonate/portlandite colloids precipitated out in the groundwater sample during transit. Another problem can be seen in Figure 10-2; the sampling site is in a narrow, dirty tunnel and dust, water dripping from the roof etc. are also potential contaminants. Both the above problems can be minimised by using a closed system for groundwater sampling (see Figure 10-3).

After clearing the tunnel wall of secondary precipitates, the rock face was examined to identify the areas of water flow. A Teflon® funnel was clamped directly to the wall over the main water conducting feature to aid collection and minimise contamination (after Degueldre et al., 1990; see also description in sub-section 4.4.2). A Teflon® tube was attached to the funnel and the groundwater was allowed to flow by gravity (approximate flow rate of 100–200 mL min^{-1}) to the sampling cell, first being passed through a 1 : m nominal pore size pre-filter (to remove any large particles dislodged from the fracture). The cell was connected to the inflow line and to a gas supply by a Teflon® three-way valve (Fig. 10-4).

When the cell was overflowing, the valve was switched to the gas line and high purity ('White Spot') N_2 at a maximum pressure of 3 bar was used to pass the water through the filter at the bottom of the cell. This was repeated three times per filter and only on the final volume was the cell fully emptied (i.e. dry filter). It was hoped that the rapid processing of several small volumes of the hyperalkaline groundwater, rather than one larger volume, would also minimise colloid production due to CO_2 uptake from the atmosphere.

The first 20 mL of filtrate was discarded for each filter to minimise filtrate contamination from the filter (McCarthy and Degueldre, 1993). After this first wash, the filtrate was collected in Teflon® bottles, the first, otherwise untreated, for major element chemistry, nutrients etc. and the second, acidified by the immediate addition of ultrapure 12M HNO_3, for trace elements and metals. Upon removal from the sampling cell, the filters were immediately placed in plastic petri dishes which were sealed with shrink plastic, placed in sealed polythene bags and stored in packing cases.

Obviously, the filter handling stage was the most crucial with respect to contamination and the utmost care was taken to avoid dust, water drips etc. touching the filters, petri dishes etc. but it is clear that, without laminar flow hoods or glove bags, it is impossible to guarantee absolute cleanliness (see Fig. 10-3).

The groundwater chemistry at site M1 has been determined previously (Milodowski et al., 1992; Milodowski et al., 1998b) and is summarised in Table 10-1. In addition, the full data set for the filtrate chemistry is presented in Appendix P.

10.2.4 Colloid Enumeration

Pre-treatment

Filters used for the laboratory tests were mounted whole onto 32 mm aluminium Cambridge type Scanning Electron Microscope (SEM) stubs using conductive carbon adhesive mounting tabs. The mounted samples were coated (by a carbon evaporative process with an Edwards 306A coater) to make them electrically conductive for SEM observation. Colloids could potentially be removed from the filter by this process and this should ideally be tested for the specific filters used here. All filters were handled in a laminar air-flow cabinet to prevent contamination during preparation and sealed in air-tight boxes after preparation.

Initial Enumeration Using a Cambridge S250 SEM

The filter specimens were then examined by SEM using a Cambridge S250 SEM. Four representative photomicrographs were taken of each filter, from the centre to the outer edge of the active filter area. This accounted for any heterogeneous distribution in colloids across the surface of the filter. The low colloid populations on the filters meant that the normal practise of counting colloids at high magnification (20 000X, for example) was abandoned as insufficient colloids could be resolved in the field of view to provide a statistically valid count. Instead, it was decided to produce the photomicrographs at a fixed magnification of approximately 2050x. The number of colloids on each photomicrograph area was counted manually and the observations scaled to determine the colloid population for the total filter. From this, knowing the volume of groundwater filtered, it was possible to calculate a colloid concentration in the groundwater.

Second Enumeration Using a LEO435VP SEM

The filters were examined under high vacuum using a LEO435VP scanning electron microscope in secondary electron mode at 5 kV, and a probe current of 15 pA and a 10 mm working distance. Four representative photomicrographs were taken of each filter, from the centre, 1/3 radial distance from the centre, 2/3 radial distance from the centre and at the outer edge of the active filter area. This accounted for any heterogeneous distribution in colloids across the surface of the filter. Magnification was optimised at 30 000X giving an individual pixel resolution of 8.47 nm. The number of colloids on each photomicrograph area was counted manually and the observations scaled to determine the colloid population for the total filter. From this, knowing the volume of groundwater filtered, it was possible to calculate a colloid concentration in the groundwater.

It has been stated that using an in-line pre-filter may remove some colloids from solution as well as larger particles (C. Degueldre, pers. comm., 1996) but, although larger particles were observed on the 1 μm and 0.1 μm nominal pore size filters, nothing could be seen in the colloid size range.

One sample was briefly analysed by analytical transmission electron microscopy (ATEM). The colloids from a portion of the filter were suspended in distilled water by

ultrasonic treatment; the suspension was then pipetted onto a TEM grid for examination and allowed to dry.

10.2.5 Colloid Size Determination

Colloid size measurement was performed using a LEO435VP scanning electron microscope and a Kontron Elektronik KS400 Image Analyser. Secondary electron images of the colloid filters were obtained under high vacuum at an accelerating voltage of 5 kV and SEM probe current of 100 pA, with the specimen working distance set to 10 mm. Optimum magnification for the images was established at 8 000X, equivalent to an individual pixel resolution of 14.32 nm. The minimum measurable object, as defined by the limits of the KS400 system, is equivalent to a 4 pixel square which in this case gives a minimum measurable colloid diameter of 40.5 nm (cf. 50–80 nm reported in Degueldre et al., 1990). Three traverses were made across each filter from the filter edge to the centre with 8 equidistant images per traverse. The SEM images were initially subjected to a shading correction procedure to remove localised variations in the grey level of the filter surface due to imaging, preparation defects or textural variations in the filter. A manual grey level discrimination was then performed to segment the colloids from the filter background, producing a binary image of the colloids only. Small artefacts, due to the filter background being mis-identified as colloids, were then removed from the segmented image. The final image was then measured automatically for all objects with a maximum dimension (equivalent to the colloid diameter) of less than 1000 nm.

The presence of mineral debris and post-filtering mineral precipitates on some regions of the filters is a potential source of errors in the size data obtained. Grey levels assigned to the colloids by segmentation were observed to occur in some of the precipitates and mineral debris on the filters, producing artefacts in the derived binary image. The influence of these artefacts was reduced by careful selection of images to minimise the volume of precipitates and mineral debris present in each image. The majority of artefacts produced were of relatively large diameter compared to the colloids, allowing them to be rejected at the measurement stage.

10.2.6 Filtrate Chemical Analysis

Techniques for analysis of the filtrate chemistry were based on those described in detail by Milodowski et al. (1998b) and only an outline of the techniques is presented here. Sample pH was determined with a Radiometer G2040B glass pH and K4040 calomel reference electrodes. The pH electrode was calibrated using Whatman standard pH 7 and 13 buffers. Major cations (Ca, Mg, Na, K and Sr) and trace cations (Si, Ba, Mn, Fe, Al, Co, Ni, Cu, Zn, Cr, Zr, Mo, Cd, Pb, V, Li), total S and Si were determined directly by inductively coupled plasma-atomic emission spectroscopy (ICP-AES). Major and trace anions (Cl^-, SO_4^{2-}, NO_3^-, NO_2^- and Br^-) were determined by ion chromatography. F^- was determined by ion-selective electrode on filtered unpreserved samples. Total organic carbon (TOC) and total inorganic carbon (TIC) were determined on filtered unpreserved samples. The technique measures total carbon (inorganic carbon plus organic carbon) and inorganic carbon in two separate stages. Inorganic carbon content represents the sum of the CO_3^{2-} and HCO_3^- present in solution. As and Se were

determined by hydride generation ICP-AES (Cave and Green, 1989). Reduced iron (Fe^{2+}) was determined by a colourimetric method using the chromogenic reagent 2,2-bipyridyl. REEs, U and Th were determined by inductively coupled plasma-mass spectrometry (ICP-MS).

10.3 RESULTS

10.3.1 Enumeration and Size Distribution

Using the Cambridge S250 SEM

Mean colloid populations do not vary between each filter set by more than their standard deviations suggesting that the field sampling and enumerations produced repeatable results (Table 10-2). The average colloid population for all waters sampled from site M1 in Adit A-6 filtered through a 30 nm filter was $1.17 \cdot 10^4 \pm 5.93 \cdot 10^3$ mL^{-1} and filtered through a 50 nm filter was $2.63 \cdot 10^4 \pm 1.42 \cdot 10^4$ mL^{-1}. A higher colloid population obtained from the 50 nm filter suggests a higher proportion of colloids were greater than 50 nm in diameter. However, closer examination of Table 10-2 indicates that there is little real variation between the mean populations. Colloid populations were also converted to a mass concentration for comparison with other studies. Here, the approach of Degueldre et al. (1990) was used and the colloid size distribution for the three 50 nm nominal pore size filters was multiplied by:

Equation 10a

$$\left[\overline{coll}\right] = [coll] \times \frac{1}{6} \rho \pi d$$

where

$\left[\overline{coll}\right]$ = colloid mass concentration (mgL^{-1})

[coll] = colloid number concentration (ptL^{-1})

ρ = colloid density

d = colloid diameter

Using the LEO435VP SEM

Here, three filters were re-examined with the new SEM and the colloid size distribution assessed. Reported data for the samples is limited to colloids with maximum diameters of 450 nm. Inspection of the processed images after measurement showed a significant proportion of false colloids in the 450–1000 nm size range generated by mis-

identification of segments of particulates as colloids with very low numbers of true colloids.

Size data for filter A4 (Table 10-3; Fig. 10-5) show a mean colloid diameter of 219.03 (±2.82) nm calculated from 2713 particle measurements. A histogram of the data suggests a bimodal size distribution. The first mode occurs at 101–125 nm and contains 8.4% of the total colloids measured, with the second mode at 201–225 nm containing 14% of the total counts. The data for filter B4 (Table 10-4; Fig. 10-5) show a mean colloid diameter of 188.8 (±6.85) nm calculated from 656 particle measurements. A histogram of the data shows a single colloid population, with a mode in the range 101–125 nm, accounting for 19.4% of colloids measured. The data for filter C4 (Table 10-5; Fig. 10-6) shows a mean colloid diameter of 173.46 (±5.43) nm calculated from 847 particle measurements. The histogram of this data shows a single size population to be present with a mode in the range 101–125 nm, with this range accounting for 21.6% of the total population. The minimum colloid diameter observed in all samples, ≈ 77 nm, was significantly higher than the minimum measurable diameter.

Total colloid concentrations and normal size distributions were calculated using three different methods. This permits comparison between calculation techniques and with colloid population data from previous studies. Each calculation method is described briefly below.

Method A (after Degueldre et al., 1990)

This method was used in the Grimsel colloid exercise (Degueldre et al., 1990) and in the Maqarin Phase I study (West et al., 1992). This provides total colloid concentrations and normal size distribution functions for the colloids in terms of both mass and particle concentrations. The method uses the number of colloids counted in each size class and a colloid diameter defined by either the upper limit or by the mean value of the size class. These data are then used to calculate particle concentrations per size class as follows:

Equation 10b: Degueldre et al., 1990)

$$\frac{d[coll]}{d\Phi} = \frac{\sum dN \cdot d\Phi^{-1}}{\sum s} \cdot \frac{S}{v}$$

where

[coll] =	concentration of colloids in size class, (colloids.L^{-1})
Φ =	colloid diameter, nm
$d\Phi$ =	width of size class, nm
Σs =	total area of filter scanned, m^2
S =	active area of filter, m^2
v =	volume of filtrate, L

Mass concentrations per size class are calculated using the following equation, assuming the colloids to be spherical in form and having a density $r = 2 \cdot 10^{-18}$ mg.nm^{-3}.

Equation 10c: (Degueldre et al., 1990)

$$\frac{d\overline{[coll]}}{d\Phi} = \frac{d[coll]}{d\Phi} \cdot \frac{\rho\pi\Phi^3}{6}$$

Data generated by Equations 10b and 10c can then be plotted against colloid diameter as histograms and log-log frequency plots to illustrate the normal distribution spectrum for the colloid system (Buffle, 1988).

If it is assumed that the principal mechanisms for colloid generation are (i) fragmentation of the rocks (or, in this case, cement) in contact with the groundwaters and (ii) erosion, then the range of colloid sizes will be continuous and may be described by Pareto's Law (Lerman, 1979; Buffle, 1988) which takes the form:

Equation 10d:

$$\frac{d[coll]}{d\Phi} = A\Phi^{-b}$$

This may also be written as:

Equation 10e:

$$\log\left(\frac{d[coll]}{d\Phi}\right) = \log(A) - (b)\log\Phi$$

where A and b are constants describing the system studied.

If the log-log frequency plots generated from Equations 10b and 10c are linear, then constants A and b may be derived directly from these to give the normal size distribution functions for the colloid system in terms of either particle or mass concentration. Total colloid concentrations for the samples can then be obtained by integration of Equation 10d between the upper and lower size limits applied during colloid measurement.

Method B

This method uses individual colloid diameters generated by image analysis to provide a more empirically correct description of the colloid size distribution in terms of colloid mass. The mass of each colloid is calculated from its measured diameter using:

Equation 10f:

$$\text{colloid mass (m)} = \frac{\rho\pi\Phi^3}{6}$$

The resulting masses are then summed according to size classes defined by colloid diameter to produce a total mass of colloids for each given class. The concentration of colloids in each class is then calculated and divided by the class width to produce values equivalent to the result of Equation 10a. These data are then used as in Method A to produce the normal distribution spectrum and the Pareto's Law coefficients for the colloid population.

Method C (direct calculation of colloid populations)

This method provides values for total colloid concentrations only, by direct calculation from the basic image analysis data. Mass concentrations are calculated by converting colloid diameters obtained by image analysis to masses using Equation 10f. The resulting data are then summed and the total concentration obtained as below.

Equation 10g:

$$\overline{[\text{coll}]} = \frac{M_T . S}{v \cdot \sum s}$$

where M_T = total mass of colloids measured.

Concentrations on a particle basis can also be calculated using Equation 10g with the total number of colloids measured (N_T) substituted for M_T.

Normal distribution spectra in the form of linear histograms and log-log plots for each 50 nm nominal cut-off filter are presented in Figures 10-6 to 10-8. Estimated colloid populations generated by the differing calculation methods are summarised in Table 10-6. Estimates for the mean colloid population for all groundwaters filtered varied from $2.42 \cdot 10^7 \pm 1.75 \cdot 10^7$ colloids.mL^{-1} using Method A, to $2.70 \cdot 10^7 \pm 1.09 \cdot 10^7$ colloids.mL^{-1} by direct calculation. This compares with a maximum population of $3.98 \cdot 10^4$ colloids.mL^{-1} for the 50 nm filters by the original method (Table 10-2), a difference of three orders of magnitude. Colloid mass concentrations were estimated as 0.081 ± 0.049 mg.L^{-1} by Method A, 0.065 ± 0.046 mg.L^{-1} by Method B, and 0.088 ± 0.072 mg.L^{-1} by direct calculation. This compares with a maximum colloid mass of $5.21 \cdot 10^{-6}$

$mg.L^{-1}$ for the 50 nm filters by the original method (Table 10-2), a difference of three orders of magnitude.

The normal size distribution functions for each filter calculated on the basis of both colloid mass and particle count are summarised in Table 10-7. A 'combined data' normal size distribution is presented; this was calculated by combining colloid measurements from each of the water samples in a single dataset and applying the three calculation methods.

10.3.2 Groundwater and Filtrate Chemistry

The existing information on the M1 site groundwater chemistry has been summarised by Milodowski et al. (1998b) and Chapter 6 (this report). Briefly, all of the hyperalkaline waters analysed to date from the Maqarin site are characterised by portlandite saturation, low concentrations of Mg, Si and Al and high concentrations of SO_4. The specific composition of the groundwaters appears to be a consequence of leaching of the minerals of the cement zone with, as yet unknown, contributions from the formation water.

Results of filtrate analyses are presented in Appendix P (Table P-2). No variations in the filtrate chemistry were detected above the experimental errors (Fig. 10-9). However, certain trends in the data are present, albeit within experimental error. For example, in samples A and C the Ca, Na and K concentrations decrease with decreasing filter size. This decrease is also reflected in the Total S analyses for samples A and C but not in the SO_4^{2-} analyses. The concentration of Si and Fe was below detection limit, and that of Al was within one order of magnitude of its detection limit, hence the higher percentage errors and lack of meaningful trends in the data.

The Ca, Na and K trends could reflect a variety of solid phases such as calcite, portlandite, clays, CSH minerals, zeolites or thermal metamorphic phases. However, ATEM analyses of this material found no evidence, in most cases, for any of these phases being present on the filters. Sample B is the exception to this, with the <50 nm and <30 nm filtrates having higher concentrations of Ca, Na and K than the filtrates from the coarser filters. This is difficult to explain except possibly as contamination during sampling.

Some of the trace elements also decrease in concentration with decreasing filter size although all variations are generally within experimental error. For example, Ba, Sr, Zn and Cr have trends similar to the major cations for samples A and C (Fig. 10-9). The exceptional sample is again sample B.

If the <30 nm filtrate is considered to be true solution, then the higher concentrations of major cations Ca, Na and K relative to the concentration in true solution, may be attributed to colloidal material. In samples A and C, the <1 μm and <0.1 μm filtrates contain higher concentrations of Ca, Na and K relative to the true solution. This suggests that some of the budget of these elements may be accounted for by particulate material. This is partially confirmed by ATEM. However, differences between the <50 nm filtrates and the true solution are very small. Similar comparisons for trace

elements are less coherent since absolute differences are very small and variations are within analytical error.

10.3.3 Analytical Transmission Electron Microscopy (ATEM)

As noted in Subsection 10.2.5., one sample was examined by ATEM. The suspensions were successfully prepared but were visibly contaminated by filter paper debris. All grids examined were covered in fine halite crystals of the order of 10–100 nm in size and are presumably a contaminant. Crystalline grains were very occasionally seen as tabular or prismatic objects approximately 0.1 : m in diameter, i.e. greater than the filter size. Chemical analyses of this material were unsuccessful. In addition, irregular, elongate particles of organic material were also present.

During analyses it was found that the copper grid dominated any X-ray microanalysis, and hence observations could not be quantified. Nevertheless, the presence of certain elements in the colloids could be reliably identified and they were found to contain relatively high concentrations of Na, Cl and Si. Minor amounts of S, K, Ca and Fe were also detected. Ca and S were sometimes associated, suggesting the presence of a sulphate phase such as gypsum or ettringite and the elongate morphology of some grains would tend to support this conclusion.

Both gypsum and ettringite are present in significant amounts in the natural cement zone (Milodowski et al., 1992; Milodowski et al., 1998a) suggesting colloid production by erosion of these phases. Other elements identified may tentatively suggest the presence of clay particles. Organic material may be microbial, although it cannot be determined whether the bacteria grew after sampling or were simply those present in the groundwater initially (Coombs et al., 1998; this report, Chapter 11). The filtrate chemistry suggests that filters may have been degrading slightly in the hyperalkaline groundwaters and so the organic particles identified by ATEM also may be artefacts of this degradation process.

10.4 DISCUSSION

The disparity between results from the two different SEMs used here is believed to arise simply from better resolution of colloids on the filter surface. The imaging conditions of the initial study, using the Cambridge S250 SEM, were chosen to optimise the number of colloids counted per micrograph to ensure statistically valid data. However the improved imaging available on the new LEO435VP SEM enabled smaller colloids (~40 nm diameter as against ~80 nm diameter originally) to be resolved and their diameters measured. Use of higher SEM magnification would allow the minimum colloid diameter measurable to be further reduced, potentially to the resolution limit of the LEO435VP. However, higher resolution measurement would result in increased time to analyse the same area of the filter surface. For example doubling the SEM magnification to 16 000x would allow a minimum colloid diameter of ~20 nm to be measured but would require 96 images to be analysed in comparison to 24 images required at 8 000x magnification as in this study.

Comparison with other data on near-field cementitious colloids is difficult due to the significantly different methodologies used to data (see Table 10-8). Even in the two batch leaching tests, large differences exist. Wieland (1997) shook the samples in synthetic cement pore waters while Gardiner et al. (1998) appear to have employed static leaching in synthetic groundwaters. The method-induced effects are apparent when the colloid populations are compared with the colloid concentrations: there are no clear relationships between populations and mass, suggesting significantly different colloid diameters are being measured in each experiment. This is clearly shown in the data of Wieland (1997) where the measured colloid concentration varies over five orders of magnitude, depending on the settling time allowed following shaking of the samples (although the author notes that immediate measurement after end-over-end shaking of the batch cement/water samples used is unrealistic).

Arguably, the Maqarin data are the most realistic in so far that the Maqarin site is a better representation of a cementitious near-field/far-field interface, but such an argument ignores the lack of a hydrogeological model for the Maqarin site as a whole, and the M1 site in particular. Such a model is needed to clarify the amount of weight which can ultimately be placed on the data reported here and, consequently, on the laboratory data reported to date.

In other, lower pH, groundwaters, populations within the range of 10^6 to 10^7 colloids.mL^{-1} are common (see Table 10-9 and Degueldre et al., 1996a,b), whereas the colloid concentrations are generally higher than observed at Maqarin (with the exception of the Alligator Rivers data). Recent investigations of the Gorleben groundwater systems (Zeh et al., 1997; Dearlove et al., 1991; Kim, 1991) have highlighted the potential importance of colloidal material in the transport of actinides. Humic colloids in a suite of groundwaters were found to bear over 75% of the natural uranium present. The lower size limit for colloids in the Gorleben studies is nominally 1 nm with the majority of the colloid population for particular waters being in the 15-1 nm size range (Dearlove et al., 1991). In light of the Gorleben study the use of nominal 30 nm membranes in the current Adit A-6 study may in fact be failing to capture a substantial part of the colloid population which may represent the largest surface area component for actinide sorption.

The Pareto's Law coefficients calculated for the colloid populations in this study differ markedly from those reported previously, giving values for b ~1.1-2.2 rather than b ~4 (West et al., 1992). For suspended particles and colloids, it has been suggested that values obtained for b can indicate the colloid elimination mechanism from the suspension (Buffle, 1988). Values of b=4 are taken to indicate stability in a given groundwater system whereas b <4 reflect elimination mechanisms based upon coagulation of particles and b >4 elimination due to filtration. Thus data from the current study could be taken to suggest that colloids in the Maqarin groundwaters should undergo elimination by coagulation processes.

It must, however, be noted that Buffle's theorem does not deal with chemical instability of colloids, as might be the case at the strong pH gradient found at the distal part of a hyperalkaline plume. Nevertheless, the low b value observed in this system is applicable within the main body of the hyperalkaline plume, where the chemical conditions will not vary dramatically over short distance. This suggests that transport away from the near-field of radionuclides irreversibly sorbed on the cementitious colloids will be insignificant.

Calculation of colloid populations by the three methods used in this study produce consistent results for a particular filter. Data generated by Method A (Degueldre et al., 1990) and Method B (this study) show good agreement, suggesting that use of a fixed colloid diameter in the derivation of colloid mass for all colloids in a particular size class does not introduce significant errors into the calculation (as long as the range of the size class is not too great). The total colloid concentrations obtained by these methods are also in good agreement with those calculated directly from the original colloid measurements, indicating that modelling of the colloid population using Pareto's Law is a valid assumption under the conditions found in this study.

Re-determination of colloid sizes on three of the existing samples shows a common population with a maximum frequency in the range 101–125 nm diameter. Data for sample A4 indicates the presence of an additional mode in the range 201–225 nm diameter which comprises 14% of the colloids measured. Filters B4 and C4 were found to have significant volumes of mineral aggregated precipitates on their surfaces. Qualitative energy dispersive X-ray analysis (EDXA) of the precipitates showed chemistries of dominantly Ca and O or Ca, S and O. In most cases these aggregated particles contain colloid particles or have colloids present on their surfaces. Any colloids in contact with the aggregates cannot be measured by the method currently employed, thus reducing the size of the measurement data set.

10.5 CONCLUSIONS

The colloid data reported here, the first that the authors are aware of for such a cementitious hyperalkaline groundwater system, indicate populations ($\sim 2 \cdot 10^7$ colloids.mL^{-1}) which are comparable with lower pH groundwaters (for example, the groundwaters at the potential Swiss repository site at Wellenberg (central Switzerland) have average colloid populations of $6 \cdot 10^6$ mL^{-1}, Degueldre et al., 1994). However, care must be taken when making direct comparisons with existing data for other fracture flow systems in that the colloid measurement cut-off is often $\geq$ 100 nm. As has clearly been shown here, re-analysis of the same groundwater with newer apparatus with better resolution could produce a significant increases in the colloid population. Until such data are available, a direct comparison of colloid populations is difficult to justify.

Comparison with data from other, laboratory based, studies of cementitious near-field colloids is also not simple, the main problems arising from significantly different experimental conditions producing different forms of colloid populations. It is of note that in a recent performance assessment (Nagra, 1994), Nagra used the colloidal concentration (rather than populations) to calculate the efficiency of colloidal transport of radionuclides. In this case, and accepting the conclusions of Wieland (1997) that the large colloid concentrations produced when end-over-end shaken systems are sampled shortly afterwards are unrealistic, it can be seen from Table 10-8 that a reasonable agreement exists between the data sets. Clearly, any future work at Maqarin and in the laboratory would benefit from a common approach which should try to minimise method inherent differences, so producing a more compatible data set for use in performance assessment.

The small amount of material collected at Maqarin has made definition of the colloid composition very difficult, although the tentative conclusion is that the colloids could originate from cement phases observed within the natural cement zone. Clearly, another attempt should be made to collect a large volume sample at site M1 (the cement/host rock interface) for further characterisation of the colloid composition.

It is worth re-emphasising at this point that, although particulate material was observed on the 1 μm and 0.1 μm nominal pore size pre-filters, nothing in the colloidal size range was visible and it is thus assumed that colloid loss on pre-filtration is not a significant problem. Similar conclusions may be tentatively drawn for the possibility of colloid repulsion by both filter types, although it is accepted that more relevant tests must be carried out with cement colloids to be completely certain.

In addition, to fully understand the colloid behaviour in the Maqarin hyperalkaline groundwaters, it is necessary to collect further samples both upstream of the cement zone (for input populations) and downstream, some distance from the cement/host rock interface to assess colloid stability within the hyperalkaline plume. This is especially important as the calculated b value of the colloidal population suggests colloid loss from the Maqarin hyperalkaline groundwater via coagulation, implying attendant retention of any radionuclides irreversibly sorbed on similar colloids within a repository hyperalkaline plume.

10.6 ACKNOWLEDGEMENTS

Thanks are due to M. Cave (BGS) for performing the filtrate analyses and setting up field equipment. B. Smith (BGS) also helped with field equipment and provided valuable advice. E. Hodgkinson and C. Hughes (University of Manchester) are thanked for performing the ATEM analyses. H. Khoury (University of Jordan) and J. Smellie (Conterra) are warmly thanked for their invaluable support during the field campaign. Many thanks to C. Degueldre (Paul Scherrer Institute and University of Geneva) for a constructive review of a previous draft of this report.

10.7 REFERENCES

Alexander, W.R. (Ed.), 1992. A natural analogue study of the Maqarin hyperalkaline groundwaters. I: Source term description and thermodynamic database testing. Nagra Tech. Rep. (NTB 91-10), Nagra, Wettingen, Switzerland.

Buffle, J., 1988. Complexation reaction in aquatic systems. E. Horwood (Ed.), Chichester.

Cave, M.R., and Green, K.A., 1989. Feasibility study of the determination of iodide, tin, arsenic, selenium, and hydrogen carbonate in groundwaters by inductively coupled plasma atomic emission spectroscopy. Atom. Spec., 4, 223–225.

Clark, I.D., Milodowski, A.E., Fritz, P., Khoury, H.N., Hall, G., Cave, M., Smith, B. and Cook, J.M., 1992. Aqueous geochemistry. In: W.R. Alexander (Ed.), A natural analogue study of the Maqarin hyperalkaline groundwaters. – I: Source term description and thermodynamic database testing. Nagra Tech. Rep. (NTB 91-10), Nagra, Wettingen, Switzerland, p. 51–69.

Coombs, P., Gardner, S.J., Rochelle, C.A. and West, J.M., 1998. Natiral analogue for geochemistry and microbiology of cement porewaters and cement porewater host rock/near-field interactions. In: C.M. Linklater (Ed.), A natural analogue study of cement-buffered, hyperalkaline groundwaters and their interaction with a repository host rock: Phase II. Nirex Science Report, S/98/003, Nirex, Harwell, U.K., p. 211–240.

Dearlove, J.P.L., Longworth, G., Ivanovich, M.,Kim, J.I., Delakowitz, B. and Zeh, P., 1991. A study of groundwater-colloids and their geochemical interactions with natural radionuclides in Gorleben aquifer systems. Radiochimica Acta, 52/53, 83–89.

Degueldre, C., Longworth, G., Moulin, V. and Vilks, P., 1990. Grimsel colloid exercise: an international intercomparison exercise on the sampling and characterisation of groundwater colloids. Nagra Tech. Rep. (NTB 90-01), Nagra, Wettingen, Switzerland.

Degueldre, C., Laube, A. and Scholtis, A., 1994. A study of colloids in groundwaters at the Wellenberg site: a status report. Unpubl. Nagra Int. Rep., Nagra, Wettingen, Switzerland.

Degueldre, C., Pfeiffer, H.-R., Alexander, W.R., Wernli, B. and Brütsch, R., 1996a. Colloid properties in granitic groundwater systems I: sampling and characterisation. Appl. Geochem. 11, 677–695.

Degueldre, C., Grauer, R., Laube, A.,Oess, A. and Silby, H., 1996b. Colloid properties in granitic groundwater systems II: stability and transport studies. Appl. Geochem. 11, 697–710.

Gardiner, M.P., Holton, G.J. and Swanton, S.W., 1998. Influence of colloids, microbes and other perturbations on the near-field source term. Submitted to "The Analyst".

Kim, J.I. 1991. Actinide colloid generation in Groundwater. Radiochimica Acta, 52/53, 71–81.

Lerman, A., 1979. Geochemical processes, water and sedimentary environments. Wiley – Interscience Publication.

Linklater, C.M. (Ed.), 1998. A natural analogue study of cement-buffered, hyperalkaline groundwaters and their interaction with a repository host rock: Phase II. Nirex Science Report, S/98/003, Nirex, Harwell, U.K.

Linklater, C.M., Albinsson, Y., Alexander, W.R., Casas, I., McKinley I.G. and Sellin, P., 1996. A natural analogue of high pH cement pore waters from the Maqarin area of northern Jordan: comparison of predicted and observed trace element chemistry of uranium and selenium. J. Contam. Hydrol. 21, 59–69.

McCarthy, J. and Degueldre, C., 1993. Sampling and characterisation of colloids and particles in groundwater for studying their role in contaminant transport. In: Environmental Particles, vol. 2. J.Buffle and H. van Leeuwn, Lewis Publishers.

Miekeley, N., Coutinho de Jesus, H., Porto de Silveira, C.L., and Degueldre, C., 1992. Chemical and physical characterisation of suspended particles and colloids in waters from the Osamu Utsumi mine and Morro do Ferro analogue study sites, Poços de Caldas, Brazil. J. Geochem. Explor., 45, 409–438.

Miller, W., Alexander, W.R., Chapman, N., McKinley, I., and Smellie, J. (1994). Natural analogue studies in the geological disposal of radioactive wastes. Elsevier, Amsterdam.

Milodowski, A.E., Khoury, H.N., Pearce, J.M. and Hyslop, E.K., 1992. Discussion of the mineralogy, petrography and geochemistry of the Maqarin source-term rocks and their secondary alteration products. In: W.R. Alexander (Ed.), A natural analogue study of the Maqarin hyperalkaline groundwaters. I: Source term description and thermodynamic database testing. Nagra Tech. Rep. (NTB 91–10), Nagra, Wettingen, Switzerland, p. 41–51.

Milodowski, A-E., Pearce, J.M., Hyslop, E.K., Huges, C.R., Ingelthorpe, S.D.J., Strong, B.E., Wheal, N., MacKenzie, A-B., Karnland, O. and Khoury, H.N., 1998a. Mineralogy and petrology. In: C.M. Linklater (Ed.), A natural analogue study of cement-buffered, hyperalkaline groundwaters and their interaction with a repository host rock: Phase II. Nirex Science Report, S/98/003, Nirex, Harwell, U.K., p. 70–145.

Milodowski, A.E., Cave, M.R., Reeder, S. Smith, B., Chenery, S.R.N. and Cook, J.M., 1998b. Aqueous geochemistry at Maqarin. In: C.M. Linklater (Ed.), A natural analogue study of cement-buffered, hyperalkaline groundwaters and their interaction with a repository host rock: Phase II. Nirex Science Report, S/98/003, Nirex, Harwell, U.K., p. 48-63.

Nagra, 1994. Bericht zur Langzeitscherheit das Endlagers SMA am Standart Wellenberg. Nagra Tech. Rep. (NTB 94-06), Nagra, Wettringen, Switzerland.

Nuttall, H., and Long, R., 1993. Mobility of radioactive colloidal particles in groundwater. Rad. Waste Manag. Nucl. Fuel Cycle, 17, 237–251.

Pearce, J.M., 1991. The changes in colloid populations with time in laboratory microcosm experiments (Progress report – November 1990). British Geological Survey, Tech. Rep. (WE/91/2C), Keyworth, U.K.

Pettersson, C. and Allard, B., 1993. Humic substances in high-pH groundwaters from Maqarin, Jordan. Linköping Univ. Int. Rep.

Smith, P., and Degueldre, C., 1993. Colloid-facilitated transport of radionuclides through fractured media. J. Contam. Hydrol. 13, 143–166.

Vilks, P., Miller, H., and Doern, D., 1991. Natural colloids and suspended particles in the Whiteshell research area, Manitoba, Canada, and their potential effect on radiocolloid formation. Appl. Geochem., 6, 565–574.

Vilks, P., Cramer, J., Bachinski, D., Doern, D., and Miller, H., 1993. Studies of colloids and suspended particles, Cigar Lake uranium deposit, Saskatchewan, Canada. Appl. Geochem., 8, 605–616.

Weres, O., Yee, A. and Tsao, L., 1982. Equations and type curves for predicting the polymerization of amorphous silica in geothermal brines. Soc. Petrol. Eng. J., 3, 9–16.

West, J.M., 1991. The effect of microbial activity on the near and far fields of a Swiss type B repository – a study of gross effects on structures, geochemistry, radionuclide sorption. Final report. British Geological Survey Tech. Rep. (WE/91/13C), Keyworth, U.K. and Nagra Tech. Rep. (NTB 97-XX), Nagra, Wettingen, Switzerland (In press).

West, J.M., Degueldre, C., Allen, M., Bruetsch, R, Gardner, S., Ince, S. and Milodowski, A.E., 1992. Microbial and colloidal populations in the Maqarin groundwaters. In: W.R. Alexander (Ed.), A natural analogue study of the Maqarin hyperalkaline groundwaters. I: Source term description and thermodynamic database testing. Nagra Tech. Rep. (NTB 91-10), Nagra, Wettingen, Switzerland, p. 70–83.

Wieland, E., 1997. Colloid concentrations in cementitious backfill: monocorn mortar and quartz in contact with hyperalkaline cement pore water. Unpubl. PSI Int. Rep., Villingen, Switzerland.

Zeh, P., Czerwinski, K.R. and Kim, J.I., 1997. Speciation of uranium in Gorleben Groundwaters. Radiochimica Acta 76, 37–44.

TABLES

Table 10-1. Representative groundwater analysis for site M1, Adit A-6 (from Milodowski et al., 1998b).

	M1
Temperature (°C)	24.8
pH (field) 12.74	–
pH (lab.) 12.67	–
Eh (field) mV	+278
Major Elements (mgL^{-1})	
Ca	674
Na	47.2
K	9.88
Cl	52.4
SO_4	305
NO_3	3.28
Trace Elements (mgL^{-1})	
Mg	0.01
NH_4	<0.10
NO_2	<0.10
Fe (total)	<0.01
Al	0.14
Si	<0.02

Table 10-2. Mean colloid populations for the 30 nm and 50 nm filters.

Filter Set	30 nm nominal pore size			50 nm nominal pore size		
	Colloid concentration (mL^{-1})		Concentration (mg/L^{-1})	Colloid concentration (mL^{-1})		Concentration (mg/L^{-1})
	Mean	Standard deviation		Mean	Standard deviation	
A	$1.07 \cdot 10^{4}$	$6.47 \cdot 10^{3}$	$3.01 \cdot 10^{-7}$	$3.98 \cdot 10^{4}$	$8.47 \cdot 10^{3}$	$5.21 \cdot 10^{-6}$
B	$1.38 \cdot 10^{4}$	$4.91 \cdot 10^{3}$	$3.89 \cdot 10^{-7}$	$2.45 \cdot 10^{4}$	$1.55 \cdot 10^{3}$	$3.21 \cdot 10^{-6}$
C	$1.05 \cdot 10^{4}$	$8.12 \cdot 10^{3}$	$2.98 \cdot 10^{-7}$	$1.44 \cdot 10^{4}$	$7.65 \cdot 10^{3}$	$1.89 \cdot 10^{-6}$

Table 10-3. Descriptive statistics and histogram classes for filter A4.

Maximum dimension/nanometer		Histogram classes	Number in class
Mean	219.03	<50	0
Count	2713	51–75	0
Range	372.25	76–100	91
Minimum	77.11	101–125	229
Maximum	449.36	124–150	157
Median	212.64	151–175	319
Standard deviation	74.84	176–200	351
Sample variance	5600.36	201–225	379
Kurtosis	0.19	226–250	329
Skewness	0.52	251–275	318
Sum	594232.96	276–300	198
Standard Error	1.44	301–325	102
Confidence interval @ α=0.05	2.82	326–350	77
		351–375	56
		376–400	43
		401–425	39
		426–450	25

Table 10-4. Descriptive statistics and histogram classes for filter B4.

Maximum dimension/nanometer		Histogram classes	Number in class
Mean	188.88	<50	0
Count	656	51–75	0
Range	363.76	76–100	73
Minimum	77.11	101–125	127
Maximum	440.87	124–150	84
Median	163.22	151–175	86
Standard deviation	89.56	176–200	63
Sample variance	8021.76	201–225	47
Kurtosis	0.35	226–250	33
Skewness	1.08	251–275	38
Sum	123905.75	276–300	14
Standard Error	3.50	301–325	17
Confidence interval @ α=0.05	6.85	326–350	12
		351–375	22
		376–400	16
		401–425	13
		426–450	11

Table 10-5. Descriptive statistics and histogram classes for filter C4.

Maximum dimension/nanometer		Histogram classes	Number in class
Mean	173.46	<50	0
Count	847	51–75	0
Range	370.29	76–100	124
Minimum	77.11	101–125	183
Maximum	447.40	124–150	127
Median	147.41	151–175	96
Standard deviation	80.67	176–200	68
Sample variance	6507.17	201–225	56
Kurtosis	0.71	226–250	42
Skewness	1.14	251–275	44
Sum	146916.62	276–300	28
Standard Error	2.77	301–325	24
Confidence interval @ α=0.05	5.43	326–350	21
		351–375	9
		376–400	12
		401–425	6
		426–450	7

Table 10-6. Calculated colloid populations and mass.

Sample	Method A (West et al., 1992)		Method B		Method C Direct calculation	
	(colloids. mL^{-1})	($mg.L^{-1}$)	(colloids.mL^{-1})	($mg.L^{-1}$)	(colloids.mL^{-1})	($mg.L^{-1}$)
A4	$1.2 \cdot 10^7$	0.150	$1.21 \cdot 10^7$	0.130	$1.24 \cdot 10^7$	0.190
B4	$4.89 \cdot 10^7$	0.043	$4.89 \cdot 10^7$	0.030	$3.00 \cdot 10^7$	0.038
C4	$1.15 \cdot 10^7$	0.051	$1.15 \cdot 10^7$	0.034	$3.87 \cdot 10^7$	0.036
Mean population	$2.42 \cdot 10^7$	0.081	$2.42 \cdot 10^7$	0.065	$2.70 \cdot 10^7$	0.088
Combined data	$1.36 \cdot 10^7$	0.083	$1.36 \cdot 10^7$	0.062	$6.42 \cdot 10^6$	0.087

Table 10-7. Normal size distribution functions.

Sample	Method A (West et al., 1992)		Method B
	Particle distribution	Mass distribution	Mass distribution
A4	$\delta[coll]/\delta\Phi = 10^{10}\Phi^{-1.1193}$	$\delta[coll]/\delta\Phi = 10^{-8}\Phi^{1.8807}$	$\delta[coll]/\delta\Phi = 3 \cdot 10^{-9}\Phi^{2.0606}$
B4	$\delta[coll]/\delta\Phi = 5 \cdot 10^{10}\Phi^{-1.6509}$	$\delta[coll]/\delta\Phi = 6 \cdot 10^{-08}\Phi^{1.3491}$	$\delta[coll]/\delta\Phi = 2 \cdot 10^{-8}\Phi^{1.4772}$
C4	$\delta[coll]/\delta\Phi = 2 \cdot 10^{12}\Phi^{-2.2446}$	$\delta[coll]/\delta\Phi = 2 \cdot 10^{-06}\Phi^{0.7554}$	$\delta[coll]/\delta\Phi = 7 \cdot 10^{-7}\Phi^{0.8742}$
Combined data	$\delta[coll]/\delta\Phi = 5 \cdot 10^{10}\Phi^{-1.5061}$	$\delta[coll]/\delta\Phi = 5 \cdot 10^{-08}\Phi^{1.4939}$	$\delta[coll]/\delta\Phi = 2 \cdot 10^{-8}\Phi^{1.6501}$

Table 10-8. Comparison of existing data on near-field cementitious colloids.

Report	Methodology	Colloid Population (mL^{-1})	Colloid Concentration ($mg.L^{-1}$)
This report	Collection of groundwater at the cement/host rock interface	$1.15 - 4.89 \cdot 10^{7}$	0.051 – 0.190
Pearce, 1991	Incubation cells containing simulated waste, containment and backfill materials in synthetic groundwater	average $5 \cdot 10^{6}$	0.017[1]
Wieland, 1997	Leaching of crushed PZHS[2] monocorn mortar and quartz aggregate with cement pore waters, solid:liquid ratio of 1:10	$0.4 - 7.0 \cdot 10^{5}$ (total)[3] $1.5 - 8.5 \cdot 10^{3}$ (undist.)[4] $2 - 5 \cdot 10^{3}$ (steady)[5]	1 – 50 0.03 – 1 0.004 – 0.021
Gardiner et al., 1998	Leaching of crushed cement with groundwaters, solid:liquid ratios of 1:5, 1:10 and 1:50	$3 - 9 \cdot 10^{6}$ (NRVB)[6] $1 - 2 \cdot 10^{5}$ (PFA:OPC)[7] $1 - 9 \cdot 10^{5}$ (BFS:OPC)[8]	As this paper is only an overview of unpublished data, full information is not available to calculate colloid mass (see equation 10c)

Note:

1. No data on colloid diameters available so smallest filter nominal pore size (15 nm) used with equation 10c. Note, however, that this calculation should be applied only to a size distribution and the error induced by using a single value for the colloid diameter may be up to two orders of magnitude (C. Degueldre, pers. comm. to WRA, 1996).
2. High Sulphate Resistance Portland Cement.
3. Total colloid concentration measured immediately after end-over-end mixing of a batch system. Experimentally defined colloid diameter $\geq$100 nm.
4. Colloid concentration measured after leaving batch system undisturbed for 24 hours. Experimentally defined colloid diameters between 100 nm and 1000 nm.
5. Colloid concentration measured after leaving batch system undisturbed for >24 hours. Experimentally defined colloid diameter $\geq$100 nm.
6. Nirex Reference Vault Backfill. No data on colloid size distribution.
7. 3:1 mix of Pulverisied Fuel Ash: Ordinary Portland Cement. No data on colloid size distribution.
8. 3:1 mix of Blast Furnace Slag: Ordinary Portland Cement. No data on colloid size distribution.

Table 10-9. Colloid populations and concentrations determined in other selected groundwaters.

Site	Type	Size cut-off (nm)	Colloid population (mL^{-1})	Colloid concentration (mL^{-1})	Reference
Maqarin	M1 site	40.5	$2.42–2.70 \cdot 10^{7}$	0.065–0.088	This report
Maqarin	M1 site	40	?	0.087–0.500	West et al., 1992
Black box experiment	Lab. high pH system	15	$5 \cdot 10^{6}$	0.017[1]	Pearce, 1991
Cigar Lake	U orebody in clay	?	?	8	Vilks et al., 1991; 1993
Poços de Caldas	Osamu Utsumi U mine	?	?	0.8	Miekeley et al., 1992
Poços de Caldas	Morro do Ferro Th ore body	?	?	3.1	Miekeley et al., 1992
Alligator Rivers	U orebody	?	?	$1.4 \cdot 10^{-3}$	Miller et al., 1994
Gorleben aquifer systems	Permian salt dome	1	$5.3 \cdot 10^{14}$	158	Dearlove et al., 1991
Gorleben aquifer systems	Permian salt dome	1	$3.4 \cdot 10^{11}$	<0.9	Kim, 1991

FIGURES

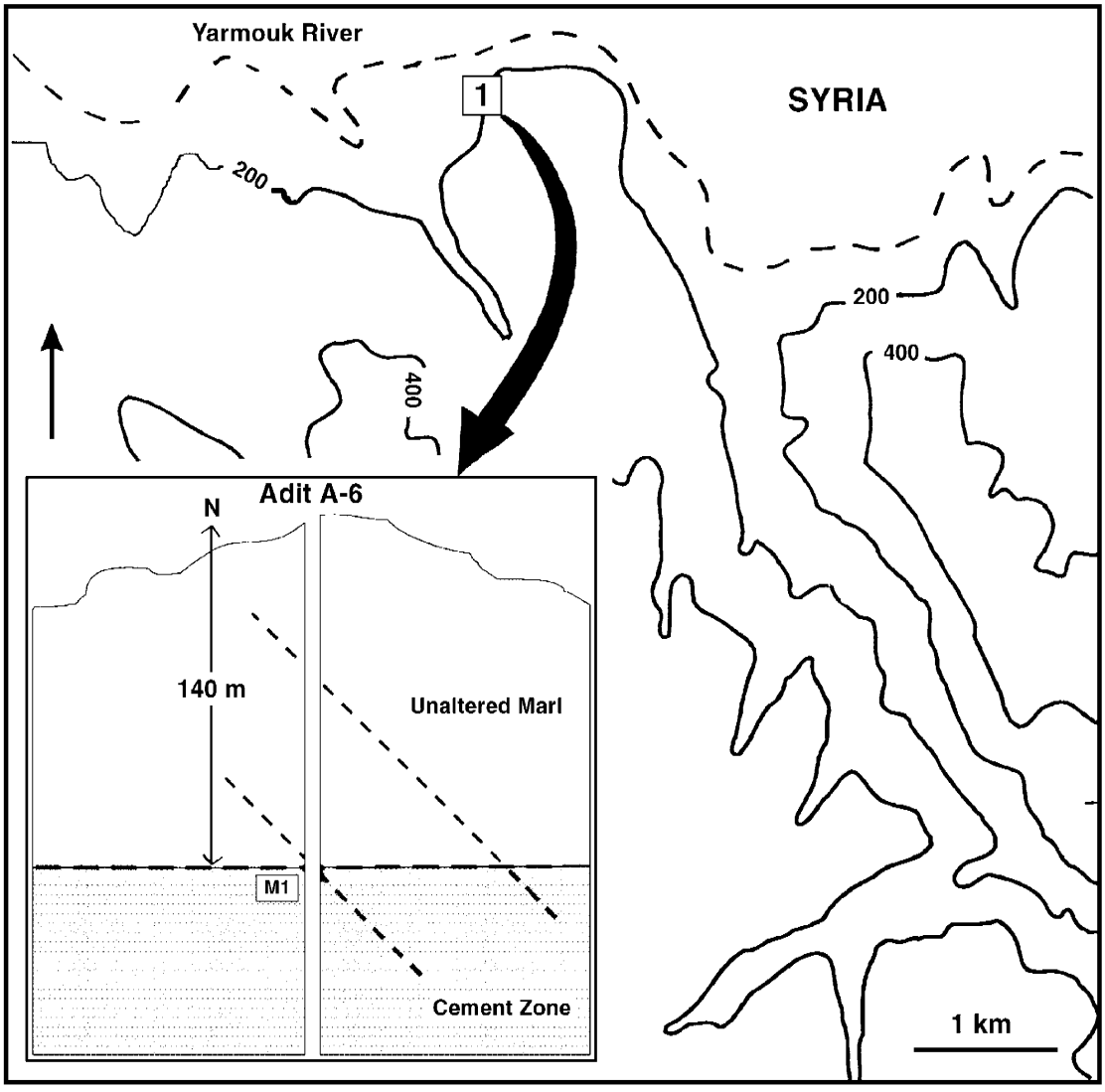

Figure 10-1. *Location of Adit A-6 and colloid sampling site M1.*

Figure 10-2. *Typical view of Adit A-6 at the M1 hyperalkaline groundwater inflow point. The secondary deposits are an intimate mixture of portlandite and carbonate.*

Figure 10-3. *M1 sampling site. Extensive secondary deposits, up to 30 cm thick, completely coat the walls of the Adit and had to be removed to fit the funnel to the rock.*

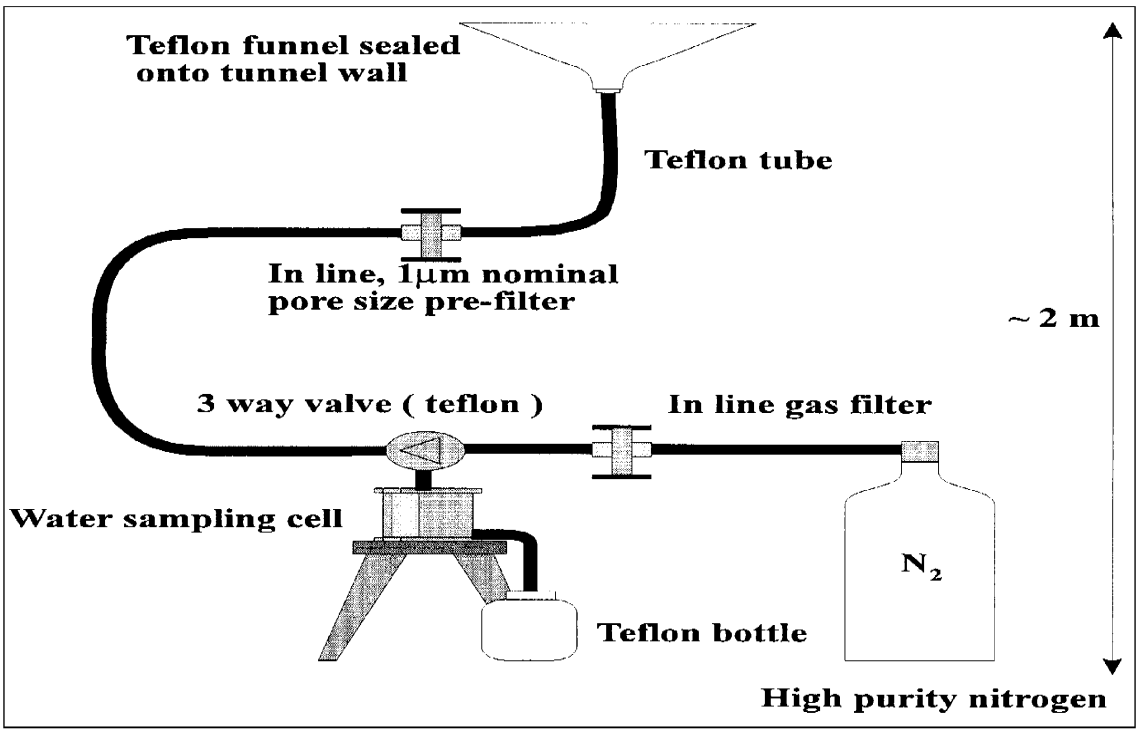

Figure 10-4. *Sketch of the sampling system set-up in the field.*

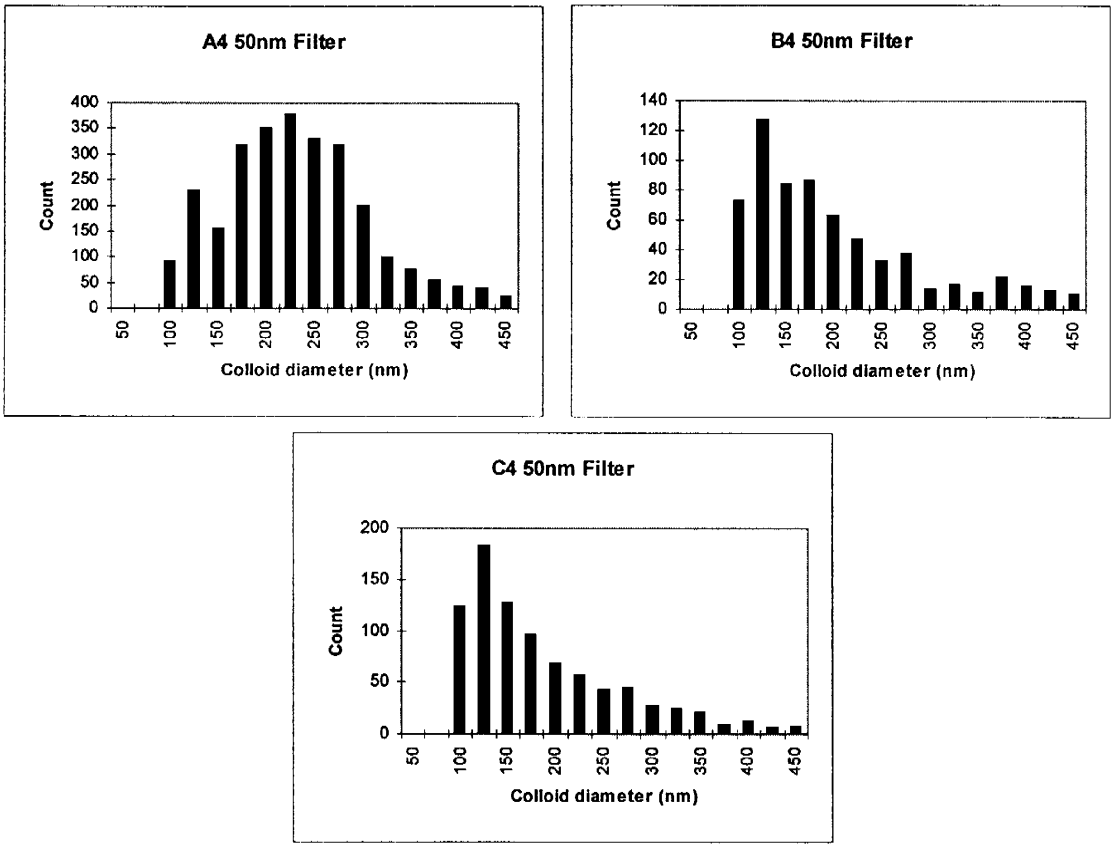

Figure 10-5. *Histograms of colloid size data.*

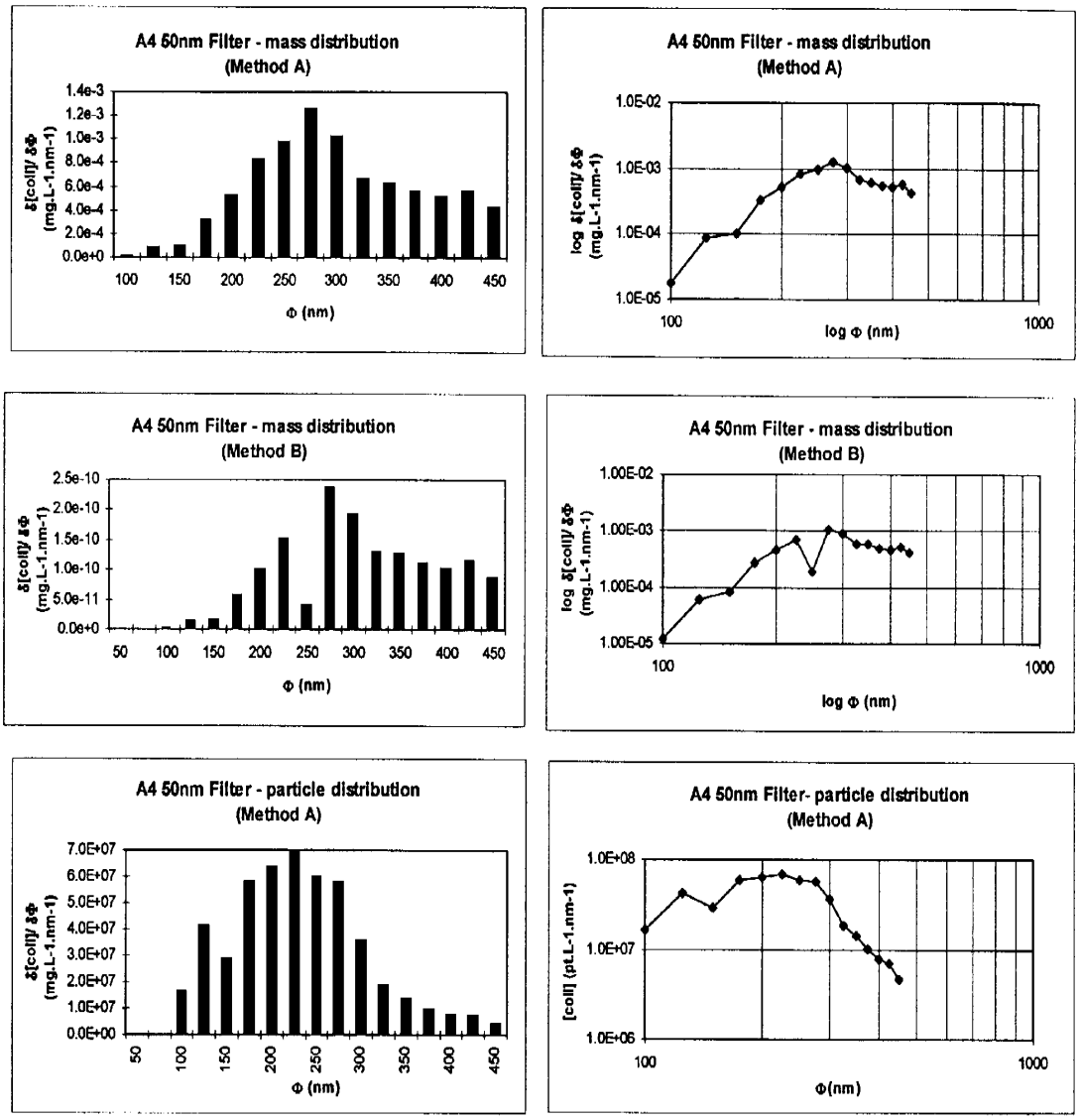

Figure 10-6. *Normal distribution spectra for filter A4.*

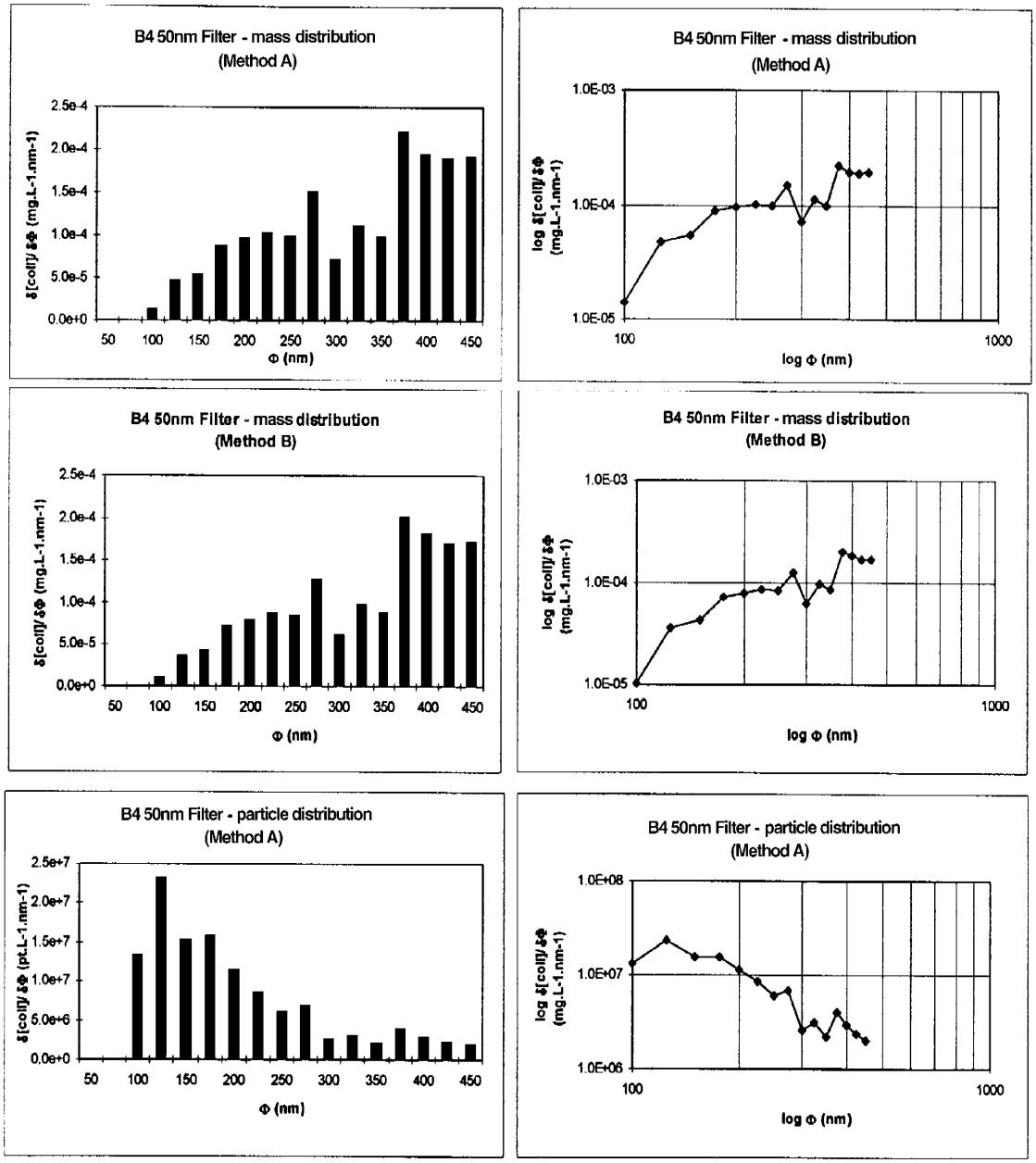

Figure 10-7. *Normal distribution spectra for filter B4.*

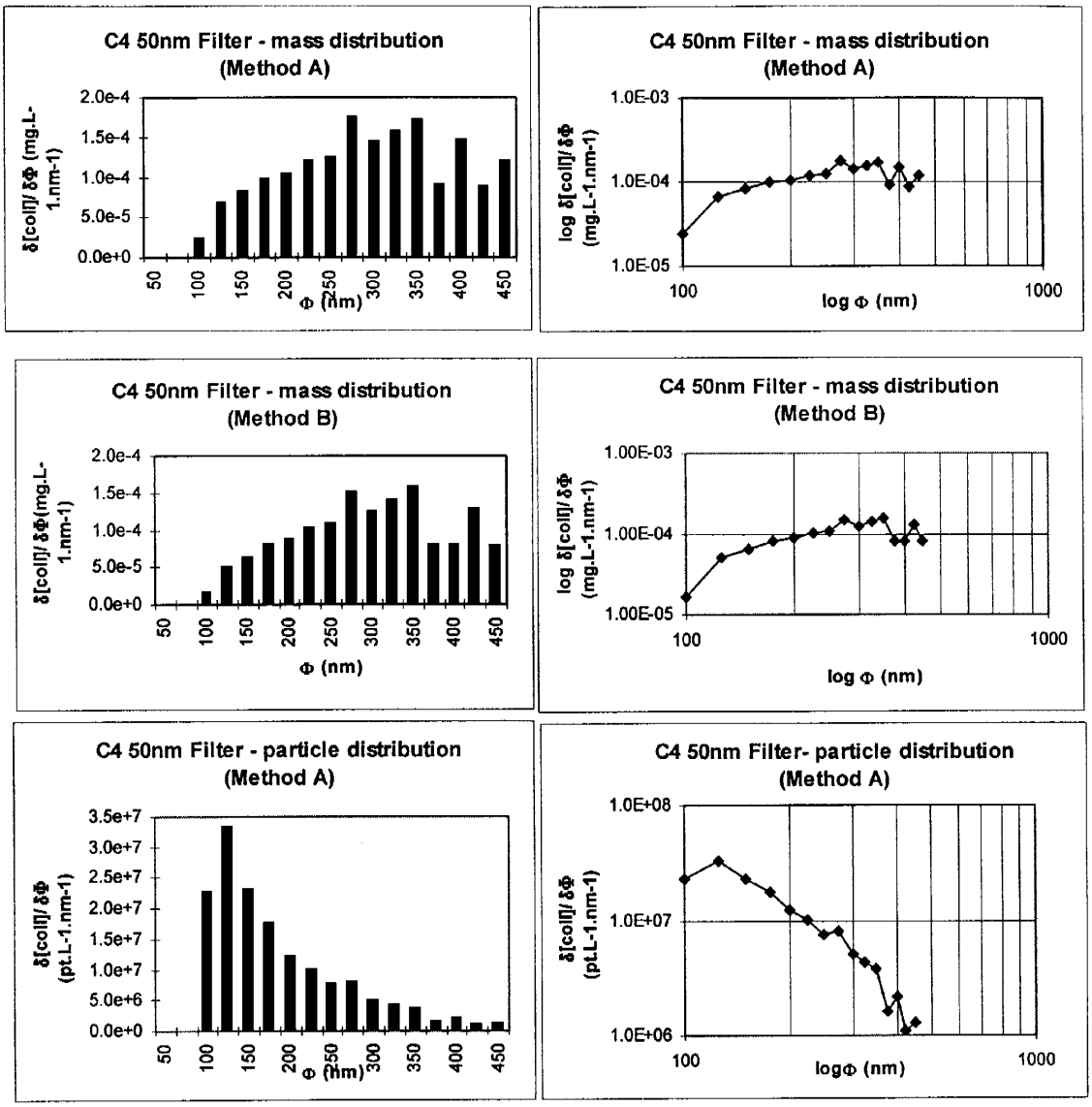

Figure 10-8. *Normal distribution spectra for filter C4.*

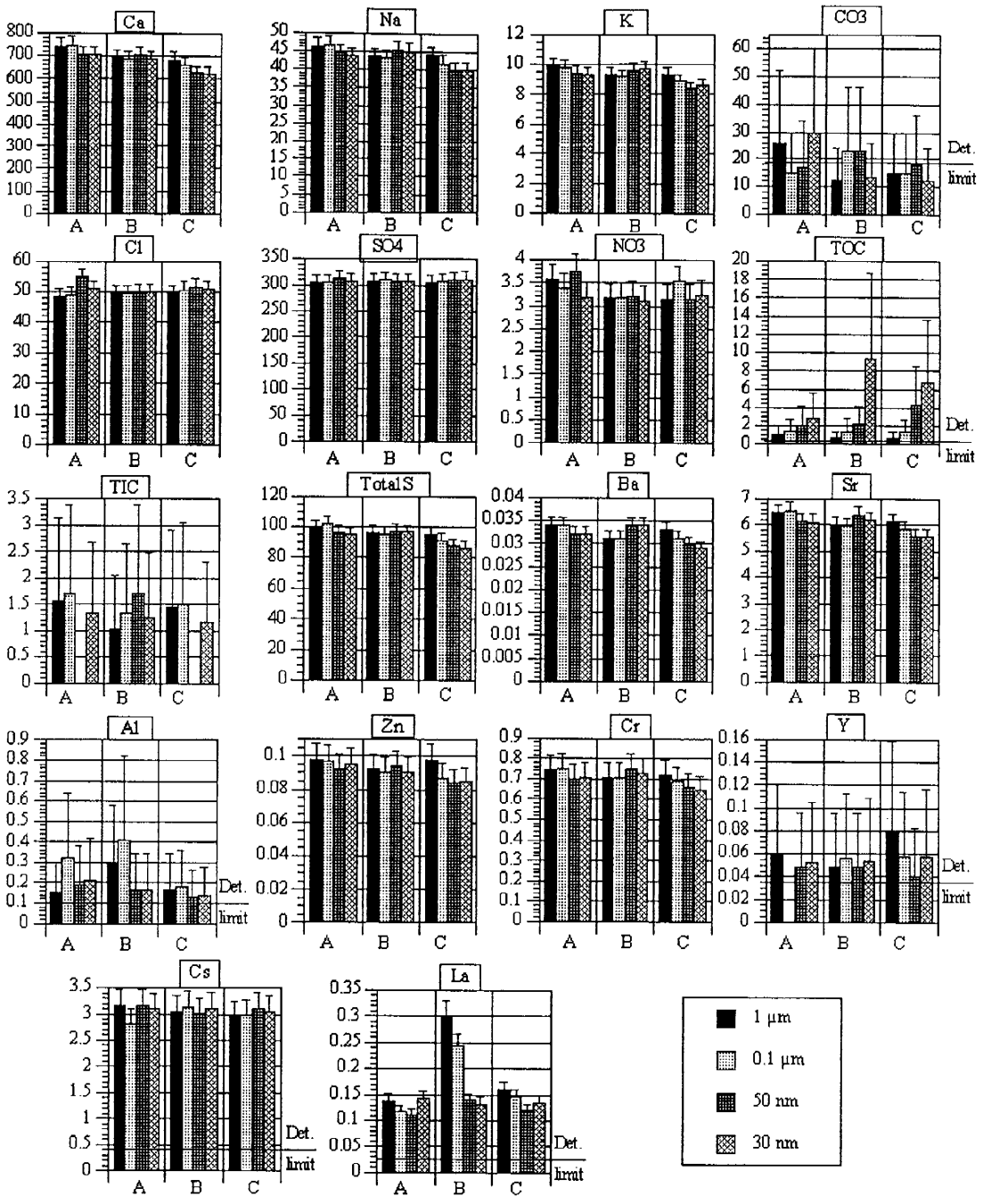

Figure 10-9. *Comparison of the filtrate chemistry between the three samples A, B and C from water sampling site M1 in Adit A-6 for the filter sizes 1.0 µm, 0.1 µm, 50 nm and 30 nm. Selected determinants plotted only. Detection limits are indicated where concentrations are within one order of magnitude. All concentrations are in* mgL^{-1}.

11 CULTURABILITY AND 16S rRNA GENE DIVERSITY OF MICRO-ORGANISMS IN THE HYPERALKALINE GROUNDWATERS OF MAQARIN

(K. Pedersen, J. Arlinger, A-C. Erlandson and L. Hallbeck)

11.1 INTRODUCTION

So-called "normal conditions" have been used to understand the foundations of bacterial cell functions and to describe the origin of physiological biochemistry. Normal conditions are usually defined as neutral pH, a temperature at 37°C, aerobic atmosphere with no over pressure, 1% salinity and with glucose as the main energy and carbon source. The conditions for life in a radioactive waste repository environment will in most respects be somewhat extreme, i.e. very different from what is understood as "normal conditions". Modelling bacterial processes in radioactive waste disposal therefore must concentrate on bacteria adapted to such environments. In comparison with what is known for bacteria living under normal conditions, detailed understanding of these repository-related bacteria is unfortunately limited when it comes to predicting bacterial processes in future waste repositories under conditions of high pH, high temperature and radiation etc. (Pedersen, 1996, 1997b). Despite wide variations in habitat pH, the internal pH of most bacteria is close to neutral. This may result from plasma membrane impermeability to protons; possibly, protons and hydroxyl ions are pumped out to maintain the proper internal pH. Extreme alkaliphiles maintain their internal pH close to neutrality by exchanging internal sodium ions for external protons (Horikoshi and Akiba, 1982). Although a high pH environment may be extreme for many bacteria, there appears to be no obvious limitation for the adaptation of bacteria to such environments.

Natural analogues and other sites with adverse conditions (e.g. radioactive waste sites) are, therefore, valuable sites to study in order to model and assess conditions that are expected to influence the performance of future radioactive waste repositories. Among the questions to be answered is whether micro-organisms can survive and be active at the extreme pH values typical for the Maqarin groundwaters.

Previous investigations have indicated the presence of micro-organisms in the hyperalkaline groundwaters of Maqarin. Culturing techniques were used to assess the populations and types of bacteria present (Alexander, 1992; Coombs et al., 1998). A diversified microbial population was found with a pH tolerance in cultures up to the highest pH studied, pH 11. However, a well documented problem when using culturing techniques to reveal microbial diversity is "the great plate count anomaly" of environmental samples as recently reviewed by Amann et al. (1995). Generally, only a few percent or less of the total microbial population in environmental samples can be successfully cultured. Non-culturing techniques, such as extraction and sequencing of the ribosomal DNA can be applied to overcome that problem (Amann et al., 1995;

Pedersen et al., 1997). Still, if both culturing results and molecular data show that microbes can be found in the Maqarin hyperalkaline waters, this does not necessarily prove that the found microorganisms were actively growing in the highly alkaline groundwater; they may have been just transported there from a neutral pH environment. Investigation of solid rock material that is exposed to high pH water to enable the growth of microbes in biofilms, or for other signs of attached growth, may be a possible way to prove that microbes can be active at these high pH values. This study describes how molecular methods, microscopy, culturing techniques and chemical analysis were used in an attempt to study the culturability and diversity of microbial populations detected in the hyperalkaline groundwater of Maqarin.

11.2 MATERIALS AND METHODS

11.2.1 Sampling Sites and Sampling Schedule

The samples analysed were collected during November 1994, April 1995 and November 1996 from three main sites; Adit A-6 (M1) and the Maqarin Station Railway Cutting (M3, M8, M18) at the Eastern Springs locality, and from the Western Springs locality (M5, M17) (Fig. 11-1). A sample was also taken from a seep within Wadi Sijin (WS). Water was collected in sterile plastic tubes and treated according to the protocol described below. The November 1994, sampling followed heavy rainfall and a period of flooding of the Yarmouk River. In contrast, the April 1995 and November 1996 sampling occurred after dry periods. Table 11-1 summarises the sampling sites and the sampling schedule; see Chapter 4 for further details. Sample M18, the Eastern Springs borehole locality, representing a mixture of hyperalkaline groundwater and precipitation, was sampled in series during the 1994 expedition. Samples were collected following the removal of 1 litre (M18-1), 2 litres (M18-2) and 25 litres (M18-3) of groundwater respectively from the borehole. It was also sampled once during the 1996 expedition, but the sample obtained was very turbid and not considered representative. Sample M1 (also Eastern Springs locality) representing an active hyperalkaline discharge from a cement zone, was sampled from Adit A-6.

At the Western Springs locality, samples M5 and M6 were collected from the seepages, together with borehole WS1 sample M17 from the unaltered Bituminous Marl Formation (characterised by a smell of H_2S). It was sampled in series in 1994 following the removal of 0 litre (i.e. start of pumping, M17-1), 2 litres (M17-2), 3.5 litres (M17-3), 5 litres (M17-4) and 20 litres (M17-5) respectively from the borehole.

11.2.2 Determination of Bacterial Populations

Samples for determination of bacterial populations were taken in sterile plastic tubes and immediately preserved with formaldehyde (2% final concentration). All samples were transported to the laboratory for counting. The total number of bacteria in the groundwater was determined by the Acridine Orange Direct Count (AODC) method (Pedersen and Ekendahl, 1992). Briefly, the groundwater samples were diluted to twice their volume with sterile filtered 0.1% oxalic acid and vigorously shaken to reduce

clogging of the filters used. A portion of the sample was filtered onto a Sudan-black stained Nuclepore filter of 0.22 μm pore size and 13 mm in diameter at -20 kPa and stained for 6 min. with acridine orange. All solutions were filter sterilised (0.22 μm). One or up to three parallel samples were analysed and two filters were counted for each water sample. The number of bacteria was counted using blue light (390–490 nm) under an epifluorescence microscope (Olympus BH-2). Between 500 and 600 cells or a minimum of 15 fields (0.0064 mm^2 each) were counted on each filter. This procedure will predict a sample mean with a precision of 5% (Niemelä, 1983; Hallbeck and Pedersen, 1990). The results were calculated as mean values of all filters from each site.

11.2.3 In Situ Hybridisation on Rock Samples

Samples of stalactites and stalagmites from the M1 site in the Adit A-6 tunnel, and rock samples from the alkaline seepages at the Western Springs locality, were collected and preserved with sterile filtered cold 4% paraformaldehyde. Care was taken to ensure that the samples had been in contact with flowing alkaline water at each respective site prior to sampling. After twenty-four hours in the 4% paraformaldehyde solution, the rock samples were removed and washed using a phosphate buffer solution (PBS) and put into a tube containing PBS and ethanol (50/50%). Autofluorescense of the samples was checked at the chosen wavelength; for the Cy5-type nucleic acid probes, the wavelength chosen is 647 nm. If the rock minerals had too high an autofluorescense, it was not possible to resolve the *in situ* hybridisation signal from the background.

11.2.4 Groundwater Composition and pH

Reference groundwater samples were collected according to the protocol described in Chapter 4.

The in situ pH was measured directly at each site using a pHep3-meter calibrated with buffers 4.01 and 7.00. The pH was also measured 3 to 4 days and 27 days after sampling, using a PHM 83 pH-meter calibrated with similar buffer solutions.

11.2.5 Sampling and Enrichment of Alkaliphilic Micro-organisms

During the 1996 sampling, a total of 100 mL of groundwater was collected directly from each location in two separate 300 mL sterile Nalgene beakers (with a screw lid) supplied with different carbon sources. The beakers were placed on a shaker at room temperature the third day after sampling. Extra water was collected in sterile, empty beakers for use during sub-culturing and for counts of the total numbers of bacteria. Two different media were used and inoculated with hyperalkaline water from the springs: 1) 100 mL of water were collected in beakers containing 0.1g peptone, 0.1g yeast extract, 0.5g glucose, and 2) 100 mL of water were collected in beakers containing 0.1g peptone, 0.1g yeast extract and 0.5 g lactate dissolved in 5 mL distilled H_2O. The enrichments were put on a shaker for 27 days at room temperature three days after sampling. Subsequently, the total number of bacteria in the cultures were assayed using the AODC technique. Enrichments with growing cells were sub-cultured in fresh media.

One mL of the cultures that were growing with lactate were inoculated into the following three different media: 1) Site relevant medium: 0.1g peptone, 0.1g yeast extract, 0.5 g lactate and 100 mL of sterile filtered water from the same source from which the original culture was inoculated. 2) Basal medium for alkaliphilic microorganisms: Lactate 10 g/L, polypeptone 5 g/L, yeast extract 5 g/L, KH_2PO_4 1 g/L, $MgSO_4 \cdot 7H_2O$ 0.2 g/L, Na_2CO_3 10 g/L, 100 mL H_2O /beaker. 3) Basal medium for alkaliphilic microorganisms: Lactate 10 g/L, polypeptone 5 g/L, yeast extract 5 g/L, KH_2PO_4 1 g/L, $MgSO_4 \cdot 7H_2O$ 0.2 g/L, Na_2CO_3 10 g/L, 100 mL H_2O /beaker. To beakers 2 and 3 10 mL sterile filtered water was added from the same source from the original culture was inoculated to ensure that necessary growth factors were included.

One mL of the cultures that were growing with glucose were sub-cultured in the following media: 1) 0.1 g peptone, 0.1 g yeast extract, 0.5 g glucose and 100 mL of sterile filtered water from the same source from which the original culture was inoculated. 2) Basal medium for alkaliphilic micro-organisms: Glucose 10 g/L, polypeptone 5 g/L, yeast extract 5 g/L, KH_2PO_4 1 g/L, $MgSO_4 \cdot 7H_2O$ 0.2 g/L, Na_2CO_3 10 g/L, 100 mL H_2O /beaker. 3) Basal medium for alkaliphilic micro-organisms: Glucose 10 g/L, polypeptone 5 g/L, yeast extract 5 g/L, KH_2PO_4 1 g/L, $MgSO_4 \cdot 7H_2O$ 0.2 g/L, Na_2CO_3 10 g/L, 100 mL H_2O /beaker. To beakers 2 and 3 10 mL sterile filtered water was added from the same source from which the original culture was inocculated from. The sub-cultures were put on a shaker at room temperature for 19 days before observed under the microscope using the AODC technique. The pH of the culture was measured simultaneously during observation.

11.2.6 DNA Extraction, PCR-amplification, Cloning and Sequencing

Groundwater for DNA analysis was sampled from M5, M8, M17-1, M17-2, M17-5 and M18-3 in November 1994, and from M1, M3 and M5 in April 1995. The groundwater was collected directly from the boreholes or seeps in sterile plastic tubes and immediately deep frozen using CO_2 ice and transported rapidly to the laboratory. Here, 10 mL samples were filtered onto sterilised 0.2 μm pore-sized Nuclepore filters. DNA extraction, PCR amplification, cloning and sequencing followed a procedure published elsewhere (Pedersen et al., 1996b). A Pfu DNA polymerase (Stratagene) was used, which has a proof reading ability that minimises the chance of chimer formation.

11.2.7 Sequence Analysis

The 16S rRNA gene clone sequences found were compared to sequences available from the European Molecular Biology Laboratory (EMBL) database using the FastA procedure described in the GCG program package (Genetic Computer Group, Wisconsin, USA). This procedure calculates identities between an unknown sequence (clone) and sequenced bacteria in the database. The phylogenetic analysis was performed using the programs contained in the PHYLIP version 3.5c package (Felsenstein, 1989) compiled for PCS. Nucleotide positions that could be unambiguously aligned for all clones were included in the analysis. The final data set comprised 301 nucleotide positions, i.e. 537-833 [*E.coli* Brosius numbering, but not including 5 inserts in the analysed data set (Brosius et al., 1978)]. The distances were calculated using the DNADIST program and a phylogenetic tree was constructed

running the KITCH program (Felsenstein, 1989) with contemporary tips. The KITCH program was run with a randomised input order of data with 10 jumbles and during execution, 60224 trees were examined. The tree was drawn by using a drawing program, DRAWTREE, also available in the PHYLIP package, and was used to differentiate the main lines of decent of the found sequences as described by Stackebrandt and Rainey (1995).

11.3 RESULTS

11.3.1 Groundwater Chemistry

Groundwater sampling and chemistry from the Maqarin area has been described earlier (Alexander, 1992; Linklater, 1998; this report, Chapters 4 and 6) and the results of sampling associated with this study are only briefly summarised below. The sampling sites M1, M3, M5 and M8 consist of hyperalkaline water with a pH between 12.3 and 12.9 while the sites M17 and M18 were close to neutral with a pH of 7.2 and 8.2 respectively. The temperature was around 25°C in all groundwaters except for M18 which had a temperature of 18.5°C. The total organic carbon contents (TOC) were 6–7 mg L^{-1} at M5, M8 and M18, with smaller amounts (1–3 mg L^{-1}) present in the other groundwaters analysed. Nitrogen was present as nitrate in all waters (0.2 up to 35 mg L^{-1}), with the lowest concentration at M17 and the highest value in M5. There were high concentrations of calcium (87-1120 mg L^{-1}) and sulphate (280 – 1410 mg L^{-1}) in all waters analysed. Phosphorus was present in all sampled groundwaters, with highest concentrations in M5 (0.12 mg L^{-1}) and lowest in M17 and M18 (less than 0.02 mg L^{-1}). The 1996 data are shown in Table 11-2. It shows that the Western Springs sampling sites, M5 and M6, are characterised by groundwater with higher pH, Ca, Na, K, NH_3, Cr, SO_4 and NO_3 concentrations than the Eastern Springs sampling site M1 in Adit A-6.

11.3.2 Total Number of Bacteria

The five samples collected in series during 1994 from borehole M17 (1-5), and the three from borehole M18 (1-3) show an initial decrease in total number of bacteria mL^{-1} that was stabilised after approximately 5 litres of water had been flowing (Fig. 11-2). The total number of bacteria was highest in the neutral pH groundwaters, M17 and M18 (Fig. 11-2 and Table 11-3), and ranged between 1 to 3 orders of magnitude higher than the total number of bacteria in water from M1, M3, M5, M8 and Wadi Sijin (WS). There was a relatively large number of bacteria in sample M8 during the 1996 expedition.

11.3.3 Enrichment of Alkaliphilic Micro-organisms

The cultures were filtered and stained for AODC and enrichments to be sub-cultured were chosen if growth could be detected. Only a few of the cultures had grown and were sub-cultured again in a new medium (Tables 11-4 and 11-5). The pH was

monitored during incubation of the enrichment cultures and decreased approximately 0.5 units in the glucose-based medium and increased about 0.5 units when lactate was used as the carbon source (Table 11-6). The pH was initially high when the Maqarin groundwater was used as the water source, but the preparation of synthetic media with a pH that was stable at around 12.5 was unsuccessful (West et al., 1992; Coombs et al., 1998).

11.3.4 Sequencing 16S rRNA of Isolated Bacteria

Two isolates were obtained from the M8 enrichments and their 16S rRNA gene could eventually be successfully sequenced; for unknown reasons, however, several difficulties with the sequencing protocol were encounted. None of the found sequences coincided with earlier obtained sequences (Table 11-7).

11.3.5 In Situ Hybridisation

A rock sample that had been in contact with the M5 seepage water was analysed using the epifluorescense microscope at wavelengths 390–490 nm and 647 nm. Unfortunately, there was so much autofluorescense at both these wavelengths that in situ hybridisation could not be performed. The same procedure was carried out using a stalactite from the tunnel, and in this case there was also too much autofluorescense at the 647 nm wavelength. The rock sample from M5 and the stalactite from the tunnel were additionally stained with acridine orange and studied under blue light, but no attached cells could be detected.

11.3.6 Distribution and Diversity of Bacteria as Analysed by 16S rRNA Gene Analysis

A total of 87 clones were sequenced, 10 from each sampling site and sample occasion except for M8 and M17-2 where 9 and 8 clones respectively were sequenced (Table 11-8). The 87 clones examined clustered into 23 different, specific sequences, each of which was given a clone group name, ranging from JN1 to JN19 for samples obtained in November 1994, to JA21-JA24 for samples obtained in April 1995. The clone group names were given clone letters ranging from "a" to "h". These letters show the sample(s) in which the clone sequence was found (Tables 11-2 and 11-8). A clone number, 1-23, is used below to identify the clones in Table 11-8. Between 1 and 5 different 16S rRNA gene sequences were detected in each sample. Some of the clone groups have several identical clone sequences, while others represent only a few or a single clone sequence. The six most commonly occurring clone sequences, Nos. 5, 6, 13, 16, 19, and 20, constituted 71 % of the sequenced clones (62 clones out of 87). Typically, each of these clone group sequences predominated at a specific site with the exception of No. 16 which predominated in three sites: M1, M3 and M5 (Table 11-8) and comprised 29% of all found sequences (25 clones out of 87). Three other clone groups were also detected at more than one site; Nos. 5, 19 and 20. The diversity was greatest in the neutral pH groundwater from M17 where five different clone groups were obtained for each of the three samples, and a total of 14 different clone groups appeared. The boreholes samples had a lower diversity with 1 or 4 clone groups per

borehole. The lowest diversity was found in Adit A-6 (M1), with all 10 clone sequences belonging to the same clone group, while four specific clone group sequences were found in M3, M5 and M8. Sampling site M18 also had a low diversity with two clone groups.

The closest related species in the database for the clones are also shown in Table 11-8. The association of a clone sequence with a species in the database at identity values below approximately 95% is meaningless because of the large phylogenetic difference at or below this level of identity. Therefore, the closest species in the database are only given for clones with an identity at or larger than 95%. Most of the found sequences clustered with the Proteobacteria Alpha, Beta and Gamma groups, one, No. 17, with Gram-positive bacteria and one, No 18, with the phylogenetic group *Thermus-Deinococcus* which is an ancient branch in the phylogenetic tree of *Bacteria* (Woese, 1987) (Table 11-8 and Fig. 11-3). Four of the clones, Nos. 20, 21, 22 and 23 were only very distantly affiliated with known bacteria and may, therefore, represent new branches in the bacterial phylogenetic tree (Fig. 11-3). No. 20, occurring in M8 and M18-3, was, however, closely related to the clone sequence G15 found in groundwater from Bangombé in Gabon (Pedersen et al., 1996b). The clone group sequence No. 13 was identical with the Bangombé sequence G21. High identities were also obtained with the genus *Acinetobacter* (Nos. 11, 12, 13, 14 and 15). Finally, one of the clone group sequence, No. 19, was closest related to an eukaryal species, a fungus, with 98.1% identity.

11.3.7 Accession Numbers

The nucleotide sequence data reported in this paper appears in the EMBL, GenBank and DDBJ Nucleotide Sequence Databases under the accession numbers Z69266 – Z69288 corresponding to JN1af – JN19e and JA21gh – JN24he, respectively.

11.4 DISCUSSION

11.4.1 Total Number of Bacteria

A first approach to most environmental microbiology studies is to assay total numbers of bacteria which will reveal if micro-organisms are present. The total number of bacteria found from Maqarin, from 10^3 up to 10^7 bacteria mL^{-1} (Table 11-3), is within the range of what has been previously reported for other subterranean sites (Pedersen, 1996). The decrease in the total number of bacteria registered in the M17 and M18 boreholes during pumping (Fig. 11-2) was probably due to the stagnant water in the borehole containing more bacteria than the aquifer water subsequently pumped up during sampling. Earlier investigations of the M1 and M3 sites (West et al., 1992; Coombs et al., 1998) indicated numbers in the same order of magnitude (M1 and M3 then had $1.7 \cdot 10^4$ [$2.6 \cdot 10^3$] and $6 \cdot 10^4$ [$2 \cdot 10^4$] bacteria mL^{-1} respectively). Using scanning electron microscopy bacteria were also found attached on solid samples from M1, and the total number of attached bacteria on solids from sites M1 and M3 were estimated to be $3.4 \cdot 10^5$ and $1.9 \cdot 10^5$ bacteria cm^{-2}, respectively. However, it should be

stressed that the identification of bacteria using SEM only as reported, is not regarded as conclusive unless structures typical for micro-organisms are also observed. The recent controversy concerning SEM images of what was suggested to be Martian microbes is a good example of the uncertainty that follows SEM identification alone (McKay et al., 1996). This present study could not find any attached bacteria using *in situ* hybridisation and light microscopy methods on samples collected during 1996. This may be due to methodological problems, such as interferences of the high pH with the hybridisation enzymes, or that attached bacteria simply did not exist. Future experiments should include artificial "blank reference" surfaces introduced in flowing hyperalkaline water. The presence of microbial biofilms after a couple of months of exposure would be conclusive evidence that microbes can be active at the very high pH in these waters, as indicated by the pH 11 results reported by Coombs et al. (1998). Absence of microbial biofilms would indicate the contrary.

11.4.2 Enrichment and Isolation of Alkaliphilic Micro-organisms

Earlier investigations (West et al., 1992; Coombs et al., 1998) reported growth of bacteria at or below pH 11, but pH above 11 could not be studied for the same reasons as noted below. Here, an attempt was made to grow bacteria at the high pH values prevailing at Maqarin with partial success. It was possible to obtain culture growth at the *in situ* pH using Maqarin groundwater as base, but it was not possible to make artificial media with pH above 12 as heavy precipitation occurred when the pH was raised. Growth occurred in *in situ* cultures with a pH above 12 (Table 11-6) but the pH did eventually decrease to below 10 after prolonged culturing (Table 11-5). It is, therefore, not possible to conclusively claim that the obtained growth occurred at high pH. Few of the enrichment cultures showed growth. It was mainly M8 that resulted in enrichment cultures coinciding with a total number of bacteria that was highest at site M8. This particular location seems to have been somewhat less well buffered at high pH, and to be a little more dilute than the other alkaline seepages (Table 11-2), and thereby possibly more inhabitable. It was not possible to continue the enrichment experiments and isolate bacteria for identification; bacteria only grew with the constant addition of Maqarin groundwater as a growth factor additive, and unfortunately, the availability of such groundwater was limited.

11.4.3 16S rRNA Gene Diversity and Distribution

A total of 23 different clone sequences was found which indicates the Maqarin area to be populated by a diverse microbial population. Most sequences were related to the Proteobacteria alpha, beta and gamma groups which agrees with what has been found at other subterranean sites (Ekendahl et al., 1994; Pedersen, 1997a; Pedersen et al., 1996a, 1997). A few were only distantly related to sequences from known, cultured and sequenced bacteria contained in the database and may, therefore, represent new branches in the phylogenetic tree. One of these showed a high identity with other sequences from subterranean sites (Table 11-8), e.g. the clone group No. 20 (12 clones) that was closely related to the Bangombé sequence, G15 frequently occurring there in two independent boreholes (13 clones) (Pedersen et al., 1996b). Also, several of the Maqarin site clone sequences had sequences from other subterranean sites as the closest

related sequence in the database (Table 11-8), implying that many of these sequences may represent a subterranean biosphere (Pedersen, 1993).

Each Maqarin sampling site generally had a clone sequence diversity that was specific and not related to the other sites, with the exception of the M1, M3 and M5 sites that shared 6 clone sequences of a *Pseudomonas* type bacterium (Table 11-8), and M8 and M18 that shared 3 sequences of the Bangombé G15 bacterium. This result is also consistent with what has been reported from three other subterranean areas investigated using a similar technique (Ekendahl et al., 1994; Pedersen et al., 1996a, 1997) and probably reflects a natural selection of species diversity due to geochemical differences between the investigated boreholes. The M17 borehole was sampled three times in series and the first sample, M17-1, did not share any similar sequences with the other two samples, M17-2 and M17-5, which shared 4 similar sequences, No. 6 (Table 11-8). The uniqueness of M17-1 seems due to the fact that stagnant water in the borehole contained bacteria different from those in the more representative aquifer water subsequently pumped up. Repeated appearances of similar sequences in aquifer water from boreholes sampled in series have been reported previously (Pedersen et al., 1996b), and probably infers that the situation has stabilised in the pumped borehole with respect to species diversity and probably also with respect to the geochemical situation.

11.4.4 Identity of the Found Sequences

There is no accepted value of the percentage identity at which two 16S rRNA genes can belong to the same genus or species. It can be quite different for different genera (Fox et al., 1992) and is also due to whether total or partial 16S rRNA genes are compared. It has been suggested, based on a comparison of rRNA sequences and on DNA-DNA reassociation, that a relation on the species level does not exist at less than 97.5% identity in the 16S rRNA sequence. At higher identity values, species identity must be confirmed by DNA-DNA hybridisation (Stackebrandt and Goebel, 1994). Accepting the 97.5% level conservatively, as identifying a sequence approximately on the genus level, some conclusions can be made about the sequences reported here. A comparison of the 16S rRNA gene sequences with EMBL in March 1996, reveals 2 clone groups that can be identified with bacteria on the genus level and one with a fungus (Table 11-8). The *Acinetobacter* type 16S rRNA No. 11 sequence and the *Candida* type 18S rRNA No. 19 sequence had identities greater than 97.5% with ribosomal rRNA sequences in the database. In addition, similarities greater than 97.4% were obtained with several sequences of other subterranean bacteria detected previously, i.e. the clones No. 5–6 and 12–16. The No. 13 sequence from the neutral pH site M17 was 100% identical with the Bangombé G21 sequence representing a clone group that occurred in 3 of the 4 boreholes investigated in Bangombé, Gabon (Pedersen et al., 1996b) (also a neutral pH groundwater).

In general, none of the closest species in the database are typical of alkaliphilic organisms (Duckworth et al., 1996) and it cannot, therefore, be concluded from the 16S rRNA data that such organisms were present at Maqarin. Two possibilities remain: 1) the found sequences represent new and unknown alkaliphilic micro-organisms that remain to sequence, and 2) The found sequences represent microorganisms that have been transported to the alkaline sites with groundwater from neutral pH environments.

11.4.5 Conclusions

- Micro-organisms were found in all of the Maqarin groundwaters but it could not be conclusively demonstrated that they were *in situ* viable and growing, rather than just transported there from other neutral groundwater sources.
- The diversity of the found micro-organisms was similar to what has been detected earlier with the 16S rRNA gene sequencing method, but none of the sequences found were typical of known alkaliphilic organisms.
- Finally, a possible hypothesis based on the results is that the investigated Maqarin groundwaters may be too extreme for active life even for the most adaptable microbe (except M8) – but this remains to be demonstrated.
- Unexplained differences between the results of this work and earlier studies at the same sites, should be investigated further. In the case of biofilms on rock surfaces, fresh sterile surfaces should be introduced to flowing, high pH waters, and examined after several months.

11.5 ACKNOWLEDGEMENTS

The authors acknowledge the much valued co-operation of Tony Milodowski (BGS), Fred Karlsson (SKB) and John Smellie (Conterra). Russell Alexander and John Smellie are thanked for editorial and technical comments on the manuscript. Expert technical assistance was provided by N. Jahromi.

11.6 REFERENCES

Alexander, W.R. (Ed.), 1992. A natural analogue study of the Maqarin hyperalkaline groundwaters. I: Source term description and thermodynamic database testing. Nagra Tech. Rep. (NTB 91-10), Nagra, Wettingen, Switzerland.

Amann, R.I., Ludwig, W. and Schleifer, K-H., 1995. Phylogenetic identification and in situ detection of individual microbial cells whiteout cultivation. Microbiol. Rev. 59, 143–169.

Coombs, P., Gardner, S.J., Rochelle, C.A. and West, J.M., 1998. Natural analogue for geochemistry and microbiology of cement porewaters and cement porewater host rock/near-field interactions. In: C.M. Linklater (Ed.), A natural analogue study of cement-buffered, hyperalkaline groundwaters and their interaction with a repository host rock: Phase II. Nirex Science Report, S/98/003, Nirex, Harwell, U.K., p. 211–240.

Duckworth, A.W., Grant, W.D., Jones, B.E. and Van-Steenbergen, R., 1996. Phylogenetic diversity of soda lake alkaliphiles. FEMS Microbiol. Ecol., 19, 181–191.

Ekendahl, S., Arlinger, J., Ståhl, F. and Pedersen, K., 1994. Characterization of attached bacterial populations in deep granitic groundwater from the Stripa research mine with 16S-rRNA gene sequencing technique and scanning electron microscopy. Microbiology, 140, 1575–1583.

Felsenstein, J., 1989. PHYLIP – phylogeny inference package. Cladistics, 5, 164–166.

Fox, G.E., Wisotzkey, J.D. and Jurtshuk, J.R.P., 1992. How close is close: 16S rRNA sequence identity may not be sufficient to guarantee species identity. Int. J. System. Bacteriol., 42, 166–170.

Hallbeck, L. and Pedersen, K., 1990. Culture parameters regulating stalk formation and growth rate of Gallionella ferruginea. J. Gen. Microbiol., 136, 1675–1680.

Horikoshi, K. and Akiba, T., 1982. A new microbial world. Alkaliphilic microorganisms. Springer-Verlag, New York., pp 1–201.

Linklater, C.M. (Ed.), 1998. A natural analogue study of cement-buffered, hyperalkaline groundwates and their interaction with a repository host rock: Phase II. Nirex Science Report, S/98/003, Nirex, Harwell, U.K.

McKay, D.S., Gibson Jr, E.K., Thomas-Keprta, K.L., Vali, H., Romaneck, C.S., Clemett, S.J., Chillier, X.D.F., Maechling, C.R. and Zare, R.N., 1996. Search for past life on mars: Possible relic biogenic activity in Martian meteorite ALH84001. Science, 273, 924–930.

Niemelä, S., 1983. Statistical evaluation of results from quantitative microbiological examinations. Nordic Committee on Food Analysis. Rep. no 1, 2nd edn, ISSN 0281–5303.

Pedersen, K., 1993. The deep subterranean biosphere. Earth-Sci. Rev., 34, 243–260.

Pedersen, K., 1996. Investigations of subterranean bacteria in deep crystalline bedrock and their importance for the disposal of nuclear waste. Can. J. Microbiol., 42, 382–391.

Pedersen, K., 1997a. Microbial life in granitic rock. FEMS Microbiol. Rev. 20, 399–414.

Pedersen, K., 1997b. The microbiology of radioactive waste disposal. In: J.H. Wolfram, R.D. Rogers and L.G. Gazso (Eds.), Microbial degradation processes in radioactive waste repository and in nuclear fuel storage areas. Kluwer Academic Publisher., Netherlands.

Pedersen, K. and Ekendahl, S., 1992. Incorporation of CO_2 and introduced organic compounds by bacterial populations in groundwater from the deep crystalline bedrock of the Stripa mine. J. Gen. Microbiol., 138, 369–376.

Pedersen, K., Arlinger, J., Ekendahl, S. and Hallbeck, L., 1996a. 16S rRNA gene diversity of attached and unattached groundwater bacteria along the Access tunnel to the Äspö Hard Rock Laboratory, Sweden. FEMS Microbiol. Ecol. 19, 249–262.

Pedersen, K., Arlinger, J., Hallbeck, L. and Pettersson, C., 1996b. Diversity and distribution of subterranean bacteria in ground water at Oklo in Gabon, Africa, as determined by 16S-rRNA gene sequencing technique. Mol. Ecol., 5, 427–436.

Pedersen, K., Hallbeck, L., Arlinger, J., Erlandson, A-C. and Jahromi, N., 1997. Investigation of the potential for microbial contamination of deep granitic aquifers during drilling using 16S rRNA gene sequencing and culturing methods. J. Microbiol. Meth. (In press).

Stackebrandt, E. and Goebel, B.M., 1994. Taxonomic note: A place for DNA-DNA reassociation and 16S rRNA sequence analysis in the present species definition in bacteriology. Int. J. Syst. Bacteriol., 44, 846–849.

Stackebrandt, E. and Rainey, F.A., 1995. Partial and complete 16S rDNA sequences, their use in generation of 16S rDNA phylogenetic trees and their implications in molecular ecological studies. In: A.D.L. Achermans, F.J. van Elsas and F.J. Bruijn (Eds.), Molecular Microbial Ecology Manual. Kluwer Academic Publishers, Dordrecht.

West, J.M., Degueldre, C., Allen, M., Bruetsch, R., Gardner, S., Ince, S. and Milodowski, A.E., 1992. Microbial and colloidal populations in the Maqarin groundwaters. In: W.R. Alexander (Ed.), A natural analogue study of the Maqarin hyperalkaline groundwaters. I: Source term description and thermodynamic database testing. Nagra Tech. Rep. (NTB 91-10), Nagra, Wettingen, Switzerland, p. 70–83.

Woese, C., 1987. Bacterial evolution. Microbiol. Rev., 51, 221–271.

Table 11-1. Site and sampling information for November 1994, April 1995, and November 1996.

Sampling site	Site description	pH	Microbiology sampling year			Groundwater chemistry
			1994	1995	1996	1996
Eastern Springs						
M3	Road cut seep	hyperalkaline		x	x	x
M8	Road cut seep	hyperalkaline	x		x	x
M18	Borehole RW 1	neutral	x		x	x
Adit A-6						
M1	Seeps 140 m inside the adit	hyperalkaline		x	x	x
Western Springs						
Wadi Sijin (WS)	Seep in valley	hyperalkaline			x	x
M5	Seep at river side	hyperalkaline	x	x	x	x
M6	Seep at river side	hyperalkaline			x	x
M17	Borehole WS1	neutral	x			–

Table 11-2. Physical conditions and chemical composition of groundwaters sampled during the 1996 expedition.

Component	Method	Units	M8	M18	M1	WS	M5	M6
Temperature at sampling	Digital instrument	C°	x	x	x	x	x	x
Colour	SS028124-2		20	brown	5	15	yellow/ green	yellow/ green
Turbidity	SSEN 27027	FNU	0.44	37	0.68	1.3	0.12	3
Smell	SLV 900101		weak	strong	none	none	weak	weak
Smell, type	SLV 900101		–	wastewater	–	–	chalky	chalky
Precipitate	SLV 900101		small	very large	rather large	rather large	small	small
Precipitate, type	SLV 900101		brown particles	brown grains	white particles	sand particles	brown grains	brown grains
COD (Mn)	SS 028118	mg/L	4	19	<1	<1	<1	<1
Conductivity 25°C	SSEN 27888	ms/m	483	203	579	764	935	927
pH	SS028122-2		12.1	7.4	12.2	12.3	12.3	12.3
Alkalinity, HCO_3	SS 028139	mg/L	1400	630	1800	2100	2300	2200
Hardness total	Calculated	odH	67.2	76.8	98	131.7	154	154
Hardness tot, Ca+Mg	Calculated	mg/L	480	549	700	941	1100	1100
Iron	FE-NI	mg/L	<0.05	0.8	<0.05	<0.05	<0.05	0.12
Manganese	MN-NI	mg/L	<0.01	0.03	<0.01	<0.01	<0.01	<0.01
Ammonium, NH_4-N	SS 028134	mg/L	0.11	0.024	<0.02	0.05	1.9	1.9
Nitrite, NO_2-N	SSEN 26777	mg/L	0.028	0.018	0.006	0.011	0.28	0.51
Nitrate, NO_3-N	SS028133-2	mg/L	2	<0.2	0.7	1.1	7.7	8.1
Phosphate, PO_4-P	SS028126-2	mg/L	<0.01	0.01	<0.01	<0.01	<0.01	<0.01
Fluoride	SS 028135	mg/L	0.39	1.7	0.34	0.45	1.0	1.1
Chloride	SS 028120	mg/L	53	163	55	87	47	48
Sulphate	SS 028182	mg/L	325	780	280	400	1300	1300
Sodium (ICP)	NA-A2I	mg/L	28	110	49	40	140	150
Potassium (ICP)	K(AIM)	mg/L	4	35	9	18	530	550
Zinc (ICP)	ZN-AIM	mg/L	<0.01	0.06	0.09	0.12	0.02	0.02
Cadmium (ICP)	CD-AIM	mg/L	<0.01	<0.01	0.01	0.01	0.01	0.01
Nickel (ICP)	NI-AIM	mg/L	<0.02	0.03	<0.02	<0.02	<0.02	<0.02
Magnesium (ICP)	MG-NI	mg/L	<0.1	54	<0.1	0.4	<0.1	<0.1
Copper (ICP)	CU-AIM	mg/L	<0.01	<0.01	<0.01	<0.01	<0.01	<0.01
Aluminium (ICP)	AL-AIM	mg/L	0.1	0.3	<0.1	0.1	0.1	0.3
Barium	BA-AIM	ug/L	30	70	30	30	20	20
Lithium (ICP)	LI-NI	mg/L	0.02	0.08	0.02	0.06	0.48	0.48
Lead, Pb (ICP)	PB-AIM	mg/L	<0.1	<0.1	<0.1	<0.1	<0.1	<0.1
Cobolt, Co (ICP)	CO	mg/L	<0.01	<0.01	<0.01	<0.01	<0.01	<0.01
Boron, B (ICP)	B-AIM	mg/L	<0.01	0.07	<0.01	<0.01	0.11	0.12
Chromium, tot, Cr (ICP)	CR-AIM	mg/L	0.88	<0.01	0.73	0.72	5.0	5.0
Calcium, Ca (ICP)	CR-A2IM	mg/L	480	460	700	940	1100	1100
Strontium, Sr (ICP)	SB-AIM	mg/L	3.7	11	6.4	15	14	14

Table 11-3. Total number of bacteria in groundwater samples from the Maqarin area in Jordan as determined by AODC.

Sampling site	Clone	pH	Total number of bacteria mL^{-1}		
	letter		Nov. 1994	Apr. 1995	Nov. 1996
Eastern Springs					
M3	h	hyperalkaline	–[a]	$2.0 \cdot 10^4$	nd[b]
M8	b	hyperalkaline	$1.2 \cdot 10^4$	–	$1.3 \cdot 10^5$
M18-3	f	neutral	$6.4 \cdot 10^6$	–	–
Adit A-6					
M1	g	hyperalkaline	–	$2.5 \cdot 10^3$	nd
Western Springs					
WS	–	hyperalkaline	–	–	$9.8 \cdot 10^3$
M5	a	hyperalkaline	nd	$3.0 \cdot 10^3$	$4.6 \cdot 10^3$
M6	–	hyperalkaline	–	–	$2.4 \cdot 10^4$
M17-1	c	neutral	$8.5 \cdot 10^6$	–	–
M17-2	d	neutral	$6.5 \cdot 10^6$	–	–
M17-5	e	neutral	$1.1 \cdot 10^6$	–	–

[a] No sampling.

[b] Not determined due to high background caused by much precipitates.

Table 11-4. Enrichment cultures with glucose or lactate as carbon source and the subsequent action taken after assessing growth of enrichment cultures at day 27 after inoculation.

Sampling site	Culture	Result	Action taken
Eastern Springs			
M3	lactate	no growth	cancelled
M3	glucose	no growth	cancelled
M8	lactate	growth	sub-cultured, see Table 11-5
M8	glucose	growth	sub-cultured; see Table 11-5
M18	lactate	no growth	cancelled
M18	glucose	no growth	cancelled
Adit A-6			
M1	lactate	growth	sub-cultured; see Table 11-5
M1	glucose	no growth	cancelled
Western Springs			
WS	lactate	no growth	cancelled
WS	glucose	no growth	cancelled
M5	lactate	no growth	cancelled
M5	glucose	no growth	cancelled
M6	lactate	no growth	cancelled
M6	glucose	no growth	cancelled

Table 11-5. Results from the sub-culturing of the selected enrichment cultures after 19 days.

Enrichment culture, from Table 11-4	Media used	pH	Result
M8-lactate	Lactate media 1	8.5	heavy growth
M8-lactate	Lactate media 2	10.1	growth
M8-lactate	Lactate media 3	10.1	weak growth
M8-glucose	Glucose media 1	8.6	no growth
M8-glucose	Glucose media 2	10.1	no growth
M8-glucose	Glucose media 3	10.0	no growth
M1-lactate	Lactate media 1	10.8	no growth
M1-lactate	Lactate media 2	10.1	no growth
M1-lactate	Lactate media 3	10.1	no growth

Table 11-6. pH of the water sampled during the 1996 expedition and the pH values that developed during culturing experiments.

Sampling Site	Measured at the sampling site	Laboratory results	After 3 days in a glucose culture	After 3 days in a lactate culture
Eastern Springs				
M3	12.1	n.a.[a]	11.6	12.7
M8	11.9	12.1	11.4	12.5
M18	7.6	7.4	n.a.	n.a.
Adit A-6				
M1	11.9	12.2	11.5	12.6
Western Springs				
M5	12.0	12.3	11.8	12.9
M6	12.0	12.3	11.7	12.9
Wadi Sijin	11.9	12.3	11.9	12.9

[a] not analysed

Table 11-7. Closest species in the EMBL database to 16S rDNA extracted from two of the enrichment cultures.

Enrichment Culture	Closest species in the EMBL database	Identity %
M8-glucose	*Sphingomonas sp.*	92.8
M8-lactate	*Rhodobacter capsulatis*	97.9

Table 11-8. Distribution of the clones between the different Maqarin sample sites, sampled in November 1994 (clone groups JN1 to JN 19 from M5, M8, M17, M18) and April 1995 (clone groups JA21 to JA24 from M1, M3 and M5). Alkaline springs are shaded.

No	Clone	Closest sequence in	Identity	Number of identical clone sequences								
				Eastern Springs			Adit A-6	Western Springs				Total
	group	the EMBL database	(%)	M3	M8	M18-3	M1	M5	M17-1	M17-2	M17-5	
		Proteobacteria Alpha group										
1	JN15d	*Agrobacterium tumefaciens*	95.4							1		1
2	JN8c	*Rhodobacter capsulatus*	97.2						1			1
3	JN9c	n.r.[a]	93.5						1			1
		Proteobacteria Beta group										
4	JN7b	Bangombé, G16 (*Rhodocyclus*)	98.0		2							2
5	JN1af	Stripa clone group II (*Pseudomonas*)	95.4			1		9				10
6	JN11de	Stripa clone group II (*Pseudomonas*)	97.4							4	5	9
7	JN6b	n.r.	92.8		1							1
8	JN12d	n.r.	92.8							1		1
9	JA22ahi	n.r.	90.3	1				1				2
10	JN13d	n.r.	89.4							1		1
		Proteobacteria Gamma group										
11	JA23h	*Acinetobacter calcoaceticus*	98.0	2								2
12	JN16e	*Acinetobacter lwoffii*	97.4								1	1
13	JN2c	Bangombé, G21 (*Acinetobacter*)	100						6			6
14	JN3c	Bangombé, G21 (*Acinetobacter*)	95.0						1			1
15	JN17e	*Äspö, S6* (*Acinetobacter*)	98.8								2	2
16	JA21agh	Äspö HRL, S25 (*Pseudomonas*)	98.8	6			10	9				25
		Gram-positive bacteria										
17	JN10c	n.r.	92.9						1			1
		***Deinococcus-Thermus* group**										
18	JA24he	n.r.	93.3	1								1
		Eukarya										
19	JN4ab	*Candida holmii*	98.1		3			1				4
		Remaing distant clones										
20	JN5bf	Bangombé, G15 (n.r.)	99.7		3	9						12
21	JN14d	n.r.	87.6							1		1
22	JN18e	n.r.	80.4								1	1
23	JN19e	n.r.	73.1								1	1
		Total no. of clone groups		4	4	2	1	2+2	5	5	5	23
		Total no. of clones		10	9	10	10	10+10	10	8	10	87

[a] To distant for a meaningful affiliation and, therefore, not relevant (n.r.).

FIGURES

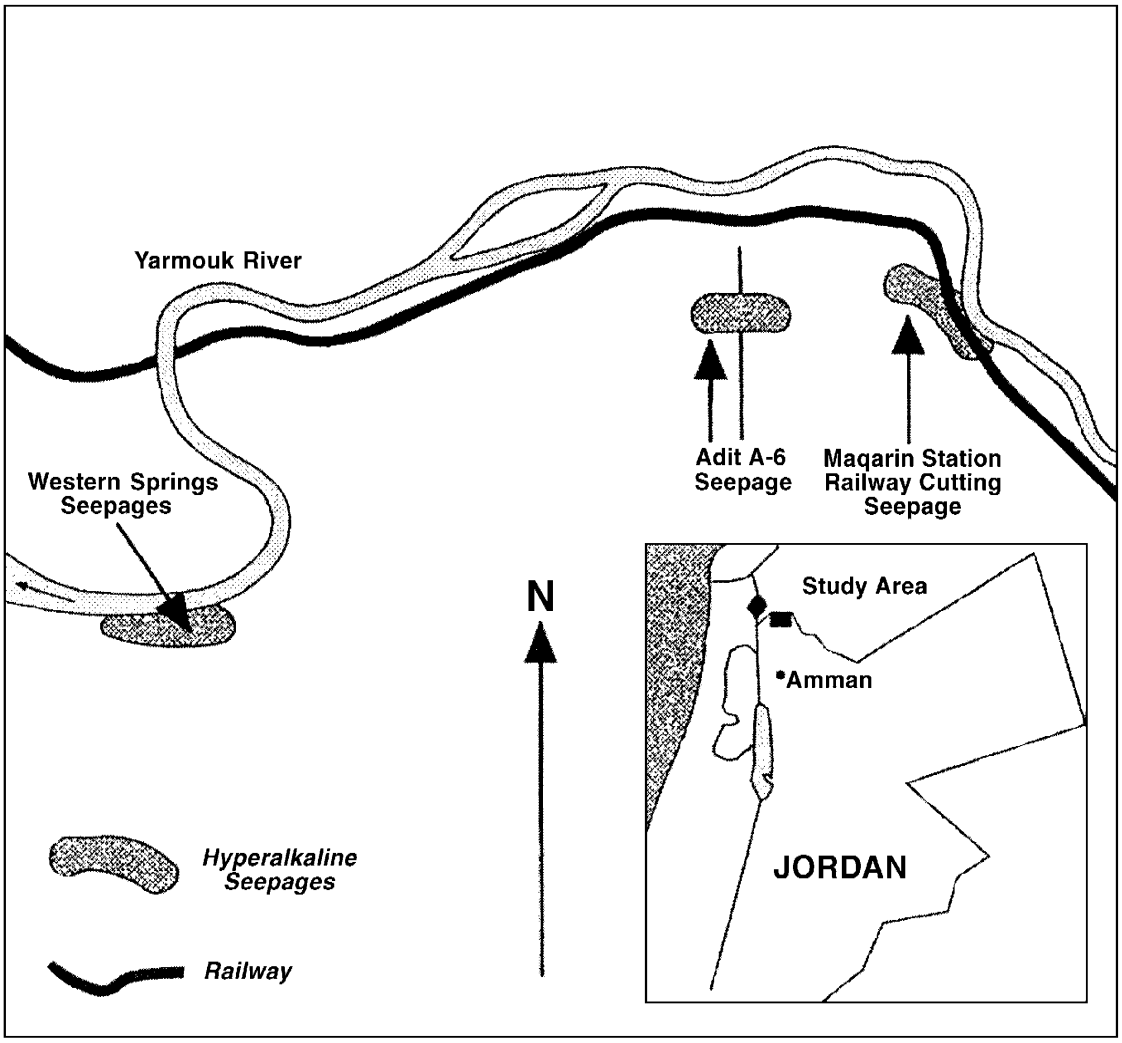

Figure 11-1. *Sample locations for microbiological studies in the Maqarin area.*

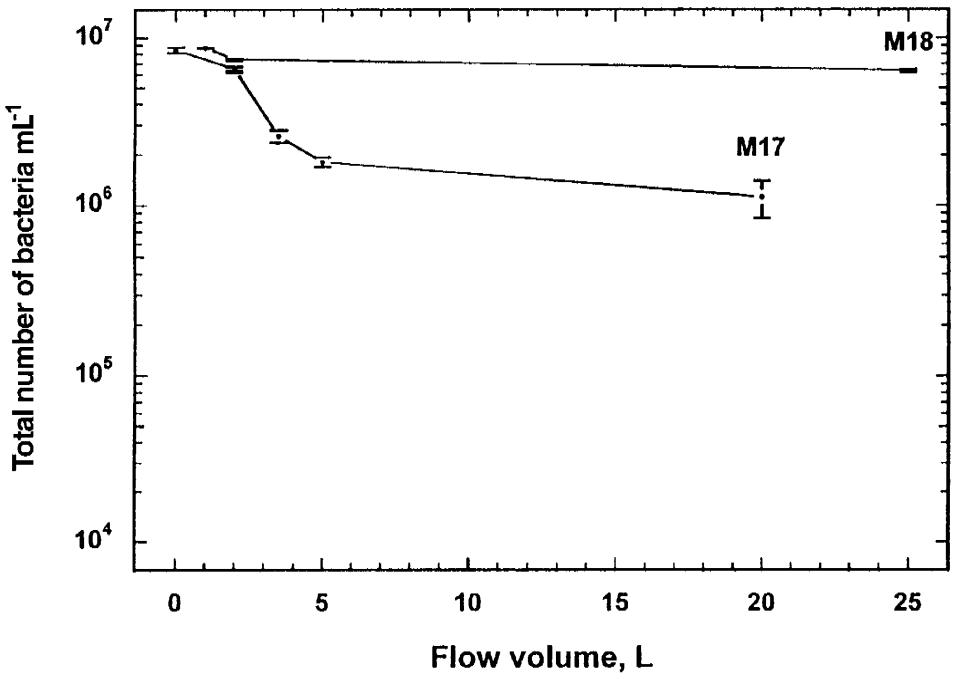

Figure 11-2. *The change in total number of bacteria in the boreholes M17 and M18 during pumping of groundwater in April 1994.*

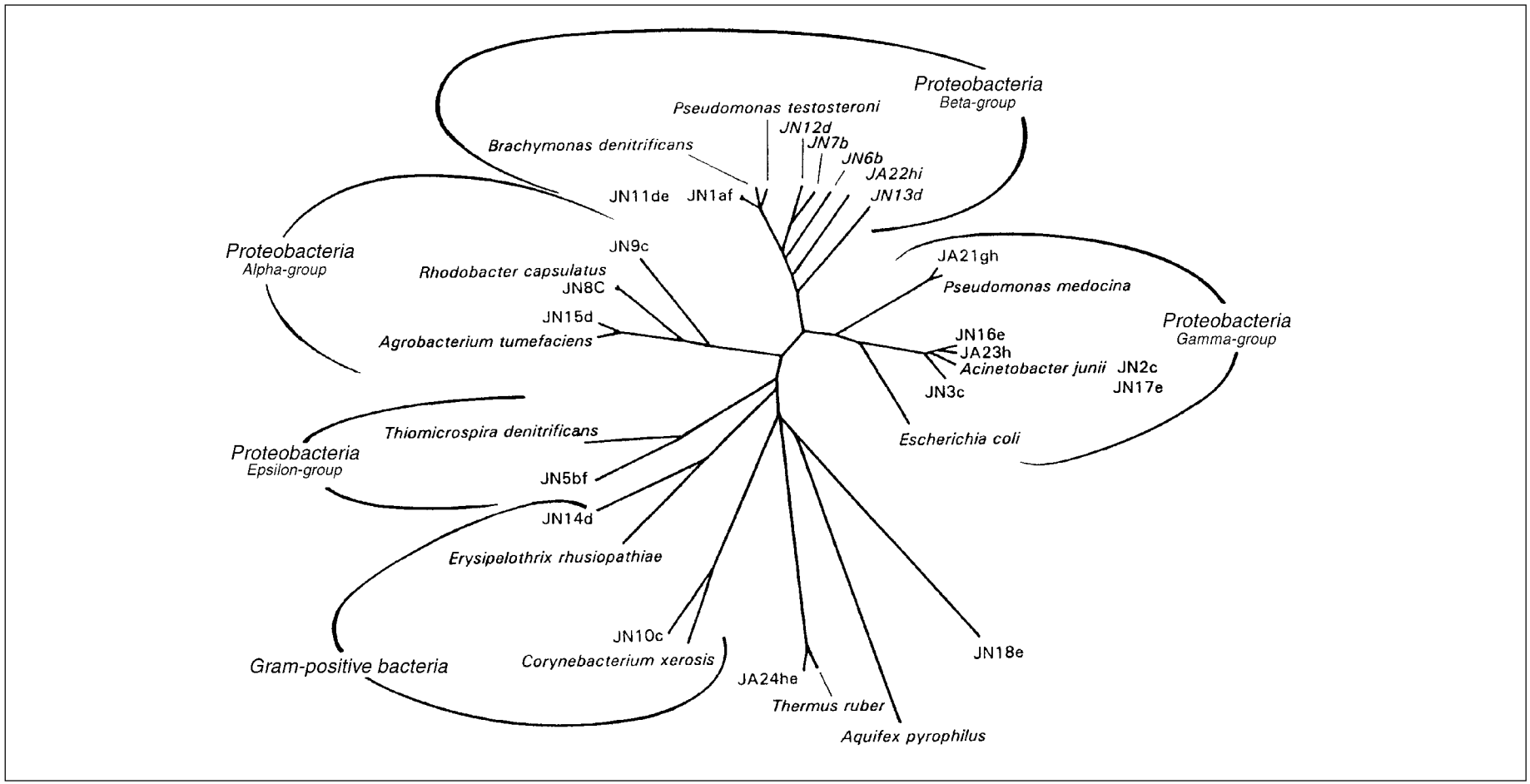

Figure 11-3. *Evolutionary distance tree based on the 16S rRNA gene sequences of clones from different localities in the Maqarin area. Four clone sequences were only very distantly related to known, sequenced and reported bacteria, and were, therefore, not affiliated in phylogenetic groups. Major phylogenetic groups of bacteria have been designated with their generally accepted names. As references, some 16S rRNA gene sequences of known bacteria from the EMBL database have been added to the tree and they are indicated with their Latin names. The tree was used to differentiate the main lines of descent of the found sequences; it will not unravel intragenic phylogeny.*

12 MAQARIN: IMPLICATIONS TO REPOSITORY PERFORMANCE ASSESSMENT

12.1 BACKGROUND

The Maqarin site now provides a consistent picture explaining the origin of the hyperalkaline waters, the persistence of some of the hyperalkaline springs/seepages and the sequence of alterations occurring when such waters react with various rock types. Additionally, the studies have produced good quality measurements of the concentration (and general speciation) of some relevant elements in high pH groundwaters, microbial populations and concentrations of colloidal material.

Information gained from the studies at Maqarin (Phases I-III) have implications for both near- and far-field processes in cementitious repositories for low- and intermediate-level ('TRU' in some concepts) radioactive wastes, and also where the use of concrete may be envisaged in repositories for high-level radioactive wastes (HLW). Current temperatures are relatively low at Maqarin, so that the effects of higher temperature (important for the TRU and HLW designs) upon the repository far-field cannot be evaluated from Maqarin data, but it may be possible to gain some understanding of the effects on repository materials by more detailed study of the (high temperature) cement zone.

The Maqarin natural analogue site is a unique location to study the mechanisms and test models of the processes associated with cementitious repositories. Features which establish Maqarin's uniqueness are the following:

- the occurrence of organic-rich (kerogenous) clayey limestones (i.e. Bituminous Marl Formation) on a regional scale in central-northern Jordan, providing a source of combustible material to generate clinker and subsequently cement minerals;
- an arid to semi-arid climate with concomitant relatively low water table, establishing the capacity for combustion of the Bituminous Marl Formation in the unsaturated zone;
- at a site level, a suitable geotectonic environment, with tensional fractures in anticlinal structures, the presence of karst features, and slumping features initiated by seismic activity and/or lateral erosion of the Yarmouk River, together enabling penetration of oxygen (and water) to depth to fuel combustion of the organic material; and
- at site level, the presence of an older, more evolved cement zone/groundwater interaction system (Eastern Springs), and a younger, less evolved system (Western Springs).

Within the cement zone itself at Maqarin, the following attributes add to the site's value as a cement analogue:

- groundwater inflow and water saturation of the combusted marls has produced cement from the clinker material;
- subsequent neutral water flow through the cement zone has resulted in leaching and the development of a high pH plume;
- interaction with the cement zone provides the possibility of studying typical cement-like minerals and their long-term stabilities;
- advection-dominated system, allowing rapid flow of the hyperalkaline water through the host marls with incomplete buffering; and
- regular reactivation of groundwater flowpaths along fractures caused by gravity sliding and/or tectonic activity.

A list of topics for which the Maqarin analogue might provide supporting data and/or information relevant to performance assessment, is given below:

Near-field processes:

- evolution of high pH pore fluids in time and space;
- solubilities (and speciation?) of radionuclide-bearing solids;
- radionuclide sorption;
- colloids;
- microbes;
- organics;
- metal (canister) corrosion;
- gas production (via metal corrosion and organic breakdown);
- stability of bentonite (used as seals in some repository concepts) in a cementitious environment;
- stability of cement-like materials used in repository construction.

Far-field processes:

- physical scale of the alkaline altered zone;
- processes at pH fronts;
  - mobilisation of radionuclides
  - colloid generation and behaviour
  - behaviour of microbial populations and organics
  - radionuclide sorption, precipitation and ion exchange;
  - matrix diffusion;
  - mobilisation of naturally-occurring organics from the host rock.

12.2 NEAR-FIELD PROCESSES

12.2.1 Evolution of High pH Pore Fluids in Time and Space

Groundwaters have been sampled from the cementitious zone in Adit A-6 above the Eastern Springs location. These groundwaters are portlandite-saturated and have a pH of around 12.5. The groundwaters at the Western Springs location have high Na^+ and K^+ levels. However, the cementitious source cannot be assessed at present. The original thought that these waters were representative of "young near-field" high pH waters seems to be borne out by the hydrogeochemical studies and supported by geomorphological criteria.

12.2.2 Solubilities of Radionuclides and Identification of Radionuclide-bearing Solids

Trace element concentrations in high pH waters were obtained during Phases I and II of the Maqarin study. Standard thermodynamic models and databases were used to predict the trace element concentration in these waters assuming solubility control by a simple oxide or hydroxide solubility limiting phase. In general, modelled data overestimate solubilities by one or more orders of magnitude and thus provide conservative estimates. The lack of any appropriate model for solid-solution behaviour prevented refinement of these models. Oxic groundwater conditions at Maqarin have been generally inferred, but the presence of organic material in the Bituminous Marls, and the existence of zeolites which include Fe^{2+}, suggest that sub-oxic conditions may be more prevalent than initially thought.

General speciation data were acquired on the Maqarin groundwaters.

12.2.3 Sorption

Mineralogical information cannot distinguish between sorption and "incorporation" in the mineral phase; furthermore, sequential extraction techniques cannot be used on such reactive minerals. The inability to distinguish between sorption and co-precipitation of chemical elements of relevance to performance assessment in the analytical data for solids in the cement zone from Maqarin means that no relevant data are available on this topic. There is some suggestion for the association of certain elements with specific minerals (e.g. uranium with zeolites), but the mechanism is unknown.

12.2.4 Colloids

Evidence from Maqarin groundwaters suggests that the amount of colloids generated in the cement zone will be no higher than those observed in most repository rocks (approx. 10^8 colloids mL^{-1}). There does appear to be a significant population of colloids in the <100 nm range and the suggestion is that the colloids are cementitious. More work is required on a better definition of the colloid chemistry and stability and in collecting colloids at a pH front. Work in Phase I demonstrated that no uranium (or other trace elements) was associated with the colloidal material characterised.

12.2.5 Microbes

Data reported during Phase I demonstrated that microbial populations were capable of withstanding hyperalkaline conditions, but no information was available concerning their activities (ability to multiply and grow). Several key groups of microbes (e.g. sulphate-reducing bacteria) have been measured in both water and rock samples; activity levels seem to be significantly lower than the values derived from simple models, implying that the latter may be unduly conservative.

Recent studies, including gene sequencing work on microbial material from Maqarin, have shown that the total number of bacteria are within the range of other subterranean sites and that there is a diverse microbial population present. However, no attached bacteria were found; absence of biofilms after a couple of months of exposure, together with the fact that few of the enrichment cultures showed positive signs of growth, would be a strong indication that microbes are not active at the high pH values prevalent at Maqarin.

12.2.6 Organics

Semi-quantitative evidence exists for the mobility of organic matter (kerogenous) and the stability of a variety of carboxylic acids in the hyperalkaline groundwater at Maqarin. The high DOC content in some groundwaters, however, cannot be explained by dissolution of organic matter from the Bituminous Marl by percolating high pH groundwaters; solution experiments show only a minor part of the organics could dissolve in the water. Organic matter does not appear therefore to play any major role in the geochemistry of the trace elements studied. Furthermore, no data were found which suggested the presence of breakdown products of cellulose (e.g. isosaccharinic acid).

12.2.7 Metal (canister) Corrosion

Metal materials in alkaline waters at Maqarin (e.g. Adit A-6; Maqarin Station Railway Cutting) have been corroded under oxic conditions and thus provide no relevant data for corrosion in the repository environment where anoxic corrosion is expected to be prevalent.

12.2.8 Gas Generation

Maqarin provides no data relevant to this topic.

12.2.9 Stability of Bentonite

The lack of identifiable smectite clays in zones of alkaline alteration precludes data from Maqarin contributing to this issue for repository performance assessment. The investigation of more clay-rich rock samples from locations such as Sweileh may provide information on this topic in the future.

12.3 FAR-FIELD PROCESSES

12.3.1 Scale of the Alkaline Disturbed Zone

The scale of the alkaline disturbed zone (ADZ) is a site-specific issue. Differences in porosity, permeability, hydraulic gradient and lithology with likely repository sites mean that evidence for the scale of alteration at Maqarin is not directly transferrable. However, the information is of value, even for those potential repository sites where transport may be dominated by diffusion (e.g. Wellenberg), as in these cases, it only takes a single fracture to allow advection away from the repository, and this will strongly influence the safety calculations. As Maqarin is dominated by fracture controlled advective flow, the site therefore provides important data for model testing and supporting information on the nature of fractures and the potential for their sealing etc. Data from Maqarin suggest alteration on the 10's to 100's m scale. Evidence uniformly suggests that fractures containing hyperalkaline groundwater will close with time due to water/rock interaction. When reactivation occurs, flowpath lengths may extend to at least 0.5 km. The hyperalkaline system at Maqarin remains active due to periodic reactivation of fractures due to slumping.

Better data on rock permeability on samples from Maqarin would help improve the comparison with repository systems.

12.3.2 Processes at pH Fronts

Mineralogical data show that pH fronts have passed through the various components of the Maqarin system (fractures, matrix, colluvium boulders), but evidence for fronts in the current groundwater system are absent.

The sequence of mineral alteration at these fronts has been modelled relatively successfully using the CHEQMATE coupled transport and chemistry computer code. For example, the model correctly predicted:

- the types of secondary phases precipitating (e.g. CSH phases, zeolites, ettringite);
- the relative amounts of different phases (e.g. zeolite distribution linked to availability of Al in the primary mineral assemblage).

However, thicknesses of alteration and migration distances were poorly simulated. These discrepancies were attributed to limitations in the way the reactions could be represented in the calculations, principally a lack of coupling between changing porosity and fluid flow/diffusion, an assumption of chemical equilibrium for all minerals, including silicates, and omission of the effects of mineral 'armouring' by reaction products. There were additional problems related to the accurate estimation of the timescale over which the alkaline water/rock interaction had been active, and a lack of data describing the physical properties of some of the rock types prior to reaction.

A kinetic representation of the reactive processes using the MARQUISS code was also able to predict the mineral sequence, but the application was limited by an inability of the computer code to scale mineral reaction rates adequately, due to numerical convergence problems.

Future work could focus on appropriate places to trace and sample reaction fronts in the pore water system at Maqarin (via borehole drilling).

12.3.3 Radionuclide Sorption, Precipitation and Ion Exchange

As for subsection 12.2.3, even though data for this topic are semi-quantitative, it is worth bearing in mind that very little other data exist in the published literature. In brief, the most important are:

Uranium:

Source: Finely dispersed organic matter/Ca-U oxycarbonate.

Sink: Portlandite, calcite, ettringite, thaumasite, jennite, tobermorite, zeolite, ferric oxyhydroxides, organic matter.

Thorium, Tin and Radium

Source: Cement zone, altered Bituminous Marl.

Sink: None specifically identified. Radium and tin are "associated" with secondary C-S-H and C-A-S-H phases; thorium is probably source-term limited in the high pH groundwaters.

Selenium

Source: Associated with sulphide (pyrite) and sulphate (gypsum) phases in the cement zone.

Sink: Solid solution of Se – ettringite; also reprecipitation in sulphides (and selenides).

Nickel

Source: Ni-Fe (selenides) and pyrite in cement zone.

Sink: Thaumasite, ettringite, vaterite, calcite.

12.3.4 Matrix Diffusion

The mineralogical alteration of wallrocks adjacent to fractures at Maqarin gives evidence that, initially at least, the rock matrix is accessible to diffusion. Evidence from ^{226}Ra profiles in the rocks adjacent to fractures suggests that the matrix continues to be accessible to fluids from fractures. This important observation implies that matrix

diffusion could continue to act as a retardation mechanism in the altered rock. Mineralogical evidence from Phase II and porosity studies from Phase III suggest an opening of porosity in the matrix, but sealing closer to the fracture wall with calcite. The general applicability of these phenomena to other rock types, however, depends on the different rock types and matrix pore waters encountered, leading to different chemical reactions and behaviour. For example, Maqarin has shown that in the absence of HCO_3 pore water, leachates may serve to reduce matrix accessibility by the precipitation of portlandite on the fracture wall.

12.4 CONCLUDING COMMENTS

The Maqarin natural analogue site is a unique location to be able to examine the mechanisms of processes associated with cementitious repositories. Evidence from Maqarin shows that:

- the conceptual model for the evolution of a hyperalkaline plume in a host rock is largely consistent with observations of the site;
- hyperalkaline pore fluid conditions generated by minerals analogous to those envisaged for cements are long-lived (in excess of several thousand years);
- predictive models of the solubility of elements of interest to radioactive waste disposal provide conservative estimates of solubility, i.e. solubilities are over-estimated;
- the amounts of colloidal material generated at the cement zone/host rock interface will be low;
- sequences of minerals predicted by thermodynamic and coupled modelling are similar to those observed in hyperalkaline alteration zones at Maqarin;
- the rock matrix may be accessible to diffusion of aqueous species;
- fractures will be probably self-healing;
- tectonic effects upon fracture sealing need to be routinely included in models of repository evolution.

However, some questions remain open:

- a pH front has not been observed directly in the groundwater system;
- to date, Maqarin reveals little about processes associated with Na, K-dominated cement pore fluids.

13 CONCLUSIONS

Phase III studies primarily addressed the regional geomorphological, hydrogeological and hydrochemical context of the Maqarin site in northern Jordan, and looked in detail at the higher pH (up to pH 12.9) groundwater system at the Western Springs locality, where the presence of Na/K enriched $Ca(OH)_2$ groundwaters have been confirmed. At this locality, the presence of more siliceous rocks (e.g. basalt, chert etc.) allowed examination of water/rock interactions of more relevance to repositories planned for crystalline host rocks. Geochemical modelling of this system (involving both equilibrium and kinetic approaches), should help to build confidence in long-term plume evolution around repositories in different geological environments. Additional objectives included a literature review of zeolite minerals of relevance to the hyperalkaline plume, an examination of colloid and microbial populations in hyperalkaline groundwaters, a study of organic material in the rock and groundwaters and an evaluation of clay stability in the presence of hyperalkaline fluids.

13.1 AGE OF THE HYPERALKALINE FLOW SYSTEMS

There seems good geomorphological evidence from the Maqarin region to support the hypothesis that lateral erosion and undercutting by the Yarmouk River, resulting in landslides and/or slumping, either triggered by seismic activity or simply gravitational mechanisms associated with heavy periods of rainfall, would provide the necessary conditions for sudden oxygen (and water) ingress and subsequent spontaneous combustion of the Bituminous Marls (i.e. limestone/clay biomicrite) to form the cement zones. The earliest combustion event probably occurred sometime between 500–800 ka, and around 600 ka would appear to be a reasonable compromise. Furthermore, land movements associated with spontaneous combustion have occurred at various times during the last 600 ka. Present studies suggest the possibility that land movements and combustion in the area which includes the Eastern Springs occurred soon after 600 ka. More hypothetically, a second, later phase of triggered landslides at the Western Springs area, might have occurred in the last 100 ka of Late Quaternary time, or even as recently as the last 10 ka, i.e. within the Holocene.

More minor earth movements have occurred and continue to occur in the Maqarin region, causing reactivation of pre-existing fractures and the formation of new ones. This accounts for many of the observations in the Eastern Springs locality, where several age generations of hyperalkaline reaction and alteration products are represented in single fracture zones, indicating periodic opening and sealing of many of the high pH groundwater pathways.

13.2 HYDROGEOCHEMICAL EVOLUTION OF THE GROUNDWATERS

Hydrochemical studies largely support the hydrogeological conceptualisation of the major groundwater flow pathways in the Maqarin region. The recharge groundwaters to the Eastern and Western Springs localities (i.e. the precursors to the high pH groundwaters) are meteoric and local in origin, recent (less than 40 a), of normal pH and dilute bicarbonate in type. Interaction of these groundwaters with the cement zones has produced two distinct types of high pH groundwaters, both older than 40 a: Eastern Springs Ca-(Na,K)-OH type and a Western Springs Ca-K-(Na)-OH-SO_4 type. Hydrochemical modelling suggests that the observed differences can be attributed to different stages of water/rock interaction and evolution. There is no convincing evidence that the high Na, K and SO_4 concentrations at the Western Springs locality are due to initial differences in the composition of the cement zones, variable infiltration conditions, or anthropogenic contamination. The Eastern Springs area is characterised simply by an older groundwater circulation system, whereby the readily soluble K/Na rich mineral phases are already completely dissolved and removed. This compares with the Western Springs area where the groundwater flow system is younger and therefore less evolved geochemically. This conclusion is supported by laboratory experiments.

These hydrochemical features are consistent with the field observations which indicate that the Eastern Springs system is geologically older than the Western Springs system. This in turn strengthens the analogy of the Maqarin system with early-stage Region 1 (Na/KOH) and late-stage Region 2 ($Ca(OH)_2$) cement leachate/host rock interaction under repository conditions.

13.3 MINERALOGICAL AND GEOCHEMICAL EVOLUTION WITHIN THE PLUME

From the Western Springs colluvium deposits, detailed examination of high pH groundwater interaction with boulders and clasts of Pleistocene basalt and limestone/clay biomicrite (including chert) showed the following general reaction sequence: basalt (glass > plagioclase/K-feldspar > augite/hypersthene/olivine) > chert/ quartz > dolomitic biomicrite > calcitic biomicrite. Calcite, apatite and Fe-oxyhydroxides are generally resistant to the high pH leachates. Mineral paragenesis of the secondary alteration phases indicates the following sequence: a) a very hydrous Ca-K-Na-Al 'zeolite-type' phase, b) a CSH gel with a variable Ca:Si ratio covering the range of CSH(I) to CSH(II) (i.e. suolinite-afwillite), c) a more Si-rich CSH gel (i.e. okenite-type), and d) a low Ca-Si ratio CSH phase (i.e. truscottite-type). The latest stage of alteration is the replacement of the CSH and CASH phases by calcite or aragonite. The development of clast reaction rims seem to be in the order of biomicrite > chert > basalt. However, this does not preclude that clast-specific mineral phases in the chert and basalt may be more altered than in the biomicrite, and also that the biomicrite may be more porous.

Based on these mineralogical observations and groundwater chemistry, geochemical modelling (both equilibrium and kinetic approaches) was carried out to predict the

extent and nature of the reaction rims around the clasts. The following conclusions can be made:

- two processes influence the suite of secondary minerals within clast reaction rims; precipitation occurring within the solutions and dissolution of primary minerals as a consequence of hyperalkaline water/rock interaction,

- the secondary minerals predicted to form using an equilibrium model (portlandite, ettringite, calcite, CSH phases and zeolites) were in reasonable agreement with those observed in the field,

- the calculations overpredicted the width of the reaction rims around the clasts,

- both the mineralogy and transport properties of the system play an important role in determining the width of the reaction rims, and

- the transport properties (porosity, diffusivity) of the clasts had the most important influence on the width of the reactions rims.

In general, the data from Western Springs present a snapshot of the likely temporal evolution of a high pH plume in any flow system where the central part of the plume may over-run the distal edge which may then be over-run by the proximal portion, with each new section of the plume replacing wholly, or in part, the previous mineral assemblage.

13.4 ROCK MATRIX POROSITY

Samples from Adit A-6 in the Eastern Springs location were studied to determine the presence and significance of porosity variations in the host rock adjacent to fracture zones in contact with reacting high pH groundwaters, and the effect this has had on geochemical diffusion into the matrix. Four profiles were selected and analysed for a suite of elements and natural decay series radionuclides along with porosity measurements. The results are highly ambiguous. Geochemical enhancement close to the fractures is most likely explained by the presence of microfracture infill minerals and by the dissolution and replacement of matrix calcite in the host rock, particularly at the fracture face. Significant variation in the natural decay series radionuclide background signatures has made it impossible to detect any potential perturbations due to hyperalkaline water/matrix interaction. However, the $^{236}Ra/^{238}U$ ratios suggest relatively young water/rock interaction up to 4-7 cm depth. Even so, these depths should be treated cautiously because of the potential influence by microfracture networks and pre-existing lithological variations (i.e. bedding) extending several centimetres into the rock.

13.5 MICROBES, ORGANICS AND COLLOIDS

Micro-organisms are present in all the hyperalkaline groundwaters studied from the Eastern and Western Springs localities (around 10^5 microbes mL^{-1}), but it could not be demonstrated conclusively that they were viable *in situ* and growing at high pH, rather than just transported to the sampling sites from the neutral groundwater system. Gene sequencing studies show that there is a diverse microbial and colloidal population within the range of that recorded at other subterranean sites.

The high DOC content in the Western Springs groundwaters cannot be fully explained by dissolution of organic matter from the Bituminous Marls by percolation of high pH groundwaters. An alternative source material may be that which has resulted from the partial combustion of bitumen; this would explain the high aromatic content and might be a contributary cause to the absence of soil-derived humic compounds in the groundwaters.

The amounts of colloids collected from the cement zone/Bituminous Marl interface in Adit A-6 were very low (10^7 colloids mL^{-1}). It was also demonstrated that no uranium (or other trace elements) is associated with the colloidal material. However, as a note of caution, sampling was carried out under oxidising conditions, which cannot be compared to the reducing conditions expected to characterise a repository environment.

13.6 PERFORMANCE ASSESSMENT CONSIDERATIONS

The Maqarin site now provides a consistent picture explaining the origin of the hyperalkaline waters, the persistence of some of the hyperalkaline springs/seepages, and the sequence of alterations occurring when such waters react with various rock-types. Additionally, the studies have produced good quality measurements of the concentration (and general speciation) of some performance assessment relevant elements in high pH groundwaters, microbial populations and concentrations of colloidal material.

The Maqarin natural analogue site is therefore a unique location for the examination of the mechanisms and processes associated with cementitious repositories. Evidence from Maqarin shows that:

- hyperakaline pore fluid conditions generated by minerals similar to those found in cements are long-lived (in excess of tens of thousands of years),

- predictive models of the solubility of several elements of interest to radioactive waste disposal provide conservative estimates of solubility (i.e. solubilities are overestimated),

- the amounts of colloidal material generated in the cement zone/host rock interface will be probably no higher than in neutral groundwaters,

- sequences of minerals predicted by thermodynamic and coupled modelling are similar to those observed in hyperalkaline alteration zones,
- the rock matrix may be accessible to diffusion of aqueous species even during the phase of on-going wallrock alteration,
- narrow aperture fractures will probably be self-healing,
- tectonic effects upon fracture sealing and the site hydrology need to be considered on a repository site-specific basis,
- the conceptual model for the evolution of a hyperalkaline plume in a host rock is largely consistent with observations at the site.

ISSN 1404-0344
CM Gruppen AB, Bromma, 1998